

**ANALYSIS AND DESIGN
OF COMPOSITE AND
METALLIC FLIGHT
VEHICLE STRUCTURES**

RICHARD ABBOTT

THIRD EDITION

THIS BOOK IS PROVIDED FREE OF CHARGE BY [ABBOTT AEROSPACE SEZC LTD.](#) WE GRANT YOU THE RIGHT TO USE, COPY AND
DISTRIBUTE THIS BOOK WITHOUT LIMITATION. TO FIND OUT MORE VISIT OUR TECHNICAL LIBRARY BY CLICKING [HERE](#).

WWW.ABBOTTAEROSPACE.COM

WWW.ABBOTTAEROSPACE.COM

REVISION HISTORY

Table of Contents

Published by: Abbott Aerospace SEZC Ltd, Bayside Plaza, 68 West Bay Road, Georgetown, Grand Cayman, PO Box 10315, KY1-1003
© Richard Abbott, 2016, 2017, 2019

This book is released as a free public domain product and every user is free to use, copy and distribute this book without limitation. Citation may be given as follows:

Abbott, Richard. Analysis and Design of Composite and Metallic Flight Vehicle Structures 3rd Edition, 2019

Notice: No responsibility is assumed by the author or publisher for an injury and/or damage to persons or property as a matter of products liability, negligence or otherwise from any use or operation of any methods, procedures, instructions, calculations, spreadsheets, source materials or ideas contained within, or linked to, the material herein.

British Library Cataloguing-in-Publication Data
A catalogue record for this book is available from the British Library.

ISBN Number: 978-1-5272-3825-1



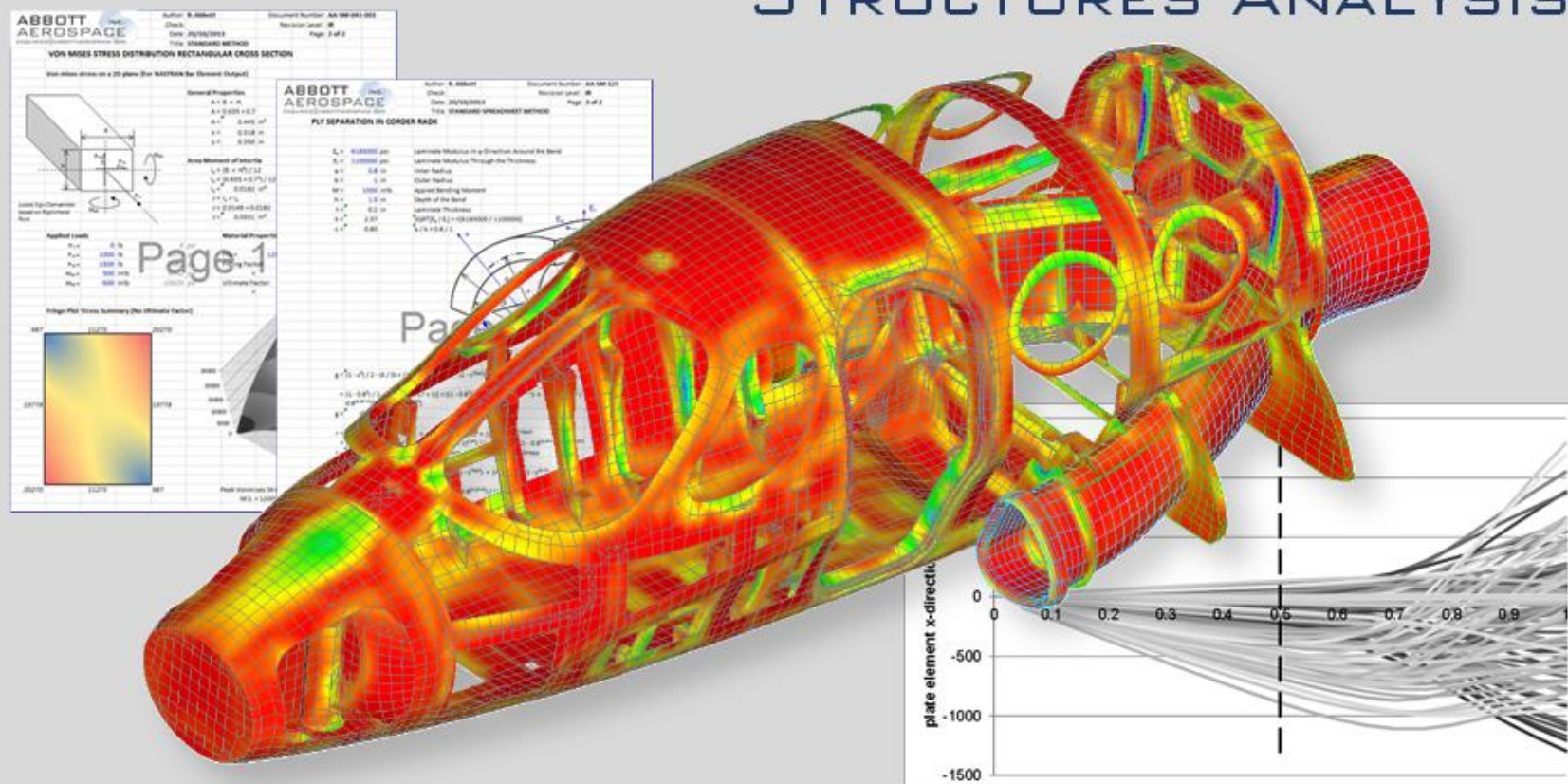
| Section # | Title | Page |
|------------|---|------------|
| 1. | Scope | 6 |
| 1.1. | Applicability | 6 |
| 1.2. | Note to the Reader | 6 |
| 1.3. | How to Help | 7 |
| 1.4. | A Note on the Analysis Spreadsheets | 7 |
| 1.5. | Note on Document Links | 7 |
| 1.6. | Updates to this Book | 8 |
| 1.7. | About the Author | 8 |
| 1.8. | Acknowledgements | 9 |
| 2. | References | 10 |
| 3. | Introduction | 13 |
| 3.1. | The Third Edition | 13 |
| 3.2. | General Approach | 13 |
| 3.3. | Load, Flow and Stress | 14 |
| 3.4. | Stress Analysis | 14 |
| 4. | Materials | 21 |
| 4.1. | Composite Materials | 21 |
| 4.2. | Metallic Materials | 46 |
| 4.3. | Other Common Aircraft Materials | 50 |
| 4.4. | Corrosion | 51 |
| 5. | Loads | 63 |
| 5.1. | Introduction | 63 |
| 5.2. | Aircraft External Loads | 63 |
| 5.3. | Internal Load Distribution | 63 |
| 6. | Section Properties | 64 |
| 6.1. | Introduction | 64 |
| 6.2. | Simple Section Properties | 66 |
| 6.3. | Section Properties of a Composite Shape | 70 |
| 7. | Stiffness | 71 |
| 7.1. | Introduction | 71 |
| 7.2. | General Terms | 71 |
| 7.3. | Axial or Direct Load Stiffness | 71 |
| 7.4. | Fastener Shear Stiffness | 73 |
| 7.5. | Torsion Stiffness | 73 |
| 8. | Beam Analysis | 74 |
| 8.1. | Introduction | 74 |
| 8.2. | Shear and Bending Moment Diagrams | 75 |
| 8.3. | Cantilevers | 76 |
| 8.4. | Single Span Beams | 81 |
| 8.5. | Multi-span Beams | 92 |
| 8.6. | Curved Beams | 92 |
| 8.7. | Other Bending Analyses | 93 |
| 9. | Torsion | 114 |
| 9.1. | Introduction | 114 |
| 9.2. | Reserved | 121 |
| 9.3. | Reserved | 121 |
| 10. | Plate Strength Analysis | 122 |
| 10.1. | Introduction | 122 |
| 10.2. | Isotropic Plates | 122 |
| 10.3. | Composite Plates | 123 |

| | |
|---|------------|
| 11. Pressure Vessels | 124 |
| 11.1. Introduction | 124 |
| 11.2. Reserved | 124 |
| 11.3. Reserved | 124 |
| 12. Joints | 125 |
| 12.1. Adhesive Joints | 125 |
| 12.2. Mechanically Fastened Joints | 128 |
| 12.3. General Treatment of Contact Stresses | 155 |
| 12.4. Strength of Brazed Joints | 160 |
| 12.5. Strength of Welded Joints | 162 |
| 13. Combined Stresses | 168 |
| 13.1. Introduction | 168 |
| 13.2. Reserved | 168 |
| 13.3. Reserved | 168 |
| 14. Ultimate Strength of Metallic Elements | 169 |
| 14.1. Introduction | 169 |
| 15. Local Stability – Isotropic Materials | 172 |
| 15.1. Introduction | 172 |
| 15.2. General Buckling Expression | 173 |
| 15.3. Column Buckling | 196 |
| 15.4. Buckling – Specific Cases | 200 |
| 15.5. Crippling | 204 |
| 16. Local Stability – Composite Materials | 205 |
| 16.1. Introduction | 205 |
| 16.2. Buckling of Laminates | 205 |
| 17. Reserved | 228 |
| 17.1. Introduction | 228 |
| 17.2. Reserved | 228 |
| 17.3. Reserved | 228 |
| 18. Reserved | 229 |
| 18.1. Introduction | 229 |
| 18.2. Reserved | 229 |
| 18.3. Reserved | 229 |
| 19. Finite Element Modelling | 230 |
| 19.1. Introduction | 230 |
| 19.2. Reserved | 230 |
| 19.3. Reserved | 230 |
| 20. Nomenclature | 231 |
| 21. Numerical Methods | 232 |
| 21.1. Common Equations | 232 |
| 21.2. Unit Conversion | 232 |
| 21.3. Quadrilateral Analysis | 232 |
| 21.4. Intersection of Two Circles | 232 |
| 21.5. Intersection of a line and a Circle | 233 |
| 21.6. Curve Fits | 233 |
| 22. Aircraft Specific Design Features and DESIGN Methods | 234 |
| 22.1. Introduction | 234 |
| 22.2. 06 Dimensions and Areas | 234 |
| 22.3. 07 Lifting and Shoring | 234 |
| 22.4. 08 Levelling and Weighing | 234 |
| 22.5. 09 Towing and Taxiing | 234 |
| 22.6. 25 Equipment and Furnishings (Interiors) | 234 |

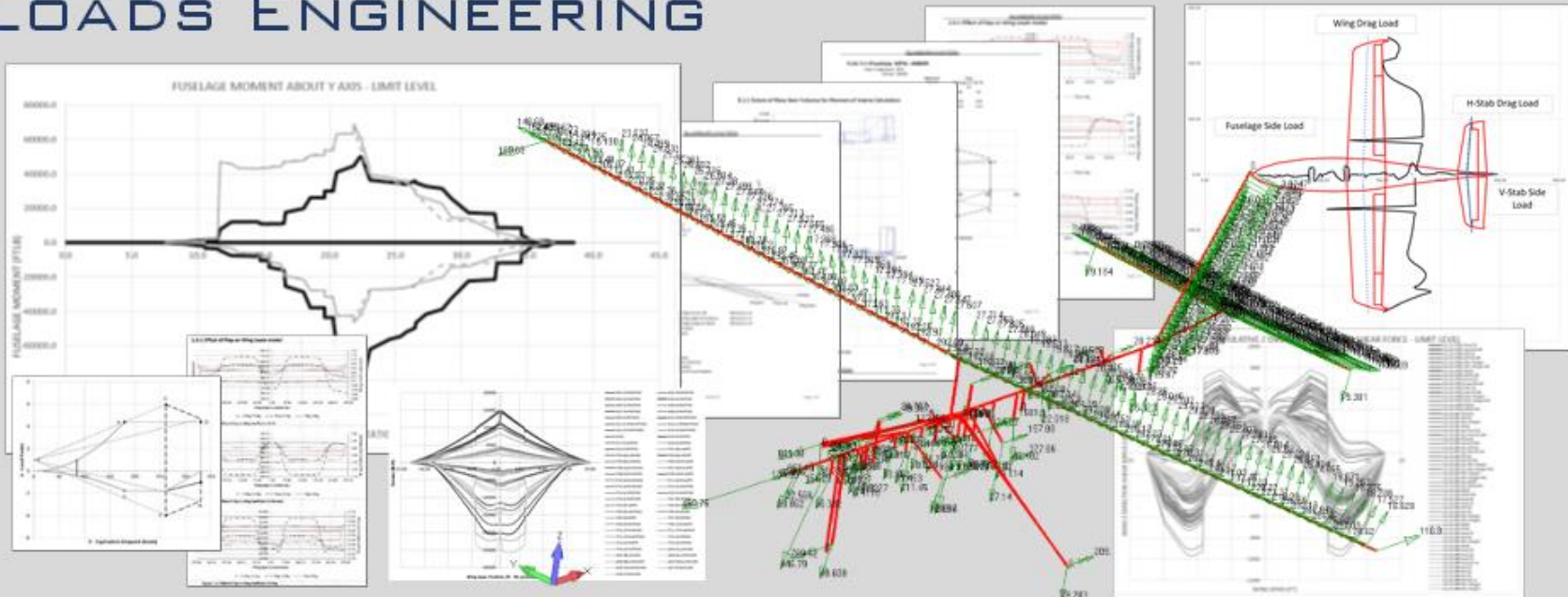
| | |
|--|------------|
| 22.7. 27 Flight Controls | 234 |
| 22.8. 28 Fuel | 234 |
| 22.9. 29 Hydraulic Power | 234 |
| 22.10. 32 Landing Gear | 234 |
| 22.11. 52 Doors | 234 |
| 22.12. 53 Fuselage | 234 |
| 22.13. 54 Nacelles & Pylons | 236 |
| 22.14. 55 Empennage/Stabilizers | 238 |
| 22.15. 56 Windows | 240 |
| 22.16. 57 Wings | 240 |
| 22.17. 71 Powerplant | 261 |
| 23. Fixed Wing Aircraft Performance | 262 |
| 23.1. Introduction | 262 |
| 23.2. Reserved | 262 |
| 23.3. Reserved | 262 |
| 24. Other Aircraft Types: Design and Analysis | 263 |
| 24.1. Introduction | 263 |
| 24.2. Reserved | 263 |
| 24.3. Reserved | 263 |
| 25. Certification | 264 |
| 25.1. Introduction | 264 |
| 25.2. Reserved | 264 |
| 25.3. Reserved | 264 |
| 26. Microsoft Excel as a Report Writing Tool | 265 |
| 26.1. Introduction | 265 |
| 26.2. Excel as a Reporting Tool – The Basics | 265 |
| 27. Common Aircraft Hardware | 272 |
| 27.1. Rivets | 272 |
| 27.2. Screws | 273 |
| 27.3. Bolts | 280 |
| 27.4. Nuts | 286 |
| 27.5. Washers | 292 |
| 27.6. Pins | 294 |

ABBOTT AEROSPACE SEZC LTD

STRUCTURES ANALYSIS



LOADS ENGINEERING



Contact us to find out how we can help you to reduce risk, maximize your potential and take flight.



CONTACT US

1. SCOPE

This document is intended to provide general structural engineering guidance for the development of metallic and fiber composite aircraft parts.

This book is not an academic textbook and does not show the mathematical theory used to derive the methods unless they add utility to the method shown. There are many fine books that provide that information. This book is a collection of practical stress analysis methods and tools; the aim is to give useful numerical methods for basic sizing that will give an engineer the means to carry out an analysis with confidence.

All methods in this document have been either cited from public domain sources or derived from first principles. Every effort has been made to cite sources and the reader is encouraged to use the links to examine the sources for a broader understanding and potential limitations of the particular method.

There are direct links to spreadsheet analysis files throughout the text. The spreadsheets have been developed by myself and others who work for and with me. Special thanks are due to Jerzy Krolkowski. Jerzy developed a set of analysis sheets for me while we both worked at Diamond Aircraft in London, Ontario, Canada. Jerzy's approach to analysis spreadsheets provided some of the inspiration for the analysis tools we produce. Sometimes the best teaching method is just to show that something can be done.

1.1. Applicability

This document is generally applicable for LSA, FARS part 23, part 25 and part 27 primary and secondary structures. However, there are varying airworthiness standards and interpretation of standards across different jurisdictions and consultation with the relevant local certification agency is essential.

When working for an OEM, if there is an OEM analysis method that is approved in the context of their compliance activities that method should always be used.

1.2. Note to the Reader

In writing this text I am standing on the shoulders of giants. Very little of the original theory in this document originates with the author. This document is a collection of the best public domain sources regarding analysis and design of composite and metallic structures that I have found over the last 25 years.

Note on source material: Attribution: Where I have lifted passages from source material directly I have given attribution. I have also tried to give reference to the origin of the methodology. In some circumstances, I have lifted some explanations from internet miscellanea which cannot be attributed to any author. If you recognize any of your work in this text please let me know, provide me with a copy of your original work and I will gladly give you attribution.

Note on source material: Copyright: I have made every effort to ensure that all the referenced material or direct use material is in the public domain. If this is not the case and I have used copyrighted or restricted materials, please contact me to resolve any copyright issue.

Note on source material: Credits: I have had correspondence with many engineers over the years and been given some extremely useful pointers and derivations. If you recognize any of the methods in this text as something you assisted me with and I have not credited you, please contact me and I will gladly give you credit.

We are all lucky to work in an environment where so much great material is in the public domain, by far the largest contributors to this store of public knowledge are the US state-funded aerospace bodies, NASA and (now defunct) NACA and the UK ARC organization. Credit and thanks are due to the generosity and public spirit of the American and the British peoples. It is a privilege to have access to this body of knowledge that stretches back almost 100 years. All the errors in this document and the accompanying products are mine and mine alone and if the reader finds any errors please contact me: textbook@abbottaerospace.com.

I would like to especially thank my wife Anna and progeny Sophia and Carl, my reasons for getting up in the morning. I would also like to thank my parents Margaret and Barrie Abbott who gave me the engineering genes and an interest in engineering that – as much as I tried to avoid it in early life – has ended up bringing me much pleasure and satisfaction.

Much gratitude for mentoring and inspiration is due to (in no particular order): Ken Whitworth, Dominique Zeoli, Paul Barrow, Paul Carter, Paul Whittle, Graham Woolley, Clayton Fox, John Vieger, Peter Maurer, Johnny Doo, Sjoerd Verhof, Hasib Nematpoor, Phil Gent, Jerzy Krolkowski, the Otto family of Otto Aviation, Carsten Sundin of Stratos Aircraft and my trusty cohorts at Abbott Aerospace, Past and Present, Knut Gjelsvik, Nirav Shukla, Peter Lebeidowicz, Santiago Perez, Tomas Chlumecky, Anthony Barr, Andrew Leibrech and Nikola Kozina. Gratitude is also due to all the companies I have worked for as well as all the engineers I have worked with over the years. Engineering is a continual process of learning on the job and that experience comes thanks to the intelligence and patience of our co-workers.

A question I am commonly asked is 'Am I allowed to print out this document'. The answer to this question is 'Yes'.



1.3. How to Help

Engineers understand the value of working as a team towards a common goal and that is how this book (and the connected resources) came about. When I started my engineering consultancy business, I considered monetizing the analysis tools that I had at that point. Instead, I made them available for free online. The free spreadsheets generated a surprising amount of goodwill and useful technical feedback and it confirmed the good-natured and generous nature of the global engineering community.

That experience inspired the creation of the Abbott Aerospace Technical Library. The Library aims to make useful engineering tools and texts freely. If you have found the material that we host and the tools we create to be useful and would like to help; you can volunteer some of your own time, work or tools, or you can donate to help maintain and expand our engineering resources. You can donate from your technical library homepage:



1.4. A Note on the Analysis Spreadsheets



Where we have a spreadsheet available for the analysis methods in this book we have provided a link to the spreadsheet in our library. You are welcome to download these spreadsheets to use, modify and redistribute them as you wish. We just ask that you provide a credit and if possible a link to the Abbott Aerospace Technical Library. These spreadsheets replace the worked examples that you would expect to find in a similar textbook so there are no worked examples shown in this book.

The spreadsheets are provided free of charge, ‘as-is’ with no guarantee. We have made every effort to make sure they are accurate and correct, but we are human and despite our best efforts as prone to error as anyone else. If you do find an error, please inform us so we can correct and share the corrected version with the rest of the library users.

Most of the spreadsheets use the XL-Viking add-in, this is available as a commercial download at this location: XL-Viking.com. This add-in displays the math in the spreadsheets in an interactive way and updates real time with the values in the spreadsheet.

If you wish to contribute an analysis spreadsheet to the library, we will gladly review any submission. If we add your sheet to the library, we will give you a permanent credit in the library and on the face of the spreadsheet.

We, like many other people and companies, have developed a way of using Microsoft Excel™ as a technical report creation tool. All spreadsheets are created (as far as possible) in what we consider to be a final report format. All of our sheets conform to the same format and layout.

The spreadsheet tools are updated on a regular basis with corrections and improvements. The user is recommended to check the [Abbott Aerospace website](http://AbbottAerospace.com) regularly to ensure they are using the latest and best version available.

1.5. Note on Document Links

This document is meant to be used only as an electronic document. It is filled with links to the source material and the analysis spreadsheets that are useful tools but also serve as worked examples.

You are welcome to print this book to make physical copies, but you will lose this important functionality.

By default, most PDF readers do not allow the use of external links from within a document. You may have to change the settings in your PDF reader.

1.5.1. Using External Links in Adobe PDF Reader

If you are using Adobe reader, you can allow the reader to access websites by going to the ‘Edit’ menu and selecting ‘Preferences’ (or just pressing ‘control-k’). Select the ‘Trust Manager’ menu item on the left-hand side and click the ‘Change Settings’ button in the main window. In the window that pops up, you can choose to allow the document to access all websites or you can add www.abbottaerospace.com to the list of allowed sites.

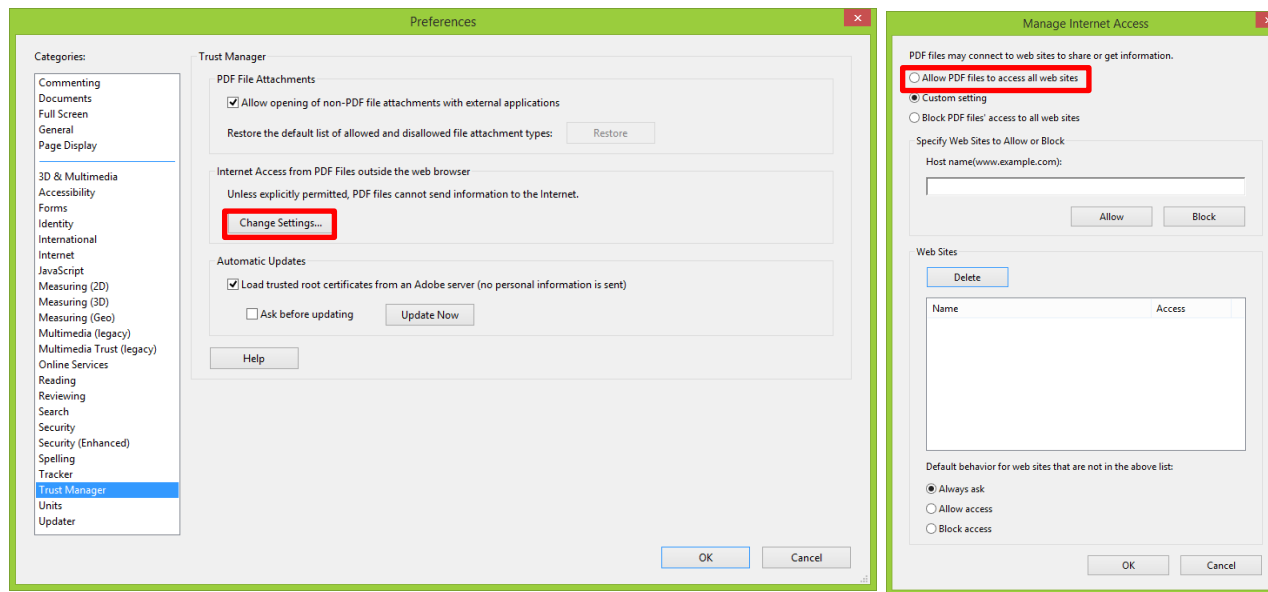


Figure 1.5.1-1: Adobe PDF Settings to Allow use of Links

Other PDF readers have similar settings that can be altered similarly.

1.6. Updates to this Book

Corrections, updates and new editions to this book will be posted on www.abbottaerospace.com. Subscribers to the Abbott Aerospace mailing list will receive notification of any updates automatically. Click [here](#) to subscribe to our mailing list.

1.7. About the Author

Richard Abbott graduated from Manchester Polytechnic (now the Metropolitan University of Manchester) in the UK in 1992. He worked as a stress engineer on multiple civil and military aircraft projects in the UK including multiple versions of the BAe Hawk, the Bombardier CRJ Aircraft and the Saab Gripen. Richard and family moved between San Antonio, Texas, USA (Sino Swearingen Aircraft Corporation), Gosselies, Belgium (Sonaca SA, the Dassault F7X program) and London, Ontario Canada (Diamond Aircraft D-Jet Program). In 2008 Richard left Diamond Aircraft and founded Abbott Aerospace with his partner Anna.

Since 2008 the Abbott Aerospace team has contributed to many projects at startup companies and established OEMs: Stratos Aircraft, Kestrel (One Aviation), Mooney, Boom, Piper, Bombardier, Solarship, CRI, PV Labs, Kopter (Marenco Swisshelicopter), ITPS, Wave Aircraft, Gore Design, Glasair, Knovel, Ampaire, M7, DeLorean Aerospace, Warrior Aircraft, Samad Aerospace, Cynergy Composites and ALP.

At the time of writing Richard holds the position of acting structures manager on the Stratos 714 program, head of structures and mechanical systems for the Otto Celera 500L program and is the acting CTO for Samad Aerospace. Richard also teaches classes on structures engineering and engineering management at the University College of the Cayman Islands.

1.8. Acknowledgements

Of particular help in the compilation and checking of this book, the following individuals deserve special recognition – in no particular order.

- Peter Lebiedowicz
- Michael Prystie
- Knut Gjelsvik
- Nirav Shukla
- Santiago Perez – Checker Extraordinaire
- Kenan Stewart
- Charles Lee
- Anna Abbott
- Mike Sharpe
- Sophia Abbott

Many thanks to the following readers of the first edition of the book who have spotted errors and provided useful feedback

- Roey Epshtein of Elbit Systems
- Stephen Rigen of Cobham Mission Systems
- Martin Zahoruyko of Altitude Aerospace
- Steve Marsan of Innoviator Flight Science
- Andrew Butcher of Pratt and Whitney
- Surya Batchu of MD Helicopters

2. REFERENCES

The following documents form a part of this document to the extent referenced herein:

- AC20-107B. (2009). *Composite Aircraft Structure*. Federal Aviation Administration.
- AC43.13-1B, A. C. (1998). *Acceptable Methods, Techniques and Practices - Aircraft Inspection and Repair*. Oklahoma City.
- AC43-4A, A. C. (1991). *Corrosion Control for Aircraft*. Federal Aviation Administration, William J White.
- AFFDL-TR-69-42. (1986). *Stress Analysis Manual*. Airforce Flight Dynamics Laboratory, Wright Patterson.
- AFWAL-TR-85-3069. (1985). *Buckling of Laminated Composite Plates and Shell Panels*. Arthur W Leissa.
- AFWL-TR-86-3035. (1986). *Design Guide for Bolted Joints in Composite Structures*. Wright Patterson Flight Dynamic Laboratory.
- AGARD-AG-278. (1985). *Aircraft Corrosion: Causes and Case Histories*. W. Wallace, D, W, Hoeppner, P. V. Kandachar.
- AGARD-CP-590. (1996). *Conference Proceedings 590: Bolted/Bonded Joints in Polymeric Composites*. Advisory Group for Aerospace Research and Development.
- ARC-CP-1380. (1977). *The Strength of Bolted Joints in Multi-Directional CFRP Laminates*. London: Aeronautical Research Council.
- ARC-CP-235. (1956). *The Buckling under Longitudinal Compression of a Simply Supported Panel that changes in Thickness across the Width*. London: E. C. Capey.
- ARC-RM-2652. (1953). *Investigation of Skin Buckling*. Bristol: D. J. Farrar.
- ARC-RM-2778. (1953). *The Elastic Stability of Sandwich Plates*. London: ARC.
- DOT/FAA/AR-01/33. (2001). *Investigation of Thick Bondline Adhesive Joints*. J. S. Tomblin, C. Yang, P. Harter.
- DOT/FAA/AR-01/57. (2001). *Investigation of Adhesive Behavior for Aircraft Applications*. Washington: Yang, Tomblin.
- DOT/FAA/AR-02/121. (2003). *Guidelines for Analysis, Testing, and Nondestructive Inspection of Impact Damaged Composite Sandwich Structures*. Federal Aviation Administration.
- DOT/FAA/AR-10/6. (2011). *Determining the Fatigue Life of Composite Aircraft Structures Using Life and Load-Enhancement Factors*. Washington: John Tomblin & Waruna Seneviratne.
- DOT/FAA/AR-99/49. (1999). *Review of Damage Tolerance for Composite Sandwich Airframe Structures*. Wichita: J. Tomblin, T. Lacy, B. Smith, S. Hooper, A. Vizzini and S. Lee.
- ECSS-E-HB-32-22A. (2011). *Insert Design Handbook*. European Cooperation for Space Standardization.
- ECSS-Q-ST-70-36C. (2009). *Material Selection for Controlling Stress Corrosion Cracking*. ECSS.
- ESA-PSS-03-1202. (1987). *Insert Design Handbook*. European Space Research and Technology Center.
- FAA-ACE100-2001-006. (2001). *Static Strength Substantiation of Composite Airplane Structure; Policy Statement*. Federal Aviation Administration.
- FAA-H-8083-25A. (2008). *Pilot's Handbook of Aeronautical Knowledge*. Oklahoma City: Federal Aviation Administration.
- FAA-H-8083-30. (2008). *Aviation Maintenance Technician Handbook*. Oklahoma City: Federal Aviation Administration.
- FAA-H-8083-31. (2012). *Aircraft Maintenance handbook Volume 1*. Oklahoma City: Federal Aviation Administration, Flight Standards Service.
- FAA-PS-ACE100-2004-10030. (2005). *Substantiation of Secondary Composite Structures*. Federal Aviation Administration.
- FAA-PS-ACE100-2005-10038. (2005). *Bonded Joints and Structures - Technical Issues and Certification Considerations*. Federal Aviation Administration.
- FPL-070. (1964). *Buckling Coefficients for Simpy Supported and Clamped Rectangular Sandwich Panels Under Edgewise Compression*. Madison, Wisconsin: US Forest Service.
- L.J. Hart-Smith. (1992). *NASA-N92-32588 A New Approach to Fibrous Composite Laminate Strength Prediction*. NASA.
- MIL-HDBK-17A. (1973). *Plastics for Aerospace Vehicles, Part II Transparent Glazing Materials*. Wright-Patterson Airforce Base, Ohio: Richard S. Hassard.
- MIL-HDBK-17F Vol 3. (2002). *Polymer Matrix Composites Volume 3: Materials Usage Design and Analysis*. Department of Defense.
- MIL-HDBK-23A. (1968). *Structural Sandwich Composites*. Department of Defense.
- MIL-HDBK-310. (1997). *Global Climatic Data for Developing Military Products*. Department of Defense.
- Mil-HNDBK-17F-Vol1. (2002). *Polymer Matrix Composites Volume 1: Guidelines for Characterization of Structural Materials*.
- MIL-HNDBK-5H. (1998). *Metallic Materials and Elements for Aerospace Vehicle Structures*. Department of Defense.
- MIL-P-5425D. (1967). *Military Specification, Plastic Sheet, Acrylic, Heat Resistant*. Department of Defense.
- MIL-PRF-25690B. (1960). *Performance Specification, Plastic, Sheeets and Formed Parts, Modified Acrylic Base, Monolithic, Crack Propagation Resistant*. Lakehurst, NJ: Department of Defense.
- MIL-S-8879C. (1991). *Screw Threads, Controlled Radius Root with Increased Minor Diameter, General Specification For*. Department of Defense.
- MIL-STD-210C. (1987). *Climatic Information to Determine Design and Test Requirements for Military Systems and Equipment*. Department of Defense.
- MIL-STD-889C. (2016). *Standard Practice - Dissimilar Metals*. Patuxent River, Maryland: US Department of Defense.
- MSFC-SPEC-3679. (2012). *MSFC Technical Standard - Process Specification - Welding Aerospace Hardware*. Alabama: George C. Marshall Space Flight Center.
- MSFC-SPEC-522B. (1987). *Design Criteria for Controlling Stress Corrosion Cracking*. George C Marshall Space Flight Center: NASA.
- NACA-Report-1027. (n.d.). *Buckling of Thin-Walled Cylinders Under Axial Compression and Internal Pressure*. Hsu Lo, Harold Crate and Edward Schwartz.
- NACA-Report-733. (n.d.). *Critical Compressive Stress for Flat Rectangular Plates Supported aLng All Edges and Elastically Restrained Against Rotation Along the Unloaded Edges*. Lundquist and Stowell.
- NACA-Report-734. (n.d.). *Critical Compressive Stress for Outstanding Flanges*. Lundquist and Stowell.
- NACA-TN-1051. (1946). *Preliminary Investigation of the Loads Carried by Individual Bolts in Bolted Joints*. Washington: NACA.
- NACA-TN-1222. (1947). *Buckling Stresses of Simply Supported Rectangular Flat Plates in Shear*. Washington: M Stein and J Neff.
- NACA-TN-1223. (1947). *Critical Combinations of Shear and Direct Stresses for Simply Supported Rectangular Flat Plates*. Langley, Virginia: Batdorf, Stein.
- NACA-TN-1261. (1947). *Effect of Variables in Welding Technique on the Strength of Direct Current Metal Arc Welded Joints in Aircraft Steel*. Washington: Voldrich, Armstrong.
- NACA-TN-1323. (1947). *Charts for the Minimum-Weight Design of Multi-web Wings in Bending*. Langley, Virginia: Langley Memorial Aeronautical Laboratory.
- NACA-TN-1344. (1947). *Critical Stress of Thin-Walled Cylinders in Torsion*. Washington: S. B. Batdorf, Manuel Stein, Murray Schildcrout.
- NACA-TN-1345. (1947). *Critical Combination of Torsion and Direct Axial Stress for Thin-Walled Cylinders*. Washington: S. B. Batdorf, Manuel Stein, Murray Schildcrout.

- NACA-TN-1990. (1949). *Plastic Buckling of a Long Flate Plate Under Combined Shear and Longitudinal Compression*. Langley, Virginia: Stowell.
- NACA-TN-2163. (1950). *Critical Stress of Plate Columns*. Washington: John C. Houbolt, Elbridge Z Stowell.
- NACA-TN-2536. (1951). *Critical Combinations of Bending Shear and Transverse Compressive Stresses for Buckling of Infinitely Long Plates*. Washington: Aldie E. Johnson, Kenneth P. Buchert.
- NACA-TN-2661. (1952). *A Summary of Diagonal Tension, Part 1, Methods of Analysis*. Washington: Paul Kuhn, James P Peterson, L. Ross Levin.
- NACA-TN-306. (1929). *Curves Showing Column Strength of Steel and Duralumin*. Washington: Orrin E. Ross.
- NACA-TN-3184. (1954). *Buckling of Long Square Tubes in Combined Compression and Torsion and Comparison with Flat Plate Buckling Theories*. Langley, Virginia: Peters.
- NACA-TN-3781. (1957). *Handbook of Structural Stability*. G. Gerard, H. Becker.
- NACA-TN-3785. (1957). *Handbook of Structural Stability Part V - Compressive Strength of Flat Stiffened Panels*. Washington: George Gerard.
- NACA-TN-578. (1936). *Full Scale Wind Tunnel and Flight Tests of a Fairchild 22 Airplane Fitted with a Fowler Flap*. Washington.
- NACA-TN-733. (1940). *Chart for Critical Compressive Stress of Flat Rectangular Plates*. Washington: H. N. Hill.
- NACA-TN-862. (1942). *An Investigation of the Effectiveness of Stiffeners on Shear Resistant Plate Girder Webs*. Washington: R L Moore.
- NACA-TN-888. (1943). *Torsion of Flanged Members with Cross Sections Retrained Against Warping*. Washington: H. N. Hill.
- NACA-TN-902. (1943). *Description of Stress-Strain Curves by Three Parameters*. Washington: Walter Ramberg, William Osgood.
- NACA-TN-927. (1944). *Determination of Stress-Strain Relations from "Offset" Yield Strength Values*. Washington: H N Hill.
- NACA-TN-930. (1944). *Tensile Tests of Round-Head, Flat-Head and Brazier-Head Rivers*. Washington: Schuette, Bartone, Mandel.
- NACA-WR-3K13. (1943). *Critical Stress for an Infinitely Long Flat Plate With Elastically Restrained Edges Under Combined Shear and Direct Stress*. Langley, Virginia: Stowell, Schwarz.
- NACA-WR-L-323. (1942). *The Strength and Stiffness of Shear Webs with Holes having 45deg Flanges*. Langley: Paul Kuhn.
- NASA 20090013076. (2009). *Evaluation of Margins of Safety in Braze Joints*. Yury Flom, Len Wang, Mollie Powell, Mathew Soffa, Monica Rommel.
- NASA 20120008193. (2012). *Failure Assessment of Braze Structures*. Yuri Flom.
- NASA 20120008328. (2012). *Failure Assessment of Braze Structures Using Failure Assessment Diagram*. Yuri Flom.
- NASA Conference Publication 3087, Part 2. (1990). *Eighth DoD/NASA/FAA Conference on Fibrous Composites- in Structural Design*. NASA.
- NASA CR-1457. (1969). *Manual For Structural Stability Analysis Of Sandwich Plates And Shells*. R. T. Sullins, G. W. Smith, and E. E. Spier.
- NASA CR-2330. (1974). *Elastic Stability of Laminated Flat and Curved, Long Rectangular Plates Subjected to In-Plane Loads*. A. Viswanathan, M. Tamekuni & L. L. Baker.
- NASA TM X-73305. (1975). *Astronautic Structures Manual Volume 1*. NASA.
- NASA TM X-73306. (1975). *Astronautic Structures Manual Volume II*. NASA.
- NASA TM X-73307. (1975). *Astronautic Structures Manual Volume III*. NASA.
- NASA/CR-1999-208994. (1999). *Facesheet Wrinkling in Sandwich Structures*. National Aeronautics and Space Administration.
- NASA/CR-2001-210661. (2001). *A Study of Failure Criteria of Fibrous Composite Materials*. F. Paris.
- NASA/TM-2006-241323. (2006). *Experimental Observations for Determining the Maximum Torque Values to Apply to Composite Components Mechanically Joined With Fasteners*. F. P. Thomas.
- NASA/TP-2011-216460. (2011). *Comparison of Open-Hole Compression Strength and Compression After Impact Strength on Carbon Fiber/Epoxy Laminates for the Ares I Composite Interstage*. A.J. Hodge, A.T. Nettles and J.R. Jackson.
- NASA-CR-112236. (1973). *Adhesive Bonded Single-Lap Joints*. Hampton, Virginia: Hart-Smith.
- NASA-CR-123772. (1972). *Materials Data Handbook, Aluminum Alloy 6061*. Alabama: R. F Muraca, J.S. Whittick.
- NASA-CR-132548. (n.d.). *Shear Buckling of Square Perforated Plates*. Ithica: Gross kurth, White, Gallagher, Thomas.
- NASA-CR-2064. (1972). *Integration of NASA Sponsored Studies on Aluminum Welding*. Cambridge, Massachusetts: NASA.
- NASA-CR-2218-1. (1974). *Analysis and Design of Advanced Composite Bonded Joints*. L. J. Hart-Smith.
- NASA-CR-3767. (1984). *Durability and Damage Tolerance of Large Composite Primary Aircraft Structure (LCPAS)*. J. E. McCarty, W. G. Roeseler.
- NASA-CR-4608. (1994). *Strength Evaluation of Socket Joints*. L.C. Rash.
- NASA-CR-4746. (1996). *High Lift System on Subsonic Airliners*. Seattle: NASA Ames Research Center.
- NASA-CR-4750. (1997). *Handbook of Analytical Methods for Textile Composites*. Langley: Brian N Cox, Gerry Flannagan.
- NASA-NAS1-19347. (1997). *A Summary and Review of Composite Laminate Design Guidelines*. J. A. Bailie, R. P. Ley, A. Pasricha.
- NASA-RP-1228. (1990). *Fastener Design Manual*. Lewis Research Center, Cleveland, Ohio.
- NASA-RP-1351. (1994). *Basic Mechanics of Laminated Composite Plates*. A. T. Nettles.
- NASA-STD-5006. (1999). *General Fusion Welding Requirements for Aerospace Materials Used in Flight Hardware*. NASA.
- NASA-STD-5020. (2012). *Requirements for Threaded Fastening Systems in Space Flight Hardware*. Washington DC: NASA.
- NASA-TM-1998-206542. (1998). *Mechanical and Thermal Buckling of Rectangular plates with Cutouts*. Dryden Flight Center: William L. Ko.
- NASA-TM-2012-217454. (2012). *Aerospace Threaded Fastener Strength in Combined Shear and Tension Loading*. B.E. Steeve and R.J. Wingate: Marshall Space Flight Center, Huntsville, Alabama.
- NASA-TM-87603. (1985). *Failure Mechanisms of Laminates Transversely Loaded by Bolt Push Through*. Langley Research Center, Langley, Virginia.
- NASA-TN-D-7855. (1975). *Analysis of Bonded Joints*. Hampton, Virginia: Srinivas.
- NASA-TN-D-7996. (1975). *Numerical Analysis and Parametric Studies of the Buckling of Composite Orthotropic Compression and Shear Panels*. J. M. Housner, M. Stein.
- NASA-TP-2528. (1986). *An Approximate Buckling Analysis for Rectangular Orthotropic Plates With Centrally Located Cutouts*. Michael P. Nemeth, Manuel Stein & Eric R. Johnson.
- NASA-TP-2935. (1989). *Weld Stresses Beyond Elastic Limit*. Alabama: V. Verderame.
- NASA-TP-3024. (1990). *Buckling and Post Buckling of Compression Loaded Isotropic Plates with Cutouts*. Langley, Virginia: Michael P. Nemeth.

NAVWEPS-REPORT-7827. (1962). *Handbook of Equations for Mass and Area Properties of Various Geometrical Shapes*. China Lake, California: U.S. Naval Ordnance Test Station.

OTS-PB-151074 DMIC Report 118. (1959). *Welding of High Strength Steels for Missile Applications*. Columbus, Ohio: Mishler, Monroe, Rieppel.

PS-ACE100-2001-006. (2001). *Static Strength Substantiation of Composite Airplane Structure*. Federal Aviation Administration.

(2013). *Pull-through Failure of Composite Joints*. Department of Mechanical Engineering, McGill University, Montreal: Zao Chen.

US Forest Service Report No . 1845. (1955). *Stresses Induced in a Sandwich Panel by Load Applied at an Insert*. Madison: United States Department of Agriculture.

3. INTRODUCTION

3.1. The Third Edition

This book will always be a work in progress and the Third Edition builds on the foundations laid by the First and Second Editions. We have added chapters covering advanced beam analysis, torsion, general aircraft design, corrosion prevention more information on composite processes and material selection.

3.2. General Approach

The aim of this document is to provide guidance to designers and stress engineers. The directions and recommendations in this document reflect the airworthiness regulations, industry best practices and the general experience of the author across several FAR part 23 & 25 metallic and composite aircraft programs.

The general approach for all analyses is shown below.

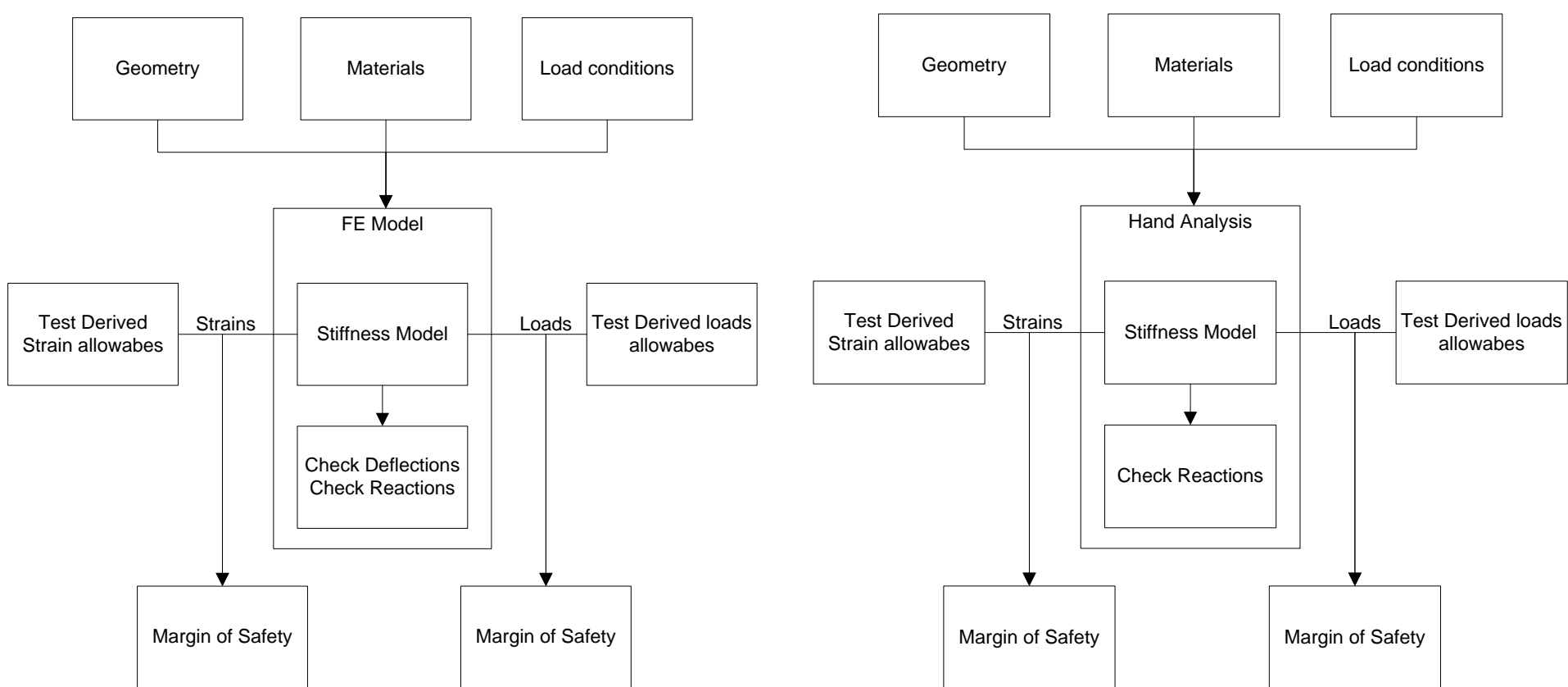


Figure 1.5.1-1: General Analysis Approach

It must be noted and understood that all analysis methods, whether a simple or a complex hand analysis or simple or a complex finite element solution, are just mathematical models of the real world. All analysis results require checking and correlation to representative testing prior to the engineered product being used for any critical application. All analysis methods should be applied with skepticism and caution.

The applicability of all analysis methods must be understood before an assessment of their likely accuracy is made. Where reference is made back to testing in the cited source material, does the tested range cover the configuration you are analyzing? If the testing is not directly applicable to your engineering problem is it reasonable to assume the method is applicable? Do you have access to any other specific company, proprietary or public domain test results to confirm the suitability of the method? Is there a subject matter expert available to consult and advise? We supply the original references so that you can check on the range of applicable situations the method does applies to. Do not take anything for granted!

If the method you have chosen for the analysis is applicable, have you applied the method correctly? Is it error free? Sanity checking of your own work and peer review is essential. Just because you have a result you expect or wanted it does not mean that it is correct. An applicable modified idiom could be "The road to hell is paved with wishful thinking". In the author's experience, it is important to trust your instincts, if you obtain an analysis result that gives you cause for suspicion or is too good to be true, trust your instincts and go back and check, reanalyze and be sure you are correct.

In the end, the analyst must have confidence in the accuracy and applicability of their selected methods. In this document, we have tried to give cited sources for all critical aspects. We encourage everyone who uses this document to go to the original sources and understand the specific limitations of each analysis method.

If you think that we have misinterpreted or misrepresented any of the source material, please let us know. If we make a change to a subsequent issue of the book we will give you footnote credit for helping us all better understand the analysis method.

3.3. Load, Flow and Stress

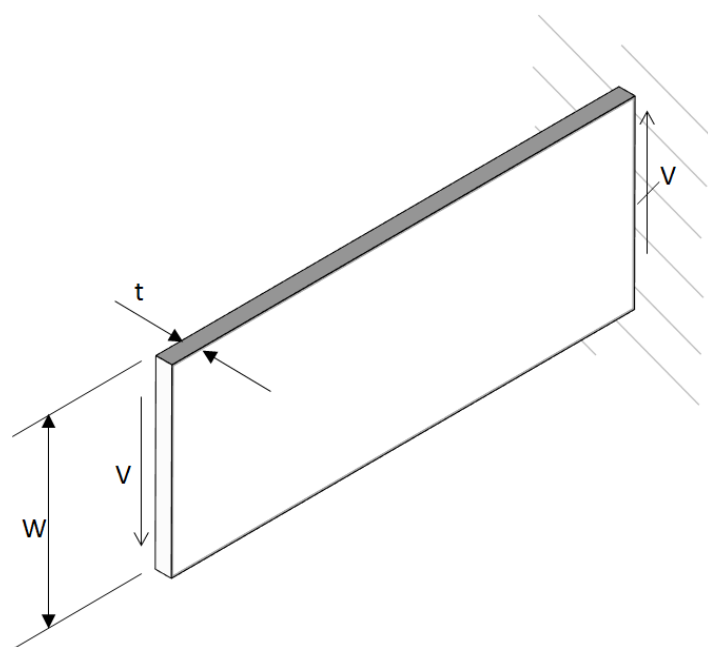
Fundamental to structures analysis are the ideas of load, flow and stress.

- **Load** is a measure of force, a moment (which is regarded as a type of applied load) is a measure of twisting or bending force.
 - lb (Load)
 - inlb (Moment)
- **Flow** is a measure of load or moment per length or width
 - lb/in (Load Flow)
 - inlb/in (Moment Flow)
- **Stress** is a measure of load per area – or stress can be thought of as flow per thickness.
 - lb/in²

The assessment of the effect of loads and moments on a structure, the derivation of relevant flows and stresses, and comparing these with appropriate failure criteria is the process of structures analysis.

The difference between load flow and stress is a useful distinction when interpreting hand analysis and finite element model results.

Using a cantilever shear beam as an example:



Consider a shear beam loaded with 'V'. The beam has a width (or depth) of 'W' and a thickness of 't'.

Note that this example is statically determinate. i.e. the load transfer through the structure is not affected by stiffness.

The reaction load, V is not changed by either W or t .

The Shear Load Flow V/W is affected by the width of the beam but not the thickness.

And finally, the average shear stress $V/(W \cdot t)$ is affected by both the width and the thickness.

Conversely:

- The reaction load is unaffected by changes in both the width and the thickness
- The Flow is unaffected by the thickness

This is particularly important when the engineer is dealing with a finite element model using plate elements. If the engineer uses plate elements (and the model is 'reasonably' statically determinate) the model need not be re-run to consider webs of different thicknesses if load flow results are used from the model – because the load flow is unaffected by the thickness.

3.4. Stress Analysis

Stress analysis is the art of determining the stress present at a location in a structure and how that level of stress affects the instantaneous strength (static) and the life (fatigue, damage tolerance) of the structure.

3.4.1. Measures of Stress

3.4.1.1. Uniaxial Stress

Uniaxial Stress is a measure of the average axial load over the cross-sectional area of a structural member. Axial stress is achieved by an axial load applied along the axis of a straight member.

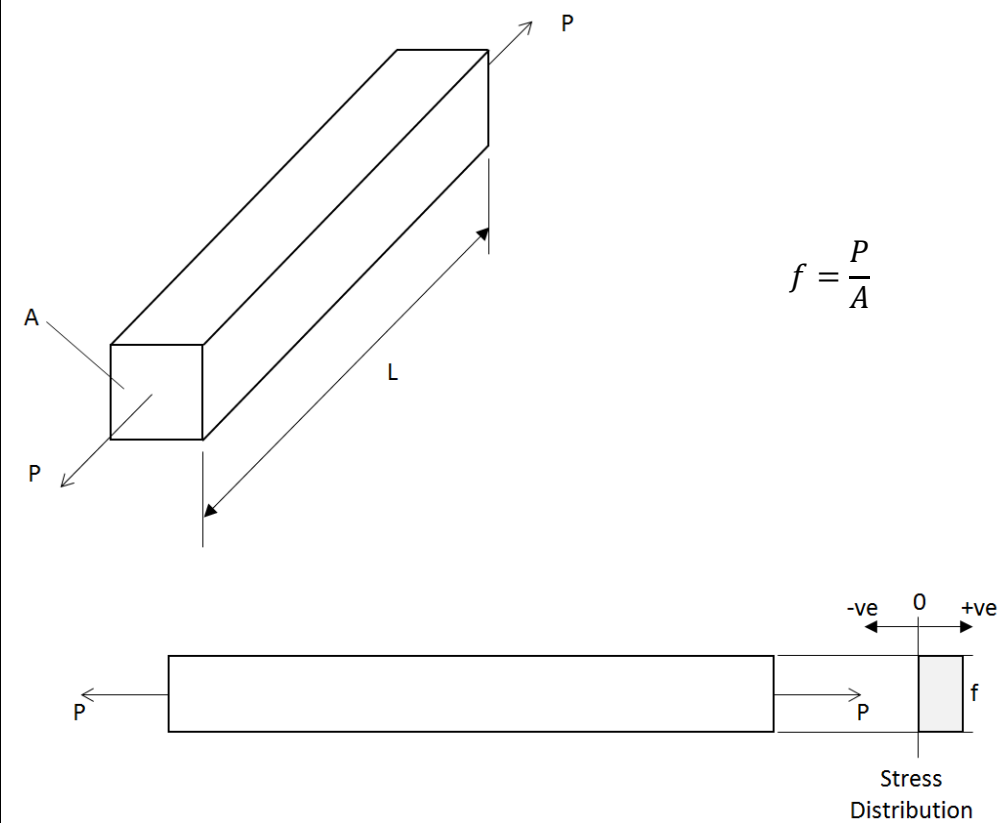


Figure 3.4.1-1: Axial Stress

Note that in this text we are using the symbol f for axial stress. The Greek letter σ (sigma) is also often used for axial stress.

For the purposes of most analyses, the change in area of the cross-section caused by Poisson's effect is not accounted for in the calculation of the value of stress.

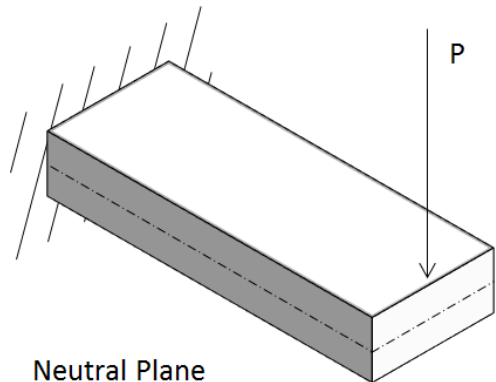
This is in part due to the fact that most material strength data is calculated from test failure loads using the original cross section of the test article used to develop the strength data.

Ref [\(MIL-HNDBK-5H, 1998\)](#) Section 1.4.4.5 "It should be noted that all stresses are based on the original cross-sectional area of the test specimen, without regard to the lateral contraction of the specimen, which actually occurs during the test."

3.4.1.2. Bending Stress

Bending stress occurs whenever a member is loaded 'off axis'. Bending stress occurs around the neutral axis of the section. The neutral axis of the section experiences no bending stress effects and lies on the centroid of the cross section. The neutral axis, or plane, stays at a constant length under bending effects as it experiences zero strain.

The outer fiber of the cross section experiences the highest bending stress. The maximum bending stress is usually calculated at the outer fiber, at a distance 'y' from the neutral axis.



$$f_b = \frac{M \cdot y}{I}$$

Note that the triangular distribution of bending stress through the thickness of the cantilever beam depends on material elasticity. In the case where the stress exceeds the proportional limit of the material plastic bending, see section 14.1.1.

For an initial assessment, it is conservative to assume the material remains perfectly elastic for predicted stress values.

3.4.1.3. Shear Stress

Shear Stress is the component of stress coplanar with the material cross section. In the case of a cantilever beam, the shear stress is constant along the length of the beam. This type of shear is called transverse shear.

Note that in this text we are using the symbol f_s for shear stress. The greek letter τ (tau) is also often used to denote shear stress.

The distribution of shear stress in a beam does not affect the bending or axial stress distribution.

It is common to assume that the shear stress is constant across a cross section.

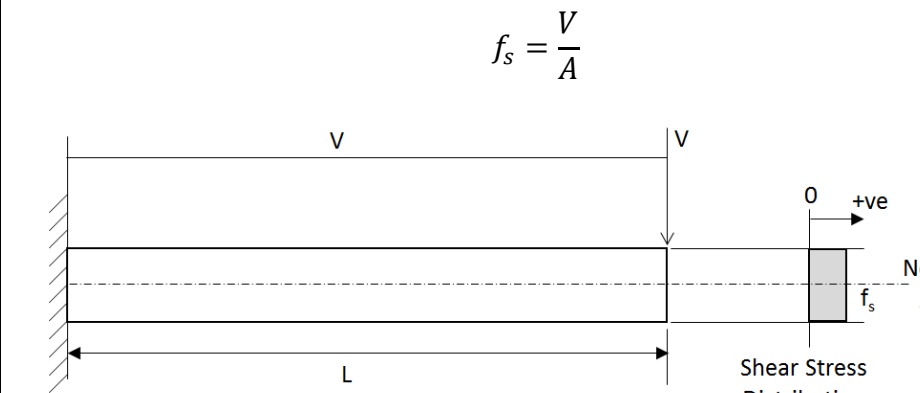


Figure 3.4.1-4: Average Shear Stress Distribution

In the figure above, the example of a cantilevers is used. In a cantilever beam, the moment is developed over the length of the beam. The moment at any point along the cantilever beam is calculated by multiplying the load by the distance from the applied load to the point along the beam of interest.

It follows that the maximum moment occurs at the furthest point (towards the support) from the applied load.

You can download a spreadsheet that calculated the shear force and bending moment for a cantilever beam with a point load applied at the free end here:

ABBOTT AEROSPACE SEZC LTD
SPREADSHEETS
ABBOTTAEROSPACE.COM

AA-SM-026-001 Beam Analysis - Cantilever - Point Load at End

A comprehensive set of beam analysis methods is defined in Section 8 of this book.

Where there is an applied moment (twist) rather than an applied out of plane load, the moment is constant along the length of cantilever.

Note that the use of the letter 'V' is used to denote a load that results in a shear reaction from the structure it is applied to. The nature of the applied load is the same whether 'P' or 'V' is used. The type of load induced in the structure from the applied load is different.

In reality, the shear stress varies across the cross section according to the following relationship:

$$f_s = \frac{V \cdot Q}{I \cdot t}$$

The shear stress distribution for a rectangular cross section beam is shown below:

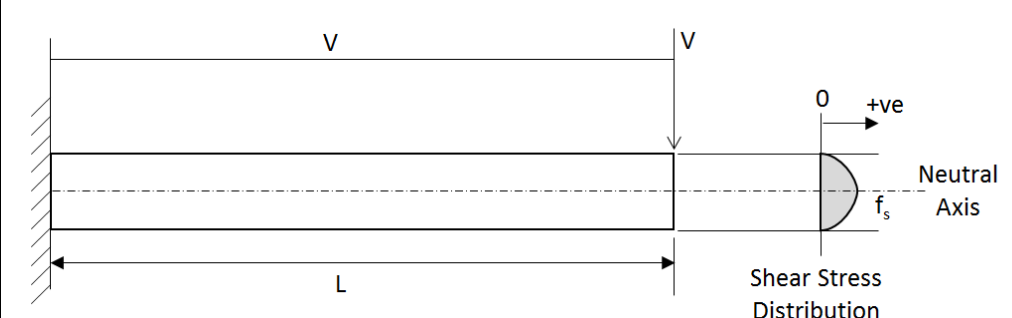


Figure 3.4.1-3: Bending Stress – Cantilever Example with Applied Moment

Figure 3.4.1-5: Actual Shear Stress Distribution

We have created several spreadsheets that calculate the parabolic shear distribution for common cross sections. These spreadsheets also calculate the average shear stress and compares the average shear stress with the peak parabolic shear stress:



AA-SM-041-011 Stress Analysis - Shear Stress in an I-Beam



AA-SM-041-012 Stress Analysis - Shear Stress in a T-Beam



AA-SM-041-013 Stress Analysis - Shear Stress in a Circular Bar



AA-SM-041-014 Stress Analysis - Shear Stress in a Rectangular Bar

3.4.2. Combined Stresses

If all structure were only loaded in one manner, or mode, failure would be relatively simple to accurately predict. In practice, a single applied point load can result in complex stress states in complex structure, and complex loading can result in complex stress states in simple structure.

There are many ways to interact stresses. In this text, the most commonly used are covered.

Note that the analyst rarely analyses three-dimensional stress states by hand. Most aircraft structures can be adequately analyzed if the structure is planar and the magnitude of stress or load in the third dimension is not significant.

Where the structure and internal loads are such that the stress state is significantly three dimensional, it is preferable to use finite element analysis to predict stresses.

Three-dimensional calculations for stress tensors are presented for information and interest only.

It is worth noting that these criteria are directly applicable to isotropic materials only.

3.4.2.1. Principal Stresses

When an element of the structure is subjected to combined stresses such as tension, compression and shear, it is often necessary to determine resultant maximum stress values and their respective principal axes.

The solution may be attained using equations or the graphical construction of Mohr's circle.

Relative Orientation and Equations of Combined Stresses. Where:

- f_x and f_y are applied normal stresses
- f_s is applied shear stress
- f_{max} and f_{min} are the resulting principal normal stresses
- f_{smax} is the resulting principal shear stress
- θ is the angle of the principal axes

Sign Convention:

- Tensile Stress is positive
- Compression Stress is negative
- Shear Stress is positive as shown
- Positive θ is counter clockwise as shown

Principal Stresses in Two Dimensions

The relationship between general and principal stresses on a plane element is shown in the following figure:

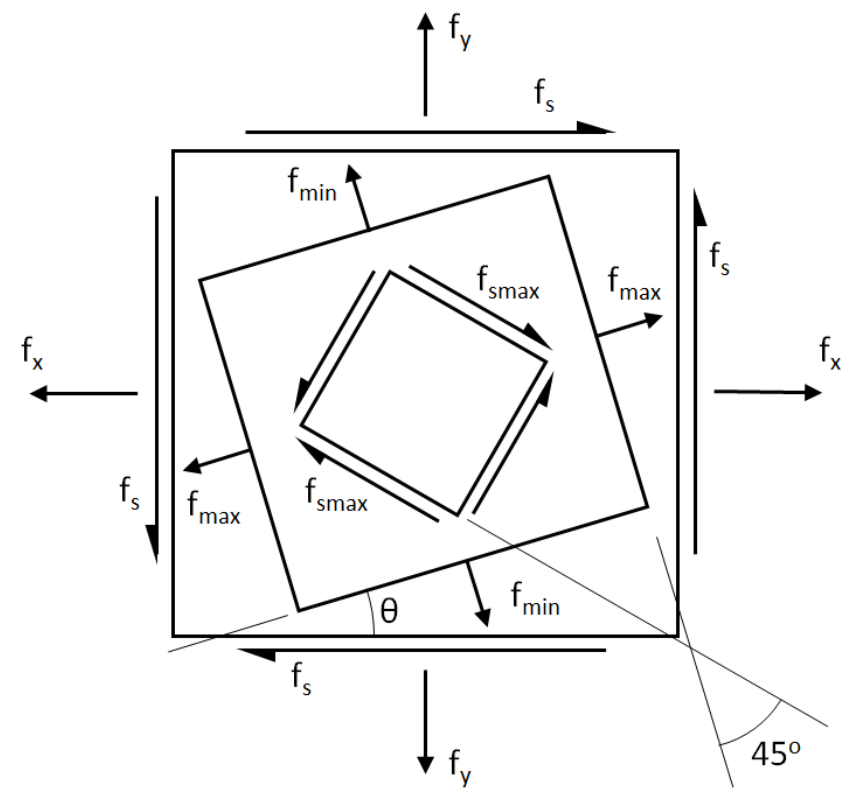


Figure 3.4.2-1: Geometric Relationship of Applied Stresses to Principal Stresses

Maximum principal stress:

$$f_{max} = \frac{f_x + f_y}{2} + \sqrt{\left(\frac{f_x - f_y}{2}\right)^2 + f_s^2}$$

Minimum Principal Stress:

$$f_{min} = \frac{f_x + f_y}{2} - \sqrt{\left(\frac{f_x - f_y}{2}\right)^2 + f_s^2}$$

The Angle of the principal stress field:

$$\tan(2\theta) = \frac{2 \cdot f_s}{f_x - f_y}$$

Maximum Shear Stress:

$$f_{smax} = \sqrt{\left(\frac{f_x - f_y}{2}\right)^2 + f_s^2}$$

The relationship between the applied and principal stresses can be visualized using Mohr's circle. See Section 3.4.3.1.

AA-SM-041-000 Stress Analysis - 2D Principal Stresses

Note. The principal strains are related to the principal stresses by the following expressions:

$$\epsilon_{max} = \frac{1}{E} \cdot (f_{max} - v \cdot f_{min})$$

$$\epsilon_{min} = \frac{1}{E} \cdot (f_{min} - v \cdot f_{max})$$

Principal Stresses in Three Dimensions

The principal stresses in 3 dimensions can be calculated using the following expression. It should be noted that these are rarely used in hand calculations and are given here for reference only.

$$f_1 = \frac{I_1}{3} + \frac{2}{3} \left(\sqrt{I_1^2 - 3 \cdot I_2} \right) \cdot \cos\phi$$

$$f_2 = \frac{I_1}{3} + \frac{2}{3} \left(\sqrt{I_1^2 - 3 \cdot I_2} \right) \cdot \cos\left(\phi - \frac{2 \cdot \pi}{3}\right)$$

$$f_3 = \frac{I_1}{3} + \frac{2}{3} \left(\sqrt{I_1^2 - 3 \cdot I_2} \right) \cdot \cos\left(\phi - \frac{4 \cdot \pi}{3}\right)$$

Where:

$$\phi = \frac{1}{3} \cdot \cos^{-1} \left(\frac{2 \cdot I_1^3 - 9 \cdot I_1 \cdot I_2 + 27 \cdot I_3}{2 \cdot (I_1^2 - 3 \cdot I_2)^{3/2}} \right)$$

$$I_1 = f_x + f_y + f_z$$

$$I_2 = f_x \cdot f_y + f_y \cdot f_z + f_z \cdot f_x - f_{xy}^2 - f_{yz}^2 - f_{zx}^2$$

$$I_3 = f_x \cdot f_y \cdot f_z - f_x \cdot f_{yz}^2 - f_y \cdot f_{zx}^2 - f_z \cdot f_{xy}^2 + 2 \cdot f_{xy} \cdot f_{yz} \cdot f_{zx}$$

There is a spreadsheet you can download for this method at this link:

AA-SM-041-001 Stress Analysis - 3D Principal Stresses

3.4.2.2. Von-Mises Stress

The Von-Mises stress is a resultant stress criterion that was initially developed to predict the point of yielding. In this case, the Von Mises stress is calculated and compared to the material yield stress allowable F_{ty} .

It is also acceptable to use the Von Mises stress to predict failure by comparison with the material ultimate stress allowable F_{tu} .

It should be noted that because Von Mises stress is a resultant stress it is always positive regardless of the nature of the stress under examination, tension or compression.

Therefore, care must be taken when the Von Mises stress is used that compression stress effects (buckling, crippling) are not ignored because the stress appears positive (or tension).

Von Mises Stress in Two Dimensions

For general stresses:

$$f_v = \sqrt{f_x^2 - f_x \cdot f_y + f_y^2 + 3 \cdot f_s^2}$$

Where the principal stresses are known:

$$f_v = \sqrt{f_1^2 - f_1 \cdot f_2 + f_2^2}$$

AA-SM-041-020 Stress Analysis - 2D Von Mises Stress

Von Mises Stress in Three Dimensions

For general stresses:

$$f_v = \sqrt{\frac{1}{2} \cdot [(f_x - f_y)^2 + (f_y - f_z)^2 + (f_z - f_x)^2 - 6 \cdot (f_{xy}^2 + f_{yz}^2 + f_{zx}^2)]}$$

Where the principal stresses are known:

$$f_v = \sqrt{\frac{1}{2} \cdot [(f_1 - f_2)^2 + (f_2 - f_3)^2 + (f_3 - f_1)^2]}$$

AA-SM-041-021 Stress Analysis - 3D Von Mises Stress

The two-dimensional Von Mises Stresses are generated for common cross-sections in the following spreadsheets:



3.4.3. Failure Criteria

General use of failure envelopes; resulting stresses inside the envelope show adequate strength, those outside show inadequate strength:

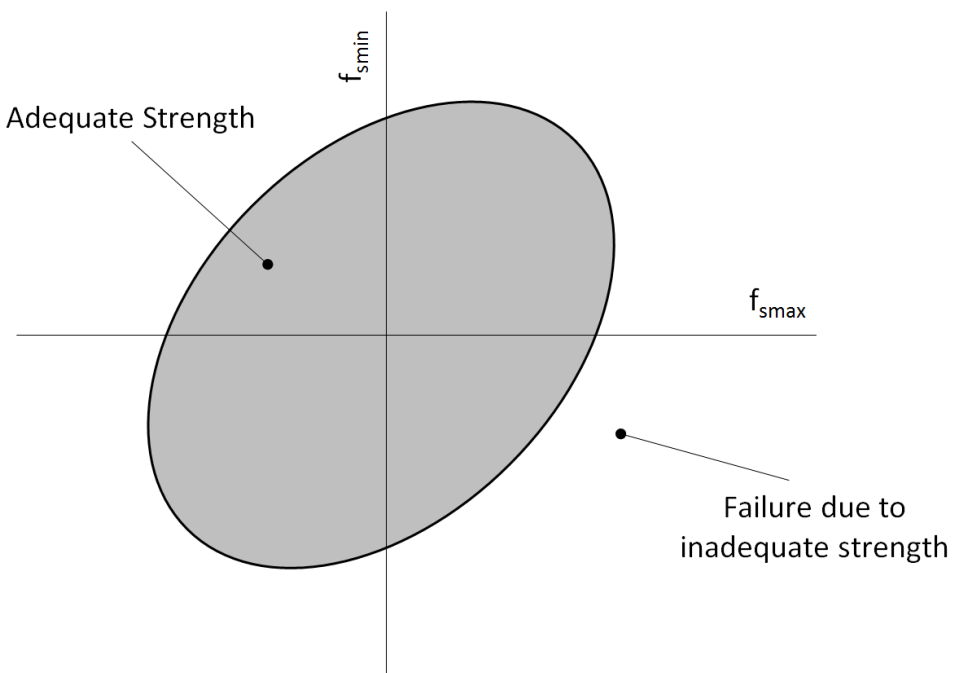


Figure 3.4.3-1: General Application of Two-Dimensional Failure Envelopes

The regions of the 2D principal stress plane correspond to the various possible modes of loading as follows (the Tresca Envelope is shown in this diagram for reference only):

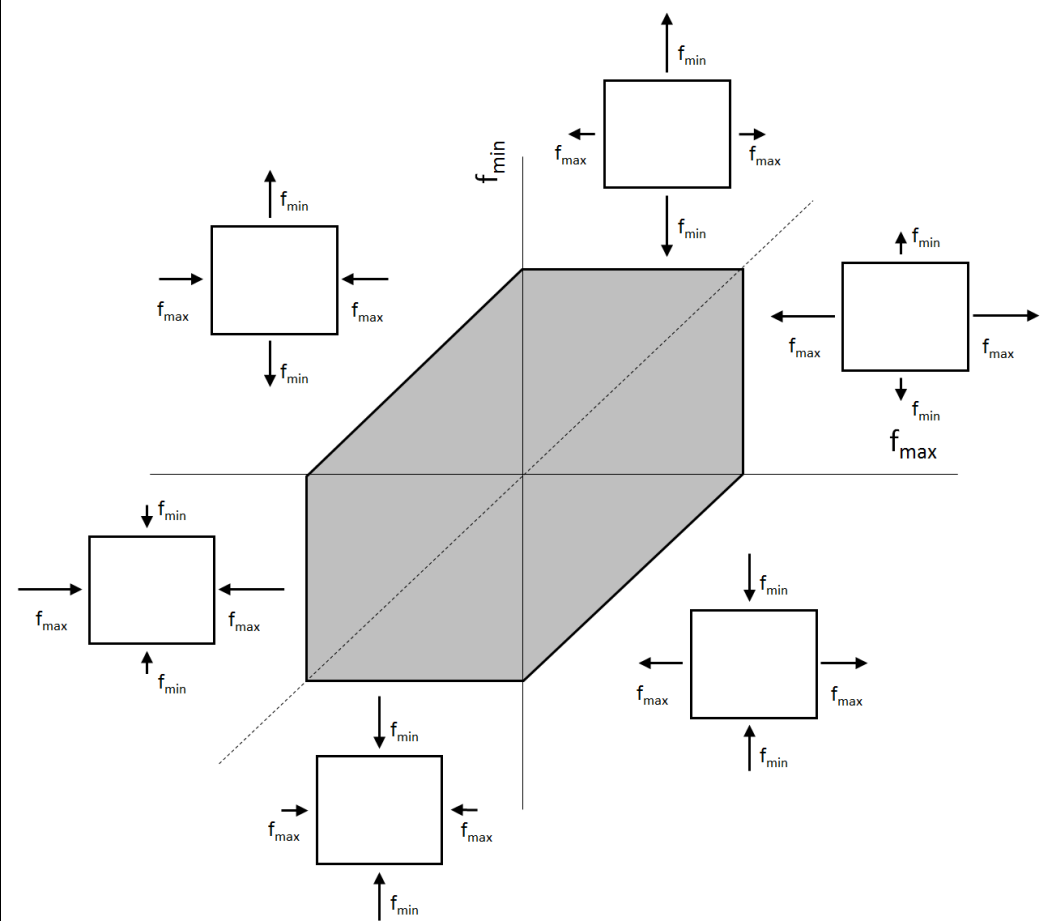


Figure 3.4.3-2: Regions of 2D Principal Stress Field

Most failure envelopes are plotted on a two-dimensional principal stress graph. This simplifies the approach as the shear stress is zero in the principal directions.

3.4.3.1. Mohr's Circle

The definition of Mohr's Circle is in part taken from [\(NASA TM X-73305, 1975\)](#).

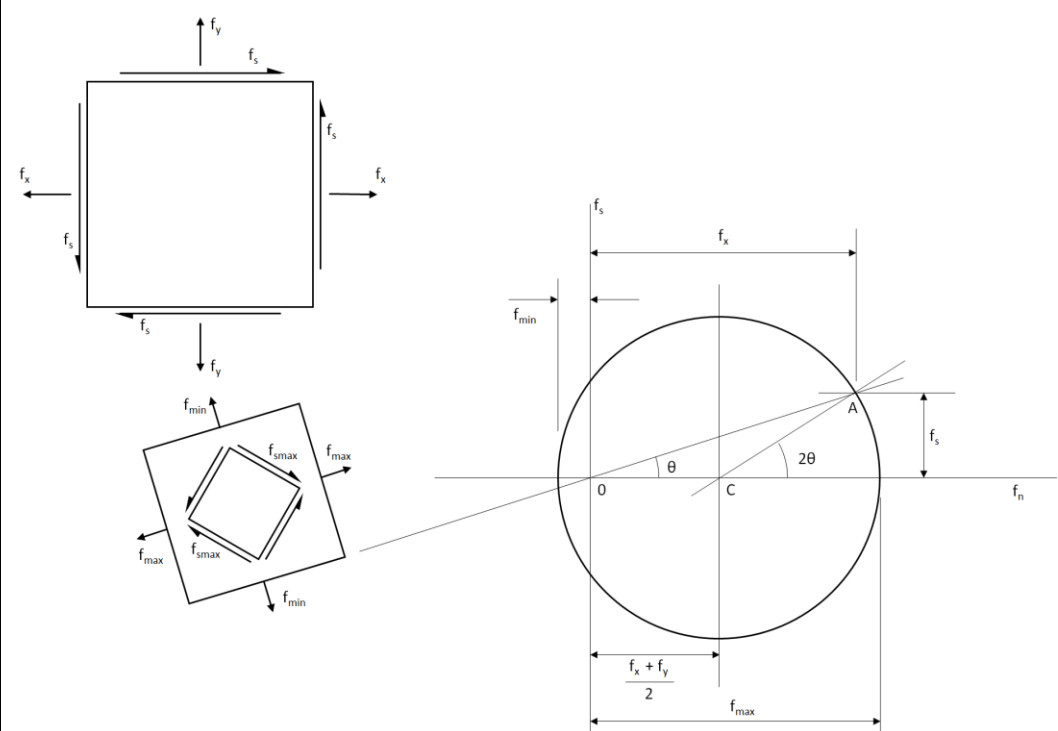


Figure 3.4.3-3: Mohr's Circle Definition

The following text is taken directly from [\(NASA TM X-73305, 1975\)](#):

1. Make a sketch of an element for which the normal and shearing stresses are known and indicate on it the proper sense of those stresses.
2. Set up a rectangular coordinate system of axes where the horizontal axis is the normal stress axis, and the vertical axis is the shearing stress axis. Directions of positive axes are taken as usual, upwards and to the right.
3. Locate the center of the circle which is on the horizontal axis at a distance of $(f_x + f_y)/2$ from the origin. Tensile stresses are positive, compressive stresses are negative
4. From the right-hand face of the element prepared in step (1), read off the values for the f_x and f_s and plot the controlling point "a". The coordinate distances to this point are measured from the origin. The sign of f_x is positive if tensile, negative if compressive; that of f_s is positive if upwards, negative if downward.
5. Draw the circle with the center found in step (3) through controlling point "a" found in step (4). The two points of intersection of the circle with the normal-stress axis give the magnitudes and sing of the two principal stresses. If an intercept is found to be positive, the principal stress is tensile, and conversely.
6. To find the direction of the principal stresses, connect point "a" located in step (4) with the intercepts found in step (5). The principal stress is given by the particular intercept found in step (5) acts normal to the line connecting this intercept point with the point "A" found in step (4)
7. The solution of the problem may then be reached by orienting an element with the sides parallel to the lines found in step (6) and by indicating the principal stresses on this element.

To determine the maximum or the principal shearing stress and the associated normal stress:

1. Determine the principal stresses and the planes on which they act per the previous procedure.
2. Prepare a sketch of an element with its corners located on the principal axes. The diagonals of this element will this coincide with the directions of the principal stresses.
3. The magnitude of the maximum (principal) shearing stresses acting on mutually perpendicular planes is equal to the radius of the circle. These shearing stresses act along the faces of the element prepared in step (2) towards the diagonal, which coincides with the direction of the algebraically normal stress.
4. The normal stresses acting on all the faces of the element are equal to the average of the principal stresses, considered algebraically. The magnitude and sign of these stresses are also given by the distance from the origin of the coordinate system to the center of Mohr's circle.



3.4.3.2. Maximum Principal Stress Envelope

The maximum principal stress envelope assumes that both the maximum and minimum principal stresses can occur at the same point simultaneously. This is likely to be optimistic and fail to predict material failure when it is likely to occur. For this reason, this envelope is not used for analysis purposes and is included here for information only.

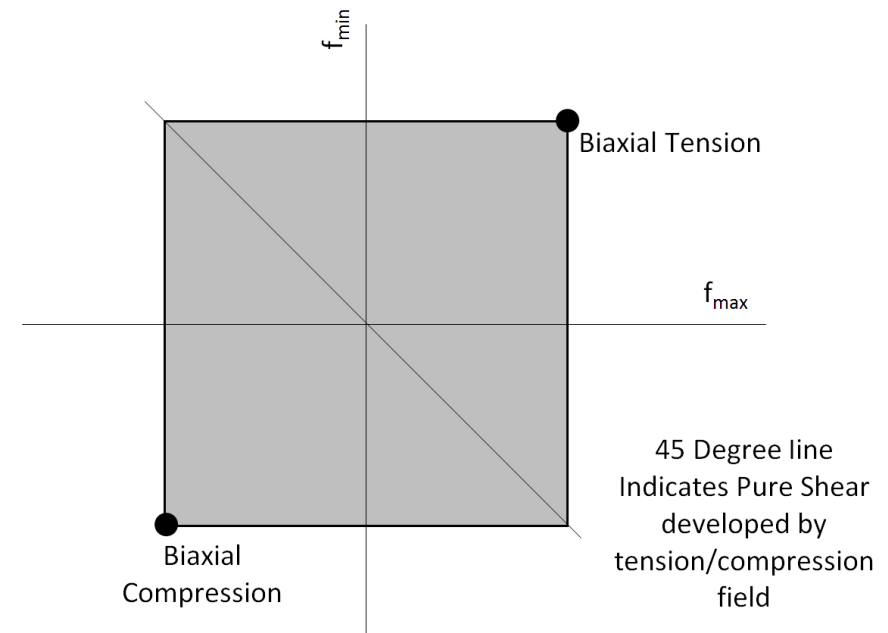


Figure 3.4.3-4: Maximum Principal Stress Envelope

In this envelope, the 45-degree line that illustrates the pure shear condition extends into a region beyond the typical shear strength of most materials.

3.4.3.3. Tresca Criterion

The Tresca Criterion is also called the maximum shear stress criteria.

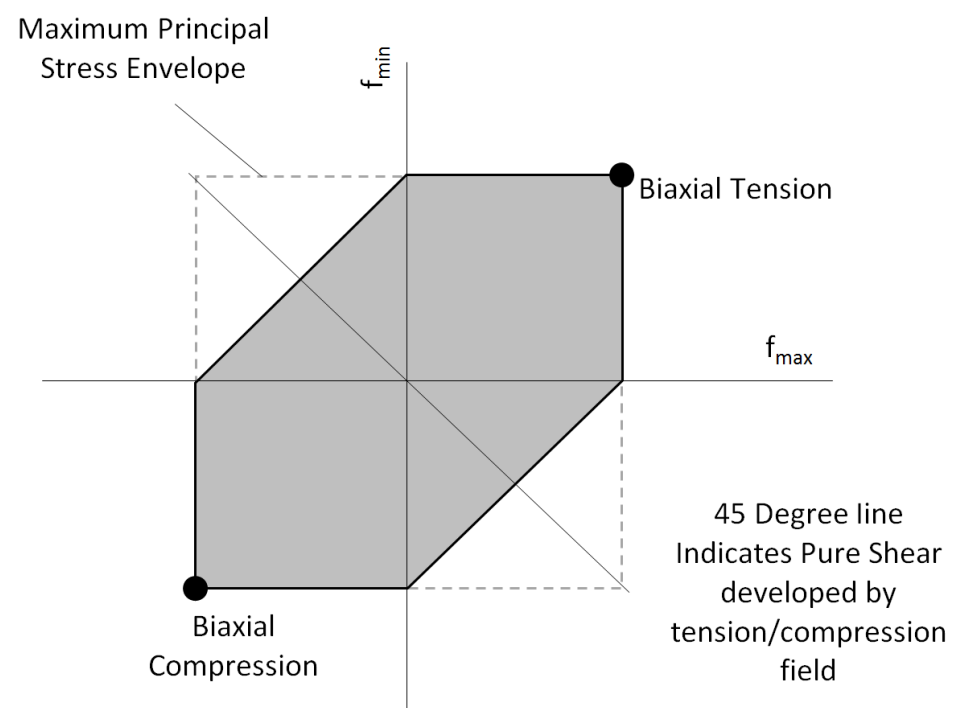


Figure 3.4.3-5: Tresca Envelope

For the Tresca Criterion, the allowable shear stress = the allowable tensile stress divided by two:

$$F_{sy} = \frac{F_{tu}}{2}$$

Or, assuming linear material behavior up to ultimate failure level:

$$F_{su} = \frac{F_{tu}}{2}$$

This criterion regarding shear stress is conservative for almost all metals as the shear strength is greater than half of the tensile strength.

The Tresca stress tensor (or the effective stress) should be compared to the allowable material strength. The Tresca stress tensor can be calculated from the principal stresses in the following way:

$$f_s = \frac{|f_{max} - f_{min}|}{2}$$



The Tresca criterion is conservative compared to the more realistic Von Mises Criterion.

3.4.3.4. Von Mises Criterion

The Von Mises criterion is also called the octahedral shear stress criterion. When plotted for plane stress states the Von Mises stress envelope is an ellipse

$$f_v = \sqrt{f_x^2 - f_x \cdot f_y + f_y^2 + 3 \cdot f_s^2}$$

For the Von Mises Criterion, the allowable shear stress = the allowable tensile stress divided by the square root of three.

$$F_{sy} = \frac{F_{ty}}{\sqrt{3}}$$

Or, assuming linear material behavior up to ultimate failure level.

$$F_{su} = \frac{F_{tu}}{\sqrt{3}}$$

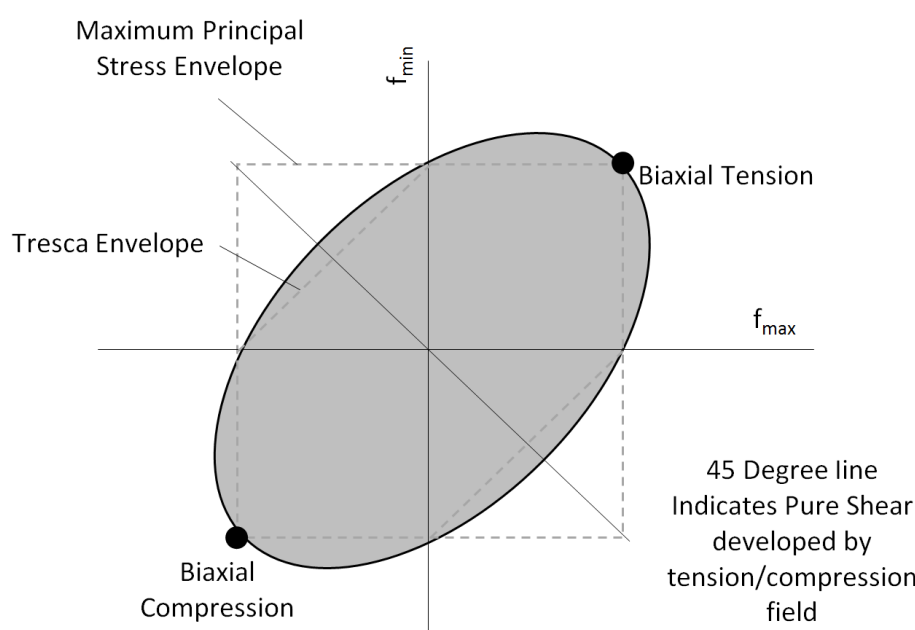


Figure 3.4.3-6: Von Mises Envelope



The Von Mises criterion is considered generally representative for ductile materials and the relationship between F_{su}/F_{sy} and F_{tu}/F_{ty} is close enough for most analysis purposes.

3.4.4. Note on Practical Stress Analysis

The various material failure criteria defined in this chapter are used for different reasons in a range of different situations. General stress analysis should not always reach for these solutions. Where the stress is predominantly uniaxial a simple comparison to F_{ty} or F_{tu} is sufficient, or where the stress is predominantly shear, a comparison to F_{sy} or F_{sy} is sufficient.

The need to go to a plane stress criterion is dependent on the complexity of the stress field and the general magnitude of the stress, and is at the discretion of the engineer.

ADVERT: ENGINEERING SERVICES

COMPOSITE DESIGN

CONTACT US ENGINEERING SERVICES

4. MATERIALS

4.1. Composite Materials

4.1.1. Introduction

Composite materials comprise of more than one material. They are a mixture. This book covers laminated composite structures. Reinforcements arranged in layers (usually Carbon or Glass) set in a rigid matrix (usually epoxy resin).

Laminate composite structure is not isotropic (the same stiffness in all directions) and can usually be described as orthotropic.

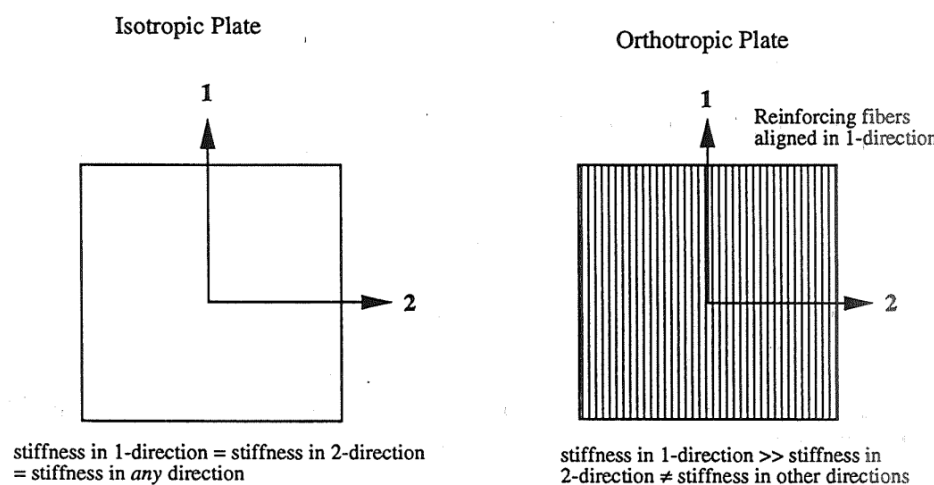


Figure 4.1.1-1: Difference between an Isotropic and an Orthotropic Panel
[\(NASA-RP-1351, 1994\)](#)

The design and substantiation of composite structure has to be integrated considering the specific compliance methods for the aircraft project. i.e. the analysis methods used are validated for specific laminates and design features that can be unique for the aircraft in question. It is important for the engineer to realize that there is no reliable universal general solution for the analysis of carbon fiber composite structures in the context of airworthiness regulations (although accepted common methodologies are evolving) and that companies develop, qualify and validate analysis methods for design features that they wish to use.

There are design conventions for composite structure and these will be covered in this book. However, this book is not to be regarded as a comprehensive composite structural design manual.

Because of the unique nature of composite laminate structures – both physical and regulatory - novel or unusual features (those that are new to the company or particular aircraft) must first be discussed with the chief engineer before incorporation into the design of components and assemblies.

In this manner, composite structures are no different to metallic structures. It is worth pointing out the obvious, that metallic structures have been around for much longer than composite structures and conventions are better established and widely known. There is a wealth of information regarding the analysis of metallic (isotropic, elasto-plastic) structure – Timoshenko, NACA, NASA and many others.

The methods and philosophies discussed in this document are generally acceptable at the time of writing to North American certification agencies.

The substantiation methods covered in this document are targeted at primary structure. They would also be acceptable for the substantiation of secondary structure but if those methods are used for the sizing of secondary structure it may result in excess weight being built into the design.

General guidance for substantiation of secondary composite structures can be found in [\(FAA-PS-ACE100-2004-10030, 2005\)](#), while specifically applicable to FAA part 23 aircraft, the standards in this document are generally applicable to all aircraft.

For clarity the definition of secondary structures from [\(FAA-PS-ACE100-2004-10030, 2005\)](#) is repeated here:

Secondary structures are those that are not primary load carrying members, and their failure would not reduce the structural integrity of the airframe or prevent the airplane from continuing safe flight and landing. This is the same definition used in AC 23-19, issued by the Small Airplane Directorate. For clarification, the secondary structure definition implies that a hazard assessment of the partial or complete failure of the structure has been performed and there is no reasonable threat to safety of flight or landing. Such an assessment should include consideration for flight stability and control. Also consider subsequent failures that are the logical result of the initial failure.

Secondary structures must be designed, fabricated, and maintained such that they will not depart the aircraft and/or cause other safety hazards. Those exterior components that meet the definition of secondary structures may include fairings, cowlings, and radomes. Non-structural components, including many interior parts, whose failure would be inconsequential, may also fit the definition of secondary structures. Clearly, engineering judgment, based on the location, design, and function of a particular secondary structure, will help determine the level of material and process evaluation needed in type certification and subsequent production controls.

Ambiguity also exists between secondary and primary structures. For differentiation purposes, we define primary structure in this policy as, "The structure that carries flight, ground, crash or pressurization loads, and whose failure would reduce the structural integrity of the airplane or may result in injury or death to passengers or crew." Interior structures that carry crash loads, as required by 14 CFR part 23, §§ 23.561 and 23.562, are primary structure. Some structures may not satisfy the definitions of secondary or primary structure as provided in this policy. This may include structure that does not carry primary loads, but its failure may impact primary structure and prevent the continued safe flight of the airplane. Further coordination with the certification engineer may be required for these structures.

Composites may be susceptible to lightning damage. Lightning protection may be needed for secondary composite structure, such as engine cowls, where the effect of strike may be detrimental to engine operation. Demonstrate that the composite structure can dissipate P-static electrical charges, provides electromagnetic protection where required, and provides an acceptable means of diverting the lightning electrical current so as not to endanger the aircraft. Consider possible deterioration and undetected damage to the lighting protection system.

Flammability and fire protection requirements also need to be substantiated for aircraft components. The use of composite structures/components should not decrease the level of safety prescribed by the existing requirements for flammability and fire protection. These

components may include some of the composite airframe structures and non-structural interior components. For certification convenience, divide the latter into two classifications: (1) non-structural components/parts that are not subject to compartment interior fire protection requirements (e.g., knobs, handles, pulleys, etc.), and (2) non-structural components/parts that are subject to compartment interior fire protection requirements.

4.1.1.1. Some Important General Notes on Composite Laminates and Aircraft

- 1) Certifiable laminate composites rarely offer any real-world weight saving when compared to an analogous aluminum part or assembly. However, if composite parts and assemblies are well designed, and during the design process manufacturing are consulted on a regular basis, they can offer significant parts reduction and manufacturing cost reduction.
- 2) Composite structure, if well designed and manufactured, in theory, should have a greater service life than metallic equivalents. However, at the time of writing, there is not enough data on aging composite aircraft in the civil or commercial sector and only time will tell if this is correct or not. These issues are not well understood and unless these important issues are acknowledged at the start of the design process the results of the design process can be disappointing.
- 3) The composite section of this book is aimed almost exclusively at carbon fiber and epoxy resin fiber laminates as this combination is the most commonly used for critical aircraft structures applications. The methods and philosophies in the manual may be applicable to other matrix and reinforcement materials but the onus is on the reader to fully characterize whatever material system they choose and check the applicability of these methods to their chosen material system.
- 4) Almost all FAR part 25 aircraft adopt a 'black metal' approach to composite aircraft design i.e sandwich structure and adhesives are not used in primary structure and the resulting structure looks, to the lay person, like an aluminum aircraft design that has been built out of carbon fiber. This is due to both manufacturing process control and damage tolerance issues of sandwich structure and adhesive joints. However, cored structure and adhesive joints are commonly used in FAR part 23 aircraft primary structure and the analyst should be aware of their unique advantages and limitations and we will try to give some insight into these issues in the relevant chapters herein.
- 5) When composite materials are used the aircraft developer takes on a greater responsibility for material processing and quality control. The engineer must work closely with manufacturing and quality to ensure that the impact of material and part variability are considered in the substantiation and compliance work.

The following sections on composite laminate nomenclature, physical characteristics, strength and durability are no more than a high level 'whistle-stop' tour of the result of decades of work done by industry, government agencies and universities. It is highly recommended that the reader follows the links to the all the cited sources and read them in full.

This will take a significant amount of time, but it is important to realize the breadth and complexity of the subject and the issues that have driven the aircraft industry to adopt the current design conventions and analysis methods.

As previously mentioned, we are all standing on the shoulders of giants. We would be helpless without the work done by those who have preceded us.

ADVERT: ENGINEERING SERVICES

LOADS ANALYSIS
ENGINEERING SERVICES

4.1.2. Basic Composite Material Primer

Composite materials are by definition made up of different types of materials. The common composites used in aircraft design are laminate composites. Laminate composites are made up of different layers (lamina or plies) which adhere to each other. The material in the individual lamina is called the **reinforcement** and the adhesive/bonding agent is called the **matrix**.

4.1.2.1. Matrix

The matrix is the 'binder' that holds the otherwise flexible reinforcement in a rigid form. Common matrix materials are Epoxy Resin, Polyester Resin and Vinyl-Ester resin. The matrix can come either applied to the reinforcement (pre-impregnated or 'pre-pregged') or can be applied to the 'dry' reinforcement manually during the lay-up process (wet layup) or infused into the reinforcement using a vacuum pump (VARTM – vacuum assisted resin transfer molding).

4.1.2.2. Reinforcement

Common forms of reinforcements are stitched or woven (containing fibers at 90 degrees to each other) and tapes (containing fibers all orientated in the same direction).

The reinforcement can contain other products such as polyester stitching or a resin binder product, but these have no effect on the final strength of the design. These products are added for ease of manufacture and it is more likely for the final product to achieve the intended strength and suffer fewer quality problems.

By far the most common reinforcement materials are glass fiber and carbon fiber. Glass fiber is cheaper, less brittle and less strong. Carbon fiber is more expensive, more brittle and stronger.

Types of Weave

The form of the cloth can be of several different weave types. The satin weave types are more flexible and easier to conform to more complex geometry during layup. Satin weave materials are also less stable as the fibers are more prone to moving and creating gaps.

The Twill weave is used for cosmetic purposes and is better suited for compound curvature than plain weave and has greater fabric stability than a harness satin weave.

2X2 Twill is in common use for many applications as it offers the best compromise.

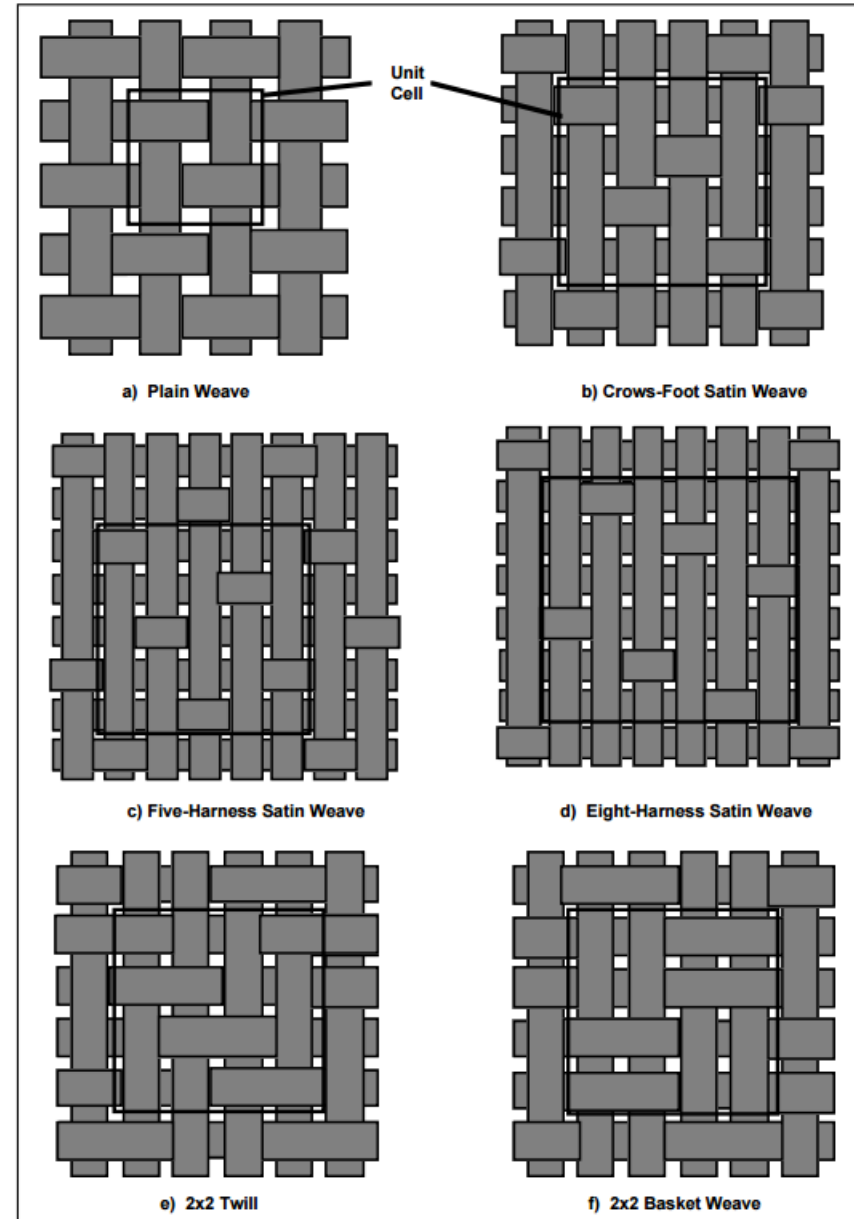


Figure 4.1.2-1: Commonly Used 2D Weave Patterns [\(NASA-CR-4750, 1997\)](#)

4.1.2.3. Combination of Reinforcement and Matrix

The reinforcement and the matrix are combined via a chemical process in the matrix, this is triggered by elevated temperature and is called **curing**. The final product takes on a unique set of physical/mechanical properties. The physical characteristics of the combination of reinforcement and matrix are related *in some ways* to the physical characteristics of the constituent parts, but it is dangerous to assume that any of these individual properties can be directly applied to the cured composite material.

The characteristics of the cured composite material must be determined by test. The critical characteristics used for sizing/analysis and the test methods used to best define them is an extensive field of study.

4.1.2.4. Composite Nomenclature

It is important that the standard terms referring to composite structures are understood. There are many ways to define composite design on the face of a drawing and to reference them in a report. The key aspects to define are the orientation of each ply relative to a clear datum, the material of each ply, the order that the plies are to be laid in and the extent of each ply.

The most common way to orient each ply relative to a datum is the use a rosette to define the 0, 45 and 90-degree directions.

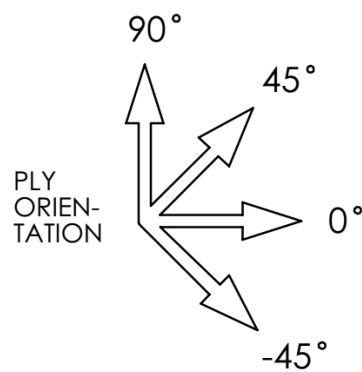


Figure 4.1.2-2: Example Ply Orientation Rosette

The individual ply directions are then defined relative to the 0-degree direction on the rosette. The individual ply directions can be defined in a table on the face of the drawing.

| LAYER NO | MATERIAL SPECIFICATION | FIBER DIRECTION | THICKNESS IN INCHES | NOTES |
|----------|--|-----------------|---------------------|----------|
| 1 | MITSUBISHI RAYON NX033115 - 7781 E-GLASS | 45 | .010 | OVER ALL |
| 2 | MITSUBISHI RAYON NX033115 - 7781 E-GLASS | 0 | .010 | OVER ALL |
| 3 | MITSUBISHI RAYON NX033115 - 7781 E-GLASS | 45 | .010 | OVER ALL |
| 4 | MITSUBISHI RAYON NX033115 - 7781 E-GLASS | 0 | .010 | OVER ALL |
| 5 | MITSUBISHI RAYON NX033115 - 7781 E-GLASS | 45 | .010 | OVER ALL |
| 6 | MITSUBISHI RAYON NX033115 - 7781 E-GLASS | 0 | .010 | OVER ALL |
| 7 | MITSUBISHI RAYON NX033115 - 7781 E-GLASS | 45 | .010 | OVER ALL |
| 8 | MITSUBISHI RAYON NX033115 - 7781 E-GLASS | 0 | .010 | OVER ALL |
| 9 | MITSUBISHI RAYON NX033115 - 7781 E-GLASS | 45 | .010 | AS SHOWN |
| 10 | MITSUBISHI RAYON NX033115 - 7781 E-GLASS | 0 | .010 | AS SHOWN |
| 11 | MITSUBISHI RAYON NX033115 - 7781 E-GLASS | 45 | .010 | AS SHOWN |
| 12 | MITSUBISHI RAYON NX033115 - 7781 E-GLASS | 0 | .010 | AS SHOWN |
| 13 | MITSUBISHI RAYON NX033115 - 7781 E-GLASS | 45 | .010 | AS SHOWN |
| 14 | MITSUBISHI RAYON NX033115 - 7781 E-GLASS | 0 | .010 | AS SHOWN |
| 15 | MITSUBISHI RAYON NX033115 - 7781 E-GLASS | 45 | .010 | AS SHOWN |
| 16 | MITSUBISHI RAYON NX033115 - 7781 E-GLASS | 0 | .010 | AS SHOWN |
| -- | PEEL PLY | -- | -- | OVER ALL |
| | | TOTAL THICKNESS | .080 | |

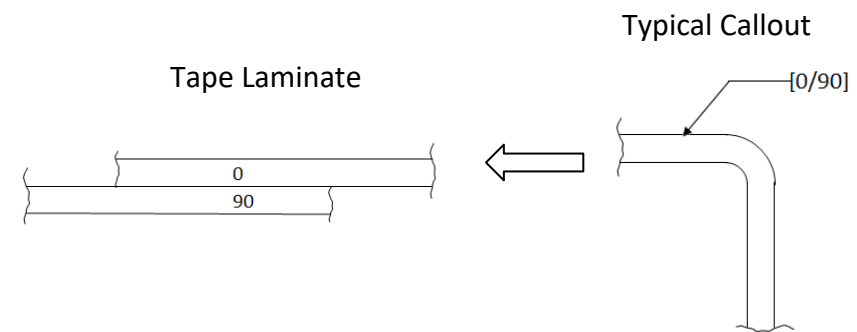
Figure 4.1.2-3: Example Ply Table

Each ply is given a number. Note that nonstructural items that are included in the manufacturing process are also specified in the ply table; peel ply in the example table above. Other items that may appear in the ply table includes film adhesive and lightning protection materials. Where the plies do not extend over all of the part the extent of each ply (where the ply 'drop' occurs) is defined on the face of the drawing.

There are alternative ways to define the stack of the plies in the part, most organizations use similar but not identical definitions. A common approach is shown below. It is important to check the documentation applicable to the project you are working on to avoid errors.

- The lamina/plies are listed in sequence, set off by brackets starting from the side indicated by the code arrow:

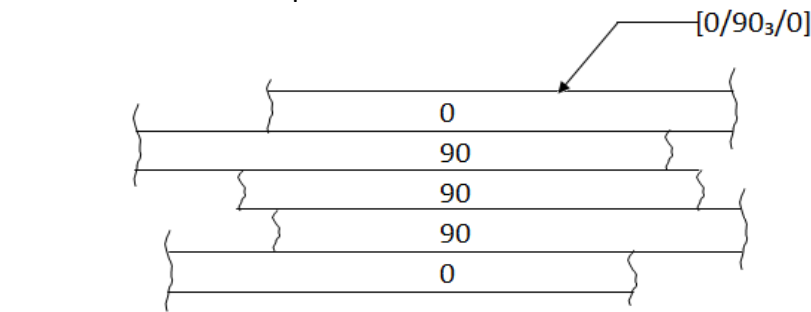
- The orientation of the plies is defined relative to the primary load direction of the part. 0° being the primary load direction.
- Adjacent plies with different angles of orientation are separated by a slash.



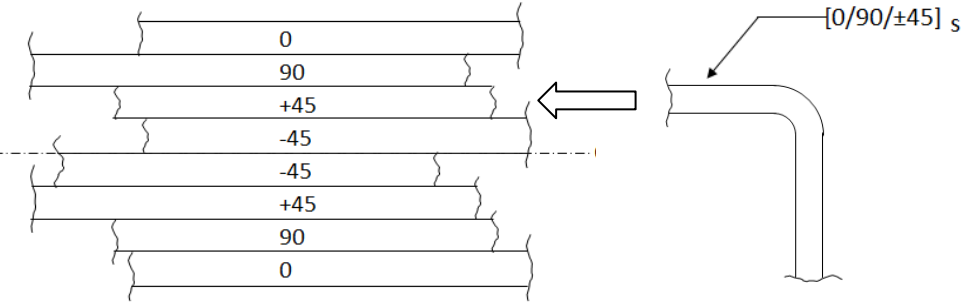
- The callout of fabric plies is differentiated from tape plies by parentheses.

Example: $[(\pm 45)/(0,90)]$

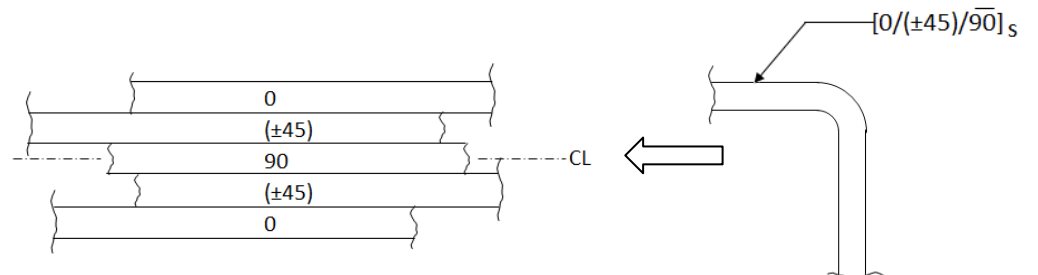
- Adjacent plies of the same angle of orientation are shown by a numerical subscript.



- For tape only when the ± is used two adjacent plies are indicated, with the top symbol being the first of the two:



- Symmetric laminates with an odd number of plies have the center one overlined to indicate this condition. Starting with this ply, the rest of the code would be a mirror-image of that part shown.



Note that these forms of laminate definition are not universally used and companies often develop their own simplified versions of these definitions.

4.1.3. Fundamental Behavior of Carbon Fiber Epoxy Resin Composite Laminates

In general, it is recommended that for cloth (woven or stitched biaxial reinforcing) 'quasi-isotropic' laminates are taken to be the default and that they be as close to balanced and symmetrical as possible. Where both balance and symmetry cannot be achieved simultaneously symmetry should be sacrificed to maintain balance. The effect of an unsymmetrical laminate on outer surface stresses and strains can be calculated and predicted.

Quasi-isotropic laminates are recommended for the following reasons:

1. They offer good load resistance in all directions and therefore require no particular effort paid to orientation in manufacturing.
2. They offer the best resistance to impact damage and damage growth.
3. They produce the best joint strength for mechanical attachments.
4. Quasi-isotropic laminates reduce the risk of parts warping when releasing from the mold due to uneven surface strains.

Where high anisotropy (tailored stiffness in a particular orientation) is required – i.e. wing spar caps - local unidirectional fiber (tape) placement is encouraged.

4.1.3.1. Stress-Strain Behavior of Common Composite Laminates

Carbon fiber laminate materials exhibit brittle (non-plastic) failure modes and typically the stress-strain plot remains linear to ultimate failure, see Figure 4.1.3-1. This behavior is different to typical aircraft metals, see Figure 4.1.3-2.

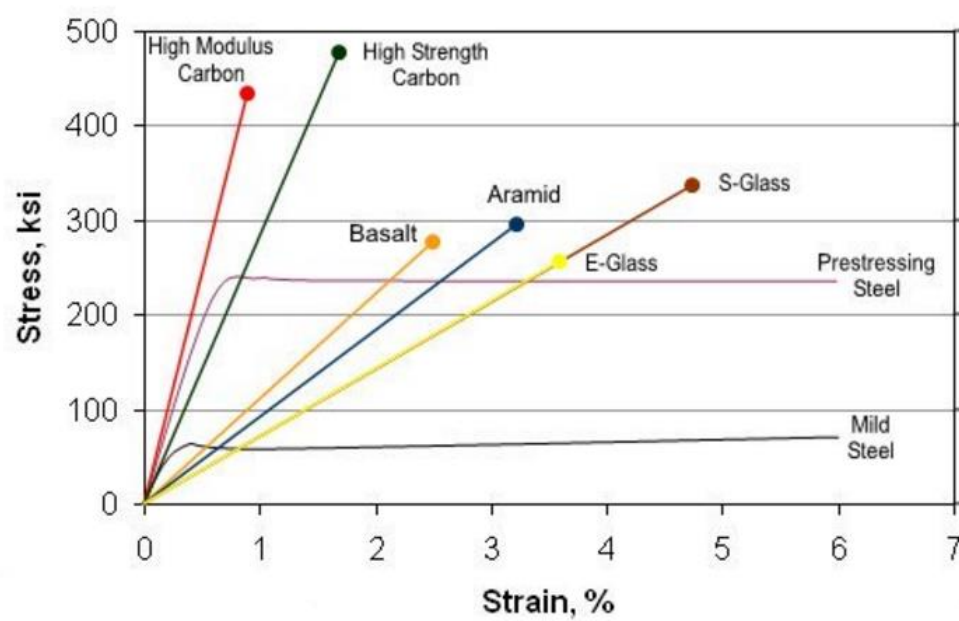
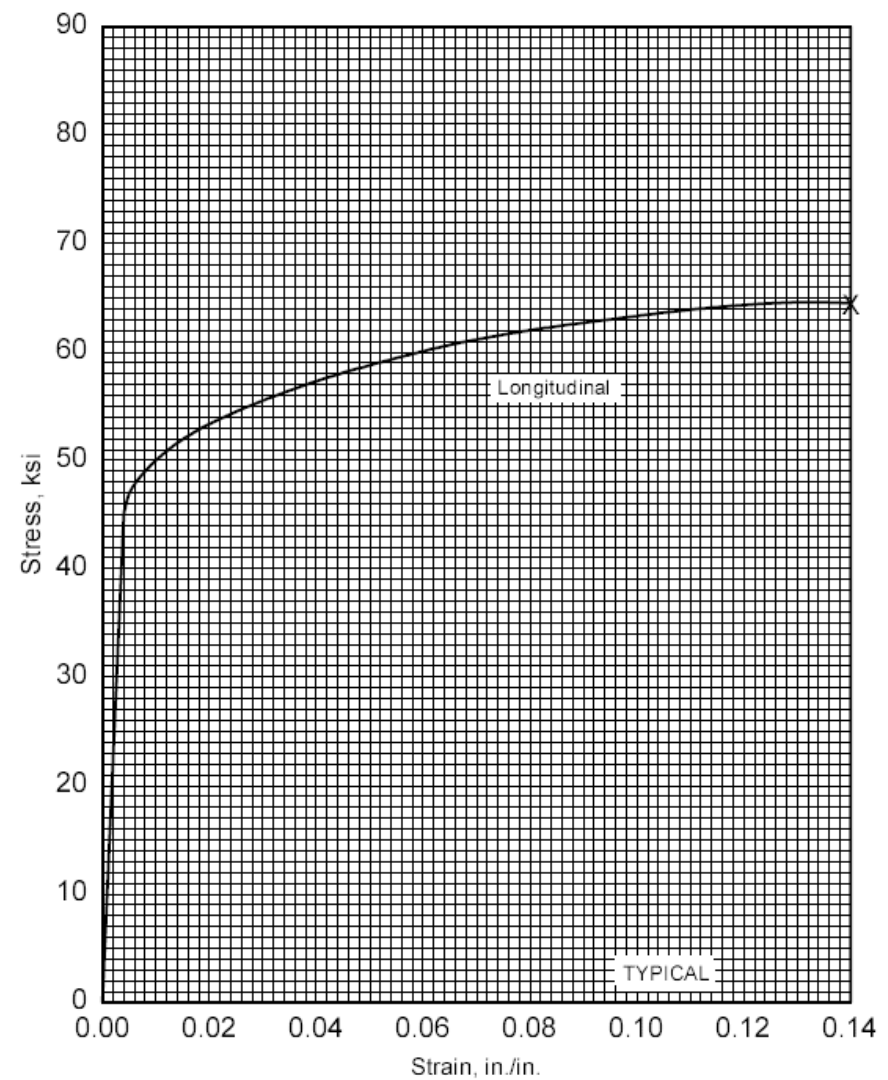


Figure 4.1.3-1: Comparison of Common Laminate Stress-Strain Behavior
(Source: [Prince Engineering](#))



2024-T351

Figure 4.1.3-2: Stress-Strain Data for 2024-T351 ([MIL-HNDBK-5H, 1998](#))

The linear stress-strain behavior for common composite materials means that 'Kt' effects (stress concentrations) that can be ignored at limit and ultimate level analysis (but not for fatigue) in ductile metals **must** be considered for carbon fiber laminates up to ultimate load level.

The behavior of carbon reinforced epoxy resin laminates also stops any redistribution of load as there is no proportional limit or yield point on the stress-strain curve to exceed. Particular attention must be paid to design; whereas in metals the ultimate strength may rely on load redistribution (plastic joint load redistribution and plastic bending are two examples) carbon fiber laminates do not allow any 'plastic redistribution'.

Any fiber laminate will exhibit the greatest strength in tension (assuming a reasonable component of 0-degree fibers in the laminate) as tension is carried directly by the fibers, loading the fibers in such a way that they are allowed to develop their ultimate tensile strength.

Fiber laminates show significantly lower strength in compression and shear. In compression, the laminate relies on the resin matrix to support the fibers and maintain their compression stability. The in-plane shear load can be described as a 45degree biaxial compression/tension load and the laminate will generally suffer a compression failure at 45degrees when loaded in shear.

The critical environmental conditions, humidity and temperature affect the resin matrix, not the fibers. This can be seen in the little variation in laminate tension strength for laminates between cold-dry and hot-wet conditions. This is in contrast to the laminate compression and shear strengths which show significant variation with different environmental conditions and a significant reduction for hot and hot wet environmental conditions, this is shown in Figure 4.1.3-3, Figure 4.1.3-4 and Figure 4.1.3-5

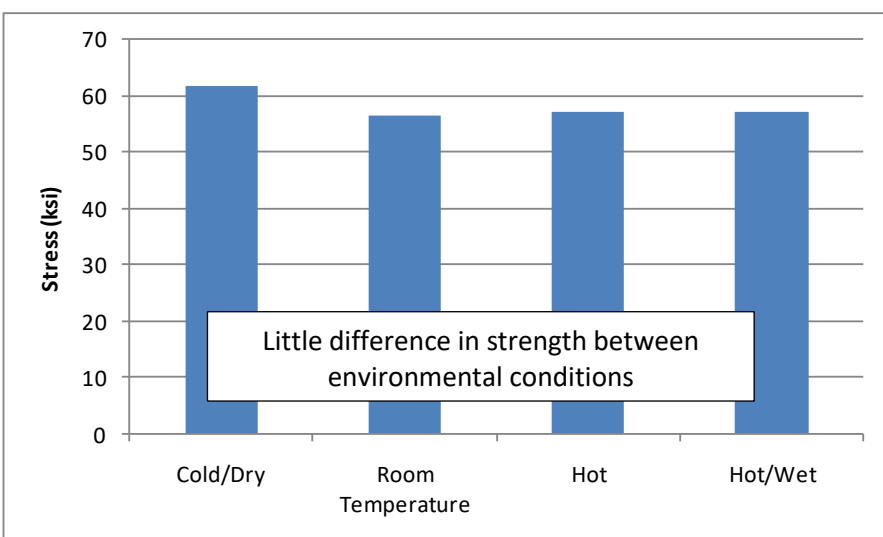


Figure 4.1.3-3: B-Basis Ultimate Tensile Strength, Lamina Strength, Various Environmental Conditions

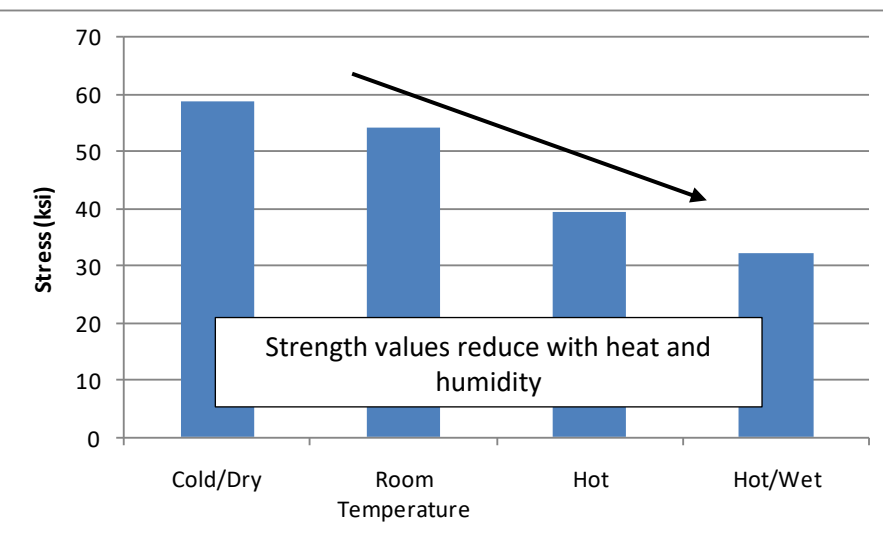


Figure 4.1.3-4: B-Basis Ultimate Compression Strength, Lamina Strength, Various Environmental Conditions

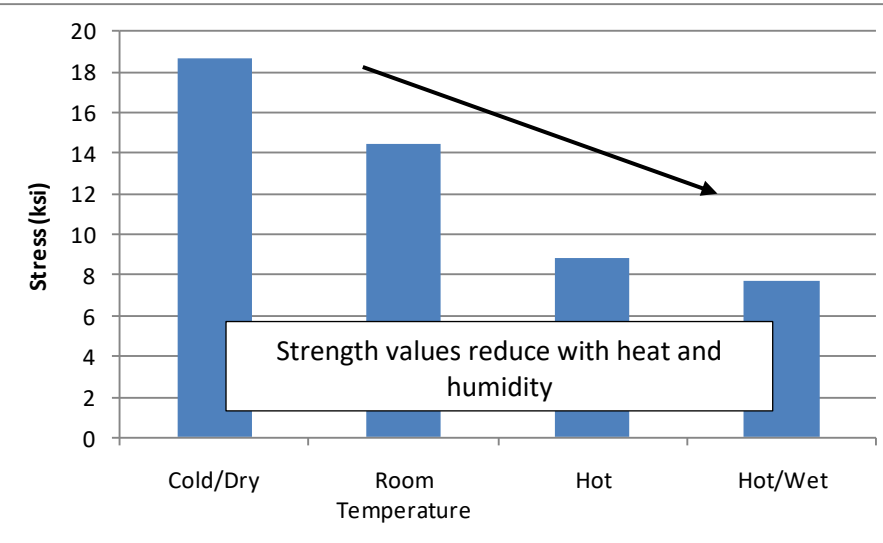


Figure 4.1.3-5: B-Basis Ultimate Shear Strength, Lamina Strength, Various Environmental Conditions

Because of how the resin matrix reacts to the critical environmental condition (hot-wet) the most common laminate failure modes occur in compression or shear.

Note: Composite laminates are known to be poor in carrying loads perpendicular to the laminate plane - the loading 'through the thickness' should be mitigated

or minimized at the design stage wherever possible. The out-of-plane load applied directly to laminate can directly drive delamination under relatively modest loads. The severity of this effect is difficult to predict and measure and so should be avoided by design. Where significant out-of-plane loading cannot be avoided, the strength of the feature in question should be determined by testing of the specific feature.

Note: Mating surfaces should be tool/mold surfaces where possible. This allows for greater geometric control over the interface. *However, extreme care must be exercised to ensure all bonding surfaces are properly prepared with no mold release residue, contamination and correct surface roughness. Control of these parameters is critical to achieving a reliable bond.*

Note: Thickness tolerance is proportional to part thickness - thicker parts require allowance for a greater thickness tolerance

4.1.3.2. On the Use of Core

Composite Sandwich structures are used where additional out-of-plane stiffness is required. This out-of-plane stiffness can be required to react direct out-of-plane loads, pressure loads or used to increase buckling stability of laminate panels.

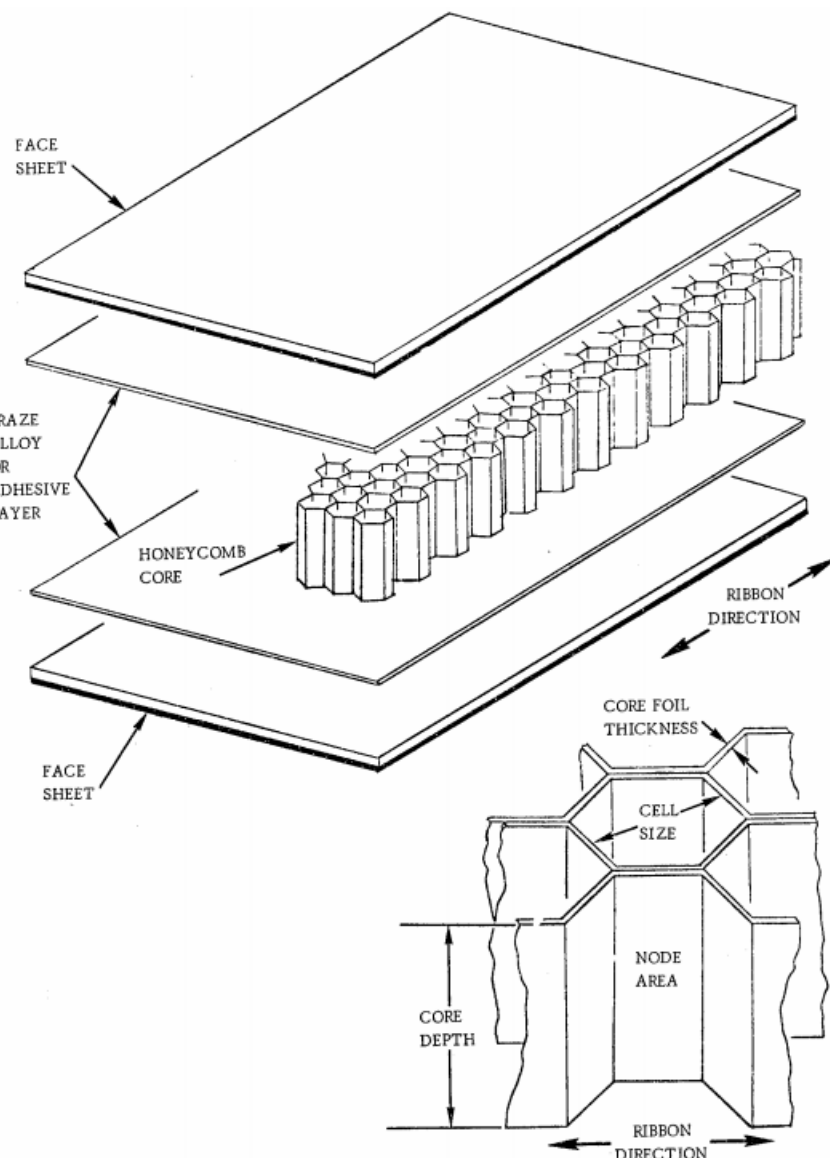


Figure 4.1.3-6: Honeycomb Sandwich Construction [\(NASA CR-1457, 1969\)](#)

The effect of core on the out of place stiffness of a laminate panel is shown below, taken from [\(FAA-H-8083-31, 2012\)](#)

| | Solid Material | Core Thickness t | Core Thickness 3t |
|-------------------|----------------|------------------|-------------------|
| Stiffness | 1.0 | 7.0 | 37.0 |
| Flexural Strength | 1.0 | 3.5 | 9.2 |
| Weight | 1.0 | 1.03 | 1.06 |

Figure 4.1.3-7: The effect of Core on Strength and Stiffness (FAA-H-8083-31, 2012) Correction to Original Material in Red

Core Materials, from (FAA-H-8083-31, 2012)

Honeycomb: Each honeycomb material provides certain properties and has specific benefits. The most common core material used for aircraft honeycomb structures is aramid paper (Nomex® or Korex®). Fiberglass is used for higher strength applications.

- **Kraft paper**—relatively low strength, good insulating properties, is available in large quantities, and has a low cost.
- **Thermoplastics**—good insulating properties, good energy absorption and/or redirection, smooth cell walls, moisture and chemical resistance, are environmentally compatible, aesthetically pleasing, and have a relatively low cost.
- **Aluminum**—best strength-to-weight ratio and energy absorption, has good heat transfer properties, electromagnetic shielding properties, has smooth, thin cell walls, is machinable, and has a relatively low cost.
- **Steel**—good heat transfer properties, electromagnetic shielding properties, and heat resistant.
- **Specialty metals** (titanium)—relatively high strength-to-weight ratio, good heat transfer properties, chemical resistance, and heat resistant to very high temperatures.
- **Aramid paper**—flame resistant, fire retardant, good insulating properties, low dielectric properties, and good formability.
- **Fiberglass**—tailorable shear properties by layup, low dielectric properties, good insulating properties, and good formability.
- **Carbon**—good dimensional stability and retention, high-temperature property retention, high stiffness, very low coefficient of thermal expansion, tailorable thermal conductivity, relatively high shear modulus, and very expensive.
- **Ceramics**—heat resistant to very high temperatures, good insulating properties, is available in very small cell sizes, and very expensive.

Honeycomb core cells for aerospace applications are usually hexagonal. The cells are made by bonding stacked sheets at special locations. The stacked sheets are expanded to form hexagons. The direction parallel to the sheets is called ribbon direction.

Honeycomb core is available with different cell sizes. Small sizes provide better support for sandwich face sheets. Honeycomb is also available in different densities. Higher density core is stronger and stiffer than lower density core.

Foam: Foam cores are used on homebuilt and lighter aircraft to give strength and shape to wing tips, flight controls, fuselage sections, wings, and wing ribs. Foam cores are not commonly used on commercial type aircraft. Foams are

typically heavier than honeycomb and not as strong. A variety of foams can be used as core material including:

- **Polystyrene** (better known as styrofoam)—aircraft grade styrofoam with a tightly closed cell structure and no voids between cells; high compressive strength and good resistance to water penetration; can be cut with a hot wire to make airfoil shapes.
- **Phenolic**—very good fire-resistant properties and can have very low density, but relatively low mechanical properties.
- **Polyurethane**—used for producing the fuselage, wing tips, and other curved parts of small aircraft; relatively inexpensive, fuel resistant, and compatible with most adhesives; do not use a hot wire to cut polyurethane foam; easily contoured with a large knife and sanding equipment.
- **Polypropylene**—used to make airfoil shapes; can be cut with a hot wire; compatible with most adhesives and epoxy resins; not for use with polyester resins, dissolves in fuels and solvents.
- **Polyvinyl chloride** (PVC) (Divinycell, Klegecell, and Airex)—a closed cell medium- to high-density foam with high compression strength, durability, and excellent fire resistance; can be vacuum formed to compound shapes and be bent using heat; compatible with polyester, vinyl ester, and epoxy resins.
- **Polymethacrylimide** (Rohacell)—a closed-cell foam used for lightweight sandwich construction; excellent mechanical properties, high dimensional stability under heat, good solvent resistance, and outstanding creep compression resistance; more expensive than the other types of foams, but has greater mechanical properties.

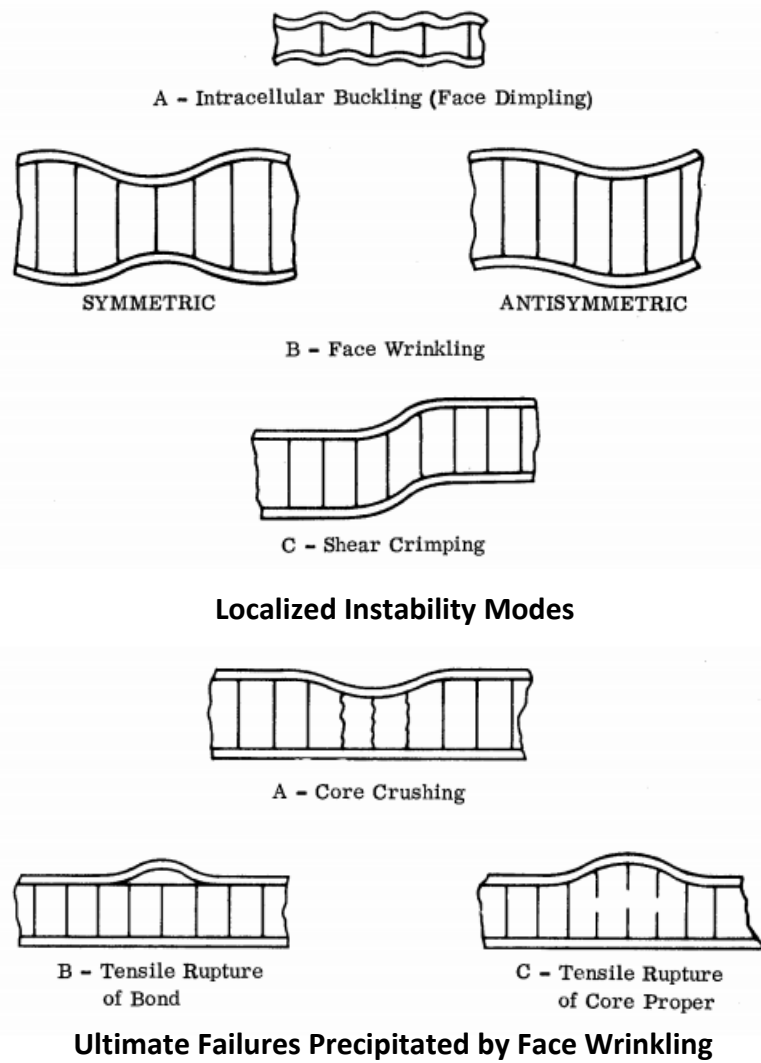
Sandwich structures are poor in damage tolerance: The step change in stiffness at the interface between the core material and the facing laminates creates an environment where damage growth is promoted. It is common for sandwich panels which have suffered damage and subsequently subjected to cyclic loads that the facing plies over the entire cored panel area can detach from the core material.

Sandwich materials are also prone to absorb moisture if the panel is improperly sealed or suffers damage to the facing plies. The repeated cycles of freezing and thawing of water absorbed into the core can detach the facing plies from the core. The failure of the rudder on Air Transat Flight 961 in 2005 was caused by this effect.

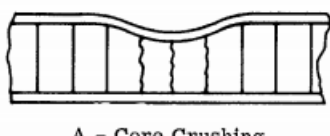


Figure 4.1.3-8: Sandwich Composite Rudder Failure due to Water Ingress
(Source: [Aero News Network](#))

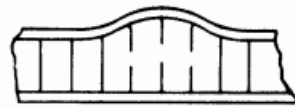
The analysis of composite laminate sandwich structures must consider different failure modes compared to solid laminates.



Localized Instability Modes



A - Core Crushing



B - Tensile Rupture of Bond

C - Tensile Rupture of Core Proper

Ultimate Failures Precipitated by Face Wrinkling

Figure 4.1.3-9: Sandwich Composite Panels, Possible Failure Modes
[\(NASA CR-1457, 1969\)](#)

Note that the tension strength of a sandwich laminate is the total strength of the structural facing plies, the inclusion of a sandwich core affects the out-of-plane bending and buckling strength. The in-plane compression and shear strength of a sandwich laminate are less than for an equivalent solid laminate (taking the facing plies alone and laminating them together) because of additional failure modes that the inclusion of more material introduces such as those shown in Figure 4.1.3-9.

For an in-depth discussion of sandwich composite specific analysis methods and failure modes see section 16.2.2.

To search the [Abbott Aerospace Technical Library](#) for 'Composite Materials'
Click the link below:

ABBOTT AEROSPACE SEZC LTD
Library Subject Search: Tag = Composite

ADVERT: SOFTWARE

EXCEL ADD-IN: SOFTWARE TOOLS **XL-VIKING**

By Aerospace Stress Engineers for Aerospace Stress Engineers

DOWNLOAD

Increase your Excel Performance

4.1.4. Environmental Conditions Considered

4.1.4.1. Temperature

The temperature that the structure may be exposed to will include maximum and minimum storage, or non-operating, temperatures and maximum and minimum operating temperatures. Note that the temperatures apply to the structure and are derived by reference to external factors. These operating and storage temperatures may not apply to systems and do not account for environmental conditions that may be caused by system operation or may not be applicable as system service conditions. The environmental conditions arising from the effect of the aircraft systems on the structure must be examined and shown not to exceed the limits below:

Hot – Operating Conditions

More details given in Section 0

For most paint colors, a default critical structural temperature of 180°F can be assumed without supporting tests or analyses. Dark colors or black, which may yield higher structural temperatures, are an exception. [\(PS-ACE100-2001-006, 2001\)](#)

Hot – Non-operating Conditions

The accepted limit of hot non-operating conditions can be assumed to be 212F.

Room Temperature

The reference ‘room temperature’ will be 73F per [\(Mil-HNDBK-17F-Vol1, 2002\)](#) Section 1.7

Cold – Operating Conditions

The accepted limit for cold operating conditions can be assumed to be -65F.

Cold - Non-operational Conditions

The lowest non-operational temperature that the aircraft could experience is defined by [\(MIL-HDBK-310, 1997\)](#), Table 5.3.1.2.1 as -90F, This shall be adopted as the temperature that the structure should be able to withstand for an indefinite period without compromising structural integrity.

4.1.4.2. Humidity

Moisture diffusion analysis and test conditioning should assume a relative humidity on the order of 85 percent as characteristic of past studies from long-term service exposure, which includes ground time in humid environments from around the world. [\(PS-ACE100-2001-006, 2001\)](#)

Note that complete saturation of all laminates in the structure may not be achieved due to the inability of water vapor to penetrate thick laminates. This implies that a blanket knockdown factor for hot/wet for all laminates is conservative for thick laminates. The extent of this conservatism can be determined by test for thick laminates and assemblies as part of the building block test program. Credit can be taken for the increased strength when it is demonstrated to the satisfaction of the certification authority.

4.1.5. Manufacturing Effects Considered

Unlike metallic materials such as steel and aluminum, the performance of composites is heavily influenced by the manufacturing process and subsequent quality assurance. Below are examples of factors that affect composite mechanical properties:

4.1.5.1. Material Storage

Composites, particularly pre-impregnated fabric (pre-preg), are sensitive to storage temperature, humidity, and time. Often pre-pregs are supplied with a shelf life based on storage temperature. Quality assurance personnel are responsible for tracking the cumulative ‘out-of-freezer’ time. Using material outside of the expiry period voids any warranty unless substantiated by test.

4.1.5.2. Material Preparation

Following removal from the freezer, pre-preg must be fully thawed and moisture removed prior to lamination. Failure to do so will result in moisture ingress and reduction in strength.

4.1.5.3. Layup Conditions

Composites are sensitive to contamination and environmental effects during the layup process. Work must be done in a clean room at set limits of temperature and humidity. These limits are set by the specific resin used.

4.1.5.4. Vacuum Bagging / De-bulk / Autoclave

Laminate strength depends on proper consolidation of the plies. Vacuum bag leaks or insufficient de-bulk frequency are likely to create pockets of entrapped air and excessive variance in laminate thickness, strength and durability.

4.1.5.5. Curing

Resins require specific curing schedules that include temperature ramp-up rate (degrees per minute), sustained time at temperature, followed by a cool down rate. Specifics are determined by the particular resin used. Falling outside of these limits may not only decrease strength but also increase brittleness in the matrix.

4.1.5.6. De-molding

Depending on the part geometry and mold design certain components require heavy persuasion to de-mold (i.e. mallet and wedges). If care is not taken, this process can introduce cracks into the matrix that are difficult to detect by the naked eye.

4.1.5.7. Trimming

When parts are trimmed manually using hand tools, care must be taken to ensure smooth edges (no frayed fibers) and avoidance of sharp stress concentrations.

4.1.5.8. Secondary Bonding

Adhesive joints are highly sensitive to contamination and surface roughness. For this reason, peel ply (consumable fiber used as facing ply on bonding surface) should be removed only immediately prior to bonding. If peel ply is not present, the surface must first be wiped with alcohol, sanded with low grit paper, followed by another alcohol wipe immediately prior to bonding. Both methods must be qualified by test.

4.1.5.9. Post Curing

Similar to curing, this step is sensitive to temperature ramp-up, time at temperature, and ramp-down. Usually, follower coupons (test sample coupons of a set laminate schedule) are placed in the same oven cycle as primary structures. These coupons are then tested to substantiate the particular post-cure cycle. Thermocouples are often placed on the thickest laminate locations to digitally log time vs. temperature. This data is also useful for determining when the structure has heat-soaked to a uniform temperature and begins the timer for the sustained temperature portion of the post-cure.

4.1.6. Strength of Laminates

4.1.6.1. Definition of Laminate Plane Element Behavior

The Strength of any structure can be determined by two means – analysis or test. The purpose of the analysis is to predict performance in real life. Real-life performance is reliably predicted by accurate testing.

There are some excellent public domain primers for analysis of composites including section 4 of [\(MIL-HDBK-17F Vol 3, 2002\)](#).

This section is largely based on [\(NASA-RP-1351, 1994\)](#). The author recommends that this document is reviewed separately by the reader. The material presented here is a summary of the reference material.

Most of the existing references concentrate on the classic laminate method which is the underlying physical model behind most analysis methods.

The aim of this analysis method is to distil the physical characteristics of the laminate to a standard method of describing the stiffness of a panel – i.e. an idealized 2D element – this form of stiffness description is called the ABD matrix and expressed in the following form:

$$\begin{bmatrix} N_x \\ N_y \\ N_{xy} \\ \hline M_x \\ M_y \\ M_{xy} \end{bmatrix} = \begin{bmatrix} A_{11} & A_{12} & A_{16} & | & B_{11} & B_{12} & B_{16} \\ A_{12} & A_{22} & A_{26} & | & B_{12} & B_{22} & B_{26} \\ A_{16} & A_{26} & A_{66} & | & B_{16} & B_{26} & B_{66} \\ \hline B_{11} & B_{12} & B_{16} & | & D_{11} & D_{12} & D_{16} \\ B_{12} & B_{22} & B_{26} & | & D_{12} & D_{22} & D_{26} \\ B_{16} & B_{26} & B_{66} & | & D_{16} & D_{26} & D_{66} \end{bmatrix} \begin{bmatrix} \epsilon_x^0 \\ \epsilon_y^0 \\ \gamma_{xy}^0 \\ \hline K_x \\ K_y \\ K_{xy} \end{bmatrix}$$

Applied Loads & Moments Stiffness Matrix Strains

Figure 4.1.6-1: ABD Matrix Equation for Plane Laminate Element
[\(NASA-RP-1351, 1994\)](#)

The inverted form of the matrix can be used to find the strains resulting from applied loads and moments

$$\begin{bmatrix} \epsilon_x^0 \\ \epsilon_y^0 \\ \gamma_x^0 \\ \hline K_x \\ K_y \\ K_{xy} \end{bmatrix} = \begin{bmatrix} A'_11 & A'_12 & A'_16 & | & B'_11 & B'_12 & B'_16 \\ A'_12 & A'_22 & A'_26 & | & B'_12 & B'_22 & B'_26 \\ A'_16 & A'_26 & A'_66 & | & B'_16 & B'_26 & B'_66 \\ \hline C'_11 & C'_12 & C'_16 & | & D'_11 & D'_12 & D'_16 \\ C'_12 & C'_22 & C'_26 & | & D'_12 & D'_22 & D'_26 \\ C'_16 & C'_26 & C'_66 & | & D'_16 & D'_26 & D'_66 \end{bmatrix} \begin{bmatrix} N_x \\ N_y \\ N_{xy} \\ \hline M_x \\ M_y \\ M_{xy} \end{bmatrix}$$

Figure 4.1.6-2: Inverted ABD Matrix Equation for Plane Laminate Element
[\(NASA-RP-1351, 1994\)](#)

Where:

N are loads, **M** are moments (expressed in flow, or load/moment per unit length), **ε** are strains and **K** are curvatures. **A_{ij}** represents extensional and shear stiffnesses, **B_{ij}** represent extension-bending coupling stiffnesses and **D_{ij}** represent bending and torsional stiffnesses.

The applied loads and moment flows are defined as follows:

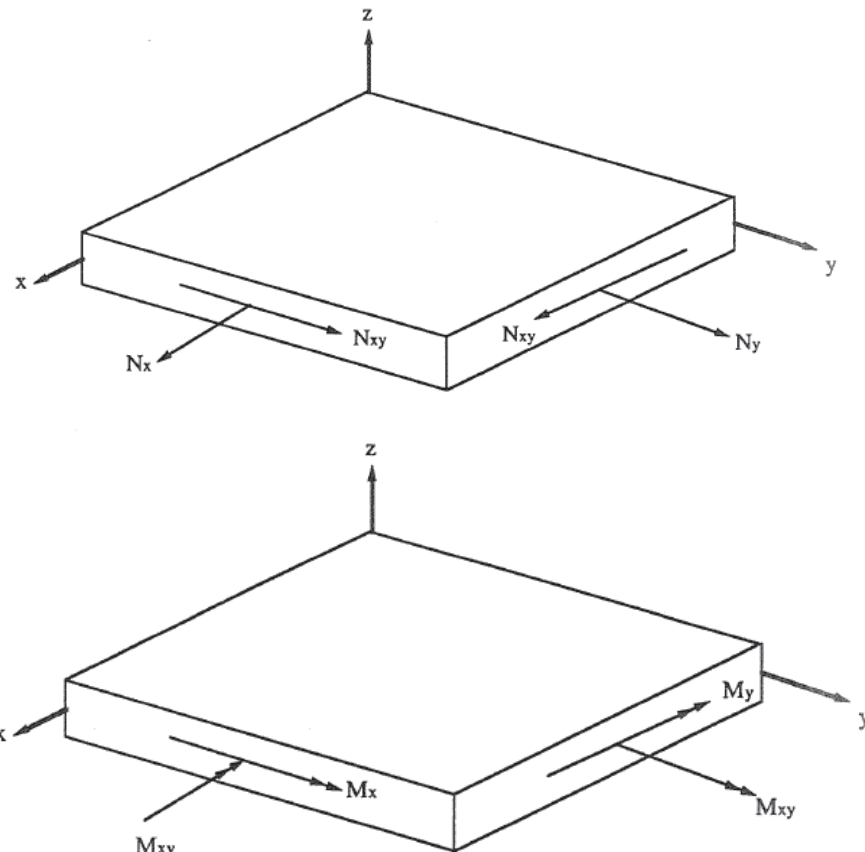


Figure 4.1.6-3: Load and Moment (flow) Definitions and Directions

A good explanation of the stiffness matrix terms is given in [\(MIL-HDBK-17F Vol 3, 2002\)](#):

The stiffness matrix **A_{ij}** in Equation 4.3.2(n) is independent of LSS (Laminate Stacking System). Inversion of the stiffness matrix [ABD] yields the compliance matrix [A'B'D']. This inversion is necessary in order to calculate strains and curvatures in terms of loads and moments. The inversion results in a relationship between LSS and extension/shear compliances. However, this relationship is eliminated if the laminate is symmetric.

Nonzero values of **A₁₆** and **A₂₆** indicates that there is extension/shear coupling (e.g., longitudinal loads will result in both extensional and shear strains). If a laminate is balanced **A₁₆** and **A₂₆** become zero, eliminating extension/shear coupling.

Nonzero values of **B_{ij}** indicates that there is coupling between bending/twisting curvatures and extension/shear loads. Traditionally, these couplings have been suppressed for most applications by choosing an LSS that minimizes the values of **B_{ij}**. All values of **B_{ij}** become zero for symmetric laminates. Reasons for designing with symmetric laminates include structural dimensional stability requirements (e.g., buckling, environmental warping), compatibility of structural components at joints and the inability to test for strength allowables of specimens that have significant values of **B_{ij}**.

In general, the values of **D_{ij}** are nonzero and strongly dependent on LSS. The average Panel bending stiffnesses, torsional rigidity and flexural Poisson's ratio

can be calculated per unit width using components of the compliance matrix [A'B'D'].

$1/D'_{11}$ = bending stiffness about y-axis
 $1/D'_{22}$ = bending stiffness about x-axis
 $1/D'_{66}$ = torsional rigidity about x- or y-axis
 $-D'_{12}/D'_{11}$ = flexural Poisson's ratio

The D'_{16} and D'_{26} terms should also be included in calculations relating midplane curvatures to moments except when considering a special class of balanced, unsymmetric laminates.

Nonzero values of D_{16} and D_{26} indicates that there is bending/twisting coupling. These terms will vanish only if a laminate is balanced and if, for each ply oriented at $+\vartheta$ above the laminate midplane, there is an identical ply (in material and thickness) oriented at $-\vartheta$ at an equal distance below the midplane. Such a laminate cannot be symmetric, unless it contains only 0° and 90° plies. Bending/twisting coupling can be minimized by alternating the location of $+\vartheta$ and $-\vartheta$ plies through the LSS.

The ABD matrix equation can be inverted and solved for strain for a given set of loads and moments as shown in Figure 4.1.6-2.

Basic laminate stiffness's (ABD matrix values) can be calculated with the following spreadsheet:



Once the ABD stiffness matrix is defined the principal strains can be calculated with this spreadsheet.



4.1.6.2. Measuring Laminate Strength

The measured strength of composite laminate and how it is compared with failure criteria is a bone of contention. A wide variety of opinion exists as to the best and most accurate way to analyze composite structures.

The aim of any analysis is to identify the load at which the structure fails, the location of failure and the mode of failure.

There are two different approaches to fiber laminate stress analysis, one is to consider each ply within the laminate and develop a failure index (common methods are Tsai-Wu or Hill) for each ply within the laminate, **this is called the lamina stress approach**. The failure of a single ply causing a sudden internal load redistribution that will cause the laminate to fail. This is a stress based approach where the load applied to a particular laminate has to be distributed onto each ply across the laminate thickness taking the direction of load in relation to the ply orientations into account. This produces a plot of stresses on each ply through the thickness that looks like this:

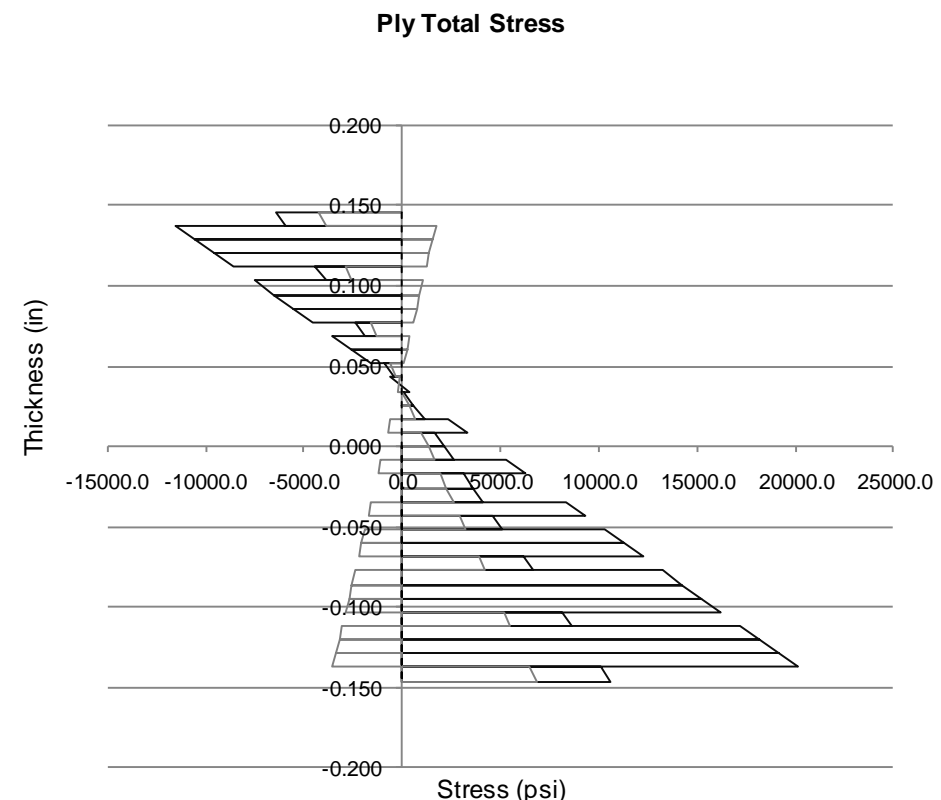


Figure 4.1.6-4: Typical 'Through the Thickness' Ply by Ply Stress Plot

The following spreadsheet calculates the individual stress in each ply of a laminate and margins of safety based on a range of failure indices.



A margin of safety can then be generated for each ply; the full Tsai-Wu failure criteria formulation is as follows:

$$F_2(\sigma_1 + \sigma_2) + F_3\sigma_3 + F_{22}(\sigma_1^2 + \sigma_2^2) + F_{33}\sigma_3^2 + F_{44}(\sigma_4^2 + \sigma_5^2) + F_{66}\sigma_6^2 + 2F_{12}\sigma_1\sigma_2 + 2F_{23}(\sigma_1 + \sigma_2)\sigma_3 \leq 1$$

While this appears complex, multiple Tsai-Wu checks on each ply in the laminate, per analysis location can easily be managed through spreadsheets or finite element post processors.

The 'ply-by-ply' stress failure approach is not commonly used in aircraft structure sizing and analysis. This is because it is difficult to correlate the actual failure of damaged composite laminates to an individual ply stress failure criterion.

The second analysis approach which is more commonly used for airframe primary structure is the **laminate strain approach**. In this method, the peak laminate strain is determined by analysis and compared with a strain allowable for a specific laminate configuration determined by test.

Classical laminate theory, the same theory that is used to distribute the loads and moments into each ply for the ply-by-ply stress analysis approach, assumes that the strain in the laminate maintains a smooth, linear distribution. There is a necessity for the laminate to operate as a coherent cross-section when reacting load. A step change in strain at a point across the thickness implies an inter-laminar failure.

Most companies developing composite structure for primary airframe applications use the strain approach. This is because testing can be done to develop laminate strain allowables that take account of manufacturing flaws and in-service damage. This is necessary to show compliance with FAR 23.573 and 25.573.

In primary structure, the level of stress raiser that is used for composite analysis is dictated by the aircraft certification regulations and has been accepted as impact damage up to the 'BVID' (Barely Visible Damage) level. The certifiable strength of laminate for the primary structure is usually derived using 'compression after impact' testing.

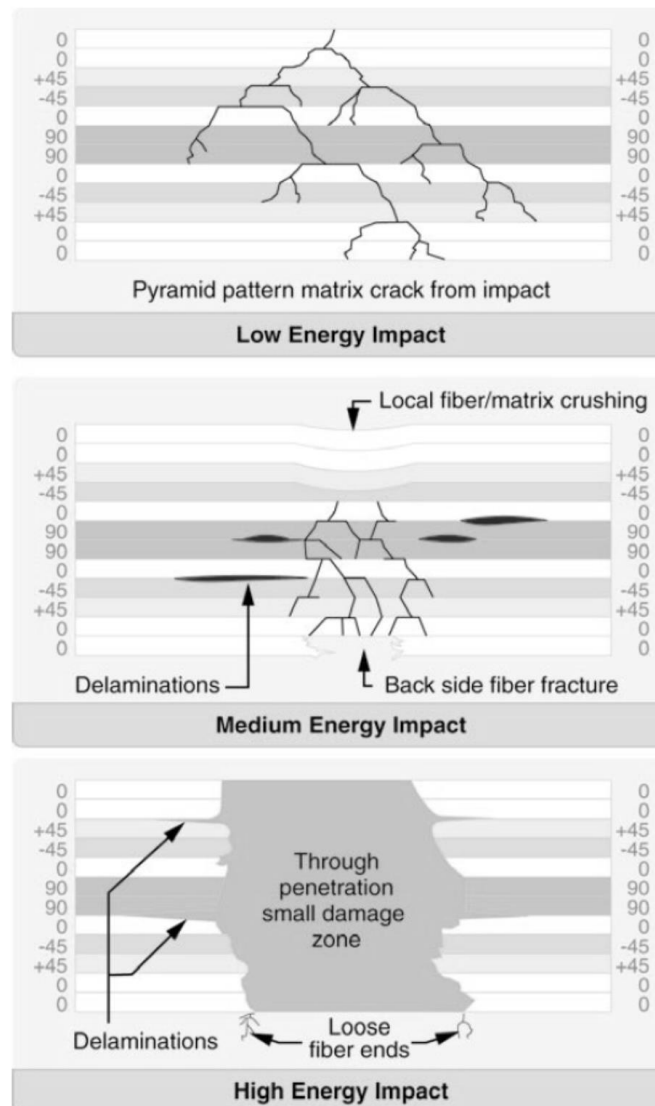


Figure 4.1.6-5: Impact Energy Levels and Relative Visibility (FAA-H-8083-25A, 2008)

Nonvisible, or BVID, or defects that are not detectable during manufacturing inspections and service inspections must withstand ultimate load and not impair operation of the aircraft for its lifetime. (DOT/FAA/AR-02/121, 2003)

Note that non-visible impacts can still cause damage through the thickness of the laminate, reference Figure 4.1.6-5. This level of damage must be able to withstand ultimate load.

The realistic test assessment of impact damage requires proper consideration of the structural details and boundary conditions. When using a visual inspection procedure, the likely impact damage at the threshold of reliable detection has been called barely visible impact damage (BVID). Selection of impact sites for static strength substantiation should consider the criticality of the local structural detail, and the ability to inspect a location. The size and shape of impactors used for static strength substantiation should be consistent with likely impact damage scenarios that may go undetected for the life of an aircraft. (AC20-107B, 2009)

To determine BVID laminate strength, a standard panel size is impacted with steel impactors of typical geometry (derived from the items in manufacture and service that are most likely to be the source of damage - tools, hail, etc) up to the point where the damage is just visibly detectable (there are established criteria for visibility of damage), these panels are then placed in a test fixture and compression load applied up to failure. The resulting compression strength is the basis for the material strength used in the structural substantiation. This type of testing is called 'Compression After Impact' testing or CAI.

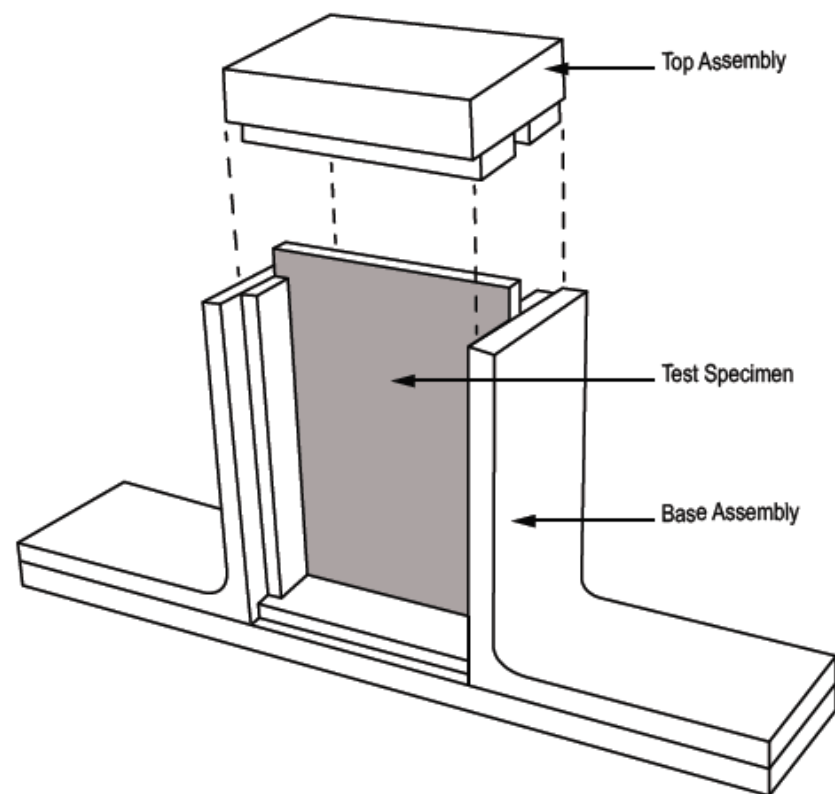


Figure 4.1.6-6: CAI Test Fixture ([NASA/TP-2011-216460, 2011](#))

The strength of any structure in a non-pristine condition is referred to as 'Residual Strength'. Composite laminate structure is brittle compared to metallic structure (no plasticity) and therefore damage, flaws and other stress/strain raising features must be accounted for in the static analysis in ways that are not considered in the static analysis of metal structure.

During the certification process, different levels of damage to the airframe are examined and the residual strength determined. This is, in part, the reason for adopting the 'pyramid' or 'building block' approach to structures substantiation through test, analysis and correlation between the two.

The aircraft developer (the applicant for the type certificate) must demonstrate an adequate level of understanding regarding strength and durability of their chosen material and the results of their processing (storage, handling, layup, cure, etc) and quality system when combined with the features within the airframe.

The progressive building block approach is taken to allow the developer to recognize potential issues and mitigate those issues at the earliest possible stage in the product development process.

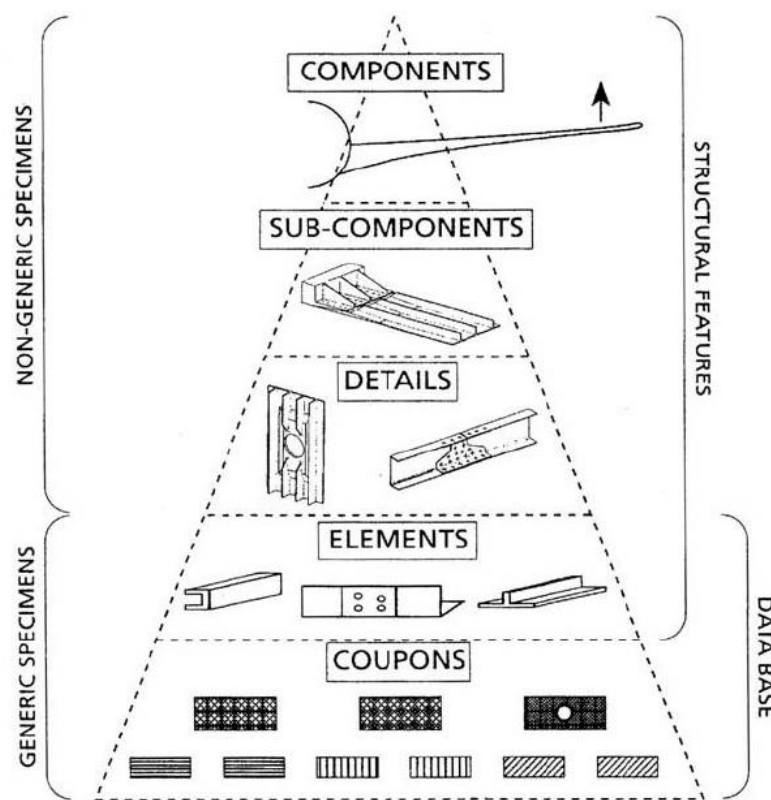


Figure 4.1.6-7: Schematic Diagram of Abuilding Block Tests for an Aircraft Wing (AC20-107B, 2009)

In composite aircraft structures development **test early and test often**.

Figure 4.1.6-8 shows the effect on structural strength of increasing levels of damage.

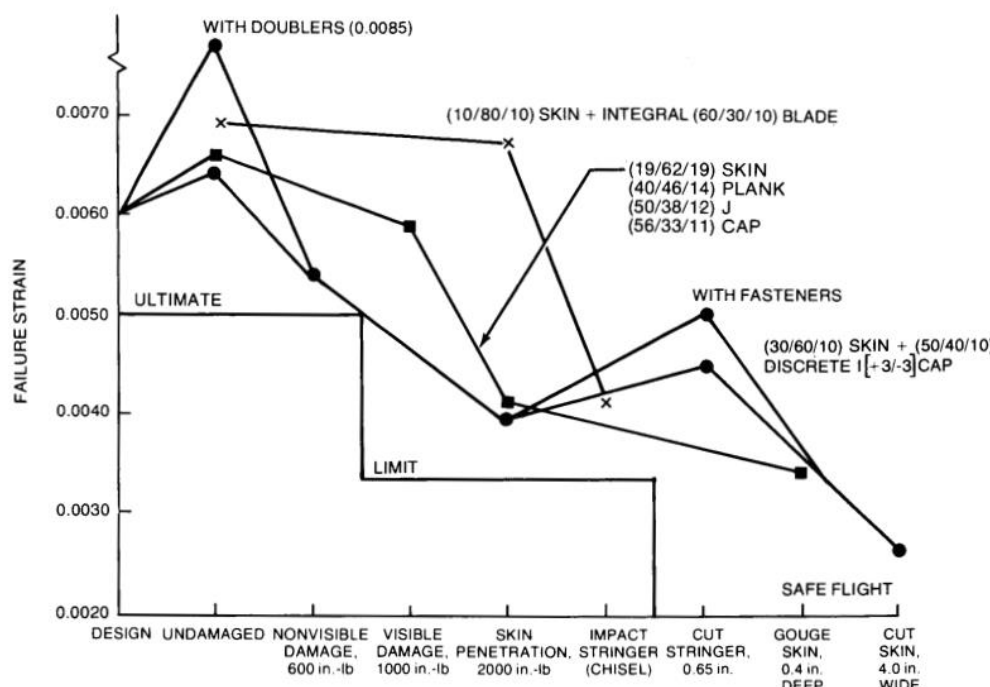


Figure 4.1.6-8: Residual Strength (expressed as failure strain) for Increasing Damage Level (NASA-CR-3767, 1984)

Note that Figure 4.1.6-8 defines the boundary between non-visible and barely visible at the point where the residual strength requirement changes from ultimate to limit.

This form of expressing strength with respect to damage level is commonly used and is a feature of modern FAA guidance material:

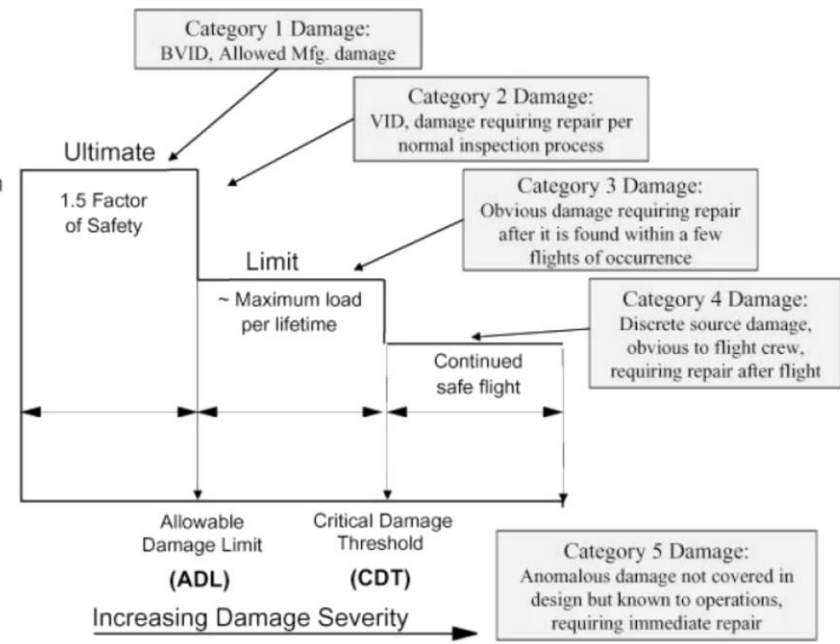


Figure 4.1.6-9: Schematic Diagram of Design Load Levels versus Categories of Damage Severity (AC20-107B, 2009)

Most of the analysis that is done is at ultimate level for BVID damage and uses strain limits developed by CAI testing or other testing to demonstrate the residual compression strength of the structure.

CAI strength values are usually the most conservative allowable values considering common features and flaws in the laminate. (See Figure 4.1.6-10). If the laminate is designed using CAI strength values, the analysis will demonstrate adequate strength for all less critical features and flaws. This can significantly simplify the structures analysis, but will provide a heavier and more robust design than an alternative method.

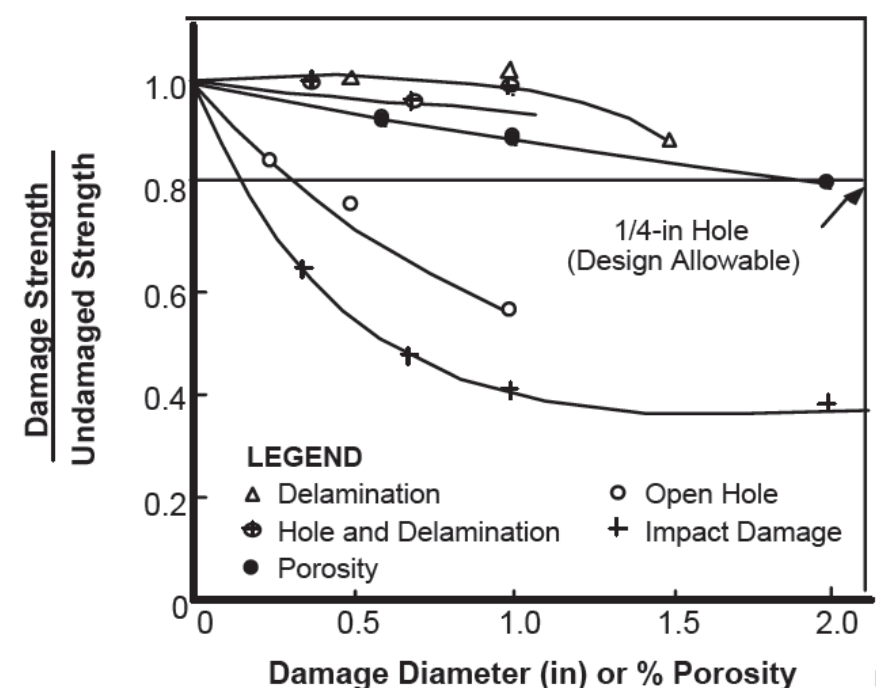


Figure 4.1.6-10: Comparison of Impact on Strength of Different Laminate Flaws and Features (NASA-NAS1-19347, 1997)

Figure 4.1.6-10 shows that of all the features, flaws and events; impact damage is critical. The critical measure of strength for fiber laminates is compression since this mode of failure is dominated by the strength of the matrix. This is the reason why compression after impact (CAI) testing is used as a basic laminate strength metric, it is a combination of the critical loading mode with the critical condition of the laminate. In general, all other loading modes and features can be passed by comparison.

Some good general data for quasi-isotropic carbon laminates is given in ([MIL-HDBK-17F Vol 3, 2002](#)) Section 4.11.2. Where a representative relationship between CAI strength and damage size and impact energy is shown graphically:

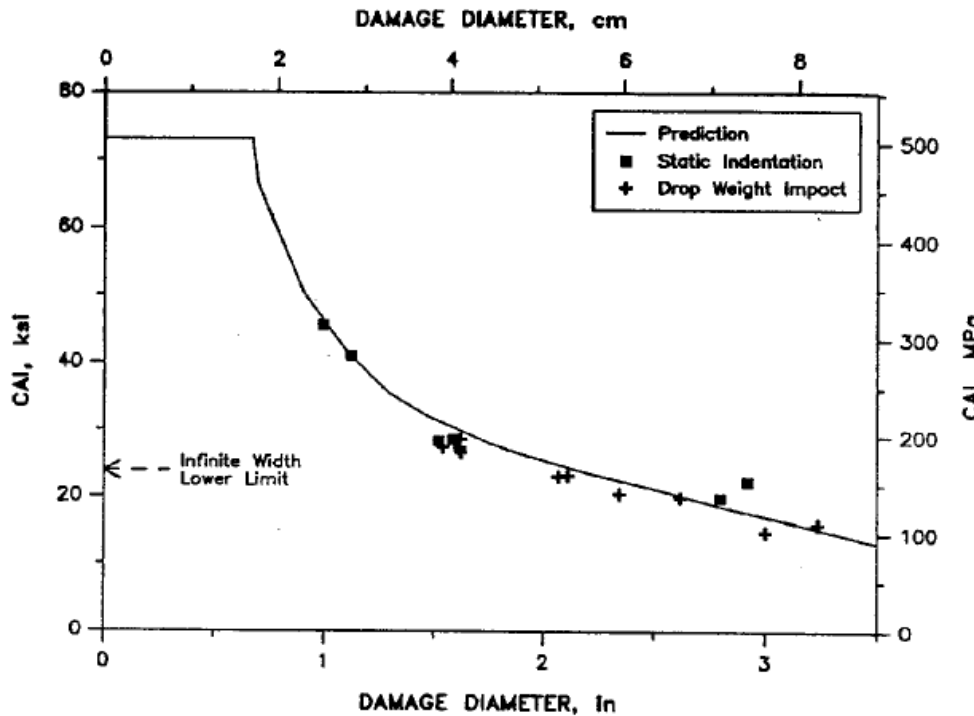


Figure 4.1.6-11: Residual Strength (expressed as failure stress) for Increasing Damage Size ([MIL-HDBK-17F Vol 3, 2002](#))

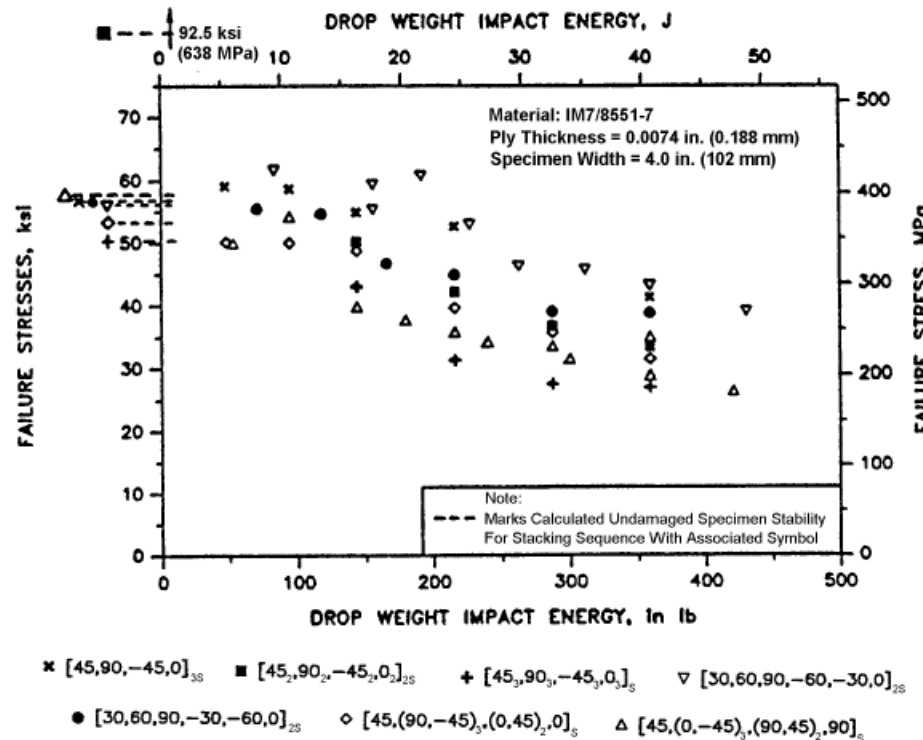


Figure 4.1.6-12: Residual Strength (expressed as failure strain) for Increasing Impact Energy ([MIL-HDBK-17F Vol 3, 2002](#))

It is worth noting that in a previous study the author has found for one material system that an ETW (Extended Temperature Wet) CAI strain limit of $3200\mu\epsilon$ for quasi-isotropic carbon fiber (epoxy resin infused) was equivalent to a von Mises stress level of approximately 25ksi for an isotropic material with the same stiffness. This is in broad agreement with the CAI stress level from Figure 4.1.6-11 for a 2in wide damaged region.

Another source gives CAI strength in terms of strain, this is in broad agreement with a CAI allowable of $3200\mu\epsilon$. This reference gives a lower value than $3200\mu\epsilon$. This diagram is for unwoven UD or tape product. Woven products generally show greater CAI strength values:

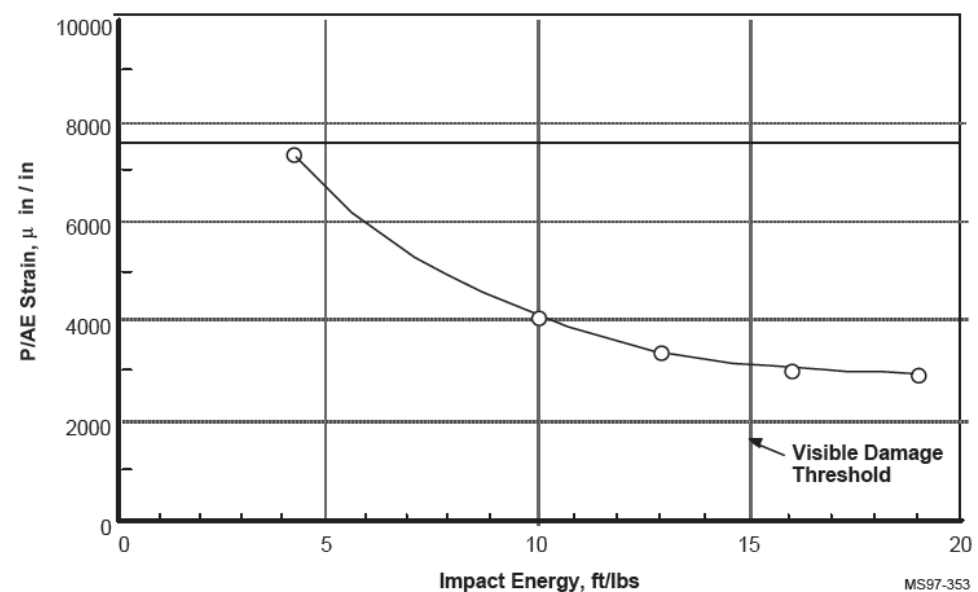


Figure 4.1.6-13: CAI Strain Values for Varying Impact Energy Levels for UD Tape Laminate ([NASA-NAS1-19347, 1997](#))

The size of impactor and the energy of the impact to create BVID is a function of a 'Damage Scenario Document' that is created by the composite structure OEM (Original Equipment Manufacturer) during the certification process. The purpose of this document is to examine the damage threat environment that the structure is exposed to through the complete lifecycle of the structure – from layup and cure to assembly and service. This document will list all potential types of damage the aircraft could experience.

These potential damage threats can be broken down into the following categories:

- Manufacturing
- Baggage handling
- Tire Fragments and stones from the landing gear
- Hail in flight
- Hail on the ground
- Damage around the door region
- Lightning strike
- Water intrusion
- Bleed air
- Rotorburst
- Engine fire
- Separation of aircraft components in flight
- Bird strike

These types of damage can occur at various levels of damage severity (refer to Figure 4.1.6-9) and a single category of damage can potentially occur at any of the 3 levels (Ultimate Residual Strength Requirement, Limit Residual Strength Requirement or Continued Safe Flight).

Frequently Asked Questions

Why is laminate compression critical? Why not tension?

In compression, the composite laminate depends on the resin matrix for its strength. In tension, the load is taken by the fibers (assuming that the engineer has aligned sufficient fibers in the primary loading direction). The fiber is many times stronger than the resin matrix.

Damage progression/growth in matrix/fiber laminates is primarily through the matrix, not caused by breaking of the fibers.

How does using CAI (Compression After Impact) allowables help with damage growth under compression loads?

There is an established relationship between the ultimate CAI strength of laminates and the non-growth of damage at normal service level loads.

If the analyst uses CAI compression allowables for an ultimate level analysis the structure will not grow damage from a BVID impact for the life of the aircraft. Proving this relationship involves a significant amount of testing. [\(DOT/FAA/AR-10/6, 2011\)](#) gives some data that support this relationship. Caution is required in assuming that data for other aircraft and material systems are directly applicable to your situation.

Figure 4.1.6-14 shows for the material considered and the fatigue spectra applied that at a limit load level in relationship to CAI (limit level = 1 / 1.5 = 0.667 or 66.7%) the structure can withstand over 100,000 cycles of limit level load. This is a significant level of robustness and can produce a structure that is not adequately optimized for weight.

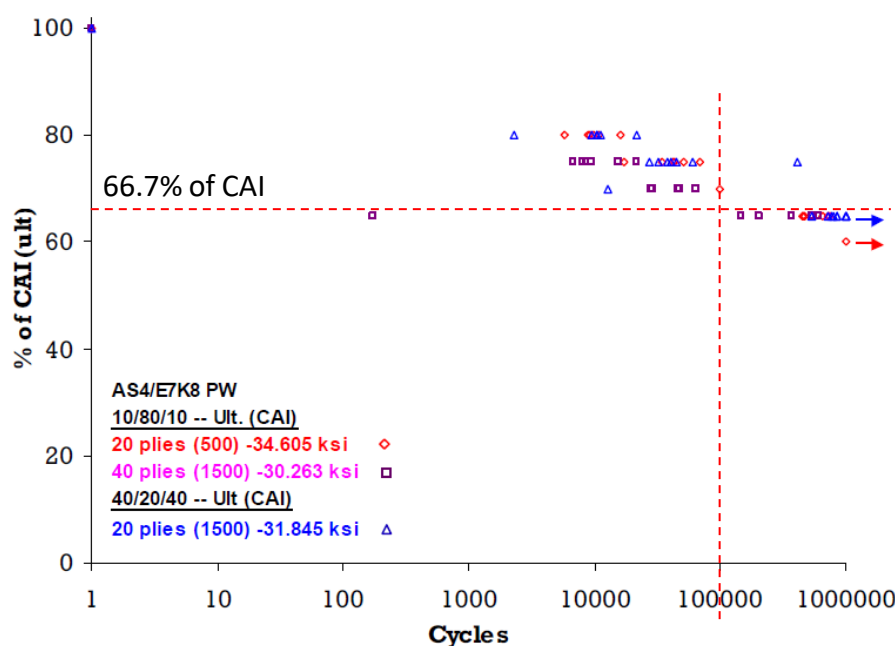


Figure 4.1.6-14: Relationship between Fatigue Life and Compression After Impact, $R = -1$ (Cytec AS4/E7K8) [\(DOT/FAA/AR-10/6, 2011\)](#)

Laminate CAI allowables look low, are they too conservative?

Permissible laminate allowable can be greater than CAI – e.g. Open Hole Compression (OHC). The risk is solely carried by the aircraft developer taking this approach as the ‘no damage growth’ design philosophy must be proven during the certification process.

Open Hole (Open Hole Tension, OHT, and Open Hole Compression, OHC) is a less conservative measure of strength and durability and still has a significant level of robustness.

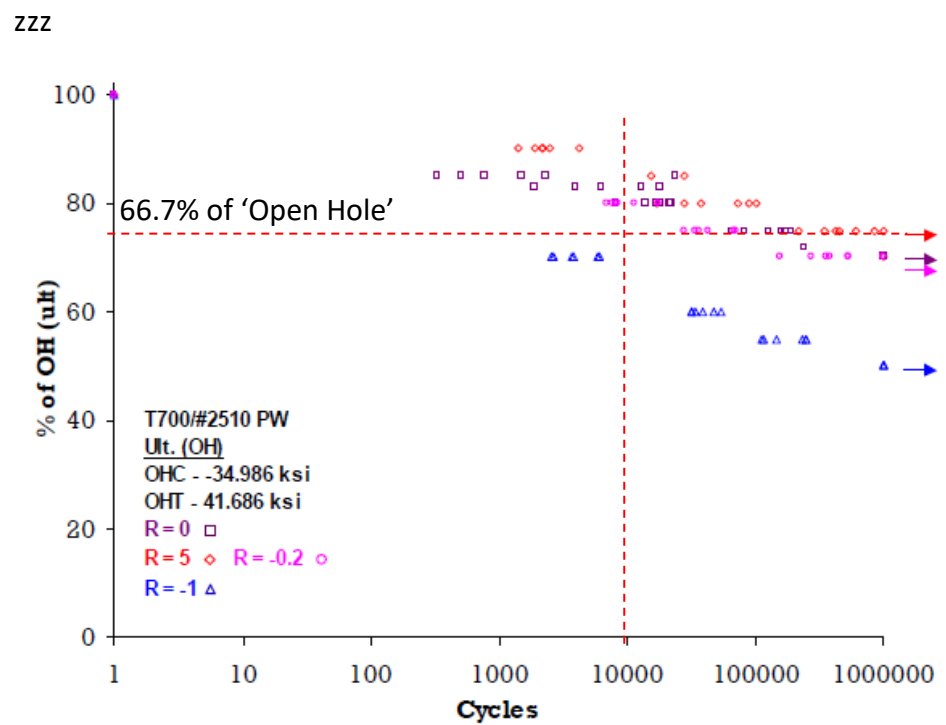


Figure 4.1.6-15: Relationship between Fatigue Life and Open Hole (Toray T700SC-12K-50C/#2510) [\(DOT/FAA/AR-10/6, 2011\)](#)

Figure 4.1.6-15 shows, for the material considered, the Open Hole sample could sustain a limit level fully reversible load for 10,000 to 20,000 cycles. Where the fatigue spectra is not fully reversed the fatigue life, for the parameters considered, is practically infinite.

4.1.6.3. Measuring the effect of Temperature on Composite Structure

Determining your Maximum Operating Temperature

You have to decide what your peak induced temperature in the airframe is likely to be - this is based on a lot of things - a review of the worst case environmental conditions out of [\(MIL-STD-210C, 1987\)](#) and other proprietary references, the color of the aircraft, the amount of glazing in the cockpit and cabin. You then choose a resin and a cure cycle that creates a wet glass transition temperature 50F above this peak induced temperature.

The actual guidance from the FAA is in document [\(FAA-PS-ACE100-2005-10038, 2005\)](#):

Reduction in strength properties at the maximum operating temperature (MOT) should be known for each application. The properties of polymer composite substrate and adhesive materials are affected by both temperature and moisture content, with a significant decrease in strength above the wet glass transition temperature($T_{g\text{ wet}}$). A simple guideline often used in selecting composite substrate materials is for the $T_{g\text{ wet}}$ to be 50 °F greater than the MOT of structural applications.

After you complete your aircraft temperature surveys you will find that the peak induced temperature for a white (or mostly white) aircraft is 180F. Airbus use 160F for their composites so the 180F value is not set in stone. But FAA policy statement [\(FAA-ACE100-2001-006, 2001\)](#) gives the following guidance regarding the 180F figure.

For most paint colors, a default critical structural temperature of 180F can be assumed without supporting tests or analyses. Dark colors or black, which may yield higher structural temperatures, are an exception.

If you want to use a MOT less than 180F you must do some justification to prove that this will be acceptable.

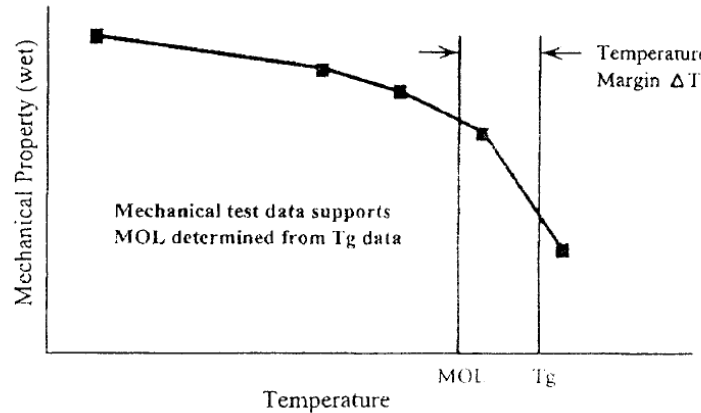


Figure 4.1.6-16: Relationship Between T_g , MOT (MOL) and Mechanical Properties [\(Mil-HNDBK-17F-Vol1, 2002\)](#)

Glass Transition Temperature (T_g)

[\(Mil-HNDBK-17F-Vol1, 2002\)](#) describes glass transition temperature as:

Glass Transition - The reversible change in an amorphous polymer or in amorphous regions of a partially crystalline polymer from (or to) a viscous or rubbery condition to (or from) a hard and relatively brittle one.

Glass Transition Temperature -- The approximate midpoint of the temperature range over which the glass transition takes place.

The most common way to measure glass transition temperature is by Dynamic Mechanical Analysis (DMA).

There are potentially multiple different values of glass transition temperature that could be derived from a DMA test.

The FAA allow the use of glass transition temperatures derived using a DMA test method per SACMA SRM-18R-94.

This method produces the following results.

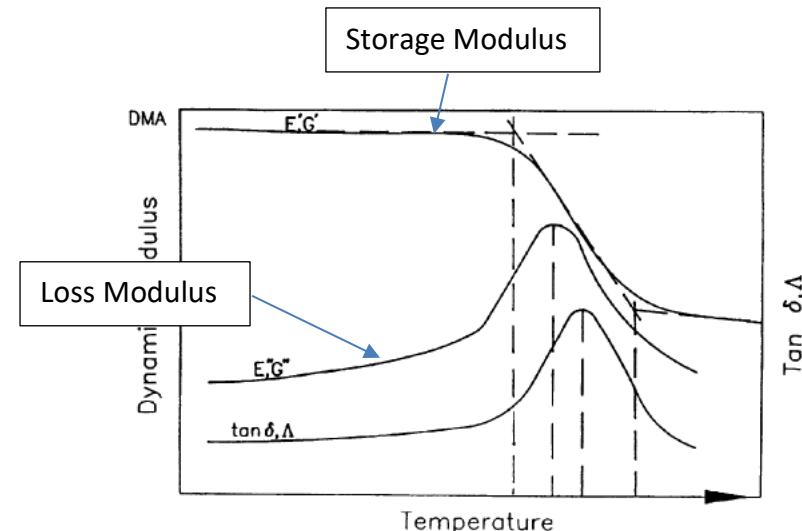


Figure 4.1.6-17: Dynamic Mechanical Analysis [\(Mil-HNDBK-17F-Vol1, 2002\)](#)

It is possible to interpret the results so that the value where any of the dashed vertical lines intersect the x-axis could be the glass transition temperature.

SACMA SRM-18R-94 specifies a forced oscillation measurement at 1 Hz, a heating rate of 5C° (9F°) per minute, and calculation of an onset T_g from the dynamic storage modulus curve.

This value for glass transition temperature is the lowest from the figure above and is shown by the red line in the figure below:

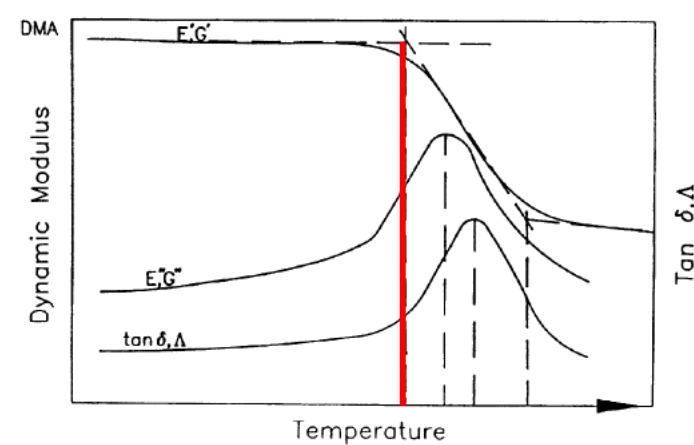


Figure 4.1.6-18: Dynamic Mechanical Analysis, T_g at Storage Modulus Onset [\(Mil-HNDBK-17F-Vol1, 2002\)](#)

Post curing raises the glass transition temperature of a polymer and therefore raises the Maximum Operating Temperature.

Moisture lowers the glass transition temperature; hence the wet glass transition temperature is lower than the dry glass transition temperature.

4.1.6.4. Commonly Asked Questions

How do I take environmental conditions into account?

CAI or any residual strength compression testing is done at RT (Room Temperature), CTD (Cold Temperature Dry), ET (Extended Temperature or 'Hot') and ETW (Extended Temperature Wet or 'Hot Wet') conditions in order to understand the effects of temperature and humidity conditions on the failure criteria. ETW will usually give the critical laminate allowable.

Do I have to do this for each different layup in the aircraft?

In theory yes, but it is normal to take a representative set of layups and materials that can be agreed to be generally applicable to the airframe. The minimum strain allowable of all the results can be used for initial sizing. The strain allowable for the local layup can be used later in the program when test results are available in order to reduce weight during detailed analysis.

What values can I use to get started when I have no test results?

WARNING: All values must be confirmed by test.

In general, for most carbon fiber composite laminates, whether UD tape, cloth or a combination of both; for ETW compression strain allowable values the following values can be used for initial sizing:

CAI: 3200 $\mu\epsilon$

OHC: 4000 $\mu\epsilon$

What do I use as a tension allowable?

It is normal to use 'Filled Hole Tension' (FHT) values for laminate tension values.

Typical value FHT: 5500 $\mu\epsilon$

If carbon fiber composite laminates have no plasticity, then are the KT effects of the damages and features from the test panels included in the static analysis?

Yes – geometric or KT effects must be accounted for in composite laminate static stress analysis.

How do I use these allowable strain values?

See the next section.

ADVERT: ENGINEERING SERVICES

STRUCTURES DESIGN
 ENGINEERING SERVICES

CONTACT US



4.1.7. General Composite Laminate Analysis Approach

4.1.7.1. Carbon Fiber Epoxy Resin Laminates - Basic Laminate Strength

The method shown in this chapter is solely concerned with laminate failure, not lamina failure. Lamina failure criteria traditionally works best when a pristine laminate is considered. For aircraft primary structure a defined project and material specific level of damage must be assumed to be present in the laminate (the Allowable Damage Limit, or ADL). At this level of damage, the structure must display ultimate strength at the worst environmental condition.

The failure criteria approach that the author has found to be the most robust and reliable is the biaxial strain envelope approach.

This has been used by several OEMs on several aircraft programs with success as part of their certification programs. The derivation and route through to choosing this method is proprietary to those organizations. A history of how this approach has been developed is given in

[\(NASA Conference Publication 3087, Part 2, 1990\).](#)

This history mirrors the author's own experience developing a certification methodology for a composite aircraft OEM.

The pertinent section of [\(NASA Conference Publication 3087, Part 2, 1990\)](#) is written by the exceptional L. J. Hart-Smith. It is not the intention to repeat his development of this approach below. It is well documented in the reference. I have attempted to give an overview. For clarification, the reference should be consulted.

Note that the original L.J Hart-Smith definition applied to fiber failure only. In the following section, the adaptation of the method to matrix failure modes is shown.

Most engineers are familiar with Mohr's circle as a visual expression of the stress or strain state of an isotropic material:

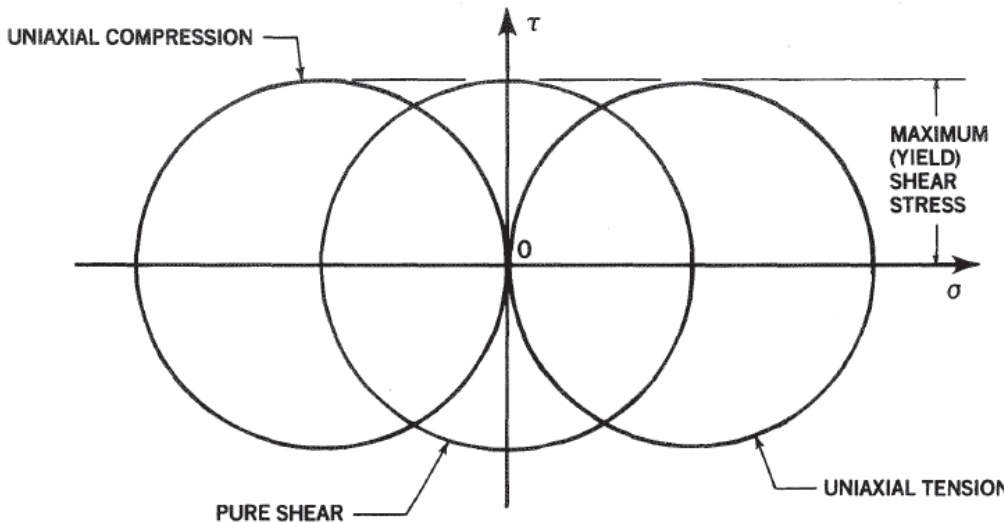


Figure 4.1.7-1: Mohr Stress Circles for Isotropic Materials
[\(NASA Conference Publication 3087, Part 2, 1990\)](#)

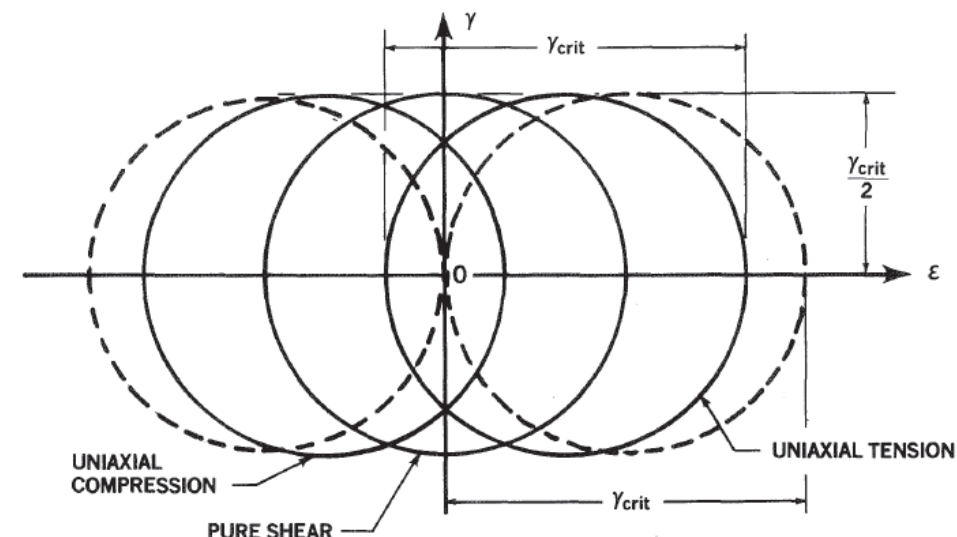


Figure 4.1.7-2: Mohr Strain Circles for Isotropic Materials
[\(NASA Conference Publication 3087, Part 2, 1990\)](#)

Unlike metallic materials, laminate composites are more prone to develop early failure modes as an interaction of the longitudinal and transverse strength of the laminate. It is, therefore, more appropriate to represent the plane strain state of the laminate in terms of the two principal strains. In this case, the strain limits can be plotted as lines at 45 degrees. The lines defined by the relationship $\epsilon_x - \epsilon_y = \gamma_{crit}$ are shown in Figure 4.1.7-3:

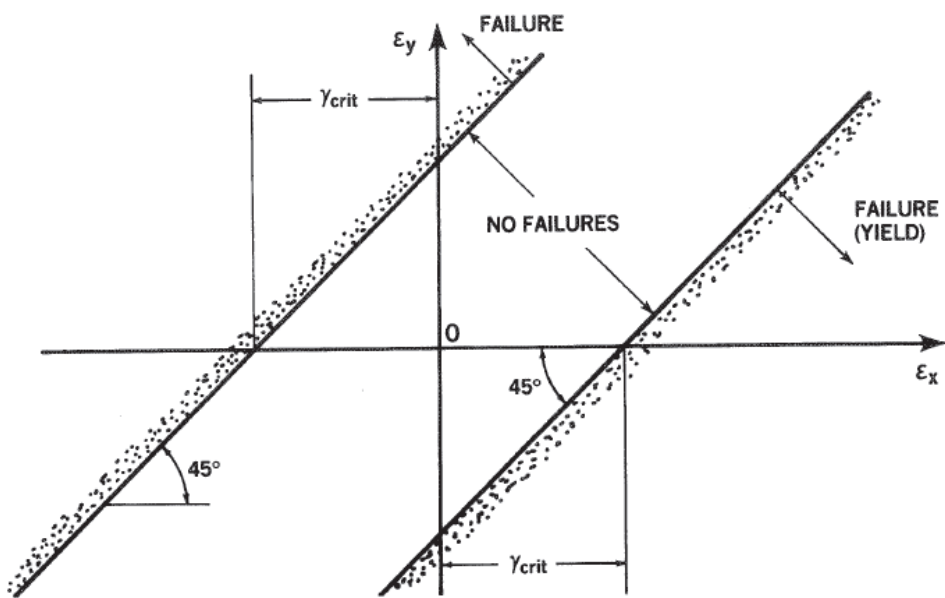


Figure 4.1.7-3: Maximum-Shear-strain Failure Criterion for Isotropic Materials
[\(NASA Conference Publication 3087, Part 2, 1990\)](#)

Additional cut offs can be added to the plot representing the following relationships:

$$\epsilon_x = (1 - \nu)\gamma_{crit} - \nu\epsilon_y$$

$$\epsilon_y = (1 - \nu)\gamma_{crit} - \nu\epsilon_x$$

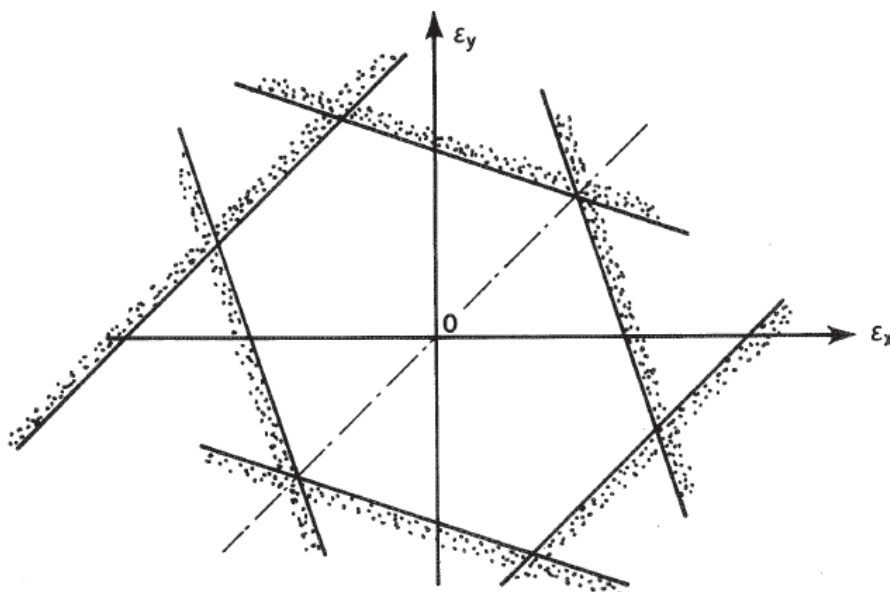


Figure 4.1.7-4: Maximum-Shear-strain Failure Criterion for Isotropic Materials
(NASA Conference Publication 3087, Part 2, 1990)

Figure 4.1.7-4 can be tidied up and shown with a definition of each region of the envelope as a useful summary in the following figure:

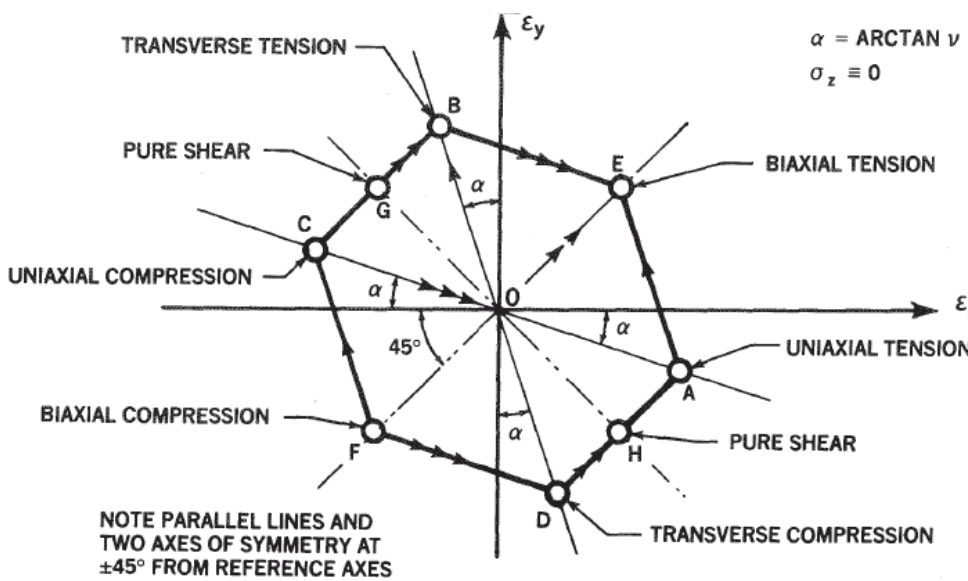


Figure 4.1.7-5: Two Dimensional Maximum Shear Strain Failure Criteria for Isotropic Materials (NASA Conference Publication 3087, Part 2, 1990)

The precise shape of the six-sided envelope depends on the value of ν (Poisson's ratio). It can be derived that the value of ν that gives an equal sided hexagon for an isotropic material is 0.2679, which is close to the typical value for most metals.

This method so far has developed a failure envelope for an isotropic material. The next section deals with how this envelope is modified to apply to a composite laminate material.

The same development will be shown for an orthotropic material considering only fiber failure:

The next step is to generalize the preceding analysis to orthotropic layers. The failure criterion to be derived should actually refer to the fiber, for fiber-dominated failures, *not* the lamina. However, the fibers and matrix obviously share a common strain along the fiber axis. For the usual case, in which strong, stiff fibers are embedded in a soft matrix, it is possible to bypass the micromechanical calculations relating the transverse strains of the fiber to those of the lamina because of the greater criticality of the fiber failure criterion.

It is assumed again that there are no normal or through-the-thickness shear stresses acting on the laminate. Using the subscripts L , T , and N to denote the longitudinal, transverse (in-plane), and normal directions, respectively. The strains for transversely isotropic materials read as follows when the axis of symmetry is longitudinal:

$$\epsilon_L = \frac{1}{E_L} (\sigma_L - \nu_{LT} \sigma_T) \\ \epsilon_T = \frac{1}{E_T} (\sigma_T - \nu_{TL} \sigma_L) = \frac{\nu_{LT} \sigma_L}{E_L} + \frac{\sigma_T}{E_T}$$

And:

$$\epsilon_N = \frac{1}{E_T} (-\nu_{TL} \sigma_L - \nu_{TN} \sigma_T)$$

For a uniaxial load along the fibers, with neither lateral nor normal applied stress, the axial strain in both the fiber and lamina will be ϵ_0 at failure and the associated lateral and normal strains will be $-\nu_{LT} \epsilon_0$ in the lamina. The corresponding orthogonal strain in the fiber, which can be presumed to have a different Poisson's ratio from the homogenized lamina, is undefined. However, for typical carbon epoxy composites, the similarity of the Poisson's ratio ν_{LT} for the unidirectional lamina and for an isotropic resin matrix, implies that the corresponding Poisson's ratio for the fiber must also be similar.

Figure 4.1.7-4 shows the traces of these uniaxial load lines, in tension and compression, on the $\epsilon_L - \epsilon_T$ in-plane strain plane. If the tension and compression strengths are the same, it is possible to locate the 45-degree sloping shear-failure lines on which the uniaxial failures are represented by individual points.

If the tensile and compressive strengths differ, the numerically greater value defines both shear-failure lines, as shown in Figure 4.1.7-6, while the lesser strength defines a cut off due to some other failure mechanism, such as micro-buckling under compression.

For a uniaxial in-plane load perpendicular to the fibers, a different Poisson's ratio, ν_{TL} , is involved and the uniaxial load line is no longer symmetric as it was for isotropic materials in Figure 4.1.7-4. The traces of this unidirectional load condition can be added to Figure 4.1.7-6, and wherever they cross the shear-failure lines denotes the points of failure of the fibers.

Note: With unidirectional laminae, the matrix may fail prematurely under transverse tension at a lower strain, but that is normally suppressed for any typical cross-plyed structural laminate and may be considered as a special case.

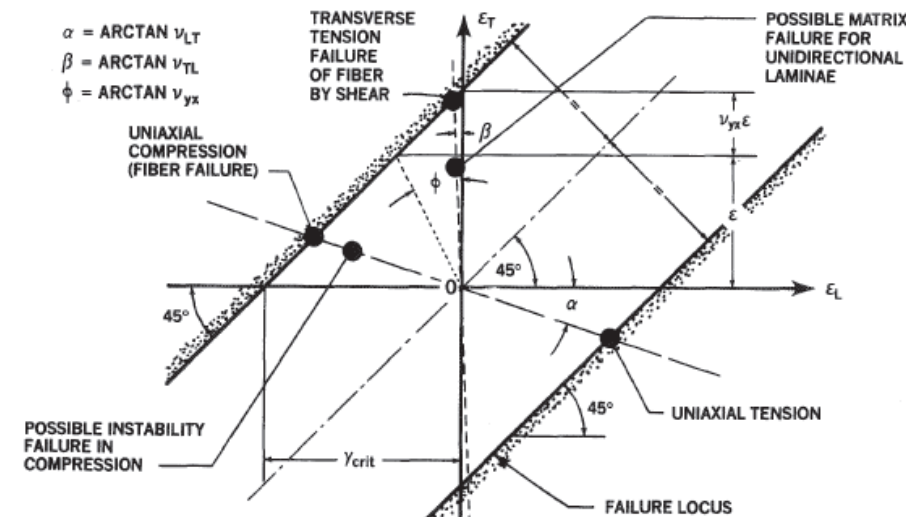


Figure 4.1.7-6: Shear Failure Loci for Orthotropic Materials (NASA Conference Publication 3087, Part 2, 1990)

It is apparent that the same critical shear strain loads through the entire region of interest since the sum of the longitudinal and orthogonal shear strains is always:

$$\epsilon_0 + \gamma\epsilon_0 = \gamma_{crit}$$

No matter what the value of Poisson's ratio for any particular cross-plyed laminate.

Adding limits to the strain envelope for arbitrary tension and compression strengths and failure envelopes for orthogonal layers of orthotropic materials the following envelope is developed.

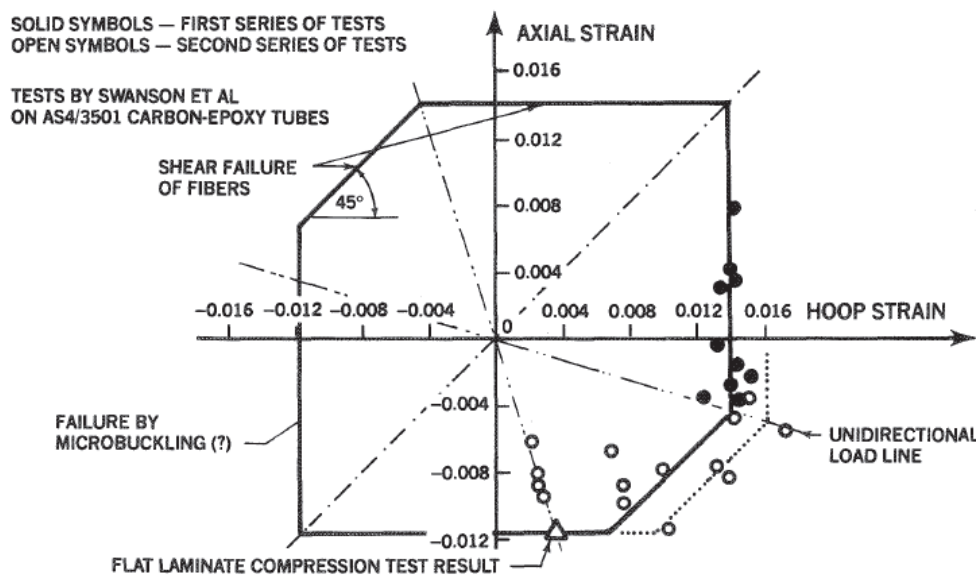


Figure 4.1.7-7: Comparison Between Test and Theory for Truncated Maximum Strain Failure Model for Carbon Epoxy Composites
(NASA Conference Publication 3087, Part 2, 1990)

This method shows good correlation for the intact laminate in the referenced paper. In the introduction, the following guidance is given: "Premature matrix failures can also be covered by appropriately truncating the fiber failure envelope".

As discussed previously, composite laminates for aircraft primary structure must be able to sustain ultimate load with damage up to the barely visible level (BVID).

It is common to use CAI (Compression After Impact) strength for the limit compression strength and open hole tension (OHT) for the limit tension strength.

For a carbon fiber laminate, the envelope is significantly truncated when compared to the pristine laminate strength:

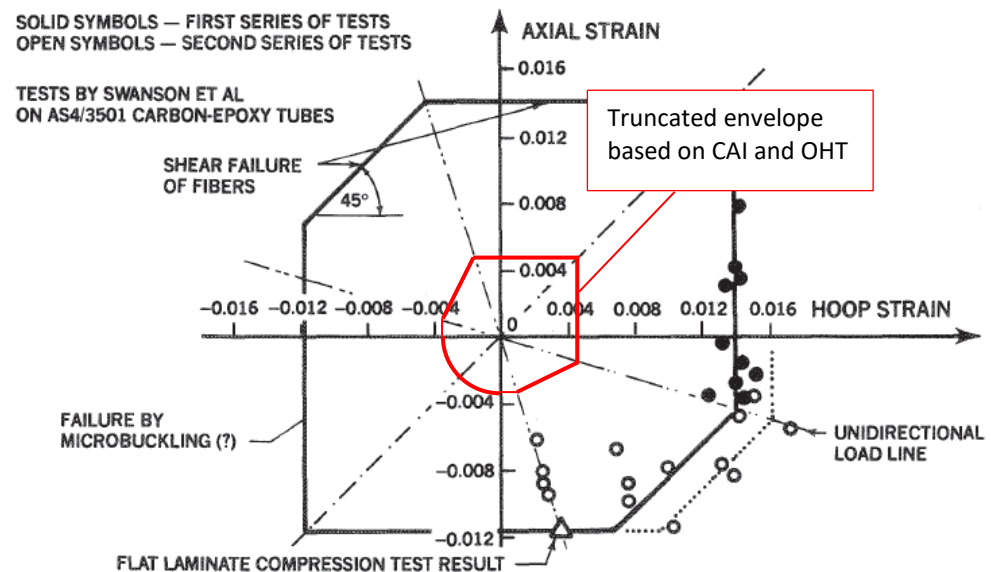


Figure 4.1.7-8: Comparison Between Typical Pristine Laminate Ultimate Strains and BVID ETW Laminate Design Strains for Aircraft Primary Structure

It can be seen from the figure above that the K_t effect from damage and features such as holes, superimposed over the effects of worst-case environmental conditioning gives a significant, if not radical, reduction in strength over the pristine laminate.

It is important that the large difference between the pristine laminate strength and the no-growth strain limit is understood. This accounts for the severe reduction or complete absence of weight saving when changing from aluminum structure to composite structure.

This underlines the potential benefits of composite structure:

- 1) If the assemblies are designed correctly there can be a large reduction in manufacturing cost.
- 2) If the structure is analyzed and sized correctly the airframe should not suffer from any damage growth in service.

The boundary of the worst case (no growth) design strain envelope is defined as shown on the next page.

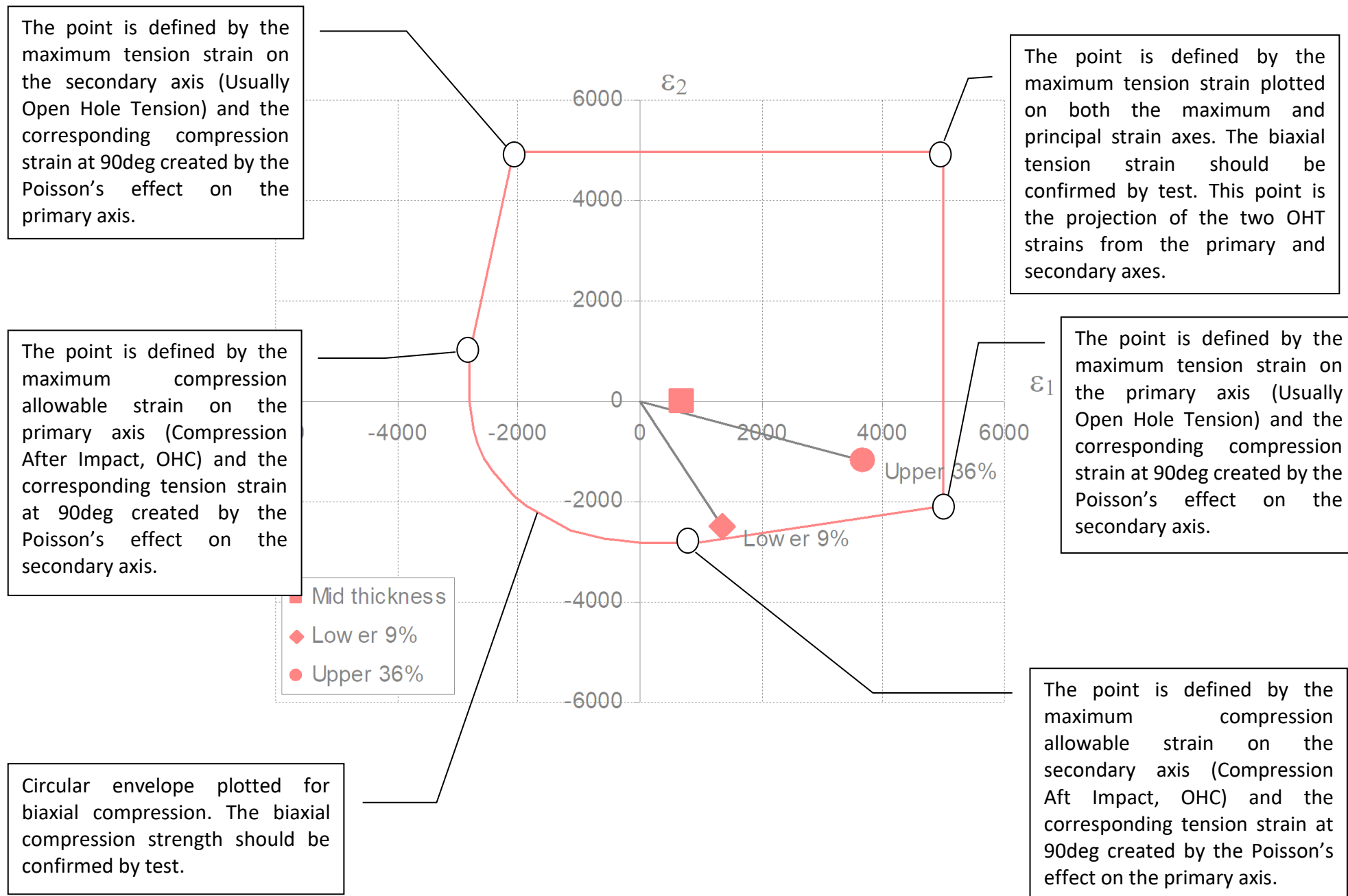


Figure 4.1.7-10: Definition of Biaxial Strain Envelope

Depending on the available budget and schedule these metrics (CAI, OHT) can be developed for multiple layups and all environmental conditions.

In general, it can be expected that the layups closest to quasi-isotropic that use woven cloth product will give the greatest CAI and OHT strain limits. The laminates with greater anisotropy and with UD rather than woven fiber product will give the lowest strain limits.

For initial conservative sizing, it can be assumed that the laminate with the most aligned UD plies at ETW condition will give you the most conservative laminate allowable strains. Initial testing can concentrate on these type of test panels and as time and budget allows, the less critical laminate configurations can be tested.

The analysis can then be refined to target specific laminates with allowables developed for that specific layup. This will allow for greater weight saving.

Note that this approach is only applicable to solid laminates and not for cored laminates.

Several 'high performance' aircraft have been certified with cored composite laminates used for primary structure. [\(DOT/FAA/AR-99/49, 1999\)](#) is a review of some of these aircraft and gives some guidance for damage tolerance of cored laminate structure.

The following points can be superimposed over the envelope described on the previous page:

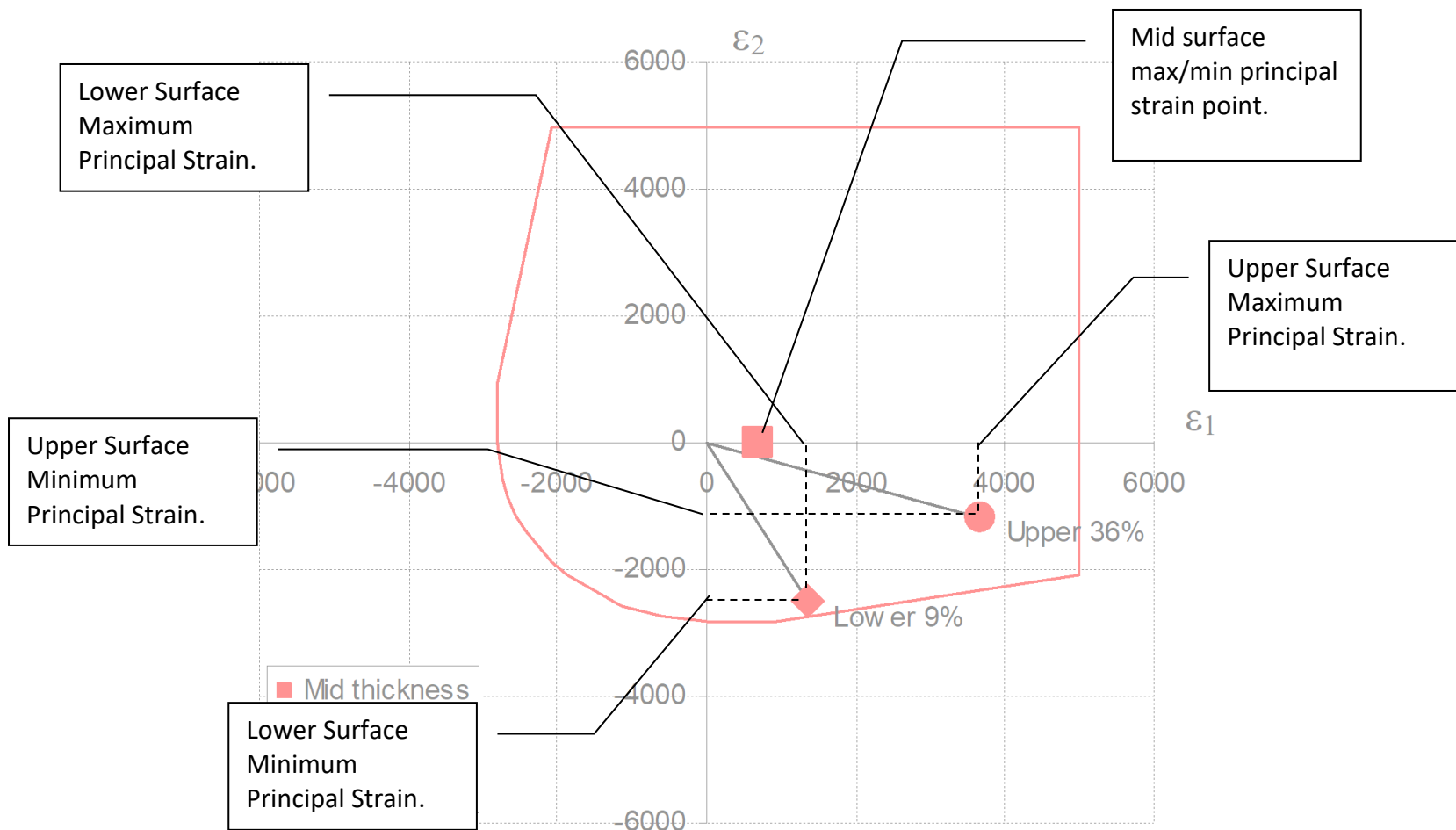


Figure 4.1.7-11: Definition of the Principal Strain Values Plotted on the Biaxial Strain Envelope

A line can then be plotted from the origin of the graph through the upper and lower plotted strain points to the perimeter of the biaxial strain envelope.

- The distance from the origin to the plotted strain point (L_1) can be determined.
- The distance from the origin through the plotted strain point to the perimeter of the envelope (L_2) can be determined.

With this information, the margin of safety can be calculated. For the upper surface:

$$MS = \frac{L_2}{L_1} - 1$$

The spreadsheet automatically calculates this margin of safety for the upper and lower surfaces.

The mid surface margin of safety is never less in magnitude than the upper or lower surface margin of safety.

This method is available in this spreadsheet:



This spreadsheet compares the calculated applied strains with a range of allowable strain values. These can be input for different environmental conditions or for any other variation and the envelope can be selected for the margin of safety calculation. If only one condition is to be considered the CAI values can be set to the same value for all environmental conditions and OHT values can be set to the same OHT strength for all environmental conditions.

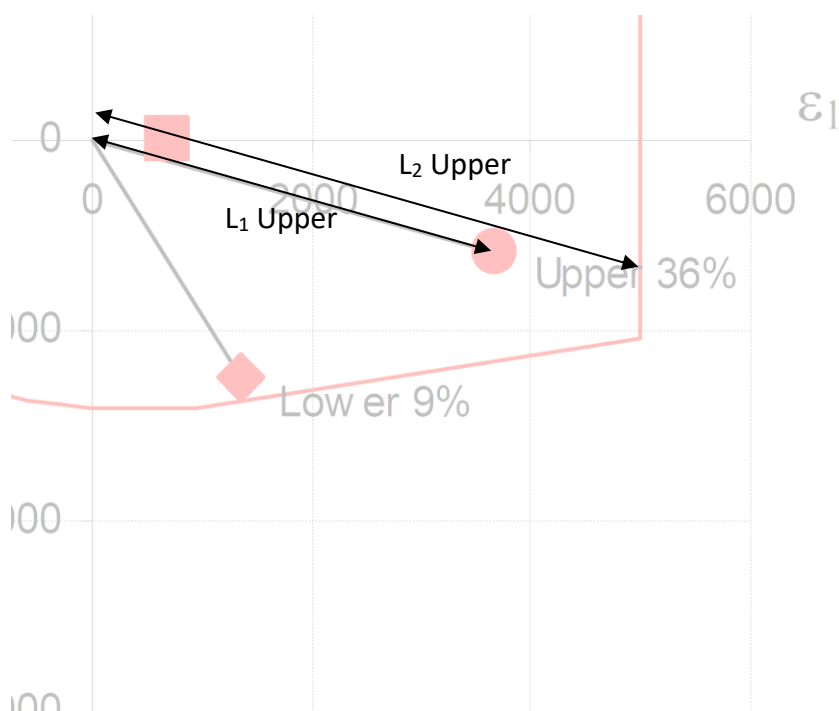


Figure 4.1.7-12: Definition of the Strain Margin of Safety

4.1.8. General Laminate Design Guidelines

This section is taken largely from [\(MIL-HDBK-17F Vol 3, 2002\)](#). Section 9.3 at the back of this reference has some excellent general guidelines for composite laminate design. Where the guidelines are obsolete or incorrect I have not included them. Some guidelines are paraphrased or changed.

4.1.8.1. General Guidelines

- In general, design for large co-cured assemblies. Large assemblies must include consideration for handling and repair.

Lower cost due to reduced part count and assembly time is one of the critical advantages associated with composite aircraft structure. If the assembly requires overly complex tooling the potential cost savings can be negated.

- Structural designs and the associated tooling should be able to accommodate design changes with the inevitable increase in design loads.
- Not all parts are suited to composite construction. Material selection should be based on a thorough analysis that includes consideration of performance, schedule and risk.
- Wherever possible, mating surfaces should be tool surfaces to help maintain dimensional control. If this is not possible precured shims can be used to take up the gap in bonded joints.
- Part thickness tolerance varies directly with part thickness. Thick parts require a larger tolerance.
- Carbon fibers must be isolated from aluminum or steel using a barrier (liquid shim, glass ply, etc).

The galvanic interaction between carbon and certain metals will cause corrosion of the metal component.

- The inspectability of structures must be considered in the design.
- Eliminate or reduce stress risers where possible.

Carbon fiber is linear up to failure and KT's directly affect static strength.

- Avoid, minimize or mitigate peel stresses within co-cured parts and especially at bonded joints.
- Thin composite laminates can be allowed to buckle with care, but most aircraft projects have a 'no buckling up to ultimate' rule. If buckling is allowed before ultimate all secondary load effects must be carefully examined.
- When adding plies, maintain balance and symmetry. Add between continuous plies in the same direction. Exterior surface plies should be continuous.

This minimizes warping and inter-laminar shear. Continuous surface plies minimize damage to edge of plies and help prevent delamination.

- Never terminate plies in fastener patterns.

It reduces profiling requirements on sub-structure. It prevents delamination caused by hole drilling and improves bearing strength.

- The stacking order of plies should be balanced and symmetrical about the laminate midplane. Any unavoidable asymmetric or unbalanced plies should be placed near the midplane.

It prevents warpage after cure and reduces residual stresses. Eliminates coupling stresses.

- Every laminate should have a minimum of 10% of fibers in each direction [0/±45/90].
- When there are multiple load conditions do not optimize the laminate for only the most severe load case.
- If the structure is mechanically fastened the laminate should be as close as possible to quasi-isotropic.
- Whenever possible, maintain a dispersed stacking sequence. Avoid grouping more than 4 plies of the same orientation together.

It minimizes the tendency to delaminate and creates a more homogenous laminate. It minimizes inter-laminar stresses.

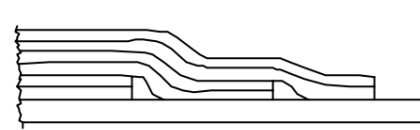
- Locate a ±45 ply at each surface of the laminate.

It minimizes splintering when drilling and protects the plies in the main load carrying direction.

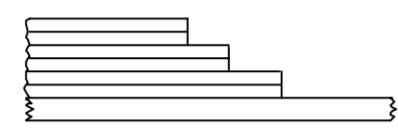
- Avoid abrupt ply terminations. Do not drop more than 2 plies at each termination. Try to drop non-adjacent plies.

Ply drops create stress concentration and load path eccentricities that cause out-of-plane load effects. Thickness transitions can cause wrinkling of fibers and delamination under load. Dropping non-adjacent plies minimizes the joggles of other plies.

- Ply drop-offs should not be less than 20 to 1 in the load direction. i.e. if a single ply is .010 in thick the minimum drop-off spacing should be one ply every 0.2in.
- Skin ply drop-offs should not occur across the width of spars, ribs or frame flanges.
- Ply drop offs should be 'protected' by outer plies.



a. Outer Plies Protecting Others



b. Plies Liable to Delamination

- Butt splice and overlaps: It is common in FAR part 23 aircraft to overlap plies; in part 25 aircraft it is common to butt splice them.

- a. For part 23 aircraft, different ply overlaps in the same laminate should not be coincident. Ply overlaps should have a minimum spacing of 4 inches and a minimum overlap length of 100 x the ply thickness. Ply overlaps should be avoided where the back side of the laminate interfaces with any other part and should be done away from interfaces with mechanical fasteners.
- b. For part 25 aircraft, a continuous ply should not be butt spliced transverse to the major load direction and may be butt spliced parallel to the major load direction if coincident plies are separated by at least 4 plies of any orientation. Joints of the plies of the same orientation separated by less than 4 plies of any orientation must be staggered by at least 0.6in. Gaps at butt spliced plies shall not exceed 0.08in.

4.1.8.2. Sandwich Design

- 1. The difference between FAR part 23 and part 25 aircraft core. In general foam core is not used in part 25 primary structures.
 - a. Foam Core: Foam core is commonly used in part 23 aircraft. Foam core is more readily processed, it is easier to machine and can often be used without any additional film adhesive product. Foam core is closed-cell and is generally less prone to moisture absorption than honeycomb core. Foam core also gives more reliable results when used 'out of autoclave'. Some brittle foam cores have poor damage tolerance characteristics and it is recommended that if possible the softer foam cores are used. Foam cores can also be used with wet laminate composites and also with infused laminates (with some significant weight penalty though). Most foam cores can be thermally pre-formed to gentle compound contours. For large sections of foam core, different foam core panels can be butt joined together with adhesive.
 - b. Honeycomb core creates sandwich panels with superior weight and durability characteristics but is more expensive and more difficult to process. Honeycomb core is more difficult to machine and often requires autoclave processing to give an adequate quality laminate.
- 2. Face sheets should be designed to minimize people-induced damage during handling or maintenance of the component.
- 3. Where possible avoid laminate buildup on the core side of the laminate.
- 4. The minimum possible core density should be used to minimize weight. The parameters to consider in selecting core density are as follows:
 - a. Out-of-plane shear strength required for service loads
 - b. Crushing Strength required for service loads
 - c. Crushing strength required to withstand process (autoclave cure)
 - d. A working temperature that can withstand the cure temperature
 - e. Thermal formability (for foam cores)
 - f. Chemical compatibility – Most commercial core materials are formulated for use with epoxy resins, regardless, this should be checked for all materials
- 5. If foam cores have been removed from the packaging or thermally formed some time prior to lamination, foam cores should be 'baked' in order to drive any moisture out of the core that may have been absorbed.
- 6. The [\(MIL-HDBK-17F Vol 3, 2002\)](#) source material states that core chamfer should be no greater than 20 degrees from the horizontal plane. In

practice, 30-degree chamfer angles have been widely used with little or no issues.

- 7. Fasteners through primary sandwich structure must always be installed using a potted insert. For secondary structure other means such as filler alone can be used.

4.1.8.3. Bolted Joints

- 1. Joint analysis should include the effects of shimming to the level permitted by the drawings.
- 2. Design bolted joints to accommodate the next larger fastener size.
- 3. Maximum Torque values should be controlled – especially with large fastener sizes. This reference [\(NASA/TM-2006-241323, 2006\)](#) shows that fasteners of $\frac{1}{4}$ diameter and below can be installed using the recommended torque/clamp up without damaging the laminate. These results agree with the author's experience of test validation on several aircraft programs.
- 4. Bolt bending is much more significant in composites than it is in metals.
- 5. Fastener Shear strength does not usually control the strength of the joint. Carbon fiber laminates have low bearing strengths compared to aluminum.
- 6. Stainless steel fasteners in carbon fiber laminate should be wet installed with a liquid sealing compound.
- 7. Use a layer of fiberglass or liquid shim between aluminum fittings and carbon fiber laminate.
- 8. Countersink depth should not exceed 70% of the laminate thickness.
- 9. Fastener edge distance should be a minimum of 3.0D in the direction of major load, otherwise, 2.5D can be used.
- 10. Use only Titanium, A286, PH13-8 MO, Monel or PH17-4 stainless steel fasteners with carbon fiber/epoxy laminates.
- 11. Do not buck rivets in composite laminate.
- 12. Interference fit fasteners should not be used. Clearance fit should be as tight as possible.
- 13. Tension head fasteners are preferred over shear head fasteners.
- 14. Avoid putting fastener threads in bearing against the laminate.

4.1.8.4. Bonded Joints

- 1. The bond should be stronger than the laminate. In shear testing of the laminate and adhesive combination, the failure should occur in the laminate. Reference Section 4.1.3.1 for recommended surface preparation for bonded joints.
- 2. Adhesive bonds should not be used to react either primary peel forces or large induced peel forces.
- 3. The strength of the joint is heavily reliant on surface preparation – mechanical means are best.

4. Bonded joints are not critical at room temperature and can be critical at cold dry - not only hot wet. Testing should be performed at all environmental conditions to confirm.
5. The edge of the adherends can be tapered/chamfered to reduce peel at the edge of the adhesive joint.
6. In general, the thinner the adhesive joint; the higher the strength. Thick laminates and thick adhesive can significantly reduce joint strength.

ADVERT: ENGINEERING SERVICES

STRESS ANALYSIS

Engineering Services

CONTACT US

SPREADSHEETS

MATHEMATICAL DERIVATION OF SHEAR BUCKLING COEFFICIENTS

LEADSHEETS

ABBOTT AEROSPACE
ABBOTTAEROSPACE.COM

4.2. Metallic Materials

4.2.1. Introduction

In general, metallic materials can be regarded as isotropic and ductile. Whereas lamina composites can be generally regarded as anisotropic and brittle.

The analysis and certification methods for metallic components and assemblies are well established. The purpose of this text is not to redefine all of the established theory and practice of metallic structure but to give a practical overview of the most useful knowledge for the structural analyst.

It is useful to highlight the difference between composite and metallic materials. In my experience the three major differences between composite and metallic structure are as follows: (note that these are not the only differences, but I believe that those are the ones that have the most impact on the development and life cycle of the aircraft product.)

Composite materials are generally linear up to failure, metallic materials generally show plastic behavior

This single aspect drives most of the design and certification difference between composite and metallic structures. It is also ironic that metals display clearly plastic behavior – especially the common aluminum alloys – whereas the most common composite primary structure material, carbon fiber, displays linear behavior up to failure.

This difference in the behavior of the two different material types fundamentally changes the analysis approach.

Composite materials are anisotropic – they exhibit different strengths and stiffness's in different directions. Metallic materials can be generally considered to be isotropic (differences between L, LT and ST properties notwithstanding).

This has most impact when considering the strength through the thickness of a laminate compared to the strength of a metal component loaded through the thickness of the part.

When manufacturing composite materials, the manufacturer takes responsibility for a large part of the materials and process quality assurance. With metallic materials, the material can be procured using a public domain and universally accepted specification from qualified vendors.

This aspect is probably the least understood by the aircraft developer. Common aircraft materials have been available to acceptable specifications from multiple vendors for decades. These metals have established and widely accepted characteristics and the processing of the metals to achieve these characteristics is all done by the material supplier. When an aircraft developer chooses to use composite materials, the material is bought in a more 'raw' form and the airframe developer takes on the responsibility for much of the material processing. This additional work includes a new quality system and new company processes to define for storing, handling, forming and curing. The engineer who develops composite structure must be aware of these new responsibilities and the new downside aspects of their ownership by the aircraft OEM.

4.2.2. Metallic Material Properties

Metallic material properties suitable for certified aircraft use have been long established. The public domain [\(MIL-HNDBK-5H, 1998\)](#) has been superseded by

the commercial MMPDS document, however, the [\(MIL-HNDBK-5H, 1998\)](#) is still relevant and an excellent resource.

This section regarding basic metallic material properties is largely taken from section 1 of [\(MIL-HNDBK-5H, 1998\)](#).

The two most common material types used in aircraft construction are steel and aluminum. With steel being used sparingly for specific high strength, high endurance or high-temperature applications because of its relatively high density (approx. 3 times that of aluminum).

4.2.2.1. Stress-Strain Curves

Both steels and aluminum exhibit plastic behavior but in slightly different ways.

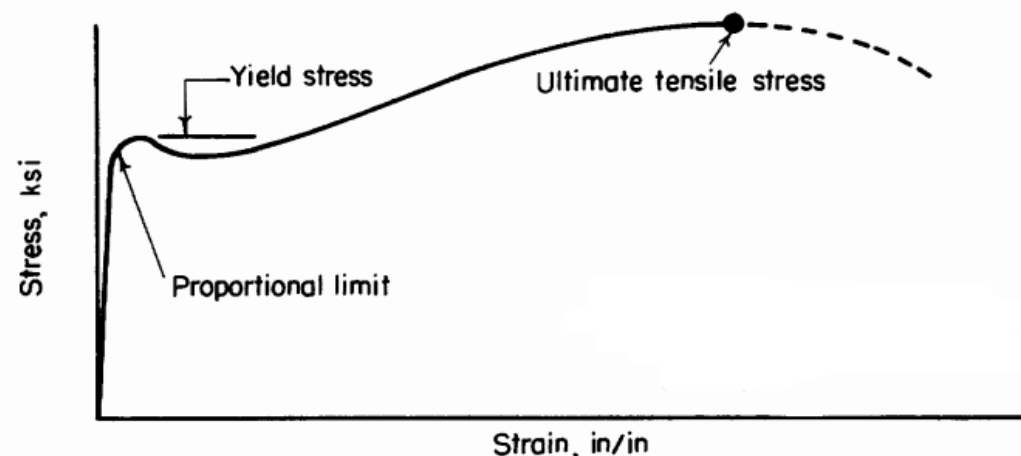


Figure 4.2.2-1: Stress-Strain Curve for a Typical Steel [\(MIL-HNDBK-5H, 1998\)](#)

Steels will typically have a defined yield point on the stress/strain curve and aluminum will generally have a smoother curve.

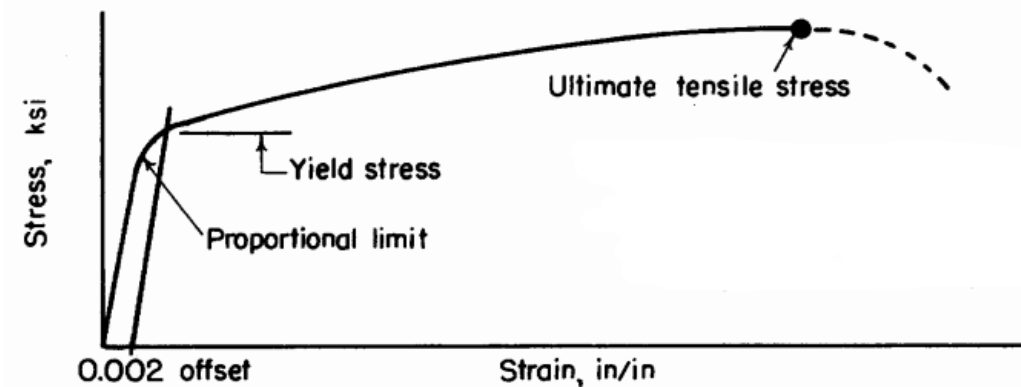


Figure 4.2.2-2: Stress-Strain Curve for a Typical Aluminum [\(MIL-HNDBK-5H, 1998\)](#)

The Stress-Strain curve can be modeled with a simple close approximation, this is called the Ramberg-Osgood method and is defined in [\(NACA-TN-902, 1943\)](#). An adaptation of the Ramberg-Osgood approach is defined in section 1.6 of [\(MIL-HNDBK-5H, 1998\)](#) and [\(NACA-TN-927, 1944\)](#). Having a simple method for modeling the stress-strain behavior of a material proves to be extremely useful when an accurate picture of how a feature may behave beyond the material yield point is required.

The model of the stress-strain curve is predicated on the following relationship:

$$e = e_e + e_p$$

Where:

$$e_e = f/E$$

And:

$$e_p = 0.002 \left(\frac{f}{F_y} \right)^n$$

i.e. the total strain is the sum of the elastic and plastic strains. This can be re-written:

$$e = \frac{f}{E} + 0.002 \left(\frac{f}{F_y} \right)^n$$

Where:

- n** Stress-strain curve shape factor (Ramberg Osgood Parameter)
- f** Applied stress
- F_y** Material yield strength

The lower the value of n, the more gradual the transition between the elastic and plastic regions of the curve. For higher values of n the transition is more abrupt. Metals with low values of n usually have a lower yield strength relative to their ultimate strength.

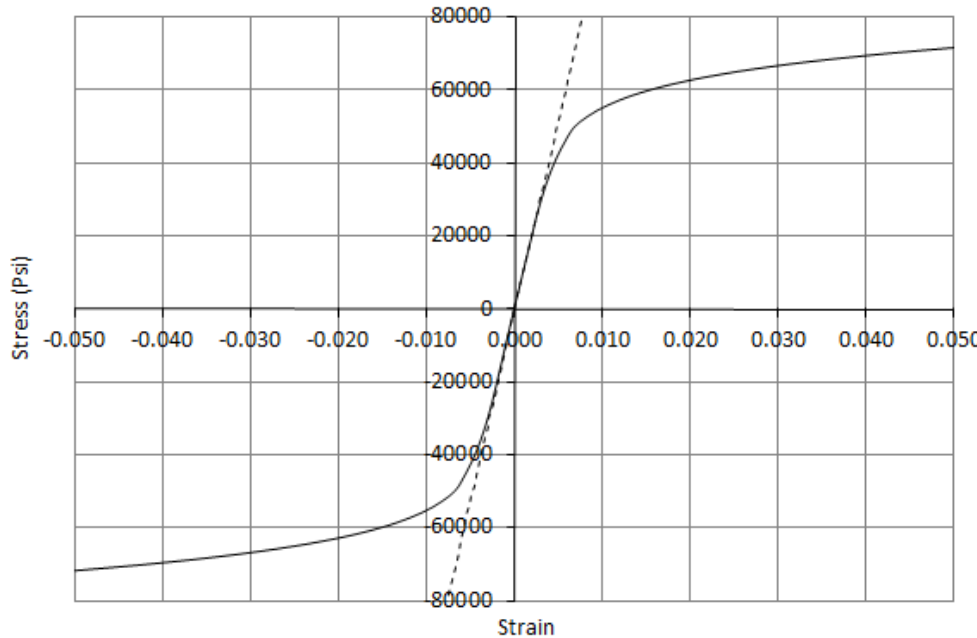


Figure 4.2.2-3: Full Range Ramberg-Osgood Approximate Stress-Strain Curve or a Sample Aluminum with a Low 'n' Value

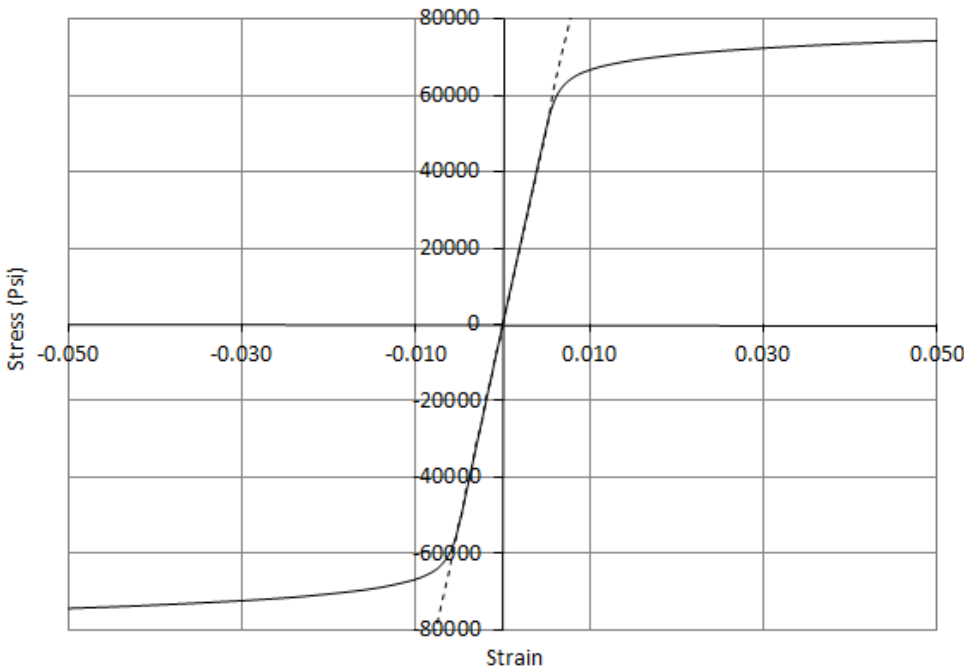


Figure 4.2.2-4: Full Range Ramberg-Osgood Approximate Stress-Strain Curve or a Sample Aluminum with a High 'n' Value

Note that metal materials also will have small differences in strength and stiffness properties for compression and tension. They also usually have a different shape factor 'n'.

The shape factor and strength can also vary with grain direction.

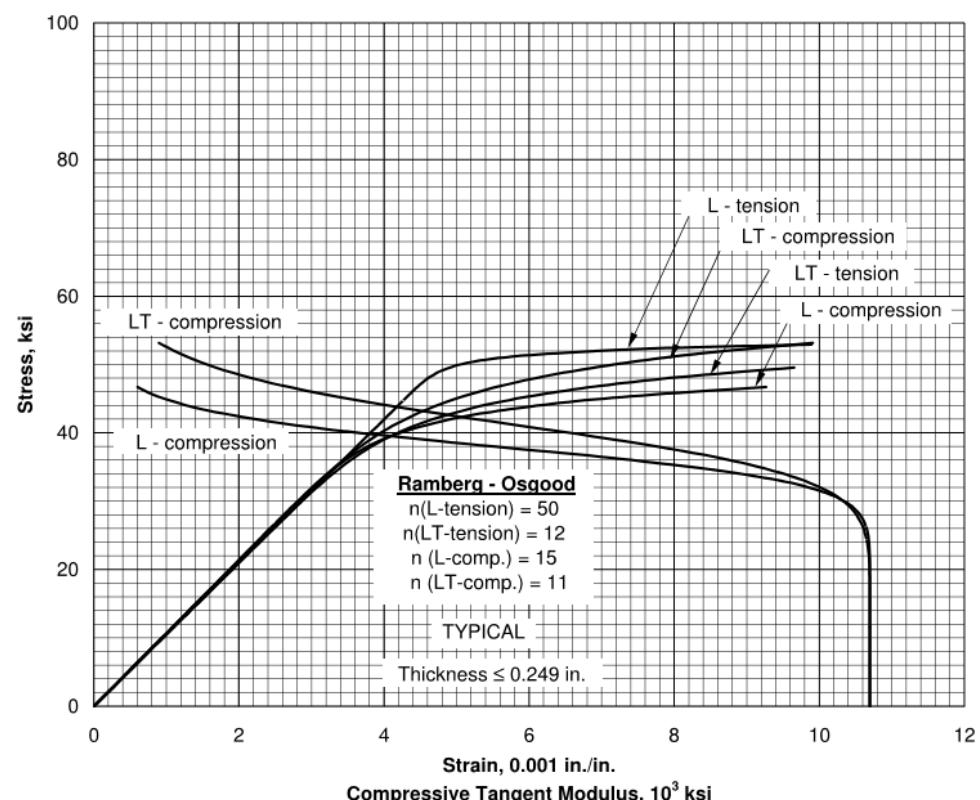


Figure 4.2.2-5: Example of 'n' Definition from (MIL-HNDBK-5H, 1998) showing Varying 'n' for Different Grain Directions and Load Direction

(MIL-HNDBK-5H, 1998) notes this about the shape factor 'n':

"While this relationship may not be exact, it is sufficiently accurate for use up to the yield strength for many materials but cannot be employed to compute full-range stress-strain curves."

An approximate method for calculating the shape factor in the plastic region can be derived from the approach in (MIL-HNDBK-5H, 1998):

$$n_u = \frac{\log \left(\frac{e_f}{0.002} \right)}{\log \left(\frac{f_{tu}}{f_{ty}} \right)}$$

Where:

- n_u** Stress-strain curve shape factor in the ultimate region
- e_f** Elongation at failure
- f_{tu}** Material ultimate tensile strength
- f_{ty}** Material yield strength

It is recommended that the ultimate shape factor is used above f_{ty}. When plotting full range stress train curves a smoothing function can be used to avoid an unnatural step in the value of 'n'.

Note that this method produces only an approximation of the shape of the true stress-strain curve of the material being examined. For the purpose of analysis, this approximation can be assumed to be accurate.

Different measures of the nonlinear nature of the stress-strain curve are useful and used in the correction of buckling allowable stresses for plastic effects. The two most commonly used are the tangent modulus and the secant modulus.

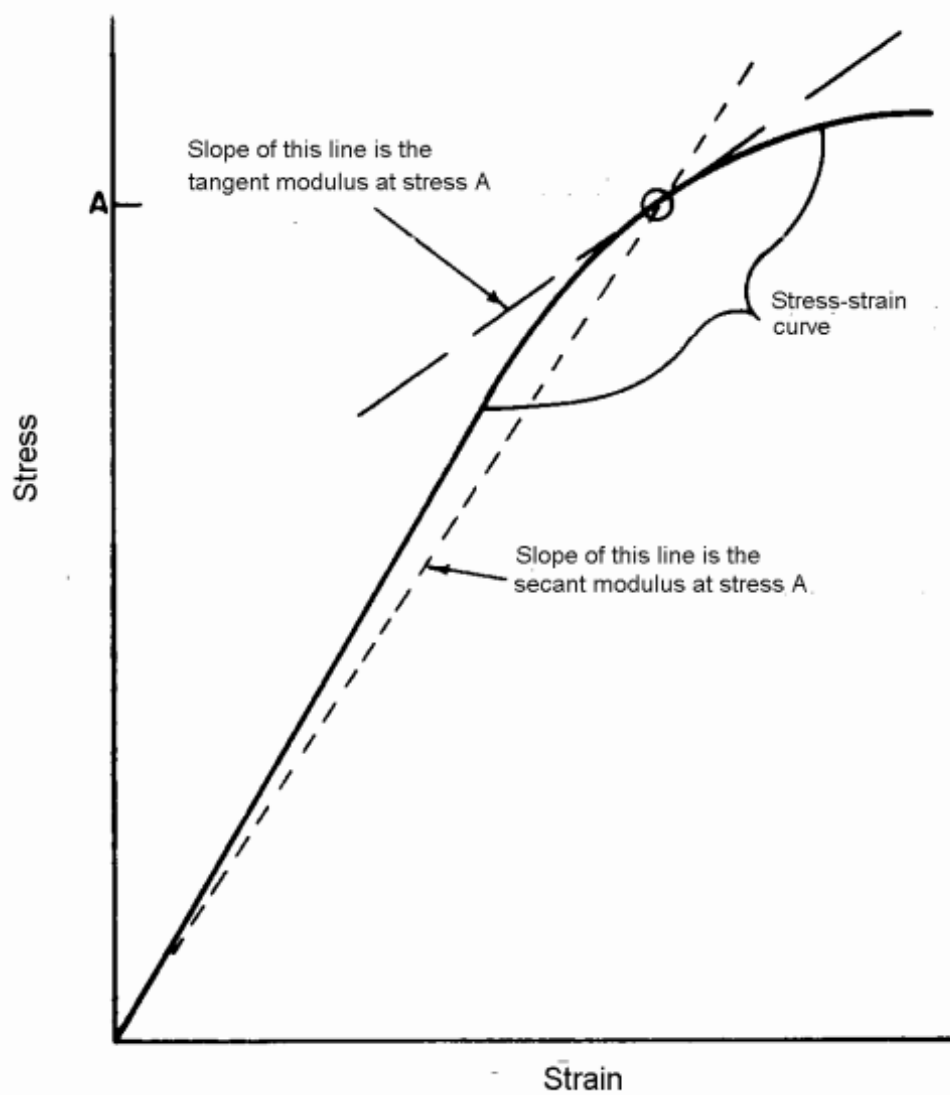


Figure 4.2.2-6: Definition of Tangent Modulus and Secant Modulus
[\(MIL-HNDBK-5H, 1998\)](#)

The tangent modulus is given by the following expression:

$$E_t = \frac{1}{\frac{1}{E} + \frac{0.002 \cdot n}{f_y} \cdot \left(\frac{f}{f_y}\right)^{n-1}}$$

The secant modulus is given by the following expression:

$$E_s = \frac{f}{\frac{f}{E} + 0.002 \left(\frac{f}{f_y}\right)^n}$$

The secant shear modulus is given by the following expression:

$$G_s = \frac{f}{\frac{f}{G} + 0.00346 \left(\frac{f}{f_{sy}}\right)^n}$$

A material property that is commonly missing from the certified, public domain material data is the shear yield strength. An approximation can be made for this value using the following expression:

$$f_{sy} = \frac{f_{ty}(L) + f_{ty}(LT) + f_{cy}(L) + f_{cy}(LT)}{4} \cdot \frac{2 \cdot f_{su}}{f_{tu}(L) + f_{tu}(LT)}$$

An acceptable approximation for the shear shape factor is:

$$n_s = \frac{n_{cL} + n_{cLT} + n_{tL} + n_{tLT}}{4}$$

We have created a spreadsheet that constructs the elasto-plastic material curves from basic material properties.



4.2.2.2. Grain Direction

While metals are generally isotropic in behavior they do show differences in static strength and, more significantly, in fracture toughness depending on the form of the metal and the direction.

Raw material is most commonly procured in sheet, panel or bar stock or as an extrusion of a specific shape.

Sheet is relatively thin; Panel is relatively thick. Bar stock is rolled with a circular cross section and extruded stock is pressed through a die with a particular cross section.

Grain direction is determined by the mill's rolling process which forms and stretches the microscopic structure and inclusions of the material. The grain direction runs parallel to the rolling direction.

For sheet or Panel stock the different directions through the raw material are defined as follows:

- | | |
|-----------|---|
| L | Longitudinal, along the length |
| LT | Longitudinal transverse, across the width |
| ST | Short transverse, through the thickness |

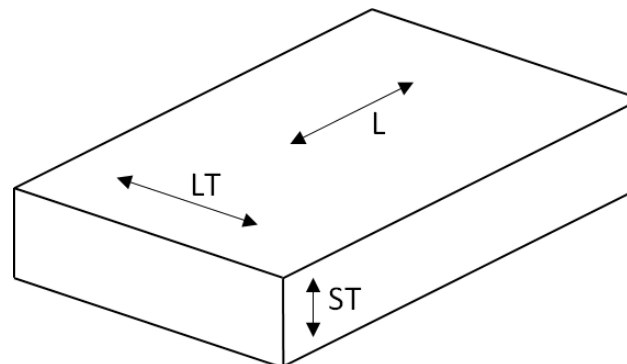


Figure 4.2.2-7: Definition of Panel Stock Grain Directions

It is advised not to align lug features in the short transverse grain direction for fittings machined from thick billets. This arrangement will show poor fatigue characteristics.

The short transverse grain direction is also more likely to demonstrate poor stress corrosion characteristics. See section 4.4.7.

Definitions of grain direction for common metallic forms are shown below:

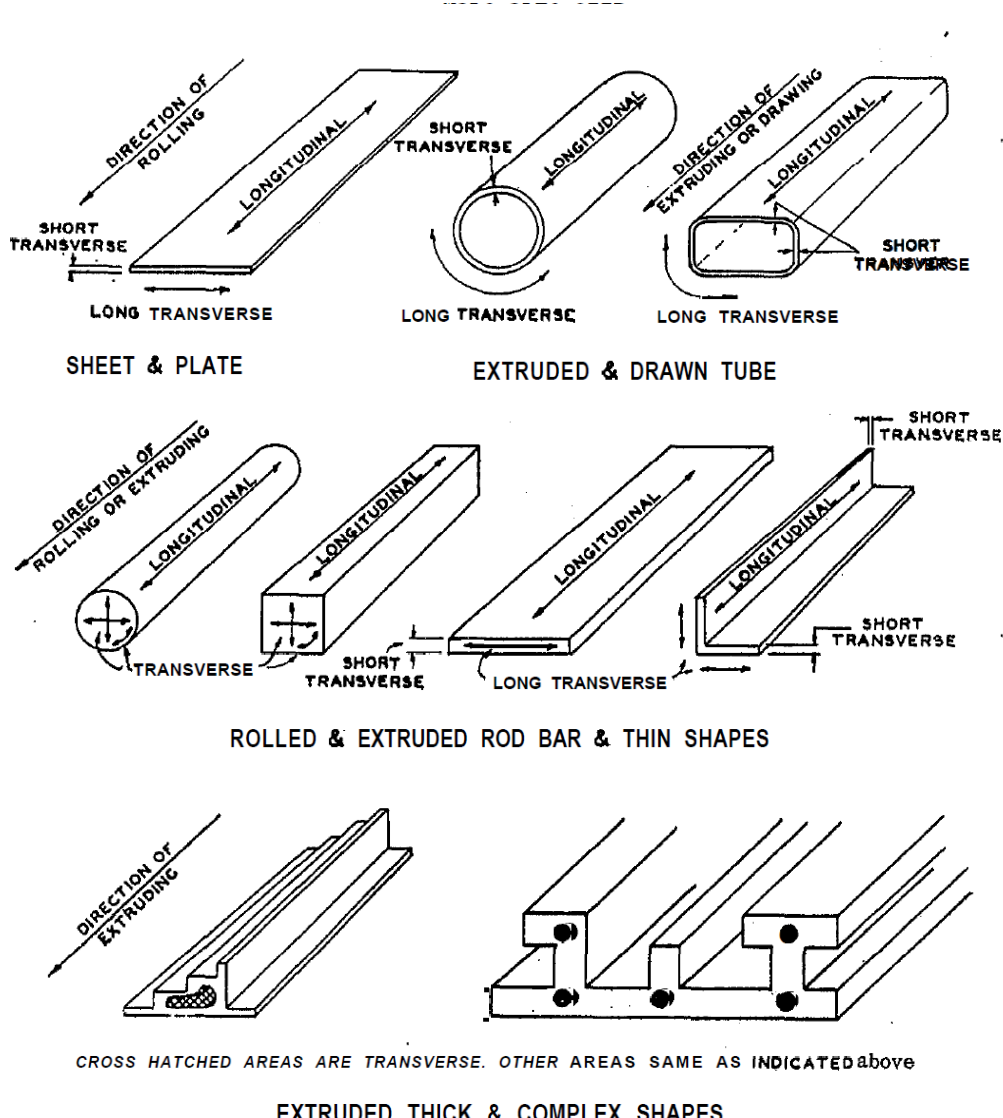


Figure 4.2.2-8: Grain Orientations in Standard Wrought Forms [\(MSFC-SPEC-522B, 1987\)](#)

ADVERT: TECHNICAL LIBRARY



We host the complete set of over 6000 NACA papers.

NACA research is a cornerstone of aerospace engineering.



4.3. Other Common Aircraft Materials

4.3.1. Stretched Acrylic

A common material used for aircraft windscreens is stretched acrylic ([\(MIL-PRF-25690B, 1960\)](#)). The strength and stiffness of this material does very significantly with temperature and therefore a conservative approach should be taken when it comes to strength and durability assessments.

The following data is taken from, or derived from data presented in [\(MIL-HDBK-17A, 1973\)](#).

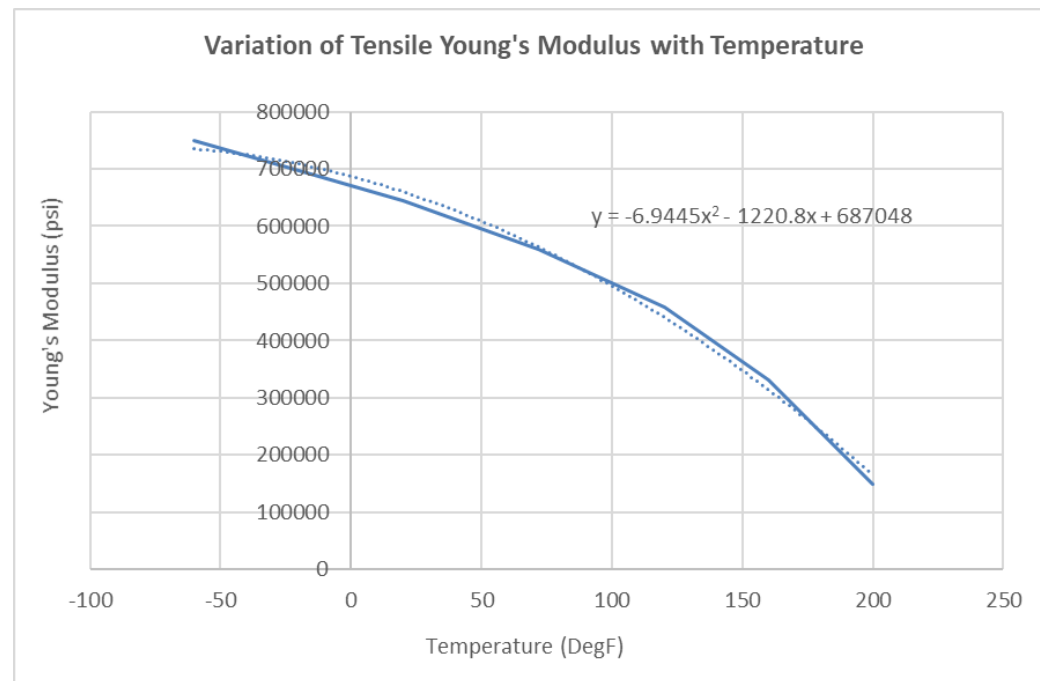


Figure 4.3.1-1: Stretched Acrylic Tensile Young's Modulus - Variation with Temperature

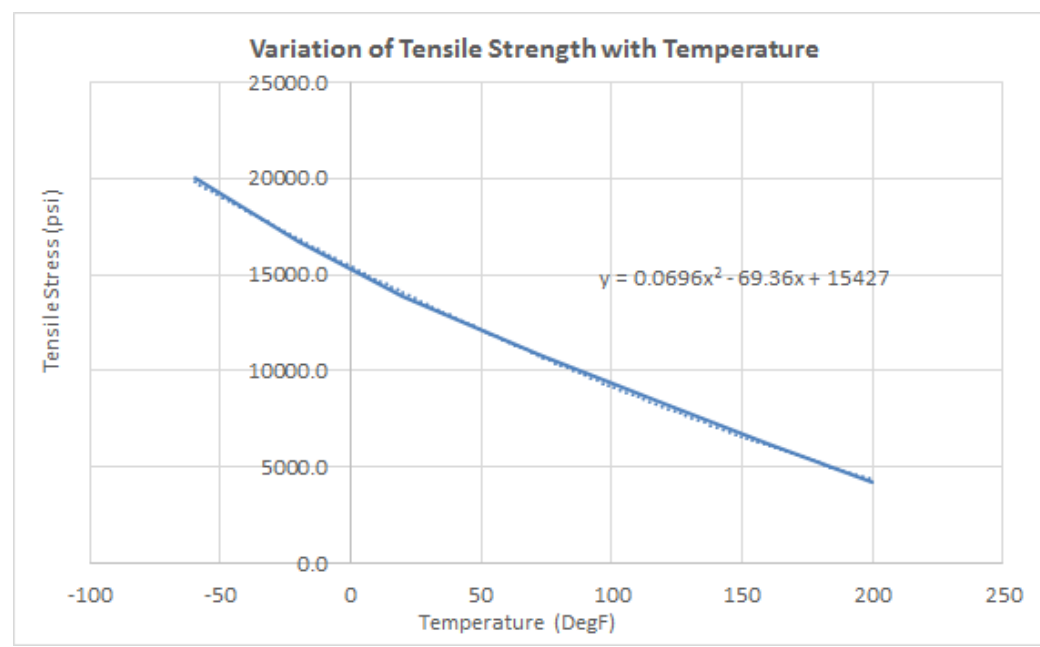


Figure 4.3.1-2: Stretched Acrylic Tensile Young's Strength - Variation with Temperature

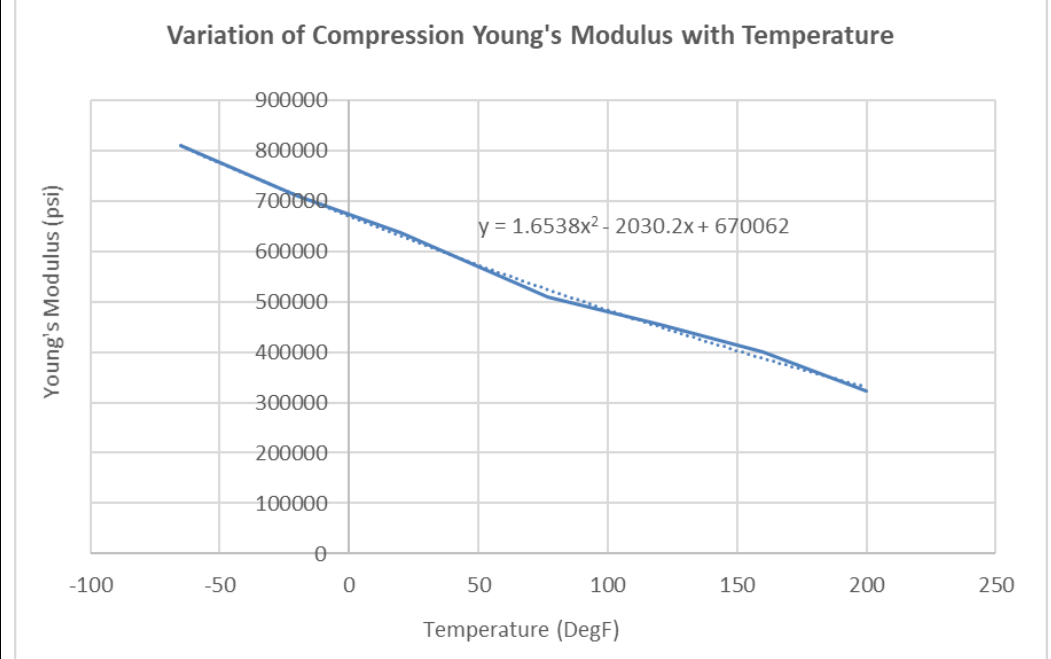


Figure 4.3.1-3: Stretched Acrylic Compression Young's Modulus - Variation with Temperature

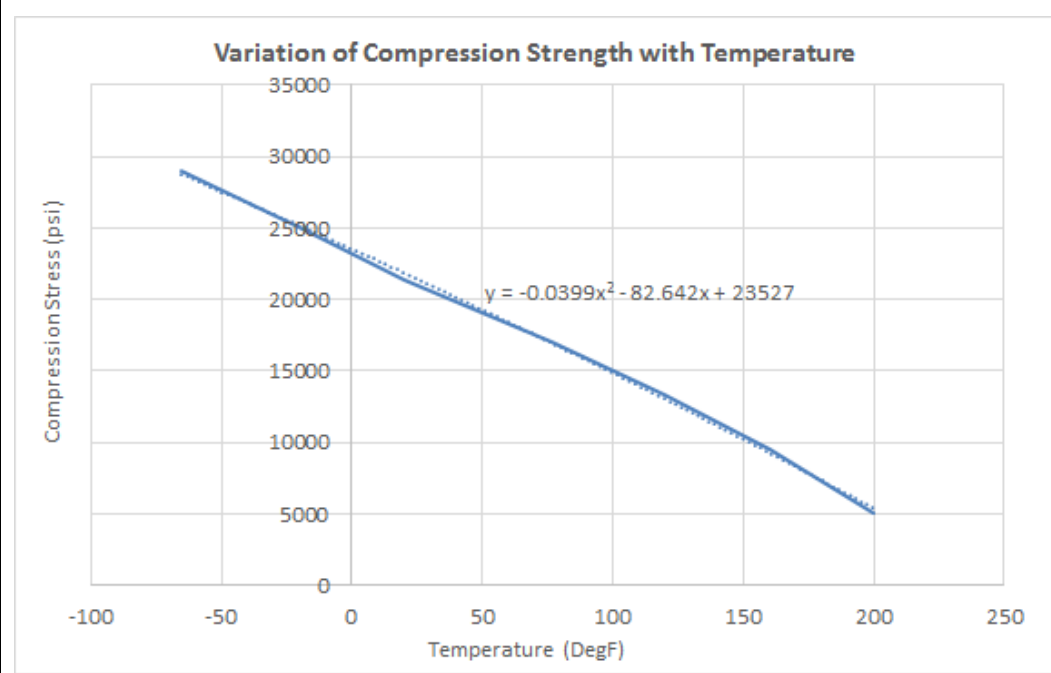


Figure 4.3.1-4: Stretched Acrylic Compression Strength - Variation with Temperature

The strength and stiffness values used for an analysis should either reflect the condition of the material at the environment at which it experiences the critical condition or a conservative approximation.

Stretched acrylic experiences the critical differential pressure load at maximum altitude and minimum temperature. At this condition the material is at the maximum strength and stiffness. As it is unusual to assume the maximum possible strength in a safety of flight or certification analysis.

The conservative minimum strength value from the basic material specification defined in [\(MIL-P-5425D, 1967\)](#) of **8000psi** can be used for the ultimate strength allowable. It is common for higher project specific allowable values to be used.

A fatigue limit stress of **2300psi**, the craze allowable from [\(MIL-PRF-25690B, 1960\)](#) Table III, can be used.

4.4. Corrosion

4.4.1. Introduction

From [\(AC43-4A, 1991\)](#):

"Corrosion is the electrochemical deterioration of a metal because of its chemical reaction with the surrounding environment. While new and better materials are continually being developed, this progress is offset, in part, by a more aggressive operational environment. This problem is compounded by the fact that corrosion is a complex phenomenon. It can take many different forms and the resistance of aircraft materials to corrosion can drastically change with only a small environmental change."

For corrosion to occur the following 4 conditions must exist

- 1) Presence of a metal that will corrode (anode)
- 2) Presence of a dissimilar conductive material (cathode) which has less tendency to corrode
- 3) Presence of a conductive liquid
- 4) Electrical contact between the anode and cathode (usually metal to metal contact or a fastener)

Elimination of any of these conditions will stop corrosion.

Factors that influence Corrosion:

- 1) Type of metal
- 2) Heat treatment and grain direction
- 3) Presence of a similar, less corrodible metal
- 4) Barrier protection
- 5) Operating Environment

Note that the only electrically inert product used in aircraft structural applications is glass fiber laminate.

This means that any other material can be used in combination with glass fiber laminates without the risk of corrosion. Glass fiber layers are used as a corrosion barrier between aluminum fittings and carbon fiber laminate back-up structure.

Electrical isolation is a good way to prevent corrosion. However, electrical isolation, especially in composite airframes can cause problems with grounding and lightning protection.

4.4.2. Forms of Corrosion

4.4.2.1. Surface Corrosion

Surface corrosion appears as a general roughening, etching, or pitting of the surface of a metal, frequently accompanied by a powdery deposit of corrosion products.



Figure 4.4.2-1: Surface Corrosion [\(FAA-H-8083-30, 2008\)](#)

Surface corrosion may be caused by either direct chemical or electrochemical attack. Sometimes corrosion will spread under the surface coating and cannot be recognized by either the roughening of the surface or the powdery deposit. Instead, closer inspection will reveal the paint or plating is lifted off the surface in small blisters which result from the pressure of the underlying accumulation of corrosion products.

Filiform corrosion gives the appearance of a series of small worms under the paint surface. It is often seen on surfaces that have been improperly chemically treated prior to painting.



Figure 4.4.2-2: Filiform Surface Corrosion [\(FAA-H-8083-30, 2008\)](#)

4.4.2.2. Galvanic or Dissimilar Metal Corrosion

Extensive pitting damage may result from contact between dissimilar metal parts in the presence of a conductor. While surface corrosion may or may not be taking place, a galvanic action, not unlike electroplating, occurs at the points or areas of contact where the insulation between the surfaces has broken down or been omitted. This electrochemical attack can be very serious because in many instances the action is taking place out of sight, and the only way to detect it prior to structural failure is by disassembly and inspection.



Figure 4.4.2-3: Dissimilar Metal (Galvanic) Corrosion. (FAA-H-8083-30, 2008)

The contamination of a metal's surface by mechanical means can also induce dissimilar metal corrosion.

The improper use of steel cleaning products, such as steel wool or a steel wire brush on aluminum or magnesium, can force small pieces of steel into the metal being cleaned, which will then further corrode and ruin the adjoining surface. Carefully monitor the use of nonwoven abrasive pads, so that pads used on one type of metal are not used again on a different metal surface.

Galvanic corrosion is covered in greater depth in section 4.4.5.

4.4.2.3. Intergranular Corrosion

This type of corrosion is an attack along the grain boundaries of an alloy and commonly results from a lack of uniformity in the alloy structure. Aluminum alloys and some stainless steels are particularly susceptible to this form of electrochemical attack. The lack of uniformity is caused by changes that occur in the alloy during heating and cooling during the material's manufacturing process. Intergranular corrosion may exist without visible surface evidence.

Very severe intergranular corrosion may sometimes cause the surface of a metal to "exfoliate." This is a lifting or flaking of the metal at the surface due to delamination of the grain boundaries caused by the pressure of corrosion residual product buildup. This type of corrosion is difficult to detect in its initial stage. Extruded components such as spars can be subject to this type of corrosion. Ultrasonic and eddy current inspection methods are being used with a great deal of success.



Figure 4.4.2-4: Intergranular Corrosion Shown as Exfoliation. (FAA-H-8083-30, 2008)

4.4.2.4. Stress Corrosion

Stress corrosion occurs as the result of the combined effect of sustained tensile stresses and a corrosive environment. Stress corrosion cracking is found in most metal systems; however, it is particularly characteristic of aluminum, copper, certain stainless steels, and high strength alloy steels (over 240,000 psi).

It usually occurs along lines of cold working and may be transgranular or intergranular in nature. Aluminum alloy bellcranks with pressed in bushings, landing gear shock struts with pipe thread type grease fittings, clevis pin joints, shrink fits, and overstressed tubing B-nuts are examples of parts which are susceptible to stress corrosion cracking.

Stress Corrosion is covered in greater depth in section 4.4.7.

4.4.2.5. Fretting Corrosion

Fretting corrosion is a particularly damaging form of corrosive attack that occurs when two mating surfaces, normally at rest with respect to one another, are subject to slight relative motion.

It is characterized by pitting of the surfaces and the generation of considerable quantities of finely divided debris. Since the restricted movements of the two surfaces prevent the debris from escaping very easily, an extremely localized abrasion occurs. The presence of water vapor greatly increases this type of deterioration.

If the contact areas are small and sharp, deep grooves resembling brinell markings or pressure indentations may be worn in the rubbing surface. As a result, this type of corrosion (on bearing surfaces) has also been called false brinelling.



Figure 4.4.2-5: Fretting. (FAA-H-8083-30, 2008)

4.4.3. Corrosion Prone Regions of the Aircraft.

(AGARD-AG-278, 1985) gives the following guidance for high risk areas for corrosion. These are not the only areas – all regions of the aircraft may corrode. Special care should be taken in the following areas to either avoid problematic material combinations or to provide additional mitigation to avoid corrosion.

- 1 UNDER DE-ICER BOOTS
Moisture may collect under the boots and result in corrosion.
- 2 FLOOR SUPPORTS AND FLOORING
Metal floors and substructure will corrode if continually in contact with moisture of any kind.
- 3 PASSENGER, CARGO, AND CREW DOORS
Floors and structure in these areas corrode as a result of exposure to rain water and condensate.
- 4 GALLEY AREAS
Spilled food, fruit juices, and other liquids in prolonged contact with metal structure will cause corrosion, particularly when protective coatings are allowed to deteriorate.
- 5 AREAS IN PATH OF EXHAUST GASES
Exhaust gases on the nacelle and wing skins and seeping into the wing structure may permeate the protective finish and cause corrosion underneath.

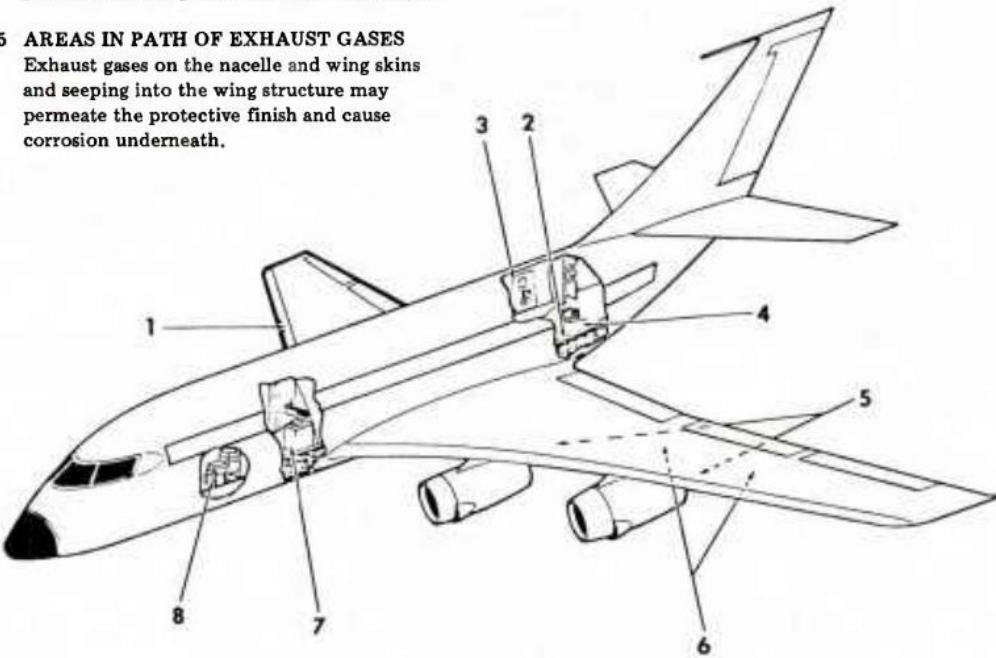


Figure 4.4.3-1: Regions of the Aircraft Susceptible to Corrosion (AGARD-AG-278, 1985)

Other regions of the aircraft also prone to corrosion:

- Landing Gear
- Flight control surface connections and any exposed hinge lines (doors, trim tabs, etc)
- High lift devices mechanisms and hinges/tracks
- Freight Doors
- Control Cables

For military aircraft:

- Cockpit Frames
- Missile and gun blast areas
- Engine Intake Areas
- Wing Fold Areas

4.4.4. Corrosion Mitigation

The requirements for corrosion prevention and control should be considered at all stages of the design process. The aim should be to ensure that the final structure will allow manufacture, assembly and in service and maintenance to be performed as easily as possible, in a manner that will maintain the quality of the structure and its ability to resist corrosion.

4.4.4.1. Corrosion Prevention By Geometric Design

The most important way to minimize the potential for corrosion by large scale geometric design is to provide adequate drain paths and avoid regions where water can collect.

The examples below are for metal structure, the same principals should be applied to composite structure.

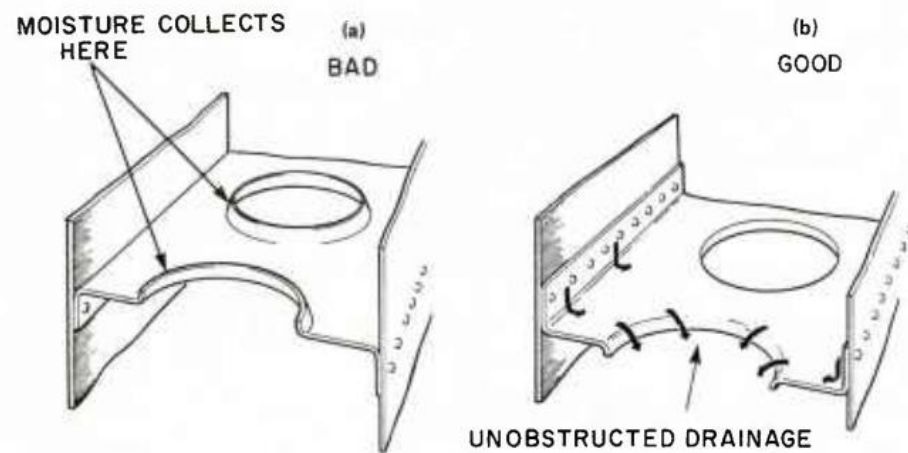


Figure 4.4.4-1: Lightening Holes in Horizontal Diaphragms (AGARD-AG-278, 1985)

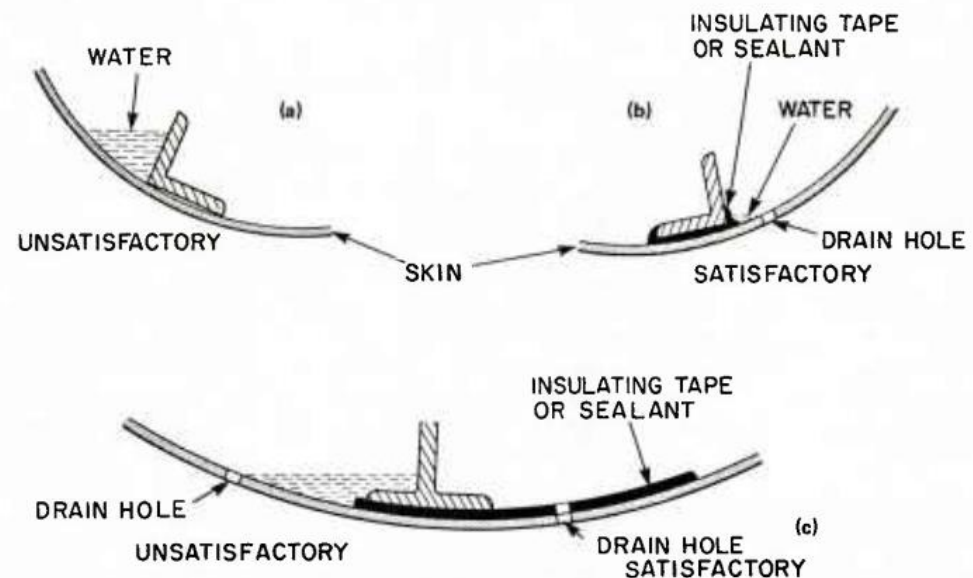


Figure 4.4.4-2: Water Traps and Faying Surfaces (AGARD-AG-278, 1985)

It is important that large assemblies are created assuming that condensation can occur on any surface. Assemblies must have managed drain paths that lead to drain holes or drain valves to avoid regions where moisture can collect and the corrosion problem this can create.

4.4.4.2. Corrosion Prevention by Surface Treatments and Protective Coatings

Exposed surfaces of the aircraft can be modified chemically to render them less susceptible to corrosion. Surfaces can also be protected with a coating or paint. Some processes (cladding) are applied at the mill stage by the manufacturer. Anodizing, chromate filming or plating are applied by the aircraft OEM after the part has been formed.

Surface pre-treatments by chemical or mechanical means are also important in creating good adhesion for paint to the surface.

Cladding

May high strength aluminum alloys are susceptible to corrosion. Corrosion resistance can be improved by metallurgically bonding to the core alloy a surface layer of pure aluminum or an alloy with good corrosion resistance. The cladding should be anodic to the core metal so if the cladding becomes damaged by or the core alloy is exposed the cladding will provide cathodic protection.

The thickness of the cladding is usually between 2% and 5% of the total sheet or plate thickness and the cladding is usually a softer or lower strength alloy. This can affect fatigue strength, abrasion resistance and buckling performance. The effect of cladding on buckling performance can be estimated using the method in section 15.2.9 of this book.

Surface Conversion Coatings

Surface conversion coatings are produced by chemical action with electrical assistance. The treatment changes the immediate surface of metal into a film of metallic oxide or compound which has greater corrosion resistance than the base metal. Surface conversion coatings also offer a good base for paint.

Anodizing: The electrolytic oxidation of a surface to produce a tightly adherent oxide scale which is thicker than the naturally occurring film. The Anodized surface is hard and abrasion resistant. Anodizing alone cannot be relied upon to provide effective corrosion resistance to corrosion prone alloys, further protection by painting is required. Anodic coatings breakdown in highly alkaline ($\text{pH} > 8.5$) and highly acid ($\text{pH} < 4.0$) solution. Anodic coatings are relatively brittle and may crack under stress, supplementary protection such as painting is particularly important with stress corrosion prone alloys.

Anodic coatings are used with aluminum, magnesium and titanium alloys.

Chromate Filming: Proprietary chromate filmings are available for aluminum, magnesium, cadmium and zinc alloys. Chromate films are usually about $5\mu\text{m}$ thick. The film contains soluble chromates which act as corrosion inhibitors and they provide a modest improvement in corrosion resistance of the base metal. Their main purpose is the provide suitable surface for sealing resins or paint.

Phosphate Coating: Several phosphate coatings have been developed for use on steel. The coatings consist of a thick porous layer of fine phosphate crystals tightly bonded to the steel. The coating does not provide effective corrosion resistance when used alone, but the coating provides an excellent base for oils waxes or paints and the help to prevent the spreading of rust under layers of paint. Phosphating is not widely used in aircraft structures.

Nitriding: Steels containing nitride forming elements such as chromium, molybdenum, aluminum and vanadium can be treated to produce hard surface layers providing improved wear resistance. The nitrides formed are not only hard but also more voluminous than the original steel and therefore they create compressive residual surface stresses which offer both improved corrosion and fatigue resistance.

Passive Films: Austenitic stainless steels and hardenable stainless steels such as martensitic, precipitation hardening and maraging stainless steels are seldom

coated but their corrosion resistance depends on the formation of naturally occurring transparent oxide films. The production of these films is inhibited by surface contaminants and treatments are available to clean and degrease surfaces to help produce uniform protective oxide films under controlled conditions.

Metallic Coatings

Metallic coatings are deposited by electroplating, electroless plating, spraying, hot dipping, chemical vapor deposition and ion vapor deposition. The most common coatings used in aircraft are cadmium, chromium, nickel, aluminum and zinc.

Cadmium: Cadmium is widely used as an electroplating on steel fasteners however it is being phased out due to the toxicity of both the product and the process. Cadmium is anodic to steel and will cathodically protect the substrate at scratches or gaps in the coating at cut edges. It also exhibits surface lubricity, conductivity, resist fretting and. Coatings are usually 5 to $25\mu\text{m}$ thick.

Chromium: Chromium is used on steel as a protective coating providing resistance to wear, abrasion and corrosion. It has a hardness in the range 900 to 1100HV, low friction characteristics and high reflectivity. It is used as a thin coating usually in the range 0.2 to $1\mu\text{m}$ thick as the final layer in a multiple-plate copper-nickel-chromium electroplating, or as a thick coating up to $300\mu\text{m}$ to provide wear resistance. The corrosion resistance is derived primarily from the barrier effect of the thick nickel plate of the chromium.

Chromium is a metal with lower cathode efficient and substantial amounts of hydrogen are deposited on the part along with the metal being plated. Because of this, parts must be baked as soon as possible after plating to drive off the hydrogen and prevent embrittlement. Baking temperatures can be used up to the tempering temperature of the steel and therefore they tend to be less effective for very high strength steels where tempering temperatures are low.

Aluminum: Aluminum coatings can be applied to steel by hot dipping, cementation, ion vapor deposition or spraying. Spraying is the only process that has been used extensively over a long period of time with airframe parts. Pack cementation is widely used for turbine engine components.

Sprayed aluminum coatings are around 100 to $150\mu\text{m}$ thick. Ion vapor coatings can be applied down to a minimum of 8 to $25\mu\text{m}$.

Zinc: Zinc coatings may be applied either by electroplating or spraying. Electroplatings are normally less than $25\mu\text{m}$ thick and may be as thin as $5\mu\text{m}$ on threaded parts. However, while they provide good protection to steel in rural atmospheres, they do not perform as well in marine or industrial environments. Zinc plating does not perform as well as cadmium in tropical and marine atmospheres, and therefore cadmium is preferred for aircraft use.

4.4.5. Galvanic Corrosion

A common form of corrosion occurs between dissimilar conductive material types. These materials include all metals and carbon fiber laminate. The extent or severity of the reaction between different materials depends on the position relative to each other on the galvanic series. The further apart the two materials are the greater their propensity to galvanically corrode.

The galvanic series is given in the figure below:



ANALYSIS AND DESIGN OF COMPOSITE AND METALLIC FLIGHT VEHICLE STRUCTURES

Doc. No.: AA-SB-001
Edition: 3rd
Date: March, 2019

| ANODIC | | GALVANIC SERIES (SEA WATER) | | | | | | | | | | | | | |
|--|--|-----------------------------|--|--|--|--|--|--|--|--|--|--|--|--|--|
| Magnesium | | | | | | | | | | | | | | | |
| Magnesium Alloys | | | | | | | | | | | | | | | |
| Beryllium | | | | | | | | | | | | | | | |
| Zinc | | | | | | | | | | | | | | | |
| Galvanized Steel | | | | | | | | | | | | | | | |
| Aluminum Alloys | | | | | | | | | | | | | | | |
| Chromium | | | | | | | | | | | | | | | |
| Gallium | | | | | | | | | | | | | | | |
| Cadmium | | | | | | | | | | | | | | | |
| Mild Steel | | | | | | | | | | | | | | | |
| Wrought Iron | | | | | | | | | | | | | | | |
| Indium | | | | | | | | | | | | | | | |
| Low-Alloy Steels | | | | | | | | | | | | | | | |
| Cast Iron | | | | | | | | | | | | | | | |
| Low-Alloy Cast Iron | | | | | | | | | | | | | | | |
| 4–6% Cr Steel | | | | | | | | | | | | | | | |
| Ni Cast Iron | | | | | | | | | | | | | | | |
| 12–14% Chromium Steel and 25–30% | | | | | | | | | | | | | | | |
| Lead-Tin Solders | | | | | | | | | | | | | | | |
| 16–18% Chromium Steel | | | | | | | | | | | | | | | |
| Austenitic Cr-Ni Stainless Steel | | | | | | | | | | | | | | | |
| Austenitic Cr-Ni-Mo Stainless Steel | | | | | | | | | | | | | | | |
| Lead | | | | | | | | | | | | | | | |
| Tin | | | | | | | | | | | | | | | |
| Manganese Bronze | | | | | | | | | | | | | | | |
| Naval Brass | | | | | | | | | | | | | | | |
| Cobalt | | | | | | | | | | | | | | | |
| Nickel | | | | | | | | | | | | | | | |
| Inconel (13% Cr, 6.5% Fe, Bal. Ni) | | | | | | | | | | | | | | | |
| Yellow Brass | | | | | | | | | | | | | | | |
| Admiralty Brass | | | | | | | | | | | | | | | |
| Aluminum Bronze | | | | | | | | | | | | | | | |
| Red Brass | | | | | | | | | | | | | | | |
| Antimony | | | | | | | | | | | | | | | |
| Copper | | | | | | | | | | | | | | | |
| Silicon Bronze | | | | | | | | | | | | | | | |
| Nickel Silver | | | | | | | | | | | | | | | |
| 70-30 Copper Nickel | | | | | | | | | | | | | | | |
| Titanium | | | | | | | | | | | | | | | |
| Monel | | | | | | | | | | | | | | | |
| Composition G Bronze (88% Cu, 2% Zn, 10% Sn) | | | | | | | | | | | | | | | |
| Composition M Bronze (88% Cu, 3% Zn, 6.5% Sn, 1.5% Pb) | | | | | | | | | | | | | | | |
| Silver Solder | | | | | | | | | | | | | | | |
| Nickel (Passive) | | | | | | | | | | | | | | | |
| 70-30 Nickel Copper | | | | | | | | | | | | | | | |
| Stainless Steels (Passive) | | | | | | | | | | | | | | | |
| Silver | | | | | | | | | | | | | | | |
| Palladium | | | | | | | | | | | | | | | |
| Gold | | | | | | | | | | | | | | | |
| Rhodium | | | | | | | | | | | | | | | |
| Platinum | | | | | | | | | | | | | | | |
| Carbon | | | | | | | | | | | | | | | |
| CATHODIC | | | | | | | | | | | | | | | |

Figure 4.4.5-1: Galvanic Series of Common Metals and Alloys (AGARD-AG-278, 1985)

It follows that direct contact of materials from different ends of the galvanic series should be avoided.

The following figure gives the appropriate level of concern and mitigation required for common material combinations.

| Table 3-3 Degree of Corrosion at Bimetallic Contacts (Ref. 3-8) | | | | | | | | | | | | | | | |
|---|--------------------------------------|---|---|--|--------------------------|-------------------|-------------------|----------------|--|------------------|-------------------|-------------------|------------------------------|-------------------|----------------|
| 1 | 2 | 3 | 4 | 5 | 6 | 7 | 8 | 9 | 10 | 11 | 12 | 13 | 14 | 15 | 16 |
| CONTACT METAL → | Gold, platinum, rhodium, silver | Monel, nickel, molybdenum, denum, aluminum alloys | Cupro-nickel, silver solder, tin, aluminum bronzes, gunmetals | Copper, brasses, nickel silver, tin and soft solders | Lead, tin, and cast iron | Steel | Cadmium | Zinc | Magnesium and magnesium alloys (chromated) | Stainless steels | Chromium | Titanium | Aluminum and aluminum alloys | | |
| METAL CONSIDERED ↓ | | | | | | | | | | | | | | | |
| 1 Gold, platinum, rhodium, silver | — | A | A | A | A | A | A | A | A | A | A | A | A | A | A |
| 2 Monel, Inconel, nickel molybdenum | B | — | A | A | A | A | A | A | A | A | A | A | A | A | A |
| 3 Cupronickels, silver solder, aluminum bronzes, tin bronzes, gunmetals | C ^k | BorC | — | A | A | A | A | A | BorC | B | A | BorC | BorC | A ^a | |
| 4 Copper, brasses, nickel silvers | C ^k | BorC | BorC ^b | — | BorC | BorC ^c | A | A | A | BorC | BorC ^d | BorC | BorC | A ^e | |
| 5 Nickel | C | B | A | A | — | A | A | A | A | BorC | BorC ^d | BorC | BorC | BorC | A |
| 6 Lead, tin and soft solders | C | BorC ^b | BorC ^c | BorC ^d | B | — | AorC ^e | A | AorC ^f | A | BorC | BorC ^d | BorC | BorC | A |
| 7 Steel and cast iron | C | C | C | C | C ^k | C ^k | — | A ^m | A ^m | A | C | C | +C | C ^k | B ^m |
| 8 Cadmium | C | C | C | C | C | B | C | — | A | A | C | C | C | C | B |
| 9 Zinc | C | C | C | C | B | C | B | — | A | C | C | C | C | C | C ⁱ |
| 10 Magnesium and magnesium alloys (chromated) b, a | D | D | D | D | D | C | D | BorC | BorC | — | C | C | C | BorC ^g | |
| 11 | Austenitic 18/8 | A | D | A | A | A | A | A | A | — | A | A | A | A ^v | A |
| 12 Stain- | less | steel | 18/2 Cr/Ni | C | AorC ^e | AorC ^f | AorC ^g | A | A | — | A | A | — | A | |
| 13 | 13% Cr | C | C | C | C | BorC | A | A | A | C | C | — | C | C | A |
| 14 | Chromium | A | A | A | A | A | A | A | A | A | A | A | A | — | A |
| 15 | Titanium | A | A | A | A | A | A | A | A | A | A | A | A | — | A |
| 16 | Aluminum and aluminum alloys n, s, w | D | C | D ^b | D ^c | C ^k | BorC | BorC | A | A ^d | BorC | BorC | BorC | BorC ^d | C |

Key A indicates the corrosion of the metal is not likely to be increased by the contact metal
B indicates the corrosion of the metal may be slightly increased by the contact metal
C indicates the corrosion of the metal may be markedly increased by the contact metal. (Accelerated corrosion, however, is likely to occur only when the metal is wetted with moisture containing an electrolyte such as salt, acid, combustion products, etc. Under less severe conditions the increase in corrosion may be slight.)
D indicates that when moisture is present this combination is inadvisable without adequate protective measures.
Superscript symbols refer to the Table notes printed below.

Figure 4.4.5-2: Degrees of Corrosion at Bimetallic Contacts (AGARD-AG-278, 1985)

The most common cause of galvanic corrosion is a dissimilarity in metals at fastener locations. The form of this corrosion is shown below:

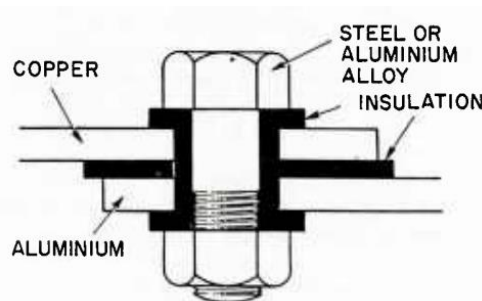


Figure 4.4.5-4: Required Sealing or Barriers for Steel Fasteners in Aluminum Joints. (AGARD-AG-278, 1985)

The behavior of aluminum fasteners in carbon fiber laminate is similar and tends to be more severe.

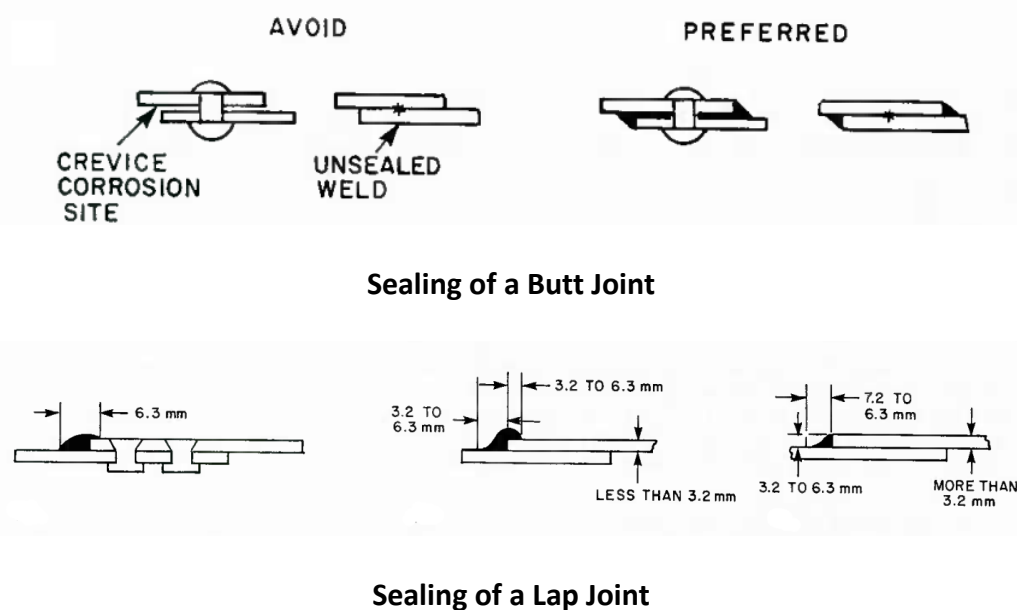


Figure 4.4.5-5: Sealing of Joints Against Moisture Ingress. (AGARD-AG-278, 1985)

4.4.5.2. Galvanic Corrosion Recommended Protective Treatments (in order of effectiveness)

This information is taken primarily from [\(MIL-STD-889C, 2016\)](#).

Treatments For Magnesium:

1. Anodic coating (ASTM D1732) post treated with an alkali-resistant paint or resin coating system.
2. Chromate conversion coating (SAE AMS-M-3171) post treated with an alkali-resistant paint or resin coating system. Alternate for general use in non-persistent wet or marine atmosphere; or anodic coating without organic coating system.
3. Metallic coating, electroless nickel (SAE AMS-C-26074, or MIL-DTL-32119 where applicable) with cadmium overplating (SAE AMS-QQ-P-416). For electrical, thermal conducting purposes, in absence of wet, saline or acidic atmospheric conditions.
4. Chromate treatment. Suitable for assured condensation-free and acid-free conditions.

Note: Bare magnesium should not be used.

Treatments for Zinc:

1. Anodic coating post treated with a paint or resin coating system, primarily for castings.
2. Chromate conversion coating (MIL-C-17711) post treated with a paint or resin coating system; or anodic coating without organic coating system. For use in non-persistent wet or marine atmosphere. For electrical, thermal conducting purposes in mild atmospheres in absence of wet, saline or acidic conditions.
3. Chromate conversion coating without paint or resin coating system.

Note: Bare, plated zinc should not be used in a marine environment.

Treatments for Cadmium or Beryllium:

1. Chromate conversion coating (SAE AMS-QQ-P-416, SAE AMS-C-8837 or SAE AMS-C-81562) post-treated with a paint or resin coating system.
2. Chromate conversion coating without organic coating system. For use in non-persistent wet or marine atmosphere. For electrical, thermal conducting purposes in mild atmospheres in absence of wet, saline or acidic conditions. Recommended for beryllium in high temperature applications to forestall catastrophic oxidation in oxygen containing atmosphere.

Treatments for Aluminum and Aluminum Alloys:

1. Anodic coating (MIL-A-8625) post treated with a paint or resin coating system.
2. Chromate conversion coating (MIL-DTL-5541) post treated with a paint or resin coating system; or anodic coating, sealed, with resin seal (when porous castings are used, impregnated with resin prior to surface treating and finishing).
3. Chromate conversion coating without paint or resin coating system, for electrical, thermal conducting purposes in mild atmospheres in absence of saline, alkaline or acidic conditions.
4. Bare aluminum - may be used when surface treating would interfere with application, under conditions free of salinity or extended wetness, or when high corrosion resistant alloys are used. Faying edges should be sealed to prevent crevice corrosion.

Treatments for Carbon and Low Alloy Steels:

1. Metallic coating (e.g., sacrificial Zn or Cd, with supplemental passivation or surface treatment or non-sacrificial, e.g., Cu or Ni), with a paint or resin coating system. For steels of strengths greater than 220ksi metallic coatings should be applied by nonelectrolytic methods. For steels of strengths up to 220ksi metallic coatings may be applied electrolytically, but the steel should be stress relieved before plating and hydrogen embrittlement relieved after plating.
2. Metallic coating (e.g., sacrificial Zn or Cd, with supplemental passivation or surface treatment or non-sacrificial, e.g., Cu or Ni), without paint or resin coating system, for direct metallic contact or for achieving least potential difference between joined metals. For metals of strengths greater than 220ksi, metallic coating, if required, should be applied by non-electrolytic methods.
3. Zinc phosphate conversion coating (TT-C-490) post treated with a paint or resin coating system. Caution, if a phosphate coating is used on steels of strengths between 150 to 220ksi, stress relief is required prior to phosphating and hydrogen embrittlement relief is required after phosphating. Zinc phosphate coatings are prohibited for steels of strength greater than 220ksi.

4. Pretreatment primer (MIL-C-8514) post treated with a paint or resin coating system.
5. Heavy phosphate conversion coating (MIL-DTL-16232) post treated with a supplemental treatment. Not for steels of strengths greater than 220ksi.

Treatments for Lead, Tin Solders and Indium Coatings:

Coatings of these materials applied to other metals by hot-dipping, fusing, or electroplating processes.

1. Coat with paint or resin coating system. Electroplated coatings should be "flowed" prior to applying coating system.
2. Electroplate with other metal to reduce the electro potential difference of metals being joined, where direct contact of metals is required for electrical purposes.

Treatments for Martensitic and Ferric Stainless Steels:

Steels with chromium contents in the region of 12 percent will undergo considerable surface staining and limited rusting in corrosive environments, but overall are appreciably less corroded than carbon steels.

1. Apply paint or resin coating system.
2. May be electroplated or used bare for use in non-persistent wet or marine atmosphere, and for electrical or thermal conducting purposes. Faying edges to be sealed to prevent crevice corrosion.

Treatments for Chromium (Plate), Molybdenum and Tungsten:

1. Paint or apply resin coating system to reduce corrosion at voids in chromium plating or staining of molybdenum or tungsten surfaces.
2. Normally may be used bare for electrical wear resistance, or thermal conducting purposes. Seal faying edges to mitigate crevice attack.

Treatments for steels stainless-austenitic, PH, super strength, heat resistant, brass leaded, bronze, brass bronze-low copper, and copper high nickel:

1. Apply metallic coating as may be required to minimize electrical potential difference between the metals to be joined and apply paint or resin coating system, primarily to diminish ion contamination from metals of this group onto more anodic metals to which they might be joined, thereby diminishing potential damage to the more anodic metal.
2. Apply metallic coating (as "a" above), use without paint or resin coating system, for electrical or thermal conducting purposes. May be expedient to overcoat completed assembly with paint or resin.
3. Apply paint or resin coating system and seal faying edges.
4. Use bare and seal faying edges for electrical and thermal conducting purposes, if more anodic metals are not directly joined or in close proximity to receive rundown of surface condensate.
5. Select galvanically compatible metals required to be coupled for high temperature applications, where metallic coatings may not be useful and paint or resin coatings are not practical.

Treatments for Titanium:

1. Anodize, for anti-galling and wear resistance.
2. Apply metallic coating (Cd, Zn prohibited, Ag over Ni acceptable) post-treated with a paint or resin coating system.
3. Apply metallic coating (Cd, Zn prohibited, Ag over Ni acceptable), seal faying edges. For electrical or thermal conducting purposes.

4. May be used bare with faying edges sealed in contact with metals other than magnesium, zinc or cadmium; for electrical or thermal conducting purposes.

Treatments for Silver:

1. Silver or silver plated parts to be used as electrical, open-close contact points, plugs and receptacles should be plated over with rhodium, palladium or gold.
2. May be used in stationary components of electrical assemblies, e.g., connectors, printed circuits, but should be enveloped by sulfur-free conformal coatings.
3. Apply chromate conversion coating post treated with a corrosion inhibiting fluid film to parts of electrical plugs, receptacles, etc.

Treatments for rhodium, palladium, gold, platinum and alloys:

Use bare, with compound sealant at edges of dissimilar metal joint, or by enveloping dissimilar metal joint in conformal coatings, where feasible.

Treatments for Graphite:

1. Plate graphite to minimize electrical potential difference between graphite and metal to be joined to it. Seal faying edges to preclude corrosion at contacting surface of the metal member, if service is electrical, or apply conformal coating.
2. May be used bare in electrical or thermal conducting service, conditions permitting. Seal faying edges.

4.4.6. Jointing Compounds and Sealants

Jointing compounds are used for protection at joints where they act by excluding dirt and moisture, and by providing a reservoir of slightly soluble chromates which act as inhibitors. Sealants are applied to joints to prevent the escape of fluids, such as fuel, but they also exclude moisture.

Common aircraft fay surface and joint sealing products are typically qualified to MIL-S-8802. These sealants are commonly used for both joint surface and edge sealing as well as for sealing fuel tanks.

Note that a liquid shim also acts as a surface seal.

Sealants can be both conductive (for grounding and lightning strike protection) and non-conductive (for electrical isolation and protection against galvanic corrosion).

Temperature resistant sealants for firewall applications are typically qualified to MIL-S-38249.

4.4.7. Stress Corrosion Cracking

Ref: [\(MSFC-SPEC-522B, 1987\)](#), [\(ECSS-Q-ST-70-36C, 2009\)](#)

Stress corrosion may be defined as the combined action of sustained tensile stress and corrosion to cause premature failure of, materials.

Certain materials are more susceptible to stress corrosion cracking (SCC) than others. If a susceptible material is placed in service in a corrosive environment under tension of sufficient magnitude, and the duration of service is sufficient to permit the initiation and growth of cracks, failure occurs at a stress lower than

that which the material is normally be expected to withstand. The corrosive environment need not be severe in terms of general corrosive attack.

Service failures due to stress-corrosion are frequently encountered in cases where the surfaces of the failed parts are not visibly corroded in a general sense.

Stresses are additive and threshold stresses for susceptibility are often low. There have been a number of stress-corrosion failures for which design stresses were intermittent and of short duration, and only of minor significance in contributing to failure. Stress-corrosion cracking in those cases occurred because of a combination of residual and assembly stresses not anticipated in design.

Resistance to stress corrosion cracking of metal alloys mainly depends on Grain Orientation (Reference Section 4.2.2.2) and Material Susceptibility to Stress Corrosion Cracking (Reference Section 0).

Protective coatings such as electroplate, anodize or chemical conversion coatings do not change the stress corrosion rating of alloys to which they are applied.

Surface treatments such as carburizing or nitriding may adversely affect the stress corrosion rating of materials to which they are applied.

4.4.7.1. Common Situations which result in Stress Corrosion Problems

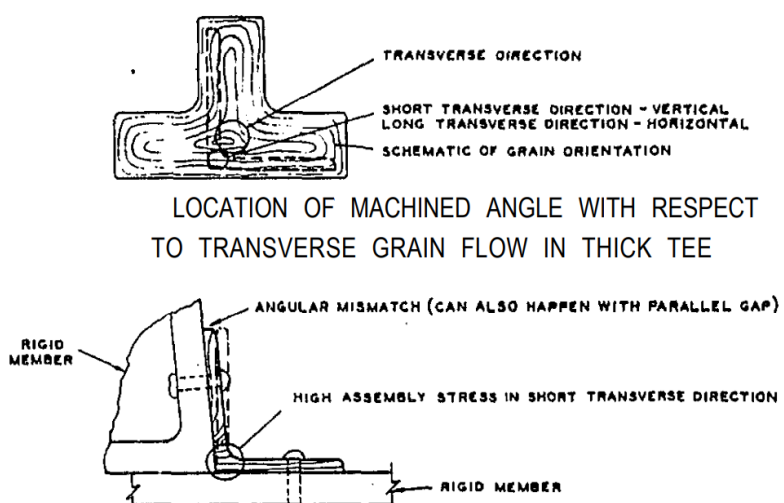


Figure 4.4.7-1: Assembly Stress Resulting from Mismatch [\(MSFC-SPEC-522B, 1987\)](#)



LOCATION OF MACHINED CHANNEL IN PLATE OR BAR

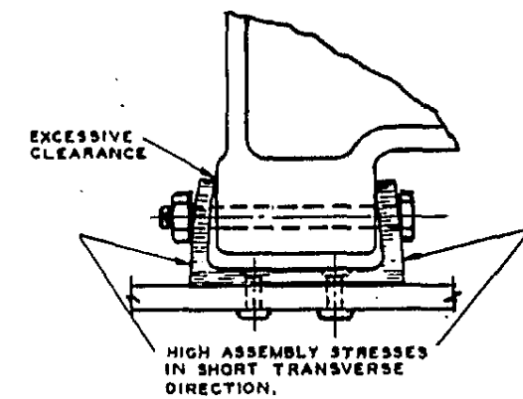
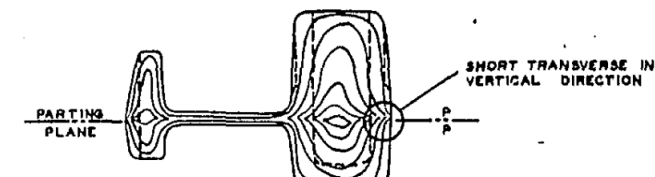


Figure 4.4.7-2: Assembly Stress Resulting from Excessive Clearance [\(MSFC-SPEC-522B, 1987\)](#)



CROSS SECTION OF DIE FORGING SHOWING OUTLINE OF MACHINED PART

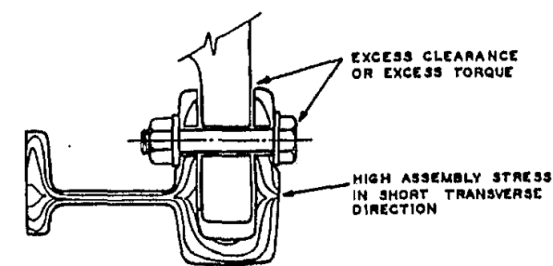


Figure 4.4.7-3: Assembly Stress in Forging with Excessive Clearance [\(MSFC-SPEC-522B, 1987\)](#)

4.4.7.2. Alloys with High Resistance to Stress Corrosion Cracking

| (a) Steel | Condition |
|--|--|
| Carbon steel (1000 series) | Below 1 225 MPa (180 ksi) UTS |
| Low alloy steel (4130, 4340, etc.) | Below 1 225 MPa (180 ksi) UTS ¹ |
| (E) D6AC, H-11 | Below 1 450 MPa (210 ksi) UTS |
| Music wire (ASTM 228) | Cold drawn |
| HY-80 steel | Quenched and tempered |
| HY-130 steel | Quenched and tempered |
| HY-140 steel | Quenched and tempered |
| 1095 spring steel | Quenched and tempered |
| 300 series stainless steel (unsensitized) ² | All |
| 400 series Ferritec stainless steel (404, 430, 431, 444, etc.) | All |
| 21-6-9 stainless steel | All |
| Carpenter 20Cb stainless steel | All |
| Carpenter 20Cb-3 stainless steel | All |
| A286 stainless steel | All |
| AM350 stainless steel | SCT 1000 ⁴ and above |
| AM355 stainless steel | SCT 1000 and above |
| Almar 362 stainless steel | H1000 ⁵ and above |
| Custom 450 stainless steel | H1000 and above |
| Custom 455 stainless steel | H1000 and above |
| 15-5 PH stainless steel | H1000 and above |
| PH 14-8 Mo stainless steel | CH900 and SRH950 and above ^{6,7} |
| PH 15-7 Mo stainless steel | CH900 |
| 17-7 PH stainless steel | CH900 |
| Nitronic 33 ³ | All |
| (E) Maraging steel MARVAL X12 | All |

Table 4.4.7-1 Steel Alloys with High Resistance to Stress-Corrosion Cracking
(ECSS-Q-ST-70-36C, 2009)

| (c) Aluminium alloys: | | | |
|------------------------|--------------------|--------------------|----------------------|
| Wrought ^{1,2} | | Cast | |
| Alloy | Condition | Alloy ³ | Condition |
| 1000 series | All | 355.0, C355.0 | T6 |
| 2011 | T8 | 356.0, A356.0 | All |
| 2024, rod bar | T8 | 357.0 | All |
| 2219 | T6, T8 | B358.0 (Tens-50) | All |
| (E) 2419 | T8 | 359.0 | All |
| (E) 2618 | T6, T8 | 380.0, A380.0 | As cast |
| 3000 series | All | 514.0 (214) | As cast ⁵ |
| 5000 series | All ^{4,5} | 518.0 (218) | As cast ⁵ |
| 6000 series | All | 535.0 (Almag 35) | As cast ⁵ |
| (E) 7020 | T6 ⁶ | A712.0, C712.0 | As cast |
| 7049 | T73 | | |
| 7149 | T73 | | |
| 7050 | T73 | | |
| 7075 | T73 | | |
| 7475 | T73 | | |

1. Mechanical stress relieved (TX5X or TX5XX) where possible.
 2. Including weldments of the weldable alloys.
 3. The former designation is shown in parenthesis when significantly different.
 4. High magnesium content alloys 5456, 5083 and 5086 should be used only in controlled tempers (H111, H112, H116, H117, H323, H343) for resistance to stress-corrosion cracking and exfoliation.
 5. Alloys with magnesium content greater than 3,0 % are not recommended for high-temperature application, 66 °C (150 °F) and above.
 6. Excluding weldments.
 (E) ESA classification - not in NASA MSFC-SPEC-522A.

Table 4.4.7-3 Aluminum Alloys with High Resistance to Stress Corrosion Cracking
(ECSS-Q-ST-70-36C, 2009)

| (b) Nickel Alloy | Condition |
|--------------------------|-----------|
| Hastelloy C | All |
| Hastelloy X | All |
| Incoloy 800 | All |
| Incoloy 901 | All |
| Incoloy 903 | All |
| Inconel 600 ³ | Annealed |
| Inconel 625 | Annealed |
| Inconel 718 ³ | All |
| Inconel X-750 | All |
| Monel K-500 | All |
| Ni-Span-C 902 | All |
| René 41 | All |
| Unitemp 212 | All |
| Waspaloy | All |
| 3. Including weldments | |

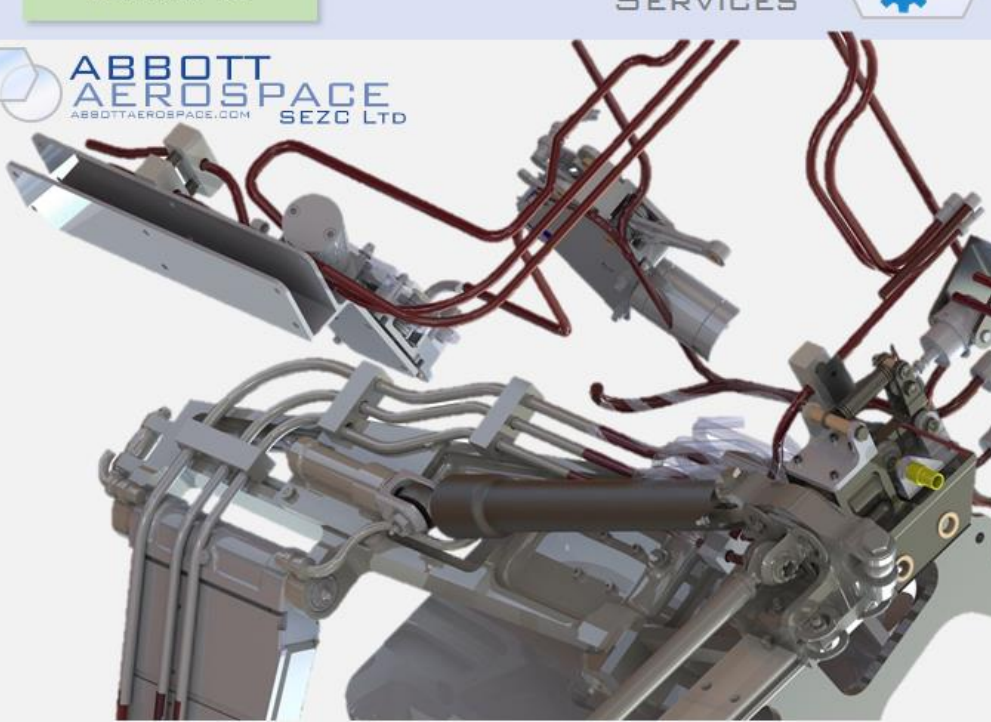
Table 4.4.7-2 Nickel Alloys with High Resistance to Stress Corrosion Cracking
(ECSS-Q-ST-70-36C, 2009)

ADVERT: ENGINEERING SERVICES

MECHANICAL SYSTEMS

CONTACT US

ABBOTT AEROSPACE SEZC LTD



| (d) Copper Alloy | |
|-----------------------------------|--|
| CDA no. ¹ | Condition (% cold rolled) ² |
| 110 | 37 |
| 170 | AT, HT ^{3,4} |
| 172 | AT, HT ^{3,4} |
| 194 | 37 |
| 195 | 90 |
| 230 | 40 |
| 422 | 37 |
| 443 | 10 |
| 510 | 37 |
| 521 | 37 |
| 619 | 40 (9 % B phase) |
| 619 | 40 (95 % B phase) |
| 688 | 40 |
| 706 | 50 |
| 725 | 50, annealed |
| 280, 524, 606, 632, 655, 704, 710 | 0 |
| 715, (E) 917, (E) 937 | 0 |

1. Copper Development Association alloy number.

2. Maximum per cent cold rolled for which stress-corrosion-cracking data are available.

3. AT - annealed and precipitation hardened.

4. HT - work hardened and precipitation hardened.

(E) ESA classification not in NASA MSFC-SPEC-522A.

| (b) Aluminium Alloys ^{1,2} | | | |
|-------------------------------------|-------------|---------------------------|-----------|
| Wrought | Cast | | |
| Alloy | Condition | Alloy | Condition |
| 2011 | T3, T4 | 295.0 (195) | T6 |
| 2014 | All | B295.0 (B195) | T6 |
| 2017 | All | 520.0 (220) | T4 |
| 2024 | T3, T4 | 707.0 (607, tern-alloy 7) | T6 |
| 2024 Forgings | T6, T62, T8 | D712.0 (D612,40E) | As cast |
| 2024 Plate | T62 | | |
| (E) Al-Li 2080 | T8 | | |
| (E) 2618 | T3, T4 | | |
| 7001 | T6 | | |
| 7005 | All | | |
| (E) 7020 | Weldments | | |
| 7039 | All | | |
| 7075 | T6 | | |
| 7175 | T6 | | |
| 7079 | T6 | | |
| 7178 | T6 | | |
| 7475 | T6 | | |
| (E) Al-Li 8090 | All | | |
| (E) BS L93 | T6 | | |
| (E) Russian Al-Li 1441 and 1460 | All | | |

1. Mechanically stress-relieved products (TX5X or TX5XX) should be specified where possible

2. Sheet, unmachined extrusions and unmachined plate are the least susceptible

(E) ESA classification - not in NASA MSFC-SPEC-522A.forms

Table 4.4.7-4 Copper Alloys with High Resistance to Stress Corrosion Cracking
(ECSS-Q-ST-70-36C, 2009)

4.4.7.3. Alloys with Low Resistance to Stress Corrosion Cracking

| (a) Steel Alloy | Condition |
|------------------------------------|------------------|
| Carbon steel (1000 series) | Above 1 370 MPa |
| Low-alloy steel (4130, 4340, etc.) | Above 1 370 MPa |
| (E) D6AC, H-11 steel | Above 1 450 MPa |
| 440C stainless steel | All |
| 18 Ni Maraging steel, 200 grade | Aged at 900 °F |
| 18 Ni Maraging steel, 250 grade | Aged at 900 °F |
| 18 Ni Maraging steel, 300 grade | Aged at 900 °F |
| 18 Ni Maraging steel, 350 grade | Aged at 900 °F |
| AM 350 stainless steel | Below SCT 1000 |
| AM 355 stainless steel | Below SCT 1000 |
| Custom 455 stainless steel | Below H1000 |
| PH 15-7 Mo stainless steel | All except CH900 |
| 17-7 PH stainless steel | All except CH900 |
| (E) Kovar | All |

(E) ESA classification not in NASA MSFC-SPEC-522A.

Table 4.4.7-6 Aluminum Alloys with Low Resistance to Stress Corrosion Cracking
(ECSS-Q-ST-70-36C, 2009)

(c) Copper alloys

| CDA no. ¹ | Condition (% cold rolled) ² |
|----------------------|--|
| 260 | 50 |
| 353 | 50 |
| 443 | 40 |
| 672 | 50, annealed |
| 687 | 10, 40 |
| 762 | A, 25, 50 |
| 766 | 38 |
| 770 | 38, 50, annealed |
| 782 | 50 |

1. Copper Development Association alloy number.

2. Rating based on listed conditions only.

Table 4.4.7-5 Steel Alloys with Low Resistance to Stress-Corrosion Cracking
(ECSS-Q-ST-70-36C, 2009)

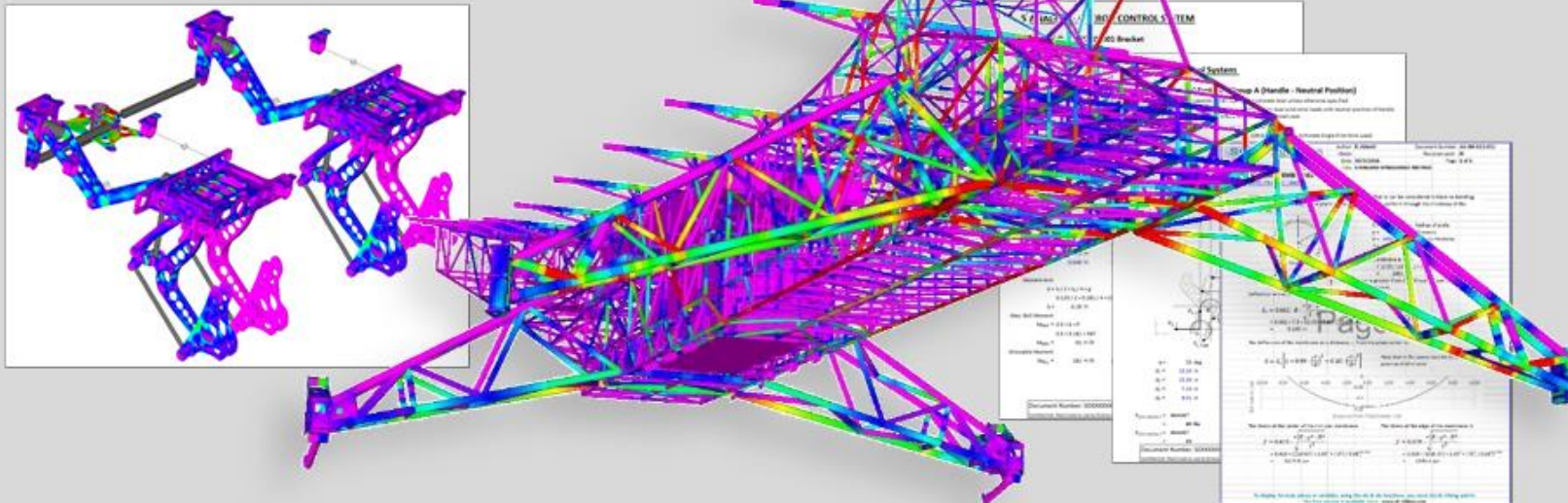
Table 4.4.7-7 Copper Alloys with Low Resistance to Stress Corrosion Cracking
(ECSS-Q-ST-70-36C, 2009)

| (d) Magnesium Alloy | Condition |
|---------------------|-----------|
| AZ61A | All |
| AZ80A | All |
| WE54 | All |
| ZCM711 | All |

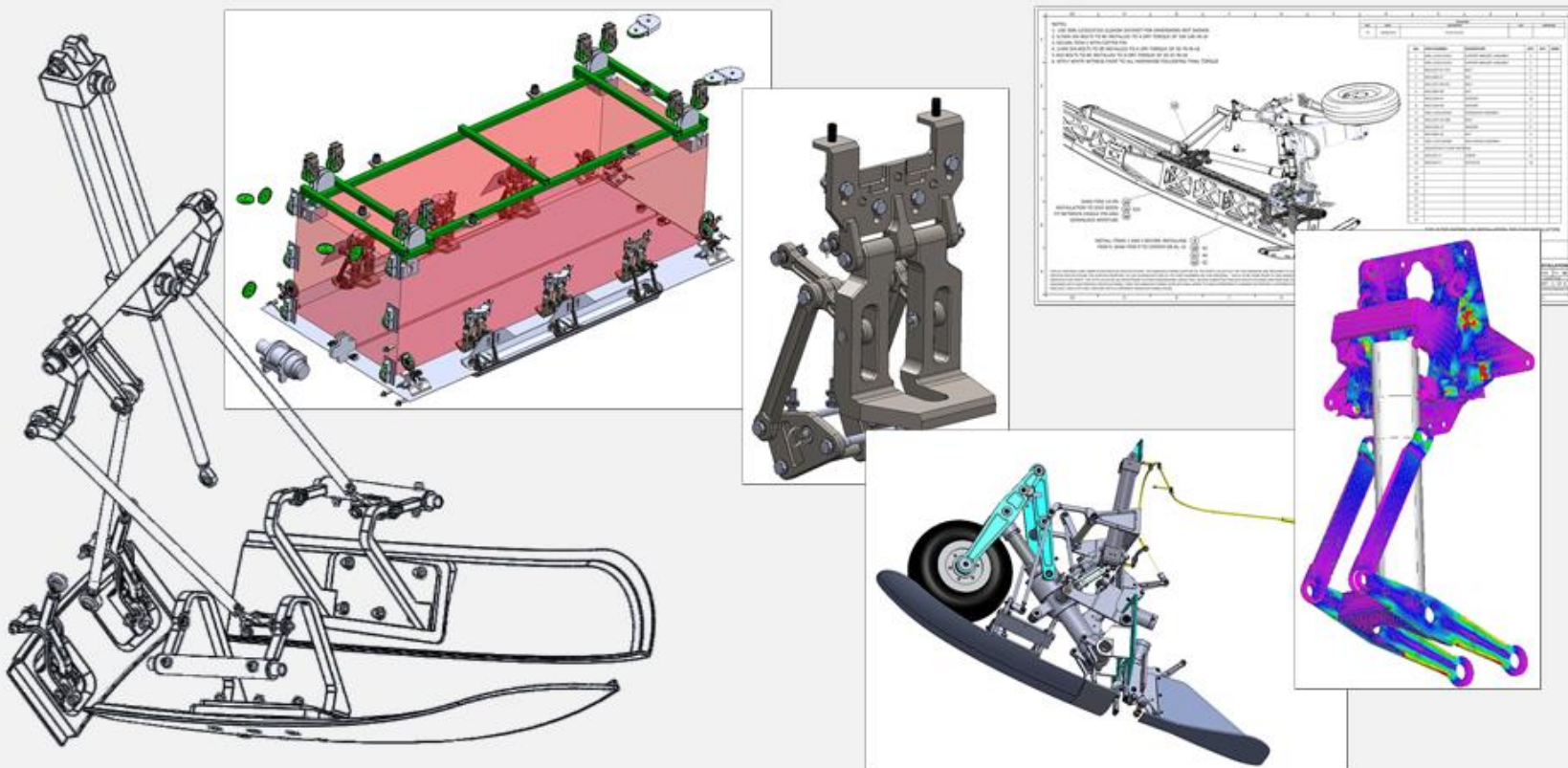
Table 4.4.7-8 Magnesium Alloys with Low Resistance to Stress Corrosion Cracking (ECSS-Q-ST-70-36C, 2009)

ABBOTT AEROSPACE SEZC LTD

STRUCTURES ANALYSIS



MECHANICAL SYSTEMS DESIGN



Contact us to find out how we can help you to reduce risk, maximize your potential and take flight.



CONTACT US

5. LOADS

5.1. Introduction

5.2. Aircraft External Loads

5.2.1. Introduction

5.2.2. Reserved

5.2.3. Reserved

5.3. Internal Load Distribution

5.3.1. Introduction

5.3.2. Reserved

5.3.3. Reserved

This section will be included in a later edition. This page is a placeholder only.

6. SECTION PROPERTIES

6.1. Introduction

This section covers basic cross section properties. In the compilation of this section the reference [\(NAVWEPS-REPORT-7827, 1962\)](#) has been used and provides good background information.

The following terms are used in this section and are in general use:

| | |
|--------------------|--|
| k | Plastic Bending Shape Factor |
| \bar{x}, \bar{y} | Centroidal Distance, in |
| R | Radius, Outer Radius, in |
| a, b, d | Major Dimensions, in |
| t | Thickness, in |
| r | Inner Radius, in |
| p | Radius of Gyration, in |
| A | Area, in ² |
| Q | First Moment of Area about the Shape Neutral Axis, in ³ |
| I | Area Moment of Inertia or Second Moment of Area, in ³ |

6.1.1. Centroid (\bar{x}, \bar{y})

The *centroid* of a shape represents the point about which the area of the section is evenly distributed. The centroidal distance is the distance from the centroid of a cross section to the extreme fiber.

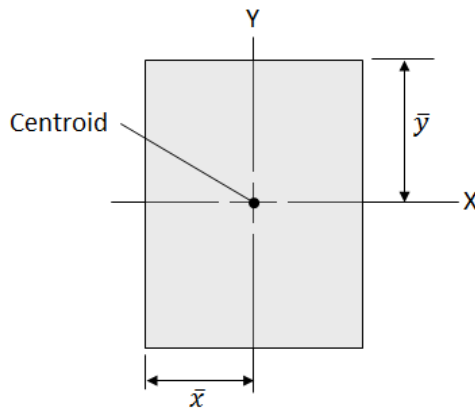


Figure 6.1.1-1: Definition of Centroid and Centroidal Distance

Centroid by Integration:

$$\bar{x} = \frac{\int x dA}{A}$$

$$\bar{y} = \frac{\int y dA}{A}$$

Centroid by Area Moment Summation for a Composite Area:

$$\bar{x} = \frac{x_1 \cdot a_1 + x_2 \cdot a_2 + \dots + x_n \cdot a_n}{a_1 + a_2 + \dots + a_n} = \frac{\sum(x \cdot a)}{A}$$

$$\bar{y} = \frac{y_1 \cdot a_1 + y_2 \cdot a_2 + \dots + y_n \cdot a_n}{a_1 + a_2 + \dots + a_n} = \frac{\sum(y \cdot a)}{A}$$

6.1.2. First Moment of Area (Q)

The *first moment of area* or *statical moment* is a measure of the distribution of the area of a shape in relation to the axis. The first moment of area is the summation of area multiplied by the distance of the centroid of that area to an axis:

$$Q_x = \int y dA$$

$$Q_y = \int x dA$$

The first moment of area is used to calculate the plastic bending shape factor. It is also used to calculate the shear stress distribution in a cross section. See Section 3.4.1.3.

6.1.3. Area Moment of Inertia (I)

The *area moment of inertia*, also known as *second moment of inertia*, *moment of inertia of a plane area* or *second area moment*.

The area moment of inertia of a plane area is referred to the second moment of area since the first moment Q is multiplied by the differential area moment arm:

$$I_x = \int y^2 dA$$

$$I_y = \int x^2 dA$$

Where the elements are integrated over the whole body.

The area moment of inertia about the Z axis (polar moment of inertia) is given by the following expression:

$$I_z = I_x + I_y$$

6.1.4. Parallel Axis Theorem

If the moment of inertia of a cross section about a centroidal axis is known, then the *parallel axis theorem* can be used to calculate the moment of inertia about any parallel axis:

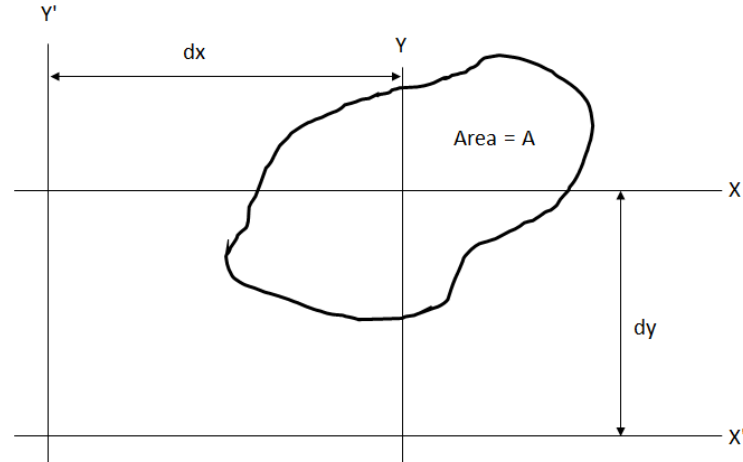


Figure 6.1.4-1: Definition of terms for Parallel Axis Theory

$$I_{x'} = I_x + Ady^2$$

$$I_{y'} = I_y + Adx^2$$

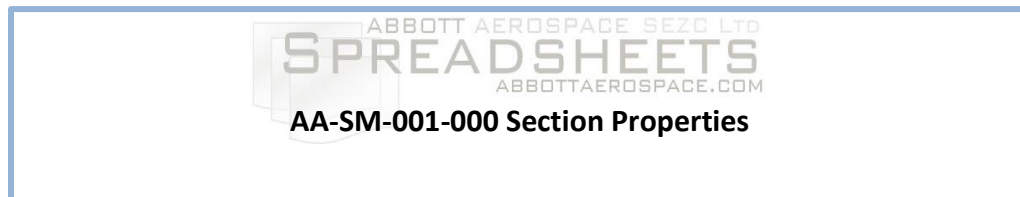
6.1.5. Radius of Gyration

The radius of gyration represents the distance from a section's centroid at which all of the area could be concentrated without having any effect on the moment of inertia. The radius of gyration of a shape with respect to each axis is given by:

$$\rho_x = \sqrt{I_x/A}$$

$$\rho_y = \sqrt{I_y/A}$$

All the section properties in the following table are calculated in this spreadsheet:



ADVERT: SOFTWARE

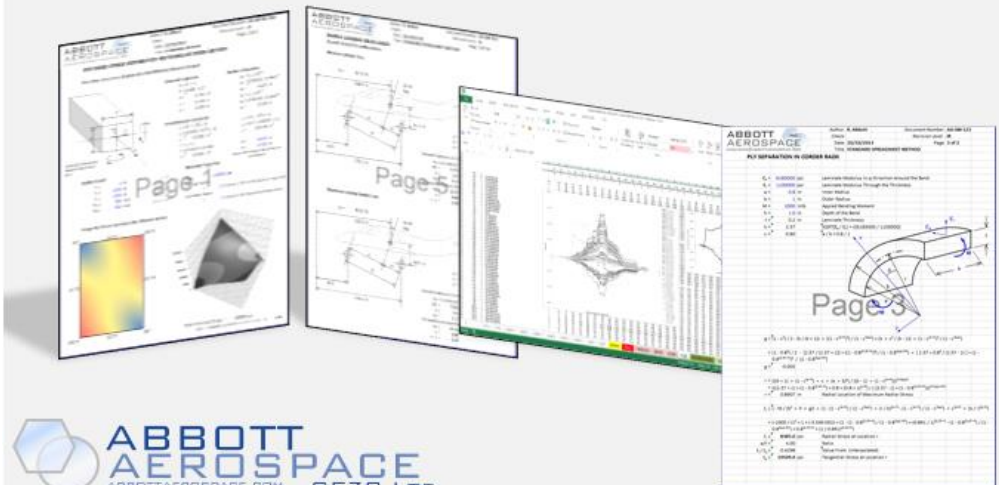
EXCEL ADD-IN: SOFTWARE TOOLS XL-VIKING

DOWNLOAD



By Aerospace Stress Engineers for Aerospace Stress Engineers

***Our Formula Viewer Makes
MS-Excel the Perfect Reporting Tool***

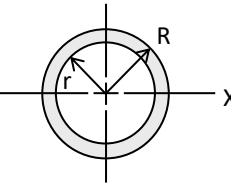
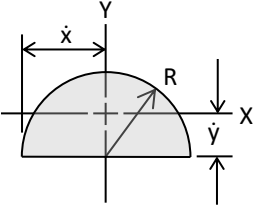
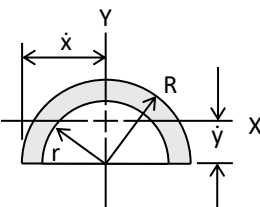
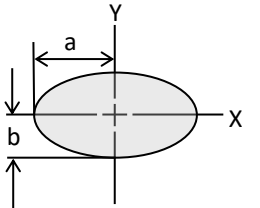
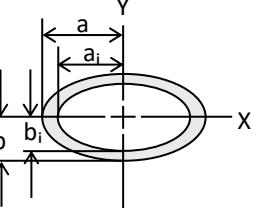


 **ABBOTT AEROSPACE**
 SEZC LTD
 ABBOTTAEROSPACE.COM

6.2. Simple Section Properties

Notes: In general, the plastic bending shape factor can be expressed using the following expressions: $k_x = 2 \cdot Q_x \cdot \bar{y} / I_x$ and $k_y = 2 \cdot Q_y \cdot \bar{x} / I_y$. Where the plastic bending shape factor is constant for a cross section is expressed as a constant value. The expression for the plastic bending shape factor is also adapted to give the correct centroid distance where appropriate. The Radius of Gyration is not given in this table as it can be calculated for all shapes about either axis using the expression: $\rho = \sqrt{I/A}$.

| Description | Area | Centroids | First Moment of Area | Second Moment of Area | Plastic Bending Shape Factor |
|----------------------------|-------------------------------------|--|--|--|--|
| 1. Square | $A = a^2$ | $\bar{x} = \frac{a}{2}$ $\bar{y} = \frac{a}{2}$ | $Q_x = \frac{a^3}{4}$ $Q_y = \frac{a^3}{4}$ | $I_x = \frac{a^4}{12}$ $I_y = \frac{a^4}{12}$ | $k_x = 1.50$ $k_y = 1.50$ |
| 2. Rectangle | $A = b \cdot d$ | $\bar{x} = \frac{b}{2}$ $\bar{y} = \frac{d}{2}$ | $Q_x = \frac{b \cdot d^2}{4}$ $Q_y = \frac{d \cdot b^2}{4}$ | $I_x = \frac{b \cdot d^3}{12}$ $I_y = \frac{d \cdot b^3}{12}$ | $k_x = 1.50$ $k_y = 1.50$ |
| 3. Hollow Rectangle | $A = b \cdot d - b_i \cdot d_i$ | $\bar{x} = \frac{b}{2}$ $\bar{y} = \frac{d}{2}$ | $Q_x = \frac{(b \cdot d^2) - (b_i \cdot d_i^2)}{4}$ $Q_y = \frac{(d \cdot b^2) - (d_i \cdot b_i^2)}{4}$ | $I_x = \frac{(b \cdot d^3) - (b_i \cdot d_i^3)}{12}$ $I_y = \frac{(d \cdot b^3) - (d_i \cdot b_i^3)}{12}$ | $k_x = \frac{3}{2} \cdot \frac{b \cdot d^3 - b_i \cdot d_i^2 \cdot d}{b \cdot d^3 - b_i \cdot d_i^3}$ $k_y = \frac{3}{2} \cdot \frac{d \cdot b^3 - d_i \cdot b_i^2 \cdot b}{d \cdot b^3 - d_i \cdot b_i^3}$ |
| 4. Circle | $A = \pi \cdot R^2$ | $\bar{x} = R$ $\bar{y} = R$ | $Q_x = \frac{(2 \cdot R)^3}{6}$ $Q_y = \frac{(2 \cdot R)^3}{6}$ | $I_x = \frac{\pi \cdot R^4}{4}$ $I_y = \frac{\pi \cdot R^4}{4}$ | $k_x = 1.698$ $k_y = 1.698$ |

| Description | Area | Centroids | First Moment of Area | Second Moment of Area | Plastic Bending Shape Factor |
|------------------------------|--|--|--|--|--|
| 5. Hollow Circle |  $A = \pi \cdot (R^2 - r^2)$ | $\bar{x} = R$ $\bar{y} = R$ | $Q_x = \frac{(2 \cdot R)^3 - (2 \cdot r)^3}{6}$ $Q_y = \frac{(2 \cdot R)^3 - (2 \cdot r)^3}{6}$ | $I_x = \frac{\pi \cdot (R^4 - r^4)}{4}$ $I_y = \frac{\pi \cdot (R^4 - r^4)}{4}$ | $k_x = \frac{16 \cdot (2 \cdot r) \cdot ((2 \cdot R)^3 - (2 \cdot r)^3)}{3 \cdot \pi \cdot (2 \cdot R)^4 - (2 \cdot r)^4}$ $k_y = \frac{16 \cdot (2 \cdot r) \cdot ((2 \cdot R)^3 - (2 \cdot r)^3)}{3 \cdot \pi \cdot (2 \cdot R)^4 - (2 \cdot r)^4}$ |
| 6. Semi-Circle |  $A = \frac{\pi \cdot R^2}{2}$ | $\bar{x} = R$ $\bar{y} = \frac{4 \cdot R}{3 \cdot \pi}$ | $Q_x = \frac{2 \cdot 0.532 \cdot R^3}{6}$ $Q_y = \frac{2 \cdot 0.532 \cdot R^3}{6}$ | $I_x = \left(\frac{\pi}{8} - \frac{8}{9 \cdot \pi}\right) \cdot R^4$ $I_y = \frac{\pi \cdot R^4}{8}$ | $k_x = 1.860$ $k_y = 1.698$ |
| 7. Hollow Semi-Circle |  $A = \frac{\pi \cdot (R^2 - r^2)}{2}$ | $\bar{x} = R$ $\bar{y} = 0.4244 \cdot \left(R + \frac{r^2}{R+r}\right)$ | $Q_x = \frac{2 \cdot 0.532 \cdot (R^3 - r^3)}{6}$ $Q_y = \bar{y} \cdot \frac{A}{2}$ | $I_x = \frac{\pi}{8} \cdot (R^4 - r^4) - \pi \cdot \bar{y}^2 \cdot \frac{(R^2 - r^2)}{2}$ $I_y = \frac{\pi}{8} \cdot (R^4 - r^4)$ | $k_x = \frac{2 \cdot Q_x \cdot (R - \bar{y})}{I_x}$ $k_y = \frac{2 \cdot Q_y \cdot \bar{x}}{I_y}$ |
| 8. Ellipse |  $A = \pi \cdot a \cdot b$ | $\bar{x} = a$ $\bar{y} = b$ | $Q_x = \frac{4 \cdot b \cdot A}{6 \cdot \pi}$ $Q_y = \frac{4 \cdot a \cdot A}{6 \cdot \pi}$ | $I_x = \frac{\pi \cdot a \cdot b^3}{4}$ $I_y = \frac{\pi \cdot b \cdot a^3}{4}$ | $k_x = \frac{2 \cdot Q_x \cdot \bar{y}}{I_x}$ $k_y = \frac{2 \cdot Q_y \cdot \bar{x}}{I_y}$ |
| 9. Hollow Ellipse |  $A = \pi \cdot (A \cdot B - a \cdot b)$ | $\bar{x} = a$ $\bar{y} = b$ | | $I_x = \frac{\pi \cdot (a \cdot b^3 - a_i \cdot b_i^3)}{4}$ $I_y = \frac{\pi \cdot (b \cdot a^3 - b_i \cdot a_i^3)}{4}$ | $k_x = \frac{1.698 \cdot (a \cdot b^3 - b \cdot a_i \cdot b_i^2)}{(a \cdot b^3 - a_i \cdot b_i^3)}$ $k_y = \frac{1.698 \cdot (b \cdot a^3 - a \cdot b_i \cdot a_i^2)}{(b \cdot a^3 - b_i \cdot a_i^3)}$ |

| Description | Area | Centroids | First Moment of Area | Second Moment of Area | Plastic Bending Shape Factor |
|---------------------------------|---|--|--|--|--|
| 10. Isosceles Triangle | $A = \frac{d \cdot b}{2}$ | $\bar{x} = 0.5 \cdot b$ $\bar{y} = \frac{2 \cdot d}{3}$ | $Q_x = \frac{b \cdot \bar{y}^2}{3} - \frac{4 \cdot b \cdot d \cdot \bar{y}}{27}$ $Q_y = (\bar{x} - \bar{x} \cdot \frac{\bar{y}}{d}) \cdot \left(\frac{d \cdot b}{4}\right)$ | $I_x = \frac{b \cdot d^3}{36}$ $I_y = \frac{d \cdot b^3}{48}$ | $k_x = \frac{2 \cdot Q_x \cdot \bar{y}}{I_x}$ $k_y = \frac{2 \cdot Q_y \cdot \bar{x}}{I_y}$ |
| 11. Equilateral Triangle | $A = 0.433 \cdot a^2$ | $\bar{x} = 0.5 \cdot a$ $\bar{y} = 0.577 \cdot a$ | $Q_x = \frac{a \cdot \bar{y}^2}{3} - \frac{4 \cdot a^2 \cdot 0.866 \cdot \bar{y}}{27}$ $Q_y = (\bar{x} - \bar{x} \cdot \frac{\bar{y}}{0.866 \cdot a}) \cdot \left(\frac{0.866 \cdot a^2}{4}\right)$ | $I_x = 0.01804 \cdot a^4$ $I_y = 0.01804 \cdot a^4$ | $k_x = \frac{2 \cdot Q_x \cdot \bar{y}}{I_x}$ $k_y = \frac{2 \cdot Q_y \cdot \bar{x}}{I_y}$ |
| 12. Tee Section | $A = t \cdot b + t_w \cdot d$ | $\bar{x} = 0.5 \cdot b$ $\bar{y} = \frac{b \cdot t^2 + t_w \cdot d \cdot (2 \cdot t + d)}{2 \cdot (t \cdot b + t_w \cdot d)}$ | $Q_x = \frac{(d + t) - \bar{y}}{2} \cdot ((d + t) - \bar{y}) \cdot t_w$ $Q_y = \frac{b^2 \cdot t}{8} + \frac{t_w^2 \cdot d}{8}$ | $I_x = \frac{b \cdot (d + t)^3}{3} - \frac{d^3 \cdot (b - t_w)}{3} - A \cdot (d + t - \bar{y})^2$ $I_y = \frac{b^3 \cdot t}{12} + \frac{t_w^3 \cdot d}{12}$ | $k_x = \frac{2 \cdot Q_x \cdot (d + t - \bar{y})}{I_x}$ $k_y = \frac{2 \cdot Q_y \cdot \bar{x}}{I_y}$ |
| 13. Channel Section | $A = t \cdot b + 2 \cdot t_w \cdot d$ | $\bar{x} = 0.5 \cdot b$ $\bar{y} = \frac{b \cdot t^2 + 2 \cdot t_w \cdot d \cdot (2 \cdot t + d)}{2 \cdot (t \cdot b + 2 \cdot t_w \cdot d)}$ | $Q_x = \frac{t^2 \cdot b}{8} + \frac{t_w \cdot d \cdot (t + d - \frac{t_w \cdot d}{b})}{2}$ $Q_y = \frac{b^2 \cdot t}{8} + \frac{t_w \cdot d \cdot (b - t_w)}{8}$ | $I_x = \frac{b \cdot (d + t)^3}{3} - \frac{d^3 \cdot (b - 2 \cdot t_w)}{3} - A \cdot (d + t - \bar{y})^2$ $I_y = \frac{b^3 \cdot (d + t)}{12} - \frac{(b - 2 \cdot t_w)^3 \cdot d}{12}$ | $k_x = \frac{2 \cdot Q_x \cdot (d + t - \bar{y})}{I_x}$ $k_y = \frac{2 \cdot Q_y \cdot \bar{x}}{I_y}$ |

| Description | Area | Centroids | First Moment of Area | Second Moment of Area | Plastic Bending Shape Factor |
|--|---|--|--|--|--|
| 14. Wide Flange Beam with Equal Flanges | <p>$A = 2 \cdot t \cdot b + t_w \cdot d$</p> | $\bar{x} = 0.5 \cdot b$ $\bar{y} = \frac{d}{2} + t$ | $Q_x = \frac{t_w \cdot d^2}{4} + b \cdot t \cdot (d + t)$ $Q_y = \frac{b^2 \cdot t}{2} + \frac{t_w^2 \cdot d}{4}$ | $I_x = \frac{b \cdot (d + 2 \cdot t)^3}{12} - \frac{d^3 \cdot (b - t_w)}{12}$ $I_y = \frac{b^3 \cdot t}{6} - \frac{t_w^3 \cdot d}{12}$ | $k_x = \frac{2 \cdot Q_x \cdot \bar{y}}{I_x}$ $k_y = \frac{2 \cdot Q_y \cdot \bar{x}}{I_y}$ |
| 15. Equal Legged Angle | <p>$A = t \cdot (2 \cdot a - t)$ $b = a - t$</p> | $\bar{x} = 0.7071 \cdot a$ $\bar{y}_1 = \frac{0.7071 \cdot (a^2 + a \cdot t - t^2)}{2 \cdot a - t}$ $\bar{y}_2 = \frac{0.7071 \cdot a^2}{2 \cdot a - t}$ | | $I_x = \frac{a^4 - b^4}{12} - \frac{0.5 \cdot t \cdot a^2 \cdot b^2}{a + b}$ $I_y = \frac{a^4 - b^4}{12}$ | |
| 16. Unequal Legged Angle | <p>$A = t \cdot (d + b - t)$</p> | $\bar{x} = \frac{b^2 + d \cdot t - t^2}{2 \cdot (b + d - t)}$ $\bar{y} = \frac{d^2 + b \cdot t - t^2}{2 \cdot (b + d - t)}$ | | $I_x = \frac{1}{3} \cdot (b \cdot d^3 - (b - t) \cdot (d - t)^3) - A \cdot (d - \bar{y})^2$ $I_y = \frac{1}{3} \cdot (d \cdot b^3 - (d - t) \cdot (b - t)^3) - A \cdot (b - \bar{x})^2$ | |

6.3. Section Properties of a Composite Shape

More complex shapes can be built up from individual rectangular sections. The section property can be calculated for each rectangle and the combined section property calculated for the combination.

The section properties of a composite shape are defined as follows:

$$\bar{y} = \frac{\sum(a \cdot y)}{A}$$

$$\bar{x} = \frac{\sum(a \cdot x)}{A}$$

The total second moment of area of the shape is determined by using the parallel axis theorem (see section 6.1.4) with I' being the 2nd moment of area of each individual component:

$$I_y = \sum I_y' + \sum(x^2 \cdot A)$$

$$I_x = \sum I_x' + \sum(y^2 \cdot A)$$

The solution is best laid out as a table, with a row for each element of the cross section. This is shown in the spreadsheet at the link below:

ABBOTT AEROSPACE SEZC LTD
SPREADSHEETS
 ABBOTTAEROSPACE.COM

AA-SM-001-002 Section Properties - General

The spreadsheet first calculates the combined section properties about the origin:

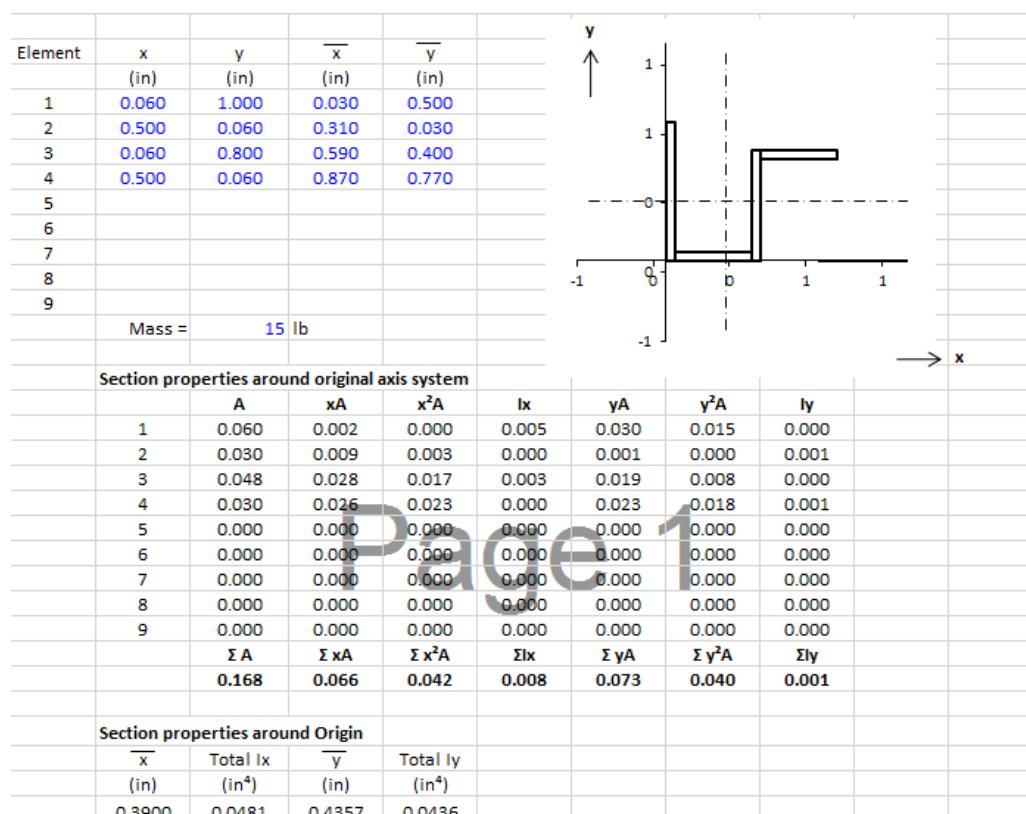


Figure 6.1.5-1: Tabular Calculation of Combined Section Properties about Origin

This table is used to determine the centroid of the combined rectangles.

The spreadsheet then recalculates the section properties about the centroid of the combined rectangles:

| Section Properties About Centroidal Axis Parallel to Original Axis | | | | | | | |
|--|-------|------------|--------------|-------|------------|--------------|-------|
| | A | $\bar{x}A$ | \bar{x}^2A | I_x | $\bar{y}A$ | \bar{y}^2A | I_y |
| 1 | 0.060 | -0.022 | 0.008 | 0.005 | 0.004 | 0.000 | 0.000 |
| 2 | 0.030 | -0.002 | 0.000 | 0.000 | -0.012 | 0.005 | 0.001 |
| 3 | 0.048 | 0.010 | 0.002 | 0.003 | -0.002 | 0.000 | 0.000 |
| 4 | 0.030 | 0.014 | 0.007 | 0.000 | 0.010 | 0.003 | 0.001 |
| 5 | 0.000 | 0.000 | 0.000 | 0.000 | 0.000 | 0.000 | 0.000 |
| 6 | 0.000 | 0.000 | 0.000 | 0.000 | 0.000 | 0.000 | 0.000 |
| 7 | 0.000 | 0.000 | 0.000 | 0.000 | 0.000 | 0.000 | 0.000 |
| 8 | 0.000 | 0.000 | 0.000 | 0.000 | 0.000 | 0.000 | 0.000 |
| 9 | 0.000 | 0.000 | 0.000 | 0.000 | 0.000 | 0.000 | 0.000 |
| ΣA | 0.168 | 0.000 | 0.017 | 0.008 | 0.008 | 0.000 | 0.009 |

| General Properties | | | | | | | |
|--------------------------|---------------------------|----------------------------------|--|--|--|--|--|
| A = | 0.168 in ² | Radius of Gyration | | | | | |
| \bar{x}_{left} = | 0.390 in | $r_x = \sqrt{0.0162 / 0.168}$ | | | | | |
| \bar{x}_{right} = | 0.730 in | = 0.3 in | | | | | |
| \bar{y}_{upper} = | 0.564 in | $r_y = \sqrt{0.0181 / 0.168}$ | | | | | |
| \bar{y}_{lower} = | 0.436 in | = 0.3 in | | | | | |
| Total Height (y) = | 1.000 in | | | | | | |
| Total Width (x) = | 1.120 in | | | | | | |
| Weight Moment of Inertia | | | | | | | |
| I_x = | 15 / 0.168 × 0.0162 | $I_x = 15 / 0.168 \times 0.0162$ | | | | | |
| | = 1.44 lb in ² | = 1.44 lb in ² | | | | | |
| Area Moment of Intertia | | | | | | | |
| I_x = | 0.0162 in ⁴ | $I_y = 15 / 0.168 \times 0.0181$ | | | | | |
| I_y = | 0.0181 in ⁴ | = 1.61 lb in ² | | | | | |
| J = | 0.0343 in ⁴ | $J = 1.61 + 1.44$ | | | | | |
| | | = 3.06 lb in ² | | | | | |

Figure 6.1.5-2: Tabular Calculation of Combined Section Properties about Section Centroidal Axis

There are different spreadsheets that allow analysis of various composite rectangular sections at the links below:

ABBOTT AEROSPACE SEZC LTD
SPREADSHEETS
 ABBOTTAEROSPACE.COM

AA-SM-001-004 Section Properties - General with Angles - moment distribution

ABBOTT AEROSPACE SEZC LTD
SPREADSHEETS
 ABBOTTAEROSPACE.COM

AA-SM-001-005 Section Properties - General with Angles - Really Small Format

ABBOTT AEROSPACE SEZC LTD
SPREADSHEETS
 ABBOTTAEROSPACE.COM

AA-SM-001-006 Section Properties - General with Angles - weighted area - moment distribution

ABBOTT AEROSPACE SEZC LTD
SPREADSHEETS
 ABBOTTAEROSPACE.COM

AA-SM-001-007 Section Properties - General with Angles - weighted area - moment distribution - small format

7. STIFFNESS

7.1. Introduction

Stiffness and the approximation of stiffness for calculation are critical for predicting the performance of structures and mechanisms.

7.2. General Terms

Axial stiffness is reliant on the value of $E \cdot A$

Where:

E Young's modulus of the member material, psi

A Cross sectional area of the member, in²

Bending stiffness is related to the value of $E \cdot I$

Where:

E Young's modulus of the member material, psi

I 2nd moment of area of the bending section, in⁴

Torsional stiffness is related to the value of $G \cdot J$

Where:

G Shear modulus of the member material, psi

J Section torsional constant, in⁴

7.3. Axial or Direct Load Stiffness

Axial or direct load stiffness is expressed in the following way:

$$k = \frac{P}{\delta}$$

Where:

P Force applied, lb

δ Change of length in the direction of the force vector, in

7.3.1. Extensional Stiffness

For a member with a constant cross section the following expression applies:

$$\delta = \frac{P \cdot L}{E \cdot A}$$

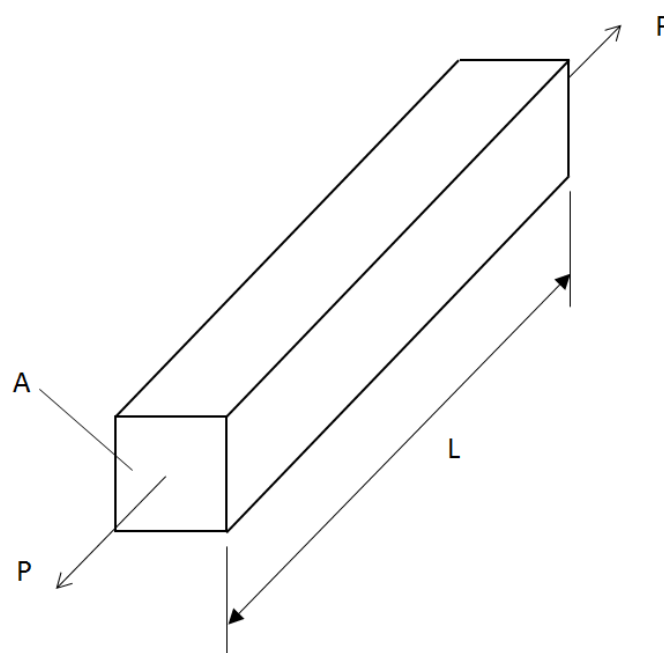


Figure 7.3.1-1: Simple Extensional Stiffness

Where:

δ Change of length in the direction of the force vector, in

P Force applied, lb

L Original length of the member, in

E Young's modulus of the member material, psi

A Cross sectional area of the member, in²

The expression for Stiffness can easily be derived as

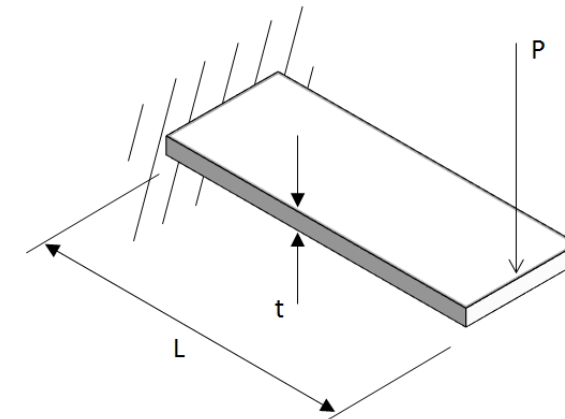
$$k = \frac{E \cdot A}{L}$$

7.3.2. Bending Stiffness

7.3.2.1. Simple Cantilever

The expression will be given in terms of stiffness per unit width:

$$\delta = \frac{4 \cdot P \cdot L^3}{E \cdot t^3}$$



Where:

δ Deflection in the direction of the force vector, in

P Force applied, lb

L Original length of the cantilever beam, in

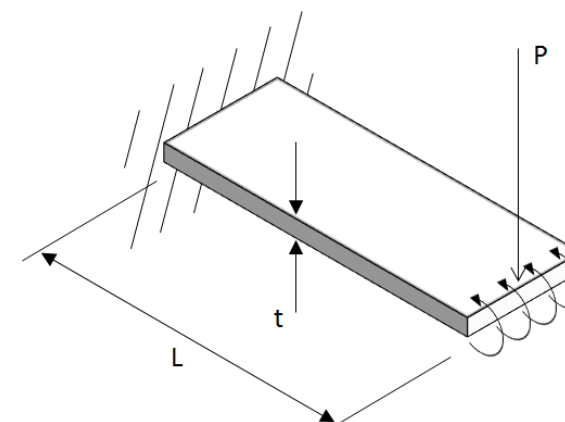
E Young's modulus of the member material, psi

t Thickness of the beam, in

The expression for stiffness per unit width of beam can easily be derived as

$$k = \frac{E \cdot t^3}{4 \cdot L^3}$$

7.3.2.2. Guided Cantilever



The expression will be given in terms of stiffness per unit width:

$$\delta = \frac{P \cdot L^3}{E \cdot t^3}$$

The expression for Stiffness can easily be derived as

$$k = \frac{E \cdot t^3}{L^3}$$

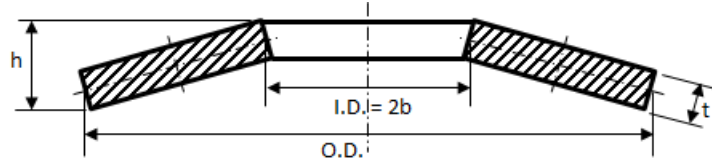


AA-SM-260 Tools - Spring Stiffness of Cantilever Beams

7.3.3. Axial Spring Design

7.3.3.1. Belleville Washer Design

This method is taken from [\(NASA TM X-73305, 1975\)](#) and is a relatively simple method.



Belleville springs are used where space requirements dictate a short range of motion.

The design depends on the following parameters:

| | |
|----------|-------------------------------------|
| P | Load, lb |
| δ | Deflection, in |
| t | Thickness of material, in |
| h | Free height minus thickness, in |
| a | One half of outside diameter, in |
| E | Young's modulus, psi |
| f | Stress at Inside Circumference, psi |
| k | Ratio of O.D./I.D. |
| v | Poisson's Ratio |

M, C₁ and C₂ are constants which can be calculated from the formulas below:

$$M = \frac{6}{\pi \cdot \log_e \cdot k} \cdot \frac{(k-1)^2}{k^2}$$

$$C_1 = \frac{6}{\pi \cdot \log_e \cdot k} \cdot \left[\frac{(k-1)}{\log_e \cdot k} - 1 \right]$$

$$C_2 = \frac{6}{\pi \cdot \log_e \cdot k} \cdot [k-1]$$

The deflection load formula using these constants is:

$$P = \frac{E \cdot \delta}{(1 - v^2) \cdot M \cdot k^2 \cdot b^2} \cdot \left[\left(h - \frac{\delta}{2} \right) \cdot (h - \delta) \cdot t + t^3 \right]$$

The stress formula is as follows:

$$f = \frac{E \cdot \delta}{(1 - v^2) \cdot M \cdot k^2 \cdot b^2} \cdot \left[C_1 \cdot \left(h - \frac{\delta}{2} \right) + C_2 \cdot t \right]$$

In the stress formula, it is possible for the term $\left(h - \frac{\delta}{2} \right)$ to become negative when δ is large. When this occurs the term inside the bracket should be changed to read $\left[C_1 \cdot \left(h - \frac{\delta}{2} \right) - C_2 \cdot t \right]$. Note that the load deflection curve for Belleville washers is not linear.

This is shown in Figure 7.3.3-1.

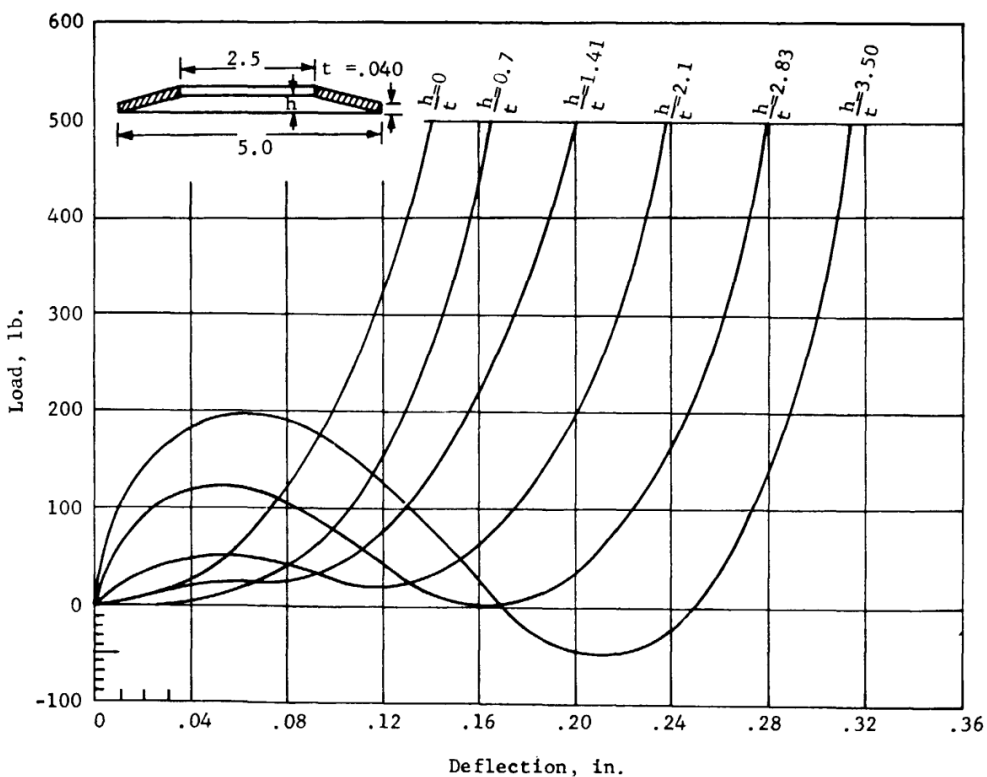


Figure 7.3.3-1: Load Deflection Characteristics of a 0.40in Thick Washer for Various h/t Ratios. [\(NASA TM X-73305, 1975\)](#)

Belleville washers can be stacked to obtain the desired load-deflection characteristics; the accepted methods are shown in the figure below:

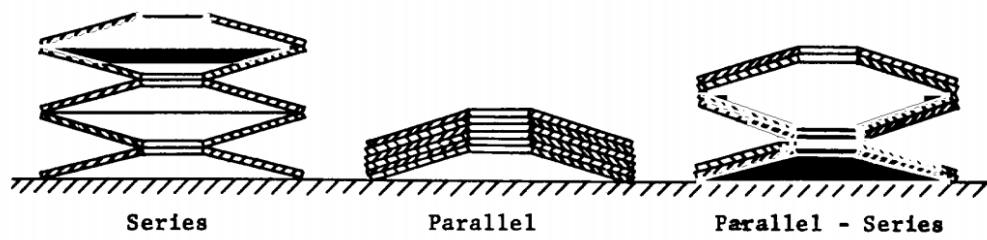


Figure 7.3.3-2: Acceptable Combination of Belleville Washers. [\(NASA TM X-73305, 1975\)](#)

As the number of washers increases so does the friction in the stacks. This may not be uniform and can result in springs which are erratic and difficult to predict.

You can download a spreadsheet for this method at the link below:

ABBOTT AEROSPACE SEZC LTD
SPREADSHEETS
ABBOTTAEROSPACE.COM

AA-SM-042-001 Rev A Stress Analysis - Disc Washer Analysis

7.4. Fastener Shear Stiffness

Fastener shear stiffness or fastener joint stiffness' are often used in bolt group models and finite element models. It is important to note that at best, fastener stiffness values are approximations. The stiffness of a joint and each fastener within the joint depends on many factors including – the condition of the joint surfaces, the clamp-up force in the joint, the clearance of the fasteners in the fastener holes, the material of the fastener, the material of the sheet, the thickness of the sheets, the size of the fastener, the fastener head size, the nut type, whether washers are used, etc.

There are a range of methods of varying complexity to calculate fastener stiffness' for use in joint analyses and they are all approximations.

It is recommended that a relatively simple approach is used.

(NACA-TN-1051, 1946) provides a rational method and experimental derivation for the critical parameters.

The flexibility of a single fastener is given by the following expression:

$$C = \frac{8}{t_{av} \cdot E_{bb}} \cdot \left\{ B_1 \cdot \left(\frac{t_{av}}{D} \right)^2 \cdot \left[B_2 + \left(\frac{t_{av}}{D} \right)^2 \right] + B_3 \right\}$$

Where:

- t_{av} Average joint plate thickness, in (see below)
- E_{bb} Young's modulus of the fastener, psi (see below)
- D Diameter of fastener, in
- B_1 Joint parameter 1 (see table below)
- B_2 Joint parameter 2 (see table below)
- B_3 Joint parameter 3 (see table below)

Average Joint Plate Thickness for a single shear joint:

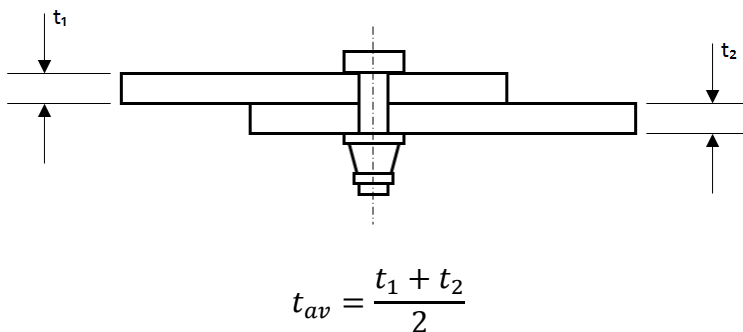


Figure 7.3.3-1: Average Thickness for a Single Shear Joint

Average Joint Plate Thickness for a Double Shear Joint:

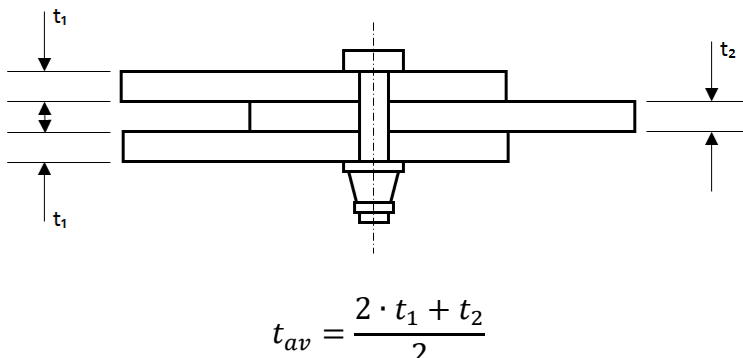


Figure 7.3.3-2: Average Thickness for a Double Shear Joint

| Case | Plate | Strap | Fastener | B ₁ | B ₂ | B ₃ |
|------|----------|----------|----------|----------------|----------------|----------------|
| 1 | Aluminum | Aluminum | Aluminum | 0.130 | 2.120 | 1.000 |
| 2 | Steel | Steel | Steel | 0.130 | 2.120 | 1.000 |
| 3 | Aluminum | Aluminum | Steel | 0.130 | 2.120 | 1.870 |
| 4 | Aluminum | Steel | Steel | 0.130 | 2.120 | 1.430 |
| 5 | Aluminum | Steel | Aluminum | 0.130 | 2.120 | 0.840 |

Table 7.3.3-1 Fastener Stiffness Joint Parameters

You can download a spreadsheet for this method at the link below:

ABBOTT AEROSPACE SEZC LTD
SPREADSHEETS
ABBOTTAEROSPACE.COM
AA-SM-028-001 Fastener Flexibility - NACA Method

7.5. Torsion Stiffness

Axial or direct load stiffness is expressed in the following way:

$$k = \frac{M}{\theta} = G \cdot J$$

Where:

- M** Moment applied, in-lb
- θ** Rotation about the moment axis, radians
- G** Material bulk or shear modulus, psi
- J** Section torsion constant, in⁴

Torsion stiffness, stress and angular deflection for common cross sections are calculated in this spreadsheet:

ABBOTT AEROSPACE SEZC LTD
SPREADSHEETS
ABBOTTAEROSPACE.COM
AA-SM-002-001 Torsion - Regular Sections - Rev B

ADVERT: ENGINEERING SERVICES
LOADS ANALYSIS
CONTACT US ENGINEERING SERVICES

FE Model Loads

ABBOTT AEROSPACE SEZC LTD

8. BEAM ANALYSIS

This section is in part taken from [\(NASA TM X-73305, 1975\)](#) Section B 4.0.0 and [\(AFFDL-TR-69-42, 1986\)](#) Section 1.

8.1. Introduction

Nomenclature:

| | |
|----------|------------------------------------|
| M | Moment, inlb |
| W | Applied Load, lb |
| w | Applied Distributed load, lb/in |
| R | Reaction Load, lb |
| V | Beam Internal Shear Load, lb |
| y | Distance perpendicular to beam, in |
| x | Distance along beam, in |
| θ | Angle of deflection, Radians |

Sign Convention:

1. x is positive to the right
2. y is positive upward
3. M is positive when the top fiber is compressed
4. W is positive in the direction of negative Y
5. V is positive when the part of the beam to the left of the section tends to move upward under the action of the resultant of the vertical force

Limiting Assumptions:

1. The material follows Hooke's law
2. Plane cross sections remain plane
3. Shear deflections are negligible
4. Deflections are small

The general equations relating load, shear, bending moment and deflection are given in the table below. These equations are given in terms of deflection and bending moments.

| Title | Y | M |
|----------------|--|--|
| Deflection | $\Delta = y$ | $\Delta = \iint \frac{M}{E \cdot I} dx dx$ |
| Slope | $\theta = \frac{dx}{dy}$ | $\theta = \int \frac{M}{E \cdot I} dx$ |
| Bending Moment | $M = E \cdot I \cdot \frac{d^2 y}{dx^2}$ | M |
| Shear | $V = E \cdot I \cdot \frac{d^3 y}{dx^3}$ | $V = \frac{dM}{dx}$ |
| Load | $W = E \cdot I \cdot \frac{d^4 y}{dx^4}$ | $V = \frac{dv}{dx} = \frac{d^2 M}{dx^2}$ |

The solutions for various single span beams are given in the tables on the following pages. The spreadsheets give worked examples that show the shear force and bending moment diagrams and a plot of beam deflection.

8.2. Shear and Bending Moment Diagrams

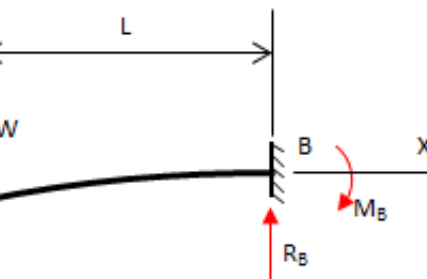
This section will be included in a later edition. This page is a placeholder only.

8.3. Cantilevers

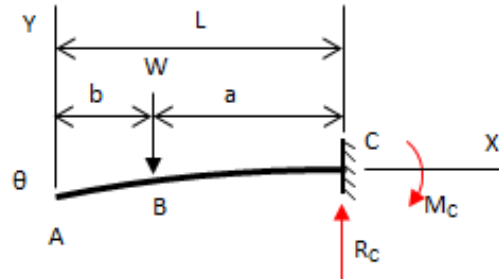
| Type of Loading | Reactions, Vertical Shear, Bending Moments, Deflection and Slope |
|---------------------------------|---|
| Simple Single Span Beams | |
| 1. Point Load at Free End | <p>$R_B = W$ $V = -W$ $M_x = -W \cdot x$ $\text{Max. } M = -W \cdot L \text{ at } B$ $y = -\frac{1}{6} \cdot \frac{W}{E \cdot I} \cdot (x^3 - 3 \cdot L^2 \cdot x + 2 \cdot L^3)$ $\text{Max. } y = -\frac{1}{3} \cdot \frac{W \cdot L^3}{E \cdot I} \text{ at } A$ $\theta = \frac{1}{2} \cdot \frac{W \cdot L^2}{E \cdot I} \text{ at } A$</p> |
| 2. Point Load Mid-Span | <p>$R_C = W$ $(A \text{ to } B) V = 0$ $(B \text{ to } C) V = -W$ $(A \text{ to } B) M = 0$ $(B \text{ to } C) M = -W \cdot (x - b)$ $\text{Max. } M = -W \cdot a \text{ at } C$ $(A \text{ to } B) y = -\frac{1}{6} \cdot \frac{W}{E \cdot I} \cdot (-a^3 + 3 \cdot a^2 \cdot L + 3 \cdot a^2 \cdot x)$ $(B \text{ to } C) y = -\frac{1}{6} \cdot \frac{W}{E \cdot I} \cdot [(x - b)^3 - 3 \cdot a^2 \cdot (x - b) + 2 \cdot a^3]$ $\text{Max. } y = -\frac{1}{6} \cdot \frac{W}{E \cdot I} (3 \cdot a^2 \cdot L - a^3) \text{ at } A$ $\theta = \frac{1}{2} \cdot \frac{W \cdot a^2}{E \cdot I} \text{ at } (A \text{ to } B)$</p> |

AA-SM-026-001 Beam Analysis - Cantilever - Point Load at End

AA-SM-026-002 Beam Analysis - Cantilever - Point Load Mid Span



2. Point Load Mid-Span



| Type of Loading | Reactions, Vertical Shear, Bending Moments, Deflection and Slope |
|-------------------------------------|---|
| 3. Distributed Load over Whole Span | <p>$R_B = W$</p> $V = -\frac{W}{L} \cdot x$ $M_x = -\frac{W}{2 \cdot L} \cdot x^2$ $\text{Max. } M = -\frac{W \cdot L}{2} \text{ at } B$ $y = -\frac{1}{24} \cdot \frac{W}{E \cdot I \cdot L} \cdot (x^4 - 4 \cdot L^3 \cdot x + 3 \cdot L^4)$ $\text{Max. } y = -\frac{1}{8} \cdot \frac{W \cdot L^3}{E \cdot I} \text{ at } A$ $\theta = \frac{1}{6} \cdot \frac{W \cdot L^2}{E \cdot I} \text{ at } A$ <div style="border: 1px solid #ccc; padding: 5px; margin-top: 10px;"> AA-SM-026-003 Beam Analysis - Cantilever - Dist Load Whole Span </div> |
| 4. Distributed Load over Part Span | <p>$R_D = W$</p> $(A \text{ to } B) V = 0$ $(B \text{ to } C) V = -\frac{W}{b-a} \cdot (x - L + b)$ $(C \text{ to } D) V = -W$ $(A \text{ to } B) M = 0$ $(B \text{ to } C) M = -\frac{1}{2} \cdot \frac{W}{b-a} \cdot (x - L + b)^2$ $(C \text{ to } D) M = -\frac{1}{2} \cdot W \cdot (2 \cdot x - 2 \cdot L + a + b)$ $\text{Max. } M = -\frac{W \cdot (a+b)}{2} \text{ at } D$ $(A \text{ to } B) y = -\frac{1}{24} \cdot \frac{W}{E \cdot I} \cdot [4 \cdot (a^2 + a \cdot b + b^2) \cdot (L - x) - a^3 - a \cdot b^2 - a^2 \cdot b - b^3]$ $(B \text{ to } C) y = -\frac{1}{24} \cdot \frac{W}{E \cdot I} \cdot \left[6 \cdot (a+b) \cdot (L-x)^2 - 4 \cdot (L-x)^3 + \frac{(L-x-a)^4}{b-a} \right]$ $(C \text{ to } D) y = -\frac{1}{12} \cdot \frac{W}{E \cdot I} \cdot [3 \cdot (a+b) \cdot (L-x)^2 - 2 \cdot (L-x)^3]$ $\text{Max. } y = -\frac{1}{24} \cdot \frac{W}{E \cdot I} \cdot [4 \cdot (a^2 + a \cdot b + b^2) \cdot (L - x) - a^3 - a \cdot b^2 - a^2 \cdot b - b^3] \text{ at } A$ $\theta = \frac{1}{6} \cdot \frac{W}{E \cdot I} \cdot (a^2 + a \cdot b + b^2) \text{ at } A \text{ to } B$ <div style="border: 1px solid #ccc; padding: 5px; margin-top: 10px;"> AA-SM-026-004 Beam Analysis - Cantilever - Dist Load Part Span </div> |

| Type of Loading | Reactions, Vertical Shear, Bending Moments, Deflection and Slope |
|---|---|
| 5. Triangular Load over Whole Span, Peak at Support | <p>$R_B = W$</p> <p>$V = -\frac{W}{L^2} \cdot x^2$</p> <p>$M_x = -\frac{W}{3 \cdot L^2} \cdot x^3$</p> <p>Max. $M = -\frac{W \cdot L}{3}$ at B</p> <p>$y = -\frac{1}{60} \cdot \frac{W}{E \cdot I \cdot L^2} \cdot (x^5 - 5 \cdot L^4 \cdot x + 4 \cdot L^5)$</p> <p>Max. $y = -\frac{1}{15} \cdot \frac{W \cdot L^3}{E \cdot I}$ at A</p> <p>$\theta = \frac{1}{12} \cdot \frac{W \cdot L^2}{E \cdot I}$ at A</p> <div style="border: 1px solid #ccc; padding: 5px; margin-top: 10px;"> SPREADSHEETS AA-SM-026-005 Beam Analysis - Cantilever - Triangle load Whole Span Peak at Support </div> |
| 6. Triangular Load over Part Span, Peak at Support | <p>$R_D = W$</p> <p>(A to B) $V = 0$</p> <p>(B to C) $V = -\frac{W}{(b-a)^2} \cdot (x - L + b)^2$</p> <p>(C to D) $V = -W$</p> <p>(A to B) $M = 0$, (B to C) $M = -\frac{1}{3} \cdot \frac{W}{(b-a)^2} \cdot (x - L + b)^3$, (C to D) $M = -\frac{1}{3} \cdot W \cdot (3 \cdot x - 3 \cdot L + b + 2 \cdot a)$</p> <p>Max. $M = -\frac{W \cdot (b+2 \cdot a)}{3}$ at D</p> <p>(A to B) $y = -\frac{1}{60} \cdot \frac{W}{E \cdot I} \cdot [(5 \cdot b^2 + 10 \cdot a \cdot b + 15 \cdot a^2) \cdot (L-x) - 4 \cdot a^3 - 2 \cdot a \cdot b^2 - 3 \cdot a^2 \cdot b - b^3]$</p> <p>(B to C) $y = -\frac{1}{60} \cdot \frac{W}{E \cdot I} \cdot \left[(20 \cdot a + 10 \cdot b) \cdot (L-x)^2 - 10 \cdot (L-x)^3 + 5 \cdot \frac{(L-x-a)^4}{b-a} - \frac{(L-x-a)^5}{(b-a)^2} \right]$</p> <p>(C to D) $y = -\frac{1}{6} \cdot \frac{W}{E \cdot I} \cdot [(2 \cdot a + b) \cdot (L-x)^2 - (L-x)^3]$</p> <p>Max. $y = -\frac{1}{60} \cdot \frac{W}{E \cdot I} \cdot [(5 \cdot b^2 + 10 \cdot a \cdot b + 15 \cdot a^2) \cdot (L-x) - 4 \cdot a^3 - 2 \cdot a \cdot b^2 - 3 \cdot a^2 \cdot b - b^3]$ at A</p> <p>$\theta = \frac{1}{12} \cdot \frac{W}{E \cdot I} \cdot (3 \cdot a^2 + 2 \cdot a \cdot b + b^2)$ at A to B</p> <div style="border: 1px solid #ccc; padding: 5px; margin-top: 10px;"> SPREADSHEETS AA-SM-026-006 Beam Analysis - Cantilever - Triangle load Part Span Peak at Support </div> |

| Type of Loading | Reactions, Vertical Shear, Bending Moments, Deflection and Slope |
|--|---|
| 7. Triangular Load over Whole Span, Peak at Free End | <p>$R_B = W$</p> $V = -W \cdot \left(\frac{2 \cdot L \cdot x - x^2}{L^2} \right)$ $M_x = -\frac{W}{3 \cdot L^2} \cdot (3 \cdot L \cdot x^2 - x^3)$ $\text{Max. } M = -\frac{2 \cdot W \cdot L}{3} \text{ at } B$ $y = -\frac{1}{60} \cdot \frac{W}{E \cdot I \cdot L^2} \cdot (-x^5 - 15 \cdot L^4 \cdot x + 5 \cdot L \cdot x^4 + 11 \cdot L^5)$ $\text{Max. } y = -\frac{11}{60} \cdot \frac{W \cdot L^3}{E \cdot I} \text{ at } A$ $\theta = \frac{1}{4} \cdot \frac{W \cdot L^2}{E \cdot I} \text{ at } A$ <div style="border: 1px solid #ccc; padding: 5px; margin-top: 10px;"> ABBOTT AEROSPACE SEZC LTD SPREADSHEETS AA-SM-026-007 Beam Analysis - Cantilever - Triangle load Whole Span Peak at Free End </div> |
| 8. Triangular Load over Part Span, Peak at Free End | <p>$R_D = W$</p> $(A \text{ to } B) V = 0$ $(B \text{ to } C) V = -W \cdot \left[1 - \frac{(L - a - x)^2}{(b - a)^2} \right]$ $(C \text{ to } D) V = -W$ $(A \text{ to } B) M = 0$ $(B \text{ to } C) M = -\frac{1}{3} \cdot W \cdot \left[\frac{3 \cdot (x - L + b)^2}{(b - a)} - \frac{(x - L + b)^3}{(b - a)^2} \right]$ $(C \text{ to } D) M = -\frac{1}{3} \cdot W \cdot (-3 \cdot L + 3 \cdot x + 2 \cdot b + a)$ $\text{Max. } M = -\frac{W \cdot (2 \cdot b + a)}{3} \text{ at } D$ $(A \text{ to } B) y = -\frac{1}{60} \cdot \frac{W}{E \cdot I} \cdot [(5 \cdot a^2 + 10 \cdot a \cdot b + 15 \cdot b^2) \cdot (L - x) - a^3 - 2 \cdot a^2 \cdot b - 3 \cdot a \cdot b^2 - 4 \cdot b^3]$ $(B \text{ to } C) y = -\frac{1}{60} \cdot \frac{W}{E \cdot I} \cdot \left[\frac{(L - x - a)^5}{(b - a)^2} - 10 \cdot (L - x)^3 + (10 \cdot a + 20 \cdot b) \cdot (L - x)^2 \right]$ $(C \text{ to } D) y = -\frac{1}{6} \cdot \frac{W}{E \cdot I} \cdot [(a + 2 \cdot b) \cdot (L - x)^2 - (L - x)^3]$ $\text{Max. } y = -\frac{1}{60} \cdot \frac{W}{E \cdot I} \cdot [(5 \cdot a^2 + 10 \cdot a \cdot b + 15 \cdot b^2) \cdot L - a^3 - 2 \cdot a^2 \cdot b - 3 \cdot a \cdot b^2 - 4 \cdot b^3] \text{ at } A$ $\theta = \frac{1}{12} \cdot \frac{W}{E \cdot I} \cdot (a^2 + 2 \cdot a \cdot b + 3 \cdot b^2) \text{ at } A \text{ to } B$ <div style="border: 1px solid #ccc; padding: 5px; margin-top: 10px;"> ABBOTT AEROSPACE SEZC LTD SPREADSHEETS AA-SM-026-008 Beam Analysis - Cantilever - Triangle load Part Span Peak at Free End </div> |

| Type of Loading | Reactions, Vertical Shear, Bending Moments, Deflection and Slope |
|-----------------------|--|
| 9. Moment at Free End | <p>$R_B = 0$ $V = 0$ $M = M_0$ $\text{Max. } M = M_0$ $y = -\frac{1}{2} \cdot \frac{M_0}{E \cdot I} \cdot (L^2 - 2 \cdot L \cdot x + x^2)$ $\text{Max. } y = -\frac{1}{2} \cdot \frac{M_0 \cdot L^2}{E \cdot I} \text{ at } A$ $\theta = \frac{M_0 \cdot L}{E \cdot I} \text{ at } A$</p> <div style="border: 1px solid #ccc; padding: 5px; margin-top: 10px;"> AA-SM-026-009 Beam Analysis - Cantilever - Moment at Free End </div> |
| 10. Moment Anywhere | <p>$R_C = 0$ $V = 0$ $(A \text{ to } B) M = 0$ $(B \text{ to } C) M = M_0$ $(A \text{ to } B) y = \frac{M_0 \cdot a}{E \cdot I} \cdot \left(L - \frac{a}{2} - x\right)$ $(B \text{ to } C) y = -\frac{1}{2} \cdot \frac{M_0}{E \cdot I} \cdot [(x - L + a)^2 - 2 \cdot a \cdot (x - L + a) + a^2]$ $\text{Max. } y = \frac{M_0 \cdot a}{E \cdot I} \cdot \left(L - \frac{a}{2}\right) \text{ at } A$ $\theta = -\frac{M_0 \cdot a}{E \cdot I} \text{ at } A$</p> <div style="border: 1px solid #ccc; padding: 5px; margin-top: 10px;"> AA-SM-026-010 Beam Analysis - Cantilever - Moment Anywhere </div> |

8.4. Single Span Beams

| Type of Loading | Reactions, Vertical Shear, Bending Moments, Deflection and Slope |
|----------------------------|--|
| 11. Point Load at Mid Span | <p>$R_A = \frac{W}{2}$, $R_C = \frac{W}{2}$</p> <p>$V = \frac{W}{2}$ at A to B, $V = -\frac{W}{2}$ at B to C</p> <p>$M = \frac{W \cdot x}{2}$ at A to B, $M = \frac{W \cdot (L-x)}{2}$ at B to C</p> <p>Max. $M = \frac{W \cdot L}{4}$ at B</p> <p>$y = -\frac{1}{48} \cdot \frac{W}{E \cdot I} \cdot (3 \cdot L^2 \cdot x + 4 \cdot x^3)$ at A to B, $y = -\frac{1}{48} \cdot \frac{W}{E \cdot I} \cdot (3 \cdot L^2 \cdot (L-x) + 4 \cdot (L-x)^3)$ at B to C</p> <p>Max. $y = -\frac{1}{48} \cdot \frac{W \cdot L^3}{E \cdot I}$ at B</p> <p>$\theta = -\frac{1}{16} \cdot \frac{W \cdot L^2}{E \cdot I}$ at A, $\theta = \frac{1}{16} \cdot \frac{W \cdot L^2}{E \cdot I}$ at C</p> |
| 12. Point Load Anywhere | <p>$R_A = \frac{W \cdot b}{L}$, $R_C = \frac{W \cdot a}{L}$</p> <p>$V = \frac{W \cdot b}{L}$, at A to B, $V = -\frac{W \cdot a}{L}$ at B to C</p> <p>$M = \frac{W \cdot b}{L} \cdot x$ at A to B, $M = \frac{W \cdot a}{L} \cdot (L-x)$ at B to C</p> <p>Max. $M = \frac{W \cdot a \cdot b}{L}$ at B</p> <p>$y = \frac{W \cdot b \cdot x}{6 \cdot E \cdot I \cdot L} \cdot (2 \cdot L \cdot (L-x) - b^2 - (L-x)^2)$ at A to B, $y = -\frac{W \cdot a \cdot (L-x)}{6 \cdot E \cdot I \cdot L} \cdot (2 \cdot L \cdot b - b^2 - (L-x)^2)$ at B to C</p> <p>Max. $y = -\frac{W \cdot a \cdot b}{27 \cdot E \cdot I \cdot L} \cdot (a + 2 \cdot b) \cdot \sqrt{3 \cdot a \cdot (a + 2 \cdot b)}$ at $x = \sqrt{\frac{a}{3}}(a + 2 \cdot b)$ when $a > b$</p> <p>$\theta = -\frac{1}{6} \cdot \frac{W}{E \cdot I} \cdot \left(b \cdot L - \frac{b^3}{L}\right)$ at A, $\theta = \frac{1}{6} \cdot \frac{W}{E \cdot I} \cdot \left(2 \cdot b \cdot L + \frac{b^3}{L} - 3 \cdot b^2\right)$ at C</p> |

| Type of Loading | Reactions, Vertical Shear, Bending Moments, Deflection and Slope |
|---|--|
| 13. Simply Supported, Uniformly Distributed Load Entire Length | <p>$R_A = \frac{W}{2}$, $R_B = \frac{W}{2}$</p> $V = \frac{W}{2} \cdot \left(1 - \frac{2 \cdot x}{L}\right)$ $M = \frac{W}{2} \cdot \left(x - \frac{x^2}{L}\right)$ $\text{Max. } M = \frac{W \cdot L}{8} \text{ at } \frac{L}{2}$ $y = \frac{W \cdot x}{24 \cdot E \cdot I \cdot L} \cdot (L^3 - 2 \cdot L \cdot x^2 + x^3)$ $\text{Max. } y = \frac{5 \cdot W \cdot L^3}{384 \cdot E \cdot I} \text{ at } x = \frac{L}{2}$ $\theta = -\frac{W \cdot L^2}{24 \cdot E \cdot I} \text{ at } A, \quad \theta = \frac{W \cdot L^2}{24 \cdot E \cdot I} \text{ at } B$ <div style="border: 1px solid blue; padding: 5px; margin-top: 10px;"> <p>ABBOTT AEROSPACE SEZC LTD SPREADSHEETS ABBOTTAEROSPACE.COM</p> <p>AA-SM-026-013 Beam Analysis - Simply Supported Both Ends - UDL along Entire Length</p> </div> |
| 14. Simply Supported, Uniformly Distributed Load Part Length | <p>$c = b - a$, $d = L - \frac{b}{2} - \frac{a}{2}$, $W = w \cdot c$</p> $R_A = \frac{W \cdot d}{L}, \quad R_D = \frac{W}{L} \cdot \left(a + \frac{c}{2}\right)$ $V = R_A \text{ at } A \text{ to } B, \quad V = R_A - \frac{W \cdot (x - a)}{c} \text{ at } B \text{ to } C, \quad V = R_A - W \text{ at } C \text{ to } D$ $M = R_A \cdot x \text{ at } A \text{ to } B, \quad M = R_A \cdot x - \frac{W \cdot (x - a)^2}{2 \cdot c} \text{ at } B \text{ to } C, \quad M = R_A \cdot x - W \left(x - \frac{a}{2} - \frac{b}{2}\right) \text{ at } C \text{ to } D$ $y = \frac{1}{48 \cdot E \cdot I} \left\{ 8 \cdot R_A \cdot (x^3 - L^2 \cdot x) + W \cdot x \cdot \left[\frac{8 \cdot d^3}{L} - \frac{2 \cdot b \cdot c^2}{L} + \frac{c^3}{L} + 2 \cdot c^2 \right] \right\} \text{ at } A \text{ to } B$ $y = \frac{1}{48 \cdot E \cdot I} \left\{ 8 \cdot R_A \cdot (x^3 - L^2 \cdot x) + W \cdot x \cdot \left[\frac{8 \cdot d^3}{L} - \frac{2 \cdot b \cdot c^2}{L} + \frac{c^3}{L} + 2 \cdot c^2 \right] - \frac{2 \cdot W \cdot (x - a)^4}{c} \right\} \text{ at } B \text{ to } C$ $y = \frac{1}{48 \cdot E \cdot I} \left\{ 8 \cdot R_A \cdot (x^3 - L^2 \cdot x) + W \cdot x \cdot \left[\frac{8 \cdot d^3}{L} - \frac{2 \cdot b \cdot c^2}{L} + \frac{c^3}{L} \right] - 8 \cdot W \cdot \left(x - \frac{a}{2} - \frac{b}{2}\right)^3 + W \cdot (2 \cdot b \cdot c^2 - c^3) \right\} \text{ at } C \text{ to } D$ $\theta = \frac{W}{48 \cdot E \cdot I} \cdot \left\{ -8 \cdot R_A \cdot L^2 + W \cdot \left[\frac{8 \cdot d^3}{L} - \frac{2 \cdot b \cdot c^2}{L} + \frac{c^3}{L} + 2 \cdot c^2 \right] \right\} \text{ at } A$ $\theta = \frac{W}{48 \cdot E \cdot I} \cdot \left\{ 16 \cdot R_A \cdot L^2 + W \cdot \left[24 \cdot d^2 - \frac{8 \cdot d^3}{L} + \frac{2 \cdot b \cdot c^2}{L} - \frac{c^3}{L} \right] \right\} \text{ at } B$ <div style="border: 1px solid blue; padding: 5px; margin-top: 10px;"> <p>ABBOTT AEROSPACE SEZC LTD SPREADSHEETS ABBOTTAEROSPACE.COM</p> <p>AA-SM-026-014 Beam Analysis - Simply Supported Both Ends - UDL Part Span</p> </div> |

| Type of Loading | Reactions, Vertical Shear, Bending Moments, Deflection and Slope |
|---|---|
| 15. Simply Supported, Triangular Load over Whole Span | <p>$R_A = \frac{W}{3}$, $R_B = \frac{2 \cdot W}{3}$</p> $V = W \cdot \left(\frac{1}{3} - \frac{x^2}{L^2} \right)$ $M = \frac{W}{3} \cdot \left(x - \frac{x^3}{L^2} \right)$ $\text{Max. } M = 0.128 \cdot W \cdot L \text{ at } x = \frac{L \cdot \sqrt{3}}{3}$ $y = \frac{-W \cdot x \cdot (3 \cdot x^4 - 10 \cdot L^2 \cdot x^2 + 7 \cdot L^4)}{180 \cdot E \cdot I \cdot L^2}$ $\text{Max. } y = -\frac{0.01304 \cdot W \cdot L^3}{E \cdot I} \text{ at } x = 0.519 \cdot L$ $\theta = -\frac{7 \cdot W \cdot L^2}{180 \cdot E \cdot I} \text{ at } A, \quad \theta = \frac{8 \cdot W \cdot L^2}{180 \cdot E \cdot I} \text{ at } B$ <div style="border: 1px solid #ccc; padding: 5px; margin-top: 10px;"> <p>ABBOTT AEROSPACE SEZC LTD SPREADSHEETS ABBOTTAEROSPACE.COM</p> <p>AA-SM-026-015 Beam Analysis - Simply Supported Both Ends - Triangle Load Whole Span</p> </div> |
| 16. Simply Supported, Triangular Load over Whole Span, Peak at Center | <p>$R_A = \frac{W}{2}$, $R_C = \frac{W}{2}$</p> $V = \frac{W}{2} \cdot \left(1 - \frac{4 \cdot x^2}{L^2} \right) \text{ at } A \text{ to } B, \quad V = -\frac{W}{2} \cdot \left(1 - \frac{4 \cdot (L-x)^2}{L^2} \right) \text{ at } B \text{ to } C$ $M = \frac{W}{6} \cdot \left(3 \cdot x - \frac{4 \cdot x^3}{L^2} \right) \text{ at } A \text{ to } B, \quad M = \frac{W}{6} \cdot \left(3 \cdot (L-x) - \frac{4 \cdot (L-x)^3}{L^2} \right) \text{ at } B \text{ to } C$ $\text{Max. } M = \frac{W \cdot L}{6} \text{ at } B$ $y = \frac{-W \cdot x}{6 \cdot E \cdot I \cdot L^2} \cdot \left(\frac{L^2 \cdot x^2}{2} - \frac{x^4}{5} - \frac{5 \cdot L^4}{16} \right) \text{ at } A \text{ to } B$ $\text{Max. } y = -\frac{W \cdot L^3}{60 \cdot E \cdot I} \text{ at } B$ $\theta = -\frac{5 \cdot W \cdot L^2}{96 \cdot E \cdot I} \text{ at } A, \quad \theta = \frac{5 \cdot W \cdot L^2}{96 \cdot E \cdot I} \text{ at } C$ <div style="border: 1px solid #ccc; padding: 5px; margin-top: 10px;"> <p>ABBOTT AEROSPACE SEZC LTD SPREADSHEETS ABBOTTAEROSPACE.COM</p> <p>AA-SM-026-016 Beam Analysis - Simply Supported Both Ends - Triangle Load Peak at Center</p> </div> |

| Type of Loading | Reactions, Vertical Shear, Bending Moments, Deflection and Slope |
|--|--|
| 17. Simply Supported, Triangular Load over Whole Span, Zero and Middle | <p>$R_A = \frac{W}{2}$, $R_C = \frac{W}{2}$</p> $V = \frac{W}{2} \cdot \left(\frac{L - 2 \cdot x}{L}\right)^2 \text{ at } A \text{ to } B, \quad V = -\frac{W}{2} \cdot \left(\frac{2 \cdot x - L}{L}\right)^2 \text{ at } B \text{ to } C$ $M = \frac{W}{2} \cdot \left(x - \frac{2 \cdot x^2}{L} + \frac{4 \cdot x^3}{3 \cdot L^2}\right) \text{ at } A \text{ to } B, \quad M = \frac{W}{2} \cdot \left((L - x) - \frac{2 \cdot (L - x)^2}{L} + \frac{4 \cdot (L - x)^3}{3 \cdot L^2}\right) \text{ at } B \text{ to } C$ $\text{Max. } M = \frac{W \cdot L}{12} \text{ at } B$ $y = \frac{W}{12 \cdot E \cdot I} \cdot \left(x^3 - \frac{x^4}{L} + \frac{2 \cdot x^5}{5 \cdot L^2} - \frac{3 \cdot L^2 \cdot x}{8}\right) \text{ at } A \text{ to } B$ $\text{Max. } y = -\frac{3 \cdot W \cdot L^3}{320 \cdot E \cdot I} \text{ at } B$ $\theta = -\frac{W \cdot L^2}{32 \cdot E \cdot I} \text{ at } A, \quad \theta = \frac{W \cdot L^2}{32 \cdot E \cdot I} \text{ at } C$ <div style="border: 1px solid blue; padding: 5px; margin-top: 10px;"> <p>ABBOTT AEROSPACE SEZC LTD SPREADSHEETS ABBOTTAEROSPACE.COM</p> <p>AA-SM-026-017 Beam Analysis - Simply Supported Both Ends - Triangle Load Zero at Center</p> </div> |
| 18. Simply Supported, Moment at One End | <p>$R_A = -\frac{M_0}{L}$, $R_B = \frac{M_0}{L}$</p> $V = R_A$ $M = M_0 + R_A \cdot x$ $\text{Max. } M = M_0 \text{ at } A$ $y = \frac{M_0}{6 \cdot E \cdot I} \cdot \left(3 \cdot x^2 - \frac{x^3}{L} - 2 \cdot L \cdot x\right)$ $\text{Max. } y = -0.0642 \cdot \frac{M_0 \cdot L^2}{E \cdot I} \text{ at } x = 0.422 \cdot L$ $\theta = -\frac{M_0 \cdot L}{3 \cdot E \cdot I} \text{ at } A, \quad \theta = \frac{M_0 \cdot L}{6 \cdot E \cdot I} \text{ at } B$ <div style="border: 1px solid blue; padding: 5px; margin-top: 10px;"> <p>ABBOTT AEROSPACE SEZC LTD SPREADSHEETS ABBOTTAEROSPACE.COM</p> <p>AA-SM-026-018 Beam Analysis - Simply Supported Both Ends - Moment at End</p> </div> |

| Type of Loading | Reactions, Vertical Shear, Bending Moments, Deflection and Slope |
|---|--|
| 19. Simply Supported, Moment at Any Point | <p>Diagram shows a beam of length L supported by pin joints at A and C. A clockwise moment M_0 is applied at point B, which is a distance a from joint A. The beam has a deflection curve. Reactions at A and C are R_A and R_C respectively. Angles at A and C are θ_A and θ_C.</p> <p>Equations:</p> $R_A = -\frac{M_0}{L}, \quad R_C = \frac{M_0}{L}$ $V = R_A$ $M = +R_A \cdot x \text{ at } A \text{ to } B, \quad M = M_0 + R_A \cdot x \text{ at } B \text{ to } C$ $\text{Max. positive } M = R_A \cdot a \text{ just right of } B$ $y = \frac{M_0}{6 \cdot E \cdot I} \cdot \left[\left(6 \cdot a - \frac{3 \cdot a^2}{L} - 2 \cdot L \right) \cdot x - \frac{x^3}{L} \right] \text{ at } A \text{ to } B$ $y = \frac{M_0}{6 \cdot E \cdot I} \cdot \left[3 \cdot a^2 + 3 \cdot x^2 - \frac{x^3}{L} - \left(2 \cdot L + \frac{3 \cdot a^2}{L} \right) \cdot x \right] \text{ at } B \text{ to } C$ $\theta = -\frac{M_0}{6 \cdot E \cdot I} \cdot \left(2 \cdot L - 6 \cdot a + \frac{3 \cdot a^2}{L} \right) \text{ at } A, \quad \theta = \frac{M_0}{6 \cdot E \cdot I} \cdot \left(L - \frac{3 \cdot a^2}{L} \right) \text{ at } C$ $\theta = \frac{M_0}{E \cdot I} \cdot \left(a - \frac{a^2}{L} - \frac{L}{3} \right) \text{ at } B$ <div style="border: 1px solid blue; padding: 5px; margin-top: 10px;"> <p>ABBOTT AEROSPACE SEZC LTD SPREADSHEETS ABBOTTAEROSPACE.COM</p> <p>AA-SM-026-019 Beam Analysis - Simply Supported Both Ends - Moment Anywhere</p> </div> |
| 20. Simply Supported, Load at Overhang | <p>Diagram shows a beam of total length L supported by pin joints at A and C. The beam has an overhang of length b beyond joint C. A downward load W is applied at the free end C. The beam has a deflection curve. Reactions at A and C are R_A and R_B respectively. Angles at A and C are θ_A and θ_C.</p> <p>Equations:</p> $R_A = -\frac{W \cdot b}{a}, \quad R_B = \frac{W \cdot L}{a}$ $V = +R_A \text{ at } A \text{ to } B, \quad V = +W \text{ at } B \text{ to } C$ $M = +R_A \cdot x \text{ at } A \text{ to } B, \quad M = R_A \cdot a + W \cdot (x - a) \text{ at } B \text{ to } C$ $\text{Max. } M = +R_A \cdot a \text{ at } B$ $y = -\frac{W \cdot b \cdot x}{6 \cdot a \cdot E \cdot I} \cdot (x^2 - a^2) \text{ at } A \text{ to } B$ $y = -\frac{W}{6 \cdot E \cdot I} \cdot [(L - x)^3 - b \cdot (L - x) \cdot (2 \cdot L - b) + 2 \cdot b^2 \cdot L] \text{ at } B \text{ to } C$ $\text{Max. } y = -\frac{W \cdot b^2 \cdot L}{3 \cdot E \cdot I} \text{ at } C$ $\theta = \frac{W \cdot a \cdot b}{6 \cdot E \cdot I} \text{ at } A, \quad \theta = -\frac{W \cdot a \cdot b}{3 \cdot E \cdot I} \text{ at } B, \quad \theta = -\frac{W \cdot b}{6 \cdot E \cdot I} \cdot (2 \cdot L + b) \text{ at } C$ <div style="border: 1px solid blue; padding: 5px; margin-top: 10px;"> <p>ABBOTT AEROSPACE SEZC LTD SPREADSHEETS ABBOTTAEROSPACE.COM</p> <p>AA-SM-026-020 Beam Analysis - Simply Supported With Overhang - Load at free end</p> </div> |

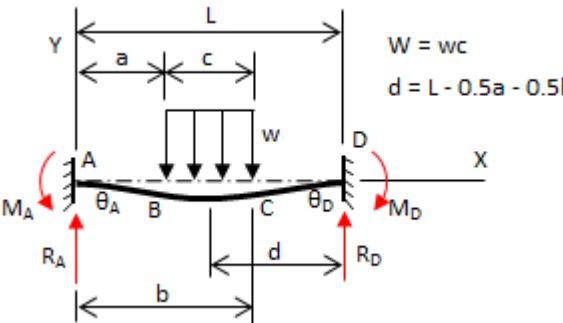
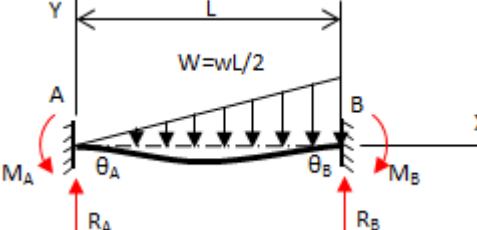
| Type of Loading | Reactions, Vertical Shear, Bending Moments, Deflection and Slope |
|--|--|
| 21. Fixed and Simply Supported, Point Load Anywhere | <p>$R_A = \frac{W}{2} \left(\frac{3 \cdot a^2 \cdot L - a^3}{L^3} \right), \quad R_C = W - R_A$</p> <p>$V = +R_A \text{ at } A \text{ to } B, \quad V = R_A - W \text{ at } B \text{ to } C$</p> <p>$M = +R_A \cdot x \text{ at } A \text{ to } B, \quad M = R_A \cdot x - W \cdot (x - L + a) \text{ at } B \text{ to } C$</p> <p>$M_C = \frac{W}{2} \left(\frac{a^3 + 2 \cdot a \cdot L^2 - 3 \cdot a^2 \cdot L}{L^2} \right)$</p> <p>$\text{Max } (-M) = -M_C \text{ at } C$</p> <p>$\text{max possible value} = -0.1927 \cdot W \cdot L, \quad \text{when } a = 0.4277 \cdot L$</p> <p>$y = \frac{1}{6 \cdot E \cdot I} \cdot [R_A \cdot (x^3 - 3 \cdot L^2 \cdot x) + 3 \cdot W \cdot a^2 \cdot x] \text{ at } A \text{ to } B$</p> <p>$y = \frac{1}{6 \cdot E \cdot I} \cdot [R_A \cdot (x^3 - 3 \cdot L^2 \cdot x) + W \cdot (3 \cdot a^2 \cdot x - (x - b)^3)] \text{ at } B \text{ to } C$</p> <p>If $a < 0.586 \cdot L$, maximum y is between A and B at $x = L \cdot \sqrt{1 - \frac{2 \cdot L}{3 \cdot L - a}}$</p> <p>If $a > 0.586 \cdot L$, maximum y is at $x = \frac{L \cdot (L^2 + b^2)}{3 \cdot L^2 - b^2}$</p> <p>If $a = 0.586 \cdot L$, maximum possible y is at B and $= -0.0098 \cdot \frac{W \cdot L^3}{E \cdot I}$</p> <p>$\theta = \frac{W}{4 \cdot E \cdot I} \cdot \left(\frac{a^3}{L} - a^2 \right) \text{ at } A$</p> |
| 22. Fixed and Simply Supported, UDL Over Entire Length | <p>$R_A = \frac{3 \cdot W}{8}, \quad R_B = \frac{5 \cdot W}{8}$</p> <p>$V = W \cdot \left(\frac{3}{8} - \frac{x}{L} \right)$</p> <p>$M = W \cdot \left(\frac{3 \cdot x}{8} - \frac{x^2}{2 \cdot L} \right)$</p> <p>$\text{Max } (+M) = \frac{9 \cdot W \cdot L}{128} \text{ at } x = \frac{3 \cdot L}{8}, \quad \text{Max } (-M) = \frac{W \cdot L}{8} \text{ at } B$</p> <p>$y = \frac{1}{48 \cdot E \cdot I \cdot L} \cdot [3 \cdot L \cdot x^3 - 2 \cdot x^4 - L^3 \cdot x], \quad \text{Max } y = -0.0054 \cdot \frac{W \cdot L^3}{E \cdot I} \text{ at } x = 0.4215 \cdot L$</p> <p>$\theta = -\frac{W \cdot L^2}{48 \cdot E \cdot I} \text{ at } A$</p> |

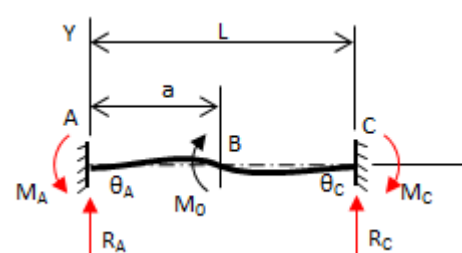
| Type of Loading | Reactions, Vertical Shear, Bending Moments, Deflection and Slope |
|--|--|
| 23. Fixed and Simply Supported, UDL Over Part Span | <p>AA-SM-026-023 Beam Analysis - Fixed and Simply Supported Ends UDL Part Span</p> $R_A = \frac{W}{8 \cdot L^3} \cdot [4 \cdot L \cdot (a^2 + a \cdot b + b^2) - a^3 - a \cdot b^2 - a^2 \cdot b - b^3], \quad R_D = W - R_A$ $V = R_A \quad \text{at } A \text{ to } B,$ $V = R_A - W \cdot \left(\frac{x-d}{c} \right) \quad \text{at } B \text{ to } C$ $V = R_A - W \quad \text{at } C \text{ to } D$ $M = R_A \cdot x \quad \text{at } A \text{ to } B,$ $M = R_A \cdot x - \frac{W \cdot (x-d)^2}{2 \cdot c} \quad \text{at } B \text{ to } C$ $M = R_A \cdot x - W \cdot \left(x - d - \frac{c}{2} \right) \quad \text{at } C \text{ to } D$ $\text{Max } (+M) = R_A \cdot \left(d + \frac{R_A \cdot c}{2 \cdot W} \right) \text{ at } x = \left(d + \frac{R_A \cdot c}{W} \right), \quad \text{Max } (-M) = M_D = -R_A \cdot L + \frac{W}{2} (a+b)$ $y = \frac{1}{E \cdot I} \cdot \left[R_A \cdot \left(\frac{x^3}{6} - \frac{L^2 \cdot x}{2} \right) + W \cdot x \cdot \left(\frac{a^2}{2} + \frac{a \cdot c}{2} + \frac{c^2}{6} \right) \right] \quad \text{at } A \text{ to } B$ $y = \frac{1}{E \cdot I} \cdot \left[R_A \cdot \left(\frac{x^3}{6} - \frac{L^2 \cdot x}{2} \right) + W \cdot x \cdot \left(\frac{a^2}{2} + \frac{a \cdot c}{2} + \frac{c^2}{6} \right) - \frac{W \cdot (x-d)^4}{24 \cdot c} \right] \quad \text{at } B \text{ to } C$ $y = \frac{1}{E \cdot I} \cdot \left[R_A \cdot \left(\frac{x^3}{6} - \frac{L^2 \cdot x}{2} + \frac{L^3}{3} \right) + W \cdot \left\{ \frac{1}{6} \cdot \left(a + \frac{c}{2} \right)^3 - \frac{1}{2} \left(a + \frac{c}{2} \right)^2 \cdot L - \frac{1}{6} \cdot \left(x - d - \frac{c}{2} \right)^3 + \frac{1}{2} \cdot \left(a + \frac{c}{2} \right)^2 \cdot x \right\} \right] \quad \text{at } C \text{ to } D$ $\theta = -\frac{1}{E \cdot I} \cdot \left[\frac{R_A \cdot L^2}{2} - W \cdot \left(\frac{a^2}{2} + \frac{a \cdot c}{2} + \frac{c^2}{6} \right) \right] \quad \text{at } A$ |

| Type of Loading | Reactions, Vertical Shear, Bending Moments, Deflection and Slope |
|--|---|
| 24. Fixed and Simply Supported, Triangle Load over Whole Span. Peak at Fixed Support | <p>$R_A = \frac{W}{5}$, $R_B = \frac{4 \cdot W}{5}$</p> <p>$V = W \cdot \left(\frac{1}{5} - \frac{x^2}{L^2} \right)$</p> <p>$M = W \cdot \left(\frac{x}{5} - \frac{x^3}{3 \cdot L^2} \right)$</p> <p>Max. $M = 0.06 \cdot W \cdot L$ at $x = 0.4474 \cdot L$</p> <p>$y = \frac{W}{60 \cdot E \cdot I \cdot L} \cdot \left(2 \cdot L \cdot x^3 - L^3 \cdot x - \frac{x^5}{L} \right)$</p> <p>Max. $y = -0.00477 \cdot \frac{W \cdot L^3}{E \cdot I}$ at $x = L \cdot \sqrt{\frac{1}{5}}$</p> <p>$\theta = -\frac{W \cdot L^2}{60 \cdot E \cdot I}$ at A</p> <div style="border: 1px solid #ccc; padding: 5px; margin-top: 10px;"> <small>ABBOTT AEROSPACE SEZC LTD AA-SM-026-024 Beam Analysis - Fixed and Simply Supported Ends Triangle Load Whole Span - Peak at Fixed</small> </div> |
| 25. Fixed and Simply Supported, Moment Anywhere | <p>$R_A = -\frac{3 \cdot M_0}{2 \cdot L} \cdot \left(\frac{L^2 + a^2}{L^2} \right)$, $R_C = \frac{3 \cdot M_0}{2 \cdot L} \cdot \left(\frac{L^2 + a^2}{L^2} \right)$</p> <p>$V = R_A$ at A to B,</p> <p>$V = R_C$ at B to C, note that this term for V is corrected from the source material</p> <p>$M = R_A \cdot x$ at A to B,</p> <p>$M = R_A \cdot x + M_0$ at B to C</p> <p>Max. $(+M) = M_0 \cdot \left[1 - \frac{3 \cdot a \cdot (L^2 - a^2)}{2 \cdot L^3} \right]$</p> <p>$y = \frac{M_0}{E \cdot I} \cdot \left[\frac{L^2 - a^2}{4 \cdot L^3} \cdot (3 \cdot L^2 \cdot x - x^3) - (L - a) \cdot x \right]$ at A to B</p> <p>$y = \frac{M_0}{E \cdot I} \cdot \left[\frac{L^2 - a^2}{4 \cdot L^3} \cdot (3 \cdot L^2 \cdot x - x^3) - L \cdot x + \frac{x^2 + a^2}{2} \right]$ at B to C</p> <p>$\theta = \frac{M_0}{E \cdot I} \cdot \left(a - \frac{L}{4} - \frac{3 \cdot a^2}{4 \cdot L} \right)$ at A</p> <div style="border: 1px solid #ccc; padding: 5px; margin-top: 10px;"> <small>ABBOTT AEROSPACE SEZC LTD ISpreadsheets AA-SM-026-025 Beam Analysis - Fixed and Simply Supported Ends Moment Anywhere</small> </div> |

| Type of Loading | Reactions, Vertical Shear, Bending Moments, Deflection and Slope |
|---|--|
| 26. Fixed and Simply Supported, Triangle Load over Whole Span. Peak at Simple Support | <p>$R_A = \frac{11 \cdot W}{20}, \quad R_B = \frac{9 \cdot W}{20}$</p> $V = W \cdot \left(\frac{11}{20} - \frac{2 \cdot x}{L} + \frac{x^2}{L^2} \right)$ $M = W \cdot \left(\frac{11 \cdot x}{20} - \frac{x^2}{L} + \frac{x^3}{3 \cdot L^2} \right)$ $\text{Max. } (+M) = 0.0846 \cdot W \cdot L \text{ at } x = 0.329 \cdot L$ $\text{Max. } (-M) = -\frac{7}{60} \cdot W \cdot L \text{ at } B$ $y = \frac{W}{120 \cdot E \cdot I \cdot L} \cdot \left(11 \cdot L \cdot x^3 - 3 \cdot L^3 \cdot x - 10 \cdot x^4 + \frac{2 \cdot x^5}{L} \right)$ $\text{Max. } y = -0.00609 \cdot \frac{W \cdot L^3}{E \cdot I} \text{ at } x = 0.402 \cdot L$ $\theta = -\frac{W \cdot L^2}{40 \cdot E \cdot I} \text{ at } A$ <div style="border: 1px solid #ccc; padding: 5px; margin-top: 10px;"> SPREADSHEETS AA-SM-026-026 Beam Analysis - Fixed and Simply Supported Ends Triangle Load Whole Span - Peak at SS </div> |
| 27. Fixed and Simply Supported, Moment at Simple Support | <p>$R_A = -\frac{3 \cdot M_0}{2 \cdot L}, \quad R_B = \frac{3 \cdot M_0}{2 \cdot L}$</p> $V = -\frac{3 \cdot M_0}{2 \cdot L}$ $M = \frac{M_0}{2} \cdot \left(2 - \frac{3 \cdot x}{L} \right)$ $\text{Max. } (+M) = M_0 \text{ at } A, \quad \text{Max. } (-M) = -\frac{M_0}{2} \text{ at } B$ $y = \frac{M_0}{4 \cdot E \cdot I} \cdot \left[2 \cdot x^2 - \frac{x^3}{L} - L \cdot x \right]$ $\text{Max. } y = -\frac{M_0 \cdot L^2}{27 \cdot E \cdot I} \text{ at } x = \frac{L}{3}$ $\theta = \frac{M_0 \cdot L}{4 \cdot E \cdot I} \text{ at } A$ <div style="border: 1px solid #ccc; padding: 5px; margin-top: 10px;"> SPREADSHEETS AA-SM-026-027 Beam Analysis - Fixed and Simply Supported Ends Moment at SS </div> |

| Type of Loading | Reactions, Vertical Shear, Bending Moments, Deflection and Slope |
|--|---|
| 28. Fixed both Ends, Point Load Mid-Span | <p>$R_A = \frac{W}{2}$, $R_C = \frac{W}{2}$</p> <p>$V = \frac{W}{2}$ at A to B, $V = -\frac{W}{2}$ at B to C</p> <p>$M = \frac{W \cdot (4 \cdot x - L)}{8}$ at A to B, $M = \frac{W \cdot (3 \cdot L - 4 \cdot x)}{8}$ at B to C</p> <p>Max. $M = \frac{W \cdot L}{8}$ at B</p> <p>$y = -\frac{1}{48} \cdot \frac{W}{E \cdot I} \cdot (3 \cdot L \cdot x^2 - 4 \cdot x^3)$ at A to B, $y = -\frac{1}{48} \cdot \frac{W}{E \cdot I} \cdot (3 \cdot L \cdot (L-x)^2 - 4 \cdot (L-x)^3)$ at B to C</p> <p>Max. $y = -\frac{1}{192} \cdot \frac{W \cdot L^3}{E \cdot I}$ at B</p> <div style="border: 1px solid #ccc; padding: 5px; margin-top: 10px;"> <p>ABBOTT AEROSPACE SEZC LTD SPREADSHEETS ABBOTTAEROSPACE.COM</p> <p>AA-SM-026-028 Beam Analysis - Fixed Both Ends - Point Load Mid Span</p> </div> |
| 29. Fixed both Ends, Point Load Anywhere | <p>$R_A = \frac{W \cdot b^2}{L^3} \cdot (3 \cdot a + b)$, $R_C = \frac{W \cdot a^2}{L^3} \cdot (3 \cdot b + a)$</p> <p>$V = R_A$ at A to B, $V = R_A - W$ at B to C</p> <p>$M = -\frac{W \cdot a \cdot b^2}{L^2} + R_A \cdot x$ at A to B, $M = -\frac{W \cdot a \cdot b^2}{L^2} + R_A \cdot x - W \cdot (x-a)$ at B to C</p> <p>Max. $(+M) = -\frac{W \cdot a \cdot b^2}{L^2} + R_A \cdot a$ at B</p> <p>$y = \frac{W \cdot b^2 \cdot x^2}{6 \cdot E \cdot I \cdot L^3} \cdot (3 \cdot a \cdot x + b \cdot x - 3 \cdot a \cdot L)$ at A to B, $y = \frac{W \cdot a^2 \cdot (L-x)^2}{6 \cdot E \cdot I \cdot L^3} \cdot [(3 \cdot b + a) \cdot (L-x) - 3 \cdot b \cdot L]$ at B to C</p> <div style="border: 1px solid #ccc; padding: 5px; margin-top: 10px;"> <p>ABBOTT AEROSPACE SEZC LTD SPREADSHEETS ABBOTTAEROSPACE.COM</p> <p>AA-SM-026-029 Beam Analysis - Fixed Both Ends - Point Load Anywhere</p> </div> |
| 30. Fixed both Ends, UDL | <p>$R_A = \frac{W}{2}$, $R_B = \frac{W}{2}$</p> <p>$V = \frac{W}{2} \cdot \left(1 - \frac{2 \cdot x}{L}\right)$</p> <p>$M = \frac{W}{2} \cdot \left(x - \frac{x^2}{L} - \frac{L}{6}\right)$</p> <p>$M_A = \frac{W \cdot L}{12}$, $M_B = \frac{W \cdot L}{12}$</p> <p>$y = -\frac{W \cdot x^2}{24 \cdot E \cdot I \cdot L} \cdot (2 \cdot L \cdot x - L^2 - x^2)$</p> <div style="border: 1px solid #ccc; padding: 5px; margin-top: 10px;"> <p>ABBOTT AEROSPACE SEZC LTD SPREADSHEETS ABBOTTAEROSPACE.COM</p> <p>AA-SM-026-030 Beam Analysis - Fixed Both Ends - UDL along Entire Length</p> </div> |

| Type of Loading | Reactions, Vertical Shear, Bending Moments, Deflection and Slope |
|--|--|
| 31. Fixed both Ends, UDL Part Span | <p></p> <p>$W = w_c$ $d = L - 0.5a - 0.5b$</p> <p>$R_A = \frac{W}{4 \cdot L^2} \cdot \left(12 \cdot d^2 - \frac{8 \cdot d^3}{L} + \frac{2 \cdot b \cdot c^2}{L} - \frac{c^3}{L} - c^2 \right), \quad R_D = W - R_A$</p> <p>$M_A = -\frac{W}{24 \cdot L} \cdot \left(\frac{24 \cdot d^3}{L} - \frac{6 \cdot b \cdot c^2}{L} + \frac{3 \cdot c^3}{L} + 4 \cdot c^2 - 24 \cdot d^2 \right)$</p> <p>$M_D = \frac{W}{24 \cdot L} \cdot \left(\frac{24 \cdot d^3}{L} - \frac{6 \cdot b \cdot c^2}{L} + \frac{3 \cdot c^3}{L} + 2 \cdot c^2 - 48 \cdot d^2 + 24 \cdot d \cdot L \right)$</p> <p>$V = R_A \text{ at } A \text{ to } B, \quad V = R_A - W \cdot \frac{x-a}{c} \text{ at } B \text{ to } C, \quad V = R_A - W \text{ at } C \text{ to } D$</p> <p>$M = -M_A + R_A \cdot x \text{ at } A \text{ to } B, \quad M = -M_A + R_A \cdot x - W \cdot \frac{(x-a)^2}{2 \cdot c} \text{ at } B \text{ to } C,$</p> <p>$M = -M_A + R_A \cdot x - W \cdot (x-L+d) \text{ at } C \text{ to } D$</p> <p>$y = \frac{1}{6 \cdot E \cdot I} \cdot (R_A \cdot x^3 - 3 \cdot M_A \cdot x^2) \text{ at } A \text{ to } B$</p> <p>$y = \frac{1}{6 \cdot E \cdot I} \cdot \left(R_A \cdot x^3 - 3 \cdot M_A \cdot x^2 - \frac{W \cdot (x-a)^4}{4 \cdot c} \right) \text{ at } B \text{ to } C$</p> <p>$y = \frac{1}{6 \cdot E \cdot I} \cdot (R_D \cdot (L-x)^3 - 3 \cdot M_D \cdot (L-x)^2) \text{ at } C \text{ to } D$</p> <p style="text-align: right;">AA-SM-026-031 Beam Analysis - Fixed Both Ends - UDL Part Span</p> |
| 32. Fixed both Ends, Triangle Load Full Span | <p></p> <p>$R_A = \frac{3 \cdot W}{10}, \quad R_B = \frac{7 \cdot W}{10}$</p> <p>$M_A = \frac{W \cdot L}{15}, \quad M_B = \frac{W \cdot L}{10}$</p> <p>$V = W \cdot \left(\frac{3}{10} - \frac{x^2}{L^2} \right)$</p> <p>$M = W \cdot \left(\frac{3 \cdot x}{10} - \frac{x^3}{3 \cdot L^2} - \frac{L}{15} \right), \quad \max(M) = 0.043 \cdot W \cdot L \text{ at } x = 0.548 \cdot L$</p> <p>$y = -\frac{W}{60 \cdot E \cdot I} \cdot \left(3 \cdot x^3 - 2 \cdot L \cdot x^2 - \frac{x^5}{L^2} \right), \quad \max y = -0.002617 \cdot \frac{W \cdot L^3}{E \cdot I} \text{ at } x = 0.525 \cdot L$</p> <p style="text-align: right;">AA-SM-026-032 Beam Analysis - Fixed Both Ends - Triangle Load Whole Span</p> |

| Type of Loading | Reactions, Vertical Shear, Bending Moments, Deflection and Slope |
|--------------------------------------|---|
| 33. Fixed both Ends, Moment Anywhere | <p>Reactions, Vertical Shear, Bending Moments, Deflection and Slope</p> <p>AA-SM-026-033 Beam Analysis - Fixed Both Ends - Moment Anywhere</p>  $R_A = -\frac{6 \cdot M_0}{L^3} \cdot (a \cdot L - a^2), \quad R_C = \frac{6 \cdot M_0}{L^3} \cdot (a \cdot L - a^2)$ $M_A = -\frac{M_0}{L^2} \cdot (4 \cdot L \cdot a - 3 \cdot a^2 - L^2), \quad M_C = \frac{M_0}{L^2} \cdot (2 \cdot L \cdot a - 3 \cdot a^2)$ $V = R_A$ $M = -M_A + R_A \cdot x \text{ at } A \text{ to } B, \quad M = -M_A + R_A \cdot x + M_0 \text{ at } B \text{ to } C$ $y = \frac{1}{6 \cdot E \cdot I} \cdot (3 \cdot M_A \cdot x^2 - R_A \cdot x^3) \text{ at } A \text{ to } B$ $y = \frac{1}{6 \cdot E \cdot I} \cdot ((M_0 - M_A) \cdot (3 \cdot x^2 - 6 \cdot L \cdot x + 3 \cdot L^2) - R_A \cdot (3 \cdot L^2 \cdot x - x^3 - 2 \cdot L^3)) \text{ at } B \text{ to } C$ |

8.5. Multi-span Beams

Reserved

8.6. Curved Beams

Reserved

8.7. Other Bending Analyses

8.7.1. Particular Solution of Bents and Semicircular Arches

This section is taken from [\(NASA TM X-73305, 1975\)](#) section B 5.1.4.

| Configuration | Reactions, Vertical Shear, Bending Moments, Deflection and Slope |
|---|--|
| 1. Vertical Concentrated Load, Simple Support | <p></p> $K = \frac{I_2 \cdot h}{I_1 \cdot L}$ $V_A = \frac{Q \cdot b}{L}, \quad V_E = Q - V_A$ $H = \frac{3 \cdot Q \cdot a \cdot b}{2 \cdot L \cdot h \cdot (2 \cdot K + 3)}$ <div style="border: 1px solid #ccc; padding: 5px; margin-top: 10px;"> SPREADSHEETS AA-SM-026-041 Beam Analysis - Framework - Vertical Concentrated Load Simple Support </div> |
| 2. Vertical Concentrated Load, Fixed Support | <p></p> $K = \frac{I_2 \cdot h}{I_1 \cdot L}$ $V_A = \frac{Q \cdot b}{L} \cdot \left[1 + \frac{a \cdot (b - a)}{L^2 \cdot (6 \cdot K + 1)} \right], \quad V_E = Q - V_A$ $H = \frac{3 \cdot Q \cdot a \cdot b}{2 \cdot L \cdot h \cdot (2 \cdot K + 3)}$ $M_A = \frac{Q \cdot a \cdot b}{L} \cdot \left[\frac{1}{2 \cdot (K + 2)} - \frac{(b - a)}{2 \cdot L \cdot (6 \cdot K + 1)} \right]$ $M_E = \frac{Q \cdot a \cdot b}{L} \cdot \left[\frac{1}{2 \cdot (K + 2)} + \frac{(b - a)}{2 \cdot L \cdot (6 \cdot K + 1)} \right]$ <div style="border: 1px solid #ccc; padding: 5px; margin-top: 10px;"> SPREADSHEETS AA-SM-026-042 Beam Analysis - Framework - Vertical Concentrated Load Fixed Support </div> |

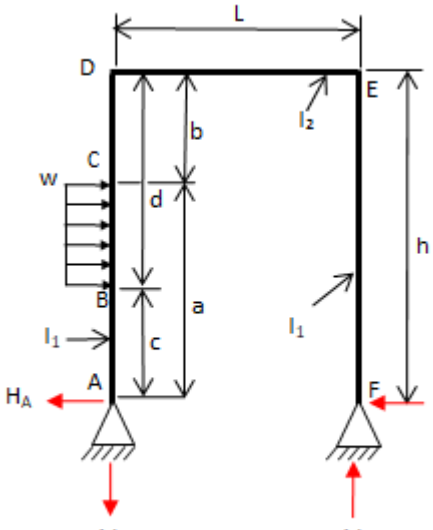
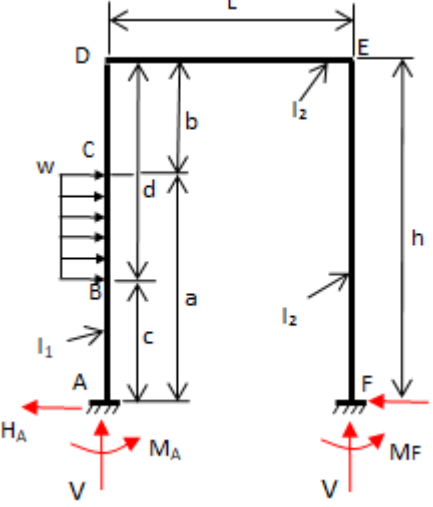
| Configuration | Reactions, Vertical Shear, Bending Moments, Deflection and Slope |
|---|--|
| 3. Horizontal Concentrated Load, Simple Support | <p></p> $K = \frac{I_2 \cdot h}{I_1 \cdot L}$ $V = \frac{Q \cdot a}{L}, \quad H_A = Q - H_E$ $H_E = \frac{Q \cdot a}{2 \cdot h} \cdot \left[\frac{b \cdot K \cdot (a + h)}{h^2 \cdot (2 \cdot K + 3)} + 1 \right]$ |
| 4. Horizontal Concentrated Load, Fixed Support | <p></p> $K = \frac{I_2 \cdot h}{I_1 \cdot L}$ $V = \frac{3 \cdot Q \cdot a^2 \cdot K}{L \cdot h \cdot (6 \cdot L + 1)}, \quad H_A = Q - H_E$ $H_E = \frac{Q \cdot a \cdot b}{2 \cdot h^2} \cdot \left[\frac{h}{b} - \frac{h + b + K \cdot (b - a)}{h \cdot (K + 2)} \right]$ $M_A = \frac{Q \cdot a}{2 \cdot h} \cdot \left[\frac{b \cdot (h + b + b \cdot K)}{h \cdot (K + 2)} + h - \frac{3 \cdot a \cdot K}{(6 \cdot K + 1)} \right]$ $M_E = \frac{Q \cdot a}{2 \cdot h} \cdot \left[\frac{-b \cdot (h + b + b \cdot K)}{h \cdot (K + 2)} + h - \frac{3 \cdot a \cdot K}{(6 \cdot K + 1)} \right]$ |

ABBOTT AEROSPACE SEZC LTD
SPREADSHEETS
ABBOTTAEROSPACE.COM
AA-SM-026-043 Beam Analysis - Framework - Horizontal
Concentrated Load Simple Support

ABBOTT AEROSPACE SEZC LTD
SPREADSHEETS
ABBOTTAEROSPACE.COM
AA-SM-026-044 Beam Analysis - Framework - Horizontal
Concentrated Load Fixed

| Configuration | Reactions, Vertical Shear, Bending Moments, Deflection and Slope |
|--|---|
| 5. Vertical Uniform Running Load, Simple Support | <p></p> $K = \frac{I_2 \cdot h}{I_1 \cdot L}$ $d = L - \frac{a}{2} - \frac{b}{2}$ $V_A = \frac{w \cdot c \cdot d}{L}, \quad V_F = w \cdot c \cdot \left(1 - \frac{d}{L}\right)$ $H = \frac{3 \cdot w \cdot c}{24 \cdot L \cdot h \cdot (2 \cdot K + 3)} \cdot [12 \cdot d \cdot L - 12 \cdot d^2 - c^2]$ <div style="border: 1px solid #ccc; padding: 5px; margin-top: 10px;"> SPREADSHEETS AA-SM-026-045 Beam Analysis - Framework - Vertical Uniform Running Load Simple Support </div> |
| 6. Vertical Uniform Running Load, Fixed Support | <p></p> $K = \frac{I_2 \cdot h}{I_1 \cdot L}$ $d = L - \frac{a}{2} - \frac{b}{2}$ $X_1 = -\frac{w \cdot c}{24 \cdot L} \cdot \left[24 \cdot \frac{d^3}{L} - 6 \cdot \frac{b \cdot c^2}{L} + 3 \cdot \frac{c^2}{L} + 4 \cdot c^2 - 24 \cdot d^2 \right]$ $X_2 = \frac{w \cdot c}{24 \cdot L} \cdot \left[24 \cdot \frac{d^3}{L} - 6 \cdot \frac{b \cdot c^2}{L} + 3 \cdot \frac{c^3}{L} + 2 \cdot c^2 - 48 \cdot d^2 + 24 \cdot L \right]$ $V_A = \frac{w \cdot c \cdot d}{L} + \frac{X_1 + X_2}{L \cdot (6 \cdot K + 1)}, \quad V_F = w \cdot c - V_A$ $H = \frac{3 \cdot (X_1 + X_2)}{2 \cdot h \cdot (K + 2)}$ $M_A = \frac{X_1 + X_2}{2 \cdot (K + 2)} - \frac{X_1 - X_2}{2 \cdot (6 \cdot K + 1)}$ $M_F = \frac{X_1 + X_2}{2 \cdot (K + 2)} + \frac{X_1 - X_2}{2 \cdot (6 \cdot K + 1)}$ <div style="border: 1px solid #ccc; padding: 5px; margin-top: 10px;"> SPREADSHEETS AA-SM-026-046 Beam Analysis - Framework - Horizontal Running Load Fixed Support </div> |

| Configuration | Reactions, Vertical Shear, Bending Moments, Deflection and Slope |
|---|---|
| 7. Vertical Triangular Running Load, Simple Support | <p>$K = \frac{I_2 \cdot h}{I_1 \cdot L}$</p> <p>$d = L - \frac{a}{2} - \frac{b}{2}$</p> <p>$V_A = \frac{w \cdot c \cdot d}{2 \cdot L}, \quad V_F = \frac{w \cdot c}{2 \cdot L} \cdot \left(a + \frac{2 \cdot c}{L} \right)$</p> <p>$H = \frac{3 \cdot w \cdot c}{4 \cdot L \cdot h \cdot (2 \cdot K + 3)} \cdot \left[d \cdot L - \frac{c^2}{18} - b^2 \right]$</p> <div style="border: 1px solid #ccc; padding: 5px; margin-top: 10px;"> AA-SM-026-047 Beam Analysis - Framework - Horizontal Triangle Dist Load Simple Support </div> |
| 8. Vertical Triangular Running Load, Fixed Support | <p>$K = \frac{I_2 \cdot h}{I_1 \cdot L}$</p> <p>$d = L - \frac{a}{2} - \frac{b}{2}$</p> <p>$X_3 = -\frac{w \cdot c}{2 \cdot L} \cdot \left[\frac{d^3}{L} - \frac{c^2}{9} + \frac{51 \cdot c^2}{810 \cdot L} + \frac{c^2 \cdot b}{6 \cdot L} - d^2 \right]$</p> <p>$X_4 = \frac{w \cdot c}{L} \cdot \left[\frac{d^3}{L} - \frac{c^2}{9} + \frac{51 \cdot c^2}{810 \cdot L} + \frac{c^2 \cdot b}{6 \cdot L} - 2 \cdot d^2 + d \cdot L \right]$</p> <p>$V_A = \frac{w \cdot c \cdot d}{2 \cdot L} + \frac{X_3 - X_4}{L \cdot (6 \cdot K + 1)}, \quad V_F = \frac{w \cdot c}{2} - V_A$</p> <p>$H = \frac{3 \cdot (X_3 + X_4)}{2 \cdot h \cdot (K + 2)}$</p> <p>$M_A = \frac{X_3 + X_4}{2 \cdot (K + 2)} - \frac{X_3 - X_4}{2 \cdot (6 \cdot K + 1)}$</p> <p>$M_F = \frac{X_3 + X_4}{2 \cdot (K + 2)} + \frac{X_3 - X_4}{2 \cdot (6 \cdot K + 1)}$</p> <div style="border: 1px solid #ccc; padding: 5px; margin-top: 10px;"> AA-SM-026-048 Beam Analysis - Framework - Horizontal Triangle Dist Load Fixed Support </div> |

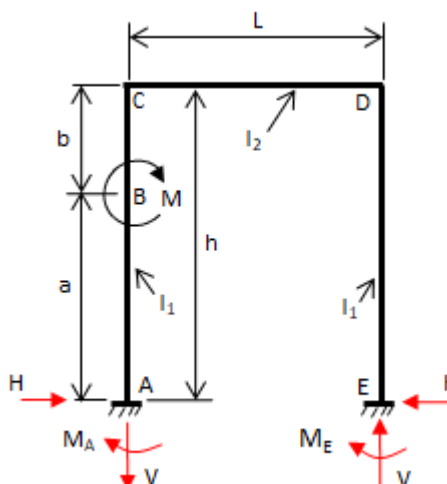
| Configuration | Reactions, Vertical Shear, Bending Moments, Deflection and Slope |
|--|--|
| 9. Horizontal Uniform Running Load, Simple Support | <p></p> $K = \frac{I_2 \cdot h}{I_1 \cdot L}$ $V = \frac{w \cdot (a^2 - c^2)}{2 \cdot L}$ $H_A = w(a - c) - H_F$ $H_F = \frac{w \cdot (a^2 - c^2)}{4 \cdot h} + \frac{K \cdot [w \cdot (a^2 - c^2) \cdot (2 \cdot h^2 - a^2 - c^2)]}{8 \cdot h^3 \cdot (2 \cdot K + 3)}$ <div style="border: 1px solid #ccc; padding: 5px; margin-top: 10px;"> <p>ABBOTT AEROSPACE SEZC LTD SPREADSHEETS ABBOTTAEROSPACE.COM</p> <p>AA-SM-026-049 Beam Analysis - Framework - Vertical Dist Load Simple Support</p> </div> |
| 10. Horizontal Uniform Running Load, Fixed Support | <p></p> $K = \frac{I_2 \cdot h}{I_1 \cdot L}$ $V = \frac{w \cdot (a^2 - c^2)}{2 \cdot L} - \frac{M_A}{L} - \frac{M_F}{L}$ $X_5 = \frac{w}{12 \cdot h^2} \cdot [d^3 \cdot (4 \cdot h - 3 \cdot d) - b^3 \cdot (4 \cdot h - 3 \cdot b)]$ $X_6 = \frac{w}{12 \cdot h^2} \cdot [a^3 \cdot (4 \cdot h - 3 \cdot a) - c^3 \cdot (4 \cdot h - 3 \cdot c)]$ $H_A = w(a - c) - H_F$ $H_F = \frac{w \cdot (a^2 - c^2)}{4 \cdot h} - \frac{X_5}{2 \cdot h} + \frac{X_6 \cdot (K - 1)}{2 \cdot h \cdot (K + 2)}$ $M_A = \frac{(3 \cdot K + 1) \cdot \left[\frac{w \cdot (a^2 - c^2)}{2} - X_5 \right]}{2 \cdot (6 \cdot K + 1)} + \frac{X_6}{2} \cdot \left[\frac{1}{K + 2} + \frac{3 \cdot K}{6 \cdot K + 1} \right] + X_5$ $M_F = \frac{(3 \cdot K + 1) \cdot \left[\frac{w \cdot (a^2 - c^2)}{2} - X_5 \right]}{2 \cdot (6 \cdot K + 1)} - \frac{X_6}{2} \cdot \left[\frac{1}{K + 2} - \frac{3 \cdot K}{6 \cdot K + 1} \right]$ <div style="border: 1px solid #ccc; padding: 5px; margin-top: 10px;"> <p>ABBOTT AEROSPACE SEZC LTD SPREADSHEETS ABBOTTAEROSPACE.COM</p> <p>AA-SM-026-050 Beam Analysis - Framework - Vertical Dist Load Fixed Support</p> </div> |

| Configuration | Reactions, Vertical Shear, Bending Moments, Deflection and Slope |
|--|---|
| 11. Horizontal Triangular Running Load, Simple Support | <p></p> $K = \frac{I_2 \cdot h}{I_1 \cdot L}$ $V = \frac{w}{6 \cdot L} \cdot (a^2 + a \cdot c - 2 \cdot c^2)$ $H_A = \frac{w(a - c)}{2} - H_F$ $X_7 = \frac{w}{120 \cdot h^2 \cdot (d - b)} \cdot [3 \cdot (4 \cdot d^5 + b^5) - 15 \cdot h \cdot (3 \cdot d^4 + b^4) + 20 \cdot h^2 \cdot (2 \cdot d^3 + b^3) - 15 \cdot b \cdot d^2 \cdot (2 \cdot h - d)^2]$ $H_F = \frac{V \cdot L}{2 \cdot h} + \frac{K \cdot X_7}{(2 \cdot K + 3) \cdot h}$ <div style="border: 1px solid blue; padding: 5px; margin-top: 10px;"> AA-SM-026-051 Beam Analysis - Framework - Vertical Triangle Dist Load Lower Peak Simple Support </div> |
| 12. Horizontal Triangular Running Load, Simple Support | <p></p> $K = \frac{I_2 \cdot h}{I_1 \cdot L}$ $V = \frac{w}{6 \cdot L} \cdot (2 \cdot a + c) \cdot (a - c)$ $H_A = \frac{w \cdot (a - c)}{2} - H_F$ $X_{10} = \frac{w}{120 \cdot h^2 \cdot (a - c)} \cdot [-12 \cdot (a^5 - c^5) + 15 \cdot c \cdot (a^4 - c^4) + 20 \cdot h^2 \cdot (a^3 - c^3) - 30 \cdot c \cdot h^2 \cdot (a^2 - c^2)]$ $H_F = \frac{V \cdot L}{2 \cdot h} + \frac{K \cdot X_{10}}{(2 \cdot K + 3) \cdot h}$ <div style="border: 1px solid blue; padding: 5px; margin-top: 10px;"> AA-SM-026-052 Beam Analysis - Framework - Vertical Triangle Dist Load Upper Peak Simple Support </div> |

| Configuration | Reactions, Vertical Shear, Bending Moments, Deflection and Slope |
|---|--|
| 13. Horizontal Triangular Running Load, Fixed Support | <p>ABBOTT AEROSPACE SEZC LTD SPREADSHEETS ABBOTTAEROSPACE.COM</p> <p>AA-SM-026-053 Beam Analysis - Framework - Vertical Triangle Dist Load Lower Peak Fixed Support</p> $K = \frac{I_2 \cdot h}{I_1 \cdot L}$ $V = \frac{w \cdot (a^2 + a \cdot c - 2 \cdot c^2)}{6 \cdot L} - \frac{M_A}{L} - \frac{M_F}{L}$ $X_8 = \frac{w}{60 \cdot h^2 \cdot (d - b)} \cdot [15 \cdot (h + b) \cdot (d^4 - b^4) - 12 \cdot (d^5 - b^5) - 20 \cdot b \cdot h \cdot (d^3 + b^3)]$ $X_9 = \frac{w}{60 \cdot h^2 \cdot (d - b)} \cdot [10 \cdot d^2 \cdot h^2 \cdot (2 \cdot d - 3 \cdot b) + 10 \cdot b \cdot h \cdot (4 \cdot d^3 + b^3 \cdot h - b^3) - d^4 \cdot (30 \cdot h + 15 \cdot b) + 12 \cdot d^5 + 3 \cdot b^5]$ $H_A = \frac{w \cdot (a - c)}{2} - H_F$ $H_F = \frac{w \cdot (a^2 + a \cdot c - 2 \cdot c^2)}{12 \cdot h} - \frac{X_8}{2 \cdot h} + \frac{X_9 \cdot (K - 1)}{2 \cdot h \cdot (K + 2)}$ $M_A = \frac{(3 \cdot K + 1) \cdot \left[\frac{w \cdot (a^2 + a \cdot c - 2 \cdot c^2)}{6} - X_8 \right]}{2 \cdot (6 \cdot K + 1)} + \frac{X_9}{2} \cdot \left[\frac{1}{K + 2} + \frac{3 \cdot K}{6 \cdot K + 1} \right] + X_8$ $M_F = \frac{(3 \cdot K + 1) \cdot \left[\frac{w \cdot (a^2 + a \cdot c - 2 \cdot c^2)}{6} - X_8 \right]}{2 \cdot (6 \cdot K + 1)} - \frac{X_8}{2} \cdot \left[\frac{1}{K + 2} - \frac{3 \cdot K}{6 \cdot K + 1} \right]$ |

| Configuration | Reactions, Vertical Shear, Bending Moments, Deflection and Slope |
|---|---|
| 14. Horizontal Triangular Running Load, Fixed Support | <p>AA-SM-026-054 Beam Analysis - Framework - Vertical Triangle Dist Load Upper Peak Fixed Support</p> $K = \frac{I_2 \cdot h}{I_1 \cdot L}$ $V = \frac{w \cdot (2 \cdot a + c) \cdot (a - c)}{6 \cdot L} - \frac{M_A}{L} - \frac{M_F}{L}$ $X_{11} = \frac{w}{60 \cdot h^2 \cdot (d - b)} \cdot [5 \cdot h \cdot d^4 - 3 \cdot d^5 - 20 \cdot h \cdot d \cdot b^3 - 12 \cdot b^4 \cdot (d + h)]$ $X_{12} = \frac{w}{60 \cdot h^2 \cdot (a - c)} \cdot [15 \cdot (h + c) \cdot (a^4 - c^4) - 12 \cdot (a^5 - c^5) - 20 \cdot c \cdot h \cdot (a^3 - c^3)]$ $H_A = \frac{w \cdot (a - c)}{2} - H_F$ $H_F = \frac{w \cdot (a^2 + a \cdot c - 2 \cdot c^2)}{12 \cdot h} - \frac{X_{11}}{2 \cdot h} + \frac{X_{12} \cdot (K - 1)}{2 \cdot h \cdot (K + 2)}$ $M_A = \frac{(3 \cdot K + 1) \cdot \left[\frac{w \cdot (2 \cdot a^2 - a \cdot c - c^2)}{6} - X_{11} \right]}{2 \cdot (6 \cdot K + 1)} + \frac{X_{12}}{2} \cdot \left[\frac{1}{K + 2} + \frac{3 \cdot K}{6 \cdot K + 1} \right] + X_{11}$ $M_F = \frac{(3 \cdot K + 1) \cdot \left[\frac{w \cdot (2 \cdot a^2 - a \cdot c - c^2)}{6} - X_{11} \right]}{2 \cdot (6 \cdot K + 1)} - \frac{X_{12}}{2} \cdot \left[\frac{1}{K + 2} - \frac{3 \cdot K}{6 \cdot K + 1} \right]$ |
| 15. Moment on Horizontal Span, Simple Support | <p>AA-SM-026-055 Beam Analysis - Framework - Horizontal Moment Simple Support</p> $K = \frac{I_2 \cdot h}{I_1 \cdot L}$ $V = \frac{M}{L}$ $H = \frac{3 \cdot \left(b - \frac{L}{2} \right) \cdot M}{L \cdot h \cdot (2 \cdot K + 3)}$ |

| Configuration | Reactions, Vertical Shear, Bending Moments, Deflection and Slope |
|---|---|
| 16. Moment on Horizontal Span Fixed Support | <p></p> $K = \frac{I_2 \cdot h}{I_1 \cdot L}$ $V = \frac{6 \cdot (a \cdot b + L^2 \cdot K) \cdot M}{L^3 \cdot (6 \cdot K + 1)}$ $H = \frac{3 \cdot (b - a) \cdot M}{2 \cdot L \cdot h \cdot (K + 2)}$ $M_A = M \cdot \left[\frac{6 \cdot a \cdot b \cdot (K + 2) - L \cdot [a \cdot (7 \cdot K + 3) - b \cdot (5 \cdot K - 1)]}{2L^2 \cdot (K + 2) \cdot (6 \cdot K + 1)} \right]$ $M_E = V \cdot L - M - M_A$ |
| 17. Moment on Vertical Span, Simple Support | <p></p> $K = \frac{I_2 \cdot h}{I_1 \cdot L}$ $V = \frac{M}{L}$ $H = \frac{3 \cdot \left(b - \frac{L}{2} \right) \cdot M}{L \cdot h \cdot (2 \cdot K + 3)}$ |

| Configuration | Reactions, Vertical Shear, Bending Moments, Deflection and Slope |
|--|---|
| 18. Moment on Vertical Span, Simple Support  | <p>AA-SM-026-058 Beam Analysis - Framework - Vertical Moment Fixed Support</p> $K = \frac{I_2 \cdot h}{I_1 \cdot L}$ $V = \frac{6 \cdot b \cdot K \cdot M}{h \cdot L \cdot (6 \cdot K + 1)}$ $H = \frac{3 \cdot b \cdot M \cdot [2 \cdot a \cdot (K + 1) + b]}{2 \cdot h^3 \cdot (K + 2)}$ $M_A = \frac{-M}{2 \cdot h^2 \cdot (K + 2) \cdot (6 \cdot K + 1)} \cdot [4 \cdot a^2 + 2 \cdot a \cdot b + b^2 + K \cdot (26 \cdot a^2 - 5 \cdot b^2) + 6 \cdot a \cdot K^2 \cdot (2 \cdot a - b)]$ $M_E = V \cdot L - M - M_A$ |

8.7.2. Tension Flexure of Beams

These beam solutions are taken from [\(NASA TM X-73305, 1975\)](#) Table B4.6.1

Where:

M The bending moment due to the combined loading, positive when clockwise, negative when counter clockwise (inlb)

M₁ & M₂ Applied external couples positive when acting as shown (inlb)

y Deflection, positive when upward, negative when downward (in)

θ Slope of the beam to horizontal, positive when upwards to the right (radians)

$$j = \sqrt{(E \cdot I) / P}$$

Where:

E Modulus of Elasticity (psi)

I Moment of Inertia of cross section about the horizontal axis (in⁴)

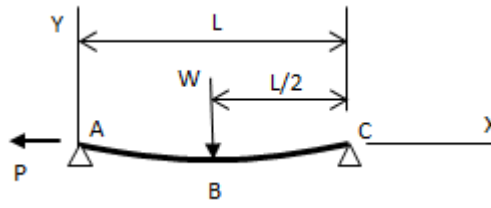
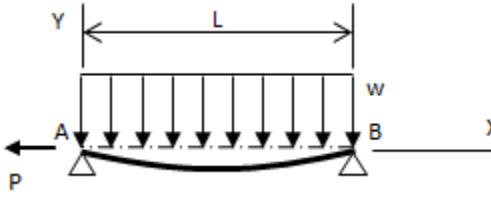
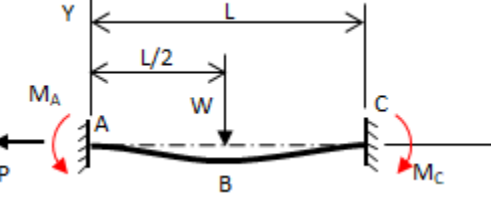
P Axial Load (lb)

$$U = L/j$$

W Transverse load (lb)

w Transverse load per unit length (lb/in)

| Configuration | Reactions, Vertical Shear, Bending Moments, Deflection and Slope |
|---|---|
| 1. Cantilever, Point load on End | <p>$Max M = -W \cdot j \cdot \tanh(U) \text{ at } B$</p> $Max y = -\frac{W}{P} \cdot (L - j \cdot \tanh(U)) \text{ at } A$ <div style="border: 1px solid blue; padding: 5px; margin-top: 10px;"> <small>ABBOTT AEROSPACE SEZC LTD</small> SPREADSHEETS <small>ABBOTTAEROSPACE.COM</small> AA-SM-026-101 Beam Analysis - Tension Flexure - Cantilever Point Load at End </div> |
| 2. Cantilever, Uniformly Distributed Load | <p>$Max M = -w \cdot j \cdot [L \cdot \tanh(U) - j \cdot (1 - \operatorname{sech}(U))] \text{ at } B$</p> $Max y = -\frac{w \cdot j}{P} \cdot \left[j \cdot \left(1 - \frac{U^2}{2} - \operatorname{sech}(U) \right) - L \cdot (\tanh(U) - U) \right] \text{ at } A$ <div style="border: 1px solid blue; padding: 5px; margin-top: 10px;"> <small>ABBOTT AEROSPACE SEZC LTD</small> SPREADSHEETS <small>ABBOTTAEROSPACE.COM</small> AA-SM-026-102 Beam Analysis - Tension Flexure - Cantilever UDL </div> |

| Configuration | Reactions, Vertical Shear, Bending Moments, Deflection and Slope |
|---|---|
| 3. Simply Supported Both Ends, Point Load in middle | $\text{Max } M = \frac{1}{2} \cdot W \cdot j \cdot \tanh\left(\frac{U}{2}\right) \text{ at } B$ $\text{Max } y = -\frac{W}{P} \cdot \left[\frac{L}{4} - \frac{1}{2} \cdot \tanh\left(\frac{U}{2}\right) \right] \text{ at } B$  |
| 4. Simply Supported Both Ends, Uniformly Distributed Load | $\text{Max } M = w \cdot j^2 \cdot \left(1 - \operatorname{sech}\left(\frac{U}{2}\right) \right) \text{ at Midspan}$ $\text{Max } y = -\frac{w}{P} \cdot \left[\frac{L^2}{8} - j^2 \cdot \left(1 - \operatorname{sech}\left(\frac{U}{2}\right) \right) \right] \text{ at Midspan}$  |
| 5. Fixed Both Ends, Point Load in Middle | $M_A = M_C = \frac{W \cdot j}{2} \cdot \left(\frac{\cosh\left(\frac{U}{2}\right) - 1}{\sinh\left(\frac{U}{2}\right)} \right) \text{ at } A \& C$ $\text{Max } + M = \frac{W \cdot j}{2} \cdot \left(\frac{1 - \cosh\left(\frac{U}{2}\right)}{\sinh\left(\frac{U}{2}\right) \cdot \cosh\left(\frac{U}{2}\right)} + \tanh\left(\frac{U}{2}\right) \right) \text{ at } B$ $\text{Max } y = -\frac{W \cdot j}{2 \cdot P} \cdot \left[\frac{U}{2} - \tanh\left(\frac{U}{2}\right) - \frac{\left(1 - \cosh\left(\frac{U}{2}\right)\right)^2}{\sinh\left(\frac{U}{2}\right) \cdot \cosh\left(\frac{U}{2}\right)} \right] \text{ at } B$  |

| Configuration | Reactions, Vertical Shear, Bending Moments, Deflection and Slope |
|--|--|
| 6. Fixed Both Ends, Uniformly Distributed Load | <p>AA-SM-026-106 Beam Analysis - Tension Flexure - Fixed Both Ends UDL</p> $M_A = M_B = w \cdot j^2 \cdot \left(\frac{\frac{U}{2} - \tanh\left(\frac{U}{2}\right)}{\tanh\left(\frac{U}{2}\right)} \right) \text{ at } A \& C$ $\text{Max } +M = w \cdot j^2 \cdot \left(1 - \frac{\frac{U}{2}}{\sinh\left(\frac{U}{2}\right)} \right) \text{ at Midspan}$ $\text{Max } y = -\frac{w \cdot j^2}{8 \cdot P} \cdot \left(\frac{4 \cdot U \cdot \left(1 - \cosh\left(\frac{U}{2}\right) \right)}{\sinh\left(\frac{U}{2}\right)} + U^2 \right) \text{ at Midspan}$ |

8.7.3. Compression Flexure of Beams

These beam solutions are taken from [\(NASA TM X-73305, 1975\)](#) Table B4.6.2

Where:

M The bending moment due to the combined loading, positive when clockwise, negative when counter clockwise (inlb)

M Applied external couples positive when acting as shown (inlb)

y Deflection, positive when upward, negative when downward (in)

θ Slope of the beam to horizontal, positive when upwards to the right (radians)

$$j = \sqrt{(E \cdot I)/P}$$

Where:

E Modulus of Elasticity (psi)

I Moment of Inertia of cross section about the horizontal axis (in^4)

P Axial Load (lb)

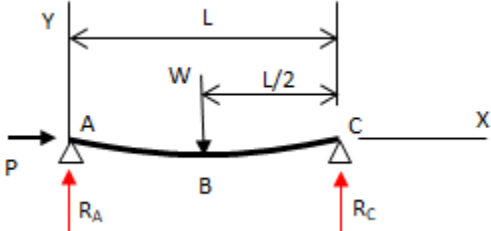
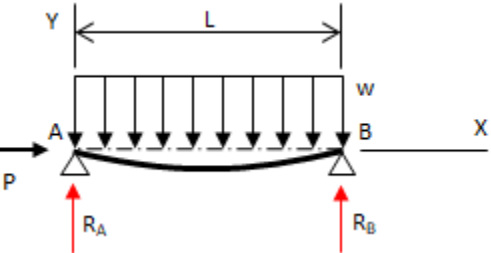
$$U = L/j$$

W Transverse load (lb)

w Transverse load per unit length (lb/in)

Note that these methods do not predict beam column failure, these methods only the internal loads and moments in the beam. To predict the stability failure of a beam column the method in section 15.3.6 should be used.

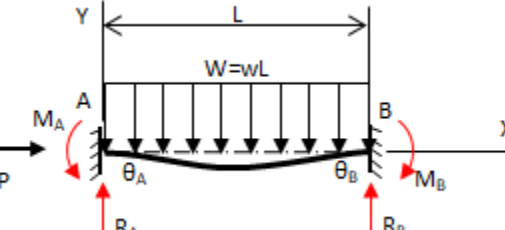
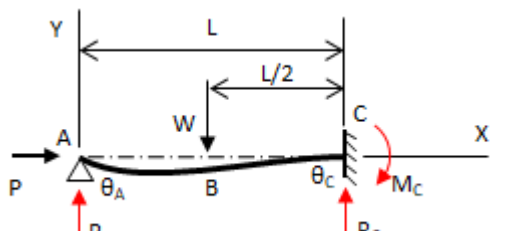
| Configuration | Reactions, Vertical Shear, Bending Moments, Deflection and Slope |
|---|--|
| 1. Cantilever, Point load on End | <p>$\text{Max } M = -W \cdot j \cdot \tanh(U) \text{ at } B$</p> <p>$\text{Max } y = -\frac{W}{P} \cdot (L - j \cdot \tanh(U)) \text{ at } A$</p> <p>$\theta = \frac{W}{P} \cdot \left(\frac{1 - \cos(U)}{\cos(U)} \right) \text{ at } A$</p> <div style="border: 1px solid #ccc; padding: 5px; margin-top: 10px;"> SPREADSHEETS AA-SM-026-111 Beam Analysis - Compression Flexure - Cantilever Point Load at End </div> |
| 2. Cantilever, Uniformly Distributed Load | <p>$\text{Max } M = -w \cdot j \cdot [L \cdot \tan(U) + j \cdot (1 - \sec(U))] \text{ at } B$</p> <p>$\text{Max } y = -\frac{w \cdot j}{P} \cdot \left[j \cdot \left(1 - \frac{U^2}{2} - \sec(U) \right) + L \cdot (\tanh(U) - U) \right] \text{ at } A$</p> <p>$\theta = \frac{w}{P} \cdot \left[\frac{L}{\cos(U)} - j \cdot \left(\frac{1 - \cos(2 \cdot U)}{\sin(2 \cdot U)} \right) \right] \text{ at } A$</p> <div style="border: 1px solid #ccc; padding: 5px; margin-top: 10px;"> SPREADSHEETS AA-SM-026-112 Beam Analysis - Compression Flexure - Cantilever, UDL </div> |

| Configuration | Reactions, Vertical Shear, Bending Moments, Deflection and Slope |
|---|---|
| 3. Simply Supported Both Ends, Point Load in middle | <p>$Max M = \frac{1}{2} \cdot W \cdot j \cdot \tan\left(\frac{U}{2}\right)$ at B</p> <p>$Max y = -\frac{W \cdot j}{2 \cdot P} \cdot \left[\tan\left(\frac{U}{2}\right) - \frac{U}{2} \right]$ at B</p> <p>$\theta = -\frac{W}{2 \cdot P} \cdot \left[\frac{1 - \cos\left(\frac{U}{2}\right)}{\cos\left(\frac{U}{2}\right)} \right]$ at A and C</p>  <div style="border: 1px solid #ccc; padding: 5px; margin-top: 10px;"> AA-SM-026-113 Beam Analysis - Compression Flexure - Simply Supported Both Ends, Midspan Point </div> |
| 4. Simply Supported Both Ends, Uniformly Distributed Load | <p>$Max M = w \cdot j^2 \cdot \left(\sec\left(\frac{U}{2}\right) - 1 \right)$ at Midspan</p> <p>$Max y = -\frac{w \cdot j^2}{P} \cdot \left[\sec\left(\frac{U}{2}\right) - 1 - \frac{U^2}{8} \right]$ at Midspan</p> <p>$\theta = -\frac{w \cdot j}{P} \cdot \left[-\frac{U}{2} + \frac{1 - \cos(U)}{\sin(U)} \right]$ at A and B</p>  <div style="border: 1px solid #ccc; padding: 5px; margin-top: 10px;"> AA-SM-026-114 Beam Analysis - Compression Flexure - Simply Supported Both Ends, UDL </div> |

| Configuration | Reactions, Vertical Shear, Bending Moments, Deflection and Slope |
|--|---|
| 5. Simply Supported Both Ends, Point Load Applied Anywhere | <p>AA-SM-026-115 Beam Analysis - Compression Flexure - Simply Supported Both Ends, Point Load</p> <p><i>Moment Equation $x = 0$ to $x = a$, $M = \frac{W \cdot j \cdot \sin\left(\frac{b}{j}\right) \cdot \sin\left(\frac{x}{j}\right)}{\sin(U)}$</i></p> <p><i>Max M at $x = \frac{\pi \cdot j}{2}$ if $\frac{\pi \cdot j}{2} < a$</i></p> <p><i>Moment Equation $x = a$ to $x = L$, $M = \frac{W \cdot j \cdot \sin\left(\frac{a}{j}\right) \cdot \sin\left(\frac{L-x}{j}\right)}{\sin(U)}$</i></p> <p><i>Max M at $x = L - \frac{\pi \cdot j}{2}$ if $(L - \frac{\pi \cdot j}{2}) > a$</i></p> <p><i>Max M is at $x = a$ if $\frac{\pi \cdot j}{2} > a$ and $(L - \frac{\pi \cdot j}{2}) < a$</i></p> <p><i>Deflection Equation $x = 0$ to $x = a$, $y = \frac{W \cdot j}{P} \cdot \left(\frac{\sin\left(\frac{b}{j}\right) \cdot \sin\left(\frac{x}{j}\right)}{\sin(U)} - \frac{b \cdot x}{L \cdot j} \right)$</i></p> <p><i>Deflection Equation $x = a$ to $x = L$, $y = \frac{W \cdot j}{P} \cdot \left(\frac{\sin\left(\frac{a}{j}\right) \cdot \sin\left(\frac{L-x}{j}\right)}{\sin(U)} - \frac{a \cdot (L-x)}{L \cdot j} \right)$</i></p> <p>$\theta = -\frac{W}{P} \cdot \left(\frac{b}{L} + \frac{\sin\left(\frac{a}{j}\right)}{\tan(U)} - \cos\left(\frac{a}{j}\right) \right) \text{ at } A$</p> <p>$\theta = \frac{W}{P} \cdot \left(\frac{a}{L} + \frac{\sin\left(\frac{a}{j}\right)}{\sin(U)} \right) \text{ at } B$</p> |

| Configuration | Reactions, Vertical Shear, Bending Moments, Deflection and Slope |
|--|---|
| 6. Simply Supported Both Ends, Triangular Distributed Load | <p><i>Moment Equation</i> $M = w \cdot j^2 \cdot \left(\frac{\sin(\frac{x}{j})}{\sin(U)} - \frac{x}{L} \right)$</p> <p><i>Max M at $x = j \cdot \arccos\left(\frac{\sin(U)}{U}\right)$</i></p> <p><i>Deflection Equation</i>, $y = -\frac{w}{P} \cdot \left(\frac{x^3}{6 \cdot L} + \frac{j^2 \cdot \sin(\frac{x}{j})}{\sin(U)} - \frac{j \cdot x}{U} - \frac{L \cdot x}{6} \right)$</p> <p>$\theta = -\frac{w}{P} \cdot \left(\frac{j}{\sin(U)} - \frac{j}{U} - \frac{L}{6} \right) \text{ at } A$</p> <p>$\theta = \frac{w}{P} \cdot \left(-\frac{j}{\tan(U)} + \frac{j}{U} - \frac{L}{3} \right) \text{ at } B$</p> <div style="border: 1px solid #ccc; padding: 5px; margin-top: 10px;"> AA-SM-026-116 Beam Analysis - Compression Flexure - Simply Supported Both Ends, Triangular Load </div> |
| 7. Simply Supported Both Ends, Similar Moment Applied at Both Ends | <p><i>Max M</i> $= M_A \cdot \sec\left(\frac{U}{2}\right) \text{ at } x = \frac{L}{2}$</p> <p><i>Max y</i> $= -\frac{M_A}{P} \cdot \left(\frac{1 - \cos\left(\frac{U}{2}\right)}{\cos\left(\frac{U}{2}\right)} \right) \text{ at } x = \frac{L}{2}$</p> <p>$\theta = -\frac{M_A}{P \cdot j} \cdot \tan\left(\frac{U}{2}\right) \text{ at } A \text{ and } B$</p> <div style="border: 1px solid #ccc; padding: 5px; margin-top: 10px;"> AA-SM-026-117 Beam Analysis - Compression Flexure - Simply Supported and Similar Moment Both Ends </div> |

| Configuration | Reactions, Vertical Shear, Bending Moments, Deflection and Slope |
|--|--|
| 8. Simply Supported Both Ends, Different Moment Applied at Both Ends | <p>AA-SM-026-118 Beam Analysis - Compression Flexure - Simply Supported and Different Moment Both Ends</p> <p>Moment Equation $M = \left(\frac{M_B - M_A \cdot \cos(U)}{\sin(U)} \right) \cdot \sin\left(\frac{x}{j}\right) + M_A \cdot \cos\left(\frac{x}{j}\right)$</p> <p>Max M at $x = j \cdot \text{atan}\left(\frac{M_B - M_A \cdot \cos(U)}{M_A \cdot \sin(U)}\right)$</p> <p>Deflection Equation, $y = \frac{1}{P} \cdot \left[M_A + (M_B - M_A) \cdot \frac{x}{L} - (M_B - M_A \cdot \cos(U)) \cdot \frac{\sin\left(\frac{x}{j}\right)}{\sin(U)} - M_A \cdot \cos\left(\frac{x}{j}\right) \right]$</p> <p>$\theta = \frac{1}{P} \cdot \left(\frac{M_B - M_A}{L} - \frac{M_B - M_A \cdot \cos(U)}{j \cdot \sin(U)} \right)$ at A</p> <p>$\theta = \frac{1}{P} \cdot \left(\frac{M_B - M_A}{L} - \frac{M_B - M_A \cdot \cos(U)}{j \cdot \sin(U)} \cdot \cos(U) + \frac{M_A}{j} \cdot \sin(U) \right)$ at B</p> |
| 9. Fixed Both Ends, Point Load in Middle | <p>AA-SM-026-119 Beam Analysis - Compression Flexure - Fixed Both Ends, Midspan Load</p> <p>$M_A = M_C = \frac{1}{2} \cdot W \cdot j \cdot \left(\frac{1 - \cos\left(\frac{U}{2}\right)}{\sin\left(\frac{U}{2}\right)} \right)$</p> <p>at $x = \frac{L}{2}$, $M = \frac{1}{2} \cdot W \cdot j \cdot \left(\tan\left(\frac{U}{2}\right) - \frac{1 - \cos\left(\frac{U}{2}\right)}{\sin\left(\frac{U}{2}\right) \cdot \cos\left(\frac{U}{2}\right)} \right)$</p> <p>$\text{Max } y = \frac{W \cdot j}{2 \cdot P} \cdot \left(\tan\left(\frac{U}{2}\right) - \frac{U}{2} - \frac{\left(1 - \cos\left(\frac{U}{2}\right)\right)^2}{\sin\left(\frac{U}{2}\right) \cdot \cos\left(\frac{U}{2}\right)} \right)$ at B</p> |

| Configuration | Reactions, Vertical Shear, Bending Moments, Deflection and Slope |
|--|--|
| 10. Fixed Both Ends, UDL along Length | <p>$M_A = M_B = W \cdot j^2 \cdot \left(1 - \frac{\left(\frac{U}{2}\right)}{\tan\left(\frac{U}{2}\right)} \right)$</p> <p>at $x = \frac{L}{2}$, $M = W \cdot j^2 \cdot \left(\frac{\left(\frac{U}{2}\right)}{\sin\left(\frac{U}{2}\right)} - 1 \right)$</p> <p>$\text{Max } y = \frac{W \cdot j^2}{P} \cdot \left(t - \left(1 - \frac{\frac{U}{2}}{\tan\left(\frac{U}{2}\right)} \right) \cdot \left(\frac{1 - \cos\left(\frac{U}{2}\right)}{\cos\left(\frac{U}{2}\right)} \right) + \sec\left(\frac{U}{2}\right) - \frac{U^2}{8} - 1 \right)$ at $\frac{L}{2}$</p> <div style="border: 1px solid #ccc; padding: 5px; margin-top: 10px;"> <p>ABBOTT AEROSPACE SEZC LTD SPREADSHEETS ABBOTTAEROSPACE.COM</p> <p>AA-SM-026-120 Beam Analysis - Compression Flexure - Fixed Both Ends, UDL</p> </div>  |
| 11. Fixed One End, Point Load Halfway Along Length | <p>$\text{Max } M = M_C = \frac{WL}{2} \cdot \left(\frac{j \cdot \tan(U) \cdot \left(\sec\left(\frac{U}{2}\right) - 1 \right)}{j \cdot \tan(U) - L} \right)$</p> <p>$R = \frac{W}{2} - \frac{M_1}{L}$</p> <p><i>Moment Equation:</i> $x = \frac{L}{2}$ to $x = L$</p> <p>$M = M_C \cdot \left(\frac{\sin\left(\frac{x}{j}\right)}{\tan(U)} - \cos\left(\frac{x}{j}\right) \right) + W \cdot j \cdot \left(\sin\left(\frac{u}{2}\right) \cdot \cos\left(\frac{x}{j}\right) - \frac{\sin\left(\frac{U}{2}\right) \cdot \sin\left(\frac{x}{j}\right)}{\tan(U)} \right)$</p> <p><i>Deflection Equation:</i> $x = \frac{L}{2}$ to $x = L$</p> <p>$Y = -\frac{1}{P} \cdot \left(M_C \cdot \left(1 - \frac{x}{L} + \frac{\sin\left(\frac{x}{j}\right)}{\tan(U)} - \cos\left(\frac{x}{j}\right) \right) - W \cdot j \cdot \left(\frac{L-x}{2 \cdot j} + \frac{\sin\left(\frac{U}{2}\right) \cdot \sin\left(\frac{x}{j}\right)}{\tan(U)} - \sin\left(\frac{U}{2}\right) \cdot \cos\left(\frac{x}{j}\right) \right) \right)$</p> <div style="border: 1px solid #ccc; padding: 5px; margin-top: 10px;"> <p>ABBOTT AEROSPACE SEZC LTD SPREADSHEETS ABBOTTAEROSPACE.COM</p> <p>AA-SM-026-121 Beam Analysis - Compression Flexure - Fixed One End, Free One End Point Load</p> </div>  |

| Configuration | Reactions, Vertical Shear, Bending Moments, Deflection and Slope |
|-------------------------------------|--|
| 12. Fixed One End, UDL Along Length | <p>Diagram: A beam of length L is fixed at end A and has a roller support at end B. A uniformly distributed load w acts downwards along the entire length. At end A, there is a horizontal force P pointing right and a reaction R_A pointing upwards. At end B, there is a reaction R_B pointing upwards and a clockwise moment M_B. The angle of deflection at end A is θ_A and at end B is θ_B.</p> <p>Equations:</p> $\text{Max } M = M_B = w \cdot L \cdot j \cdot \left(\frac{\tan(U) \cdot \left(\tan\left(\frac{U}{2}\right) - \frac{U}{2} \right)}{\tan(U) - U} \right)$ $R = \frac{w \cdot L}{2} - \frac{M_1}{L}$ <p>Moment Equation: $x = 0$ to $x = L$</p> $M = M_B \cdot \left(\cot(U) \cdot \sin\left(\frac{x}{j}\right) - \cos\left(\frac{x}{j}\right) \right) + W \cdot j^2 \cdot \left(\frac{\sin\left(\frac{x}{j}\right)}{\sin(U)} \cdot (1 - \cos(U)) + \cos\left(\frac{x}{j}\right) - 1 \right)$ <p>Deflection Equation: $x = \frac{L}{2}$ to $x = L$</p> $Y = -\frac{1}{P} \cdot \left(M_1 \cdot \left(1 - \frac{x}{L} + \cot(U) \cdot \sin\left(\frac{x}{j}\right) - \cos\left(\frac{x}{j}\right) \right) - W \cdot j^2 \cdot \left(\cot(U) \cdot \sin\left(\frac{x}{j}\right) - \frac{\sin\left(\frac{x}{j}\right)}{\sin(U)} - \cos\left(\frac{x}{j}\right) + \frac{L \cdot x - x^2}{2 \cdot j^2} + 1 \right) \right)$ |

ABBOTT AEROSPACE SEZC LTD
SPREADSHEETS
ABBOTTAEROSPACE.COM
AA-SM-026-122 Beam Analysis - Compression Flexure -
Fixed One End, Free One End, UDL

9. TORSION

This section is in part taken from [\(NASA TM X-73306, 1975\)](#) Section B 8.0.0 and [\(AFFDL-TR-69-42, 1986\)](#) Section 1.5.

9.1. Introduction

The following section considers the torsion stress and deflection of closed regular cross sections.

Nomenclature:

| | |
|----------------------|---|
| T | Moment, inlb |
| a | Width of Section, in (Generally the major dimension) |
| b, H | Height of Section, in (Generally the minor dimension) |
| R, r | Radius, in |
| A | Length of Side, in |
| D | Distance, in |
| t | Thickness, in |
| f_s | Shear Stress, psi |
| L | Length of Rod/Bar, in |
| J | Section Torsion Constant, in ⁴ |
| α | Dimensioned Angle, Degrees |
| θ | Angle of deflection, Radians |

9.1.1. Torsion Modulus of Rupture for Round Steel Tubes

For circular cross sections the following figures give the torsion modulus of rupture for a range of steels:

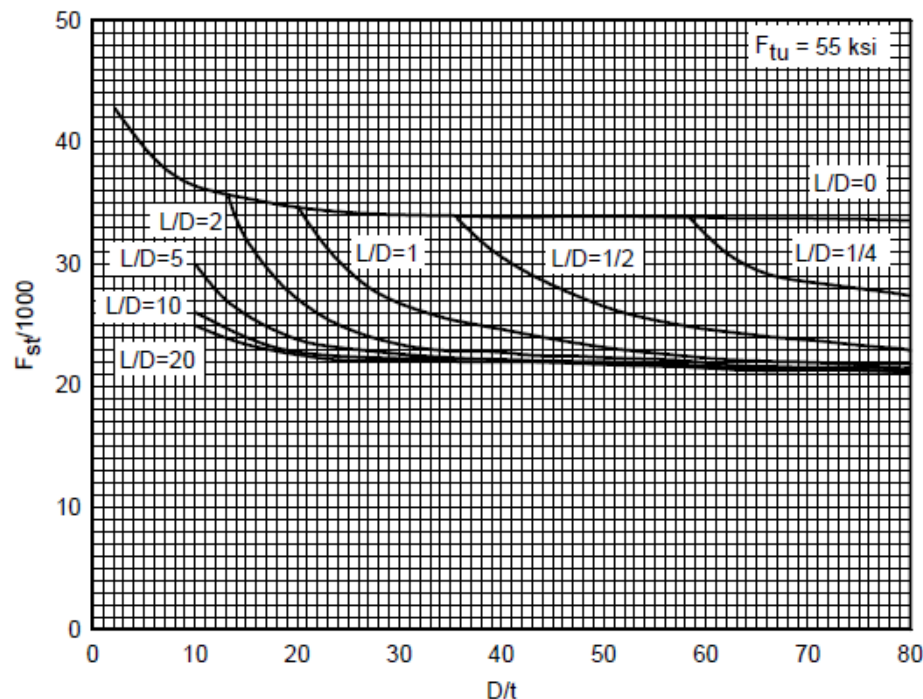


Figure 9.1.1-1: Torsional Modulus of Rupture – Plain Carbons Steels F_{tu} = 55ksi [\(MIL-HNDBK-5H, 1998\)](#)

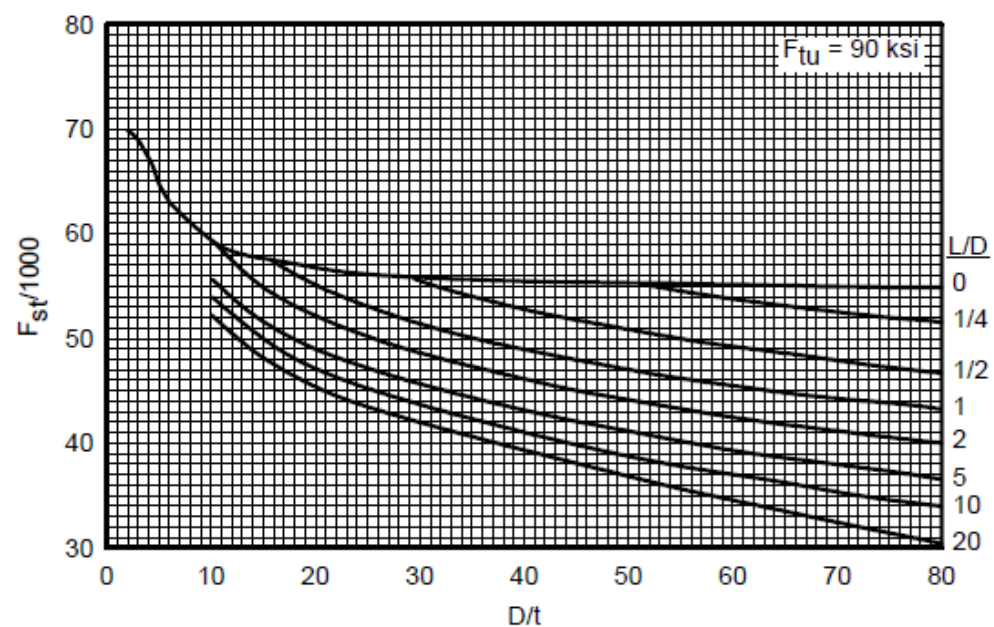


Figure 9.1.1-2: Torsional Modulus of Rupture – Low Alloy Steels Treated to F_{tu} = 90ksi [\(MIL-HNDBK-5H, 1998\)](#)

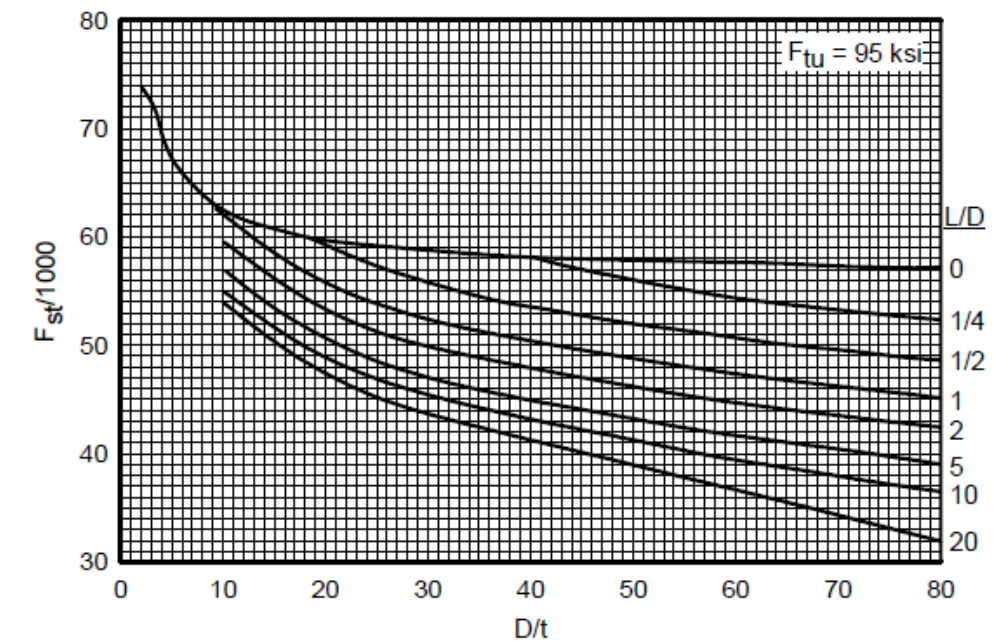


Figure 9.1.1-3: Torsional Modulus of Rupture – Low Alloy Steels Treated to F_{tu} = 95ksi [\(MIL-HNDBK-5H, 1998\)](#)

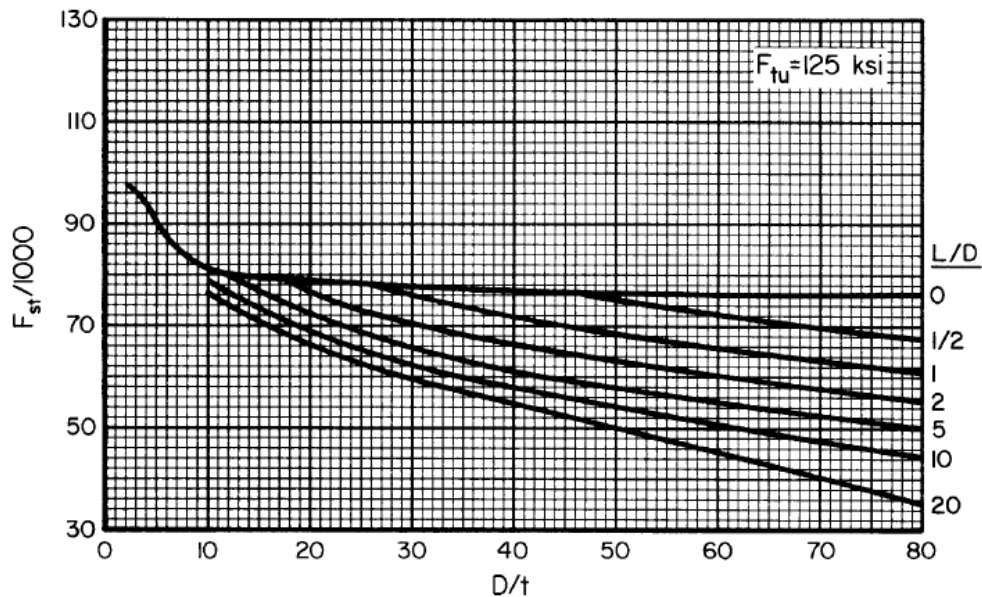


Figure 9.1.1-4: Torsional Modulus of Rupture – Low Alloy Steels Heat Treated to $F_{tu} = 125\text{ksi}$ [\(MIL-HNDBK-5H, 1998\)](#)

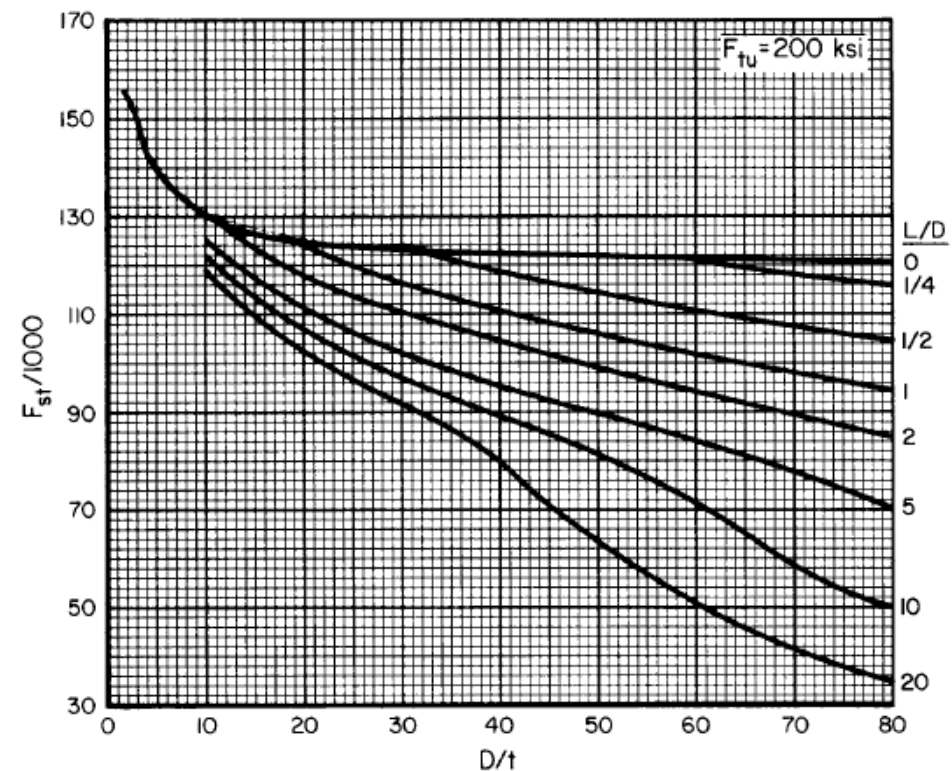


Figure 9.1.1-7: Torsional Modulus of Rupture – Alloy Steels Heat Treated to $F_{tu} = 200\text{ksi}$ [\(MIL-HNDBK-5H, 1998\)](#)

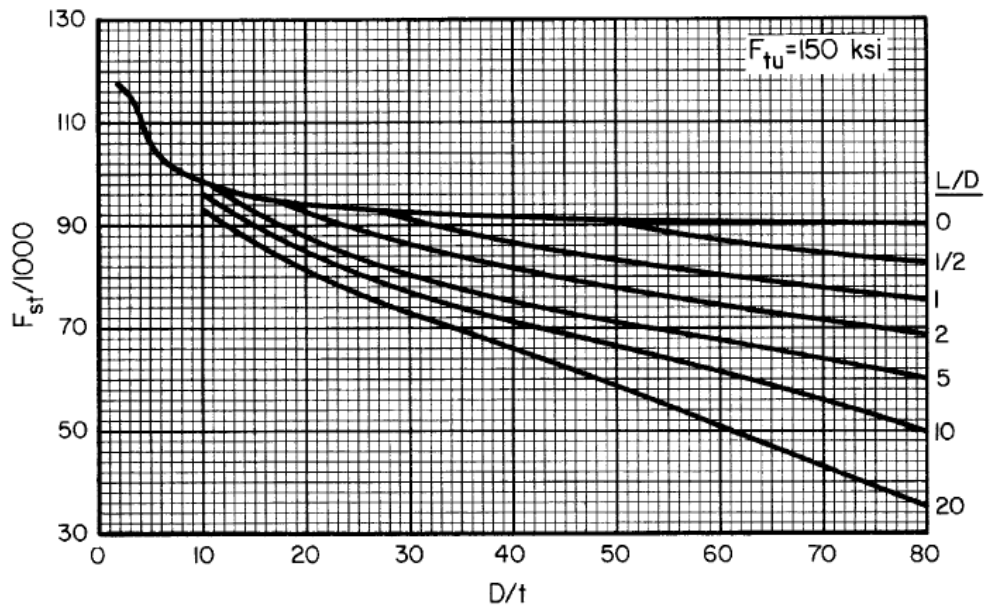


Figure 9.1.1-5: Torsional Modulus of Rupture – Low Alloy Steels Heat Treated to $F_{tu} = 150\text{ksi}$ [\(MIL-HNDBK-5H, 1998\)](#)

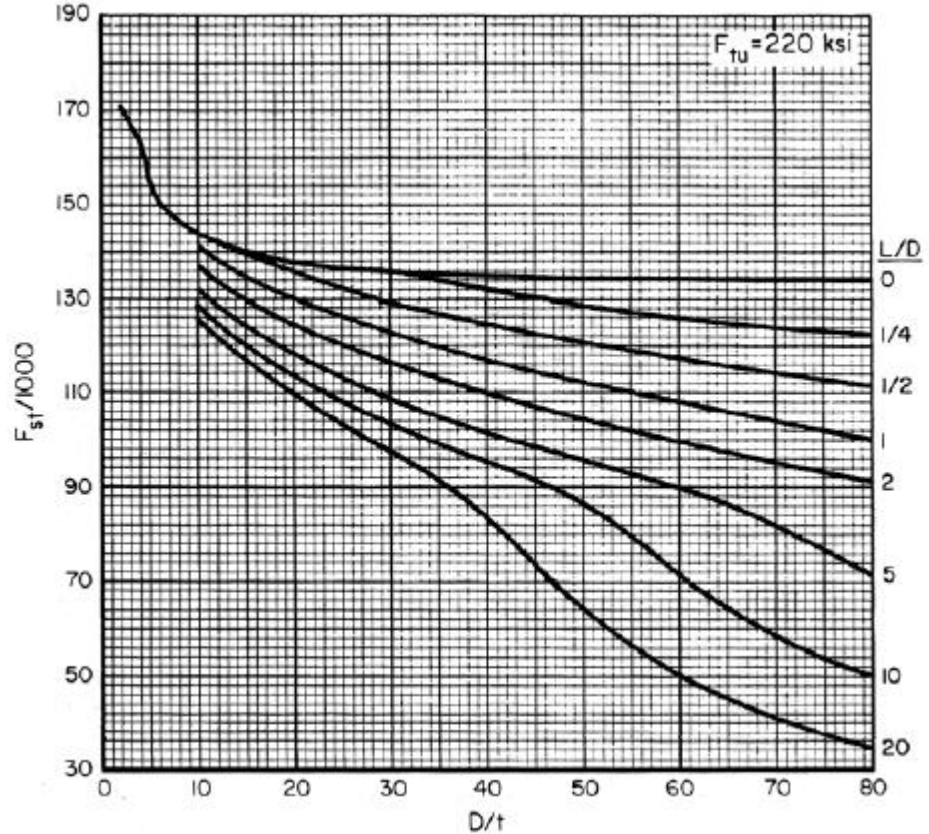


Figure 9.1.1-8: Torsional Modulus of Rupture – Alloy Steels Heat Treated to $F_{tu} = 220\text{ksi}$ [\(MIL-HNDBK-5H, 1998\)](#)

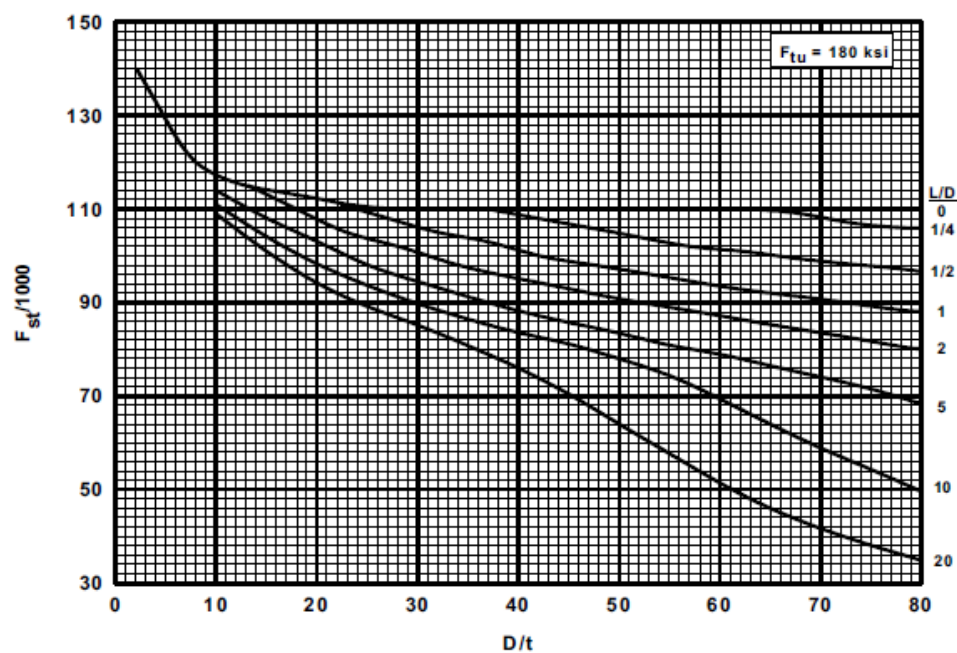


Figure 9.1.1-6: Torsional Modulus of Rupture – Alloy Steels Heat Treated to $F_{tu} = 180\text{ksi}$ [\(MIL-HNDBK-5H, 1998\)](#)

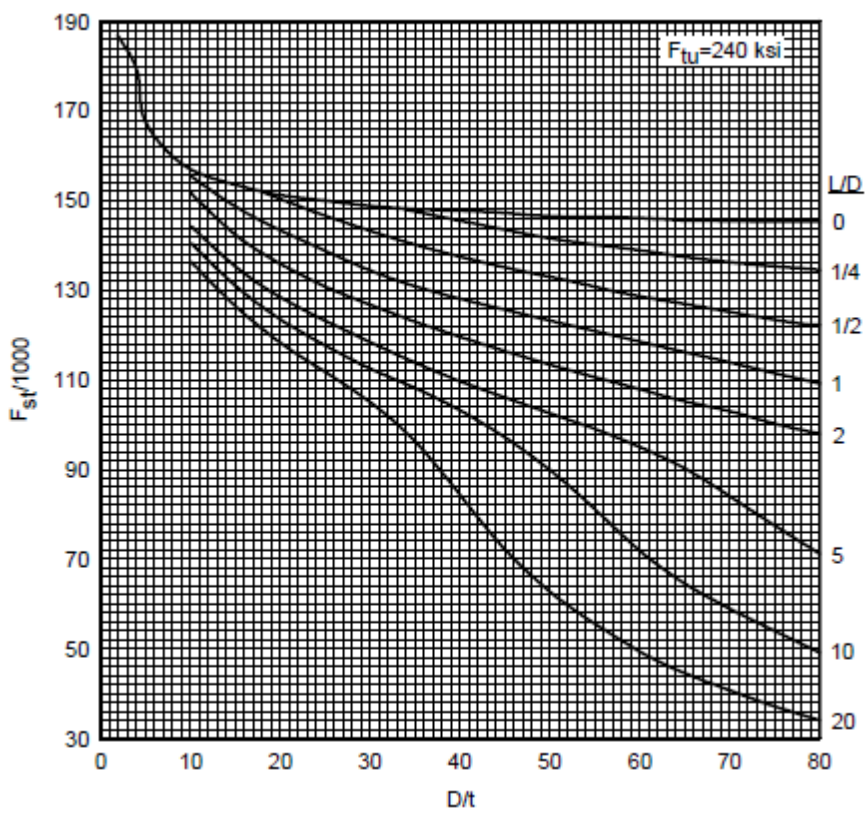


Figure 9.1.1-9: Torsional Modulus of Rupture – Alloy Steels Heat Treated to $F_{tu} = 240\text{ksi}$ [\(MIL-HNDBK-5H, 1998\)](#)

9.1.2. Torsion Modulus of Rupture for Round Aluminum Tubes

For circular cross sections the following figures give the torsion modulus of rupture for a range of Aluminum Alloys.

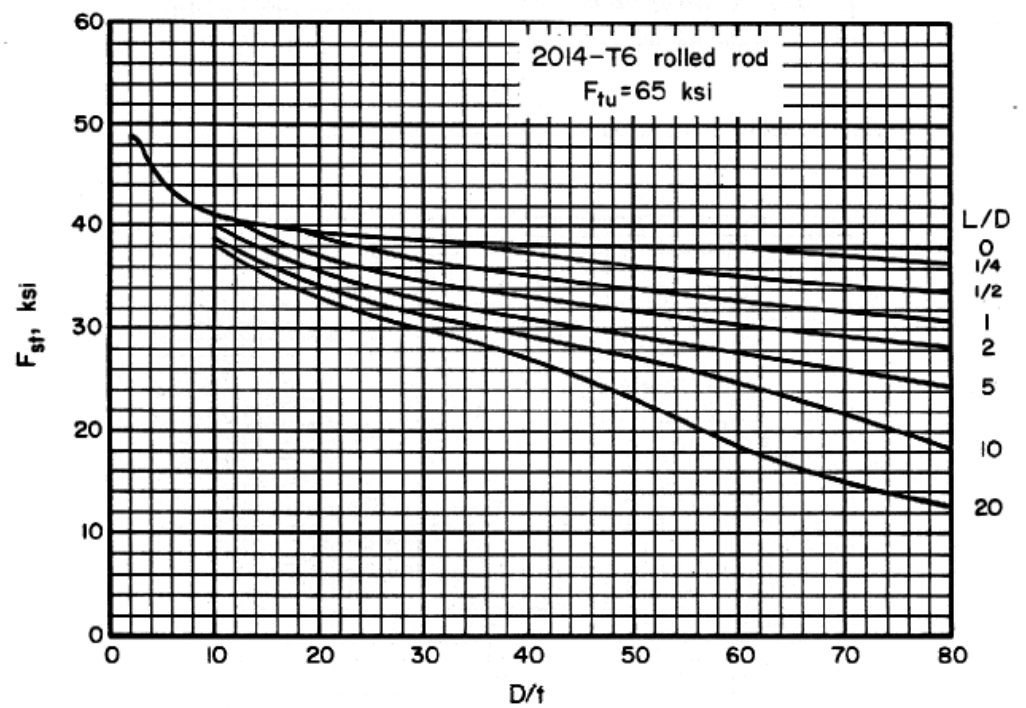


Figure 9.1.2-1: Torsional Modulus of Rupture – 2014-T6 Aluminum Alloy Rolled Rod [\(MIL-HNDBK-5H, 1998\)](#)

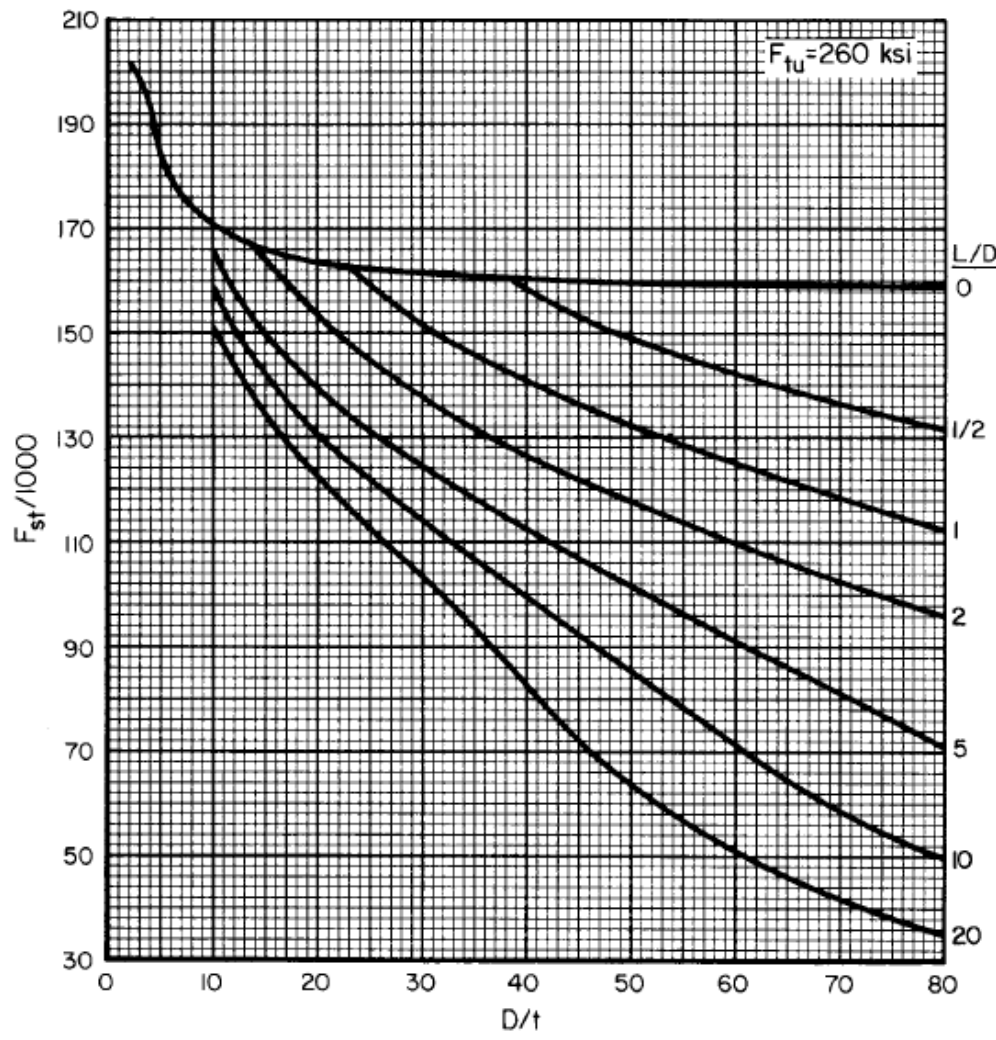


Figure 9.1.1-10: Torsional Modulus of Rupture – Alloy Steels Heat Treated to $F_{tu} = 260\text{ksi}$ [\(MIL-HNDBK-5H, 1998\)](#)

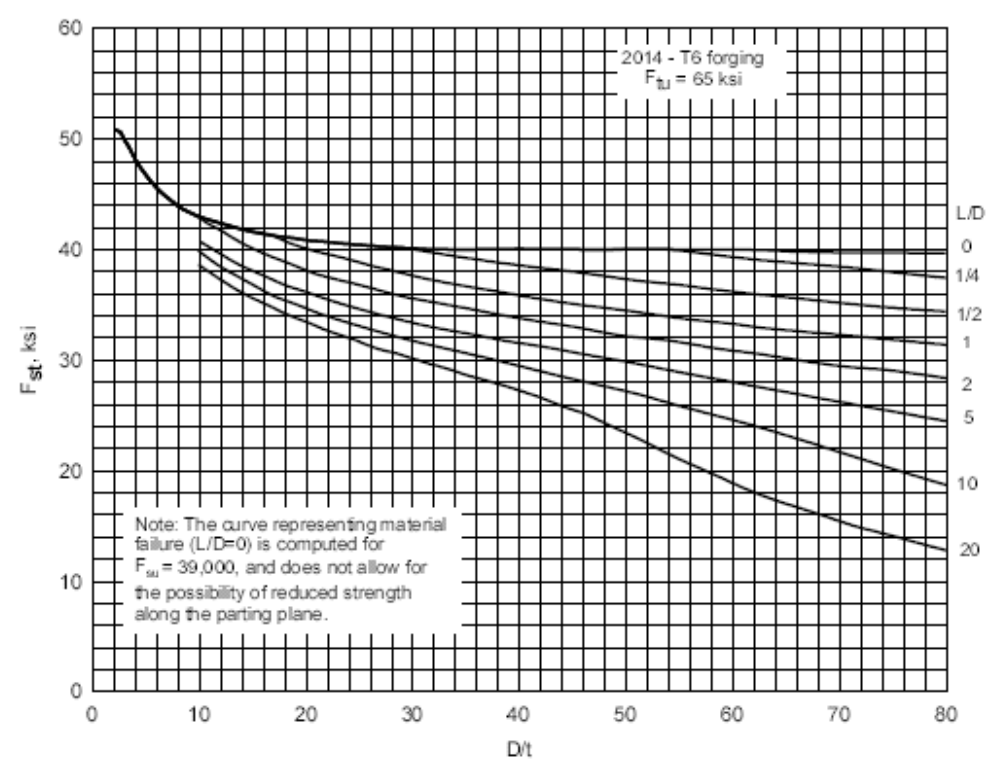


Figure 9.1.2-2: Torsional Modulus of Rupture – 2014-T6 Aluminum Alloy Forging [\(MIL-HNDBK-5H, 1998\)](#)

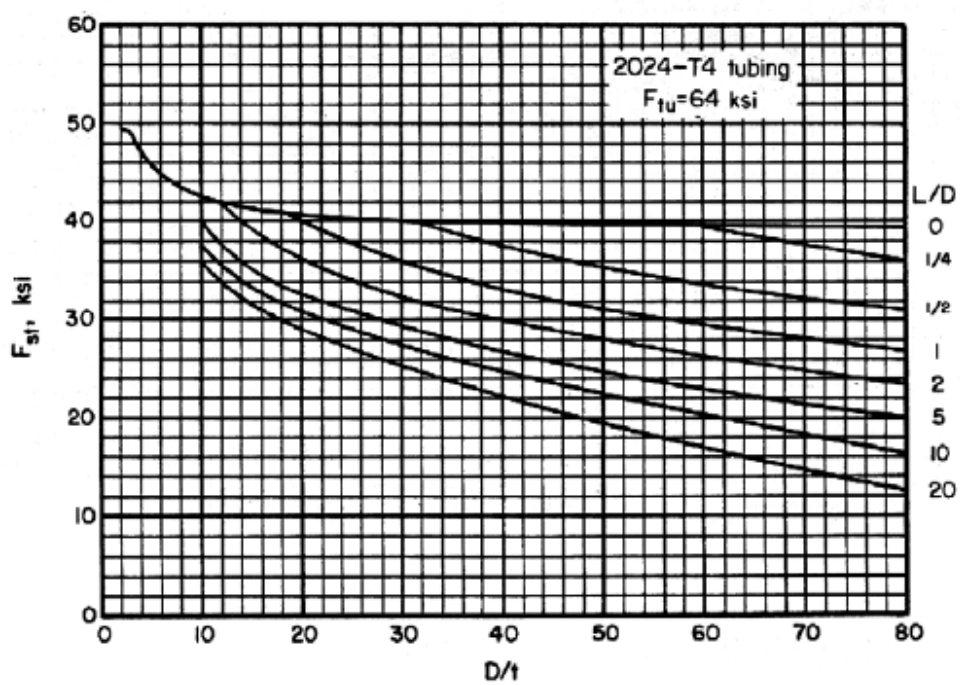


Figure 9.1.2-3: Torsional Modulus of Rupture – 2024-T4 Aluminum Alloy Tubing [\(MIL-HNDBK-5H, 1998\)](#)

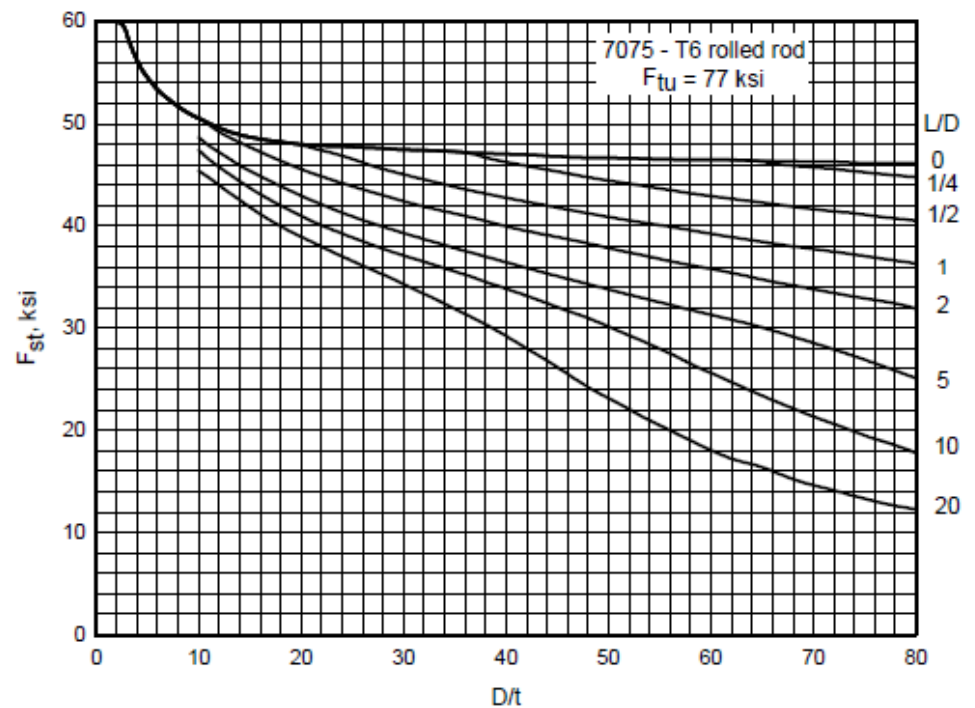


Figure 9.1.2-5: Torsional Modulus of Rupture – 7075-T6 Aluminum Alloy Rolled Rod [\(MIL-HNDBK-5H, 1998\)](#)

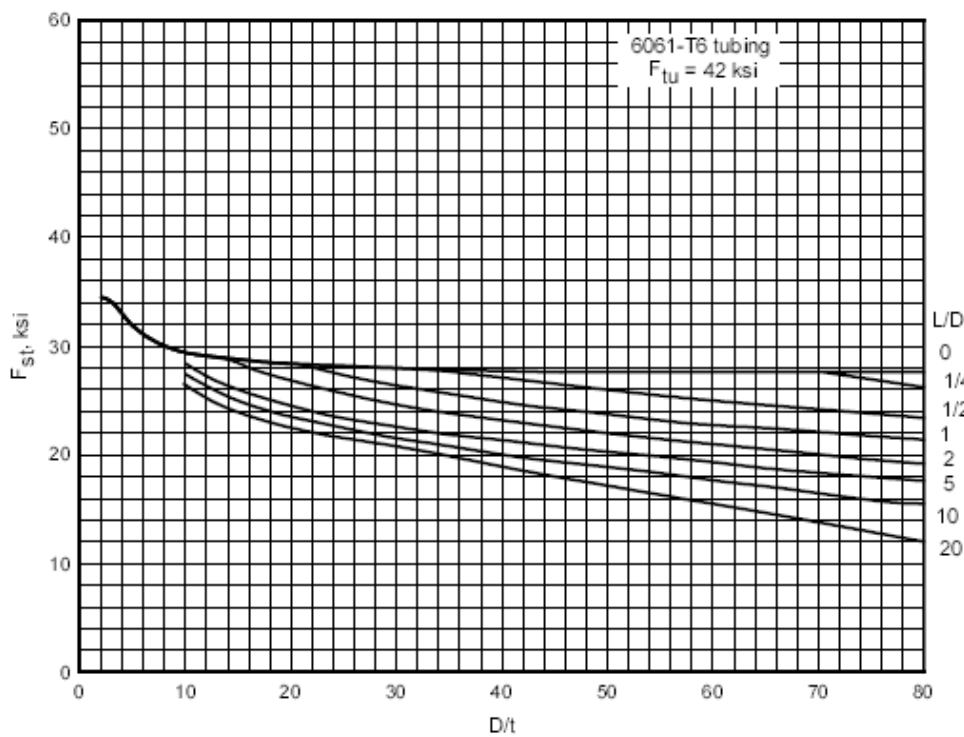


Figure 9.1.2-4: Torsional Modulus of Rupture – 6061-T6 Aluminum Alloy Tubing [\(MIL-HNDBK-5H, 1998\)](#)

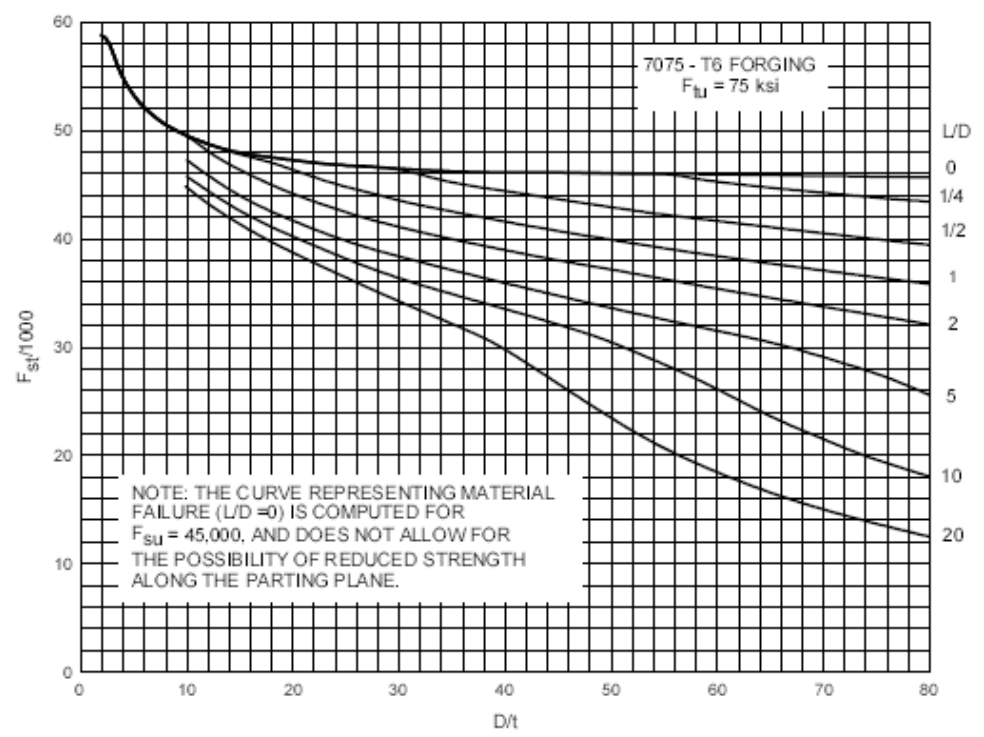


Figure 9.1.2-6: Torsional Modulus of Rupture – 7075-T6 Aluminum Alloy Forging [\(MIL-HNDBK-5H, 1998\)](#)

9.1.3. Torsion Modulus of Rupture for Round Magnesium Tubes

For circular cross sections the following figures give the torsion modulus of rupture for a single Magnesium Alloy.

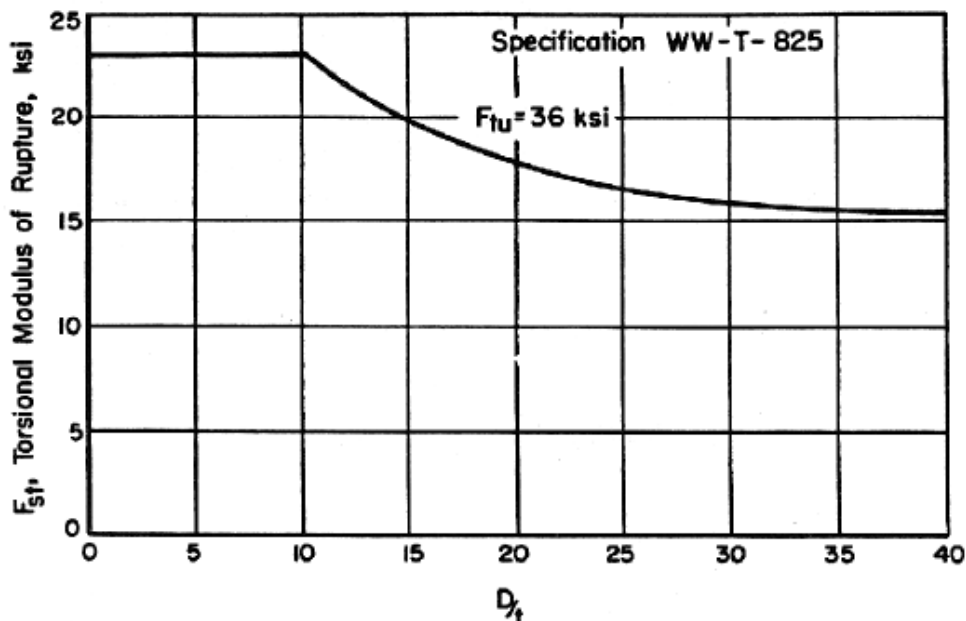
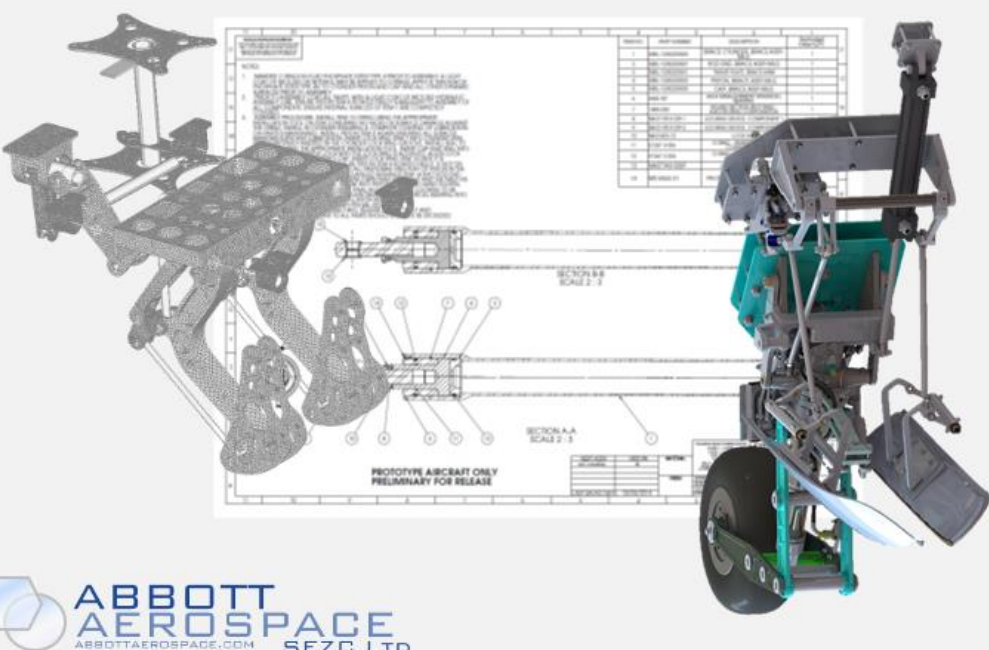


Figure 9.1.3-1: Torsional Modulus of Rupture – AZ61A-F Magnesium Alloy Round Tubing ([MIL-HNDBK-5H, 1998](#))

ADVERT: ENGINEERING SERVICES



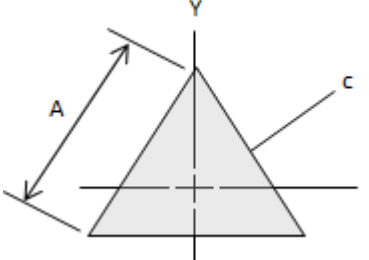
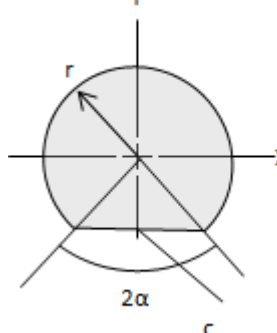
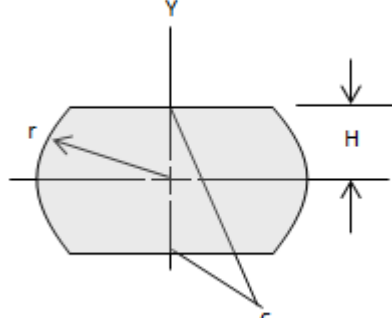
 **ABBOTT AEROSPACE**
 ABBOTTAEROSPACE.COM SEZC LTD

9.1.4. Torsion Stresses and Deflections of Regular Closed and Solid Shapes

The equations in the table below are valid for the elastic range of the material considered.

| Cross Section | Section Torsion Constant, Peak Shear Stress, Angular Deflection |
|------------------------------------|--|
| 1. Solid Round Rod | $J = \frac{\pi \cdot R^4}{2}$ $f_s = \frac{T \cdot R}{J}$ $\theta = \frac{T \cdot L}{J \cdot G}$ <div style="border: 1px solid #ccc; padding: 5px; margin-top: 10px;"> ABBOTT AEROSPACE SEZC LTD SPREADSHEETS AA-SM-002-011 Torsion – Regular Sections – Solid Round Rod </div> |
| 2. Thick-walled Round Tube | $J = \frac{\pi \cdot (R^4 - r^4)}{2}$ $f_s = \frac{T \cdot R}{J}$ $\theta = \frac{T \cdot L}{J \cdot G}$ <div style="border: 1px solid #ccc; padding: 5px; margin-top: 10px;"> ABBOTT AEROSPACE SEZC LTD SPREADSHEETS AA-SM-002-012 Torsion – Regular Sections – Thick Walled Round Tube </div> |
| 3. Thin-walled Round Tube | $J = 2 \cdot \pi \cdot t \cdot R^3$ $f_s = \frac{T \cdot R}{J}$ $\theta = \frac{T \cdot L}{J \cdot G}$ <div style="border: 1px solid #ccc; padding: 5px; margin-top: 10px;"> ABBOTT AEROSPACE SEZC LTD SPREADSHEETS AA-SM-002-013 Torsion – Regular Sections – Thin Walled Round Tube </div> |
| 4. Solid Rectangular or Square Bar | <div style="border: 1px solid #ccc; padding: 5px; margin-bottom: 10px;"> ABBOTT AEROSPACE SEZC LTD SPREADSHEETS AA-SM-002-014 Torsion – Regular Sections – Solid Rectangular and Square </div> $J = a \cdot b^3 \cdot \left[\frac{16}{3} - 3.36 \cdot \frac{b}{a} \cdot \left(1 - \frac{b^4}{12 \cdot a^4} \right) \right] \text{ for } a > b$ $f_s = \frac{3 \cdot T}{8 \cdot a \cdot b^2} \cdot \left[1 + 0.6095 \cdot \frac{b}{a} + 0.8865 \left(\frac{b}{a} \right)^2 - 1.8023 \cdot \left(\frac{b}{a} \right)^3 + 0.9100 \cdot \left(\frac{b}{a} \right)^4 \right]$ $\theta = \frac{T \cdot L}{J \cdot G}$ |

| Cross Section | Section Torsion Constant, Peak Shear Stress, Angular Deflection |
|-----------------------------------|---|
| 5. Solid Elliptical Section | $J = \frac{2 \cdot t_2 \cdot t_1 \cdot (a - t_2)^2 \cdot (b - t_1)^2}{a \cdot t_2 + b \cdot t_1 - t_1^2 - t_2^2}$ $f_{s1} = \frac{T}{2 \cdot t_1 \cdot (a - t_2) \cdot (b - t_1)}$ $f_{s2} = \frac{T}{2 \cdot t_2 \cdot (a - t_2) \cdot (b - t_1)}$ $\theta = \frac{T \cdot L}{J \cdot G}$ <div style="border: 1px solid #ccc; padding: 5px; margin-top: 10px;"> <p>ABBOTT AEROSPACE SEZC LTD SPREADSHEETS ABBOTTAEROSPACE.COM</p> <p>AA-SM-002-015 Torsion – Regular Sections – Thin Walled Rectangular or Square</p> </div> |
| 6. Solid Elliptical Section | $J = \frac{\pi \cdot a^3 \cdot b^3}{a^2 + b^2}$ $f_s = \frac{2 \cdot T}{\pi \cdot a^3 \cdot b^3}$ $\theta = \frac{T \cdot L}{J \cdot G}$ <div style="border: 1px solid #ccc; padding: 5px; margin-top: 10px;"> <p>ABBOTT AEROSPACE SEZC LTD SPREADSHEETS ABBOTTAEROSPACE.COM</p> <p>AA-SM-002-016 Torsion – Regular Sections – Solid Elliptical Section</p> </div> |
| 7. Thin Walled Elliptical Section | $C = \pi \cdot (a + b - t) \cdot \left[1 + 0.27 \cdot \frac{(a - b)^2}{(a + b)^2} \right]$ $J = \frac{4 \cdot \pi^2 \cdot t \cdot \left[\left(a - \frac{t}{2} \right)^2 \cdot \left(b - \frac{t}{2} \right)^2 \right]}{U}$ $f_s = \frac{T}{2 \cdot \pi \cdot t \cdot \left(a - \frac{t}{2} \right)^2 \cdot \left(b - \frac{t}{2} \right)^2}$ $\theta = \frac{T \cdot L}{J \cdot G}$ <div style="border: 1px solid #ccc; padding: 5px; margin-top: 10px;"> <p>ABBOTT AEROSPACE SEZC LTD SPREADSHEETS ABBOTTAEROSPACE.COM</p> <p>AA-SM-002-017 Torsion – Regular Sections – Thin Walled Elliptical Section</p> </div> |
| 8. Solid Hexagonal Rod | $J = 0.133 \cdot D^3$ $f_s = \frac{T}{0.217 \cdot \pi \cdot \frac{D^3}{4}}$ $\theta = \frac{T \cdot L}{J \cdot G}$ <div style="border: 1px solid #ccc; padding: 5px; margin-top: 10px;"> <p>ABBOTT AEROSPACE SEZC LTD SPREADSHEETS ABBOTTAEROSPACE.COM</p> <p>AA-SM-002-018 Torsion – Regular Sections – Solid Hexagonal Rod</p> </div> |

| Cross Section | Section Torsion Constant, Peak Shear Stress, Angular Deflection |
|--|---|
| 9. Circular Section with One Side Flattened | <p></p> $J = \frac{\sqrt{3}}{80} \cdot A^4$ $f_s = \frac{20 \cdot T}{A^3}$ $\theta = \frac{T \cdot L}{J \cdot G}$ <div style="border: 1px solid #ccc; padding: 5px; margin-top: 10px;"> <p>ABBOTT AEROSPACE SEZC LTD SPREADSHEETS ABBOTTAEROSPACE.COM</p> <p>AA-SM-002-019 Torsion – Regular Sections – Solid Triangular Rod</p> </div> |
| 10. Circular Section with One Side Flattened | <p></p> $z = 1 - \cos(\alpha)$ $k_1 = 1.5708 - 0.0666 \cdot z - 5.2366 \cdot z^2 + 8.319 \cdot z^3 - 6.1538 \cdot z^4 + 1.8598 \cdot z^5$ $k_2 = \frac{1}{0.6366 + 1.7598 \cdot z - 5.4897 \cdot z^2 + 14.062 \cdot z^3 - 14.51 \cdot z^4 + 6.434 \cdot z^5}$ $J = k_1 \cdot r^4$ $f_s = \frac{T}{k_2 \cdot r^3}$ $\theta = \frac{T \cdot L}{J \cdot G}$ <div style="border: 1px solid #ccc; padding: 5px; margin-top: 10px;"> <p>ABBOTT AEROSPACE SEZC LTD SPREADSHEETS ABBOTTAEROSPACE.COM</p> <p>AA-SM-002-020 Torsion – Regular Sections – Circular Section with One Side Flattened</p> </div> |
| 11. Circular Section with Opposite Sides Flattened | <p></p> $z = \frac{r - H}{r}$ $k_3 = 1.5708 - 0.8106 \cdot z - 7.162 \cdot z^2 + 10.5416 \cdot z^3 - 4.1544 \cdot z^4$ $k_4 = \frac{1}{0.6366 + 2.5303 \cdot z - 11.157 \cdot z^2 + 49.568 \cdot z^3 - 85.886 \cdot z^4 + 69.849 \cdot z^5}$ $J = k_3 \cdot r^4$ $f_s = \frac{T}{k_4 \cdot r^3}$ $\theta = \frac{T \cdot L}{J \cdot G}$ <div style="border: 1px solid #ccc; padding: 5px; margin-top: 10px;"> <p>ABBOTT AEROSPACE SEZC LTD SPREADSHEETS ABBOTTAEROSPACE.COM</p> <p>AA-SM-002-021 Torsion – Regular Sections – Circular Section with Opposite Sides Flattened</p> </div> |

9.2. Reserved

9.3. Reserved

10. PLATE STRENGTH ANALYSIS

10.1. Introduction

10.2. Isotropic Plates

10.2.1. Membrane Action of Plates under Uniform Pressure

This section is taken substantially from [\(AFFDL-TR-69-42, 1986\)](#) which has a good succinct summary of relevant analysis methods.

A membrane is a plate that has no bending rigidity, all stresses and in the plane of the surface and are usually tension.

This section uses the following nomenclature:

Where:

| | |
|--------------------------------------|---|
| a | Longitudinal dimension of membrane, in |
| D | Diameter, in |
| E | Material modulus of elasticity, psi |
| f | Calculated stress, psi |
| f_{max} | Calculated maximum stress, psi |
| n₁ – n₇ | Coefficients |
| p | Pressure, psi |
| R | Outside radius of circular membrane, in |
| t | Thickness of membrane, in |
| x, y | Rectangular coordinates, in |
| δ | Deflection, in |
| δ_c | Deflection at center of circular membrane, in |
| μ | Poisson's Ratio |

10.2.1.1. Circular Membranes

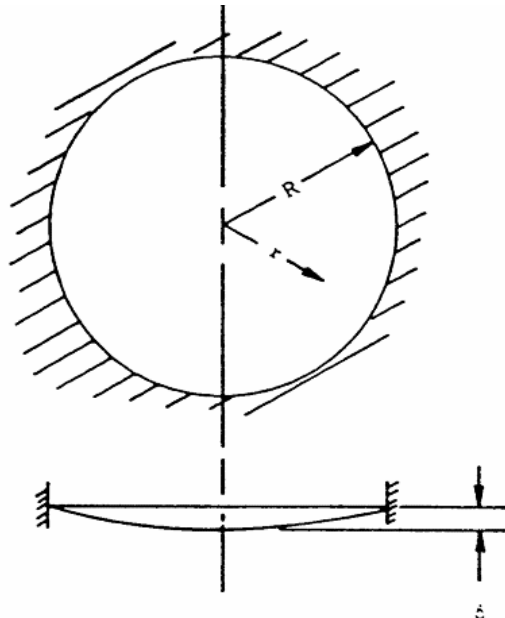


Figure 10.2.1-1: Circular Membrane with a Clamped Edge

The maximum deflection of a circular membrane with a clamped edge is given by:

$$\delta_c = 0.662 \cdot R \cdot \sqrt[3]{\frac{p \cdot R}{E \cdot t}}$$

The deflection of the membrane at a distance, r, from the center of the plate is:

$$\delta = \delta_c \cdot \left[1 - 0.09 \cdot \left(\frac{r}{R} \right)^2 - 0.10 \cdot \left(\frac{r}{R} \right)^5 \right]$$

The stress at the center of the membrane is:

$$f = 0.423 \cdot \sqrt[3]{\frac{E \cdot p^2 \cdot R^2}{t^2}}$$

The stress at the edge of the membrane is:

$$f = 0.328 \cdot \sqrt[3]{\frac{E \cdot p^2 \cdot R^2}{t^2}}$$

This method is available in a spreadsheet:

ABBOTT AEROSPACE SEZC LTD
SPREADSHEETS
ABBOTTAEROSPACE.COM

AA-SM-013-051 Circular Membranes

10.2.1.2. Rectangular Membranes

For a long membrane, the behavior will be such that the plate will behave the same whether the short edges are restrained.

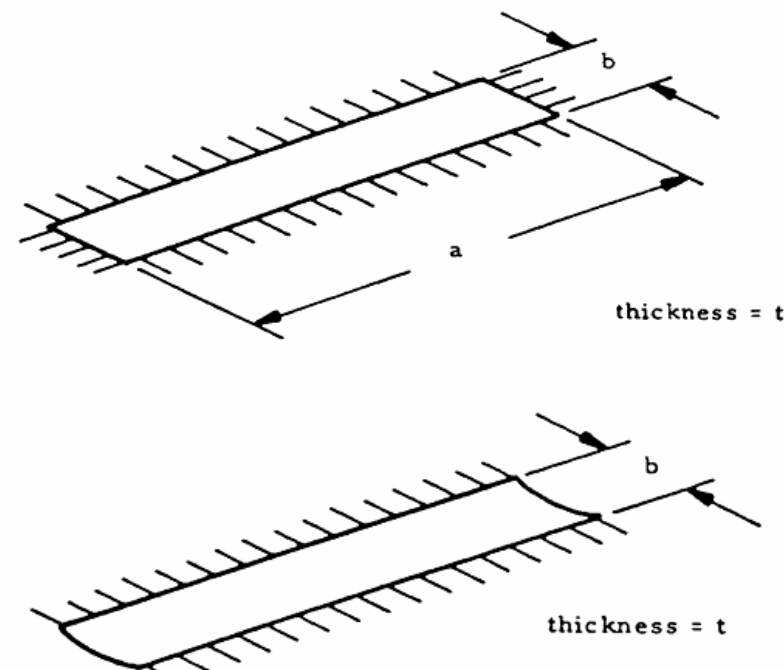


Figure 10.2.1-2: Equivalence of Simplified Long Plate

A membrane is assumed to be 'long' if $a/b > 5$.

A long plate is considered to be a membrane if $p/E \cdot (b/t)^4$ is greater than 100.

The maximum deflection at the center of the membrane is given by:

$$\delta = \frac{1}{8} \cdot b \cdot \left[\frac{24 \cdot (1 - \mu^2) \cdot p \cdot b}{E \cdot t} \right]^{1/3}$$

The stress at the center of the membrane is:

$$f_{max} = \left[\frac{p^2 \cdot E \cdot b^2}{24 \cdot (1 - \mu^2) \cdot t^2} \right]^{1/3}$$

ABBOTT AEROSPACE SEZC LTD
SPREADSHEETS
ABBOTTAEROSPACE.COM
AA-SM-013-052 Long Rectangular Membranes

For a short membrane, $a / b < 5$

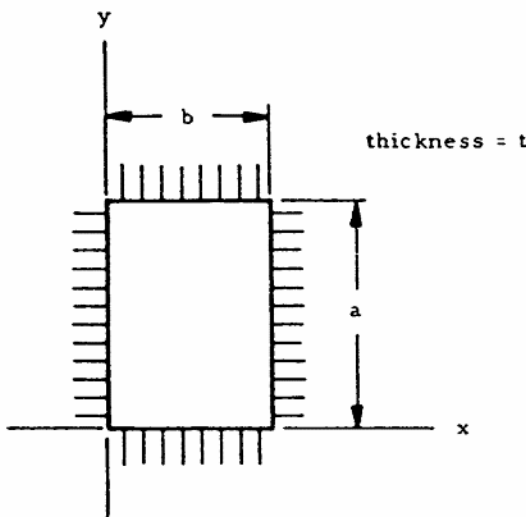


Figure 10.2.1-3: Short Rectangular Plates Clamped on Four Sides

Where n_1 thru n_7 are coefficients determined using the following figure:

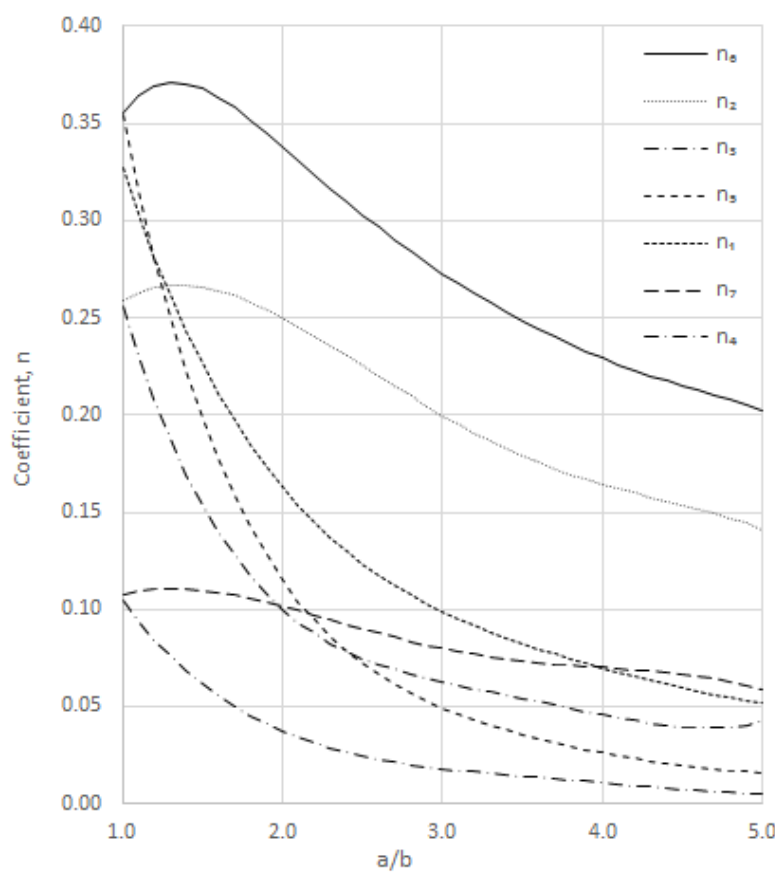


Figure 10.2.1-4: Short Rectangular Plate Coefficients

The deflection at the center of the membrane is given by:

$$\delta = n_1 \cdot a \cdot \sqrt[3]{\frac{(p \cdot a)}{(E \cdot t)}}$$

The stresses at the center of the membrane are given by:

$$f_x = n_2 \cdot \sqrt[3]{p^2 \cdot E \cdot (a/t)^2}$$

$$f_y = n_3 \cdot \sqrt[3]{p^2 \cdot E \cdot (a/t)^2}$$

The stresses at the center of the short side are given by:

$$f_x = n_4 \cdot \sqrt[3]{p^2 \cdot E \cdot (a/t)^2}$$

$$f_y = n_5 \cdot \sqrt[3]{p^2 \cdot E \cdot (a/t)^2}$$

The stresses at the center of the long side are given by:

$$f_x = n_6 \cdot \sqrt[3]{p^2 \cdot E \cdot (a/t)^2}$$

$$f_y = n_7 \cdot \sqrt[3]{p^2 \cdot E \cdot (a/t)^2}$$

The maximum stresses occur at the center of the long side of the plate.

This method is available as a spreadsheet here:

ABBOTT AEROSPACE SEZC LTD
SPREADSHEETS
ABBOTTAEROSPACE.COM
AA-SM-013-053 Short Rectangular Membranes

10.3. Composite Plates

10.3.1. Rectangular Plates

10.3.2. Circular Plates

ADVERT: TECHNICAL LIBRARY

TECHNICAL LIBRARY

SEE MORE

PUBLIC DOMAIN
TECHNICAL DATA



AERONAUTICAL RESEARCH COUNCIL

REPORTS AND MEMORANDA

We host a complete set of ARC Reports

ABBOTT
AEROSPACE
SEZC LTD

11. PRESSURE VESSELS

11.1. Introduction

11.2. Reserved

11.3. Reserved

This section will be included in a later edition. This page is a placeholder only.

12. JOINTS

12.1. Adhesive Joints

12.1.1. Introduction

The standard terms used to describe the components and parameters of bonded joints will be used throughout this section. They are defined below:

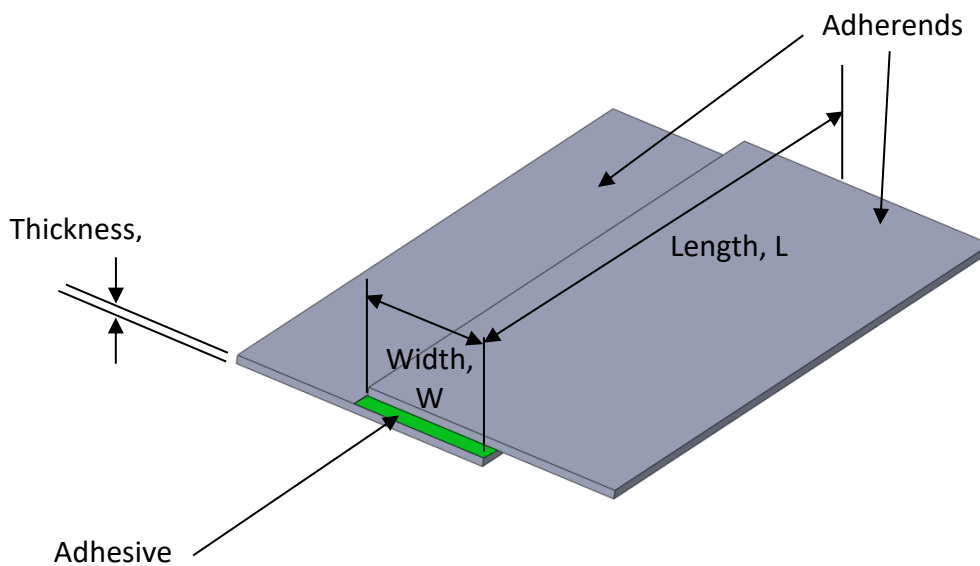


Figure 12.1.1-1: Adhesive Lap Joint Terms

- Adherends** – The panels joined by the adhesive
- Adhesive** – The glue that joins the panels together
- Width** – The overlap length of the joint
- Thickness** – The depth of the adhesive between the two panels
- Length** – The distance the two panels are joined

Types of Joints:

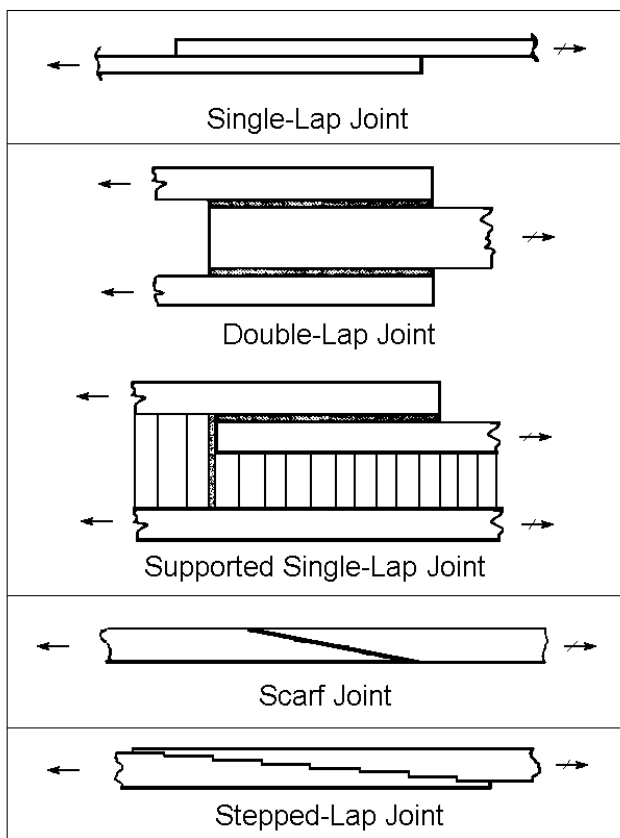


Figure 12.1.1-2: Types of Adhesive Joints

The most common type of adhesive joints in aircraft applications are single shear or single lap joints. These are the weakest joint configuration but it is the simplest to manufacture. They typically occur in wing ribs and wing spars to wing skin joints, fuselage frames to fuselage skins.

Single shear joints seem like the lazy option but in many circumstances, the simplicity and cost of design and manufacture make single shear joints prevalent in part 23 aircraft. In part 25 aircraft it is unusual to rely on the strength and reliability of an adhesive joint alone for primary load transfer. The discussion in this chapter is, therefore, concerning part 23 adhesive joint applications.

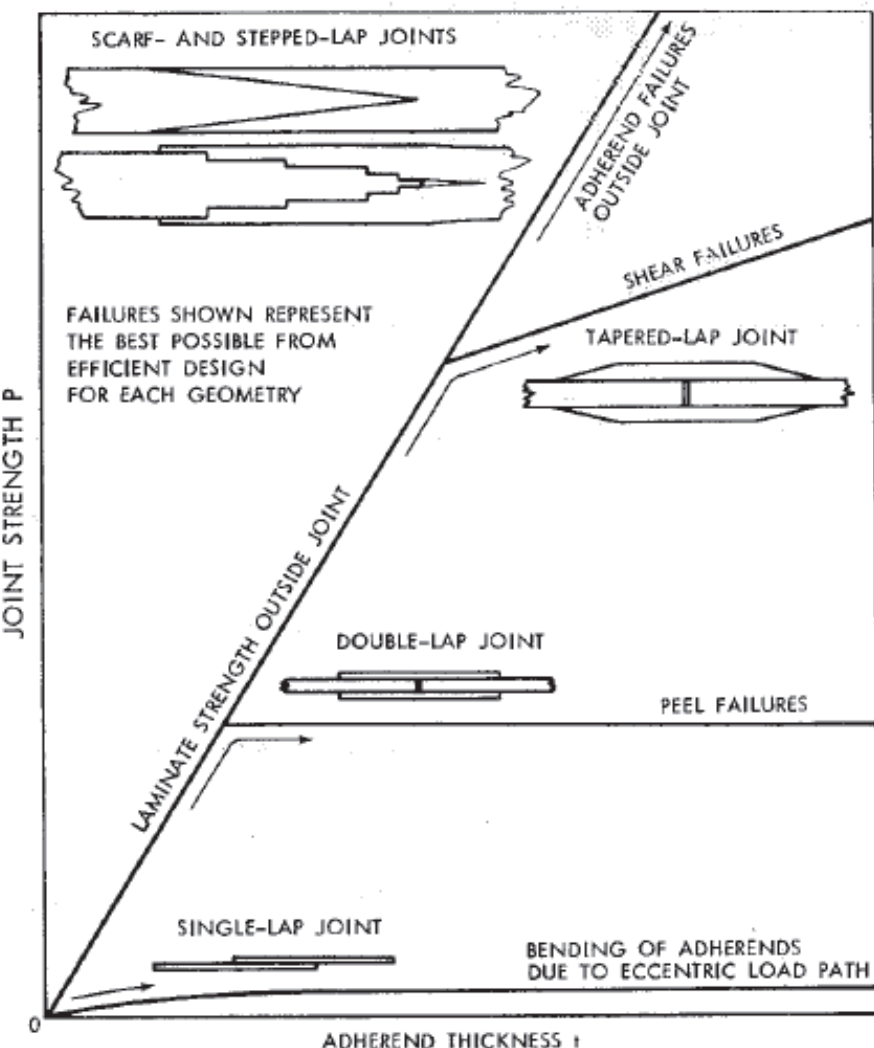


Figure 12.1.1-3: Effect of Joint Configuration and Adhesive Thickness on Joint Strength (NASA-CR-2218-1, 1974)

Note that in Figure 12.1.1-3 the single shear lap joint shows very low strength in comparison to the other pictured joint configurations.

The strength of adhesive joints depends on several factors:

- Strength of the adhesive.
- Adhesion to the surface by the adherends.
 - This is governed by the composite material and the condition of the surface of the composite material. Use of peel ply can help this aspect of the joint strength.
- Thickness of the adhesive in the joint.
 - The Thicker the joint, the lower the strength.
- Width of the joint.
 - The wider the joint, the stronger it is.
- Environmental conditions.
 - The critical condition can either be ETW (Extended Temperature Wet) or CTD (Cold Temperature Dry) depending on the response of the laminate and the adhesive to environmental conditions.

- Other factors such as the chemical compatibility of the adhesive with the resin matrix and the environmental conditions at the time the joint was manufactured.

The thickness of the adhesive (and of the composite panels) in the joint increases the offset in the joint, this offset creates a bending moment that causes peel stresses in the adhesive. This one aspect of the joint that the designer can influence affects joint stack up. Tooling and fixturing tolerances should all be carefully considered.

[\(DOT/FAA/AR-01/33, 2001\)](#) gives valuable test data on the effect of adhesive thickness on the single shear strength of joints using common composite and metallic materials.

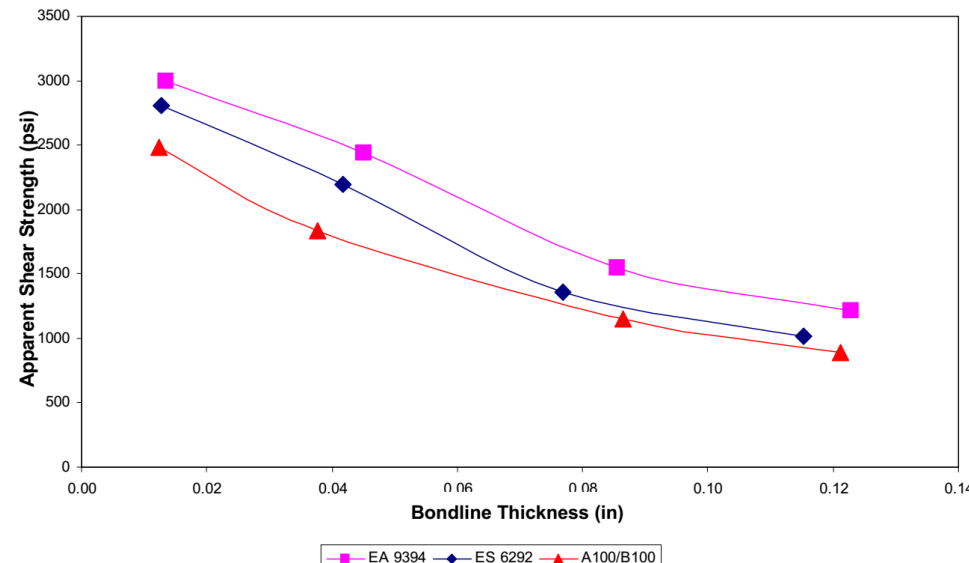


Figure 12.1.1-4: Apparent Shear Strength of 3 Adhesives with Aluminum Adherends [\(DOT/FAA/AR-01/33, 2001\)](#)

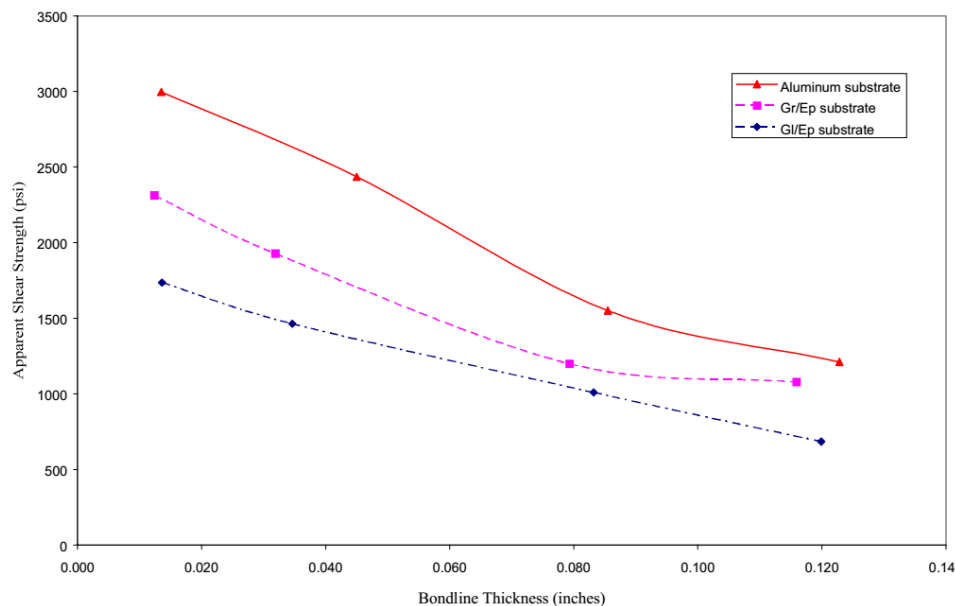


Figure 12.1.1-5: Apparent Shear Strength of 3 different Adherends for Hysol EA9394 Paste Adhesive [\(DOT/FAA/AR-01/33, 2001\)](#)

The strength values from the above figures should not be used without confirmation by test for the materials and processes specific to the application you are considering.

Note that the above figures use the term 'Apparent Shear Strength', this is the simplest measure of the shear strength of the joint. It is the load applied on test divided by the area of the bond.

For the apparent shear strength to be used, the general configuration of the joint tested must be representative of, or conservative compared to, the design intended for the final application. A range of situations should be tested – varying adherend and adhesive thicknesses - to determine the minimum joint strength at the critical environmental condition.

The moment that creates peel load is reacted over the width of the joint. The wider the joint, the smaller the peel effect on the adhesive.

It follows that the geometry of the adhesive joint should be controlled to maximize adhesive width and minimize adhesive thickness.

12.1.2. Desired Failure Mode

On test and in service; the desired failure mode is that the first ply (or more) should separate from the surface of the adherend.

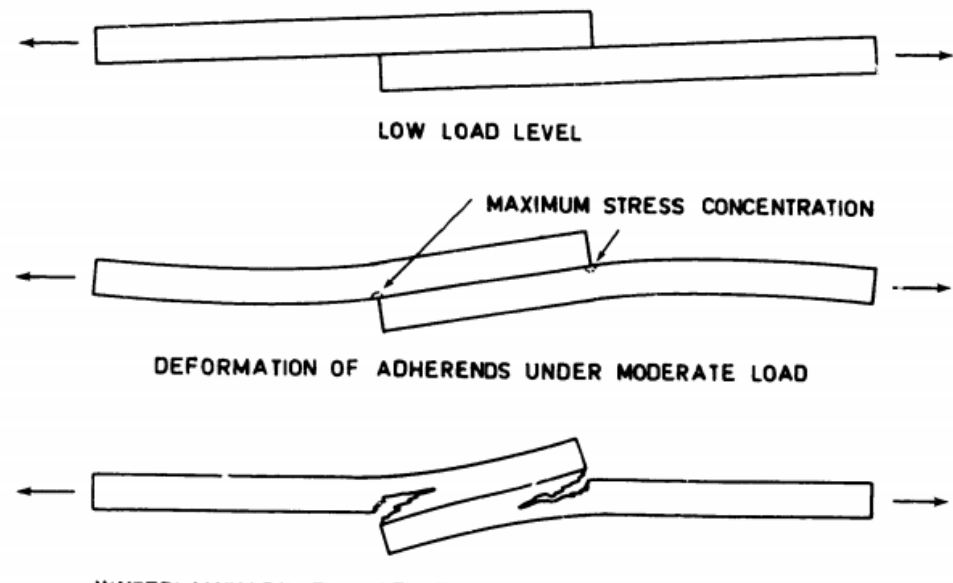


Figure 12.1.2-1: Single Adhesive Lap Joint Desired Failure Modes [\(NASA-CR-112236, 1973\)](#)

The joint geometry affects the shear and peel stress in the joint; both of which peak at the edge of the adhesive.

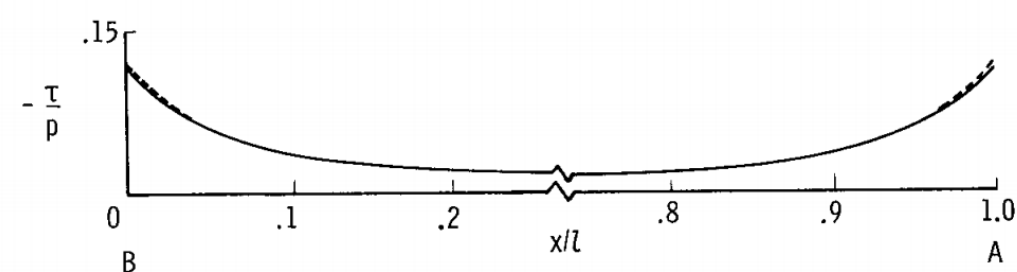


Figure 12.1.2-2: Single Shear Joint Shear Stress Distribution [\(NASA-TN-D-7855, 1975\)](#)

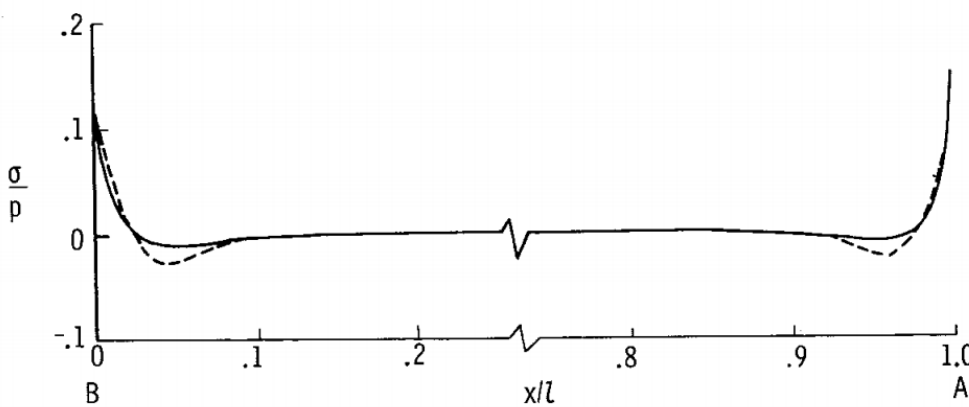


Figure 12.1.2-3: Single Shear Joint Peel Stress Distribution
(NASA-TN-D-7855, 1975)

12.1.3. Mitigation for Critical Joint Failure mode

(NASA-CR-112236, 1973) gives the following example of a way to reduce the peak peel stresses in a single lap shear adhesive joint.

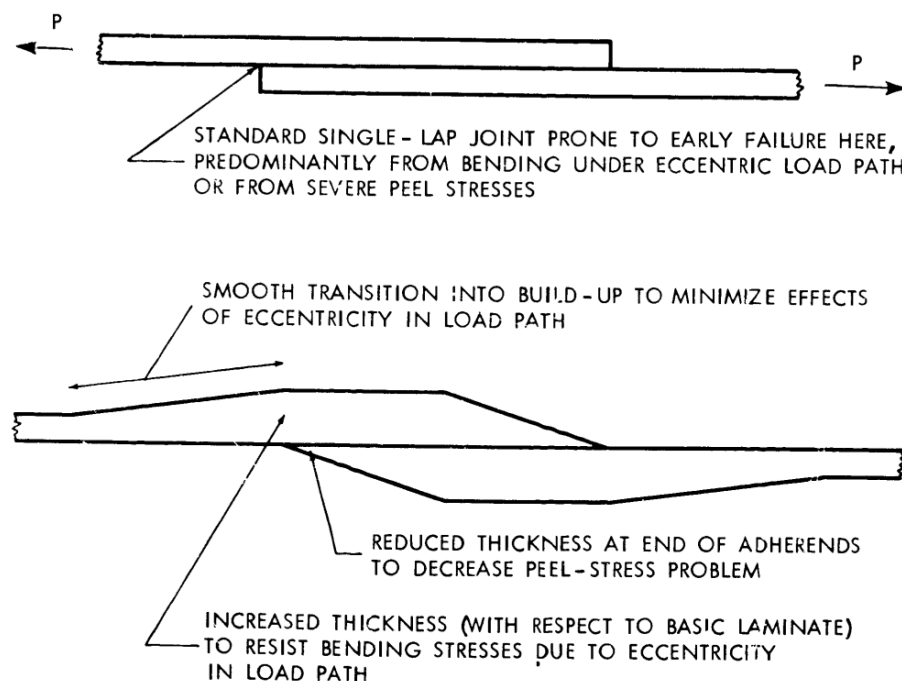


Figure 12.1.3-1: Peel Stress Mitigation in Single Shear Joint
(NASA-CR-112236, 1973)

It is not practical to increase the thickness as shown in the figure above, but the inclusion of a chamfer feature at the free edge of the adherend can increase apparent joint shear strength by 15% or more.

The analysis of adhesive joints can be complex and there are many theoretical methods and software/finite element methods and solutions proposed for the analysis of adhesive joints. However, adhesive joints are prone to a high level of strength variability in real life due to manufacturing variability and an inability to predict the precise load effects that the joint experiences.

Experience has shown that a simple conservative apparent lap shear analysis has sufficient accuracy for most structural application if the joint conforms to preferred design guidelines.

In our experience, a suitable preliminary working value for the apparent shear strength of an adhesive joint at worst case environment condition is 1000psi. This value must be confirmed by test before being used in a critical application in service.

Complete list of bonded joint references at the [Abbott Aerospace Technical Library](#):



ADVERT: SOFTWARE

EXCEL ADD-IN: SOFTWARE TOOLS

XL-VIKING

By Aerospace Stress Engineers for Aerospace Stress Engineers

Get More Out Of MS Excel

Fully Comptible with all of our Analysis Spreadsheets

12.2. Mechanically Fastened Joints

12.2.1. Introduction

'Joint strength' considers the failure of all the components and all failure modes within the joint. Joint strength is determined by the first critical failure mode of the joint.

Achieving full joint strength depends on good composition of the joint and selecting the correct hardware. Correct grip length, threaded portion length and use of washers will affect the static strength and durability of the joint.

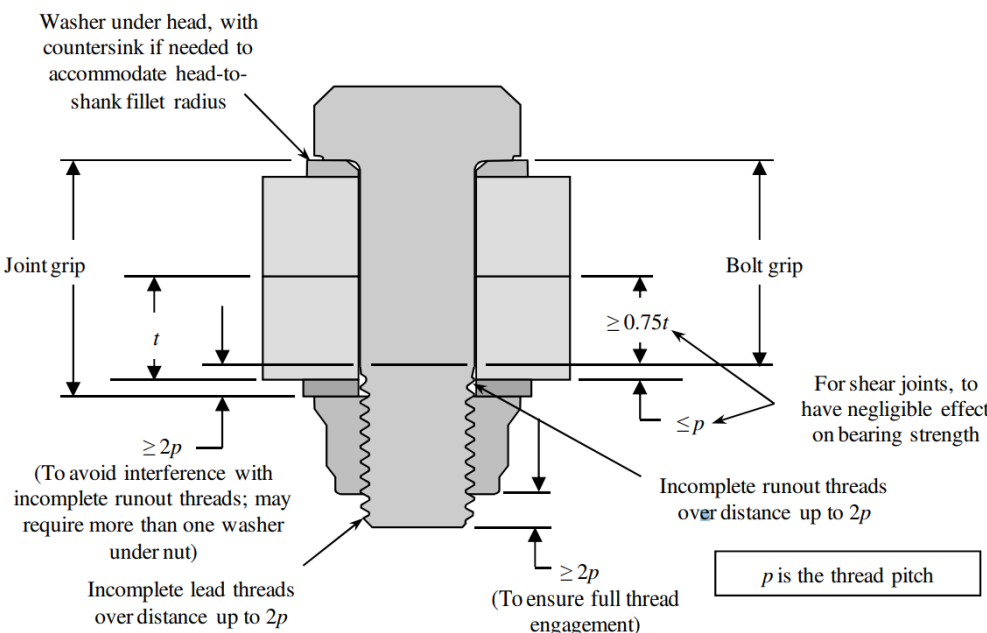


Figure 12.2.1-1: Mechanical Joint Composition and Geometric Considerations (NASA-STD-5020, 2012)

The designer also must be aware of galvanic corrosion potential between all the items in the joint. The plates or components being fastened, the bolt, nut and washers should be chosen with care. Reference section 4.4.

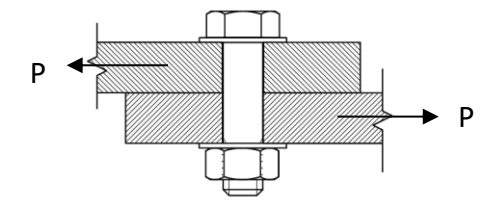
In mechanical joints involving composite structure the torque applied during bolt installation can damage the components fastened by the joint. In the authors experience, up to $\frac{1}{4}$ in diameter fasteners can be installed in carbon fiber composite structure with standard installation torque. Larger fasteners require mitigations such as a reduction in installation torque or large washers or plates. For more design guideline on mechanical joints in composite structure see section 12.2.4.1.

12.2.2. Mechanical Joint Strength

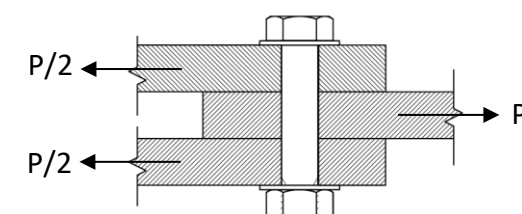
The **in-plane or shear strength** of a mechanically fastened joint includes consideration of the bearing failure of all items in the joint and the shear failure of the shank of the mechanical fastener. Depending on the joint configuration the in-plane strength may also include consideration of the bending failure of the shank of the mechanical fastener. If large out-of-plane deflections occur before failure; the fastener head can pull through the panels in the joint. The critical failure load of the joint will often include a combination of all of the above effects – but we call it bearing strength and assume the propensity for failure varies proportionally to the thickness (within limits).

The calculation of the in-plane strength of a joint may not include friction between items in the joint, the adhesive effects of liquid shim or fay surface sealant. *This is not because these effects do not exist but rather that there is no*

process control applied during manufacturing to these aspects of the joint that guarantee any level of strength..



Single Shear



Double Shear

Figure 12.2.2-1: Mechanically Fastened Shear (in-plane) Loaded Joints

The out-of-plane or tension strength of the joint includes the pull-out strength of the sheets, the tension strength of the fastener (the least of the minimum tension area strength of the fastener shank/threaded portion and the shear out of the threads) and the tension/pullout strength of the nut, nut-panel or collar.

Note: There is a more complex method of determining the joint tension strength where the fastener pre-tension is accounted for. However, the effect of the fastener pre-load on the joint strength is not considered significant in this methodology.

Note: The published tension strengths for rivets are usually higher than the desirable tension load. A tension load in excess of 20% of the rivet shear strength can result in the deformation of the formed tail of the rivet and loss of joint clamp-up which significantly degrades the fatigue life of the riveted joint.

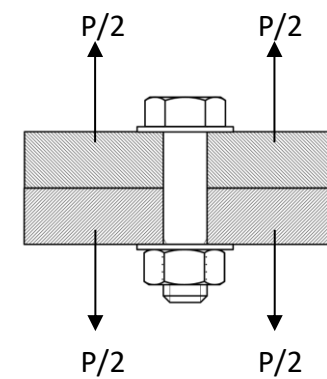


Figure 12.2.2-2: Mechanically Fastened Tension (out-of-plane) Loaded Joints

Note: The strength of each joint is subjected to the 1.5 ultimate load factor used for all structural analysis per FAR 23.303/25.303. Joints at fittings are also subjected to an additional 1.15 fitting factor per FAR 23.625/25.625.

Engineering judgment should be used when considering which checks to apply to a joint. If the tension load is low and it is not likely to significantly affect the overall margin of safety of the joint then is it acceptable to quote the shear strength margin of safety without considering the tension load effects - and vice-versa, if the applied shear load is much less than the tension load the tension margin of safety may be quoted without considering shear load effects.

The lower the overall load magnitude is, the greater the margin and the more leeway may be used in discriminating against particular lesser load effects in order to simplify the stress analysis. The converse is also true, if the margin of safety from one load effect alone is low then the other, much smaller, load effect may have to be considered and interacted with the primary load in order to ensure the structural integrity of the joint.

The following diagram shows how the in-plane strength of a mechanical joint varies with the thickness of the fastener sheets for protruding head and countersunk fastener in metal and for a general fastener in a fiber composite laminate.

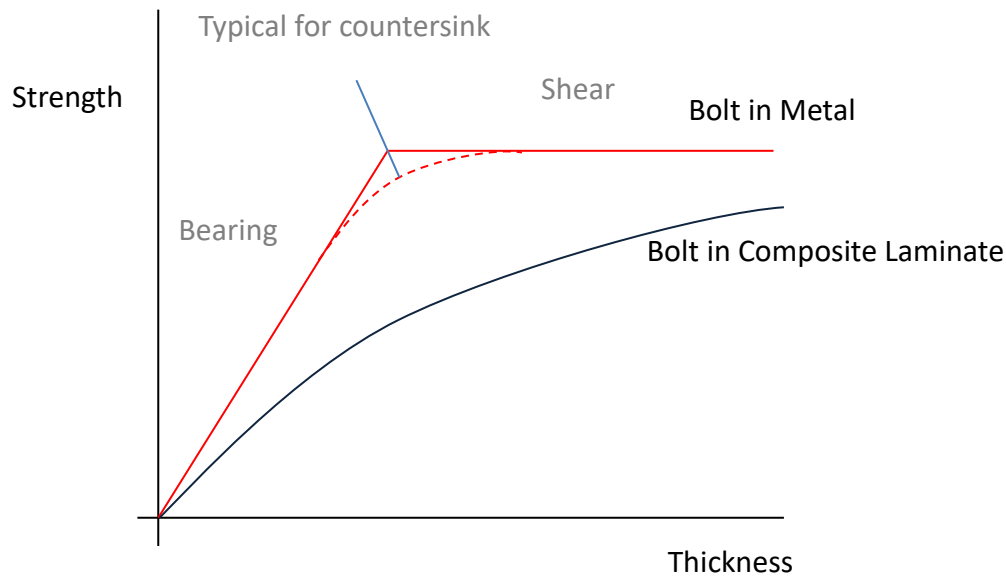


Figure 12.2.2-3: How in-plane Joint Strength Changes with Thickness

- The bearing strength (for protruding head fasteners) in metal components can be reliably calculated by the bearing area (Sheet Thickness x Fastener Diameter) multiplied by the bearing strength of the sheet material (F_{bru}).
- Note that the shear strength portion of Figure 12.2.2-3 for metal joints is solely a function of the strength of the fastener shank in shear. That is the cross-sectional area of the shank multiplied by its ultimate shear strength (F_{su}). This strength value is not affected by the thickness of the sheets in the joint.
- Note that in a typically formulated joint between sheets of composite laminate the fastener shank shear strength is not reached. The implication of this is that in a mechanically fastened joint between composite laminate sheets the joint failure mode will always be a failure in the composite laminate sheets. This is not always the case (it depends on the precise joint configuration: sheet thickness, sheet material, environmental condition, hole fit, fastener size and fastener material) but for typical mechanical joints in composite laminate components, it is a reasonable assumption.
- It can also be seen that the failure behavior of a mechanical fastener in a composite laminate sheet is not a simple bearing failure like that seen in metal sheets - the failure mode can be a combination of bolt bending and local bearing failure due to non-uniform bearing stresses combined with brittle bearing failure of the composite laminate material. There is no

accurate way to develop these failure loads theoretically, therefore the strength of mechanical fasteners in composite laminates must be determined by test – or conservative assumptions must be applied where applicable test data does not exist.

12.2.2.1. Aircraft Rivet Identification

See Section 27.1 for a more comprehensive definition of rivet types.

| Material Head Marking | 1100 | 2117T | 2017T | 2017T-HD | 2024T | 5056T | 7075-T73 |
|--------------------------------------|-------|--------|--------|----------|--------|-------|----------|
| AN Material Code | A | AD | D | D | DD | B | |
| AN425 78# Counter-Sunk Head | X | X | X | X | X | | X |
| AN426 100# Counter-Sunk Head MS20426 | X | X | X | X | X | X | X |
| AN427 100# Counter-Sunk Head MS20427 | | | | | | | |
| AN430 Round Head MS20470 | X | X | X | X | X | X | X |
| AN435 Round Head MS20613 MS20615 | | | | | | | |
| AN 441 Flat Head | | | | | | | |
| AN 442 Flat Head MS20470 | X | X | X | X | X | X | X |
| AN 455 Brazier Head MS20470 | X | X | X | X | X | X | X |
| AN 456 Brazier Head MS20470 | X | X | X | X | X | X | X |
| AN 470 Universal Head MS20470 | X | X | X | X | X | X | X |
| Heat Treat Before Using | No | No | Yes | No | Yes | No | No |
| Shear Strength psi | 10000 | 30000 | 34000 | 38000 | 41000 | 27000 | |
| Bearing Strength psi | 25000 | 100000 | 113000 | 126000 | 136000 | 90000 | |

Figure 12.2.2-4: Aircraft Rivet Markings [\(AC43.13-1B, 1998\)](#)

| Material | Carbon Steel | Corrosion-Resistant Steel | Copper | Monel | Monel Nickel-Copper Alloy | Brass | Titanium |
|--------------------------------------|-------------------|---------------------------|--------|-------|---------------------------|-------|------------------------------|
| Head Marking | Recessed Triangle | Recessed Dash | Plain | Plain | Recessed Double Dots | Plain | Recessed Large and Small Dot |
| AN Material Code | | F | C | M | C | | |
| AN425 78# Counter-Sunk Head | | | | | | | |
| AN426 100# Counter-Sunk Head MS20426 | | | | | | | MS 20426 |
| AN427 100# Counter-Sunk Head MS20427 | X | X | X | X | | | |
| AN430 Round Head MS20470 | | | | | | | |
| AN435 Round Head MS20613 MS20615 | X | X | X | | X X | | |
| | MS20613 | MS20613 | | | MS20615 MS20615 | | |
| AN 441 Flat Head | X | | X | X | | | X |
| AN 442 Flat Head MS20470 | | | | | | | |
| AN 455 Brazier Head MS20470 | | | | | | | |
| AN 456 Brazier Head MS20470 | | | | | | | |
| AN 470 Universal Head MS20470 | | | | | | | |
| Heat Treat Before Using | No | No | No | No | No | No | No |
| Shear Strength psi | 35000 | 65000 | 23000 | 49000 | 49000 | | 95000 |
| Bearing Strength psi | 90000 | 90000 | | | | | |

Figure 12.2.2-5: Aircraft Rivet Markings [\(AC43.13-1B, 1998\)](#)

12.2.2.2. Aircraft Bolt Identification

See Section 27.3 for a more comprehensive definition of bolt types.

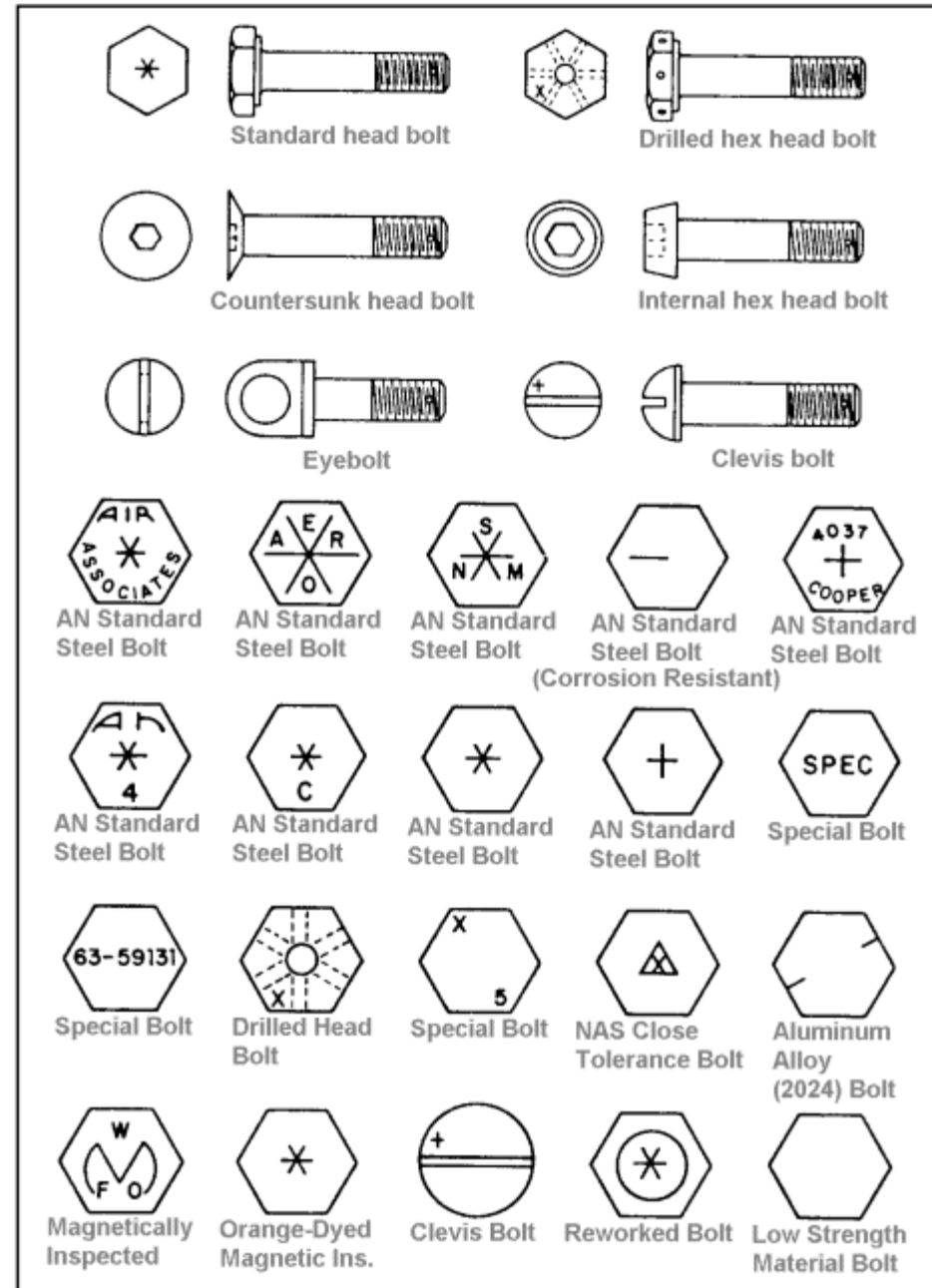


Figure 12.2.2-6: Typical Aircraft Bolt Markings [\(AC43.13-1B, 1998\)](#)

12.2.2.3. Bolt Installation Torque Values

Threaded fasteners, unless specified on the drawing, must be torqued at installation to provide a pretension on the joint.

From [\(AC43.13-1B, 1998\)](#):

"The importance of correct torque application cannot be overemphasized. Undertorque can result in unnecessary wear of nuts and bolts, as well as the parts they secure. Overtorque can cause failure of a bolt or nut from overstressing the threaded areas. Uneven or additional loads that are applied to the assembly may result in wear or premature failure. The following are a few simple, but important procedures, that should be followed to ensure that correct torque is applied"

| CAUTION THE FOLLOWING TORQUE VALUES ARE DERIVED FROM OIL FREE CADMIUM PLATED THREADS. | | | | | |
|--|---|---|--|--|--|
| | | MAXIMUM ALLOWABLE TIGHTENING TORQUE LIMITS | | | |
| Thread Size | Tension type nuts MS20365 and AN310 (40,000 psi in bolts) | Shear type nuts MS20364 and AN320 (24,000 psi in bolts) | Nuts MS20365 and AN310 (90,000 psi in bolts) | Nuts MS20364 and AN320 (54,000 psi in bolts) | |
| FINE THREAD SERIES | | | | | |
| 8-36 | 12-15 | 7-9 | 20 | 12 | |
| 10-32 | 20-25 | 12-15 | 40 | 25 | |
| 1/4-28 | 50-70 | 30-40 | 100 | 60 | |
| 5/16-24 | 100-140 | 60-85 | 225 | 140 | |
| 3/8-24 | 160-190 | 95-110 | 390 | 240 | |
| 7/16-20 | 450-500 | 270-300 | 840 | 500 | |
| 1/2-20 | 480-690 | 290-410 | 1100 | 660 | |
| 9/16-18 | 800-1000 | 480-600 | 1600 | 960 | |
| 5/8-18 | 1100-1300 | 600-780 | 2400 | 1400 | |
| 3/4-16 | 2300-2500 | 1300-1500 | 5000 | 3000 | |
| 7/8-14 | 2500-3000 | 1500-1800 | 7000 | 4200 | |
| 1-14 | 3700-5500 | 2200-3300* | 10,000 | 6000 | |
| 1-1/8-12 | 5000-7000 | 3000-4200* | 15,000 | 9000 | |
| 1-1/4-12 | 9000-11,000 | 5400-6600* | 25,000 | 15,000 | |
| COARSE THREAD SERIES | | | | | |
| 8-32 | 12-15 | 7-9 | 20 | 12 | |
| 10-24 | 20-25 | 12-15 | 35 | 21 | |
| 1/4-20 | 40-50 | 25-30 | 75 | 45 | |
| 5/16-18 | 80-90 | 48-55 | 160 | 100 | |
| 3/8-16 | 160-185 | 95-100 | 275 | 170 | |
| 7/16-14 | 235-255 | 140-155 | 475 | 280 | |
| 1/2-13 | 400-480 | 240-290 | 880 | 520 | |
| 9/16-12 | 500-700 | 300-420 | 1100 | 650 | |
| 5/8-11 | 700-900 | 420-540 | 1500 | 900 | |
| 3/4-10 | 1150-1600 | 700-950 | 2500 | 1500 | |
| 7/8-9 | 2200-3000 | 1300-1800 | 4600 | 2700 | |
| The above torque values may be used for all cadmium-plated steel nuts of the fine or coarse thread series which have approximately equal number of threads and equal face bearing areas. | | | | | |
| * Estimated corresponding values. | | | | | |

Figure 12.2.2-7: Recommended Bolt Torque Values ([AC43.13-1B, 1998](#))

12.2.3. Mechanical Joints in Metal Panels

The in-plane strength of mechanical joints in metal panels can be reliably predicted using available and approved strength data for the bearing strength of the sheet and the shear and tension strengths of the fasteners. The best source for this data is [\(MIL-HNDBK-5H, 1998\) Chapter 8.1](#).

Useful data is shown below.

12.2.3.1. In-Plane Shear Strength of Rivets

Ref [\(MIL-HNDBK-5H, 1998\) Table 8.1.2\(a\) and Table 8.1.2\(b\)](#)

| Rivet Size [in] | Rivet Size [in] | Drill No. | Nominal Hole Dia. [in] | Single Shear Strength [lbs] | | | |
|-----------------|-----------------|-----------|------------------------|-----------------------------|-----------|------------|---------|
| | | | | AD 2117-T4 | D 2017-T4 | DD 2024-T4 | M Monel |
| 1/16 | 0.063 | 51 | 0.067 | 106 | 134 | 145 | 183 |
| 3/32 | 0.094 | 41 | 0.096 | 217 | 275 | 297 | 376 |
| 1/8 | 0.125 | 30 | 0.1285 | 389 | 493 | 532 | 674 |
| 5/32 | 0.156 | 21 | 0.159 | 596 | 755 | 814 | 1030 |
| 3/16 | 0.188 | 11 | 0.191 | 860 | 1085 | 1175 | 1490 |
| 1/4 | 0.250 | F | 0.257 | 1555 | 1970 | 2125 | 2695 |
| 5/16 | 0.313 | P | 0.323 | 2455 | 3115 | 3360 | 4260 |
| 3/8 | 0.375 | W | 0.386 | 3510 | 4445 | 4795 | 6085 |

In calculating protruding-head rivet design shear strengths, the shear strength values obtained from Table 8.1.2(b) should be multiplied by the correction factors given in Table 8.1.2.1(b) – given below. This allows for the reduction in rivet shear strength resulting from high bearing stresses on the rivet at t/D ratios less than 0.33 for single-shear joints and 0.67 for double-shear joints.

| Sheet Thickness [in] | Single-Shear Rivet Strength Factors | | | | | | | |
|----------------------|-------------------------------------|-------|-------|-------|-------|-------|-------|-------|
| | 1/16 | 3/32 | 1/8 | 5/32 | 3/16 | 1/4 | 5/16 | 3/8 |
| 0.016 | 0.964 | | | | | | | |
| 0.018 | 0.981 | 0.912 | | | | | | |
| 0.020 | 0.995 | 0.933 | | | | | | |
| 0.025 | 1.000 | 0.970 | 0.920 | | | | | |
| 0.032 | 1.000 | 1.000 | 0.964 | 0.925 | | | | |
| 0.036 | 1.000 | 1.000 | 0.981 | 0.946 | 0.912 | | | |
| 0.040 | 1.000 | 1.000 | 0.995 | 0.964 | 0.933 | | | |
| 0.045 | 1.000 | 1.000 | 1.000 | 0.981 | 0.953 | | | |
| 0.050 | 1.000 | 1.000 | 1.000 | 0.995 | 0.970 | 0.920 | | |
| 0.063 | 1.000 | 1.000 | 1.000 | 1.000 | 1.000 | 0.961 | 0.922 | |
| 0.071 | 1.000 | 1.000 | 1.000 | 1.000 | 1.000 | 0.979 | 0.944 | 0.909 |
| 0.080 | 1.000 | 1.000 | 1.000 | 1.000 | 1.000 | 0.995 | 0.964 | 0.933 |
| 0.090 | 1.000 | 1.000 | 1.000 | 1.000 | 1.000 | 1.000 | 0.981 | 0.953 |
| 0.100 | 1.000 | 1.000 | 1.000 | 1.000 | 1.000 | 1.000 | 0.995 | 0.972 |
| 0.125 | 1.000 | 1.000 | 1.000 | 1.000 | 1.000 | 1.000 | 1.000 | 1.000 |

| Sheet Thickness [in] | Double-Shear Rivet Strength Factors | | | | | | | |
|----------------------|-------------------------------------|-------|-------|-------|-------|-------|-------|-------|
| | 1/16 | 3/32 | 1/8 | 5/32 | 3/16 | 1/4 | 5/16 | 3/8 |
| 0.016 | 0.687 | | | | | | | |
| 0.018 | 0.744 | 0.518 | | | | | | |
| 0.020 | 0.789 | 0.585 | | | | | | |
| 0.025 | 0.870 | 0.708 | 0.545 | | | | | |
| 0.032 | 0.941 | 0.814 | 0.687 | 0.560 | | | | |
| 0.036 | 0.969 | 0.857 | 0.744 | 0.630 | 0.518 | | | |
| 0.040 | 0.992 | 0.891 | 0.789 | 0.687 | 0.585 | | | |
| 0.045 | 1.000 | 0.924 | 0.834 | 0.744 | 0.653 | | | |
| 0.050 | 1.000 | 0.951 | 0.870 | 0.789 | 0.708 | 0.545 | | |
| 0.063 | 1.000 | 1.000 | 0.937 | 0.872 | 0.808 | 0.679 | 0.550 | |
| 0.071 | 1.000 | 1.000 | 0.966 | 0.909 | 0.852 | 0.737 | 0.622 | 0.508 |
| 0.080 | 1.000 | 1.000 | 0.992 | 0.941 | 0.891 | 0.789 | 0.687 | 0.585 |
| 0.090 | 1.000 | 1.000 | 1.000 | 0.969 | 0.924 | 0.834 | 0.744 | 0.653 |
| 0.100 | 1.000 | 1.000 | 1.000 | 0.992 | 0.951 | 0.870 | 0.789 | 0.708 |
| 0.125 | 1.000 | 1.000 | 1.000 | 1.000 | 1.000 | 0.935 | 0.870 | 0.805 |
| 0.160 | 1.000 | 1.000 | | | | | | |

However, the tension strength of a joint can be significantly less than this based on the shape of the fastener head and the fastener material. [\(NACA-TN-930, 1944\)](#) shows how much variation can occur between different type of rivets in pull-through strength. In the figure below the AN430 rivet is the equivalent of the common MS20470 solid rivet in use today.

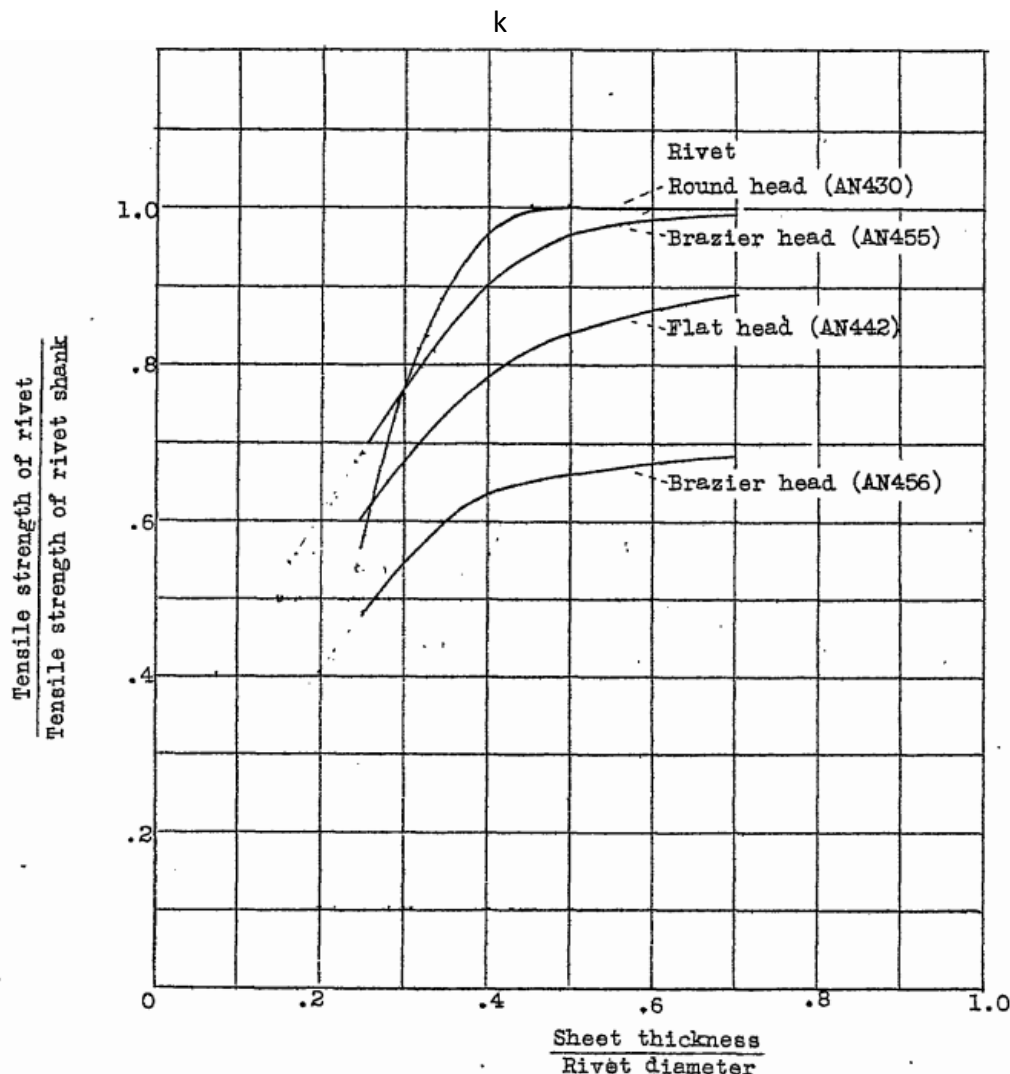


Figure 12.2.3-1: Variation in Rivet Pull-through Strength for Head Type and Fastener Diameter and Sheet Thickness [\(NACA-TN-930, 1944\)](#)

It should also be noted that rivets should not be used as a primary tension load path. Even small tension loads can cause permanent deformation of the formed rivet tail. This can reduce the amount of clamp-up in the joint and significantly reduce the fatigue life of a riveted joint. For this reason, **tension load on rivets should be limited to 20% of the ultimate shear strength of the rivet installation.**

12.2.4. Mechanical Joints in Composite Panels

In general; composite mechanical joint strength must be based on a comprehensive test program. Specific strength data cannot be provided as there are many different materials and layup combinations.

However, general design guidelines are provided, and analysis methodologies can be discussed.

12.2.4.1. Mechanical Joints in Composite Panels – Design Guidelines

The makeup of the laminate is critical. In general, quasi-isotropic laminate is preferred, although deviations from perfect quasi-isotropy are permissible and will have limited effect on joint strength.

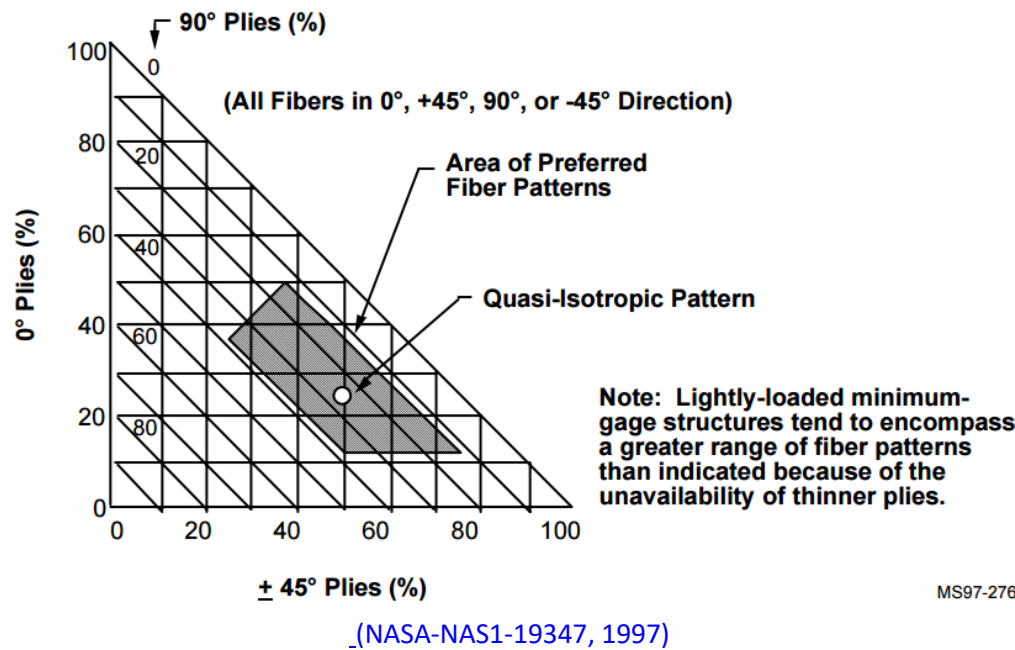
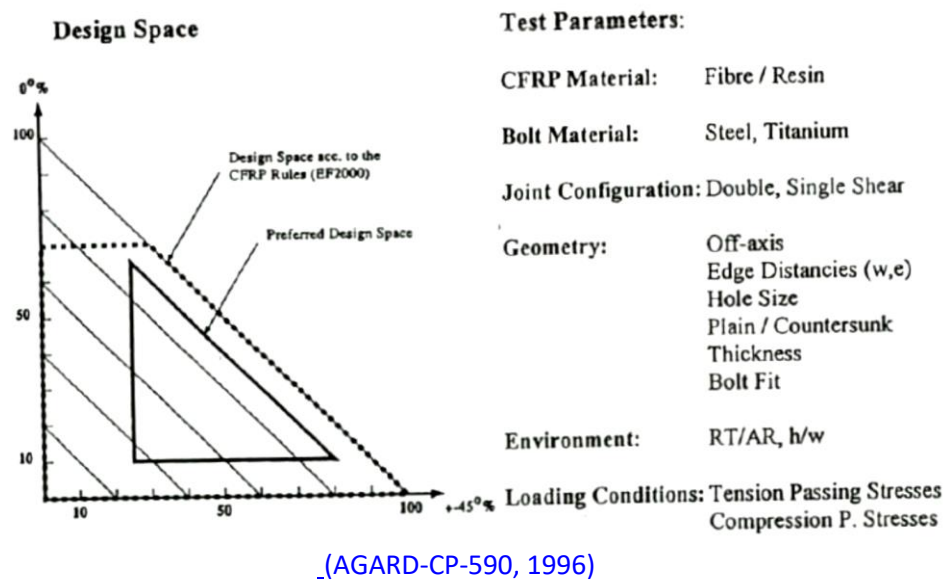


Figure 12.2.4-1: Lay-up Suitability for Bolt Installation

There are several versions of the appropriate envelope to use for layups (examples shown in the figures above). The recommended layup range is given in Figure 12.2.4-2 and the following spreadsheet.

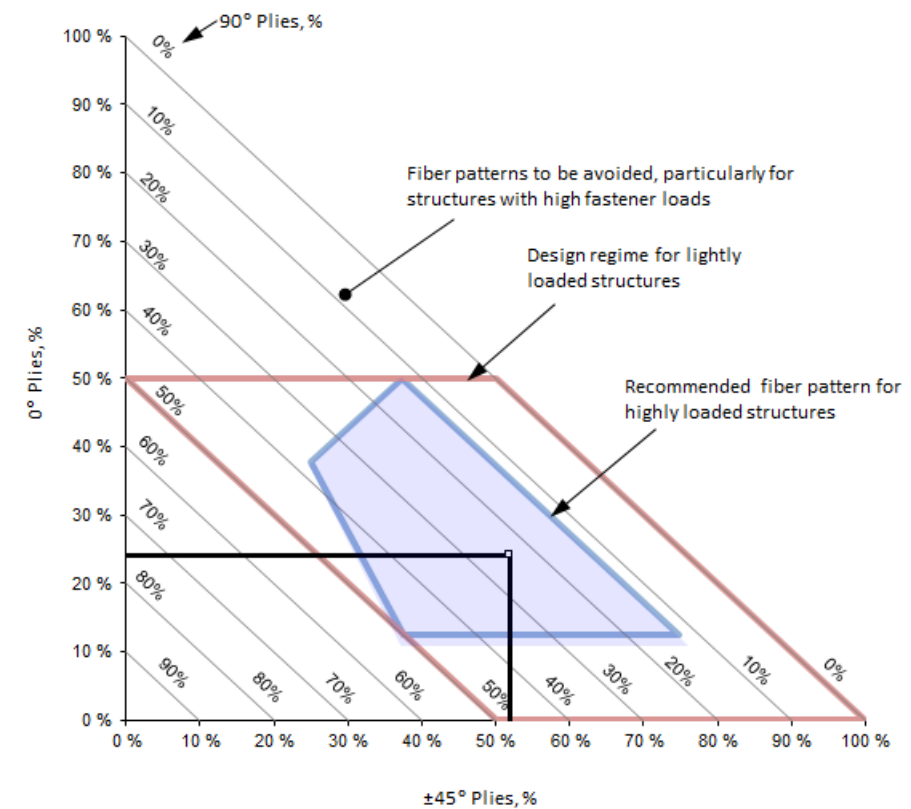
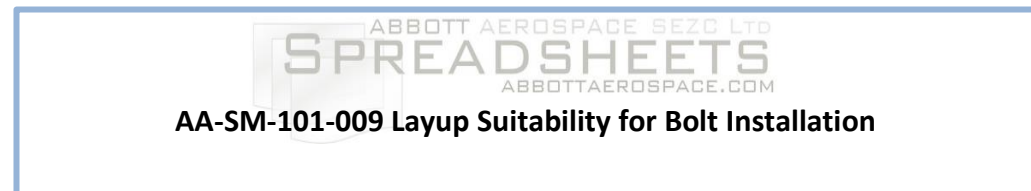


Figure 12.2.4-2: Recommended Lay-up Suitability for Bolt Installation



Bearing failure in a composite plate is progressive and non-linear, this is shown in the following figure.

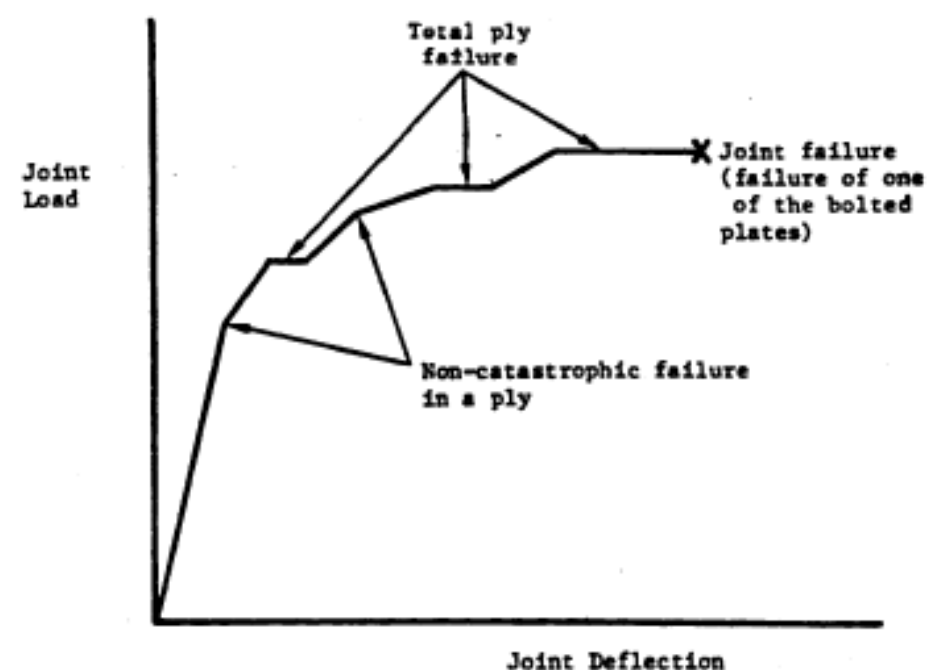


Figure 12.2.4-3: Failure Sequence of Mechanical Fastener in Composite Panel
(AFWL-TR-86-3035, 1986)

When testing and assessing specific joint configurations, it is recommended that the first failure is taken as the limit load level for the joint. This approach will demonstrate compliance with FAR 23.305(a) - *The structure must be able to support limit loads without detrimental, permanent deformation. At any load, up to limit loads, the deformation may not interfere with safe operation.*

The final joint failure load level can be taken as the ultimate strength.

Note on Shear-Out Strength of Mechanical Joints in Composite Panels

[\(ARC-CP-1380, 1977\)](#) gives some excellent data for shear-out vs bearing strength for a series of tests on a range of laminate configurations.

The first figure below is for a laminate close to quasi isotropic and below that is comparison data for biased laminate layups.

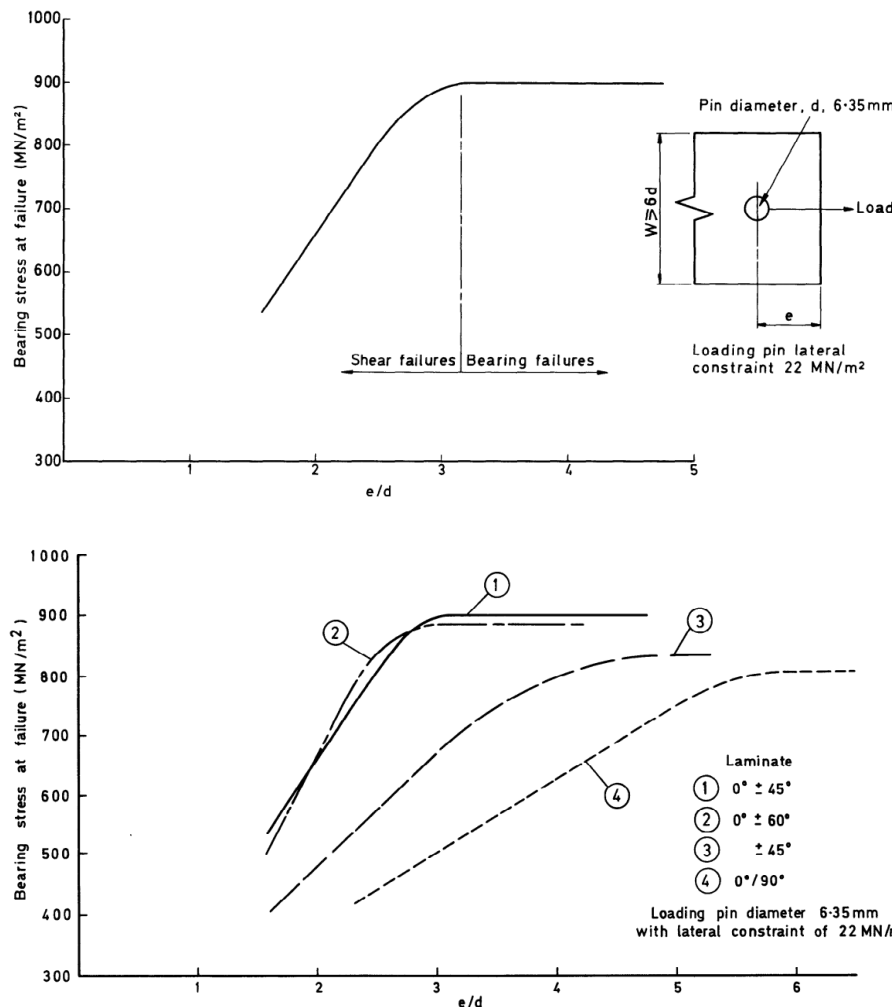


Figure 12.2.4-4: Effect of E/D and Laminate Definition on Shear-Out Strength of Mechanical Joint in Composite [\(ARC-CP-1380, 1977\)](#)

This same behavior is duplicated in [\(AFWL-TR-86-3035, 1986\)](#)

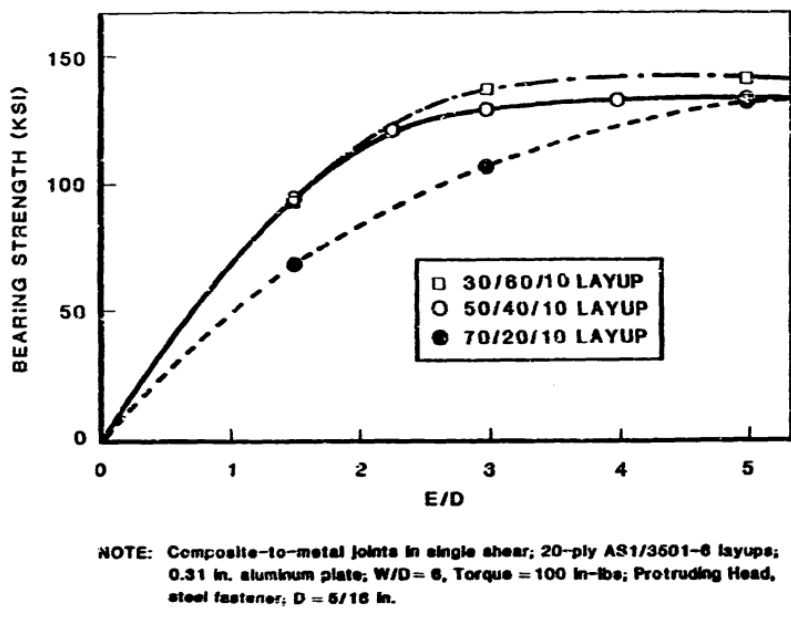


Figure 12.2.4-5: Effect of E/D and Laminate Definition on Shear-Out Strength of Mechanical Joint in Composite [\(AFWL-TR-86-3035, 1986\)](#)

This shows that for quasi-isotropic carbon laminates (and laminates close to quasi-isotropic) and E/D of 3.0 will allow the joint to develop the bearing strength of the laminate.

12.2.4.2. In-Plane Strength for Mechanical Joints in Composite Sheets

For most structures the following simple joint strength for composite laminates can be used:

If the fastener size or joint configuration is not included in the specific project-approved test results, 50ksi can be used as a general bearing stress allowable for carbon fiber laminates in their worst environmental condition and 40ksi for glass fiber laminates in their worst environmental condition. As long as the t/D (thickness/Diameter) ratio is between 0.5 and 2 and the E/D (Edge Distance/Diameter) is greater than 3.0.

Note that the in-plane strengths for composite laminate sheets for protruding head fasteners can be applied to countersunk fasteners without modification.

12.2.4.3. Out-of-Plane Strength for Mechanical Joints in Composite Sheets

There is no reliable analytical method to determine the pull-through strength of fasteners in laminated composites. There is some public domain data that can serve as a useful sizing guide. [\(NASA-TM-87603, 1985\)](#) is one of these.

The allowable data in this reference is slightly greater than that I have seen from test on several programs. Be sure to use the 1.15 fitting factor for calculations using values from this reference.

This data is developed using a 3/16in diameter 100° countersunk head titanium Huck fastener.

This testing was done with laminates from .244in to .317in thick and also for 2000 and 7000 series aluminum for comparison.

This testing was done at room temperature. Environmental factors should be applied to these results.

| System | Material | Laminate | Nominal Thickness, Inch |
|--------|--------------------|--|-------------------------|
| 1 | T300/5208 | $[(\pm 45/0_2)_2/\pm 45/0/90]_{2S}$ | 0.244 |
| 2 | AS4/3502 | $[(\pm 45/0_2)_2/\pm 45/0/90]_{2S}$ | 0.257 |
| 3 | T300/5208 | $[(\pm 45/0_2)_2/\pm 45/0/90]_{2S}$ | 0.312 |
| | | (Kevlar Stitch) | |
| 4 | AS4/3502 | $[(\pm 45/\pm 45)_2/+45/0_2/-45_2/0_2/+45_2/\pm 45_2/-45_2/0_2/+45_2/-45_2]_S$ | 0.298 |
| 5 | Kevlar 29/3501-6 | $[(\pm 45/0_2)_2/\pm 45/0/90]_{2S}$ | 0.246 |
| 6 | Kevlar 49/3501-6 | $[(\pm 45/0_2)_2/\pm 45/0/90]_{2S}$ | 0.256 |
| 7 | Kevlar 49/SP328 | $[(\pm 45/\pm 45)_2/90_2/\pm 45/\pm 45/\pm 45/\pm 45]_S$ | 0.312 |
| 8 | T300/CIBA-4 | $[(\pm 45/0_2)_2/\pm 45/0/90]_{2S}$ | 0.317 |
| 9 | AS4/PEEK (APC2) | $[+45/0/-45/90]_{6S}$ | 0.254 |
| 10 | HSCelion/CIBA-2566 | $[+45/0/-45/90]_{6S}$ | 0.265 |
| 11 | AS4/3502/FM1000 | $[+45/0/-45/90]_{5S}^{\theta}$ | 0.309 |
| 12 | Aluminum 2024-T4 | | 0.251 |
| 13 | Aluminum 7075-T651 | | 0.256 |
| 14 | AS4/3502 (0, 90) | $[(\pm 45/0_2)_2/\pm 45/0/90]_{2S}$ | 0.246 |
| | | Kevlar 285 Fabric/5208 (± 45) | |

Table 12.2.4-1 Laminate Definition for Fastener Push-Through Testing [\(NASA-TM-87603, 1985\)](#)

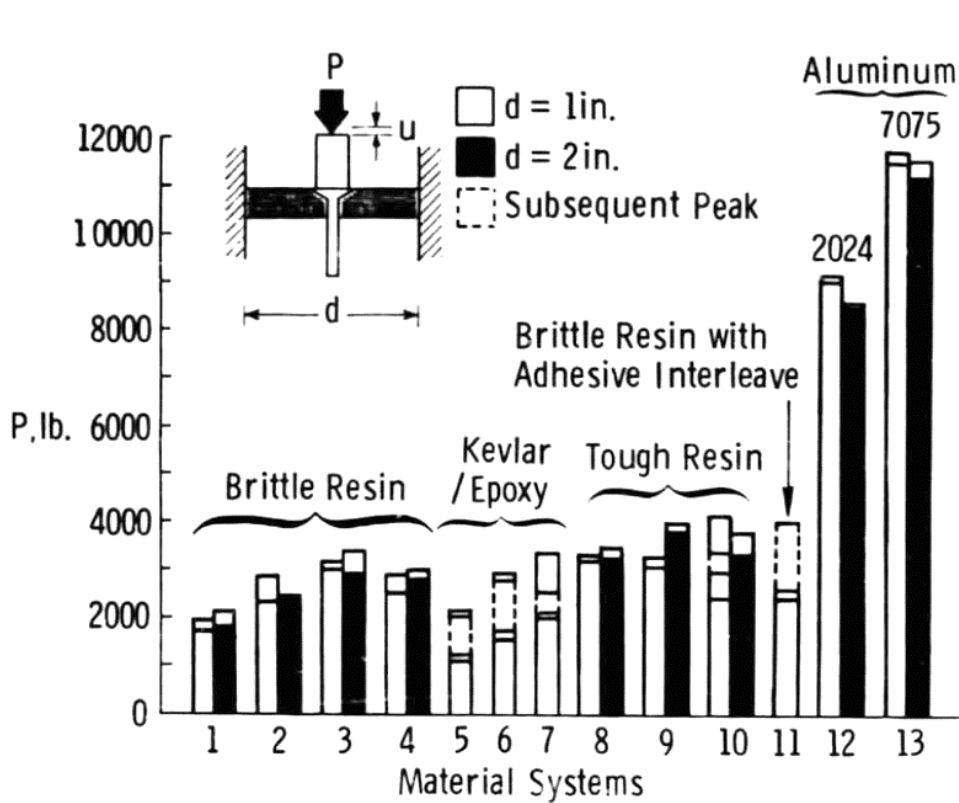


Figure 12.2.4-6: Results for 3/16 Fastener Push Through Test
(NASA-TM-87603, 1985)

It is recommended that when considering a 3/16in countersunk fastener in 1/4in thick carbon laminate at room temperature strength of 1000lb is used.

The results of (NASA-TM-87603, 1985) compare well with more recent reference that compares test results with a semi empirical hand method in (Pull-through Failure of Composite Joints, 2013).

This method is defined as follows:

$$\text{Pull Through Strength} = \frac{(2 \cdot \pi \cdot D_{fastener} \cdot t \cdot \tau_{max})}{\left(2.9 - 0.018 \cdot \frac{t}{D} - 0.51 \cdot \left(\frac{t}{D}\right)^2\right)} \cdot Mat$$

Where:

- t** Thickness of Laminate, in
- D** Diameter of the Bolt Shank, in
- D_{fastener}** Diameter of the Bolt Head or Washer, in
- τ_{max}** Material interlaminar shear stress, psi
- Mat** Factor to account for reinforcement material (see note below)

Note that this reference was solely concerned with pullout strength in carbon fiber laminate. This method correlated joint failure to the interlaminar shear strength of the laminate. It is noted that the interlaminar shear strength of a glass fiber laminate is similar to the interlaminar shear strength of a carbon fiber laminate with the same resin. Due to the increased flexibility of glass it is recommended that a 0.75 factor is applied.

The reference gives some correlation data to validate the method:

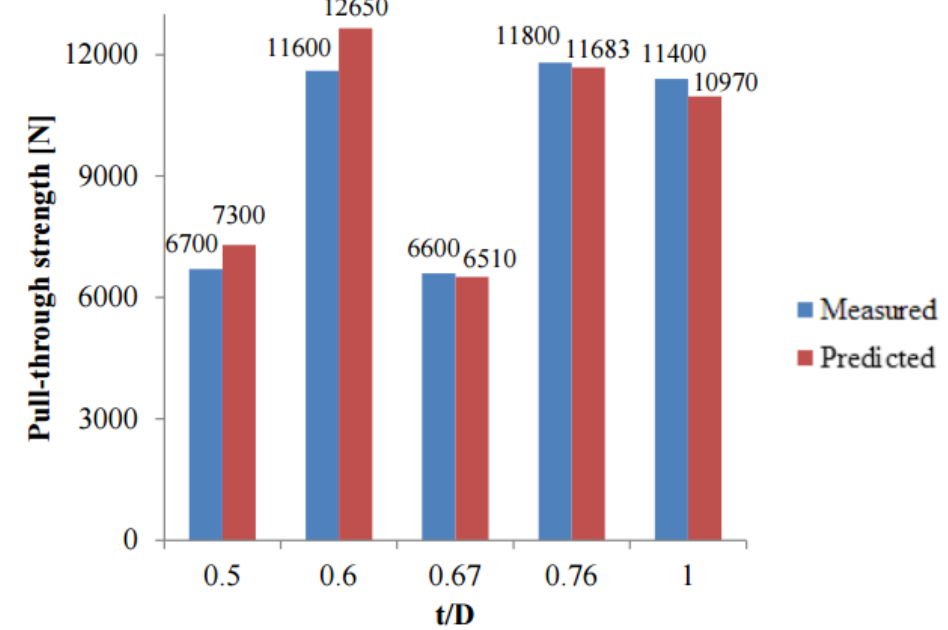


Figure 12.2.4-7: Correlation data for Fastener Push Through Strength
(Pull-through Failure of Composite Joints, 2013)

- The reader is reminded to make sure that if the interlaminar shear strength of the material at ETW is not available it should be derived in a conservative manner from available data.
- It is noted that in the available data countersunk fasteners show no appreciable difference in pull through strength when compared to protruding head bolts when the difference in head diameter between the types are accounted for.
- It is also noted that the reference considered largely quasi isotropic laminates. It is recommended that the local layup be as close to quasi-isotropic as possible.

This method is available in a spreadsheet here:

ABBOTT AEROSPACE SEZC LTD
SPREADSHEETS
ABBOTTAEROSPACE.COM
AA-SM-101-025 Bolt Pull Through Failure Load in Laminate

12.2.4.4. Mechanical Joint Design Check List

- Solid rivets and blind rivets should not be used to react significant tension loads.
- The tail diameter for solid rivets can be assumed to be 1.5 x the shank diameter.
- Note that aluminum (commonly used for solid rivets and blind rivets) has galvanic corrosion potential with carbon fiber and steel. Galvanic corrosion potential is increased by the presence of moisture and further increased by the presence of salt water.
- Do not mix different types of fasteners (i.e. solid rivets and bolts) in the same joint.
- In access panels and removable doors use a consistent grip length for all fasteners.
- Avoid design that places fastener threads in bearing for joints that carry a significant load. (See Section 12.2.7)
- In both metal and laminate composites that carry significant in-service loads, the countersunk depth should not exceed 70% of the sheet thickness.
- The edge distance in metal panels should be 2 x fastener shank diameter + positional tolerance.
- Where the service loads are low, the fastener edge distance in metal components may be reduced to 1.5 x the nominal fastener shank diameter + positional tolerance.
- 'Spot facing' in internal radii of machined metal components to allow for adequate fastener head/tail/collar/nut clearance is not recommended.
- Fastener pitch should be no less than 4 x the nominal fastener shank diameter.

Design Guidance Specific to Mechanically Fastened Laminate Composite Joints:

Note: The ideal laminate for mechanical joints is quasi-isotropic.

- Fastener edge distance in composite components should be a minimum of 3x the nominal fastener shank diameter with allowance for hole positional tolerance. This gives a minimum fastener edge distance in composite laminate components of 3x Diameter + .05in.
- In special circumstances, the fastener edge distance in composite laminate components may be reduced to 2.5x the nominal fastener shank diameter + .05in, in this case, additional analysis or other substantiation is required.
- Interference fits may not be used in composite components. It is recommended that clearance fit holes are used in all mechanical joints in composite laminate sheets.

- When using large diameter bolts (>0.25in) in composite laminates the installation torque should be limited, or other mitigations used, to avoid crushing the laminate.
- To avoid galvanic corrosion, it is recommended fastener materials used in carbon laminate composite sheets be Titanium, A286, PHI13-8MO, Monel or PH17-4. Titanium fasteners are preferred as they are the most galvanically compatible with carbon fiber composite.
- In composite-to-metal locations, corrosion barriers like fiberglass layers must be used.
- Do not buck rivets in composite structure.
- Countersunk fasteners develop greater in-plane strength than shear head fasteners in composite laminate joints.
- In fuel containment areas, joints must be sealed to be leak-proof. Fasteners must also be sealed to prevent arcing within the fuel cell in the event of a lightning strike.
- Fastener pitch must not be less than 4 x shank diameter as the interaction of the KT effect around each hole will interact and cause premature failure.

Note: Effort should be made to follow these guidelines. Deviation will require additional analysis and/or testing to validate.

12.2.5. Mechanical Joints, Examination of the Fastener

12.2.5.1. Fastener Thread Pull-Out/Shear-Out:

The fastener and nut/collar combination can fail at the minimum tension area location of the shank or thread. The fastener or collar/nut threads can also pull out.

The minimum tension strength for fasteners and nuts/collars is usually stated on the specification for the fastener, nut or collar. If the tension strength is not given for the fastener nut or collar, or the attachment is using a custom tapped thread in a part, the pull out strength can be calculated using [\(NASA-RP-1228, 1990\)](#) page 21 'Calculating Pullout Load for Threaded Bolt':

$$P = \frac{\pi d_m F_s L}{3}$$

Where:

- P** Pull-out strength, lb
- d_m** Mean diameter of threaded hole, in (can be taken as the thread pitch diameter)
- F_s** Material ultimate shear stress, psi
- L** Thread engagement, in

A spreadsheet method is available at the link below:

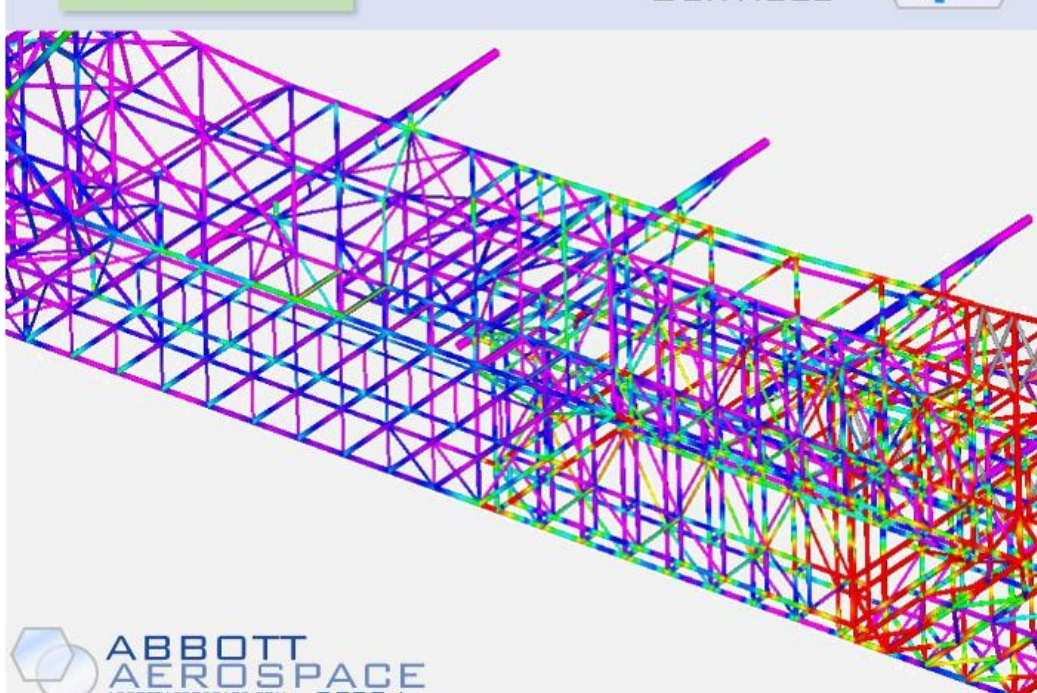


The joint in tension should also be checked against the published tension strength of both the fastener and the nut, nut-plate or collar.

ADVERT: ENGINEERING SERVICES

STRESS ANALYSIS
 ENGINEERING SERVICES

CONTACT US



 ABBOTT AEROSPACE SEZC LTD
 ABBOTTAEROSPACE.COM

12.2.6. Potted Inserts in Cored Laminates

12.2.6.1. Authors Note:

This chapter uses two main sources [\(ECSS-E-HB-32-22A, 2011\)](#) and [\(ESA-PSS-03-1202, 1987\)](#).

The 2011 document is a rewrite of the original 1987 document and the general descriptions are an improvement but the numerical analysis includes many errors that are not in the 1987 original.

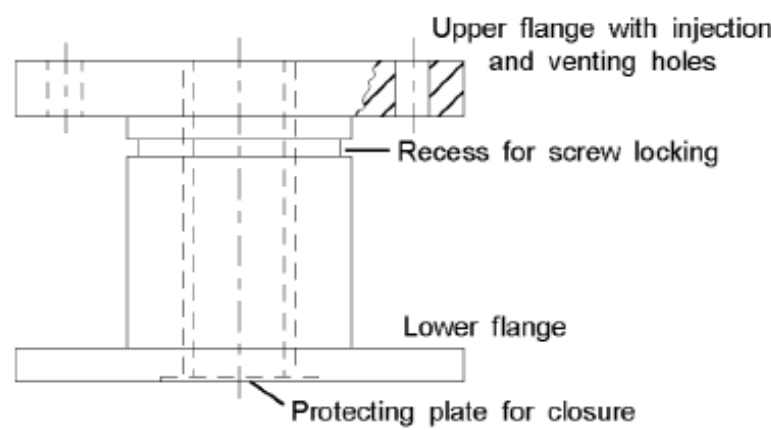
However, much of the graphical strength data in the 1987 original reference is incorrect. Issue 1 of the 1987 report includes a note at the start of this report to this effect. This incorrect graphical data is omitted from the 2011 rewritten report.

Because of the condition of the two main references used for this report much of the descriptive material and illustrations are taken from [\(ECSS-E-HB-32-22A, 2011\)](#), the analytical methods are taken from [\(ESA-PSS-03-1202, 1987\)](#).

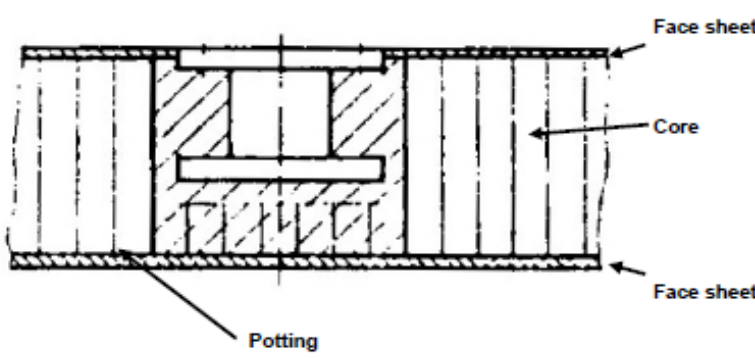
Another, older reference [\(US Forest Service Report No . 1845, 1955\)](#) has a method derived for out plane loading with some correlation between analysis and test which produces a similar load distribution with respect to radial distance as the method shown in section 12.2.6.6.

12.2.6.2. Explanation:

The most common means of mechanical attachment in sandwich panels is potted inserts. The potting procedure involves drilling through one or both face sheets, excavating the local core material, inserting the 'insert' and then injecting potting compound that sets it in place. Thus locking the insert to the cored panel in all six degrees of freedom.



A - Typical standard-type insert



Honeycomb panel
[See also: 8.1] "Structural sandwich concept"

Figure 12.2.6-1: Typical Insert and Installation Configuration
[\(ECSS-E-HB-32-22A, 2011\)](#)

There are 4 basic loading modes that a potted insert can react:

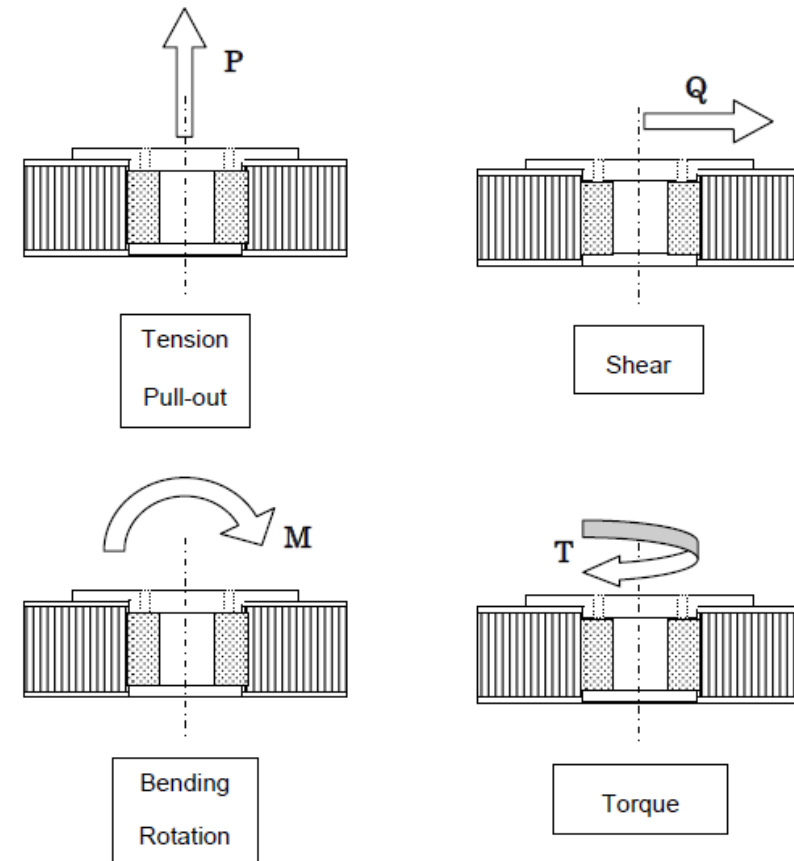


Figure 12.2.6-2: Summary of Loading Modes [\(ECSS-E-HB-32-22A, 2011\)](#)

There are 3 different types of potted insert installation configurations:

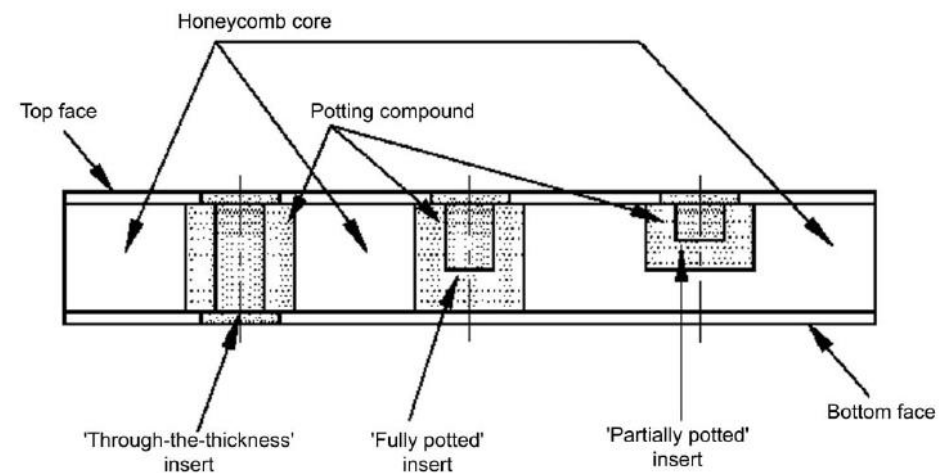


Figure 12.2.6-3: Different Potting Configurations [\(ECSS-E-HB-32-22A, 2011\)](#)

Inserts can be installed in any type of sandwich panel, with composite or isotropic face sheets. This section concentrates on potted inserts in sandwich structures with composite face sheets.

12.2.6.3. Nomenclature:

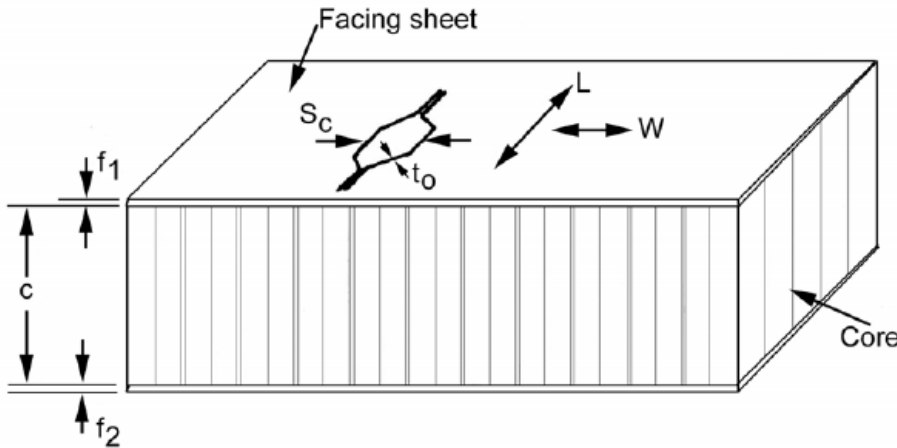
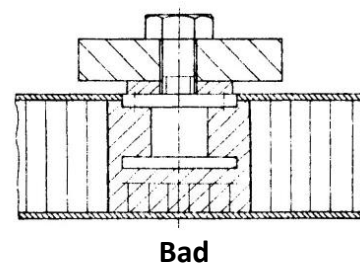
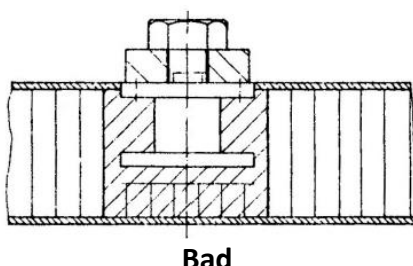
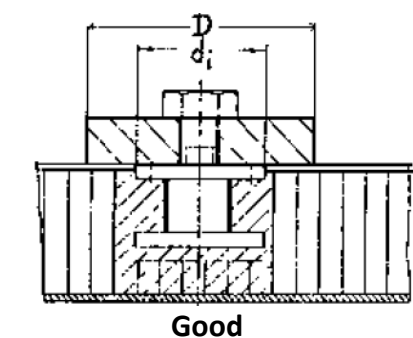


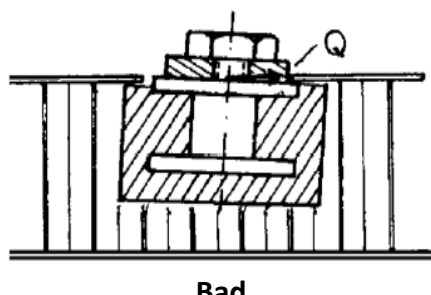
Figure 12.2.6-4: Potted Insert Analysis Nomenclature
(ECSS-E-HB-32-22A, 2011)

12.2.6.4. General Design Guidelines

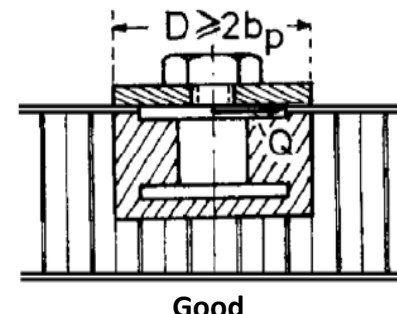
- Compressive loads are transmitted via the face sheet in the area of the potting. The bracket or foot of the attaching member needs to exceed at least the maximum extension of the potting.



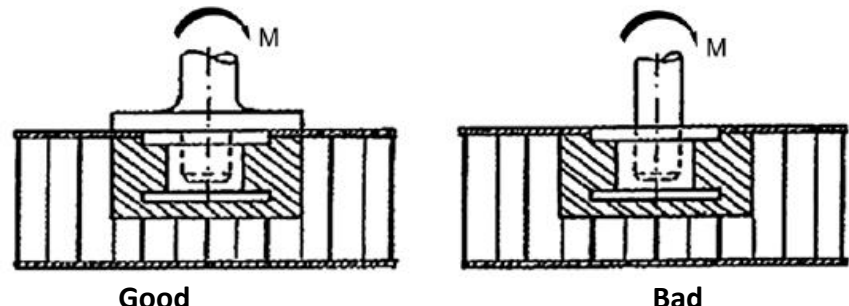
- The insert flange remains parallel to the face sheet such that under in-plane loads it cannot move below the face sheet.



- Loads in the plane of the face sheet are usually transmitted by bearing pressure between the outer insert flange and the face sheet.
- The border of the face sheet around the insert is well supported to accommodate a high bearing stress, created inside by the potting and outside by the bracket or foot:



- Under a sufficient pre-load of the insert bolt, minor or secondary bending moments are correctly reacted.



12.2.6.5. Guidelines Specific to Composite Face Sheets

For a sandwich panel with thin CFRP (Carbon Fiber Reinforced Plastic – a common term for carbon fiber laminates) face sheets, machining can be seen as problematical, although a thorough finishing of the protruding parts of the inserts is considered necessary in order to avoid damaging the surface ply. The machining process needs to be carefully investigated and reflected in the definition of the manufacturing procedure.

For thin face sheets made of CFRP with a flush mounted insert, another problem needs to be avoided under loads in-plane in the face sheet. If the outer insert flange has even a small chamfer, possibly non-intentional, the load transfer is reduced by bearing stress. The insert tends to undercut the face sheet.

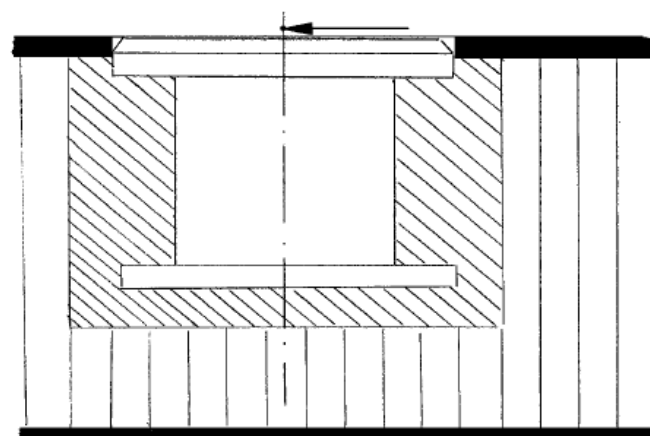


Figure 12.2.6-5: Effect of small Chamfer on Insert Flange in Load Transfer to Face Sheets (ECSS-E-HB-32-22A, 2011)

This analysis method has been developed for honeycomb core but is also applicable for foam core.

Much of the analysis methods that follow rely on the determination of the potting radius – the diagram below shows how this can prove difficult:

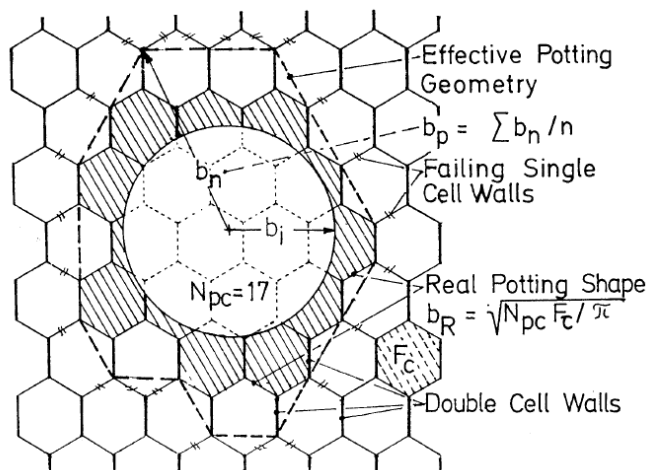


Figure 12.2.6-6: Potting Geometry (ESA-PSS-03-1202, 1987)

The effective minimum potting radius is given by the two following expressions for perforated and non-perforated core.

Where:

b_i Insert radius
 S_c Size of core cell

For perforated core:

$$b_{pmin} = 0.93192 \cdot b_i + 0.874 \cdot S_c - 0.66151$$

For non-perforated core:

$$b_{pmin} = 0.9 \cdot b_i + 0.7 \cdot S_c$$

For inserts in foam core panels the process used to install the insert should be reviewed, the amount of core excavation assessed and a conservative estimate of the likely effective potting radius should be made.

The minimum 'real' potting radius is a more conservative estimate of the potting radius and is determined using this expression:

$$b_R = b_i + 0.35 \cdot S_c$$

This expression is valid for perforated and non-perforated cores.

A spreadsheet to calculate these key parameters is available below:

ABBOTT AEROSPACE SEZC LTD
SPREADSHEETS
ABBOTTAEROSPACE.COM

AA-SM-140 Composites - Potted Insert Strength – Key Parameters

12.2.6.6. Tension/Compression Loading

This method gives the maximum axial tension or compression load that a potted insert can carry. This method is based on determining the maximum core shear

stress just outside of the potting compound radius. The assumption inherent in the method is that the core strength is significantly less than the shear strength of the potting compound and therefore the potential shear-out failure modes in the potting compound are ignored (the shear stress is assumed to be zero until the core is responsible for through-the-thickness shear transfer).

This method is suitable for a fully potted insert:

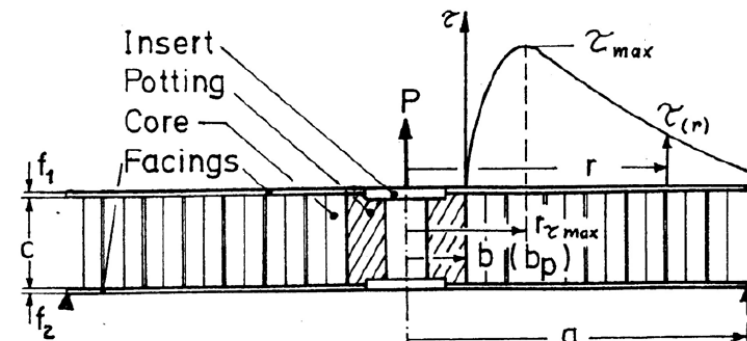


Figure 12.2.6-7: Shear Stress Distribution for Insert Loaded Out-of-Plane (ESA-PSS-03-1202, 1987)

Analysis Terms:

| | |
|-------|---|
| c | Core thickness, in |
| f | face sheet thickness – it is assumed that both face sheets are the same thickness, in |
| P | Applied tension/compression load, lb |
| G_c | Shear modulus of core, psi |
| E_f | Young's modulus of facings, psi |
| N_f | Poissons ratio of facings |
| r | Radial distance from the insert axis, in |
| b | Potting radius, in (b_p , the effective potting radius can be used) |

First, the ratio of core thickness to face sheet thickness must be determined. For this method to be accurate $\beta > 10$ is recommended.

$$\beta = c/f$$

α is the ratio of out-of-plane stiffness between the core and the face sheets:

$$\alpha = \frac{1}{f} \sqrt{\frac{G_c}{E_f} \cdot 12 \cdot (1 - \nu_f^2) \cdot \left(1 + \frac{\beta}{2}\right)}$$

K is a factor that determines the distribution of shear stress in the core with distance from the insert axis:

$$K = \frac{b}{r} \cdot \left[1 - \sqrt{\frac{r}{b}} \cdot e^{\alpha \cdot (b-r)} \right]$$

The shear stress in the core at any distance (r) from the insert axis is given by the following expression:

$$\tau(r) = \tau_{nom} \cdot C^* \cdot K$$

With the terms calculated as follows:

$$\tau_{nom} = \frac{P}{2 \cdot \pi \cdot b \cdot c}$$

$$C^* = \frac{\beta}{\beta + 1}$$

It is recommended that the shear stress is plotted for a range of (r) values and the resulting set of values surveyed to determine the maximum stress in the core (τ_{max}).

The critical shear stress can be compared with the shear strength of the core, it is recommended that a 1.15 fitting factor is used for all potted inserts for general robustness and regulatory compliance:

$$MS = \frac{\tau_{crit}}{(\tau_{max} \cdot 1.15)} - 1$$

Ref. [\(ESA-PSS-03-1202, 1987\)](#) gives a method for converting the critical core shear stress into an allowable out-of-plane load:

$$P_{crit} = \frac{(2 \cdot \pi \cdot b \cdot c \cdot \tau_{crit})}{(C^* \cdot K_{max})}$$

In which case the margin of safety is calculated as follows:

$$MS = \frac{P_{crit}}{(P \cdot 1.15)} - 1$$

[\(ESA-PSS-03-1202, 1987\)](#) has an approximate mathematical solution to determine the critical stress and critical radial distance from the hole. In the author's experience, this method is not accurate and it is better to graphically determine the critical stress.

This spreadsheet uses this approach:

ABBOTT AEROSPACE SEZC LTD
SPREADSHEETS
ABBOTTAEROSPACE.COM
AA-SM-140-001 Composites - Potted Insert Strength - Tension-Compression

12.2.6.7. Inserts Loaded with In-Plane Shear Load

This method is for a partially potted insert. It can be used for a fully potted insert as it is conservative to do so.

It is required that the diameter D of the foot of the attached part is at least as great as the typical potting diameter.

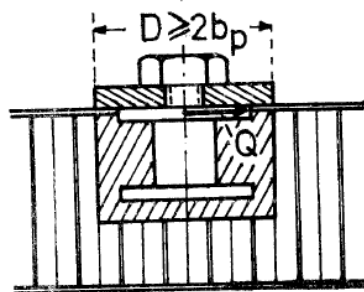


Figure 12.2.6-8: Required Clamping Conditions for Shear (Q) loaded inserts
[\(ESA-PSS-03-1202, 1987\)](#)

The shear load to which the insert can be submitted is given by the semi-empirical formula:

$$Q_{ss} = 8 \cdot b_p^2 \cdot \tau_{wcrit} + 2 \cdot f \cdot b_p \cdot \sigma_{fy}$$

Where:

b_p Effective potting radius, in

τ_{wcrit} Shear strength of core, psi (if honeycomb core, use W direction, lowest strength value)

σ_{fy} Yield strength of the facing material, psi, Note that a yield strength is not applicable for composite face sheets and it is recommended that the interlaminar shear strength of the composite face sheet is used.

f Thickness of the upper sheet, in

A spreadsheet method is available at the link below:

ABBOTT AEROSPACE SEZC LTD
SPREADSHEETS
ABBOTTAEROSPACE.COM
AA-SM-140-002 Composites - Potted Insert Strength – In plane Shear

12.2.6.8. Inserts Loaded with a Moment

Similar to the shear load determination, this method is for a partially potted insert. It can be used for a fully potted insert as it is conservative to do so.

It is required that the diameter D of the foot of the attached part is at least as great as the typical potting diameter.

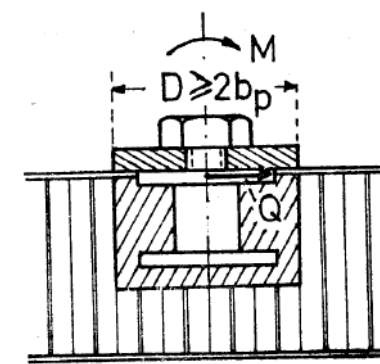


Figure 12.2.6-9: Required Clamping Conditions for Moment (M) Loaded Inserts
[\(ESA-PSS-03-1202, 1987\)](#)

The allowable moment on the insert – given the installation in Figure 12.2.6-9 – is defined by:

$$M_{ss} = P_{ssc} \cdot b_i$$

Where:

b_i Radius of insert, in

P_{ssc} Permissible compression load, psi

Ref. [\(ESA-PSS-03-1202, 1987\)](#) states that the value for P_{ss} should be derived using the graphical solutions in the reference. However, the reference states that the graphical solutions are partly in error and should not be used. The tension/compression strength developed in 12.2.6.6 can be used. This approach is conservative.

Note that as this analysis is simple no individual spreadsheet has been developed for it.

12.2.6.9. Inserts Loaded with Torsion

In general, torsion loads on a single insert should be avoided by the use of coupled inserts or groups of inserts. As with shear and moment, the foot of the attachment should be no less than the potting diameter of the insert.

For metallic honeycomb core sandwich panels, the torsional load to which the single insert in a metallic core can be submitted is given by the formula:

$$T_{ss} = 4 \cdot \pi \cdot b_R^2 \cdot t_o \cdot \tau_{ocrit}$$

Where:

b_R Real potting radius, in

τ_{ocrit} Shear strength of core base material, psi

t_o Foil thickness of the core, in

For non-metallic honeycomb core, the torsion strength should be determined by test.

A spreadsheet for this method is available at the link below:



AA-SM-140-003 Composites – Torsion Strength of Potted Inserts

12.2.6.10. Inserts Under Combined Loads

For inserts subject to combined out-of-plane and in-plane loads:

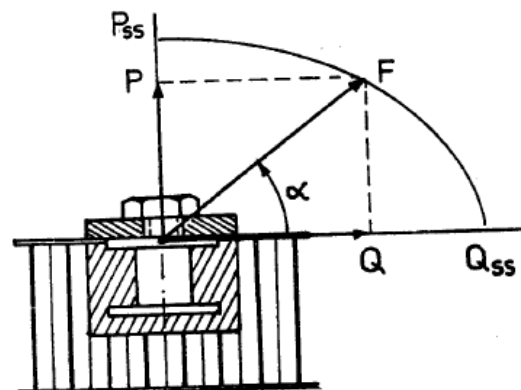


Figure 12.2.6-10: Insert Subject to Combined Out-of-Plane and Shear
(ESA-PSS-03-1202, 1987)

The interaction of these two load effects is given by the following interaction:

$$\left(\frac{P}{P_{ss}} \right)^2 + \left(\frac{Q}{Q_{ss}} \right)^2 \leq 1$$

Where:

P_{ss} Permissible tensile or compressive load

Q_{ss} Permissible shear load

Therefore, the margin of safety is given by the following expression:

$$MS = \left(\left(\frac{P}{P_{ss}} \right)^2 + \left(\frac{Q}{Q_{ss}} \right)^2 \right) - 1$$

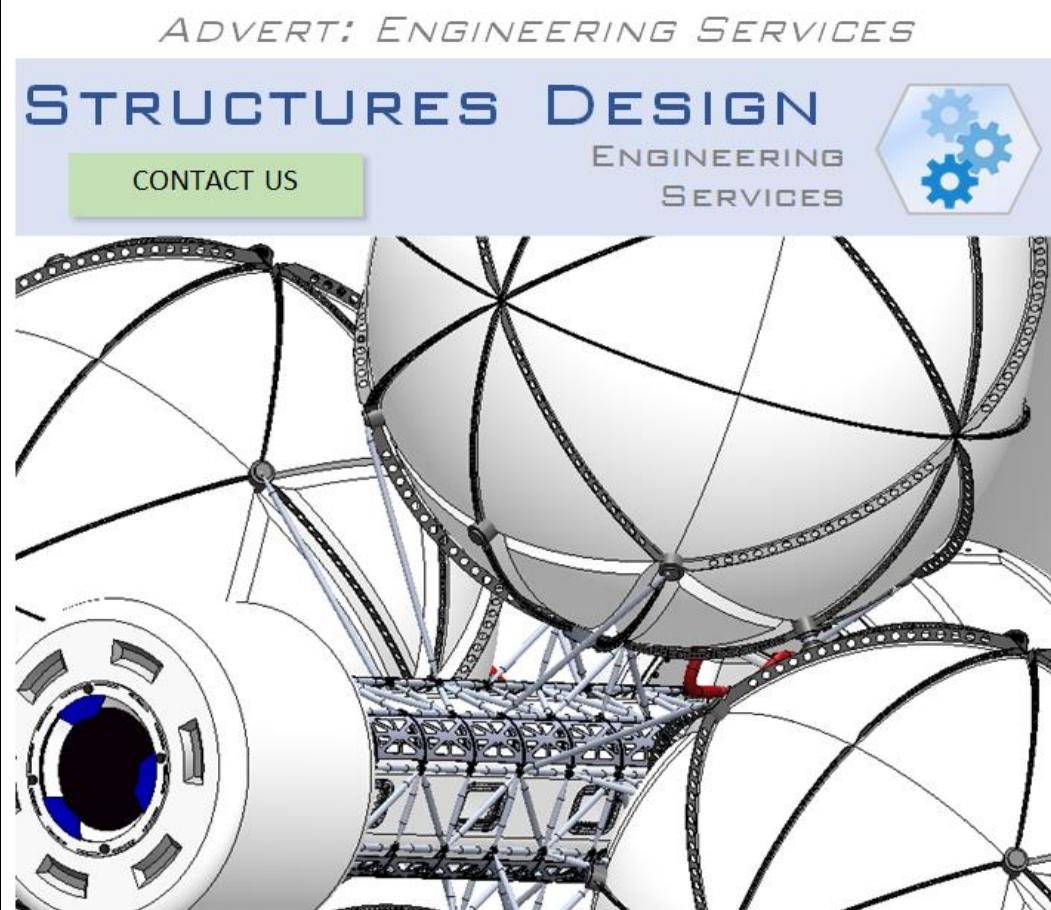
For Inserts subjected to combined out-of-plane load, shear load, moment and torsion:

The interaction of all of the possible load effects is given by the following expression:

$$\left(\left(\frac{P}{P_{ss}} \right)^2 + \left(\frac{Q}{Q_{ss}} \right)^2 + \left(\frac{M}{M_{ss}} \right)^2 + \left(\frac{T}{T_{ss}} \right)^2 \right) \leq 1$$

Therefore, the margin of safety is given by the following expression:

$$MS = \left(\left(\frac{P}{P_{ss}} \right)^2 + \left(\frac{Q}{Q_{ss}} \right)^2 + \left(\frac{M}{M_{ss}} \right)^2 + \left(\frac{T}{T_{ss}} \right)^2 \right) - 1$$



12.2.7. Fastener Interaction of Shear Load and Tension Load Effects

12.2.7.1. Interaction of Shear and Tension for Bolts

Traditional analysis methods only cover the interaction effects of shear on the shank of the fastener and tension alone on the threaded portion. The most recent and best reference for this interaction effect can be found in [\(NASA-TM-2012-217454, 2012\)](#).

This analysis is valid for bolts installed in metal and composite components as it considers only the fastener in isolation.

This reference examines fasteners loaded at the shank in combined shear and tension loads and also, in the threaded portion in combined shear and tension loads.

All of the testing represented in this reference was on 3/8in diameter bolts and lubricant was used to minimize the potential for load transfer by friction.

The first round of testing done was to compare the ultimate combined strength of the bolt with and without preload.

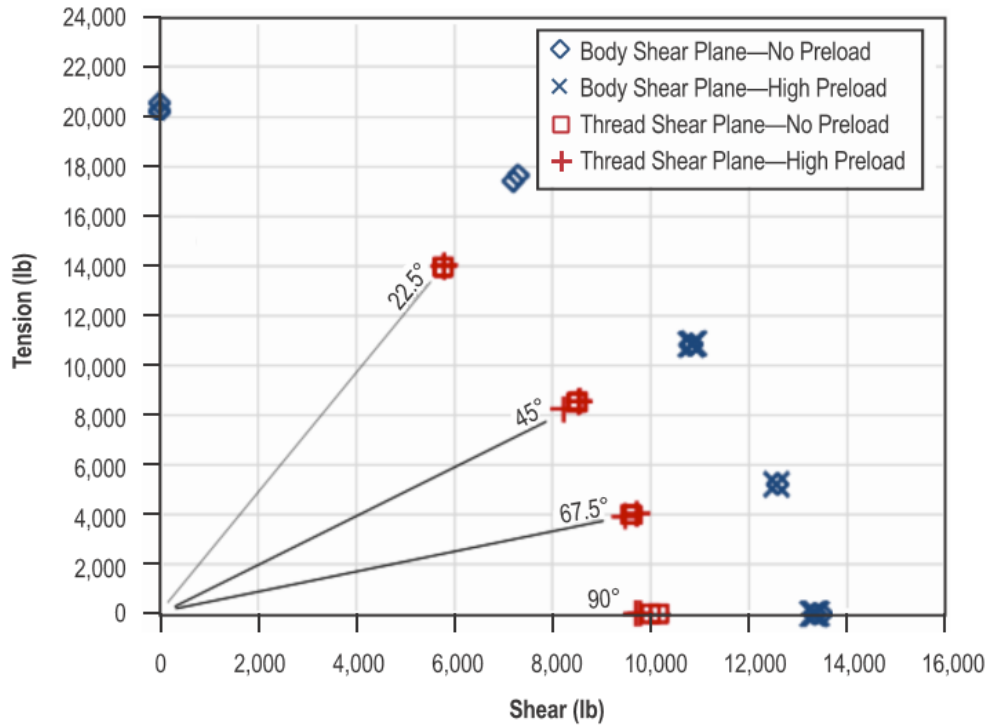


Figure 12.2.7-1: Bolt Shear and Tension Combined Test Results, With and Without Preload [\(NASA-TM-2012-217454, 2012\)](#)

When a fastener is subjected to both tensile and shear loading simultaneously, the combined load must be compared with the total strength of the fasteners. Load ratios and interaction curves are used to make this comparison, the load ratios are:

$$R_s(\text{or } R_1) = \frac{\text{Actual shear load}}{\text{Allowable shear load}} \quad R_t(\text{or } R_2) = \frac{\text{Actual tensile load}}{\text{Allowable tensile load}}$$

From Figure 12.2.7-1 two clear conclusions can be drawn:

1. The presence or lack thereof of preload does not affect the ultimate strength of the joint in tension or shear (although it is critical for the fatigue life of the joint).
2. The strength of the joint is significantly affected if the fastener is loaded in the threaded area.

The reference [\(NASA-TM-2012-217454, 2012\)](#) gives some further guidance on the definition of the interaction of shear and tension.

For fasteners loaded in the unthreaded shank:

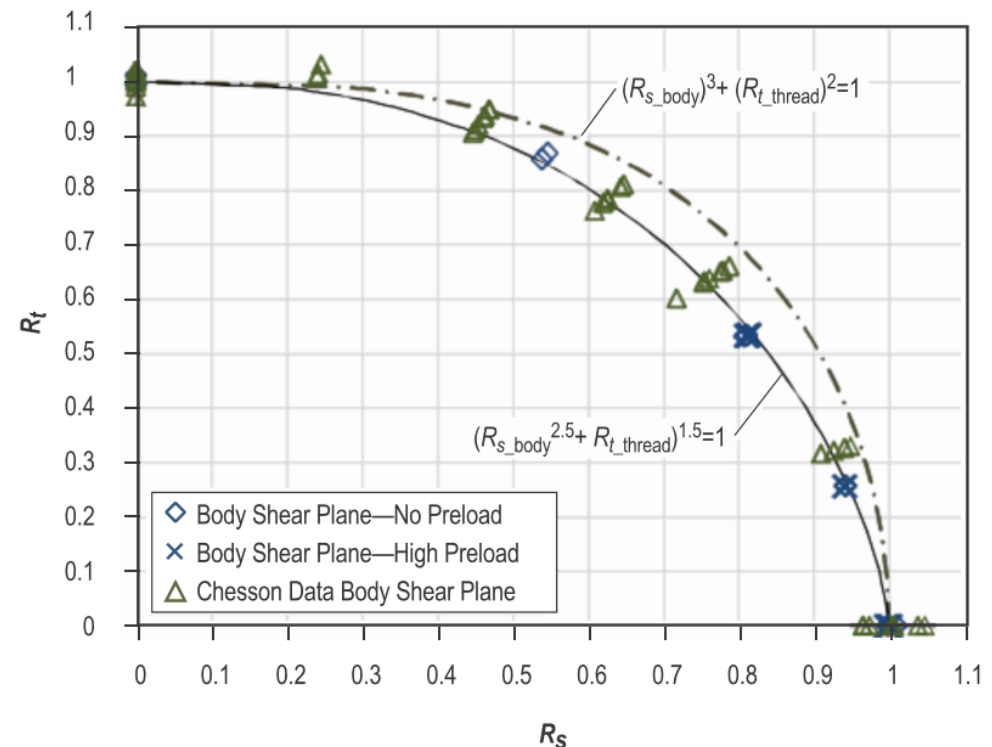


Figure 12.2.7-2: Interaction Curves for Shear Plane in the Shank of the Fastener [\(NASA-TM-2012-217454, 2012\)](#)

The interaction equation for fasteners loaded in the unthreaded shank (recommended for primary structure) is:

$$R_{s_body}^{2.5} + R_{t_thread}^{1.5} = 1$$

A spreadsheet for this interaction is available at the link below:

ABBOTT AEROSPACE SEZC LTD
SPREADSHEETS
ABBOTTAEEROSPACE.COM

AA-SM-005-001 Bolted Connections - Combined Shear and Tension on Shank

For fasteners loaded in the threaded portion:

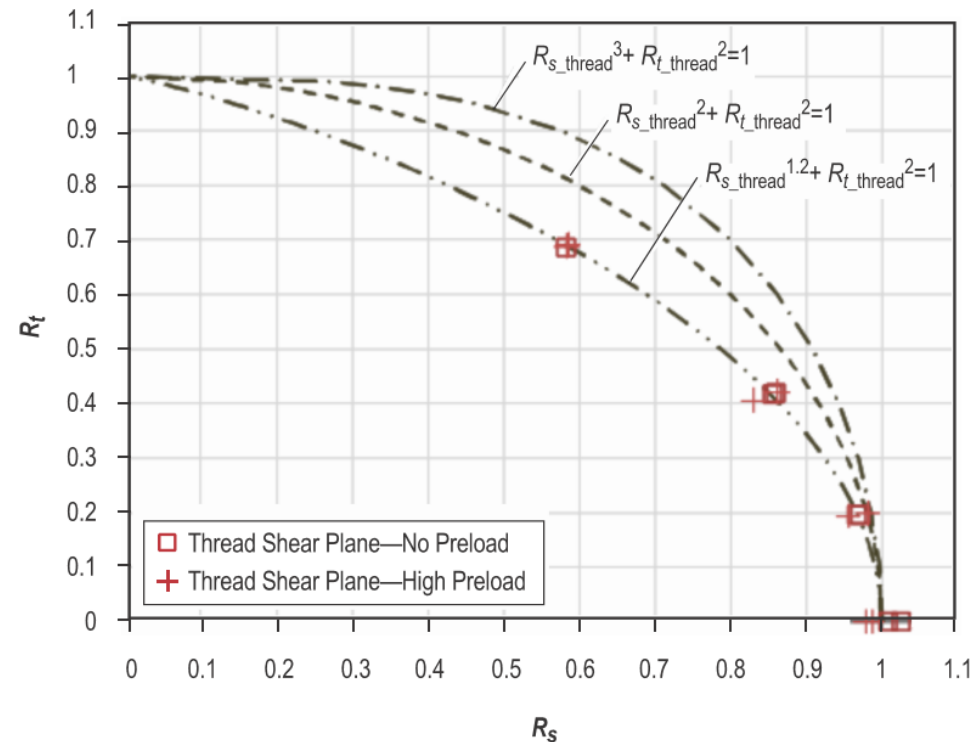


Figure 12.2.7-3: Interaction Curves for Shear Plane in the Threaded Portion of the Fastener [\(NASA-TM-2012-217454, 2012\)](#)

The interaction equation for fasteners loaded in the thread is:

$$R_{s_thread}^{1.2} + R_{t_thread}^2 = 1$$

A spreadsheet for this interaction is available at the link below:



12.2.7.2. Interaction of Shear and Tension for Rivets

The established method for interacted load effects on rivets is:

$$R_s^2 + R_t^2 = 1$$

Therefore, the margin of safety can be calculated directly using the following expression:

$$M.S = \frac{1}{\sqrt{(R_s)^2 + (R_t)^2}} - 1$$

12.2.7.3. Fastener Bending

When very thick sheets are fastened together and non-working shims are used, the offset introduced can create a bending effect on the fasteners in the joint.

These effects rarely occur in a well-designed joint using a field of fasteners. In a fastener field, the bending moment caused by an offset between load paths is carried over the area of the joint and not by an individual fastener or fasteners.

For a joint that relies on a single highly loaded fastener or has very few fasteners, has unusual geometry, has a poor fastener fit (for example, a slotted hole), with low installation torque, in thick items; then bolt bending may be considered, but it is almost always conservative to do so. Bolt bending is more typically considered for lug analyses, see section 12.2.10.1.

ADVERT: TECHNICAL LIBRARY

TECHNICAL LIBRARY
 PUBLIC DOMAIN
 TECHNICAL DATA

SEE MORE

We have collected over 900 useful FAA technical, regulatory, advisory and policy documents.





12.2.8. Mechanical Joints – Tension Clip Installations

Tension clips are used when it is not possible to transfer load as shear in a fastener. There are two basic types, single angle and double angle.

- Clips are only used when the load is small. Machined tension fittings should be used for applications in the primary load path.
- Thin clips tend to fail in bending of the clip. Thick clips tend to fail the fastener in the base of the clip due to prying action tension.
- Tension fasteners (not rivets) should be used.
- Keep the bolt head as close to the radius as possible.

A tension clip installation has two significant failure modes, failure of the clip in bending and tension failure of the fastener.

12.2.8.1. Tension Clip - Flange Bending Strength Failure

The analytical methods to determine the strength of tension clip installation has been limited to proprietary data. There is a well-known Lockheed stress memo that provides a method for the analyst and in recent years "Aircraft Stress Analysis and Sizing" by Michael Niu has given an analogous analysis method.

In the development of this book both of these methods were examined, and it was determined that the curves in these two methods were not derived by test but were analytically derived.

The derivation of the tension clip strength method is below:

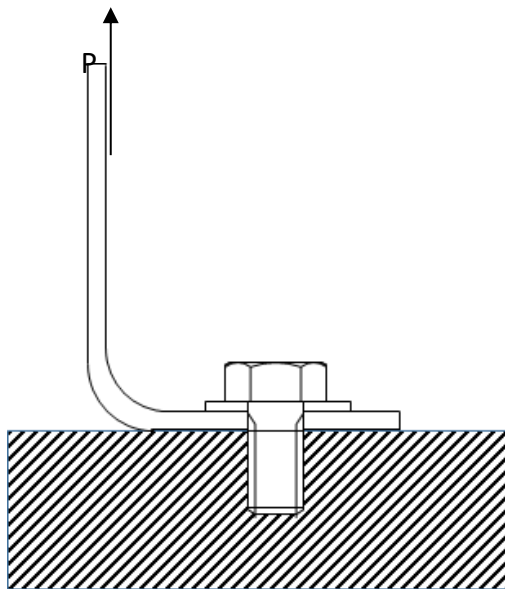


Figure 12.2.8-1: Tension Clip Idealized Installation

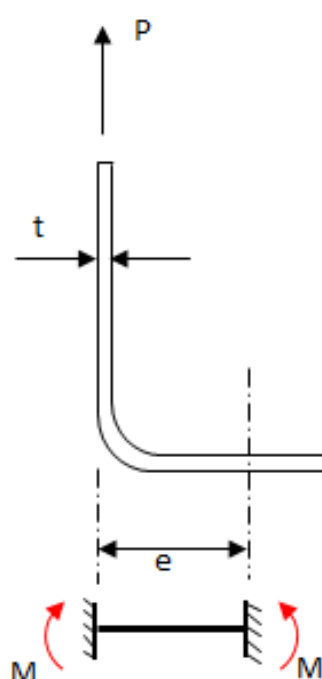
The methodology assumes that the clip is installed onto an effectively rigid foundation, and that the loaded outstanding flange is also restrained in rotation.

Therefore, the clip can be idealized as a simple beam built at the fastener and restrained in rotation at the loaded flange:

The eccentricity of the clip (e) is the length of the idealized beam and P is the load applied at the end restrained in rotation only.

For this arrangement, the critical bending moment occurs at both ends of the beam and is equal to:

$$M = P \cdot e / 2$$



The allowable load is calculated per one inch of angle. The allowable load per fastener is the allowable load from this method multiplied by the fastener pitch.

The 2nd moment of area for a unit length of angle flange is equal to:

$$I = 1 \cdot t^3 / 12$$

And the distance from the flange cross section neutral axis to the outer fiber:

$$y = t/2$$

Taking the material yield strength F_{ty} , the allowable moment to yield is given by:

$$M_0 = F_{ty} \cdot I/y$$

Therefore, the allowable applied load to yield the angle is:

$$P_0 = 2 \cdot M_0/e$$

Formed Sheet Aluminum Tension Clips

The allowable load for formed sheet aluminum clips can be found with the following factors:

The factor from yield allowable to ultimate allowable (general minimum for aluminum) is 1.33, the shape factor for a rectangular section is 1.5. The combination of these two factors is 2.00. Therefore, the P_0 term above can be multiplied by 2.0 to give an ultimate allowable.

Figure 12.2.8-2 should be used for formed sheet aluminum with $F_{ty} = 40,000\text{psi}$. The values from this figure can be modified for other grades and tempers of aluminums in the following way:

$$P'_0 = P_0 \cdot \frac{F_{ty}'}{40,000}$$

Allowable curves are shown on the next page.

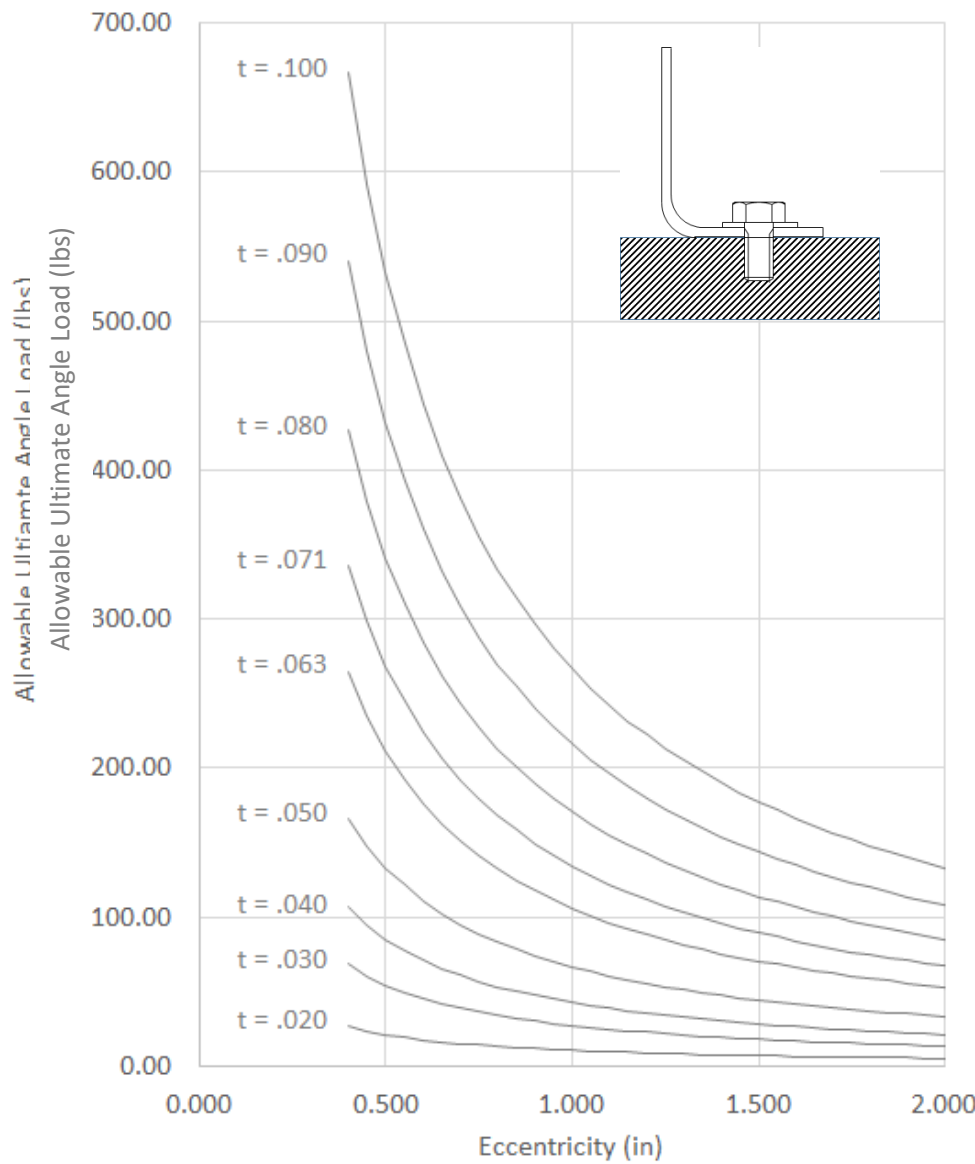


Figure 12.2.8-2: Allowable Ultimate Load for Formed Sheet Aluminum Tension Clip

A spreadsheet for this method is available at the link below:

ABBOTT AEROSPACE SEZC LTD
SPREADSHEETS
ABBOTTAEROSPACE.COM
AA-SM-027-003 Tension Clips - Formed Aluminum - Abbott Aerospace Method

Extruded Aluminum Tension Clips

The allowable load for extruded aluminum clips can be found with the following factors:

Factor from yield allowable to ultimate allowable (minimum for extruded aluminum) is 1.167, the shape factor for a rectangular section is 1.5. The combination of these two factors is 1.75. The P_0 term above can be multiplied by 1.75 to give an ultimate allowable.

Figure 12.2.8-2 should be used for formed sheet aluminum with $F_{ty} = 42,000\text{psi}$. The values from this figure can be modified for other grades and tempers of aluminum in the following way.

$$P'_0 = P_0 \cdot \frac{F_{ty}'}{42,000}$$

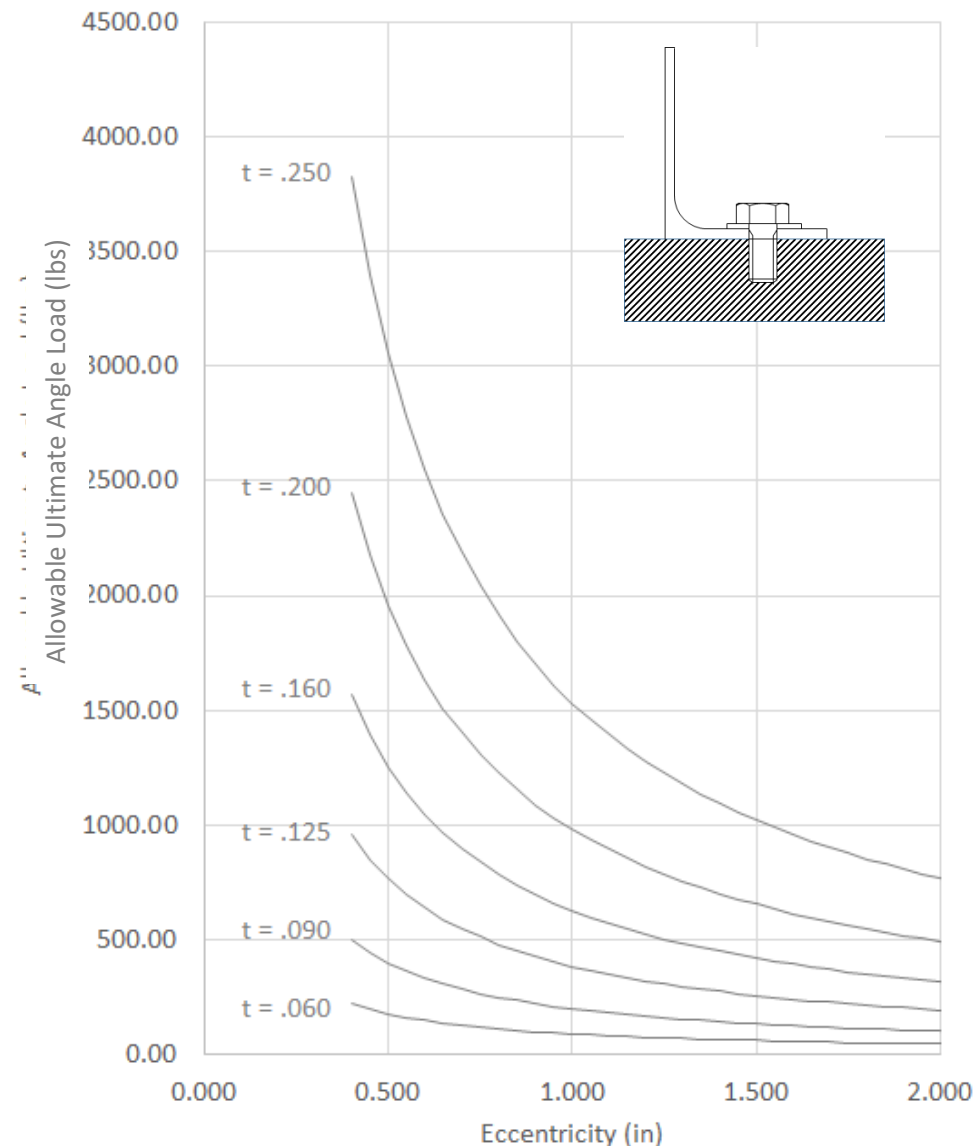


Figure 12.2.8-3: Allowable Ultimate Load for Extruded Aluminum Tension Clip

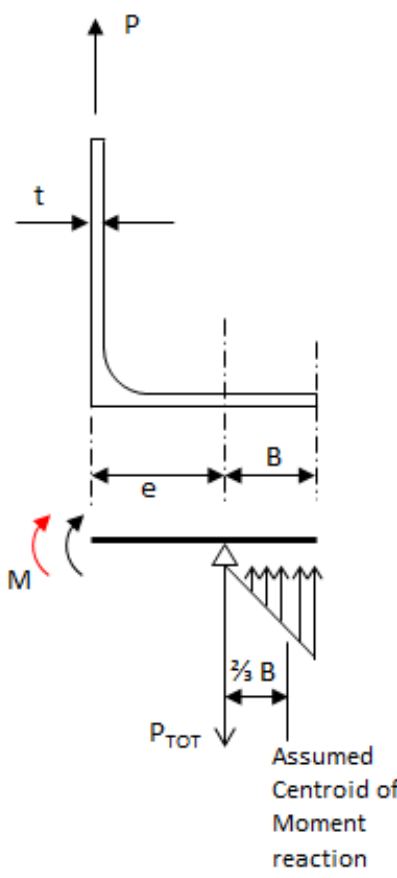
A spreadsheet for this method is available at the link below:

ABBOTT AEROSPACE SEZC LTD
SPREADSHEETS
ABBOTTAEROSPACE.COM
AA-SM-027-004 Tension Clips - Extruded Aluminum - Abbott Aerospace Method

12.2.8.2. Tension Clip - Fastener Tension Failure

The second failure mode of a tension clip installation is a tension failure of the fastener. A fastener tension failure is only likely, for a well-designed joint, by consideration of the heel-toe effect of the fastener location and the edge of the angle flange.

For this load amplification effect to be significant the clip has to have a relatively high bending stiffness. This failure mode is less likely for thinner angles. However, there is no way to determine (other than comprehensive testing) when this effect becomes significant, so it is cautious to check this effect in every case.



The assumption of how the flange reacts a moment created by the applied load is the same as for the bending check.

The moment reaction at the fastener location is replaced by a couple reaction between the fastener position and an assumed triangular bearing reaction between the underside of the clip and the support structure.

Simplistically, the moment is calculated at the fastener position assuming rotational fixity at the fastener position and the outstanding web. This can be described by the following equation:

$$M = P \cdot e / 2$$

The additional force due to the couple reaction is calculated as:

$$P_{add} = M / \left(\frac{2}{3} B \right)$$

Where $2/3B$ is the centroid of the assumed triangular reaction force.

The total bolt load is the sum of the applied load and the additional load:

$$P_{tot} = P + P_{add}$$

A spreadsheet for this method is available at the link below:



AA-SM-027-005 Tension Clips - Fastener Tension - Abbott Aerospace Method

ADVERT: SOFTWARE

EXCEL ADD-IN: XL-VIKING SOFTWARE TOOLS

[DOWNLOAD](#)

By Aerospace Stress Engineers for Aerospace Stress Engineers

| | | |
|---|--|-----------------------------|
| $M_x =$ | 300000 Nmm | Bending Moment About x-Axis |
| $M_y =$ | -80000 Nmm | Bending Moment About y-Axis |
| $I_x =$ | 81.18 mm ⁴ | Moment of Inertia |
| $I_y =$ | 153.58 mm ⁴ | Moment of Inertia |
| $I_{xy} =$ | -21.33 mm ⁴ | Product of Inertia |
| $A =$ | $2 \times I_{xy} / (I_y - I_x)$ $= 2 \times (-21.3) / (154 - 81.2)$ $A = -0.589$ | |
| $\Phi =$ | $0.5 \times \text{ATAN}[A]$ $= 0.5 \times \text{ATAN}[-0.589]$ $\Phi = -0.266$ radians $\Phi = -15.25$ degrees | |
| Moment of Inertia about principal axes | | |
| $I_{x1} =$ | $I_x \times (\cos[\Phi])^2 + I_y \times (\sin[\Phi])^2 - 2 \times I_{xy} \times \sin[\Phi] \times \cos[\Phi]$ $= 81.2 \times (\cos[-0.266])^2 + 154 \times (\sin[-0.266])^2 - 2 \times (-21.3) \times \sin[-0.266] \times \cos[-0.266]$ $I_{x1} = 75.36$ mm ⁴ | |
| $I_{y1} =$ | $I_x \times (\sin[\Phi])^2 + I_y \times (\cos[\Phi])^2 + 2 \times I_{xy} \times \sin[\Phi] \times \cos[\Phi]$ | |

Math Formulas change and update in real time

12.2.9. Mechanical Joints - Lugs

Most of this section can be cited to [\(NASA TM X-73305, 1975\)](#) although the method in the quoted reference is essentially the same as the original 1953 lug analysis paper by Melcon and Hoblit.

- A lug can be described as a 'single bolt fitting' - typically used to transmit large loads and provide a joint that can quickly be disconnected.
- In a typical bolted joint, the hole created by the presence of the bolt does not play a significant role in the overall strength of the joint - i.e. the net section strength of the sheet item is not significantly less than the gross strength of the sheet, and in any case the tension strength of the sheet is typically not the critical measure of strength in a typical bolted joint. However, in a lug the bolt hole has a significant effect on the strength of the joint.

Lug Load Nomenclature:

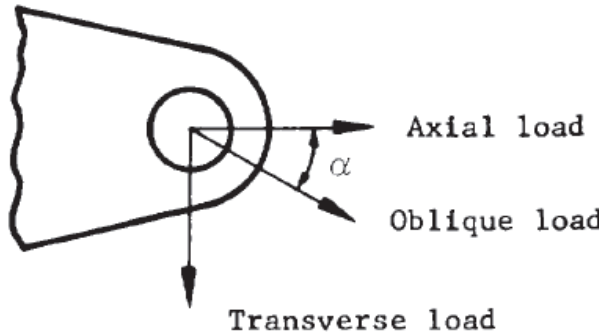


Figure 12.2.9-1: Lug Load Direction Nomenclature

It is recommended that for all lug analyses a 10% off axis load effect is considered combined with the major load direction. This gives allowance for misalignment on installation and the effect of deflection under load of the wider structural assembly.

The lug can fail in any of the following failure modes:

- Tension across the net section
- Shear tear out or bearing
- Shear of the pin
- Bending of the pin
- Side load on the lug (checked by conventional beam method)

Lug dimension nomenclature:

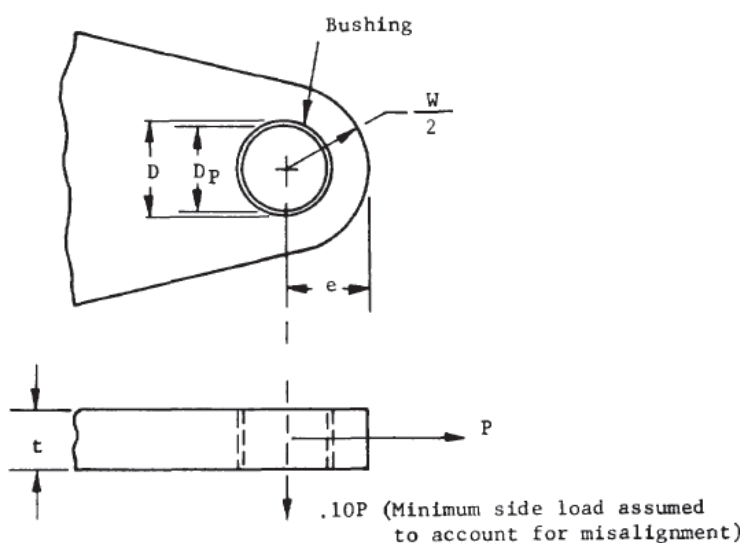


Figure 12.2.9-2: Lug Dimension Nomenclature

Derived Lug dimensional terms:

$$\text{Bearing Area: } A_{br} = D \cdot t$$

$$\text{Net Tension Area: } A_t = (W - d) \cdot t$$

12.2.9.1. Shear Tear-Out or Bearing Failure

The ultimate allowable load for shear bearing failure: $P'_{bru} = K_{br} \cdot F_{tux} \cdot A_{br}$

Where:

F_{tux} = Ultimate tensile strength of lug material in the transverse direction.

K_{br} is taken from the following figure:

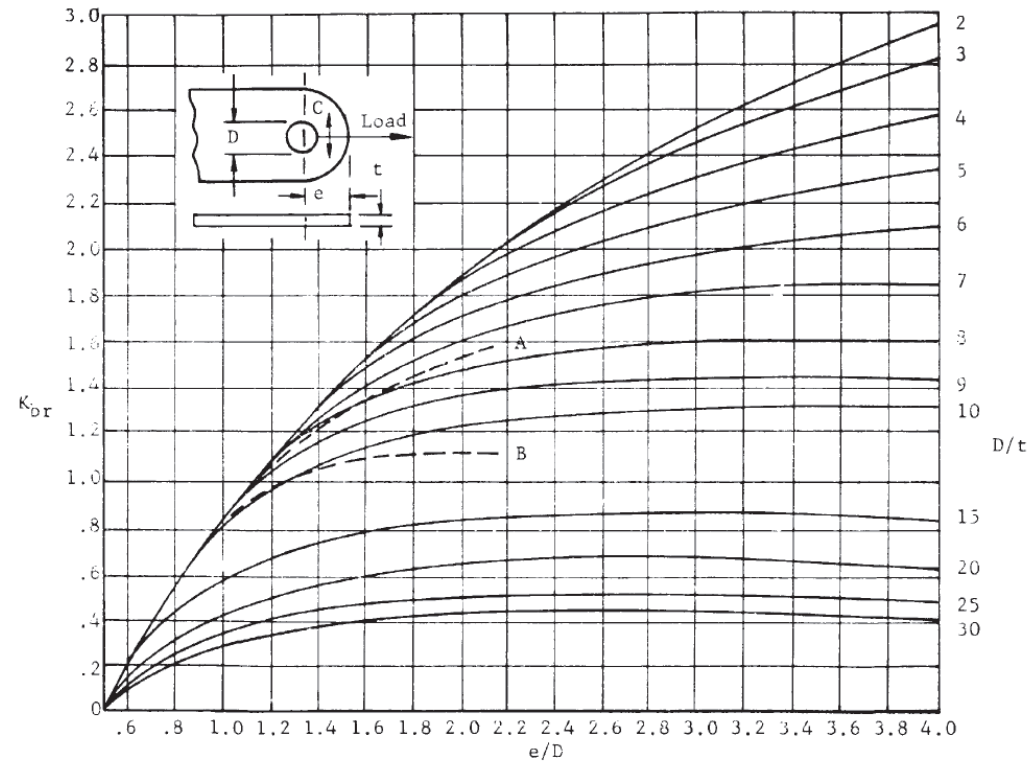


Figure 12.2.9-3: Shear Bearing Kt [\(NASA TM X-73305, 1975\)](#)

A spreadsheet for this method is available at the link below:

ABBOTT AEROSPACE SEZC LTD
SPREADSHEETS
ABBOTTAEROSPACE.COM

AA-SM-009-001 Lug Analysis - Shear Bearing Strength

12.2.9.2. Tension Across the Net Section

The ultimate allowable for tension failure: $P'_{tu} = K_t \cdot F_{tu} \cdot A_t$

Where:

F_{tu} = Ultimate tensile strength of lug material.

K_t is taken from the following figure:

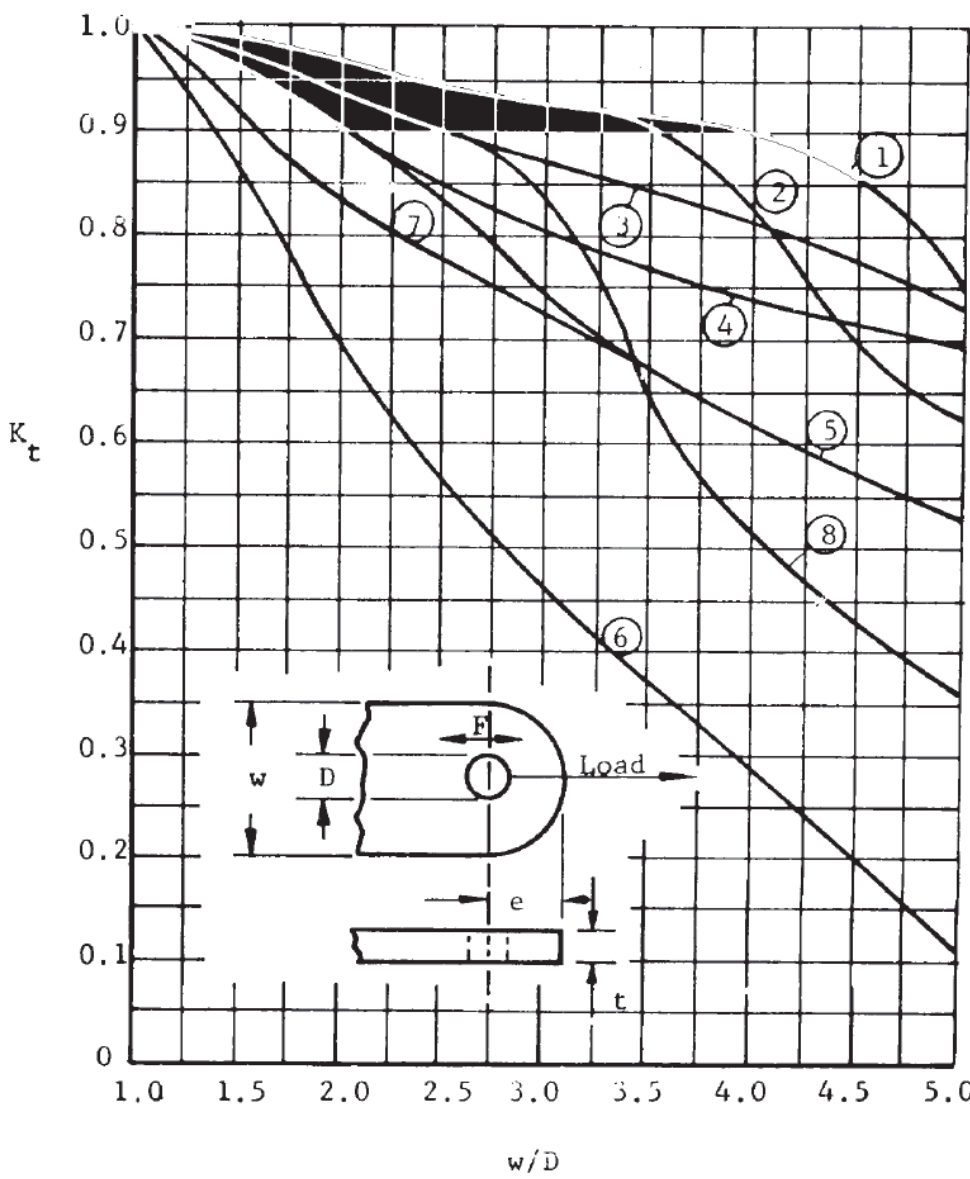


Figure 12.2.9-4: Axial Loading K_t (NASA TM X-73305, 1975)

Notes for Figure 12.2.9-4:

L = longitudinal, T = long transverse, N = short transverse (normal)

Curve 1:

4130, 4140, 4340 and 8630 steel

2014-T6 and 7075-T6 Panel ≤ 0.5 in (L,T)

7075-T6 bar and extrusion (L)

2014-T6 hand forged billet ≤ 144 sq. in. (L)

2014-T6 and 7075-T6 die forgings (L)

Curve 2:

2014-T6 and 7075-T6 Panel > 0.5 in., ≤ 1 in.

7075-T6 extrusion (T,N)

7075-T6 hand forged billet ≤ 36 sq.in. (L)

2014-T6 hand forged billet > 144 sq.in. (L)

2014-T6 hand forged billet ≤ 36 sq.in. (T)

2014-T6 and 7075-T6 die forgings (T)

17-4 PH, 17-7 PH-THD

Curve 3:

2024-T6 Panel (L,T)

2024-T4 and 2024-T42 extrusion (L,T,N)

Curve 4:

2024-T4 Panel (L,T), 2024-T3 Panel (L,T)

2014-T6 and 7075-T6 Panel > 1 in.(L,T)

2024-T4 bar (L,T)

7075-T6 hand forged billet > 36 sq.in. (L)

7075-T6 hand forged billet ≤ 16 sq.in. (T)

Curve 5:

195T6, 220T4, and 356T6 aluminum alloy casting

7075-T6 hand forged billet > 16 sq.in. (T)

2014-T6 hand forged billet > 36 sq.in. (T)

Curve 6:

Aluminum alloy panel, bar, hand forged billet, and die forging (N). Note: for die forgings, N direction exists only at the parting plane. 7075-T6 bar (T)

Curve 7:

18-8 stainless steel, annealed

Curve 8:

18-8 stainless steel, full hard, Note: for 1/4, 1/2 and 3/4 hard, interpolate between Curves 7 and 8.

A spreadsheet for this method is available at the link below:

ABBOTT AEROSPACE SEZC LTD
SPREADSHEETS
ABBOTTAEROSPACE.COM
AA-SM-009-002 Lug Analysis - Axial Strength

12.2.9.3. Transverse Lug Strength

The ultimate allowable for transverse failure: $P'_{tru} = K_{tru} \cdot F_{tux} \cdot A_{br}$

The transverse strength of the lug depends on the shape parameter of the lug. This parameter is expressed as:

Shape parameter =

$$\frac{A_{av}}{A_{br}}$$

Where

A_{br} is the bearing area – Dt

A_{av} is the weighted average area given by:

$$A_{av} = \frac{6}{\left(\frac{3}{A_1}\right) + \left(\frac{1}{A_2}\right) + \left(\frac{1}{A_3}\right) + \left(\frac{1}{A_4}\right)}$$

The areas A_1 , A_2 , A_3 and A_4 are defined as:

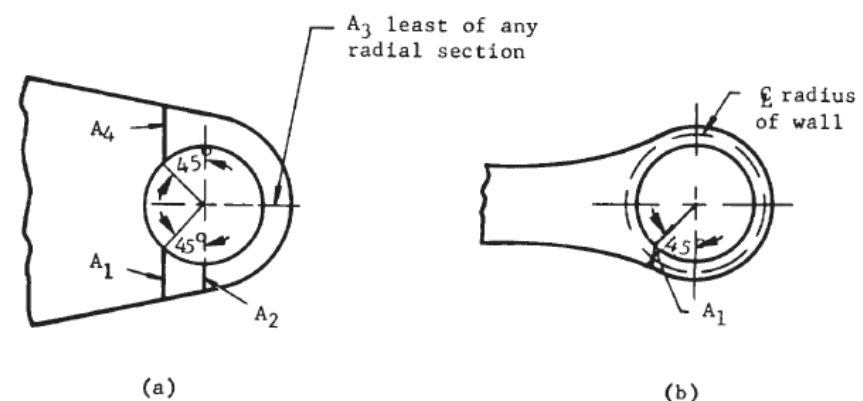


Figure 12.2.9-5: Idealization of Typical Lug for Transverse Load
(NASA TM X-73305, 1975)

A_3 is the least area on any radial section around the hole.

Thought should always be given to assure that the areas A_1 , A_2 , A_3 and A_4 adequately reflect the strength of the lug. For lugs with an unusual shape or a sudden change in cross section a conservative equivalent lug should be assumed.

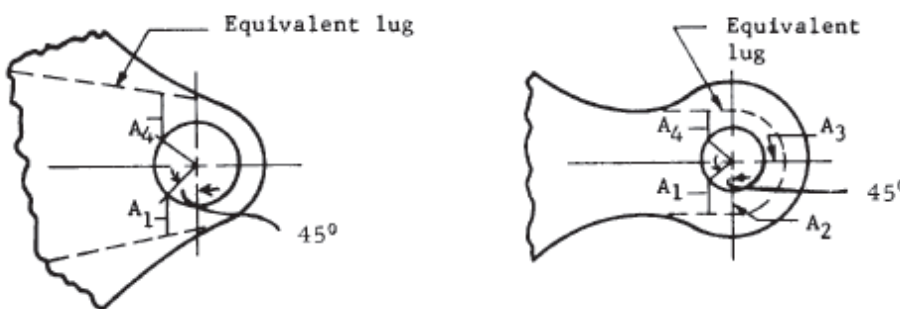


Figure 12.2.9-6: Idealization of Unusual Lugs for Transverse Load
(NASA TM X-73305, 1975)

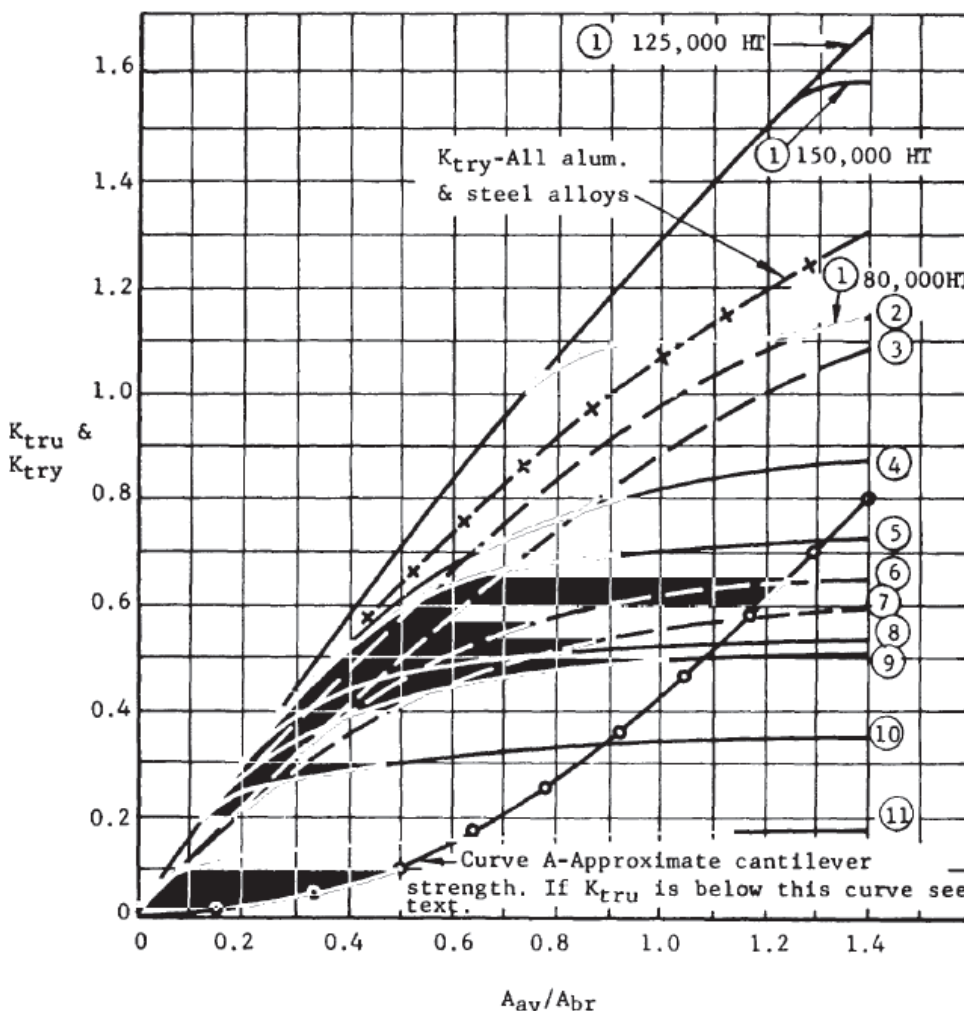


Figure 12.2.9-7: Transverse Loading Kt (NASA TM X-73305, 1975)

Notes for Figure 12.2.9-7:

Curve 1:

4130, 4140, 4340, and 8630 steels, heat treatment as noted. - Curve (a) for 125Ksi HT, Curve (b) for 150Ksi HT, Curve (c) for 80Ksi HT

Curve 2:

2024-T4 and 2024-T3 Panel \leq 0.5 in.

Curve 3:

220-T4 aluminum alloy casting

Curve 4 :

17-7 PH (THD)

Curve 5 :

2014-T6 and 7075-T6 Panel \leq 0.5 in.

Curve 6:

2024-T3 and 2024-T4 Panel $>$ 0.5 in., 2024-T4 bar

Curve 7:

195-T6 and 356-T6 aluminum alloy casting

Curve 8:

2014-T6 and 7075-T6 Panel $>$ 0.5 in., \leq 1 in.

7075-T6 extrusion

2014-T6 hand forged billets \leq 36 sq. in.

2014-T6 and 7075-T6 die forgings

Curve 9:

2024-T6 Panel

2024-T4 and 2024-T42 extrusion

Curve 10:

2014-T6 and 7075-T6 Panel $>$ 1 in.

7075-T6 hand forged billet \leq 16 sq. in.

Curve 11:

7075-T6 hand forged billet $>$ 16 sq. in.

2014-T6 hand forged billet $>$ 36 sq. in.

12.2.9.4. Lugs – Combined Axial and Transverse (Oblique) Load

In analyzing a lug, the load applied should be broken into axial and transverse components (denoted by subscripts "a" and "tr" respectively) relative to the idealized lug. The two separate cases should be analyzed and the results combined using the interaction equation:

$$R_a^{1.6} + R_{tr}^{1.6} = 1$$

Where:

$$R_a = \frac{P_a}{\min(P'_{bru}, P'_{tu})}$$

And:

$$R_{tr} = \frac{P_{tr}}{P'_{tru}}$$

The Margin of Safety is calculated as follows:

$$MS = \frac{1}{[R_a^{1.6} + R_{tr}^{1.6}]^{0.625}} - 1$$

A spreadsheet for this method is available at the link below:

ABBOTT AEROSPACE SEZC LTD
SPREADSHEETS
ABBOTTAEROSPACE.COM

AA-SM-009-005 Lug Analysis - Compact Oblique

12.2.10. Mechanical Joints - Lugs - Additional checks

12.2.10.1. Pin Bending

The pin used in the lug joint should be checked for pin bending. To obtain the effective moment arm of the pin compute the following for the inner lug:

$$r = \left[\left(\frac{e}{D} \right) - \frac{1}{2} \right] \cdot \frac{D}{t_2}$$

Where e , D and t_2 are the lug edge distance, hole/pin diameter and thickness respectively defined in Figure 12.2.9-2.

Take the smaller of P'_{bru} and P'_{tu} for the inner lug as $(P'_u)_{min}$ and compute the following expression:

$$(P'_u)_{min}/(A_{br} \cdot F_{tux})$$

Obtain the reduction factor 'y' from the following figure:

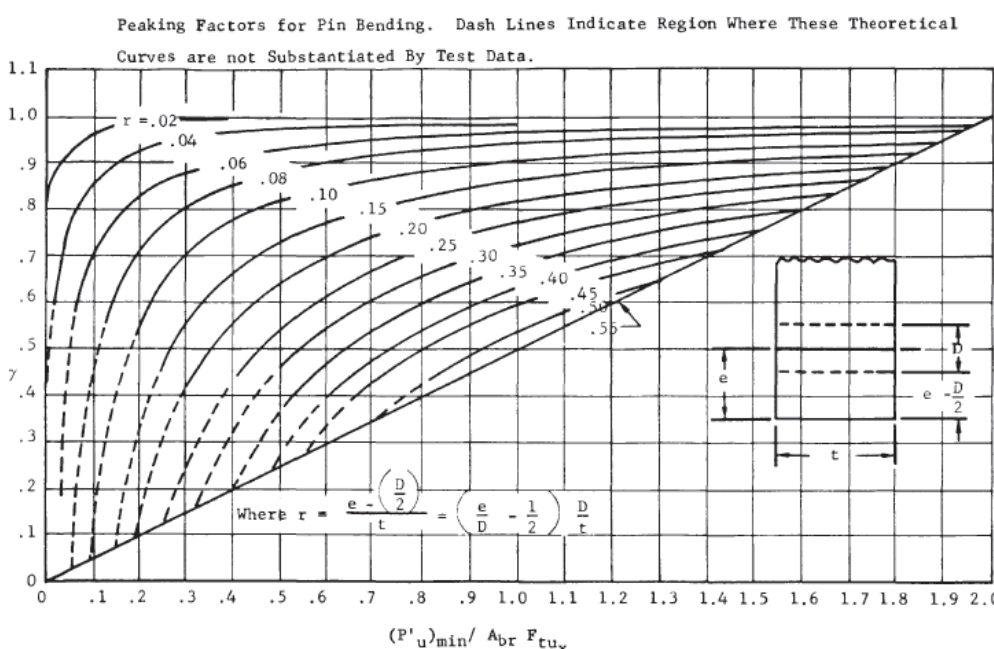


Figure 12.2.10-1: Peaking Factors for Pin Bending [\(NASA TM X-73305, 1975\)](#)

The effective moment arm can then be calculated using the following expression:

$$b = \frac{t_1}{2} + g + \gamma \left(\frac{t_1}{4} \right)$$

Where the terms in the expression are defined in the figure below:

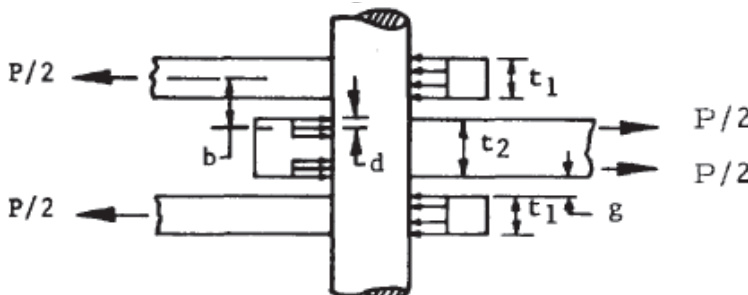


Figure 12.2.10-2: Parameters to Calculate Effective Moment Arm for Pin Bending [\(NASA TM X-73305, 1975\)](#)

Calculate pin bending moment from the equation:

$$M = P \cdot \left(\frac{b}{2} \right)$$

Calculate the bending stress resulting from "M" assuming the standard My/I distribution.

The resulting bending stress can be compared to the pin plastic bending allowable.

Note: A fitting factor per the regulations of at least 1.15 should be used. Some OEMs require a minimum margin of safety of 0.25 for lugs, or an effective fitting factor of 1.25.

A spreadsheet for this method is available at the link below:

ABBOTT AEROSPACE SEZC LTD
SPREADSHEETS
ABBOTTAEROSPACE.COM
AA-SM-009-004 Lug Analysis - Pin Bending

12.2.10.2. Stresses due to Press Fit Bushings

The method in this section is referenced to [\(AFFDL-TR-69-42, 1986\)](#) Section 9.16. Note that several errors in the source material have been corrected. *The expression for the maximum tangential stress for the bushing: The 'p' and 'B' should be in regular font, therefore the numerator becomes '2pB²' and the denominator of this expression should read 'B²-A²'.*

The pressure between a lug and a bushing assembly having negative clearance can be determined by consideration of the radial displacements. This method assumes the lug acts as if it is a uniform ring around the bushing. After assembly, the increase in the inner radius of the ring (lug), plus the decrease in the outer radius of the bushing equals the difference between the radii of the bushing and ring (lug) before assembly.

$$\delta = u_{ring} - u_{bushing}$$

Where:

δ Difference between outer radius of bushing and inner radius of the ring

u Radial displacement, positive away from the axis of the ring or bushing

Radial displacement at the inner surface of a ring subjected to internal pressure p is:

$$u = \frac{D_p}{E_{ring}} \cdot \left[\frac{C^2 + D^2}{C^2 - D^2} - \mu_{ring} \right]$$

Radial displacement at the outer surface of a bushing subjected to external pressure p is:

$$u = - \frac{B_p}{E_{bush}} \cdot \left[\frac{B^2 + A^2}{B^2 - A^2} - \mu_{bush} \right]$$

Where:

A Inner radius of bushing, in

B Outer radius of bushing, in

C Outer radius of ring, in (lug)

D Inner radius of ring, in (lug)

E Modulus of elasticity, psi
 μ Poisson's ratio

Combining these equations and substituting into the first equation and solving for p gives the following expression:

$$p = \frac{\delta}{\frac{D}{E_{ring}} \cdot \left(\frac{C^2 + D^2}{C^2 - D^2} + \mu_{ring} \right) + \frac{B}{E_{bush}} \cdot \left(\frac{B^2 + A^2}{B^2 - A^2} - \mu_{bush} \right)}$$

Maximum radial and tangential stresses for a ring (lug) subjected to internal pressure occur at the inner surface of the ring (lug).

Maximum radial stress for lug (the pressure on the interface between the lug and the bushing):

$$F_r = -p$$

Maximum tangential stress for lug:

$$F_t = p \cdot \left[\frac{C^2 + D^2}{C^2 - D^2} \right]$$

Positive sign indicates tension. The maximum shear stress at this point in the lug is:

$$F_s = \frac{F_t - F_r}{2}$$

The maximum radial stress for a bushing subjected to external pressure occurs at the outer surface of the bushing and is:

$$F_r = -p$$

The maximum tangential stress for a bushing subjected to external pressure occurs at the inner surface of the bushing and is:

$$F_t = -\frac{2 \cdot p \cdot B^2}{B^2 - A^2}$$

Acceptable stress levels:

- Stress corrosion. This maximum allowable press fit stress in magnesium alloys should not exceed 8000psi. For all aluminum alloys, the maximum press fit stress should not exceed 0.50F_{ty}.
- Static fatigue. For steels heat treated to above 200ksi, where there is any risk of hydrogen embrittlement the press fit stress should not exceed 0.25F_{tu}.
- Ultimate strength. F_{tu} should not be exceeded. However, it is rare to create stresses of this magnitude in a press fit bushing installation.

A spreadsheet for this method is available at the link below:

ABBOTT AEROSPACE SEZC LTD
SPREADSHEETS
ABBOTTAEROSPACE.COM
AA-SM-010 Stress Due to Interference fit bushing installation

ADVERT: ENGINEERING SERVICES

STRESS ANALYSIS

ENGINEERING SERVICES

CONTACT US

12.2.11. Other Mechanical Connections

12.2.11.1. Beam in a Socket Analysis

A beam in a socket type analysis is usually applicable for cantilevered (single shear) pins in fittings. The nature of these joints means that the engagement length of the pin in the 'socket' is usually some multiple of the pin diameter. This is required to reduce the peak bearing load between the pin and the socket to an acceptable level.

The method is predicated on a continuous contact between the pin and the socket and a uniform bearing load distribution between the pin and the socket. This method is referenced to R. Burandt in 1959, and an expanded method (that gives essentially the same results) is defined in [\(NASA-CR-4608, 1994\)](#). This method was provided to me by Bosko Zdanski in October 2013.

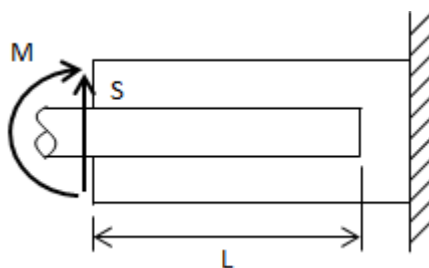


Figure 12.2.11-1: Beam in a Socket Configuration

Distributed socket reaction to shear load:

$$w_s = \frac{S}{L}$$

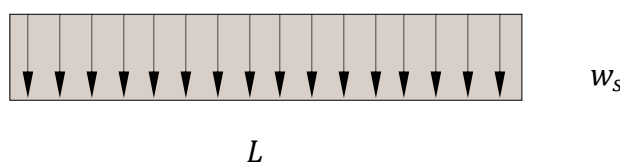


Figure 12.2.11-2: Beam in a Socket – Distributed Shear Load

Moment at Socket Center:

$$M_T = M + S \cdot \frac{L}{2}$$

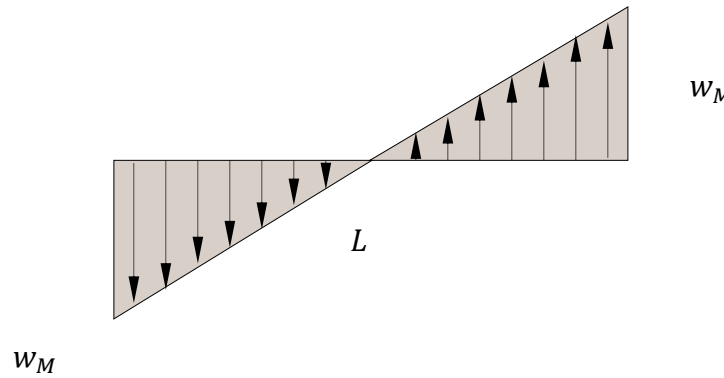


Figure 12.2.11-3: Beam in a Socket – Distributed Moment Load

Distributed socket reaction to Moment Load at Socket Center:

$$w_M = \frac{6}{L^2} \cdot \left(M + S \cdot \frac{L}{2} \right)$$

Socket Reaction at Outer End:

$$w_1 = w_M + w_s$$

This expands to:

$$w_1 = \frac{M}{L^2} \cdot \left(4 \cdot \frac{S \cdot L}{M} + 6 \right)$$

Introducing:

$$K_1 = 4 \cdot \frac{S \cdot L}{M} + 6$$

The resulting expression is:

$$w_1 = K_1 \cdot \frac{M}{L^2}$$

Socket reaction at bottom end:

$$w_2 = w_M - w_s$$

This expands to:

$$w_2 = \frac{M}{L^2} \cdot \left(2 \cdot \frac{S \cdot L}{M} + 6 \right)$$

Introducing:

$$K_2 = 2 \cdot \frac{S \cdot L}{M} + 6$$

The resulting expression is:

$$w_2 = K_2 \cdot \frac{M}{L^2}$$

From a linear load distribution, it follows that:

$$\frac{a}{w_2} = \frac{L - a}{w_1}$$

$$a = L \cdot \frac{w_2}{w_1 + w_2}$$

Introducing:

$$K_a = \frac{w_2}{w_1 + w_2} = \frac{1 + \frac{S \cdot L}{3 \cdot M}}{2 + \frac{S \cdot L}{M}}$$

The resulting expression is:

$$a = K_a \cdot L$$

Where 'a' is the distance from the 'bottom' of the socket to the point of zero shear load:

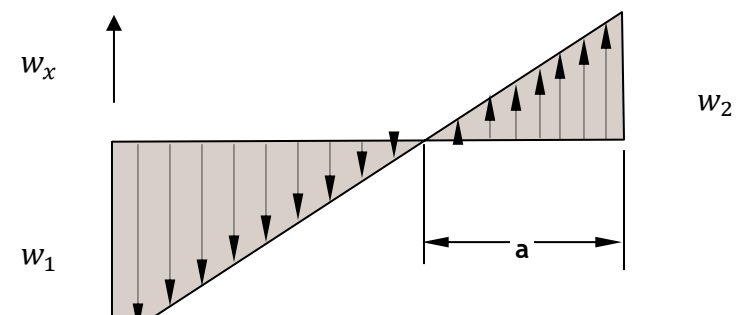


Figure 12.2.11-4: Beam in a Socket – Bearing Load Summation

Local distributed reaction along socket is given by:

$$w(x) = \frac{w_1 + w_2}{L} \cdot x - w_1$$

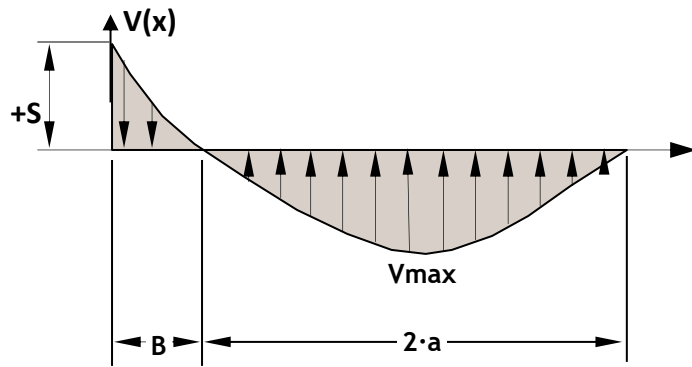


Figure 12.2.11-5: Beam in a Socket – Pin Internal Shear Load

Pin maximum shear load:

$$V_{MAX} = -\frac{a \cdot w_2}{2}$$

Introducing:

$$K_V = \frac{K_2 \cdot K_a}{2} = \frac{2 \cdot \frac{S \cdot L}{M} + 6}{2} \cdot \frac{1 + \frac{1}{3} \cdot \frac{S \cdot L}{M}}{2 + \frac{S \cdot L}{M}}$$

The resulting expression is:

$$V_{MAX} = -K_V \cdot \frac{M}{L}$$

The point of pin zero shear load is given by:

$$B = L - 2 \cdot a = L \cdot (1 - 2 \cdot K_a)$$

Introducing:

$$K_B = 1 - 2 \frac{\frac{1}{3} \cdot \frac{S \cdot L}{M}}{2 + \frac{S \cdot L}{M}} = \frac{\frac{S \cdot L}{M}}{2 + \frac{S \cdot L}{M}}$$

The resulting expression is:

$$B = K_B \cdot \frac{L}{3}$$

The location 'B' is also where the maximum pin internal moment occurs.

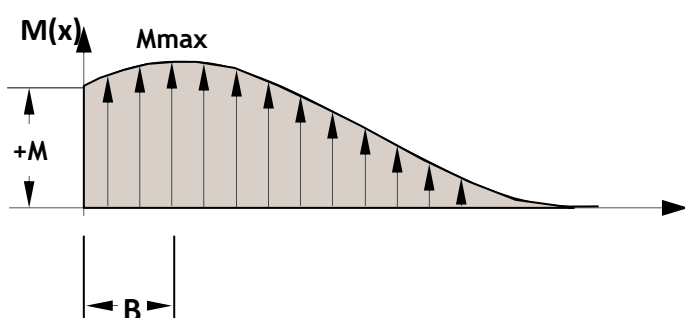


Figure 12.2.11-6: Beam in a Socket – Pin Internal Moment

The expression for the pin internal shear load is:

$$V(x) = S + \int_0^x w(x) dx$$

This can be expanded to:

$$V(x) = S + \frac{M}{L^2} \cdot \left[\left(3 \cdot S \cdot \frac{L}{M} + 6 \right) \cdot \frac{x^2}{L} - \left(4 \cdot S \cdot \frac{L}{M} + 6 \right) \cdot x \right]$$

The expression for the pin internal shear Moment is:

$$M(x) = M + \int_0^x V(x) dx$$

This can be expanded to:

$$M(x) = M + S \cdot x + \frac{M}{L^2} \cdot \left[\left(S \cdot \frac{L}{M} + 2 \right) \cdot \frac{x^3}{L} - \left(2 \cdot S \cdot \frac{L}{M} + 3 \right) \cdot x^2 \right]$$

The maximum pin moment occurs at point 'B' coincidental with the point of zero internal pin shear:

$$M_{MAX} = M \cdot \left[1 + \frac{K_B}{3} \cdot \frac{S \cdot L}{M} + \left(\frac{K_B}{3} \right)^3 \cdot \left(\frac{S \cdot L}{M} + 2 \right) - \left(\frac{K_B}{3} \right)^2 \cdot \left(2 \cdot \frac{S \cdot L}{M} + 3 \right) \right]$$

This method is available in our standard spreadsheet format here:

ABBOTT AEROSPACE SEZC LTD
SPREADSHEETS
ABBOTTAEEROSPACE.COM
AA-SM-003 Beam in a Socket

12.3. General Treatment of Contact Stresses

This section is largely adapted from [\(AFFDL-TR-69-42, 1986\)](#) chapter 11. The analysis methods in this section are applicable only to isotropic materials in the elastic range. The methods are applicable for static load only and cannot be used for dynamic contact.

The stresses that develop when two elastic bodies are forced together are termed bearing stresses, the stresses are localized on the surface of the material and can be high due to the small areas in contact.

For specialized or ball or roller bearings, the vendor information/product specification should be consulted for allowable load levels.

12.3.1. Formulas for Stress and Deformations Due to Pressure Between Elastic Bodies

12.3.1.1. Sphere on Sphere

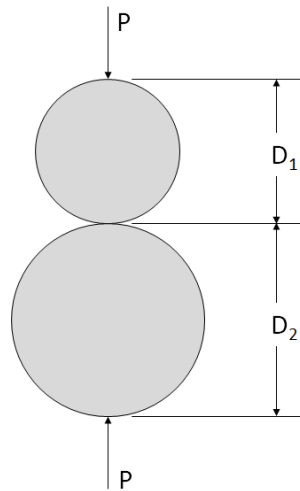
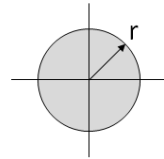


Figure 12.3.1-1: Sphere on Sphere Contact

Shape of Contact Area:



$$r = 0.721 \cdot \sqrt[3]{P \cdot \left(\frac{D_1 \cdot D_2}{D_1 + D_2}\right) \cdot \left[\frac{1 - \mu_1^2}{E_1} + \frac{1 - \mu_2^2}{E_2}\right]}$$

Deflection:

$$d = 1.04 \cdot \sqrt[3]{\frac{P^2 \cdot (D_1 + D_2)}{D_1 \cdot D_2} \cdot \left[\frac{1 - \mu_1^2}{E_1} + \frac{1 - \mu_2^2}{E_2}\right]^2}$$

Maximum Bearing Compression Stress:

$$f_{brc} = 0.918 \cdot \sqrt[3]{\frac{P \cdot \left(\frac{D_1 - D_2}{D_1 \cdot D_2}\right)^2}{\left[\frac{1 - \mu_1^2}{E_1} + \frac{1 - \mu_2^2}{E_2}\right]^2}}$$

A spreadsheet for this method is available at the link below:

ABBOTT AEROSPACE SEZC LTD
SPREADSHEETS
ABBOTTAEROSPACE.COM
AA-SM-008-001 Contact Stresses - Sphere on a Sphere

12.3.1.2. Sphere in Spherical Socket

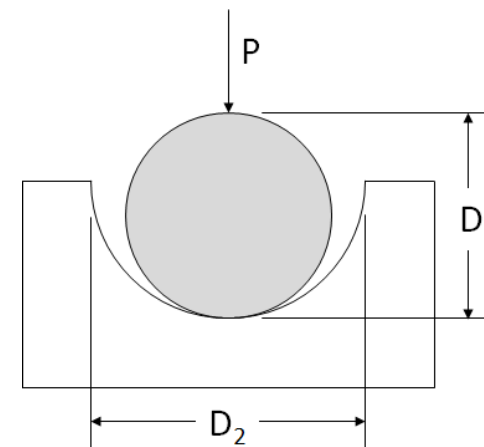
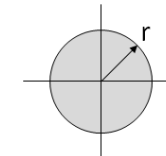


Figure 12.3.1-2: Sphere in Spherical Socket Contact

Shape of Contact Area:



$$r = 0.721 \cdot \sqrt[3]{P \cdot \left(\frac{D_1 \cdot D_2}{D_1 - D_2}\right) \cdot \left[\frac{1 - \mu_1^2}{E_1} + \frac{1 - \mu_2^2}{E_2}\right]}$$

Deflection:

$$d = 1.04 \cdot \sqrt[3]{\frac{P^2 \cdot (D_1 - D_2)}{D_1 \cdot D_2} \cdot \left[\frac{1 - \mu_1^2}{E_1} + \frac{1 - \mu_2^2}{E_2}\right]^2}$$

Maximum Bearing Compression Stress:

$$f_{brc} = 0.918 \cdot \sqrt[3]{\frac{P \cdot \left(\frac{D_1 + D_2}{D_1 \cdot D_2}\right)^2}{\left[\frac{1 - \mu_1^2}{E_1} + \frac{1 - \mu_2^2}{E_2}\right]^2}}$$

A spreadsheet for this method is available at the link below:

ABBOTT AEROSPACE SEZC LTD
SPREADSHEETS
ABBOTTAEROSPACE.COM
AA-SM-008-002 Contact Stresses - Sphere in a Spherical Socket

12.3.1.3. Sphere on a Flat Panel

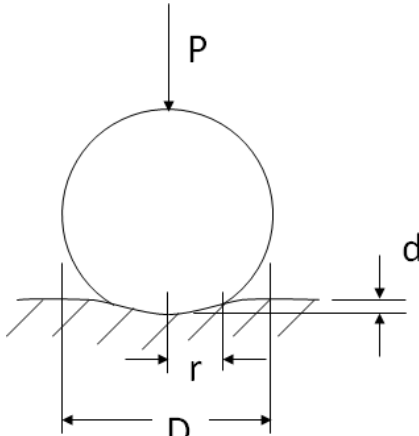
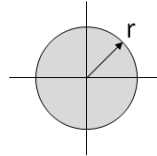


Figure 12.3.1-3: Sphere on Flat Panel Contact

Shape of Contact Area:



$$r = 0.721 \cdot \sqrt[3]{P \cdot D \cdot \left[\frac{1 - \mu_1^2}{E_1} + \frac{1 - \mu_2^2}{E_2} \right]}$$

Maximum Bearing Compression Stress:

$$f_{brc(max)} = 0.918 \cdot \sqrt[3]{\frac{P}{D^2 \cdot \left[\frac{1 - \mu_1^2}{E_1} + \frac{1 - \mu_2^2}{E_2} \right]^2}}$$

Distribution of normal pressure in the contact area as a function of distance (r') from the center of the circle:

$$f_{brc}(r') = f_{brc(max)} \sqrt{\left(1 - \frac{r'^2}{r^2}\right)}$$

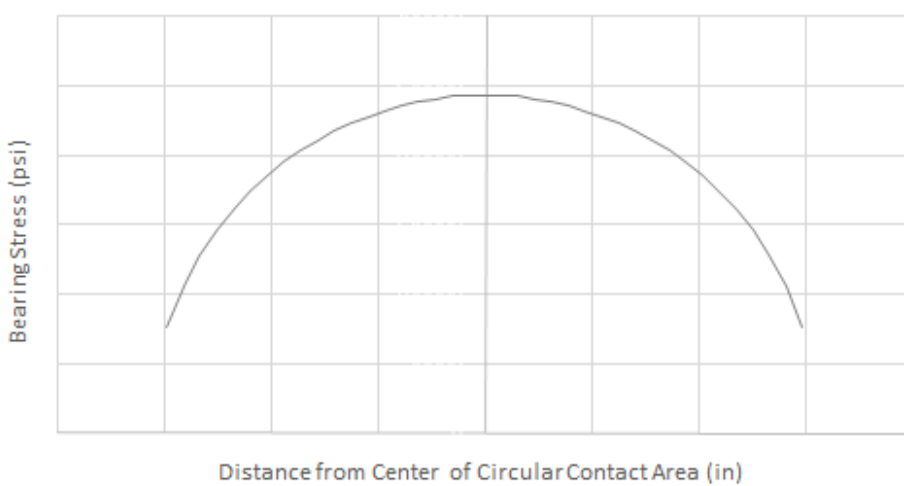


Figure 12.3.1-4: Sphere on Flat Panel Contact – Bearing Stress Distribution

Depth of Indentation:

$$d = \frac{r^2}{(D/2)}$$

A spreadsheet for this method is available at the link below:

ABBOTT AEROSPACE SEZC LTD
SPREADSHEETS
ABBOTTAEEROSPACE.COM

AA-SM-008-003 Contact Stresses - Sphere on a Flat Plate

12.3.1.4. Cylinder on a Cylinder with Axes Parallel

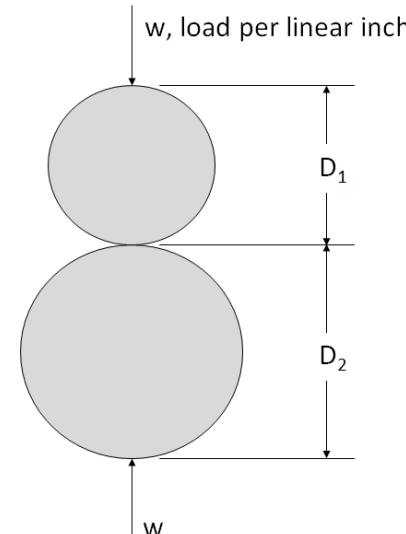
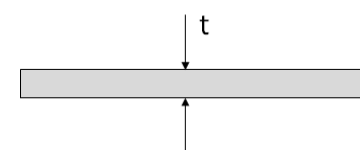


Figure 12.3.1-5: Cylinder on Cylinder Axes Parallel Contact

Shape of Contact Area:



$$t = 1.6 \cdot \sqrt{\frac{w \cdot D_1 \cdot D_2}{D_1 + D_2} \cdot \left[\frac{1 - \mu_1^2}{E_1} + \frac{1 - \mu_2^2}{E_2} \right]}$$

Maximum Bearing Compression Stress:

$$f_{brc} = 0.798 \cdot \sqrt{\frac{\frac{w \cdot (D_1 + D_2)}{D_1 \cdot D_2}}{\left[\frac{1 - \mu_1^2}{E_1} + \frac{1 - \mu_2^2}{E_2} \right]^2}}$$

A spreadsheet for this method is available at the link below:

ABBOTT AEROSPACE SEZC LTD
SPREADSHEETS
ABBOTTAEEROSPACE.COM

AA-SM-008-004 Contact Stresses - Cylinder on a Cylinder - Parallel

12.3.1.5. Cylinder in a Cylindrical Groove

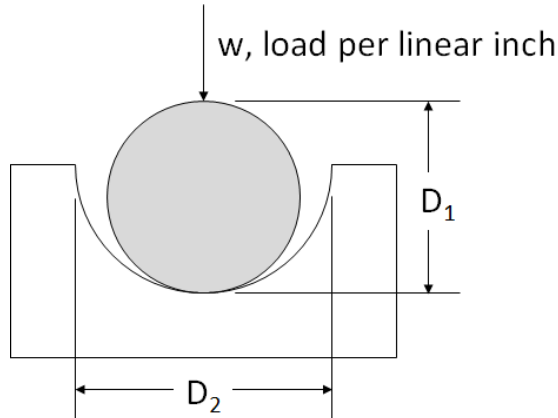
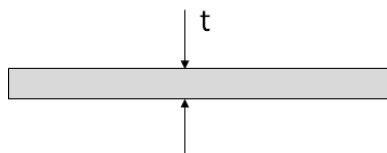


Figure 12.3.1-6: Cylinder in Cylindrical Groove Contact

Shape of Contact Area:



$$t = 1.6 \cdot \sqrt{\frac{w \cdot D_1 \cdot D_2}{D_1 - D_2} \cdot \left[\frac{1 - \mu_1^2}{E_1} + \frac{1 - \mu_2^2}{E_2} \right]}$$

Maximum Bearing Compression Stress:

$$f_{brc} = 0.798 \cdot \sqrt{\frac{\frac{w \cdot (D_1 - D_2)}{D_1 \cdot D_2}}{\left[\frac{1 - \mu_1^2}{E_1} + \frac{1 - \mu_2^2}{E_2} \right]^2}}$$

A spreadsheet for this method is available at the link below:

ABBOTT AEROSPACE SEZC LTD
SPREADSHEETS
ABBOTTAEROSPACE.COM
AA-SM-008-005 Contact Stresses - Cylinder in a Cylindrical Groove

12.3.1.6. Cylinder on a Flat Panel

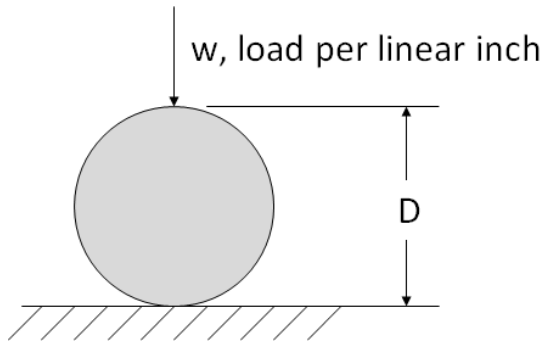
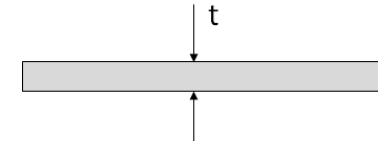


Figure 12.3.1-7: Cylinder on Flat Panel Contact

Shape of Contact Area:



$$t = 1.6 \cdot \sqrt{w \cdot D \cdot \left[\frac{1 - \mu_1^2}{E_1} + \frac{1 - \mu_2^2}{E_2} \right]}$$

Maximum Bearing Compression Stress:

$$f_{brc} = 0.798 \cdot \sqrt{\frac{w}{D \cdot \left[\frac{1 - \mu_1^2}{E_1} + \frac{1 - \mu_2^2}{E_2} \right]^2}}$$

A spreadsheet for this method is available at the link below:

ABBOTT AEROSPACE SEZC LTD
SPREADSHEETS
ABBOTTAEROSPACE.COM
AA-SM-008-006 Contact Stresses - Cylinder on a Flat Plate

12.3.1.7. Cylinder on a Cylinder with Axes Perpendicular

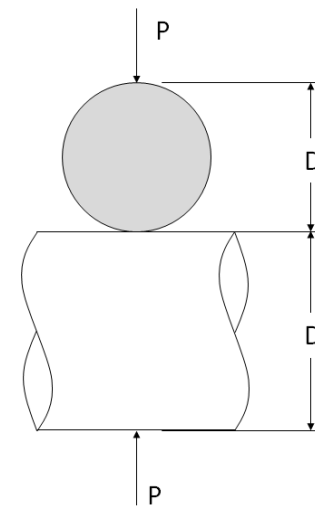
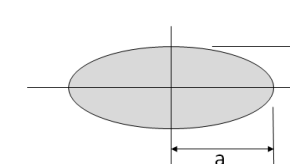


Figure 12.3.1-8: Cylinder on Cylinder Axes Perpendicular Contact

Shape of Contact Area:



The contact area between the two cylinders is derived using the following 3 parameters: K₁, K₂ and K₃.

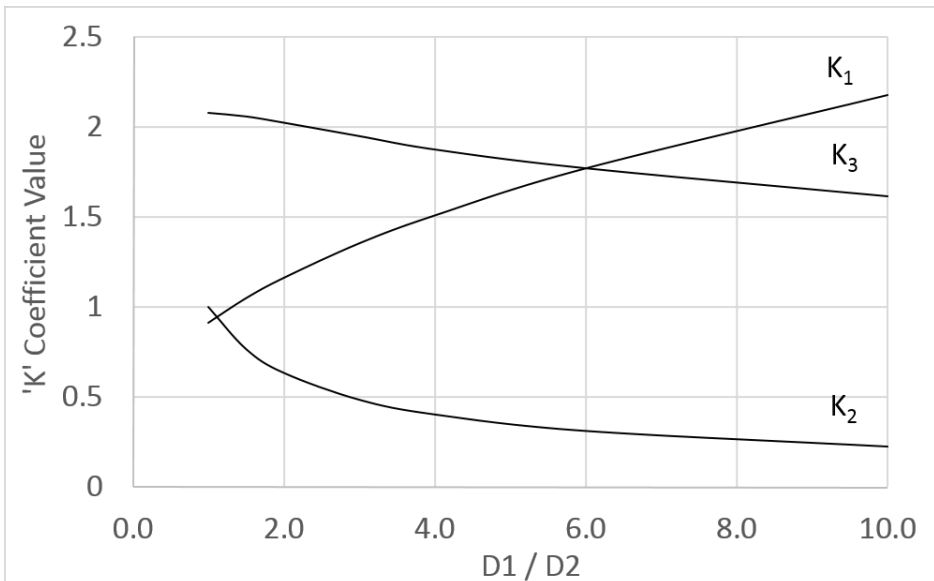


Figure 12.3.1-9: Contact Regions Parameters

$$a = K_1 \cdot \sqrt[3]{P \cdot \left(\frac{D_1 \cdot D_2}{D_1 + D_2} \right) \cdot \left[\frac{1 - \mu_1^2}{E_1} + \frac{1 - \mu_2^2}{E_2} \right]}$$

$$b = K_2 a$$

Deflection:

$$\delta = K_3 \cdot \sqrt[3]{\frac{(D_1 + D_2)}{D_1 \cdot D_2} \cdot \frac{P^2}{\left[\frac{E_1}{1 - \mu_1^2} + \frac{E_2}{1 - \mu_2^2} \right]^2}}$$

Maximum Bearing Compression Stress:

$$f_{brc} = \frac{1.5 \cdot P}{\pi \cdot a \cdot b}$$

A spreadsheet for this method is available at the link below:

ABBOTT AEROSPACE SEZC LTD
SPREADSHEETS
ABBOTTAEROSPACE.COM

AA-SM-008-007 Contact Stresses - Cylinder on a Cylinder - Perpendicular

12.3.1.8. Rigid Knife Edge on a Panel

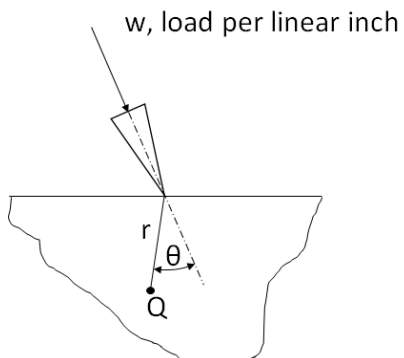


Figure 12.3.1-10: Rigid Knife Edge on a Panel Contact

Maximum Bearing Compression Stress, at any point Q:

$$f_{brc} = \frac{2 \cdot w \cdot \cos \theta}{\pi \cdot r}$$

A spreadsheet for this method is available at the link below:

ABBOTT AEROSPACE SEZC LTD
SPREADSHEETS
ABBOTTAEROSPACE.COM

AA-SM-008-008 Contact Stresses - Rigid Knife Edge on Plate

12.3.1.9. Rigid Cone on a Panel

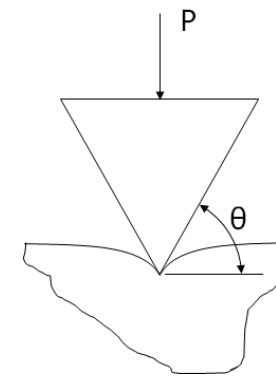


Figure 12.3.1-11: Rigid Cone on a Panel Contact

Maximum Deflection:

$$d = \sqrt{\frac{P \cdot \pi \cdot (1 - \nu^2) \cdot \tan \theta}{2 \cdot E}}$$

Depth of the Contact Region:

$$\epsilon = \frac{2 \cdot d}{\pi}$$

Radius of the Contact Region:

$$r = \frac{\epsilon}{\tan \theta}$$

Distribution of normal pressure in the contact area as a function of distance (r') from the center of the circle:

$$f_{brc}(r') = \frac{E \cdot d}{\pi \cdot r \cdot (1 - \nu^2)} \cdot \cosh^{-1} \left(\frac{r}{r'} \right)$$

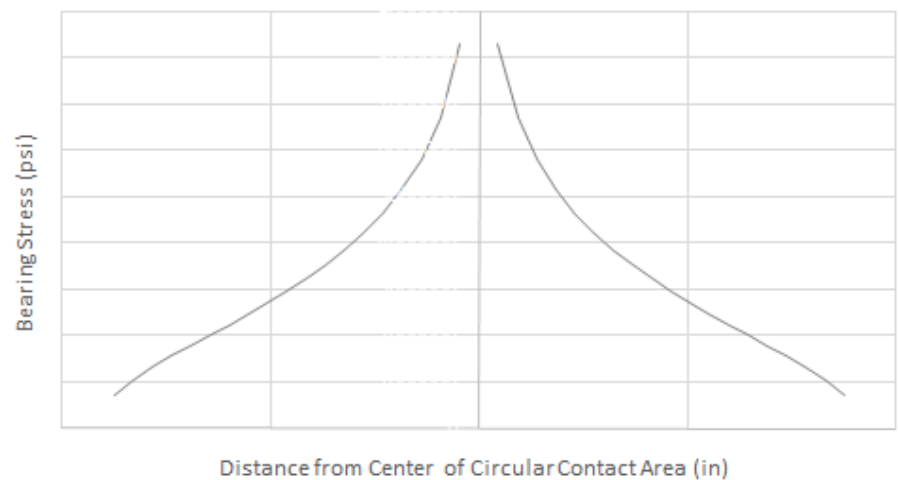


Figure 12.3.1-12: Rigid Cone on a Panel – Bearing Stress Distribution

The pressure distribution has a singularity at the center of the contact region.

A spreadsheet for this method is available at the link below:

ABBOTT AEROSPACE SEZC LTD
SPREADSHEETS
 ABBOTTAEROSPACE.COM
AA-SM-008-009 Contact Stresses - Rigid Cone on Plate

12.3.2. Allowable Stresses for Contacts

The Allowable stress for bearing compression stress is the material bearing allowable stresses, F_{bry} at yield or limit level and F_{bru} at ultimate level.

There is also a failure mode caused by a failure of the material below the surface in a shearing mode.

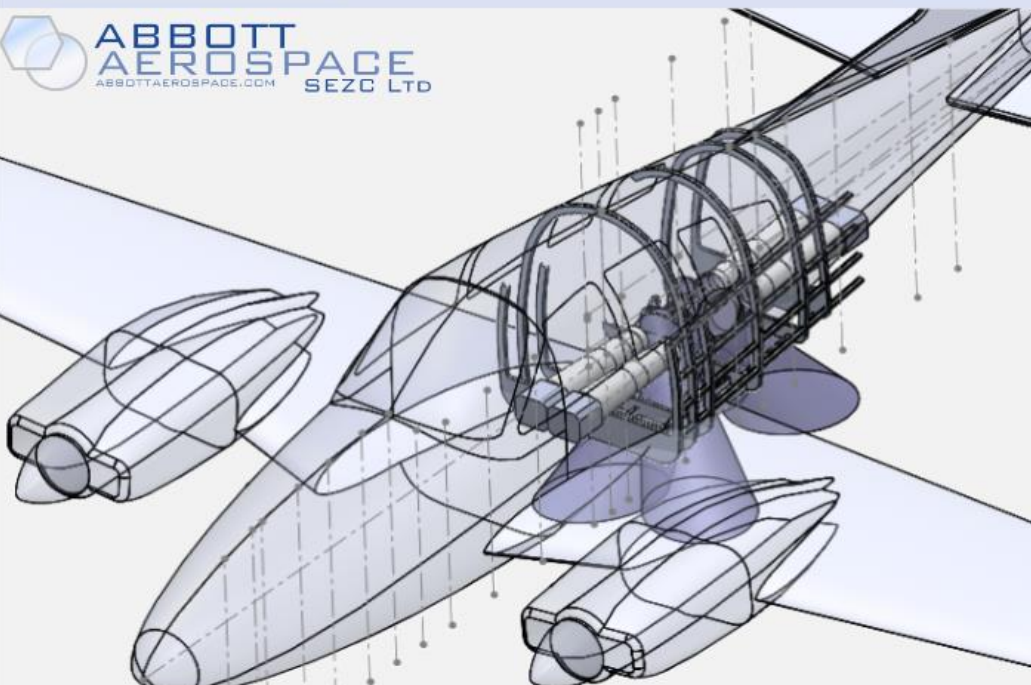
In general, the peak compression bearing stress can be divided by 3 and compared with the material shear allowable stresses, F_{sy} at yield or limit level and F_{su} at ultimate level.

ADVERT: ENGINEERING SERVICES

STRUCTURES DESIGN
 ENGINEERING SERVICES

CONTACT US

ABBOTT AEROSPACE SEZC LTD



12.4. Strength of Brazed Joints

Brazing is a joining process that is not in general use for larger structure for aerospace applications because of process cost. There is no standard method for analysis of a brazed joint, however, NASA has made some efforts to create a reliable analysis methodology. This work has been under the stewardship of Dr. Yuri Flom and his work forms the basis for most of this section.

The prevailing opinion is that the brazed joint (if the joint is well designed and the parent materials and the filler metal are well selected) has an equal or greater strength than the parent metal.

12.4.1. Practical Joint Strength and Accounting for Variability

This level of joint strength depends on the braze being 'perfect'. The work that Flom has done at NASA covers the interaction of direct and shear load effects and gives a simple assumption to cover the likely quality variability of the brazed joint.

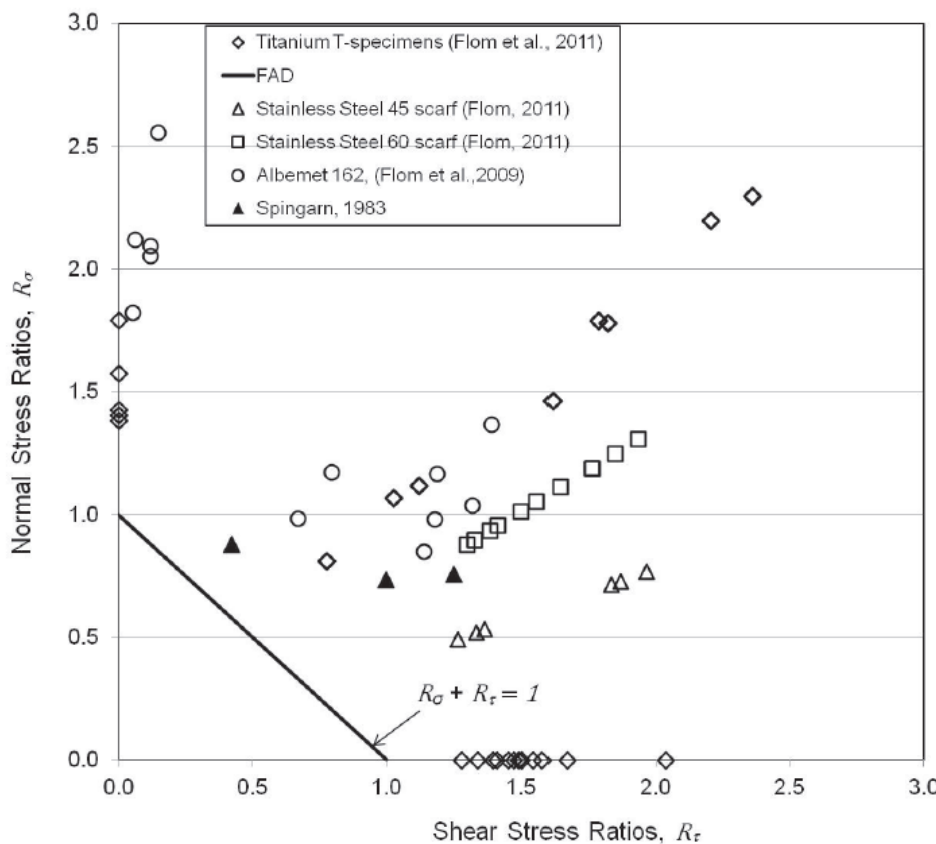


Figure 12.4.1-1: Combined Result for Studies of Brazed Joints under Combined Axial and Shear Loads [\(NASA 20120008328, 2012\)](#)

Where:

$$R_\sigma = \frac{\sigma}{\sigma_0} \text{ and } R_\tau = \frac{\tau}{\tau_0}$$

The test results used for this figure are determined by test in the following way.

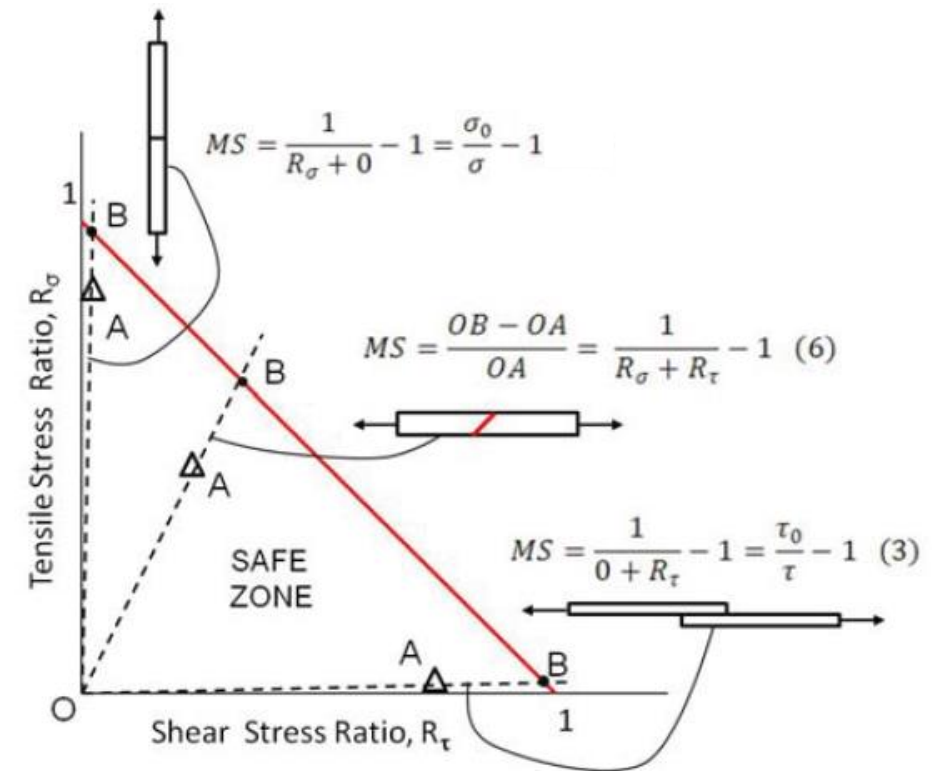


Figure 12.4.1-2: Graphical Representation of Margin of Safety for Butt Brazed, Scarf and Lap Shear Brazed Joints [\(NASA 20120008328, 2012\)](#)

Determination of appropriate allowable shear strength values is given as follows: [\(NASA 20120008193, 2012\)](#) gives the following guidance for the relationship between brazed strength test mean values and B-basis strength:

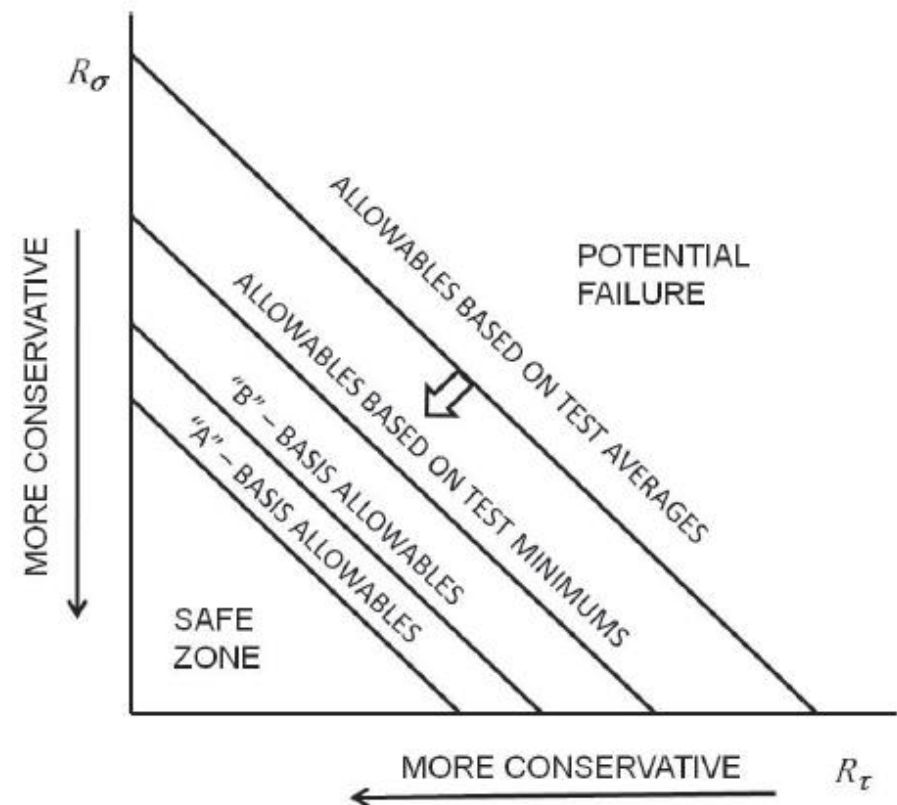


Figure 12.4.1-3: Relationship of Average Test Results to Statistical Basis Allowables for Brazed Joints [\(NASA 20120008193, 2012\)](#)

The effective B-basis brazed strength should be assumed to be 0.5 of the test mean strength for both tension strength and shear strength.

If it can be assumed that the pristine brazed joint develops the same strength of the parent material, preliminary margins of safety at ultimate load level can be generated with the following expression:

$$MS = \frac{1}{\frac{\sigma}{0.5 \cdot F_{tu}} + \frac{\tau}{0.5 \cdot F_{su}}} - 1$$

Where F_{tu} and F_{su} are the material strength of the parent material. Note that the normalized strength of the parent material should be used.

Note: This analysis method is approximate only. All critical joint strengths must be based on relevant test data.

A spreadsheet for this method is available at the link below:



Note: [\(MIL-HNDBK-5H, 1998\)](#) section 8.2 and [\(NASA TM X-73305, 1975\)](#) section B 1.3.1 and B 1.3.2 states that the allowable shear strength used for both copper and silver brazed joints in steel alloys should be limited to 15ksi. If the brazing is done without particular process control the following modified and conservative margin of safety for shear strength should be used:

$$MS = \frac{15000}{\tau_{Applied}} - 1$$

Complete list of brazing references at the Abbott Aerospace Technical Library:



ADVERT: SOFTWARE

EXCEL ADD-IN: SOFTWARE TOOLS

XL-VIKING

DOWNLOAD

By Aerospace Stress Engineers for Aerospace Stress Engineers

Add new functionality to Excel - Easily create Math Expressions

Upper Case Greek Letters Insert Math Symbols Make Numbers Superscript Make Numbers Subscript Make Numbers Normal Script Superscript and Subscript Superscript Numbers Subscript Numbers Subscript Symbols

ΑΔΗΚΝΩΤΧ ΒΕΒΛΕΡΥΨ ΓΖΙΜΟΣΦΩ

xyr p (avi @) ευβχ

ABBOTT AEROSPACE SEZC LTD ABBOTTAEROSPACE.COM

12.5. Strength of Welded Joints

12.5.1. Introduction

Welding two pieces of like metal together will result in a joint that contains the following elements:

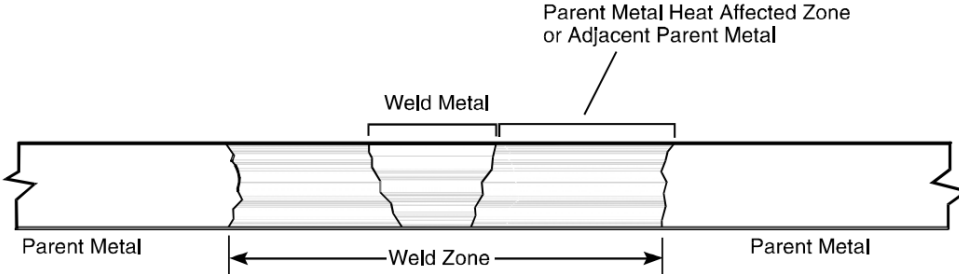


Figure 12.5.1-1: Identification of Regions in a Welded Joint
(MIL-HNDBK-5H, 1998)

Like any other design feature the actual strength of the feature depends on how well the assembly is designed for manufacture. Consultation between the engineer and the welder is a very good idea and will help both the designer and analyst avoid either designs that are likely to fail in service or designs that require rework in manufacture.

Where possible, welded joints should be designed to carry shear load rather than tension load.

In general, the information in this section is applicable to TIG welded joints.

12.5.2. Strength of Welded Steel Alloys

12.5.2.1. General Strength of Fusion Welded Joint of Steel Alloys

Allowable fusion weld-metal strengths of steel alloys are shown below. Design allowable stresses for the weld metal are based on 85% of the respective minimum tensile ultimate value.

| Material | Heat Treatment Subsequent to Welding | Welding Rod or Electrode | F_{su} , ksi | F_{tu} , ksi |
|----------------------------|--------------------------------------|---------------------------------------|----------------|----------------|
| Carbon and alloy steels .. | None | AMS 6457 | 32 | 51 |
| | | AWSA5.1 classes E6010 and E6013 | 32 | 51 |
| Alloy steels | None | AMS 6452 | 43 | 72 |
| Alloy steels | Stress relieved | AWSA5.5 class E10013 | 50 | 85 |
| | | MIL-E-22200/10, classes MIL-10018-M1 | | |

Table 12.5.2-1 Allowable Fusion Weld-Metal Strength of Steel Alloys
(MIL-HNDBK-5H, 1998)

Strength of steel in the heat affected zone:

| Section Thickness 1/4 inch or less | |
|--|------------------------------|
| Type of Joint | Ultimate Tensile Stress, ksi |
| Tapered joints of 30° or less ^b | 90 |
| All others | 80 |

Table 12.5.2-2 Strength of Steel in the Heat Affected Zone
(MIL-HNDBK-5H, 1998)

[\(NASA TM X-73305, 1975\)](#) Table B 1.2.3.1 gives the following general allowable strengths for welded steel joints. Additional data for specific steel alloys is shown in the following sections:

Table B 1.2.3.1 Strengths of Welded Joints

| Material | Heat treatment subsequent to welding | Welding rod or electrode | F_{su} , ksi | F_{tu} , ksi | |
|---------------------------|--------------------------------------|---|---|----------------|-------------------|
| Carbon and alloy steels.. | None | MIL-R-5632, class 1 MIL-E-15599, classes E-6010 and E-6013 | 32 32 | 51 51 | |
| Alloy steels | None | MIL-R-5632, class 2 | 43 | 72 | |
| Alloy steels | Stress relieved | MIL-E-6843, class 10013 MIL-E-18038, classes E-10015 and E-10016 | 50 | 85 | |
| Alloy steels | Stress relieved | MIL-E-18038, classes E-12015 and E-12016 | 60 | 100 | |
| Steels | Quench and temper ... | | | | |
| 4130 | | 125 ksi | MIL-E-8697, classes HT-4130, HT-4140, and HT-4340 | 63 75 90 | 105 125 150 |
| 4140 | | 150 ksi | | | |
| 4340 | | 180 ksi | | | |

Figure 12.5.2-1: Allowable Strength of Welded Joints
(NASA TM X-73305, 1975)

12.5.2.2. Strength of Welded 4130 Steel

The most common steel used for welded applications in aircraft, and in general strength-critical applications outside of the aircraft industry is 4130 alloy Steel. There is surprisingly little useful data on the strength of welded 4130 in the public domain. This NACA paper [\(NACA-TN-1261, 1947\)](#) has some useful information. The values in this reference are not statistical basis allowable values. It is recommended that a minimum margin of safety of 15% be maintained when using the values from these tables.

| Position of Welding | Preheat °F. | Average Ultimate Tensile Strength, p.s.i. (1) | | | | | | | |
|---------------------|-------------|---|--------------------|-----------|--------------------|-----------------------|---------|---------|---------|
| | | Carbon Steel Electrode | | | | Alloy Steel Electrode | | | |
| | | As Welded | Quenched and Drawn | As Welded | Quenched and Drawn | Cont. | Inter. | Cont. | Inter. |
| Flat | 70 | 103,600 | 88,800 | 131,900 | 113,200 | 98,700 | 101,200 | 158,600 | 146,100 |
| Flat | 300 | 102,100 | 82,900 | 125,200 | 123,300 | 98,900 | 103,300 | 153,700 | 136,600 |
| Vertical | 70 | 102,200 | 83,600 | 150,100 | 132,300 | 103,100 | 99,200 | 143,600 | 130,700 |
| Overhead | 70 | 105,400 | 98,400 | 140,800 | 98,000 | 108,400 | 98,100 | 160,500 | 145,100 |

Figure 12.5.2-2: Ultimate Tensile Strength of Continuous and Interrupted Single Head Butt Welds in 1/8in Thick 4130 Sheet
(NACA-TN-1261, 1947)

The ratio of F_{tu} to F_{ty} and to F_{su} can be assumed to be the same as for the weld as it is for the original stock 4130 alloy.

12.5.2.3. Strength of Welded 17-4 Steel

The following tables are taken from [\(OTS-PB-151074 DMIC Report 118, 1959\)](#). Some care should be taken in using these values as they are not statistical basis allowable values. It is recommended that a minimum margin of safety of 15% be maintained when using the values from these tables.

| Welding Process | Heat-Treated Condition of Weld Joint ^(a) | | Mechanical Properties ^(b) | | | | |
|---------------------------------------|---|----------------|--------------------------------------|---------------------|------------|------|-----------------------------|
| | Annealing Temp., F | Aging Temp., F | Ultimate Tensile Strength, psi | Yield Strength, psi | Elongation | | Reduction of Area, per cent |
| | | | In 2 Inches, per cent | In 1 Inch, per cent | | | |
| Manual covered electrode | 1900 | 900 | 200,000 | 185,000 | 6.5 | 13.0 | 28.8 |
| | 1900 | 950 | 186,000 | 175,000 | 6.0 | 12.0 | 29.7 |
| | 1900 | 1025 | 178,000 | 162,000 | 6.0 | 12.0 | 31.7 |
| | 1850 | 900 | 189,000 | 170,000 | 6.0 | 10.0 | 19.8 |
| | 1850 | 950 | 180,000 | 188,000 | 6.0 | 12.0 | 27.2 |
| | 1850 | 1025 | 163,000 | 154,000 | 6.0 | 12.0 | 39.0 |
| Manual inert-gas tungsten arc | 1900 | 900 | 202,000 | 187,000 | 7.5 | 13.0 | 29.0 |
| | 1900 | 950 | 193,000 | 180,000 | 7.2 | 13.5 | 28.5 |
| | 1900 | 1025 | 176,000 | 167,000 | 8.2 | 16.5 | 32.0 |
| | 1850 | 900 | 193,500 | 178,300 | 5.5 | 11.0 | 25.5 |
| | 1850 | 950 | 189,900 | 173,700 | 6.0 | 12.0 | 23.9 |
| | 1850 | 1025 | 169,600 | 154,500 | 6.0 | 12.0 | 26.6 |
| Semiautomatic inert-gas tungsten arc | 1900 | 900 | 198,000 | 183,000 | 9.0 | 17.0 | 34.9 |
| | 1900 | 950 | 195,500 | 182,000 | 9.0 | 18.0 | 42.4 |
| | 1900 | 1025 | 176,000 | 166,000 | 0.2 | 17.0 | 45.3 |
| | 1850 | 900 | 200,300 | 174,500 | 9.0 | 16.0 | 32.7 |
| | 1850 | 950 | 183,000 | 164,300 | 9.0 | 18.0 | 35.7 |
| | 1850 | 1025 | 170,600 | 160,400 | 9.0 | 18.0 | 40.9 |
| Manual inert-gas consumable electrode | 1900 | 900 | 202,600 | 181,000 | 7.0 | 14.0 | |
| | 1900 | 950 | 186,000 | 174,000 | 7.5 | 14.0 | |
| | 1900 | 1025 | 173,000 | 163,000 | 7.5 | 15.0 | |
| | 1850 | 900 | 189,200 | 178,300 | 7.0 | 14.0 | |
| | 1850 | 950 | 179,000 | 165,000 | 6.5 | 13.0 | |

(a) All welds were annealed and aged after welding.

(b) Tensile specimens cut transverse to weld joints.

Figure 12.5.2-3: Tensile Properties of Weld Joints in 0.188in Thick 17-4 Stainless Steel [\(OTS-PB-151074 DMIC Report 118, 1959\)](#)

Welds deposited manually with 17-4PH covered electrodes.

| Heat-Treated Condition of Weld Joint | Mechanical Properties ^(a) | | | | |
|--|--------------------------------------|---------------------|--------------------------------|-----------------------------|---------------------|
| | Ultimate Tensile Strength, psi | Yield Strength, psi | Elongation in 1 Inch, per cent | Reduction of Area, per cent | Location of Failure |
| As welded | 138,000 | 74,000 | 2.0 | 5.0 | Weld metal |
| Aged 900 F, 1 hr | 178,000 | 154,000 | 10.0 | 32.0 | Base metal |
| Aged 1000 F, 1 hr | 160,000 | 136,000 | 11.0 | 29.0 | Weld metal |
| Aged 1100 F, 1 hr | 159,000 | 112,000 | 13.5 | 50.0 | Base metal |
| Aged 1200 F, 1 hr | 142,000 | 98,000 | 11.5 | 63.0 | Base metal |
| Annealed 1800 F | 146,000 | 102,000 | 11.0 | 64.0 | Base metal |
| Annealed 1800 F, aged 900 F, 1 hr | 187,000 | 172,000 | 11.0 | 48.0 | Weld metal |
| Annealed 1800 F, aged 1000 F, 1 hr | 170,000 | 161,000 | 12.0 | 48.0 | Weld metal |
| Annealed 1800 F, aged 1100 F, 1 hr | 168,000 | 134,000 | 12.0 | 54.0 | Weld metal |
| Annealed 1800 F, aged 1200 F, 1 hr | 144,000 | 105,000 | 18.5 | 64.0 | Base metal |
| Annealed 1800 F, refrigerated -100 F, 1 hr, aged 900 F, 1 hr | 204,000 | 189,000 | 11.5 | 44.0 | Weld metal |

(a) Tensile specimens cut transverse to weld joint.

Figure 12.5.2-4: Tensile Properties of Weld Joints in 3/8in Thick 17-4 Stainless Steel [\(OTS-PB-151074 DMIC Report 118, 1959\)](#)

Welds deposited manually with 17-4PH covered electrodes.

| Heat-Treated Condition of Weld Joint | Mechanical Properties ^(a) | | | | |
|--|--------------------------------------|---------------------|----------------------------------|-----------------------------|---------------------|
| | Ultimate Tensile Strength, psi | Yield Strength, psi | Elongation in 2 Inches, per cent | Reduction of Area, per cent | Location of Failure |
| As welded | 140,000 | 96,000 | 4.5 | 10.5 | Weld metal |
| Aged 900 F, 1 hr | 158,000 | 118,000 | 8.0 | 21.0 | Weld metal |
| Aged 1000 F, 1 hr | 155,000 | 108,000 | 9.5 | 27.0 | Weld metal |
| Aged 1100 F, 1 hr | 155,000 | 111,000 | 7.5 | 18.5 | Weld metal |
| Aged 1200 F, 1 hr | 148,000 | 105,000 | 15.0 | 52.0 | Base metal |
| Annealed 1900 F | 145,000 | 91,000 | 10.0 | 46.5 | Base metal |
| Annealed 1900 F, aged 900 F, 1 hr | 188,000 | 163,000 | 9.5 | 36.0 | Weld metal |
| Annealed 1900 F, aged 1000 F, 1 hr | 187,000 | 148,000 | 9.5 | 39.0 | Weld metal |
| Annealed 1900 F, aged 1100 F, 1 hr | 158,000 | 129,000 | 11.0 | 38.0 | Weld metal |
| Annealed 1900 F, aged 1200 F, 1 hr | 143,000 | 100,000 | 14.0 | 54.0 | Base metal |
| Annealed 1900 F, refrigerated -100 F, 1 hr, aged 900 F, 1 hr | 201,000 | 178,000 | 10.0 | 34.0 | Weld metal |

(a) Tensile specimens cut transverse to weld joint.

Figure 12.5.2-5: Tensile Properties of Weld Joints in 1.0in Thick 17-4 Stainless Steel [\(OTS-PB-151074 DMIC Report 118, 1959\)](#)

Note that the as-welded data in the table above has a low elongation at failure (4.5%) which indicates brittleness and a propensity to crack. It is recommended that at least the minimal 1 hour of aging at 900F is done for all welded joints in 17-4 stainless steel. This increases the strength and durability of the weld.

Effect of temperature on the strength of 17-4PH weld:

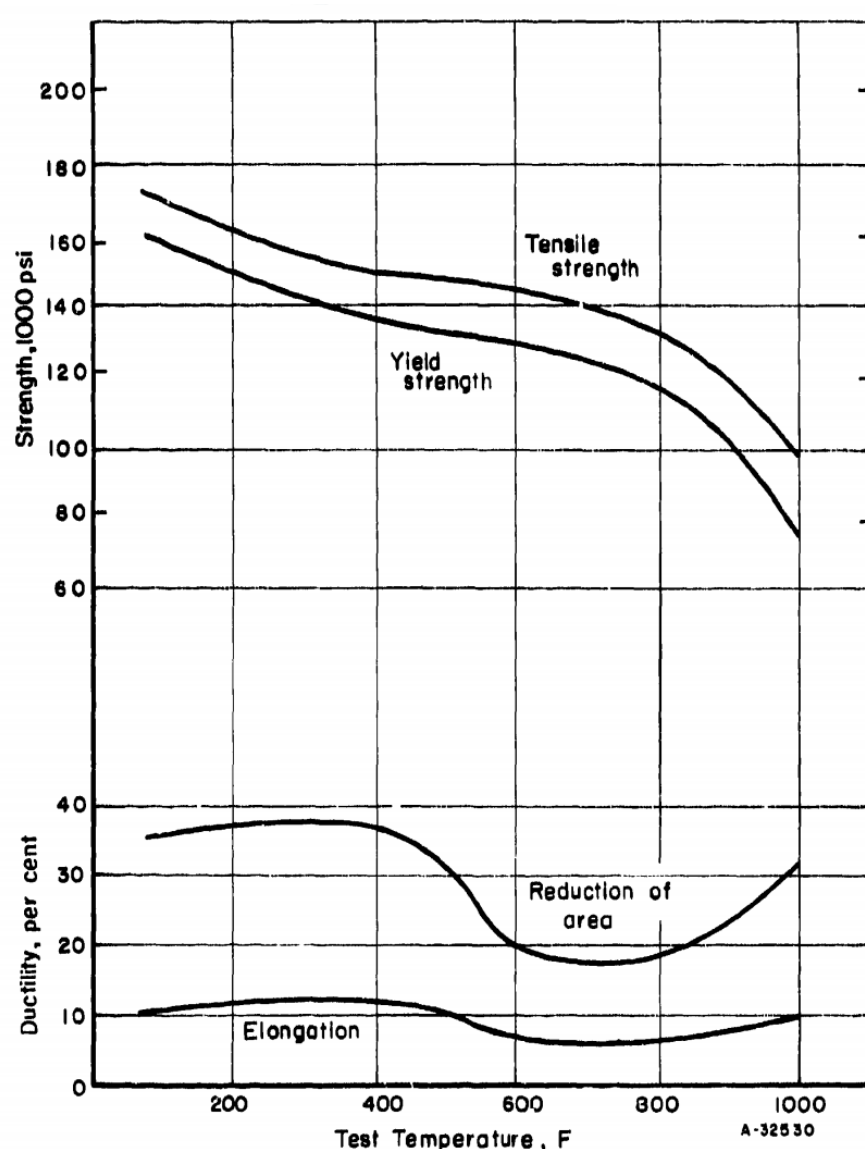


Figure 12.5.2-6: Transverse-Tensile Properties of Inert Gas Arc Welded Weld Joints in 1.0in Thick 17-4 Stainless Steel, Welded joints aged at 952F for 1 Hour Following Welding [\(OTS-PB-151074 DMIC Report 118, 1959\)](#)

12.5.2.4. Strength of Welded 17-7 Steel

The following tables are taken from [\(OTS-PB-151074 DMIC Report 118, 1959\)](#). As previously, some care should be taken in using these values as they are not statistical basis allowable values. It is recommended that a minimum margin of safety of 15% be maintained when using the values from these tables.

| Welds made by inert-gas tungsten-arc process using 17-7PH filler wire. | | | | | | |
|--|-----------------------|--------------------------------|----------------|------------------------------|------------------------------|----------------|
| Test Temperature, F | Sheet Thickness, inch | Ultimate Tensile Strength, psi | | | | |
| | | Base Metal, RH-950 | Welded, RH-950 | 1750 F, Welded -100 F, 950 F | 1750 F, -100 F Welded, 950 F | RH-950, Welded |
| RT | 0.080 | 220,000 | 211,000 | 134,000 | 133,000 | 125,000 |
| | 0.032 | 220,000 | 196,000 | 122,000 | 136,000 | 115,000 |
| 300 | 0.080 | 200,000 | 184,000 | 85,000 | 88,000 | 82,000 |
| | 0.032 | 204,000 | 190,000 | 88,000 | 93,000 | 83,000 |
| 500 | 0.080 | 187,000 | 181,000 | 84,000 | 89,000 | 75,000 |
| | 0.032 | 190,000 | 178,000 | 83,000 | 84,000 | 75,000 |
| 800 | 0.080 | 161,000 | 152,000 | 82,000 | 79,000 | 67,000 |
| | 0.032 | 158,000 | 150,000 | 84,000 | 82,000 | 76,000 |

Figure 12.5.2-7: Tensile Properties of Weld Joints in 17-7 Stainless Steel at Various steps is RH-950 Heat Treatment
[\(OTS-PB-151074 DMIC Report 118, 1959\)](#)

| Sheet Thickness, inch | Direction of Testing | Test Temp, F | Tensile Properties | | | |
|-----------------------|----------------------|--------------|--------------------------------|----------------------------------|--------------------------------|----------------------------------|
| | | | Parent Metal | | Weld Joint | |
| | | | Ultimate Tensile Strength, psi | Elongation in 2 Inches, per cent | Ultimate Tensile Strength, psi | Elongation in 2 Inches, per cent |
| 0.018 | Transverse | RT | 182,600 | 10.8 | 143,900 | 2.1 |
| 0.050 | Transverse | RT | 177,700 | 10.4 | 140,500 | 3.8 |
| 0.080 | Transverse | RT | 187,500 | 9.0 | 156,700 | 4.7 |
| 0.050 | Longitudinal | RT | 184,200 | -- | 151,400 | 4.0 |
| 0.078 | Longitudinal | RT | 189,000 | -- | 145,800 | 5.6 |
| 0.078 | Longitudinal | 300 | 175,800 | 9.1 | 96,000 | 4.9 |
| 0.050 | Longitudinal | 500 | 181,300 | 4.7 | 90,100 | 2.8 |
| 0.050 | Longitudinal | 700 | 152,400 | 6.5 | 92,300 | 3.0 |
| 0.050 | Longitudinal | 900 | 116,700 | 22.0 | 81,200 | 3.2 |

Figure 12.5.2-8: Tensile Properties of Weld Joints in Various Thicknesses 17-7 Stainless Steel After TH=1075 Heat Treatment
[\(OTS-PB-151074 DMIC Report 118, 1959\)](#)

12.5.2.5. Strength of Welded 15-7 Steel

The following tables are taken from [\(OTS-PB-151074 DMIC Report 118, 1959\)](#). As previously, it is recommended that a minimum margin of safety of 15% be maintained when using the values from these tables.

| Heat-Treated Condition of Welded Joint | Ultimate Tensile Strength, psi | Yield Strength, psi | In 2 Inches, per cent | In 1 Inch, per cent |
|--|--------------------------------|---------------------|-----------------------|---------------------|
| <u>Weld Reinforcement Intact(a)</u> | | | | |
| Welded, TH-1050 | 210,000 | 205,000 | 6.0 | -- |
| Welded, TH-1100 | 190,000 | 175,000 | 8.0 | -- |
| Welded, RH-950 | 240,000 | 225,000 | 5.0 | -- |
| Welded, RH-1075 | 215,000 | 205,000 | 5.0 | -- |
| <u>Weld Reinforcement Removed(b)</u> | | | | |
| Base metal TH-1050, as welded | 122,000 | 88,000 | 7.0 | 25.0 |
| Base metal RH-950, as welded | 115,000 | 87,000 | 6.0 | 22.0 |
| Welded, TH-1050 | 205,000 | 185,000 | 2.0 | 8.0 |
| Welded, TH-1100 | 175,000 | 165,000 | 4.0 | 14.0 |
| Welded, RH-950 | 230,000 | 215,000 | 2.0 | 8.0 |
| Welded, RH-1075 | 200,000 | 195,000 | 2.5 | 13.0 |
| Welded, annealed, TH-1050 | 210,000 | 205,000 | 2.0 | 8.0 |
| Welded, annealed, TH-1100 | 185,000 | 175,000 | 4.0 | 12.0 |
| Welded, annealed, RH-950 | 235,000 | 210,000 | 2.0 | 7.0 |
| Welded, annealed, RH-1075 | 210,000 | 200,000 | 2.0 | 10.0 |

(a) All specimens failed in base metal.

(b) All specimens failed in weld metal.

Figure 12.5.2-9: Tensile Properties of Weld Joints in 15-7 Stainless Steel
[\(OTS-PB-151074 DMIC Report 118, 1959\)](#)

12.5.3. Strength of Welded Aluminum Alloys

In general, welded aluminum is not used for certified aircraft primary structure. This is due to concerns over meeting quality requirements with regard to weld porosity and the resulting fatigue life. Welded aluminum is commonly used for secondary structure and some systems applications.

The availability of data for the strength of welded aluminum is limited. The following data is compiled from several sources.

12.5.3.1. Strength of Welded 2000 Series Aluminum

This data is derived for a 2219 aluminum Panel TIG welded to a 2219 aluminum forging and heat treated to the T87 condition. The following results are based on the average of 24 specimens.

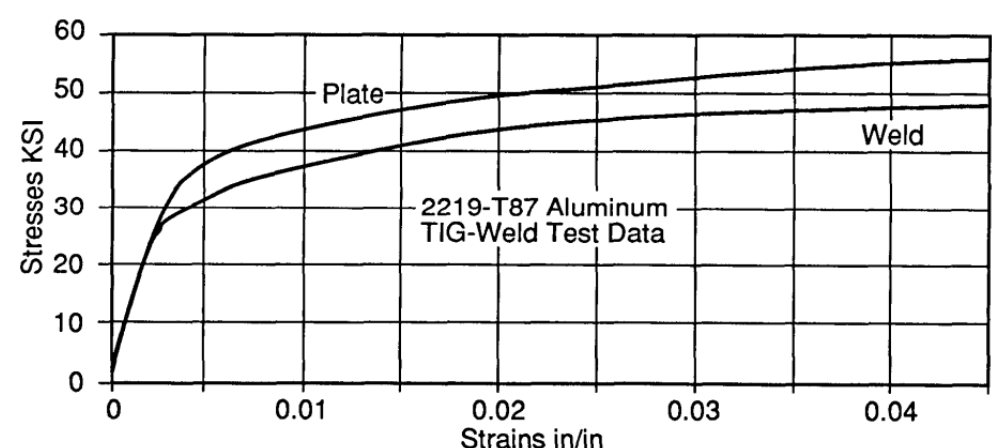


Figure 12.5.3-1: Identification of Regions in a Welded Joint
[\(NASA-TP-2935, 1989\)](#)

This data is average (and not A or B basis) but does give a good indication of the reduction in strength. This reduction in strength can be considered to apply to the available statistical basis material data.

In addition, NASA gives the following guidance for minimum ultimate tensile strength of butt welds ([NASA-CR-2064, 1972](#)):

Alloy 2219-T87, Minimum UTS = 35000 psi
Alloy 2014-T6, Minimum UTS = 38000 psi

12.5.3.2. General Guidance for the Strength of Welded 5000 and 6000 series Aluminums

5000 series aluminum is work hardened and cannot be heat treated. Therefore, the immediate post weld strength of the 5000 series aluminum material cannot be improved upon.

([MIL-HNDBK-5H, 1998](#)) has data for 5052 in the O condition and these values can be assumed to apply for 5052 aluminum in the welded state.

$$F_{ty} = 9500 \text{ psi}$$

$$F_{tu} = 25000 \text{ psi}$$

6061 series aluminum can be heat treated post weld to increase strength. ([NASA-CR-123772, 1972](#)) gives good guidance on the correct approach and some useful strength data.

6061 should be procured in the T4 condition, welded and then aged to the T6 condition after welding.

| Alloy | 6061-T4 aged to T6 | | | | | | | | | | | |
|---------------------|-----------------------|------|-----------------------|------|----------------------|-----|-----------------------|------|-----------------------|------|------|-----|
| | 0.050 inch (12.7 mm) | | | | 0.125 inch (31.8 mm) | | | | | | | |
| Thickness | F _{tu} , ksi | | F _{ty} , ksi | | e, % | | F _{tu} , ksi | | F _{ty} , ksi | | e, % | |
| | L | T | L | T | L | T | L | T | L | T | L | T |
| Weld Process | | | | | | | | | | | | |
| Manual TIG | 27.3 | 26.9 | 22.0 | 21.5 | 2.8 | 2.2 | 28.1 | 29.0 | 20.3 | 20.3 | 5.6 | 3.8 |
| Auto-TIG | 43.1 | 42.3 | 38.8 | 37.2 | 6.7 | 7.0 | 50.1 | 50.2 | 46.8 | 45.4 | 8.3 | 9.8 |
| (a) | 39.4 | 39.1 | 36.3 | 36.1 | 3.4 | 3.4 | 37.1 | 33.0 | 33.9 | 27.5 | 3.0 | 3.2 |
| (b) | 38.0 | 35.5 | 35.3 | 32.7 | 2.2 | 2.0 | 33.5 | 32.7 | 27.5 | 27.1 | 4.0 | 4.0 |
| MIG Welds | - | - | - | - | - | - | 42.0 | 41.9 | 39.2 | 38.3 | 3.9 | 4.0 |
| (c) | - | - | - | - | - | - | 35.2 | 36.3 | 30.4 | 32.4 | 3.0 | 3.0 |
| (d) | - | - | - | - | - | - | 32.4 | 32.7 | 25.7 | 26.8 | 3.5 | 3.8 |

(a) Automatic TIG welded plus one repair weld.
(b) Automatic TIG welded plus two repair welds. (e) 1 ksi = 0.70307 kg/mm²
(c) MIG welded plus one repair weld.
(d) MIG welded plus two repair welds.
Each value is average of 6 tests. 4043 filler wire was used for all welds.
Aging treatment: 340°-355°F(171°-179°C), 8 hrs. After welding, no solution treatment was employed.

Figure 12.5.3-2: Strength of Welded 6061, Aged to T6 condition ([NASA-CR-123772, 1972](#))

12.5.4. Welded Joints Analysis Approach

The analysis of welded joints depends on an assessment of the various features of the welded joint. The minimum weld geometry is in part based on the quality assessments contained in ([NASA-STD-5006, 1999](#)).

12.5.4.1. Estimation of the Weld Throat thickness, a

The weld throat thickness is the effective thickness that should be used to calculate the geometric properties to calculate section stresses.

For full penetration welds:

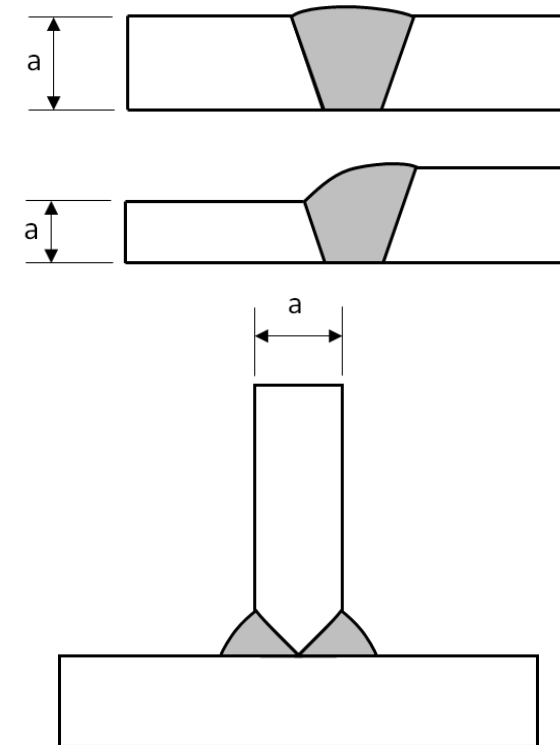
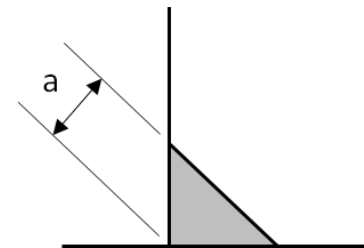
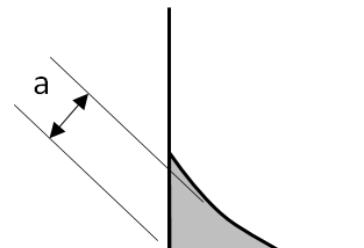


Figure 12.5.4-1: Effective Throat Thickness for Full Penetration Welded Joints

Partial Penetration welds:



Concave weld:



Convex weld:

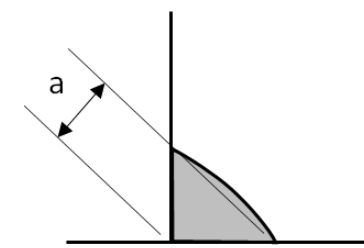


Figure 12.5.4-2: Effective Throat Thickness for Partial Penetration Welded Joints

Note that for primary structure the weld must always be full penetration. Partial penetration welds are suitable for secondary structure only.

12.5.4.2. Estimation of the Effective Weld Length, L'

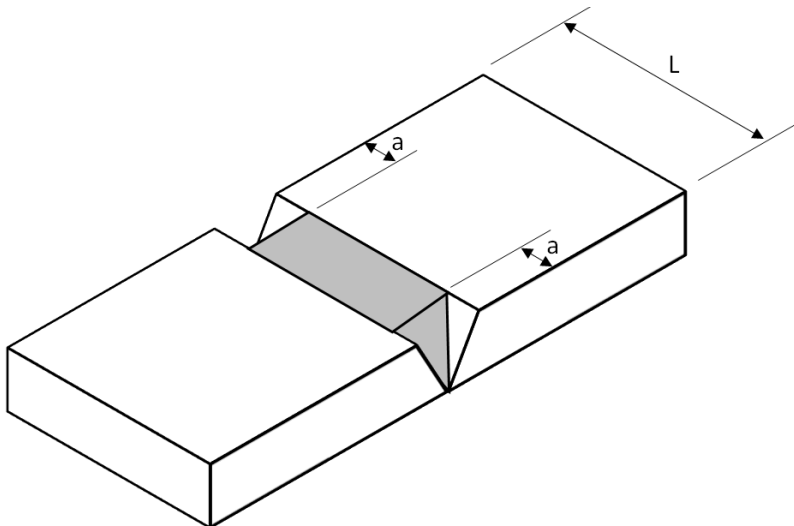


Figure 12.5.4-3: Effective Weld Length, L'

It is conservative to assume that a length equal to the throat thickness is missing from each end of the weld. Therefore, the effective weld length:

$$L' = L - 2 \cdot a$$

Other Useful References for Welding:

[NASA-MSFC-SPEC-3679 Process Specification - Welding Aerospace Hardware](#)

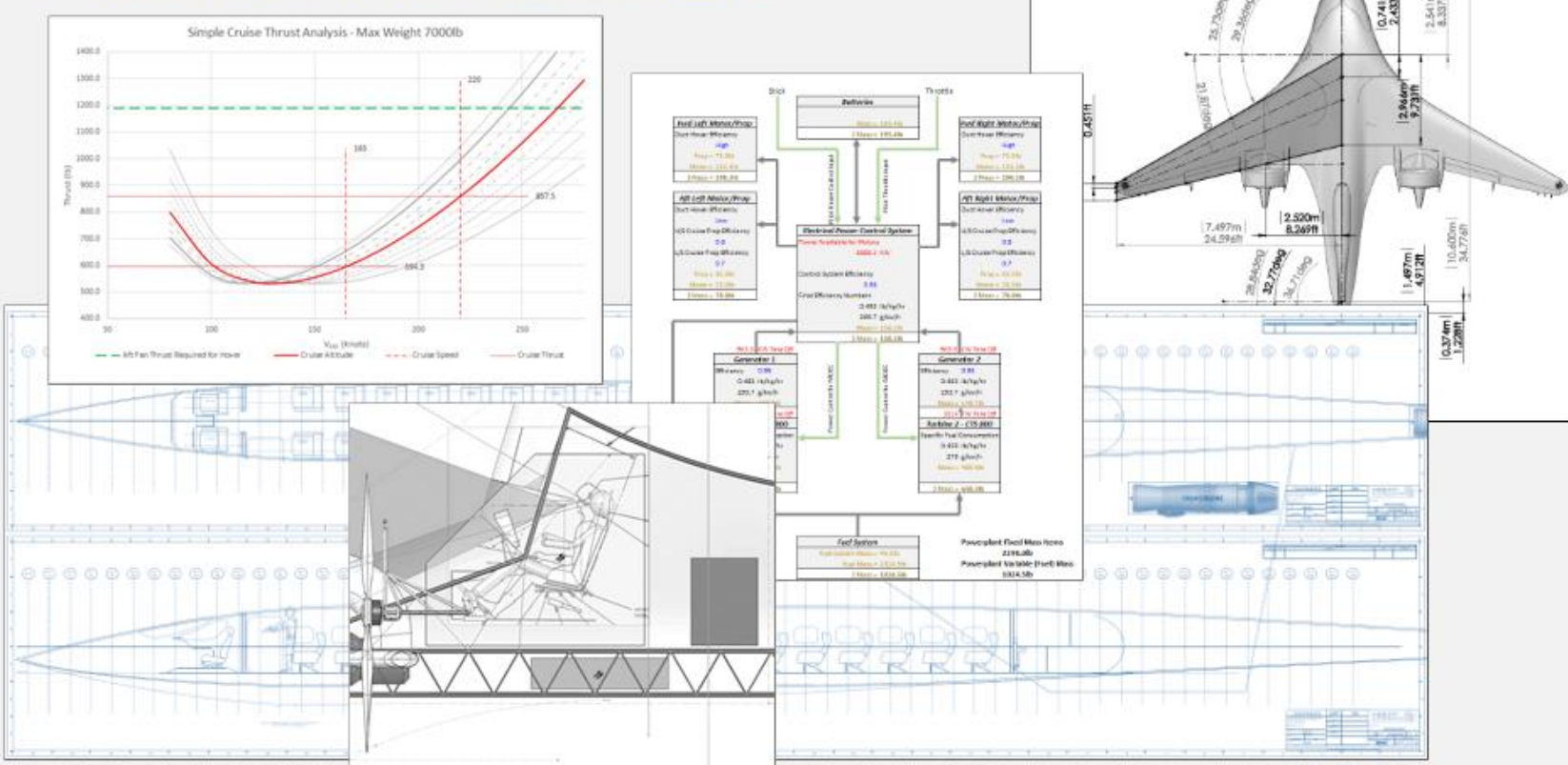
[NAVSEA-S9074-AQ-GIB-010-248 Requirements for Welding and Brazing Procedures and Performance Qualification](#)

Complete List of Welding references at the Abbott Aerospace Technical Library:

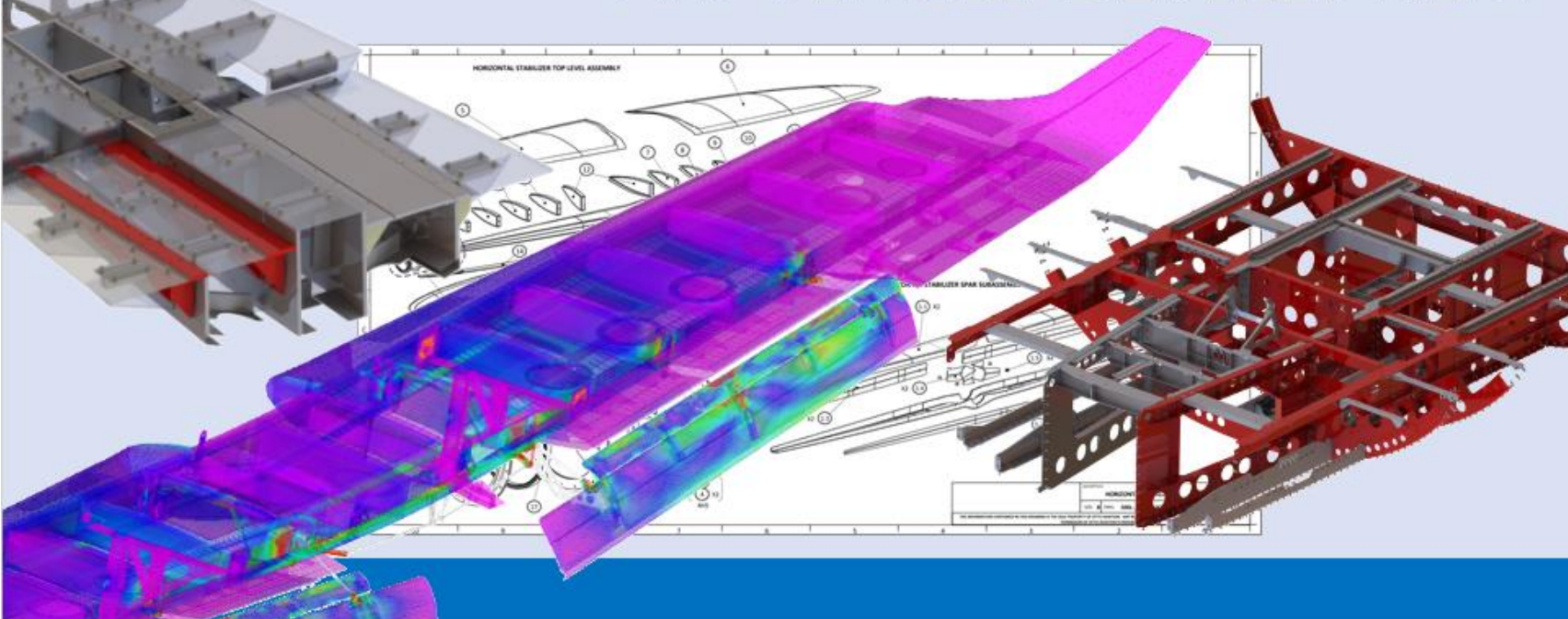
ABBOTT SEZC LTD
 AEROSPACE
 ENQ Library Subject Search: Welding

ABBOTT AEROSPACE SEZC LTD

PRELIMINARY DESIGN



AIR VEHICLE DEVELOPMENT



Contact us to find out how we can help you to reduce risk, maximize your potential and take flight.



CONTACT US

13. COMBINED STRESSES

13.1. Introduction

13.2. Reserved

13.3. Reserved

This section will be included in a later edition. This page is a placeholder only.

14. ULTIMATE STRENGTH OF METALLIC ELEMENTS

14.1. Introduction

Most common metallic alloys used in aircraft structures can seemingly exceed the ultimate strength of the material.

This illusion depends on stresses derived using an elastic analysis. The material cannot exceed its ultimate stress but as the material is stressed beyond the proportional limit the local load can be redistributed.

This redistribution relies on local material at a lower strain (and therefore stiffer) for the load to locally transfer to.

Local regions of high strain, beyond the elastic limit, are generally caused by two situations: a) Significant bending and b) Geometric features causing stress concentrations.

14.1.1. Plastic Bending

These two different situations are dealt with by two different methods:
 The classic bending hand analysis (or linear finite analysis) assumes a linear distribution of bending stress and strain through the thickness. Considering a rectangular section:

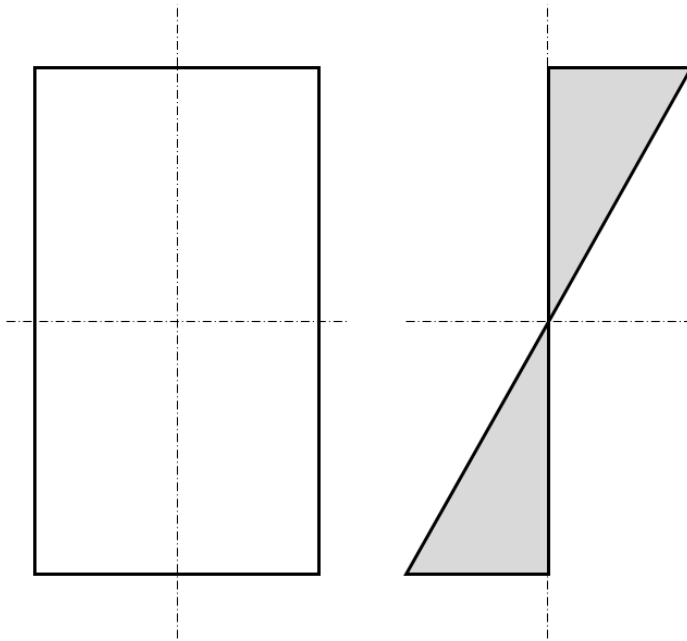


Figure 14.1.1-1: Linear Bending Stress and Strain Distribution Through the Thickness of a Rectangular Section

For ductile materials, almost all metals, stress and strain are not linear up to the point of failure. As the proportional limit is exceeded the young's modulus of the material reduces. As the peak stress regions at the surface of the bending member exceed yield, the strain and the stress does not increase at the same rate. The outer fiber does not reach ultimate strength until material closer to the neutral axis sees an increased level of stress.

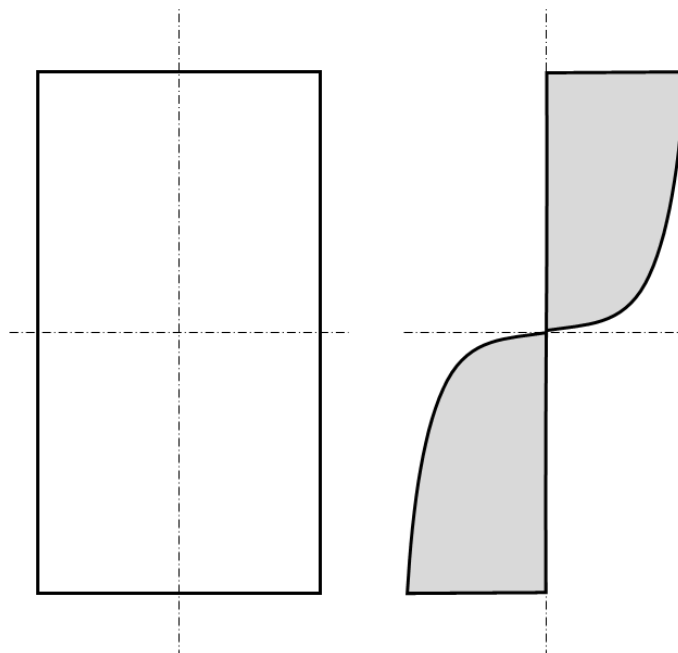


Figure 14.1.1-2: Bending Stress Distribution Through the Thickness of a Rectangular Section Including Material Plasticity Effects.

The plastic stress distribution can be approximated with the following stress distribution:

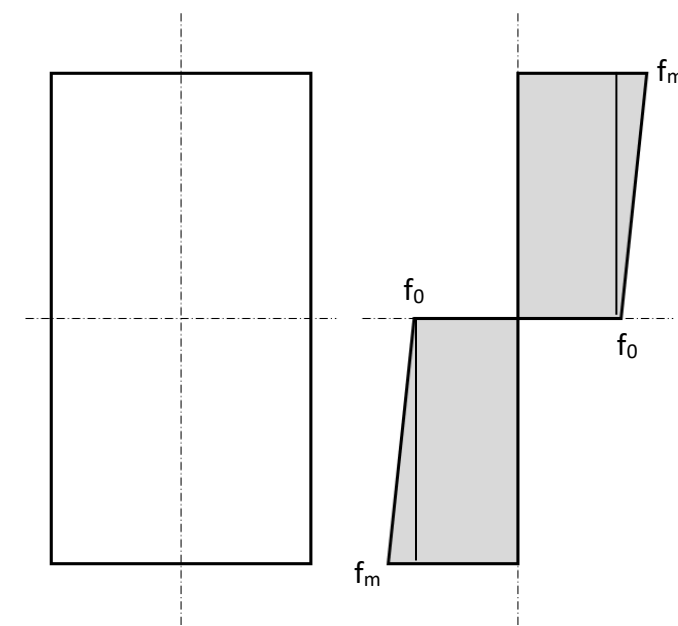


Figure 14.1.1-3: Assumed Trapezoidal Plastic Bending Stress Distribution Through the Thickness of a Rectangular Section.

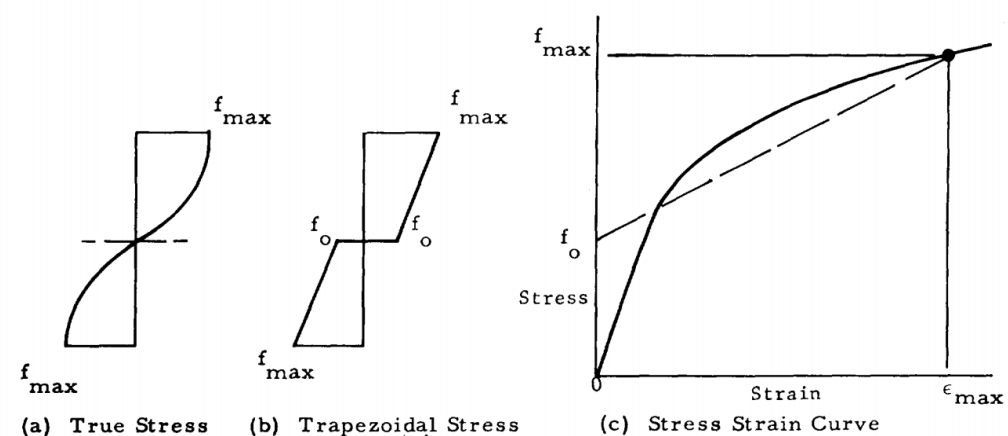


Figure 14.1.1-4: Pictorial Representation of f_0 (NASA TM X-73305, 1975)

f_m can be assumed to be equal to the ultimate strength (F_{tu}) of the material. From Section 4.2.2.1 the stress-strain curve can be modelled in the following way:



f_0 is the fictional stress which is assumed to exist at the neutral axis or at zero strain. The value of f_0 is determined by making the requirement that the internal moment of the true stress variation must equal the moment of the assumed trapezoidal stress variation.

The total strain at failure can be expressed as the elastic strain added to the plastic strain. This is called the Ramberg-Osgood relationship [\(MIL-HNDBK-5H, 1998\)](#) Section 9.3.2.4 and [\(NACA-TN-902, 1943\)](#):

$$e_u = \frac{F_{tu}}{E} + 0.002 \left(\frac{F_{tu}}{F_y} \right)^n$$

The Ramberg-Osgood shape factor can be derived using the following relationship:

$$n = \frac{\log\left(\frac{e'_u}{0.002}\right)}{\log\left(\frac{F_{tu}}{F_y}\right)}$$

Where the plastic component of the total strain at failure is given by:

$$e'_u = e_u - \frac{F_{tu}}{E}$$

The ratio between f_0 and a reference stress level f_m is given by the following expression:

$$\frac{f_0}{f_m} = \frac{6}{e_u^2} \cdot \left[\frac{1}{3} \cdot \left(\frac{f_m}{E} \right)^2 + e'_u \cdot \left(\frac{n+1}{n+2} \right) \cdot \left(\frac{f_m}{E \cdot F_{tu}} \right)^{n+1} + \frac{n}{2 \cdot n+1} \cdot e'_u^2 \cdot \left(\frac{f_m}{F_{tu}} \right)^{2n} \right] - 2$$

When f_m is set to F_{tu} , the f_0 for ultimate plastic material strength can be found.

Once f_0 has been found it can be used in the following expression to give the value of the ultimate bending strength:

$$F_b = F_{tu} + f_0 \cdot (k - 1)$$

Where F_b is the ultimate bending strength and k is a factor between 1.0 and 2.0 that depends on the geometry of the cross section.

A spreadsheet of this analysis method is given at the link below:

ABBOTT AEROSPACE SEZC LTD
SPREADSHEETS
ABBOTTAEROSPACE.COM
AA-SM-025-001 Cozzone Theory of Plastic Bending

Note that in some references K (capital 'k') = $k - 1$ (lowercase 'k')

The shape factor k (lowercase) is calculated by dividing the plastic section modulus by the elastic section modulus. This can also be expressed as:

$$k = \frac{2 \cdot Q \cdot c}{I}$$

Where:

I 2nd moment of area

c Distance from centroidal axis to the extreme fiber

$$Q = \int_0^c y \, dA$$

The shape factor calculations methods for common shapes is now included in Section 6 of this book.

The following spreadsheet calculates 'k' for common cross sections:

ABBOTT AEROSPACE SEZC LTD
SPREADSHEETS
ABBOTTAEROSPACE.COM
AA-SM-001-000 Section Properties

The following spreadsheet calculates shape factor, 'k', of compound sections made up of rectangles as well as basic section properties:

ABBOTT AEROSPACE SEZC LTD
SPREADSHEETS
ABBOTTAEROSPACE.COM
AA-SM-001-008 Section Properties - Cozzone Shape Factor 'k'

14.1.2. Neuber Plastic Strain Method

The Neuber method for plasticity is based on the idea that the stress levels produced by finite element models that use a linear material model, in some circumstances, when they exceed the proportional limit, or yield stress, will be conservative and unrealistic.

This method is applicable to the stresses caused by stress concentrations created by geometric features and for the method to be applicable the following must be true:

- 1) The finite element mesh should be fine enough to accurately predict the actual peak stress at the features.
- 2) The material should be ductile enough to allow for local redistribution.
- 3) There must be enough local material at a lower stress level to allow for local redistribution.
- 4) The stress field should be largely linear, or uniaxial in nature.

The strain energy at the peak elastic stress should be calculated. The strain energy is the area under the linear stress-strain curve:

$$SE = \frac{\sigma_{LE} \cdot \varepsilon_{LE}}{2}$$

The intercept where the line of constant strain energy crosses the elasto-plastic stress-strain curve is taken to be the corrected plastic stress/strain state that will occur in the actual material, such that:

$$\frac{\sigma_{LE} \cdot \varepsilon_{LE}}{2} = \frac{\sigma_c \cdot \varepsilon_c}{2}$$

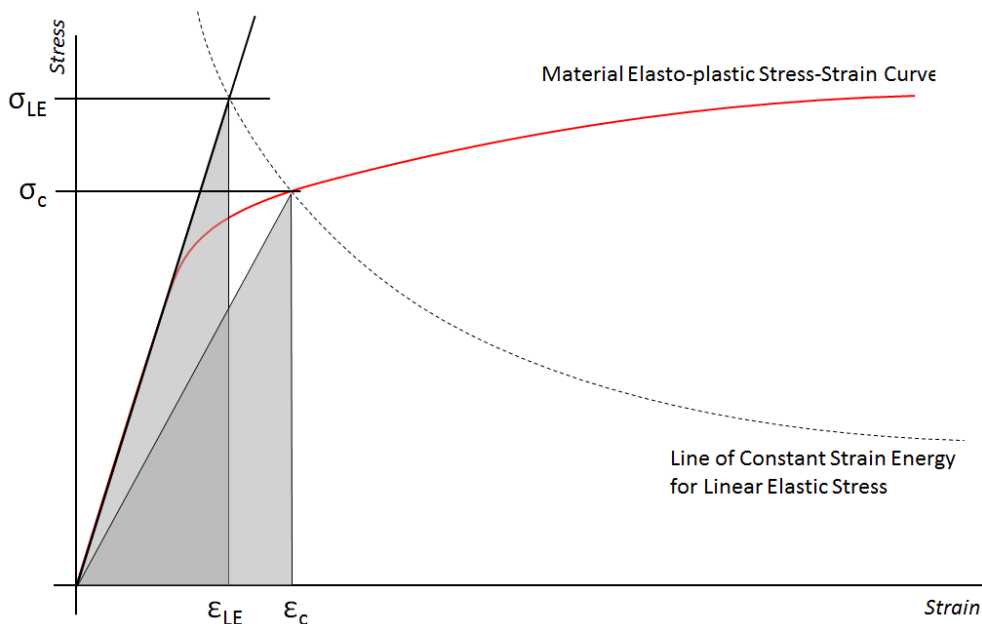


Figure 14.1.2-1: Neuber Method for Correction of Plastic Stress from Linear Models

It can be seen that the actual area under the elasto-plastic stress-strain curve is greater than the triangle given by the Neuber stress level and so this method is potentially conservative.

A spreadsheet of this analysis method is given at the link below:

ABBOTT AEROSPACE SEZC LTD
SPREADSHEETS
 ABBOTTAEROSPACE.COM
AA-SM-030 Neuber Elastic Stress Correction

ADVERT: ENGINEERING SERVICES

STRUCTURES DESIGN **ENGINEERING SERVICES**

CONTACT US

ABBOTT AEROSPACE
 SEZC LTD
 ABBOTTAEROSPACE.COM

15. LOCAL STABILITY – ISOTROPIC MATERIALS

15.1. Introduction

Local stability refers to thin local features that fail to carry shear and/or compression loads. Local stability failure does not imply a break or rupture, although uncontrolled local stability failure can lead to component, sub-assembly or complete installation failure.

Stability failures refer to a situation where the loaded item tends to move out-of-plane while carrying an in-plane load. The ability to resist stability failure depends on the out-of-plane stiffness of the feature, both in terms of the simple thickness of the feature or other design features that add out-of-plane stiffness such as stiffeners and gussets.

In this section the terms **sheet**, **plate** and **panel** are used interchangeably as they are all features that could be analyzed as a **web**. In general terms, a **plate** is usually thicker than a **sheet** and a **panel** is a removable feature that can be thick or thin.

Web refers to a panel that is restrained along all edges and can carry shear, compression and/or bending.

Flange refers to a panel with one edge free and can carry compression and/or bending.

Column refers to a feature that carries compression and/or bending and is restrained at the ends only.

Stiffeners and gussets are features that add out of plane stiffness to a web or flange.

To search the [Abbott Aerospace Technical Library](#) for 'Buckling' Clink the link below:

ABBOTT SEZC LTD
AEROSPACE
ENQ

Library Subject Search: Buckling

15.1.1. Different Types of Stability Failures

There are two levels of stability failures - buckling and crippling.

Definition of a buckle:

A buckle can be generally defined as a compression (or shear) failure in a feature (web or flange) or column that occurs in multiples of wavelengths over the whole length of the feature.

Definition of a crippling failure:

A cripple is a failure, of a corner feature or compound shape that is not reversible on the removal of the load. A crippling failure is usually considered an ultimate failure with no residual strength remaining after failure and occurs within a very local area rather than over a significant length.

When a panel is in the buckled state it continues to carry shear load (usually significantly greater load than the load at which the feature buckles) and the structure can be said to have residual strength in the post-buckled state.

However, a buckled panel or web cannot continue to carry compression load after it has buckled.

Note that a buckle is not necessarily reversible. For a ductile material if the plastic limit is exceeded during the buckling process then permanent buckling occurs and the structure will not return to the unbuckled state. Flange compression buckling is usually permanent.

A compression buckled flange or column cannot continue to carry compression loads and effectively has no residual strength. However, a flange or web that is part of a load carrying section can fail in buckling and the section can continue to carry compression load until crippling failure of the section.

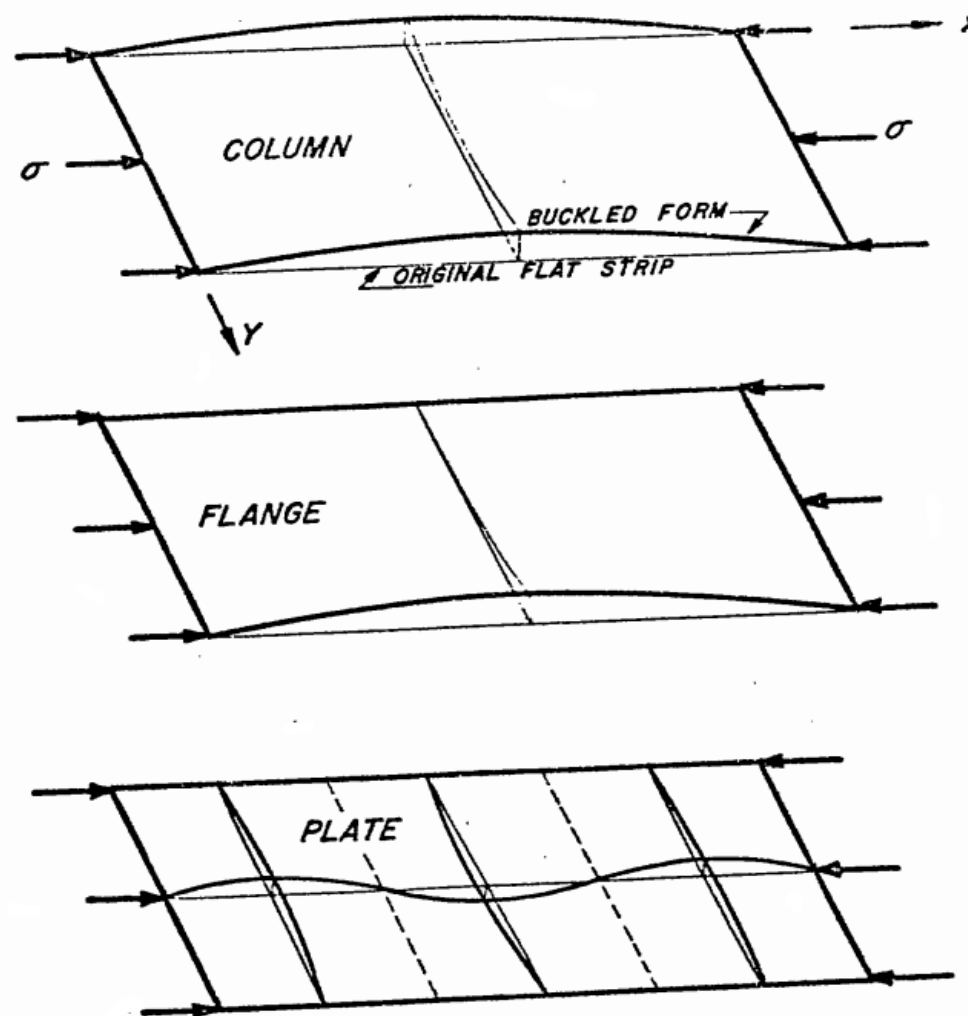


Figure 15.1.1-1: Illustration of Buckling Shapes of Different Features
[\(NACA-TN-3781, 1957\)](#)

Important design considerations for Stability Critical Structures:

- Note that the secondary loads developed in the post-buckling mode are proportional to the out-of-plane stiffness of the buckling feature.
- For features that have a significant out-of-plane stiffness (such as thick panels, thick flanges or sandwich panels) it is undesirable to allow them to buckle at all.
- For stiffer features, the secondary loads can be so large that critical failure modes can be induced in the local structure at the point of initial buckling that can cause widespread collapse or total failure of the assembly.
- Stiffer features may buckle at a stress above the yield stress level of the material. This is more complex to predict and is explained in this chapter.

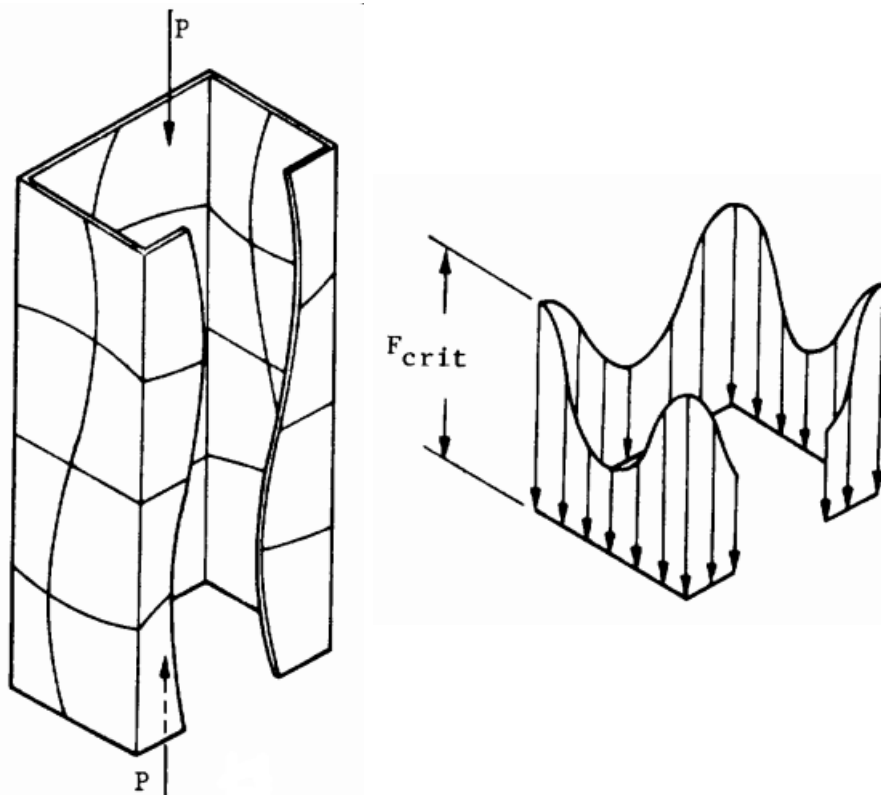


Figure 15.1.1-2: Illustration of Load Distribution on a Section After Buckling has Occurred but Prior to Crippling (NASA TM X-73306, 1975)

In addition, having features that buckle at service level loads is undesirable as the act of buckling creates a load reversal from compression to tension and therefore the act of buckling and returning to the unbuckled state imposes damaging fatigue cycles on the buckling structure.

Also, note that once a feature has buckled and returned to its original state it tends to return to the buckled state at a lower load than initiated the original buckle.

For most aircraft structures, buckling occurs before a crippling failure. In the post-buckled state, the loads are transferred from the buckling webs and flanges to the stable corners. The corners of a component or assembly are prone to crippling failure in the post-buckled state. Crippling of corners is covered in section 15.5.

15.2. General Buckling Expression

15.2.1. Introduction

The general buckling equation used for webs and flanges is as shown below:

$$F_{cr} = \eta \cdot k \cdot \frac{\pi^2 \cdot E}{12 \cdot (1 - \nu_e^2)} \left(\frac{t}{b}\right)^2$$

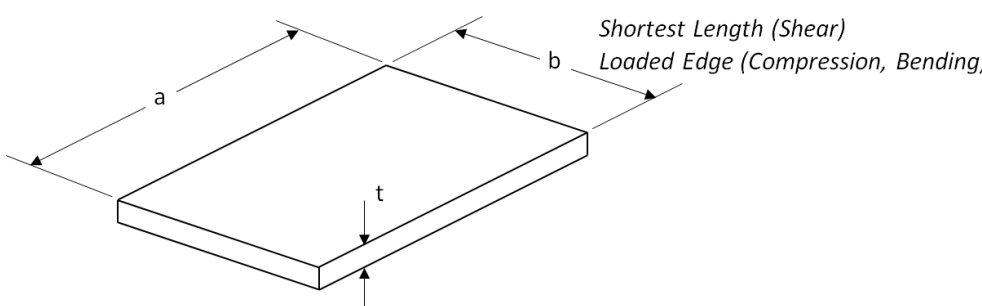


Figure 15.2.1-1: Panel Dimension Definition

Where:

| | |
|----------|---|
| F_{cr} | Buckling stress allowable, psi |
| η | Plasticity reduction factor (=1 in elastic range) |
| k | Buckling coefficient, includes allowance or panel edge fixity, related to panel aspect ratio a/b |
| E | Young's modulus of panel material, psi |
| ν_e | Poisson's ratio of panel material |
| t | Thickness of panel, in |
| b | Panel edge dimension, in – for shear buckling this is the minimum edge distance, for compression and bending buckling this is the loaded edge |

The expression for web and flange buckling is built around the flexural stiffness of the panel, which can be expressed as:

$$D = \frac{E \cdot t^3}{12 \cdot (1 - \nu_e^2)}$$

This term is equivalent to D_{11} from the composite laminate ABD matrix. Expressing the general buckling equation in terms of D, the equation becomes:

$$F_{cr} = \eta \cdot k \cdot \frac{\pi^2 \cdot D}{b^2 \cdot t}$$

This general equation holds for shear, compression and bending buckling. The 'k' value and the meaning of the 'b' term changes for each form of buckling.

The value of 'k' depends on the level of torsional restraint at the edge of the panel. If it can be considered to act like a hinge – i.e. zero torsional restraint, then the panel is said to be 'simply supported', this creates low allowable values. If the edges have a high level of torsional restraint, the edges are said to be 'clamped' or 'built-in', this creates high allowable values.

Note that all the analysis presented in this section is for symmetrical buckling modes. In almost all cases the symmetrical buckling modes yield lower allowable than the antisymmetric buckling modes. Therefore, the analysis method presented in this section omit anti-symmetric buckling.

15.2.2. Buckle Wavelength

Every buckle has a wavelength and in the derivation of buckling allowable values the value λ , the buckle half wave length is an important value. λ is also used later in this section for the calculation of the panel rotational edge fixity.

The value of λ varies depending on the type of loading.

15.2.2.1. Shear Buckle Wavelength

[\(NACA-TN-2536, 1951\)](#) provides some basic data on half wavelengths/panel width for a range of buckling situations. Note that this reference is concerned with the combination of transverse and not axial shear. Therefore, the cases where k_s has a non-zero and k_b and k_c are zero are pure shear.

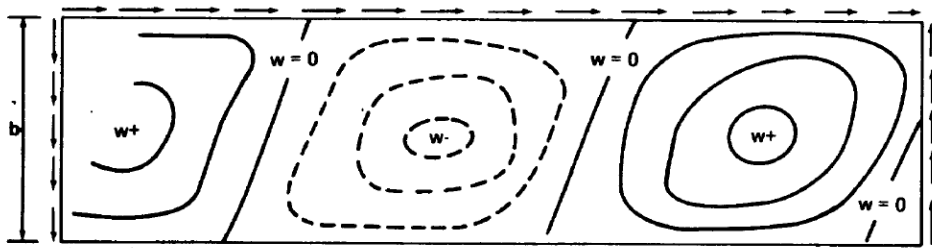


Figure 15.2.2-1: Shear Buckling Wavelength [\(NASA TM X-73306, 1975\)](#)

Note that the half wavelength is measured in the panel axial direction and NOT perpendicular to the 45-degree buckle.

CALCULATED BUCKLING STRESS COEFFICIENTS AND HALF-WAVE-LENGTH RATIOS
FOR INFINITELY LONG FLAT PLATE WITH BOTH EDGES SIMPLY SUPPORTED

| k_B | k_T | k_C | λ/b |
|-------|-------|-------|-------------|
| 23.90 | 0 | 0 | 0.7 |
| 22.82 | 2.00 | 0 | .8 |
| 18.38 | 4.00 | 0 | .9 |
| 9.60 | 5.14 | 0 | 1.1 |
| 0 | 5.36 | 0 | 1.2 |

CALCULATED BUCKLING STRESS COEFFICIENTS AND HALF-WAVE-LENGTH RATIOS
FOR INFINITELY LONG FLAT PLATE WITH LOWER EDGE SIMPLY
SUPPORTED AND UPPER EDGE CLAMPED

| k_B | k_T | k_C | λ/b |
|-------|-------|-------|-------------|
| 39.96 | 0 | 0 | 0.5 |
| 36.51 | 4.700 | 0 | .6 |
| 20.00 | 7.963 | 0 | 1.1 |
| 0 | 6.637 | 0 | 1.2 |

Figure 15.2.2-2: Shear Buckle Half Wavelength as a Ratio of Panel Width for Varying Edge Constraints [\(NACA-TN-2536, 1951\)](#)

From this reference, a first approximation for the λ/b ratio can be assumed to be 1.2 for all states of panel rotational edge fixity.

15.2.2.2. Compression Buckle Wavelength

[\(ARC-RM-2652, 1953\)](#) gives a range of good experimental data for compression buckle wavelength:

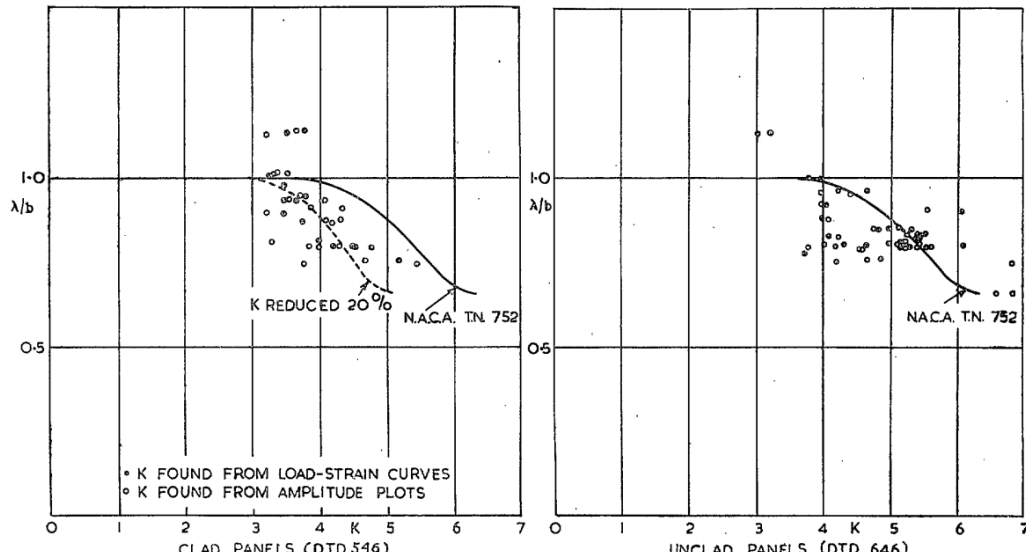


FIG. 50. Comparison of K and λ/b with results of N.A.C.A. T.N. 752.

Figure 15.2.2-3: Variation of Compression Half Buckle Wavelength with Panel Edge Fixity Coefficient [\(ARC-RM-2652, 1953\)](#)

It is noted that the λ/b ratio varies between 0.6 and 1.0.

The wavelength decreases with increasing panel edge rotational fixity.

15.2.2.3. Bending Buckle Wavelength

Using the reference for the shear buckle wavelength [\(NACA-TN-2536, 1951\)](#) the wavelength for the bending buckle can be found from the case where k_s and k_c are equal to zero:

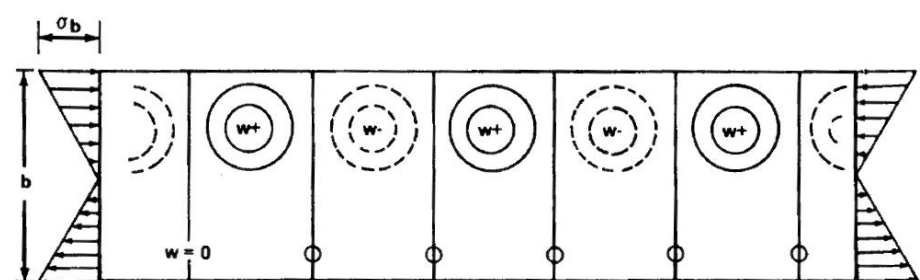


Figure 15.2.2-4: Bending Buckling Wavelength [\(NASA TM X-73306, 1975\)](#)

CALCULATED BUCKLING STRESS COEFFICIENTS AND HALF-WAVE-LENGTH RATIOS
FOR INFINITELY LONG FLAT PLATE WITH BOTH EDGES SIMPLY SUPPORTED

| k_B | k_T | k_C | λ/b |
|-------|-------|-------|-------------|
| 23.90 | 0 | 0 | 0.7 |
| 22.82 | 2.00 | 0 | .8 |
| 18.38 | 4.00 | 0 | .9 |
| 9.60 | 5.14 | 0 | 1.1 |
| 0 | 5.36 | 0 | 1.2 |

CALCULATED BUCKLING STRESS COEFFICIENTS AND HALF-WAVE-LENGTH RATIOS
 FOR INFINITELY LONG FLAT PLATE WITH LOWER EDGE SIMPLY
 SUPPORTED AND UPPER EDGE CLAMPED

| k_B | k_T | k_C | λ/b |
|-------|-------|-------|-------------|
| 39.96 | 0 | 0 | 0.5 |
| 36.51 | 4.700 | 0 | .6 |
| 20.00 | 7.963 | 0 | 1.1 |
| 0 | 6.637 | 0 | 1.2 |

Figure 15.2.2-5: Bending Buckle Half Wavelength as a Ratio of Panel Width for Varying Edge Constraints (NACA-TN-2536, 1951)

For a simply supported panel the λ/b ratio can be assumed to equal **0.70**, and for a panel with clamped edges **0.50**.

As with the compression buckle the wavelength decreases with increasing panel edge rotational fixity.

These compression, bending and shear buckling wavelengths can be estimated using the following spreadsheet:



ADVERT: ENGINEERING SERVICES

COMPOSITE DESIGN

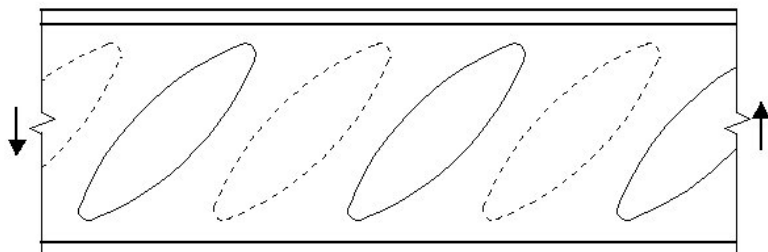
CONTACT US

ENGINEERING SERVICES

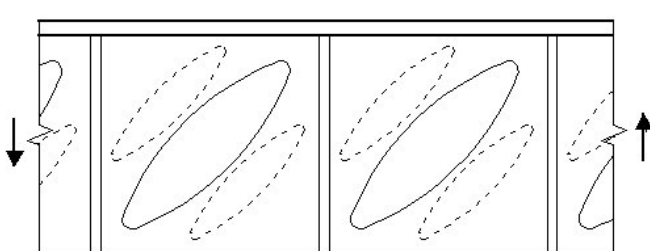
ABBOTT AEROSPACE SEZC LTD

15.2.3. Web Shear Buckling (Rectangular)

A web is a panel supported along all 4 sides, it can be the typical shear web component of an I or C-section beam. A web can be continuous or broken into smaller panels by vertical stiffeners.



(a) Unstiffened web



(b) stiffened web

Figure 15.2.3-1: Web Shear Buckling

15.2.3.1. Shear Buckling Allowable Stress

The shear buckling coefficient, k_s , can be found once the panel aspect ratio is known from the following figure:

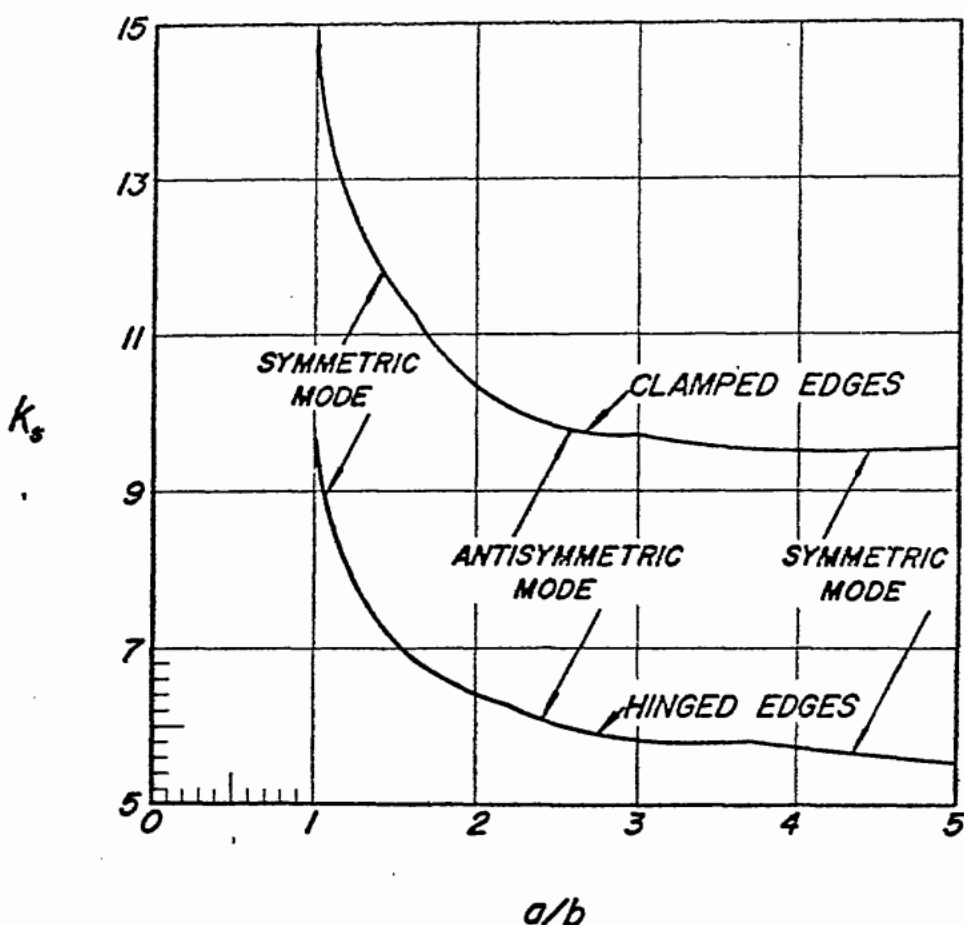


Figure 15.2.3-2: Web Shear Buckling Coefficient [\(NACA-TN-3781, 1957\)](#)

There are some good theoretical approximations to the shear buckling coefficient curves. These are as follows:

For a panel simply supported on four edges:

$$k_s = 5.34 + \frac{4.00}{r^2}$$

For a panel clamped on four edges:

$$k_s = 8.98 + \frac{5.6}{r^2}$$

For a panel clamped on the long edges and simply supported on short edges:

$$k_s = 8.98 + \frac{5.61}{r^2} - \frac{1.99}{r^3}$$

For a panel clamped on the short edges and simply supported on long edges:

$$k_s = 5.34 + \frac{2.31}{r} - \frac{3.44}{r^2} + \frac{8.39}{r^3}$$

Where: $r = a/b$

The theoretical curves are shown in the following figure:

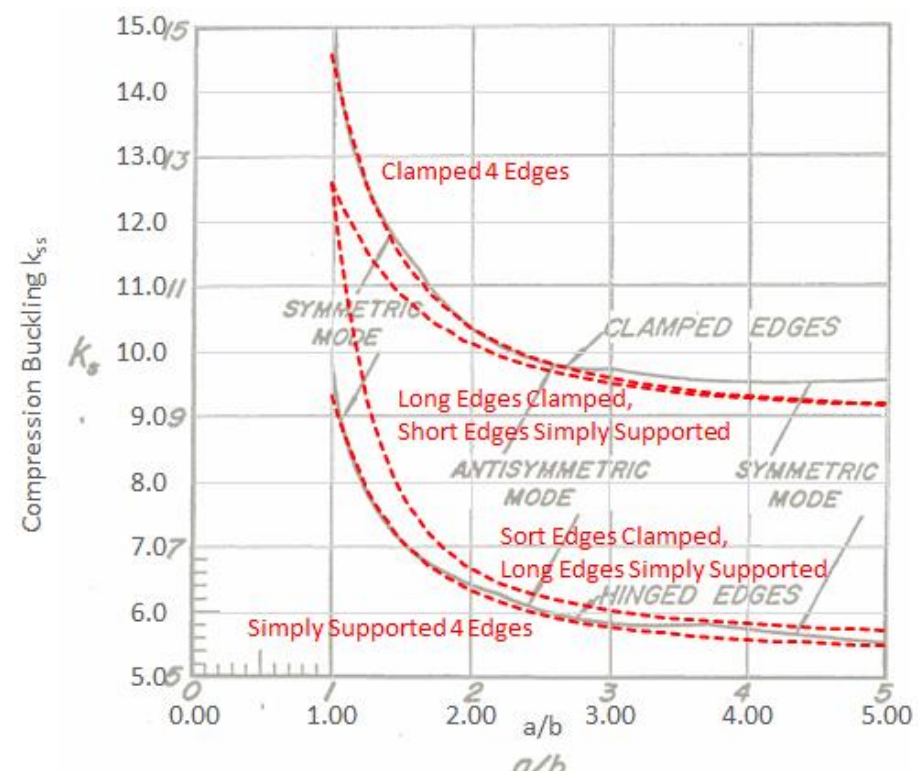


Figure 15.2.3-3: Web Shear Buckling Coefficient – Theoretical Approximations, Comparison to Figure 15.2.3-2

These Curves are plotted and compared with the 'classic' curves from [\(NACA-TN-3781, 1957\)](#) in the following spreadsheet:

ABBOTT AEROSPACE SEZC LTD
SPREADSHEETS
ABBOTTAEOSPACE.COM

AA-SM-007-091 Mathematical Derivation of Shear Buckling Coefficients

Figure 15.2.3-3 shows that the theoretical approximations are a good fit to the existing curves. It is recommended that the theoretical approximations are used.

The spreadsheets for derivation of the shear buckling allowable use the theoretical approximations for k in the following expression:

$$F_{cr} = \eta \cdot k \cdot \frac{\pi^2 \cdot E}{12 \cdot (1 - \nu_e^2)} \left(\frac{t}{b} \right)^2$$

The simplest approach to determine the panel shear buckling allowable, and the approach that is commonly used for initial sizing, is to assume that $\eta = 1$ and the panel is simply supported.

$$F_{cr} = k_{ss} \cdot \frac{\pi^2 \cdot E}{12 \cdot (1 - \nu_e^2)} \left(\frac{t}{b} \right)^2$$

Using this simple approach if F_{cr} exceeds F_{sy} , the shear yield allowable stress for the panel, then limit F_{cr} to F_{sy} . A comparison between this simple assumption and the calculated elasto-plastic shear buckling allowable for a typical aluminum is shown in Figure 15.2.3-7.

A spreadsheet method for simple shear buckling of a web is given at the link below:

Note that when R_a and R_b are equal to 1.62 (corresponding to fully fixed) the k value is close to, but not exactly the same value as the upper line in Figure 15.2.3-2. This is acceptable, and the difference is not significant.

The values for R_a and R_b can be estimated from the following chart. Where:

t_a Thickness of the stiffener along edge 'a', in
 t_b Thickness of the stiffeners long edge 'b', in
 t Thickness of the web, in

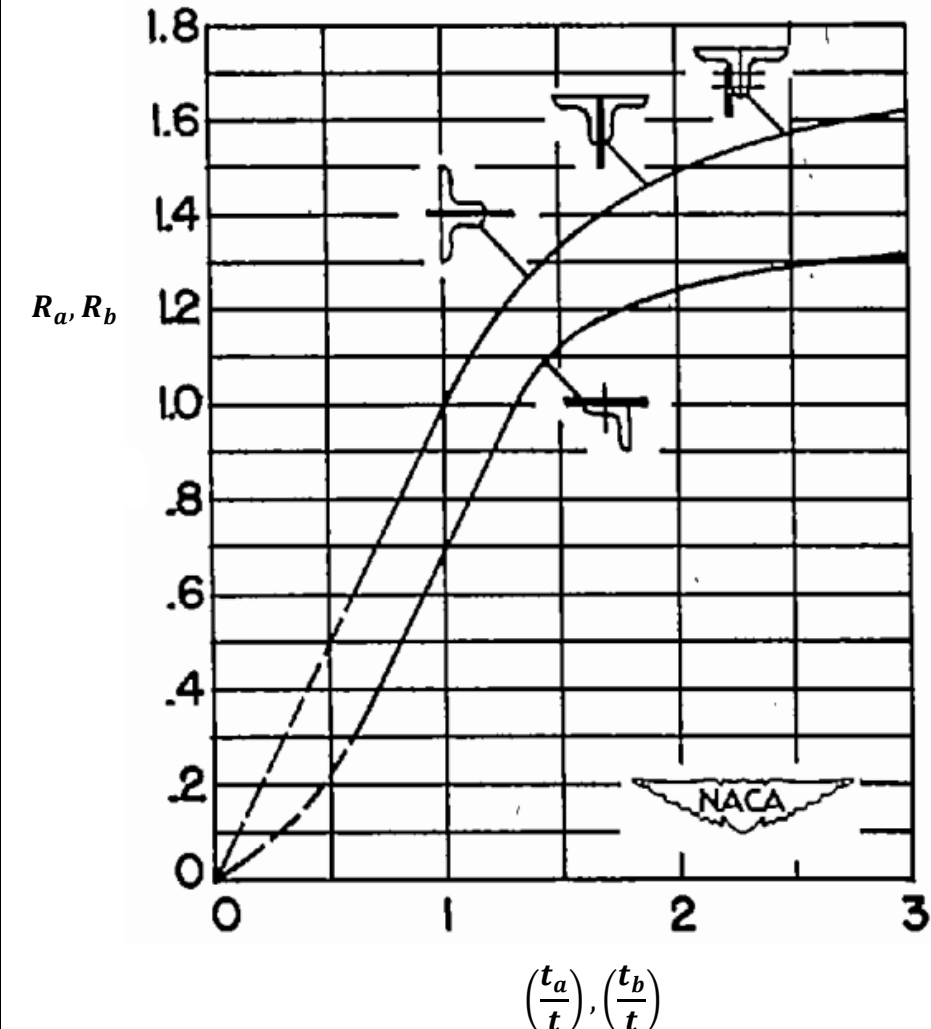


Figure 15.2.3-4: Empirical edge restraint coefficients [\(NACA-TN-2661, 1952\)](#)

15.2.3.2. Shear Buckling Allowable Stress with Varying Panel Rotational Edge Fixity

The method can be refined in the following way for panel edge rotational fixity:

Panel edge fixity is a measure of edge rotational stiffness relative to the out-of-plane stiffness of the web being considered. What could be considered to provide adequate out-of-plane stiffness in translation and rotation for a 0.025in thick aluminum web may not be considered to provide any support at all for a 0.25in thick steel web. A rational measure of relative panel edge stiffness is required.

According to [\(NACA-TN-2661, 1952\)](#) Section 3.6 the simply supported panel shear buckling coefficient can be modified for a range of edge rotational fixity from simply supported to built-in with the following expression:

$$F_{cr} = k_{ss} \cdot \frac{\pi^2 \cdot E}{12 \cdot (1 - \nu_e^2)} \left(\frac{t}{b} \right)^2 \cdot \left[R_a + \frac{1}{2} \cdot (R_b - R_a) \cdot \left(\frac{b}{a} \right)^3 \right]$$

Where R_a and R_b are the rotational edge fixity coefficients for sides a and b of the web respectively. Where 1 = simply supported and 1.62 = fully fixed.

The simply supported shear buckling coefficient can be modified using the following expression:

$$k = k_{ss} \cdot \left[R_a + \frac{1}{2} \cdot (R_b - R_a) \cdot \left(\frac{b}{a} \right)^3 \right]$$

The modifier to the simply supported shear buckling coefficient can be expressed as:

$$\frac{k}{k_{ss}} = \left[R_a + \frac{1}{2} \cdot (R_b - R_a) \cdot \left(\frac{b}{a} \right)^3 \right]$$

As before, if F_{cr} exceeds F_{sy} then limit F_{cr} to F_{sy} .

Note that, according to Figure 15.2.3-4, the values of R_a and R_b can be less than one. This would reduce the k value to below the value for the simply supported edge. This implies that if the panel edge members are not sufficiently thick, the translational stiffness of the panel edge is not sufficient.

If results for R_a and R_b are less than 1.0 this is considered to be a failing structure; redesign is required to improve the translational stiffness of the panel edge members.

A spreadsheet method for shear buckling of a web with varying edge rotational restraints is given at the link below:



15.2.3.3. Shear Buckling Allowable Stress with Full Elasto-Plastic Material Data

If the calculated shear buckling stress is approaching the shear yield stress (F_{sy}) of the material, the elastic shear buckling allowable could be optimistic. If a more nuanced approach than limiting the buckling stress to F_{sy} is required, the shear buckling allowable should be modified using the plasticity correction factor η .

For Shear buckling the plasticity correction factor is G_s/G – that is the secant shear modulus divided by the material shear modulus. This data can be plotted for a range of stresses and an ‘elastic vs plastic’ buckling stress for any material can be plotted.

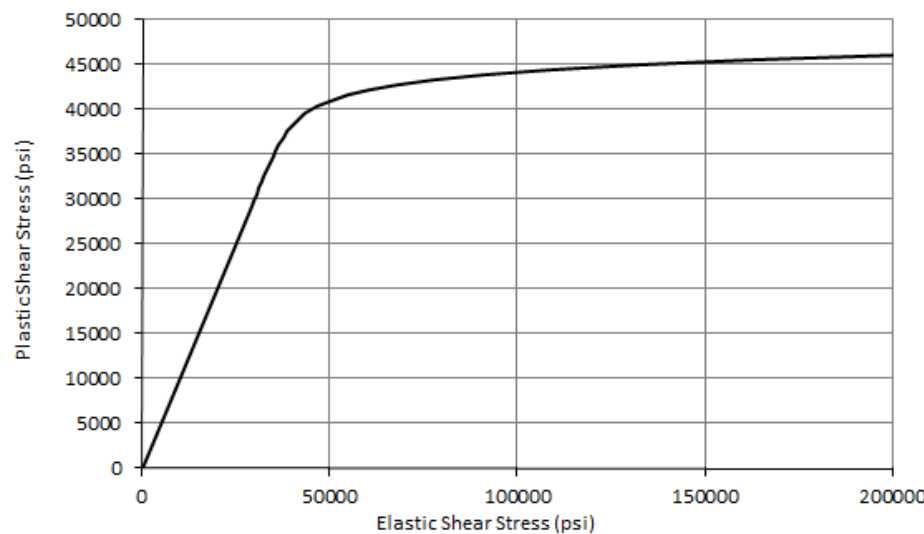


Figure 15.2.3-5: Elastic vs Plastic Shear Buckling Stress for Sample Material

Once the graph has been plotted the elastic shear buckling allowable can be plotted on the x-axis, project upwards to the curve and read across to the Y-axis to give the shear buckling allowable corrected for plasticity.

This is shown on the figure below where the elastic shear buckling stress of 70636 psi is corrected to 42848 psi.

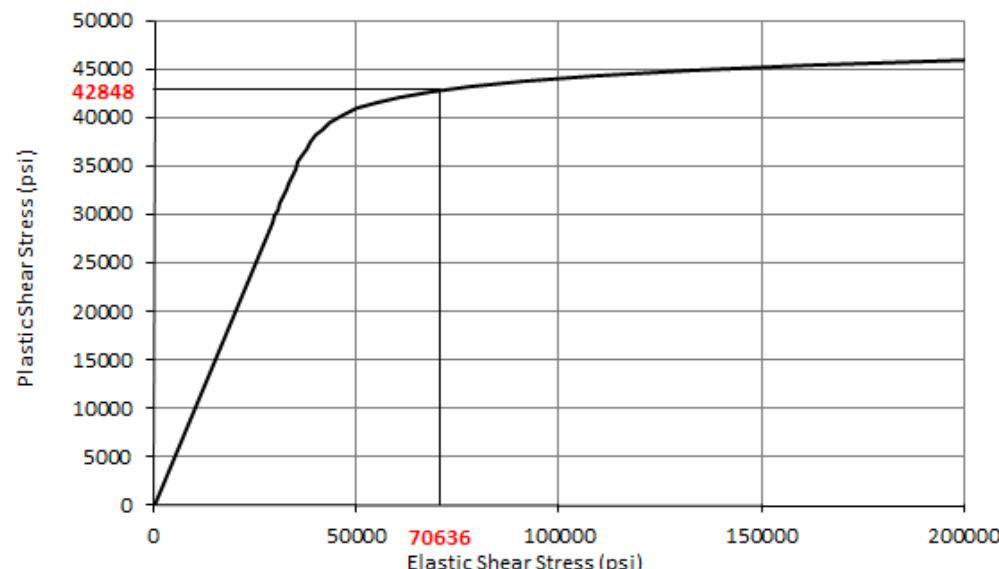


Figure 15.2.3-6: Elastic vs Plastic Shear Buckling Stress for Sample Material with Correction to Elastic Shear Buckling Allowable shown

Superimposing the simpler approach of limiting F_{cr} to F_{sy} over the elastic vs plastic shear buckling stress curve gives the following result:

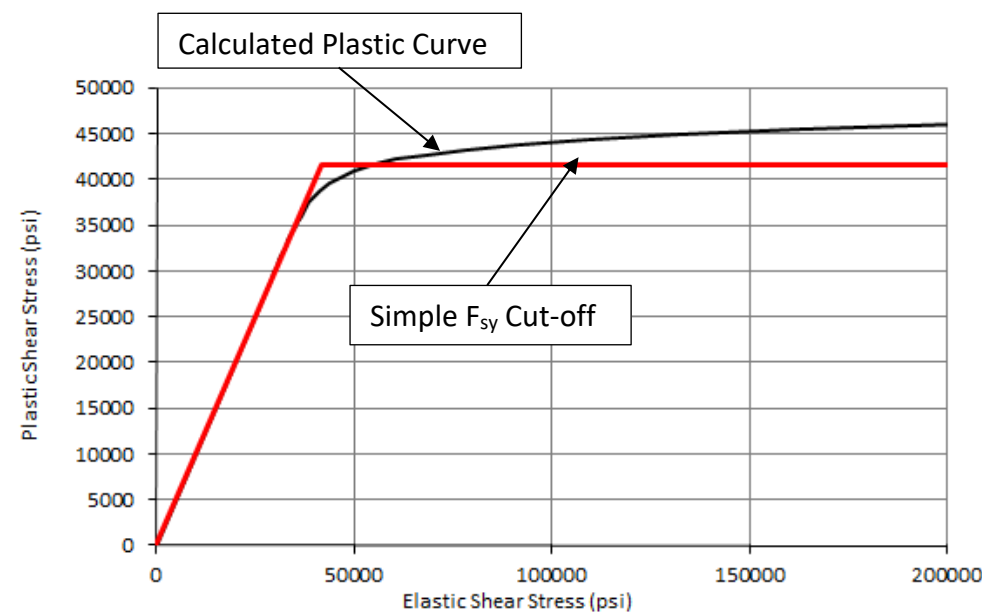


Figure 15.2.3-7: Elastic vs Plastic Shear Buckling Stress for Sample Material with Comparison to Simple Elastic and F_{sy} Cut off Value

For the sample material (and for most ductile materials) the simple approach does give a reasonable approximation to the correctly calculated plastic buckling allowable. A spreadsheet for this method is available at the link below:

ABBOTT AEROSPACE SEZC LTD
SPREADSHEETS
ABBOTTAEROSPACE.COM

AA-SM-007-003 Buckling of Flat Isotropic Plates - Plastic Shear Buckling

ADVERT: ENGINEERING SERVICES

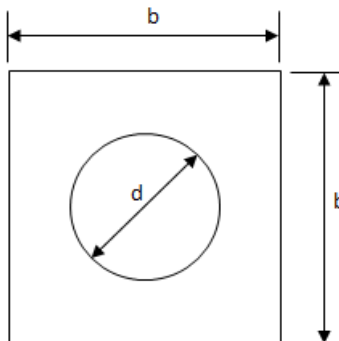
STRUCTURES DESIGN ENGINEERING SERVICES

CONTACT US

ABBOTT AEROSPACE SEZC LTD

15.2.3.4. Effect of Central Hole on Panel Shear Buckling Allowable

This section is based on the work in [\(NASA-CR-132548\)](#). The reduction in shear buckling allowable is related to the ratio of the hole size to the panel size, or the d/b ratio.



Where 'd' is the circular hole diameter and 'b' is the ruling dimension of the panel. When the panel is not square the dimension 'b' can be assumed to be the minimum panel dimension.

A good curve fit to the experimental test results in [\(NASA-CR-132548\)](#) is the function:
 $K/K_0 = e^{-1.585 \times d/b}$. This relationship is shown in the following figure and the linked spreadsheet.

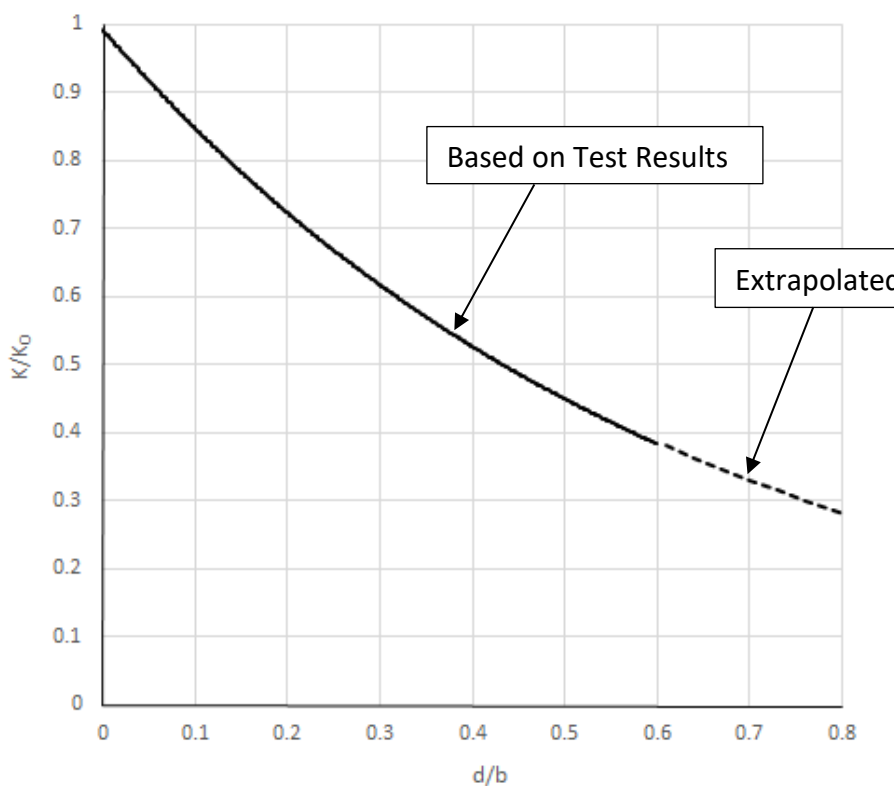


Figure 15.2.3-8: Reduction in Shear Buckling allowable for Square Panels with Centrally Located Holes

AA-SM-007-004 Effect of Central Hole on Plate Shear Buckling Allowable

15.2.3.5. Collapse of Shear webs with Flanged Circular Holes

This section is based on [\(NACA-WR-L-323, 1942\)](#). The collapsing shear stress of a rectangular web is given by the following expression:

$$\tau_{coll} = \left[\tau_h \left(1 - \left(\frac{D}{h} \right)^2 \right) + \tau_c \sqrt{\frac{D}{h}} \right] \frac{c'}{b}$$

Where the parameters are defined as follows:

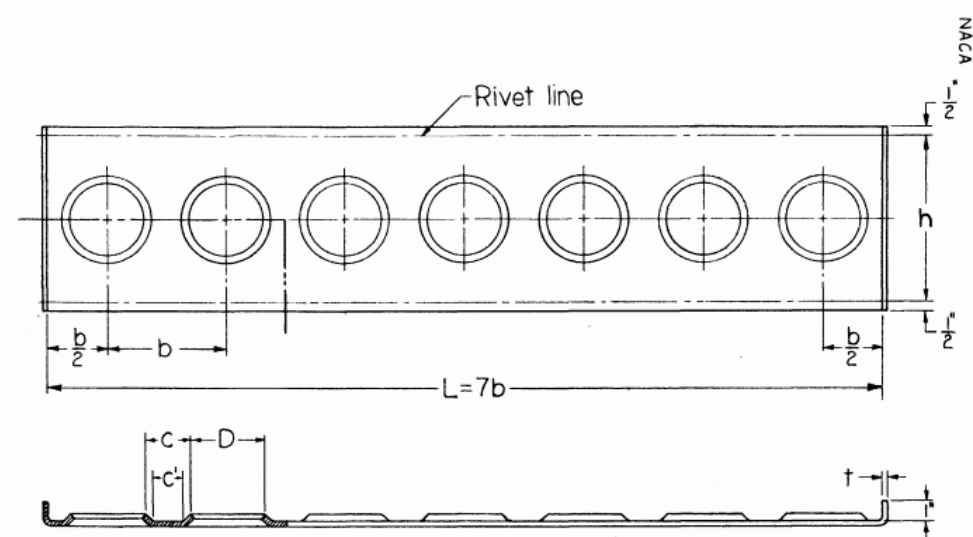


Figure 15.2.3-9: Collapse of shear web with flanged Circular Holes [\(NACA-WR-L-323, 1942\)](#)

This method is available in spreadsheet form here:

ABBOTT AEROSPACE SEZC LTD
SPREADSHEETS
ABBOTTAEROSPACE.COM
AA-SM-007-011 Collapse Of Shear Web with Holes

15.2.3.6. Assessment of Panel Breaker Effectivity

This section is largely taken from [\(NACA-TN-862, 1942\)](#). This reference comprises of an experimental study of 60 different tests of 17S-T built-up aluminum shear beams. This material is equivalent to a modern 2017 aluminum alloy.

This reference examined a range of different panel configurations and notes the effect of the stiffener configuration on the extent of the out-of-plane deflection of the web and the stiffener.

The reference then proposes a rule that governs the acceptable stiffener 2nd moment of area based on the web panel dimensions and the web thickness.

$$\lambda = \frac{12 \cdot E \cdot I \cdot (1 - \mu^2)}{E \cdot b \cdot t^3}$$

Where:

I 2nd moment of area of stiffener, in⁴

E Modulus of elasticity, psi

b Stiffener spacing, in

t Web thickness, in

v Poisson's ratio

And:

$$\lambda = \frac{14}{\left(\frac{b}{d}\right)^3}$$

d Depth of the shear web, in

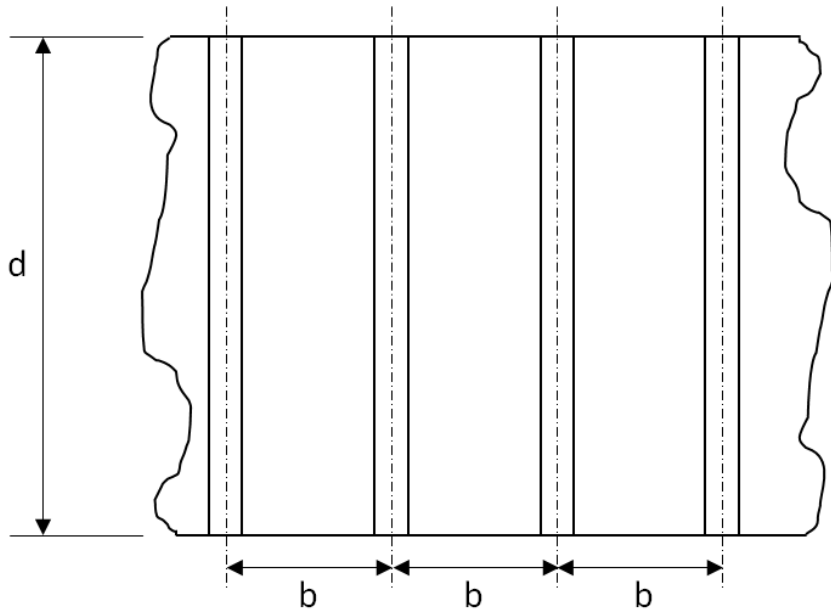


Figure 15.2.3-10: Web Panel Size Definition for Stiffener Check

The expressions can be combined and arranged to give a criterion for the required stiffener 2nd moment of area:

$$I = \frac{1.166 \cdot d^3 \cdot t^3}{b^2 \cdot (1 - \nu^2)}$$

It is recommended that this check is used as a rough sizing approximation only, but it can be considered applicable to web buckling in shear, compression and bending. It is recommended that component testing or a higher order analysis is carried out to confirm the results of this analysis.

A spreadsheet method is given at the link below:

ABBOTT AEROSPACE SEZC LTD
SPREADSHEETS
 ABBOTTAEROSPACE.COM

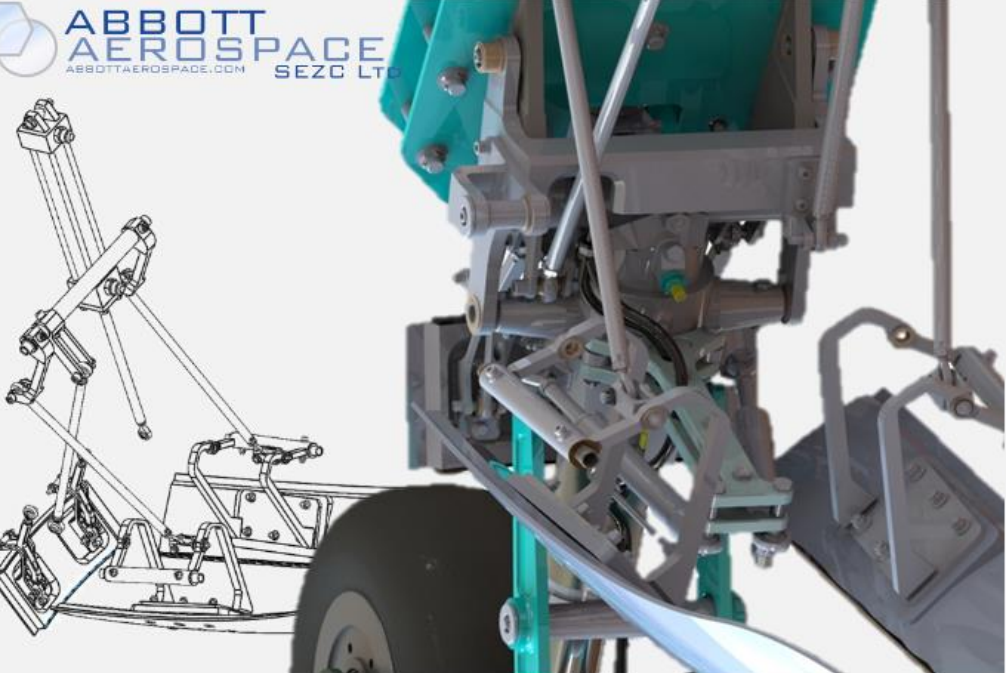
AA-SM-007-010 Assessment of Panel Breaker Effectivity

ADVERT: ENGINEERING SERVICES

MECHANICAL SYSTEMS 

CONTACT US

 **ABBOTT AEROSPACE** SEZC LTD
 ABBOTTAEROSPACE.COM



15.2.4. Panel Compression Buckling (Rectangular)

Panel compression buckling is common when considering the primary failure mode of the upper wing skin panels, horizontal tail skins and vertical tail skins. Compression also contributes to the failure of other parts of the structure in combined failure modes.



Figure 15.2.4-1: Panel Compression Buckling [\(NACA-TN-3781, 1957\)](#)

15.2.4.1. Compression Buckling Allowable Stress

The compression buckling coefficient, k_c , can be found once the panel aspect ratio is known from the following figure taken from [\(NACA-Report-733\)](#):

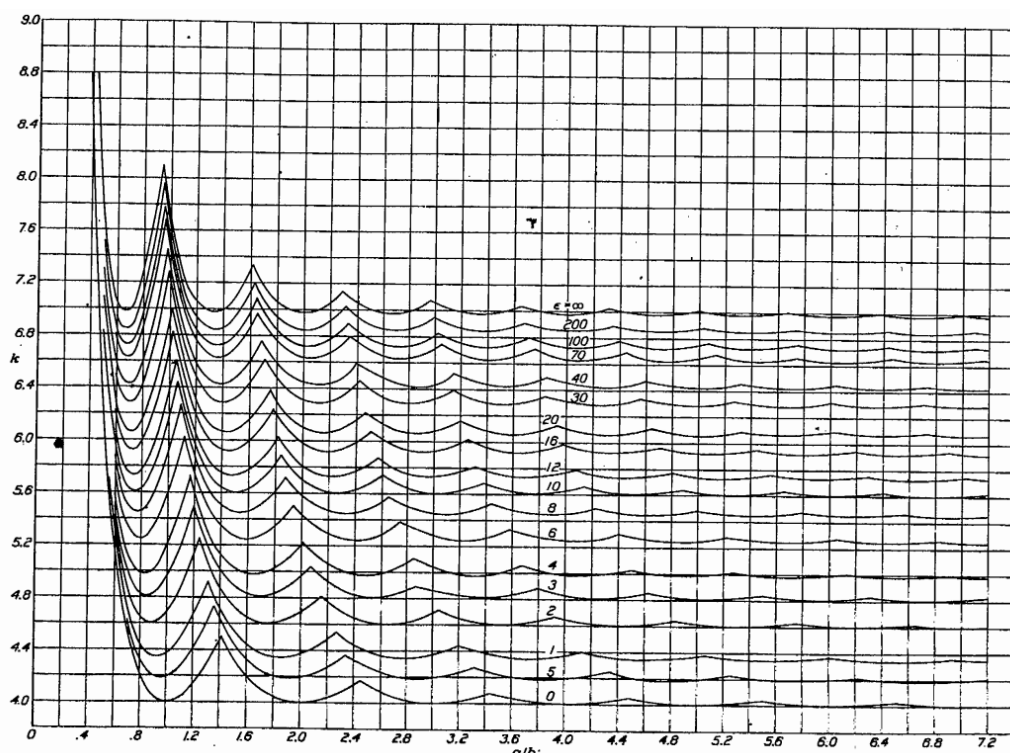


Figure 15.2.4-2: Web Compression Buckling Coefficient [\(NACA-Report-733\)](#)

$$F_{cr} = \eta \cdot k \cdot \frac{\pi^2 \cdot E}{12 \cdot (1 - \nu_e^2)} \left(\frac{t}{b}\right)^2$$

The compression buckling coefficient in the figure above is derived using the following expression:

$$k = \frac{\left[\left(\frac{\pi b}{\lambda} \right)^2 + \frac{1}{\left(\frac{\pi b}{\lambda} \right)^2} + \frac{1}{6} \right] \epsilon^2 + \left(1 + \frac{\epsilon}{2} \right) \left(\frac{b}{\lambda} + \frac{\lambda}{b} \right)^2 \left[\frac{1}{2} \left(1 + \frac{\epsilon}{2} \right) - \frac{4\epsilon}{\pi^2} \right] + \frac{2\epsilon}{\left(\frac{\pi b}{\lambda} \right)^2}}{\frac{\pi^2 \epsilon^2}{120} + \frac{4\epsilon}{\pi^2} \left(1 + \frac{\epsilon}{2} \right) + \frac{1}{2} \left(1 + \frac{\epsilon}{2} \right)^2}$$

Where:

- k Panel Compression Buckling Coefficient
- λ Half wave length of the buckle pattern
- b Panel width, in

ϵ Restraint coefficient

$$\epsilon = \frac{4 \cdot S_0 \cdot b}{D}$$

Where:

S_0 Stiffness per unit length of elastic restraining medium, or moment required to rotate a unit length of elastic medium through one-fourth radian

D Flexural rigidity of Panel per unit length

$$D = \frac{E \cdot t^3}{12 \cdot (1 - \nu_e^2)}$$

b Width of loaded edge of panel, in

t Panel thickness, in

E Panel material young's modulus, psi

ν_e Panel material elastic Poisson's ratio

This is covered in greater depth in section 15.2.4.3.

15.2.4.2. Panel with Simply Supported Edges

The simplest approach to panel compression buckling and the approach that is commonly used for initial sizing is to assume that $\eta = 1$ and the panel is simply supported:

$$F_{cr} = k_{ss} \cdot \frac{\pi^2 \cdot E}{12 \cdot (1 - \nu_e^2)} \left(\frac{t}{b}\right)^2$$

The coefficient for the simply supported edge condition is given by the following expression:

$$k_{ss} = \left(\frac{\lambda}{r} + \frac{r}{\lambda} \right)^2$$

Where:

r Panel aspect ratio, a/b

λ Half wave length of the buckle pattern

The minimum values of this curve for successive values of λ is shown below:

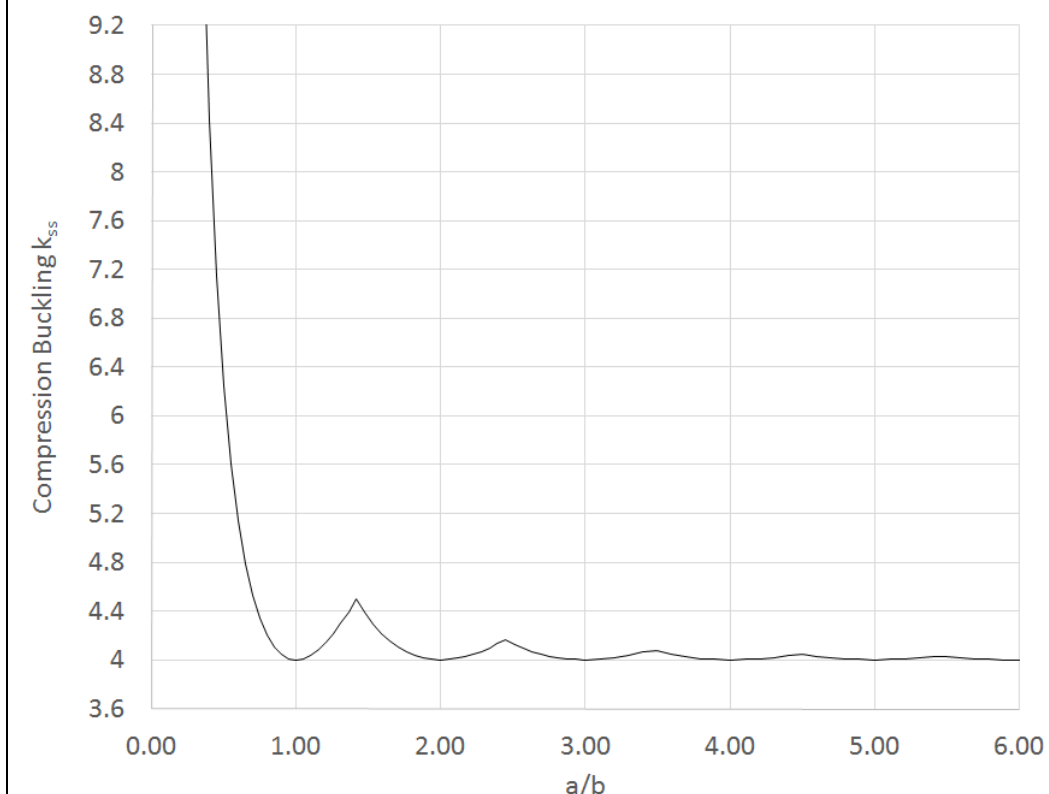


Figure 15.2.4-3: Web Compression Buckling Coefficient – Simply Supported

The simple and the general Panel compression buckling coefficients are calculated in this spreadsheet:



The simple approach to panel compression buckling is given in this spreadsheet: Using this simple approach, to account for panel material plasticity if F_{cr} exceeds F_{cy} then limit F_{cr} to F_{cy} .



15.2.4.3. Compression Buckling Allowable Stress with Varying Panel Rotational Edge Fixity

A simplified method allows for a quantified measure of the panel rotational edge stiffness, ϵ , this is defined by the following expression:

$$\epsilon = \frac{4 \cdot S_0 \cdot b}{D}$$

Where:

S_0 Stiffness per unit length of elastic restraining medium, or moment required to rotate a unit length of elastic medium through one-fourth radian

D Flexural rigidity of panel per unit length:

$$D = \frac{E \cdot t^3}{12 \cdot (1 - \nu_e^2)}$$

b Width of loaded edge of Panel, in

The value of ϵ can be calculated by taking the following approach. This approach is taken in part from [\(NACA-TN-888, 1943\)](#).

The term S_0 can be calculated from this expression:

$$4 \cdot S_0 = \frac{\pi^2}{\lambda^2} \cdot \left(G \cdot J - f \cdot I_p + \frac{\pi^2}{\lambda^2} \cdot E_s \cdot C_{BT} \right)$$

When this is combined with the initial expression for ϵ the expression for evaluating ϵ becomes:

$$\epsilon = \frac{\pi^2 \cdot b}{\lambda^2 \cdot D} \cdot \left(G \cdot J - f \cdot I_p + \frac{\pi^2}{\lambda^2} \cdot E_s \cdot C_{BT} \right)$$

Where:

C_{BT} Torsion-bending constant of stiffener sectional area about axis of rotation at or near edge of plate (see below) and

λ Half buckle wavelength, Ref Section 15.2.2

G Material modulus of rigidity, psi

J Section torsional constant, in⁴

Of all these terms the C_{BT} is a relatively little used cross section property and

[\(NACA-TN-888, 1943\)](#) is one of the few references that gives a method to determine this value.

C_{BT} is defined using the following expression:

$$C_{BT} = \int_A u^2 dA$$

and is described as "where u is the unit warping of the element of area dA from a reference plane through the shear center and normal to the axis when the angle of twist per unit length ($d\theta/dx$) is unity".

Thankfully the reference gives a set of expressions for C_{BT} for common cross sections:

$$\text{I Beam: } \frac{I_F \cdot h^2}{2}$$

$$\text{Channel: } \frac{I_F \cdot h^2}{2} \left(4 - 6 \cdot \frac{e}{b} \right)$$

$$\text{Z Section: } \frac{I_F \cdot h^2}{2} \left(4 - 6 \cdot \frac{A_F}{A} \right)$$

Where:

A_F Area of one flange ($A_F = b \cdot t_F$), in²

b Width of flange, in

t_F Flange thickness, in

A_W Area of web ($A_W = h \cdot t_W$), in²

h Height of web, in

t_W Web thickness, in

A Area of cross section ($A = A_W + 2 \cdot A_F$), in²

I_F Moment of inertia of one flange ($I_F = b^3 \cdot t_F/12$), in⁴

Further explained in the figure below:

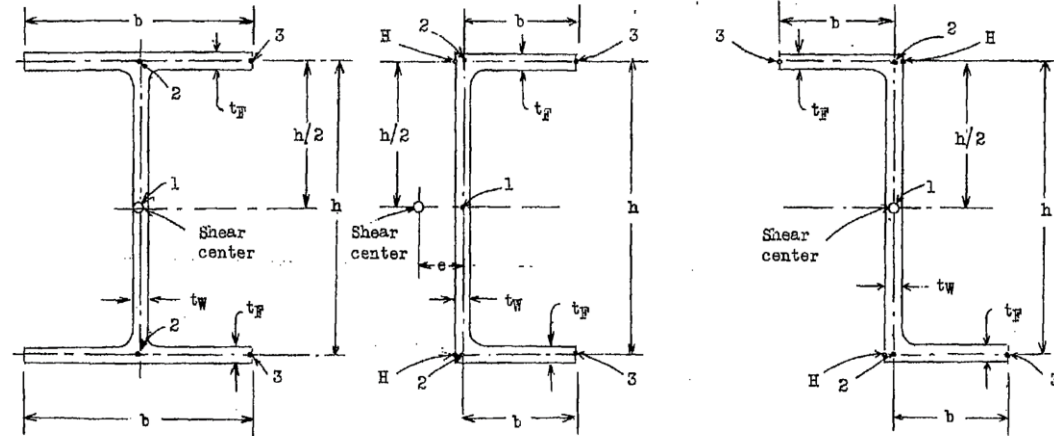


Figure 15.2.4-4: Parameters for Torsion-Bending Constant

The spreadsheet for this method is at the link below:

ABBOTT AEROSPACE SEZC LTD
SPREADSHEETS
ABBOTTAEROSPACE.COM

AA-SM-007-070 Buckling - Edge Rotational Restraint

A view of how the simply supported compression buckling coefficient, k , changes with the value of ϵ is given in Figure 17 of [\(NACA-TN-3781, 1957\)](#):

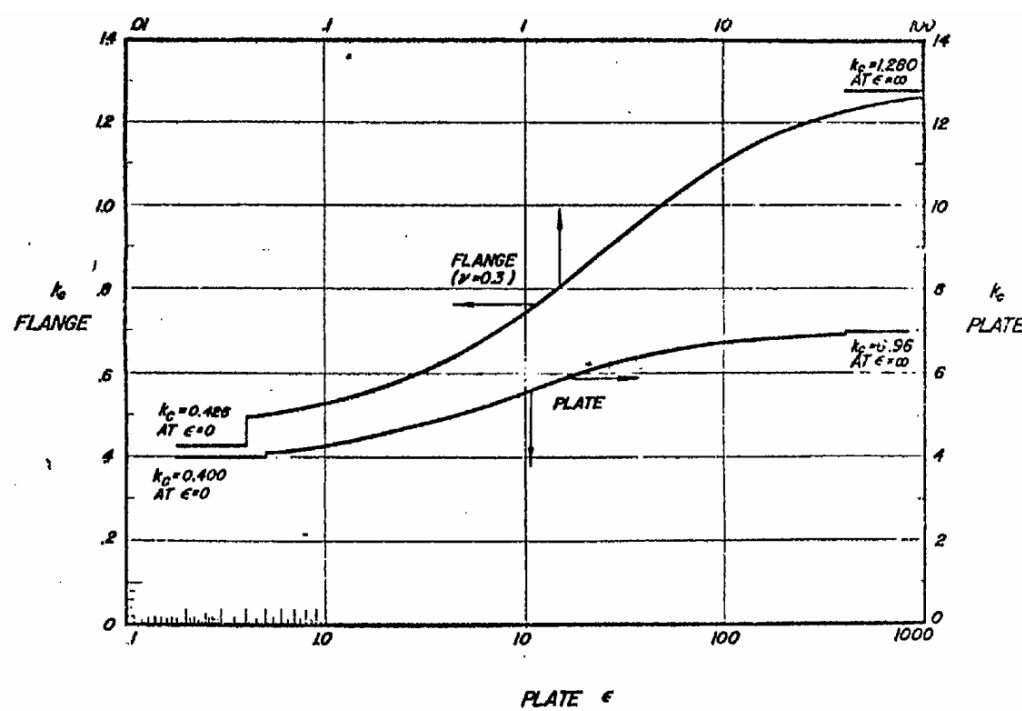


Figure 15.2.4-5: The relationship between k and ϵ [\(NACA-TN-3781, 1957\)](#)

The lower line on the graph above defines the relationship between k and ϵ for a panel in compression buckling.

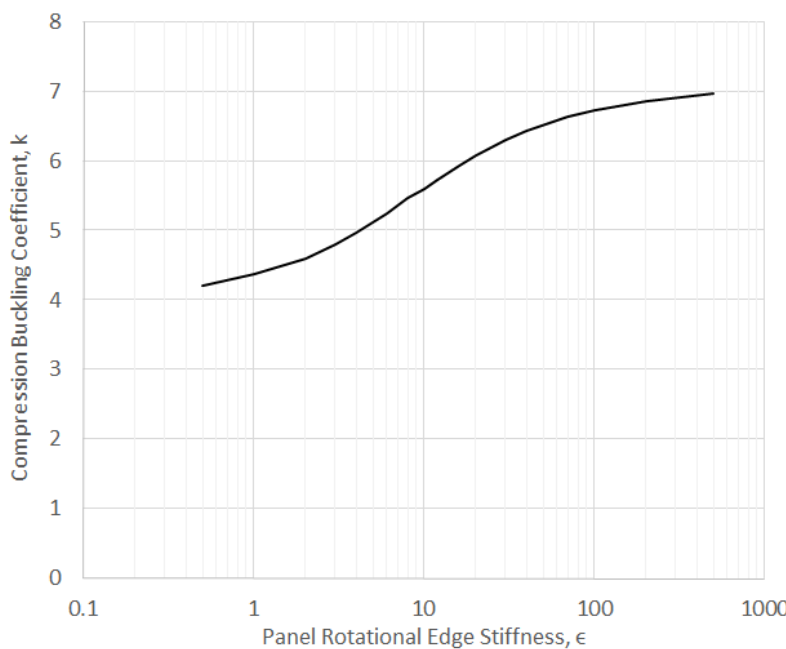


Figure 15.2.4-6: The relationship between k and ϵ - Clarified

The spreadsheet method for estimating the effect on k for edge rotational edge fixity is given at the link below:



Note that this method of accounting for panel edge fixity correlates well to the value of k calculated using the general expression which is shown in Figure 15.2.4-2.

15.2.4.4. Compression Buckling Allowable Stress with Full Elasto-Plastic Material Data

If the calculated compression buckling stress is approaching the compression yield stress (F_{cy}) of the material the elastic compression buckling could be optimistic. If a more nuanced approach than limiting the buckling stress to F_{cy} is required, the compression buckling allowable should be modified using the plasticity correction factor η .

From [\(NACA-TN-3781, 1957\)](#) for compression buckling the plasticity correction factor for a long simply supported panel is:

$$\eta_{ss} = \left[\left(\frac{E_s}{E} \right) \cdot \frac{(1 - \nu_e^2)}{(1 - \nu^2)} \right] \cdot \left\{ 0.500 + 0.250 \cdot \sqrt{1 + \left(\frac{3 \cdot E_t}{E_s} \right)} \right\}$$

the plasticity correction factor for a long, clamped panel is:

$$\eta_{cl} = \left[\left(\frac{E_s}{E} \right) \cdot \frac{(1 - \nu_e^2)}{(1 - \nu^2)} \right] \cdot \left\{ 0.352 + 0.324 \cdot \sqrt{1 + \left(\frac{3 \cdot E_t}{E_s} \right)} \right\}$$

Where:

ν_e Poisson's ratio in the elastic range

ν Poisson's ratio at any point on the material stress strain curve, given by the expression:

$$\nu = 0.5 - (0.5 - \nu_e) \cdot \left(\frac{E_s}{E} \right)$$

E_t Tangent modulus, psi (Section 4.2.2.1)

E_s Secant modulus, psi (Section 4.2.2.1)

E Young's modulus, psi

Plotting these two plasticity correction factors for a typical aluminum give the following result:

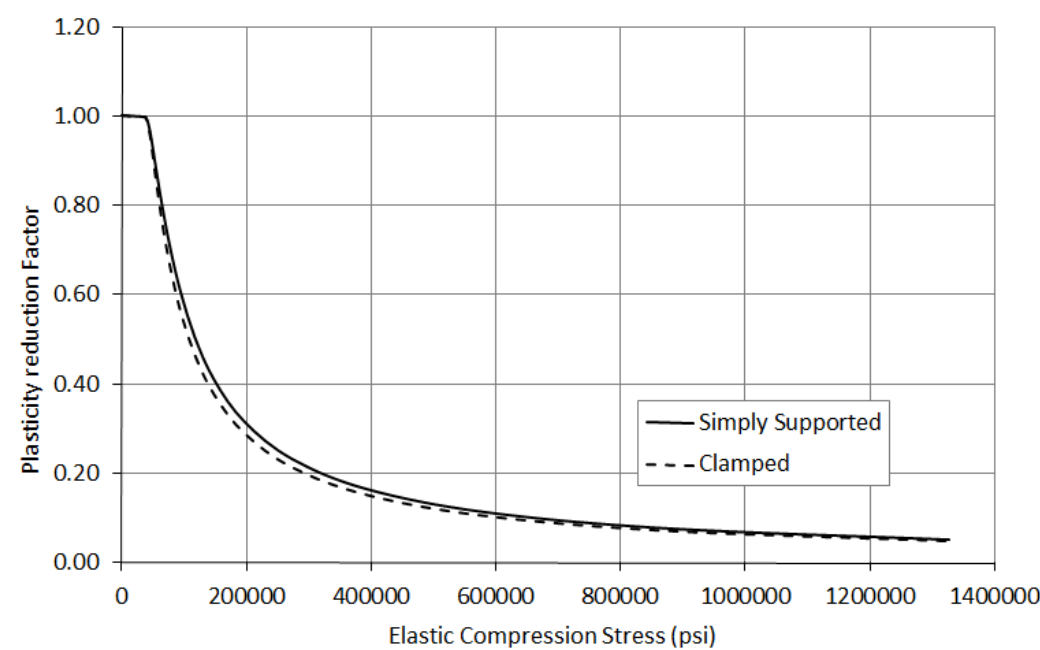


Figure 15.2.4-7: Plasticity Correction Factors Compression buckling for Typical Aluminum Material

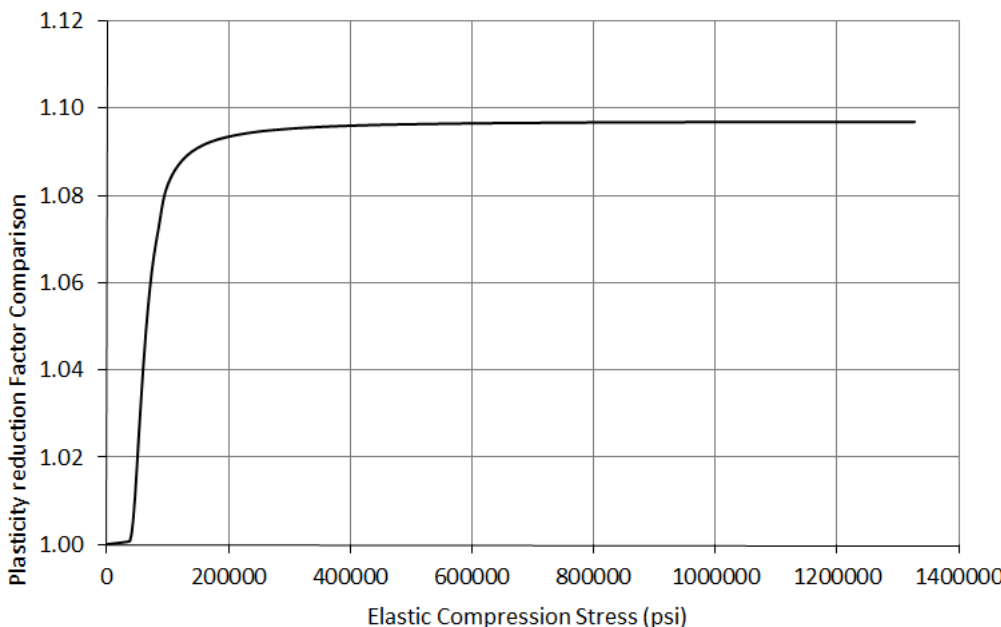


Figure 15.2.4-8: Difference Between Different Edge Fixity Conditions for Plasticity Correction Factors for a Typical Aluminum Material

There is only a small difference between the two factors (less than 10%). It is recommended that the plasticity correction factor for clamped panels is used for all panels as it provides a simpler, conservative solution.

Like the shear buckling allowable corrected for material plasticity, the plasticity correction factor for compression buckling can be used to produce a curve that relates the elastic buckling stress with the plastic buckling stress.

Once the graph has been plotted the elastic shear buckling allowable can be plotted on the x-axis, project upwards to the curve and read across to the Y-axis to give the compression buckling allowable corrected for plasticity.

Superimposing the simpler approach of limiting F_{cr} to F_{cy} over the Elastic vs Plastic shear buckling stress curve gives the following result:

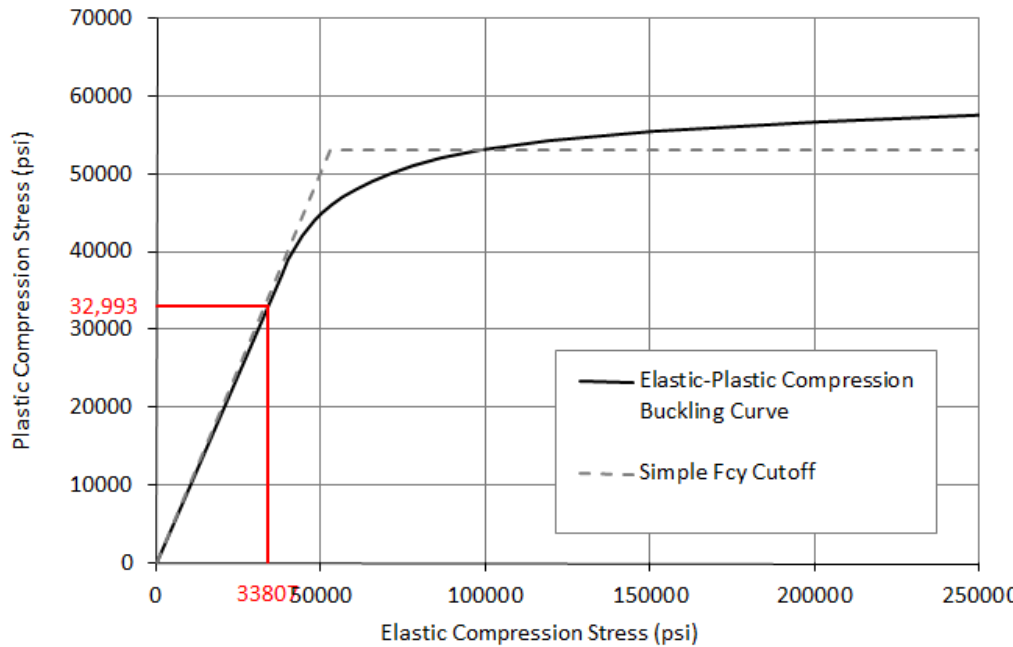


Figure 15.2.4-9: Elastic vs Plastic Compression Buckling Stress for Sample Material with Comparison to Simple Elastic and F_{cy} Cut off Value

For the sample material (and for most ductile materials) the simple approach does give a reasonable approximation to the correctly calculated plastic buckling allowable. A spreadsheet is available for this method at the link below:

ABBOTT AEROSPACE SEZC LTD
SPREADSHEETS
ABBOTTAEROSPACE.COM

AA-SM-007-023 Buckling of Flat Isotropic Plates - Plastic Compression Buckling

15.2.4.5. Effect of Central Hole on Panel Compression Buckling Allowable

In the process of writing this section many references were reviewed. The single best summary of results is contained in [\(NASA-TM-1998-206542, 1998\)](#). This paper is a summary of the results of a Finite Element study looking at the effect of circular and square holes on isotropic Panel buckling. Other references that are in general agreement include [\(NASA-TP-3024, 1990\)](#).

The figures in [\(NASA-TM-1998-206542, 1998\)](#) are given in terms of changes in absolute buckling values. These results have been reinterpreted to give a reduction factor for compression buckling factor k.

In the following figures the most onerous reduction from either the symmetric buckling or antisymmetric buckling modes have been used.

Note: The reduction factors are based on Figure 17 of [\(NASA-TM-1998-206542, 1998\)](#). This is reported as having 'free' edges – edges which are free to move in-plane. However, the results for a hole diameter of 0in agree with the results for a simply supported panel without a hole from table 4 of the same reference. This result also agrees with independent checking done for panels with edges restrained in translation and free in rotation during the compilation of this section. It is therefore assumed that the reference is in error and Figure 17 is representative of panels with a hole where the edges are restrained for in-plane translation.

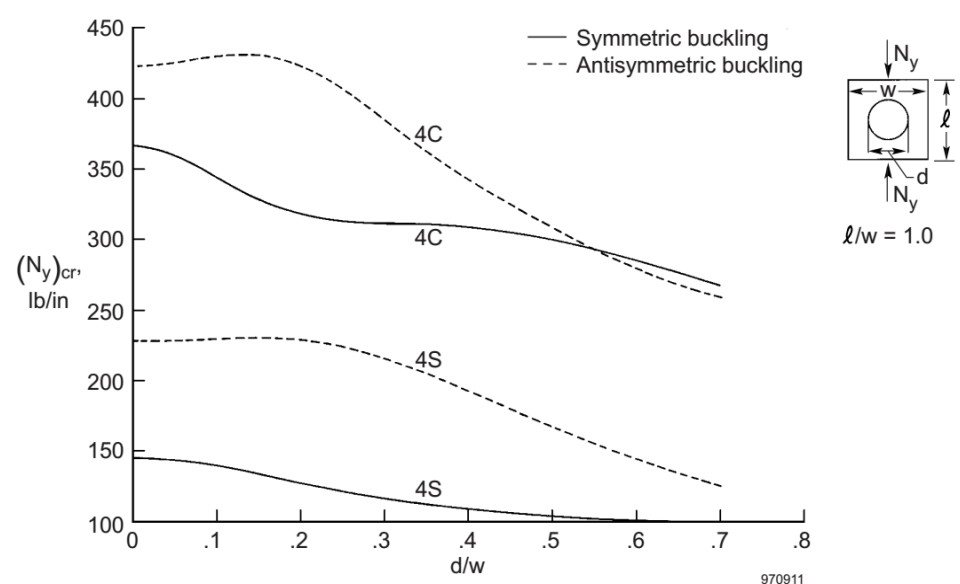


Figure 15.2.4-10: Reduction in Compression Buckling Allowable for Square Panels with Centrally Located Holes [\(NASA-TM-1998-206542, 1998\)](#)

It was found that the critical panel aspect ratio was 1:1 (square). As long as the panel is loaded in compression aligned with the long dimension, use of the square panel data is conservative.

This method is not applicable for panels loaded in compression across the short dimension.

As noted, the ratio of greatest reduction in buckling strength for each of the clamped and simply supported curves was calculated and plotted:

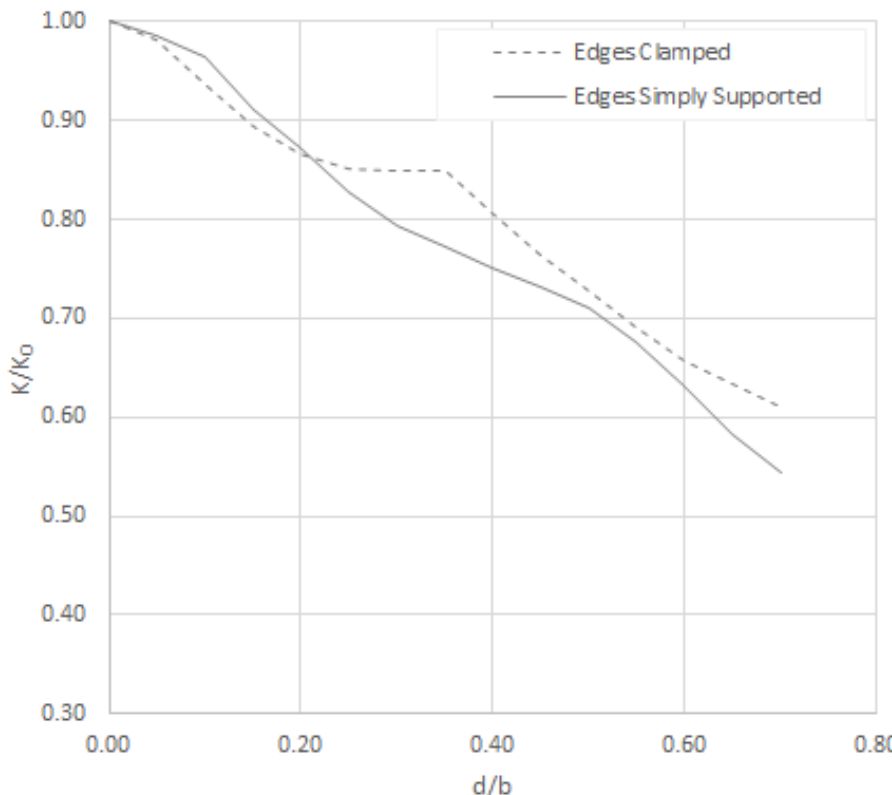


Figure 15.2.4-11: Ratio of Reduction in Compression Buckling Strength of Clamped and Simply Supported Square Panels with Varying Sizes of Central Hole

A simple conservative linear approximation can be used that is applicable to both simply supported and clamped panels.

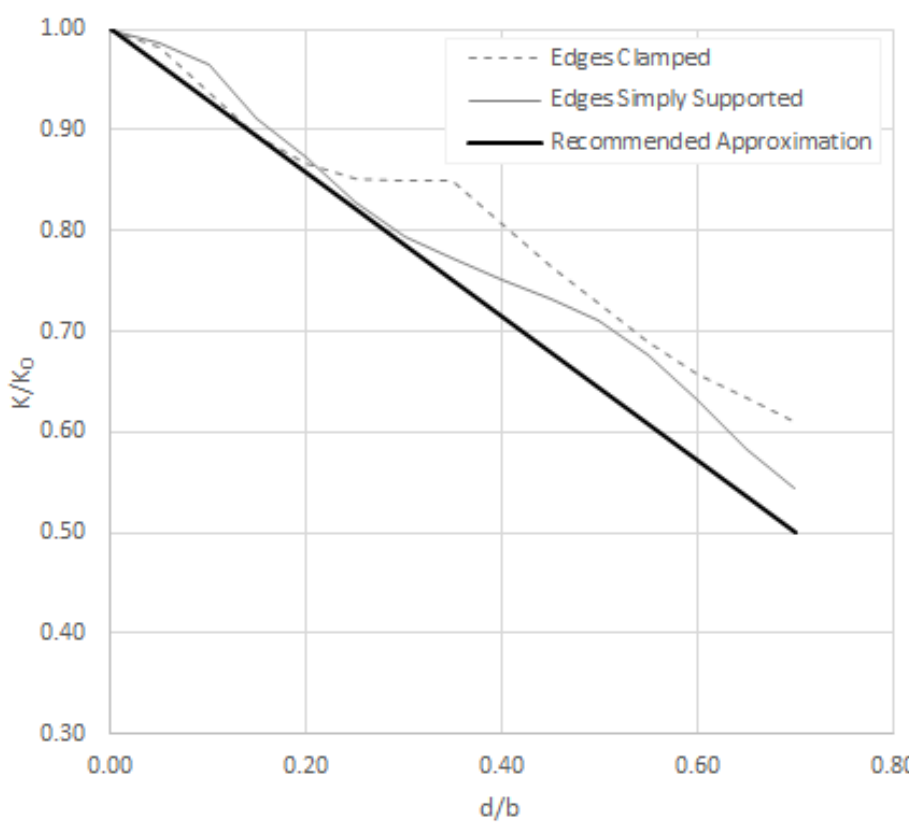


Figure 15.2.4-12: Ratio of Reduction in Compression Buckling Strength of Clamped and Simply Supported Square Panels with Varying Sizes of Central Hole – Simple Approximation

The equation for this linear approximation is:

$$\frac{K}{K_0} = -0.714 \cdot \frac{d}{b} + 1$$

A spreadsheet method is available at the link below:

ABBOTT AEROSPACE SEZC LTD
SPREADSHEETS
ABBOTTAEROSPACE.COM

AA-SM-007-024 Effect of Central Hole on Plate Compression Buckling Allowable

15.2.5. Interaction of Shear and Compression Buckling (Rectangular)

In considering a general method for the interaction of shear and compression buckling several parameters need to be reviewed or considered:

- 1) Will the same interaction hold for interaction of elastic and plastic buckling effects?
- 2) Will the same interaction hold for simply supported panel edges and clamped edges?
- 3) Will the same interaction hold for all panel aspect ratios?
- 4) Will the same interaction hold for flat and curved panels?
- 5) As the presence of tension assists resistance to shear buckling is there a way to account for the buckling interaction in the positive axial load domain as well?

(NACA-TN-3184, 1954) examines elastic vs plastic buckling for 'long' Panels:

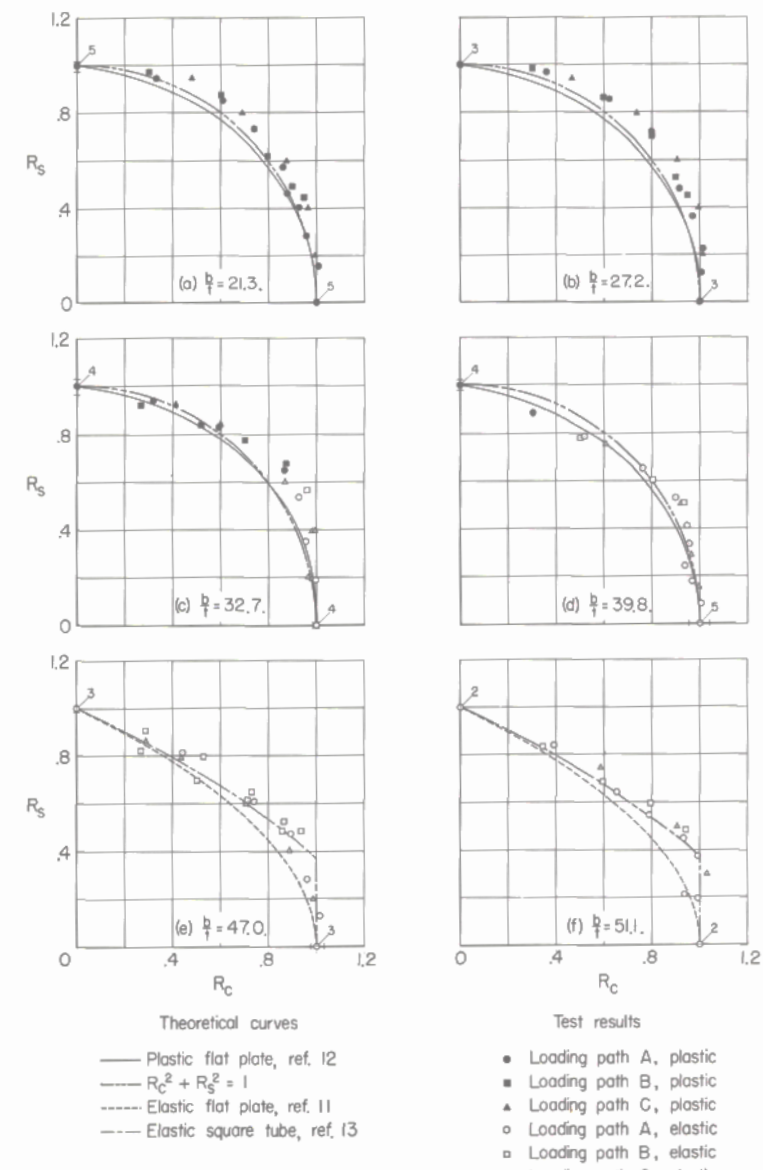


Figure 15.2.5-1: Interaction of Shear and Compression Elastic Buckling for a Long Panel (NACA-TN-3184, 1954)

[\(NACA-TN-3184, 1954\)](#) refers to the references [\(NACA-WR-3K13, 1943\)](#) and [\(NACA-TN-1990, 1949\)](#) which have the derivations for the elastic and plastic interaction curves. From a review of these references it can be seen that the elastic interaction is conservative compared to the plastic interaction. Therefore, the elastic interaction can be used for both elastic and plastic buckling interactions.

[\(NACA-TN-2661, 1952\)](#) figure 37 shows the interaction curve for a general curved panel:

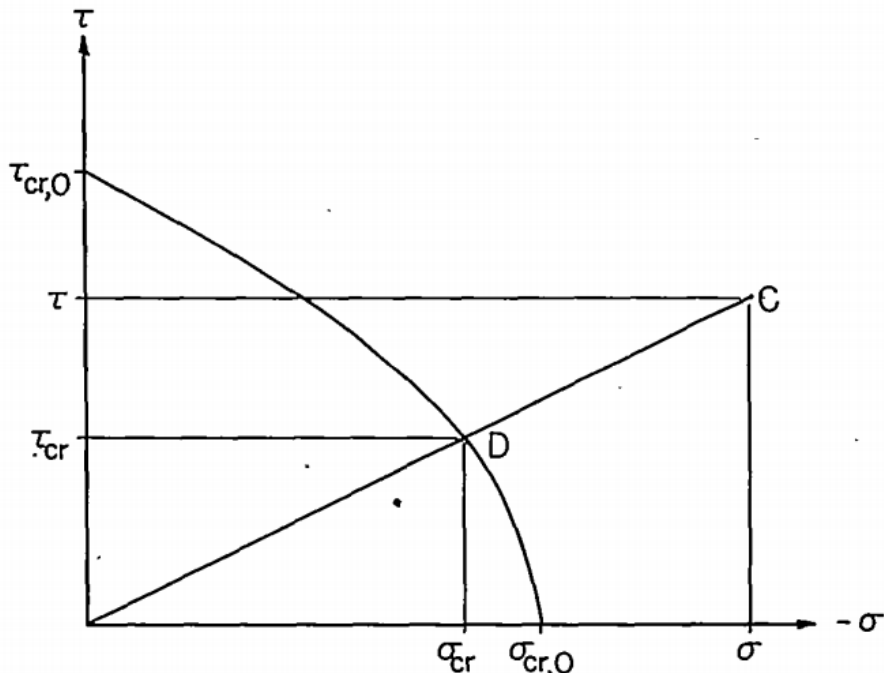


Figure 15.2.5-2: Interaction of Shear and Compression Buckling for a Curved Panel (NACA-TN-2661, 1952)

This interaction is described by the following equation:

$$\frac{\sigma_{cr}}{\sigma_{cr,0}} + \left(\frac{\tau_{cr}}{\tau_{cr,0}}\right)^2 = 1$$

As the methods in [\(NACA-TN-2661, 1952\)](#) are generally applicable to panels with all edge restraints it is reasonable to assume this interaction is likewise applicable. This interaction is in agreement with the interaction for a flat panel in [\(NACA-WR-3K13, 1943\)](#).

[\(NACA-TN-1223, 1947\)](#) gives both the extension into the positive axial load domain and a comparison of shear and compression buckling interaction for panels of different aspect ratios for panels loaded along the long edge and the short edge in compression.

A review of all of these references shows that for flat and curved panels, with simply supported or clamped edge restraint, for any aspect ratio, loaded in compression along the short or the long edge and applicable in the tension end load domain the following interaction is appropriate and/or conservative:

$$\frac{\sigma_{cr}}{\sigma_{cr,0}} + \left(\frac{\tau_{cr}}{\tau_{cr,0}}\right)^2 = 1$$

This function is graphed in the following figure:

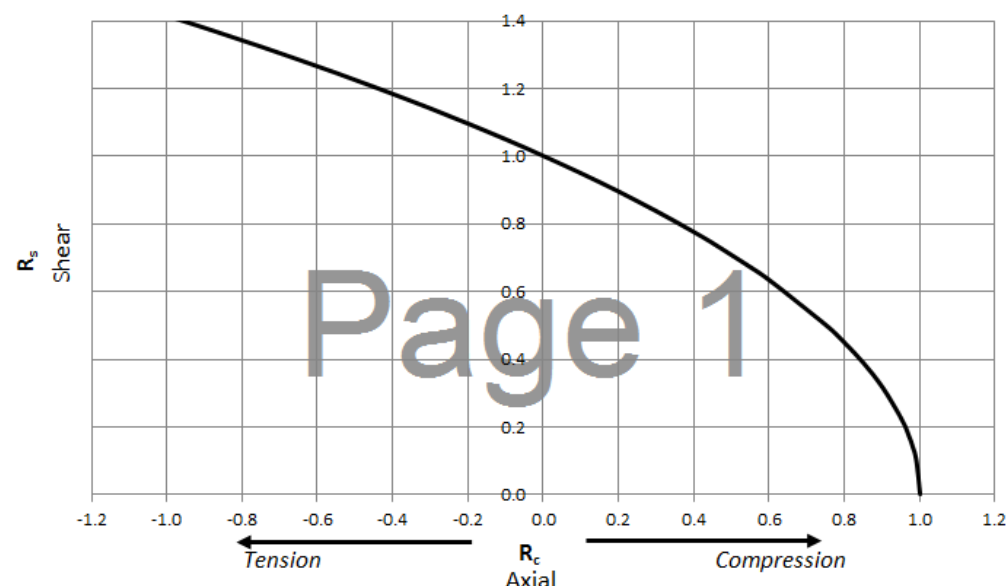


Figure 15.2.5-3: Interaction of Shear Buckling and Axial Loads (Positive Load is Compression Buckling)

A spreadsheet with this curve and a plotted margin of safety calculation is available here:

ABBOTT AEROSPACE SEZC LTD
SPREADSHEETS
 ABBOTTAEROSPACE.COM
 AA-SM-007-050 Interaction of Shear and Compression Buckling

ADVERT: TECHNICAL LIBRARY

TECHNICAL LIBRARY

SEE MORE

PUBLIC DOMAIN
 TECHNICAL DATA



We host hundreds of NASA
 research papers and books

ABBOTT
 AEROSPACE
 SEZC LTD

15.2.6. Flange Compression Buckling

Flange compression buckling is a subset of compression buckling. The form of the physical detail is different and there are two other important differences.

- 1) Generally, flanges are not considered to carry shear and so the interaction of shear and compression on flanges is usually not considered.
- 2) Because flanges are usually relatively narrow there exist no methods for the effect of a (non-fastener) hole on the flange buckling stress. A hole in a flange would usually take up much of the flange cross section and render the flange ineffective as a structural detail.

15.2.6.1. Flange Compression Buckling Allowable Stress

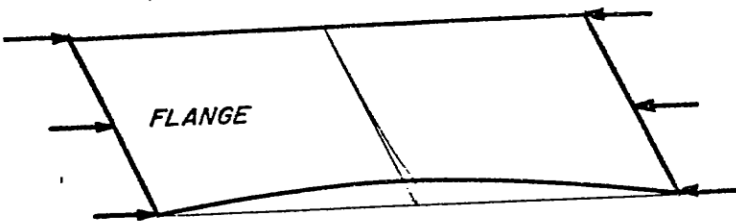


Figure 15.2.6-1: Definition of Flange Structural Detail [\(NACA-TN-3781, 1957\)](#)

The simplest approach to flange compression buckling and the approach that is commonly used for initial sizing is to assume that $\eta = 1$ and the panel is simply supported:

$$F_{cr} = k_{ss} \cdot \frac{\pi^2 \cdot E}{12 \cdot (1 - \nu_e^2)} \left(\frac{t}{b}\right)^2$$

The k_{ss} for a flange of infinite length can be assumed to be 0.407 (Ref Figure 15.2.6-2). Therefore, for a simple first check the following expression can be used:

$$F_{cr} = 0.407 \cdot \frac{\pi^2 \cdot E}{12 \cdot (1 - \nu_e^2)} \left(\frac{t}{b}\right)^2$$

For finite length flanges the following approach can be used. The first figure is from [\(NACA-TN-3781, 1957\)](#) and gives the buckling coefficients for flanges considering all edge conditions:

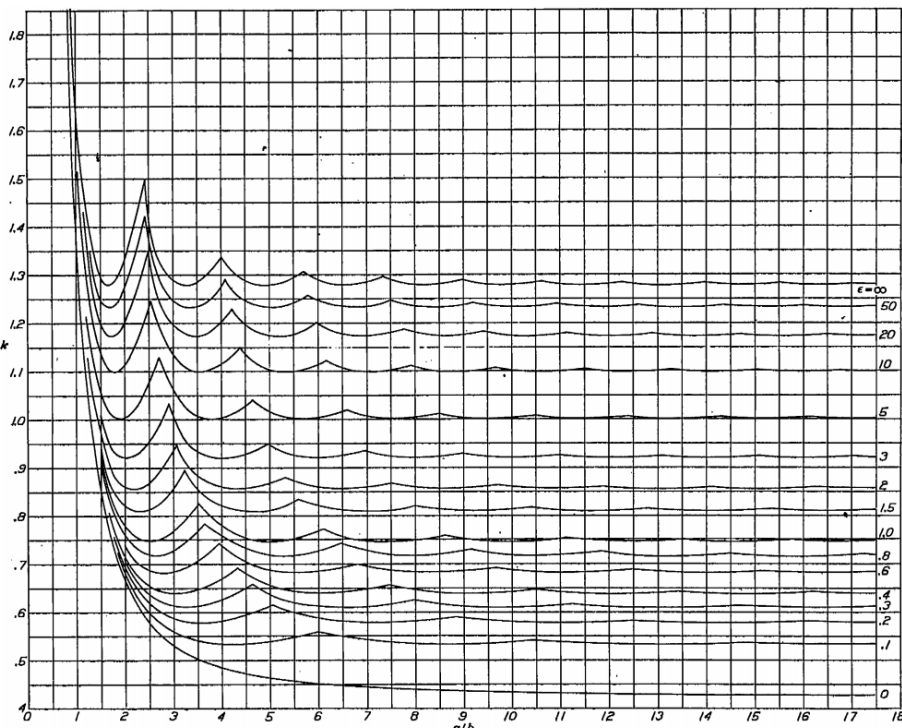


Figure 15.2.6-2: Compressive Buckling Stress Coefficient of Flanges as a function of a/b for various amounts of edge rotational restraint [\(NACA-Report-734\)](#)

The full expression for the flange compression buckling coefficient is given by the following expression [\(NACA-Report-734\)](#) equation B-17:

$$k = \frac{2}{\pi^2} \cdot \left\{ \frac{1 - \mu + \frac{1}{6} \cdot \left(\frac{\pi \cdot b}{\lambda}\right)^2 + \frac{\epsilon}{2} \cdot \left[\frac{c_1}{2} \cdot \left(\frac{\pi \cdot b}{\lambda}\right)^2 + c_2 - \mu \cdot c_3\right] + \frac{\epsilon^2}{4} \cdot \left[\frac{c_4}{2} \cdot \left(\frac{\pi \cdot b}{\lambda}\right)^2 + \frac{c_5}{2 \cdot \left(\frac{\pi \cdot b}{\lambda}\right)^2} + c_6 - \mu \cdot c_7\right] + \frac{\epsilon}{2 \cdot \left(\frac{\pi \cdot b}{\lambda}\right)^2}}{\frac{1}{3} + \frac{c_8 \cdot \epsilon}{2 \cdot a_3} + \frac{c_9 \cdot \epsilon^2}{4 \cdot a_3^2}} \right\}$$

The coefficients are defined in the source reference.

This is plotted and shown on the next page compared to the simple coefficient expressions shown below.

The flange compression buckling coefficient for a simply supported flange can be approximated by the following simple expressions:

$$k_{ss} = 0.456 + \left(\frac{b}{a}\right)^2$$

[\(NACA-TN-3781, 1957\)](#) gives the following expression for the flange buckling coefficient for a simply supported edge:

$$k_{ss} = \left(\frac{6}{\pi^2}\right) \cdot \left\{ (1 - \nu_e) + \frac{\left(\pi \cdot b / \lambda\right)^2}{6} \right\}$$

Where λ = The buckle half wave length, can be set to 1 for first buckling mode.

The flange compression buckling coefficient for a finite length simply supported flange can be found using Figure 15.2.6-3 below:

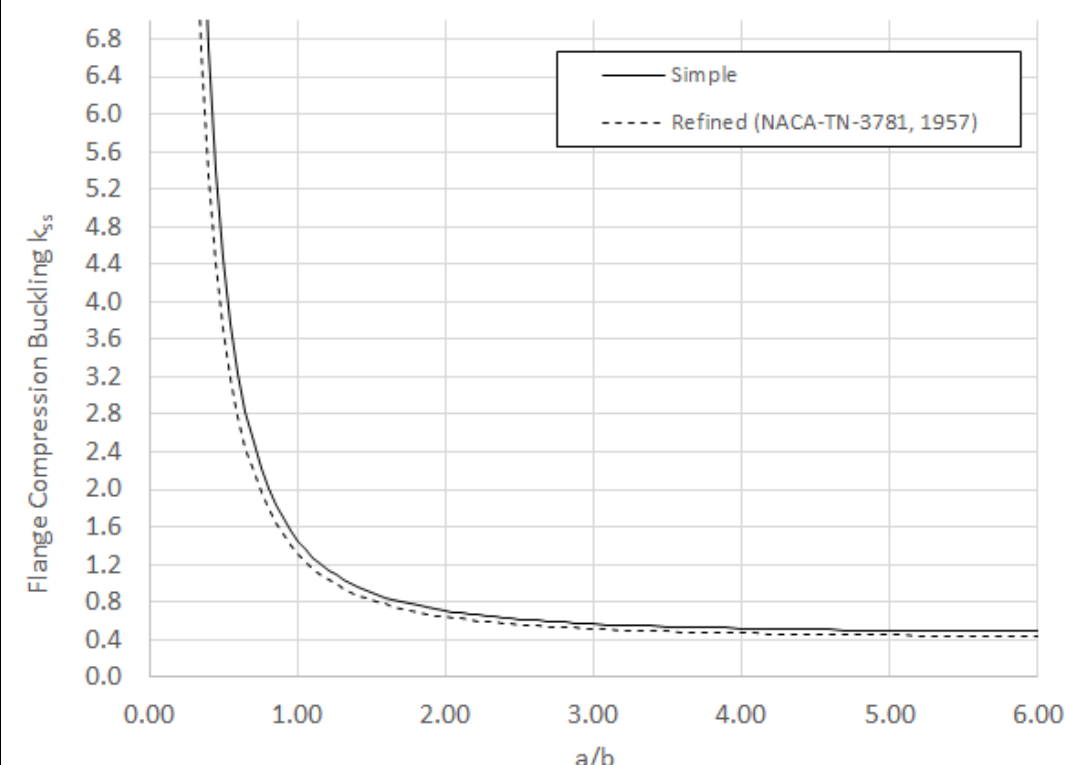


Figure 15.2.6-3: Flange Compression Buckling Coefficient – Simply Supported

Comparison of the simple expressions for a simply supported flange and the general expression per [\(NACA-Report-734\)](#) equation B-17 is shown on the following figure:

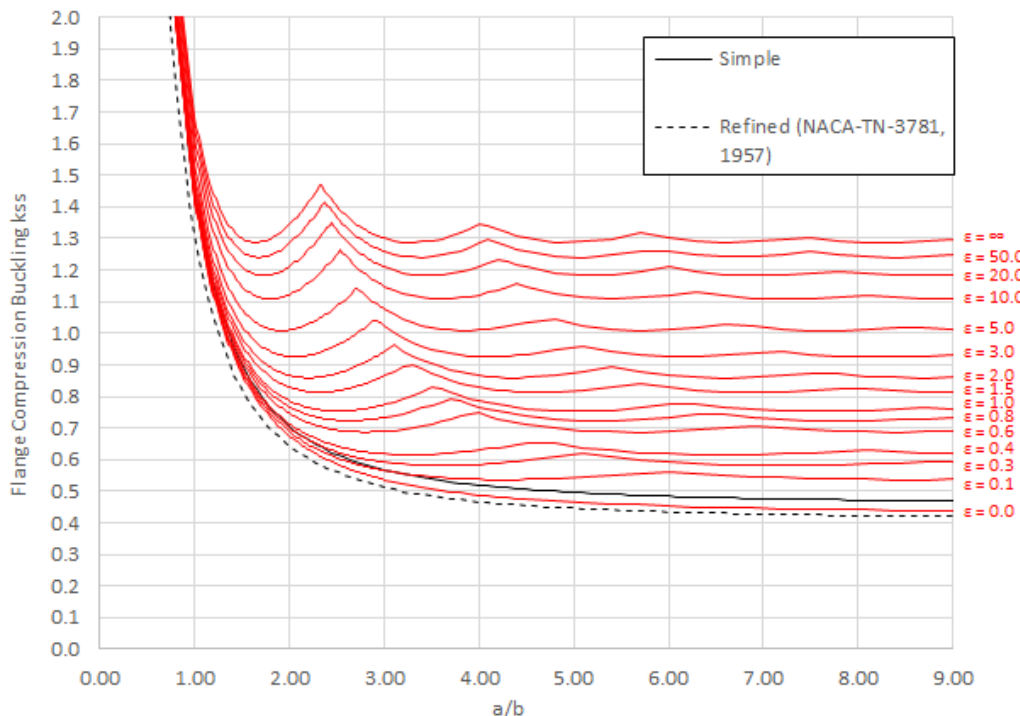


Figure 15.2.6-4: Flange Compression Buckling Coefficient – Comparison of Simple and General Method

The flange compression buckling coefficients for a simply supported edge is calculated in the spreadsheet at the link below:



AA-SM-007-093 Mathematical Derivation of Flange Compression Buckling Coefficients

The refined simple method gives, presumably, a more accurate and conservative approach that is asymptotic to .407. This approximation will be used.

The simple approach to flange compression buckling is given in this spreadsheet: Using this simple approach if F_{cr} exceeds F_{cy} then limit F_{cr} to F_{cy} .

A spreadsheet for the simple flange buckling method is available at the link below:



AA-SM-007-031 Buckling of Flat Isotropic Flanges - Compression Buckling - Simple

The modification for the buckling analysis is the same approach as defined for compression panel in section 15.2.4.3. The change in k for flange buckling for differing levels of edge restraint is shown below:

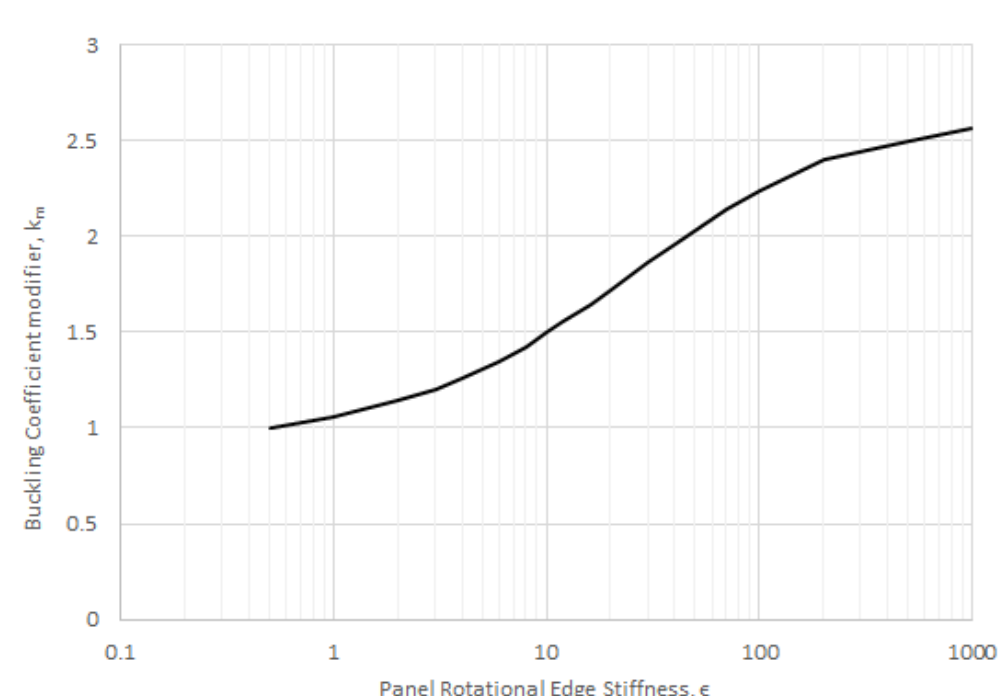


Figure 15.2.6-5: The relationship between k and ε – Flange Buckling

A spreadsheet for the flange buckling method for varying amounts of edge rotational restraint is available at the link below:



AA-SM-007-032 Buckling of Flat Isotropic Flanges - Compression Buckling

15.2.6.2. Flange Compression Buckling Allowable Stress with Full Elasto-Plastic Material Data

If the calculated flange compression buckling stress is approaching the compression yield stress (F_{cy}) of the material the elastic flange compression buckling allowable could be optimistic. If a more nuanced approach than limiting the buckling stress to F_{cy} is required, the compression buckling allowable should be modified using the plasticity correction factor η .

From [\(NACA-TN-3781, 1957\)](#) for compression buckling the plasticity correction factor for a simply supported flange is:

$$\eta_{ss} = \left[\left(\frac{E_s}{E} \right) \cdot \frac{(1 - \nu_e^2)}{(1 - \nu^2)} \right]$$

the plasticity correction factor for a long, clamped flange is:

$$\eta_{cl} = \left[\left(\frac{E_s}{E} \right) \cdot \frac{(1 - \nu_e^2)}{(1 - \nu^2)} \right] \cdot \left\{ 0.330 + 0.335 \cdot \sqrt{\left[1 + \left(\frac{3 \cdot E_t}{E_s} \right) \right]} \right\}$$

Where:

ν_e Poisson's ratio in the elastic range

ν Poisson's ratio at any point on the material stress strain curve, given by the expression:

$$\nu = 0.5 - (0.5 - \nu_e) \cdot \left(\frac{E_s}{E} \right)$$

E_t Tangent modulus, psi (Section 4.2.2.1)

E_s Secant modulus, psi (Section 4.2.2.1)
 E Young's modulus, psi

Plotting these two plasticity correction factors for a typical aluminum gives the following result:

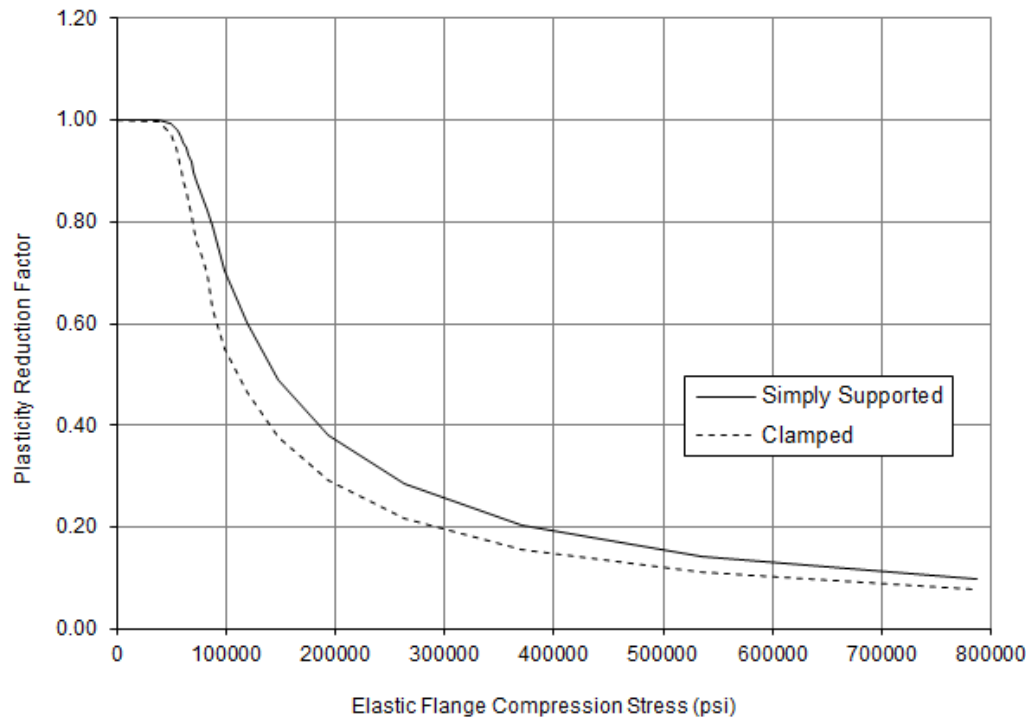


Figure 15.2.6-6: Plasticity Correction Factors for Compression buckling for Typical Aluminum Material

This shows that the reduction factor for a clamped flange is greater than for a simply supported flange. It is recommended that the plasticity reduction factor for the clamped flange is used for all edge conditions.

Superimposing the simpler approach of limiting F_{cr} to F_{cy} over the Elastic vs Plastic shear buckling stress curve for a clamped flange gives the following result:

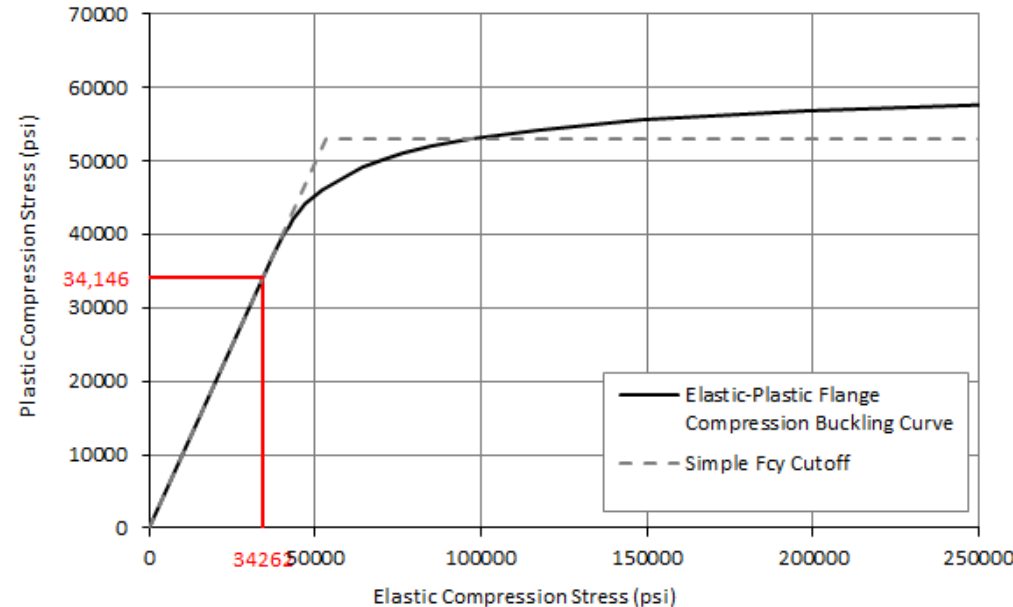


Figure 15.2.6-7: Elastic vs Plastic Compression Flange Buckling Stress for Sample Material with Comparison to Simple Elastic and F_{cy} Cut off Value

Similar to shear and compression buckling for panels, for the sample material (and for most ductile materials) the simple approach does give a reasonable approximation to the correctly calculated flange plastic buckling allowable.

A spreadsheet for flange buckling that incorporates varying edge rotational restraint and elasto-plastic material behavior is available at the link below:

ABBOTT AEROSPACE SEZC LTD
SPREADSHEETS
ABBOTTAEROSPACE.COM

AA-SM-007-033 Buckling of Flat Isotropic Flange - Plastic Compression Buckling

ADVERT: ENGINEERING SERVICES
LOADS ANALYSIS
ENGINEERING SERVICES

Airframe Loads

CONTACT US

8.3 Control Surface Flight Loading
8.3.9 Elevator Surface and Tab Loads
Elevator Trailing Edge Up, Tab Trailing Edge Up

LIMIT LEVEL

T ABOUT Y AXIS - LIMIT LEVEL

Aircraft Balance
Principal External Load Balance

Sum of Forces and Moments
 $F_x = F_{x0} + \rho V^2 S C_D + P_{atm} A_D$
 $M_y = M_{y0} + \rho V^2 S C_M + P_{atm} A_M$
 $M_z = M_{z0} + \rho V^2 S C_M + P_{atm} A_M$

PLUGGAGE STATION 37
connected vertical tail method

Wind DIRECTION

Wind Zero Wind Limit Wind Datum

Wind Angle of Attack
 $\alpha_w = \alpha_a + \alpha_r$
 $\alpha_a = 0^\circ$ Wind angle of incidence
 $\alpha_r = 1.5^\circ$ Engine angle of attack
 $\alpha_w = 1.5^\circ$ Wind angle of attack
 $\alpha_w = \alpha_r = 4.85^\circ$

Ref Section 2.2
Ref Section 2.2
Ref Section 2.6
Ref Section 2.6

15.2.7. Bending Buckling

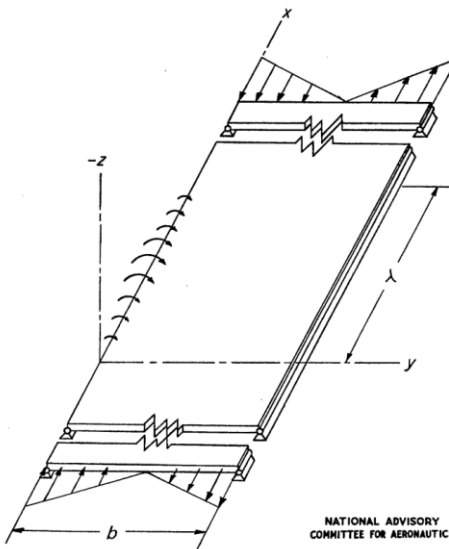


Figure 15.2.7-1: Definition of Flange Structural Detail (NACA-TN-1323, 1947)

The simplest approach to panel bending buckling and the approach that is commonly used for initial sizing is to assume that $\eta = 1$ and the panel is simply supported.

$$F_{cr} = k_{ss} \cdot \frac{\pi^2 \cdot E}{12 \cdot (1 - \nu_e^2)} \left(\frac{t}{b}\right)^2$$

The k_{ss} for a panel of infinite length can be assumed to be 24 (Ref Figure 15.2.7-2). Therefore, for a simple first check the following expression can be used.

$$F_{cr} = 24 \cdot \frac{\pi^2 \cdot E}{12 \cdot (1 - \nu_e^2)} \left(\frac{t}{b}\right)^2$$

In general, the buckling 'k' value for panel bending buckling is approximately 6 times the panel compression buckling coefficient. The k value is given by the figure below:

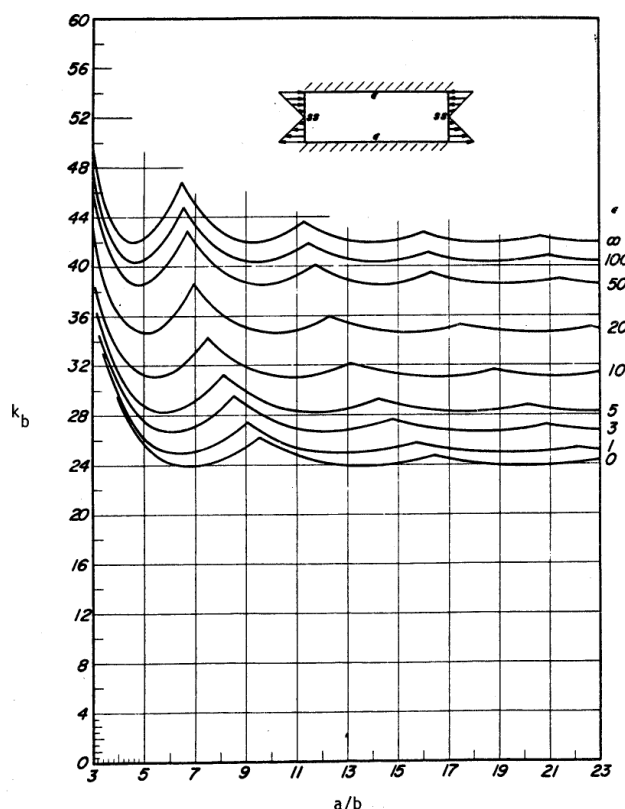


Figure 15.2.7-2: Bending Buckling Stress Coefficient of a Panel as a Function of a/b for Various Amounts of Edge Rotational Restraint (AFFDL-TR-69-42, 1986)

The bending buckling coefficient for a simply supported Panel can be approximated by the following expression:

$$k_{ss} = 24 + \left(\frac{1}{0.05 \cdot \frac{a}{b}} - 2 \right)^3 \cdot 0.175$$

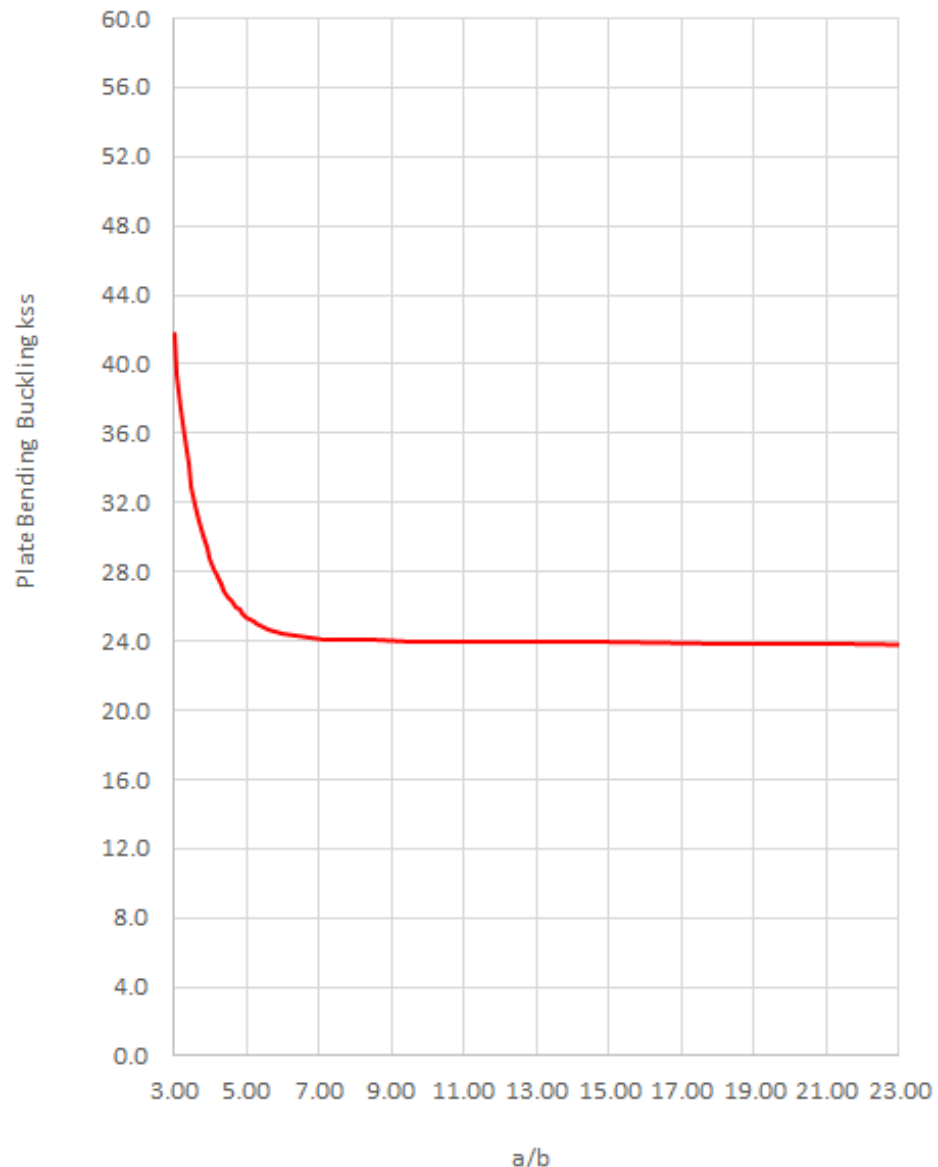


Figure 15.2.7-3: Approximation for Bending Buckling Stress Coefficient of a Panel as a Function of a/b

The flange compression buckling coefficients for a simply supported edge is shown in the spreadsheet:

ABBOTT AEROSPACE SEZC LTD
SPREADSHEETS
ABBOTTAEROSPACE.COM
AA-SM-007-094 Mathematical Derivation of Bending Buckling Coefficients

The simple approach to panel bending buckling is given in this spreadsheet: Using this simple approach if F_{cr} exceeds F_{cy} then limit F_{cr} to F_{cy} .

ABBOTT AEROSPACE SEZC LTD
SPREADSHEETS
ABBOTTAEROSPACE.COM
AA-SM-007-041 Buckling of Flat Isotropic Plates - Bending Buckling - Simple

15.2.7.1. Bending Buckling Allowable Stress with Varying Panel Rotational Edge Fixity

The effect of differing levels of edge restraint on the buckling allowable is proportionally the same as that shown in Figure 15.2.4-6 and section 15.2.4.3 for the compression panel. This relationship will be adapted for bending buckling. This approach is given in a spreadsheet form at the link below:



AA-SM-007-042 Buckling of Flat Isotropic Plates - Bending Buckling

15.2.7.2. Bending Buckling Allowable Stress with Full Elasto-Plastic Material Data

The plasticity reduction factor for panels in bending buckling can be assumed to be the same as for the flange compression buckling allowable as recommended in [\(NACA-TN-3781, 1957\)](#). These plasticity reduction factors are defined in section 15.2.6.2. The spreadsheet for this method is given at the link below:



AA-SM-007-043 Buckling of Flat Isotropic Plates - Plastic Bending Buckling

15.2.8. Buckling of Triangular Panels

15.2.8.1. Compression Buckling of Triangular Panels

This method is briefly covered in the excellent general reference: [\(NACA-TN-3781, 1957\)](#). There is little information given but it is worth including in this text.

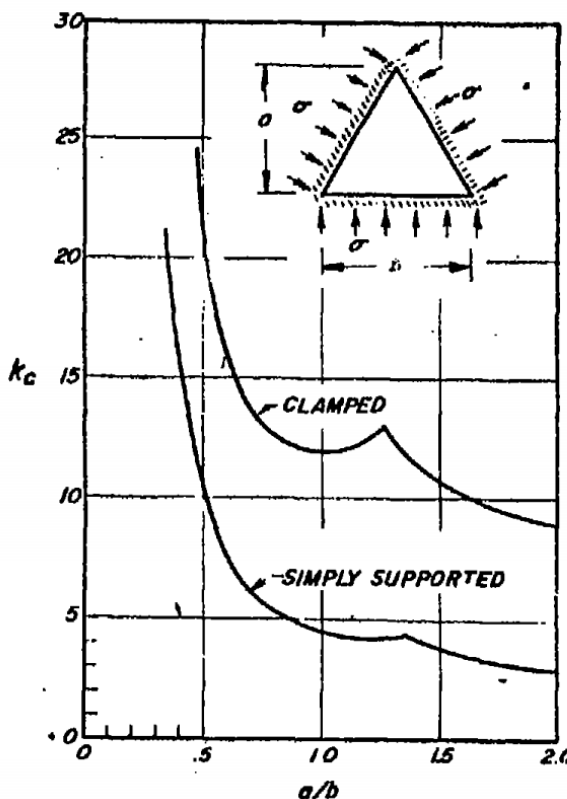


Figure 15.2.8-1: Compression Buckling Coefficient for Isosceles Triangular Panel in Compression. [\(NACA-TN-3781, 1957\)](#)

General curve fits have been done for the curves in Figure 15.2.8-1.

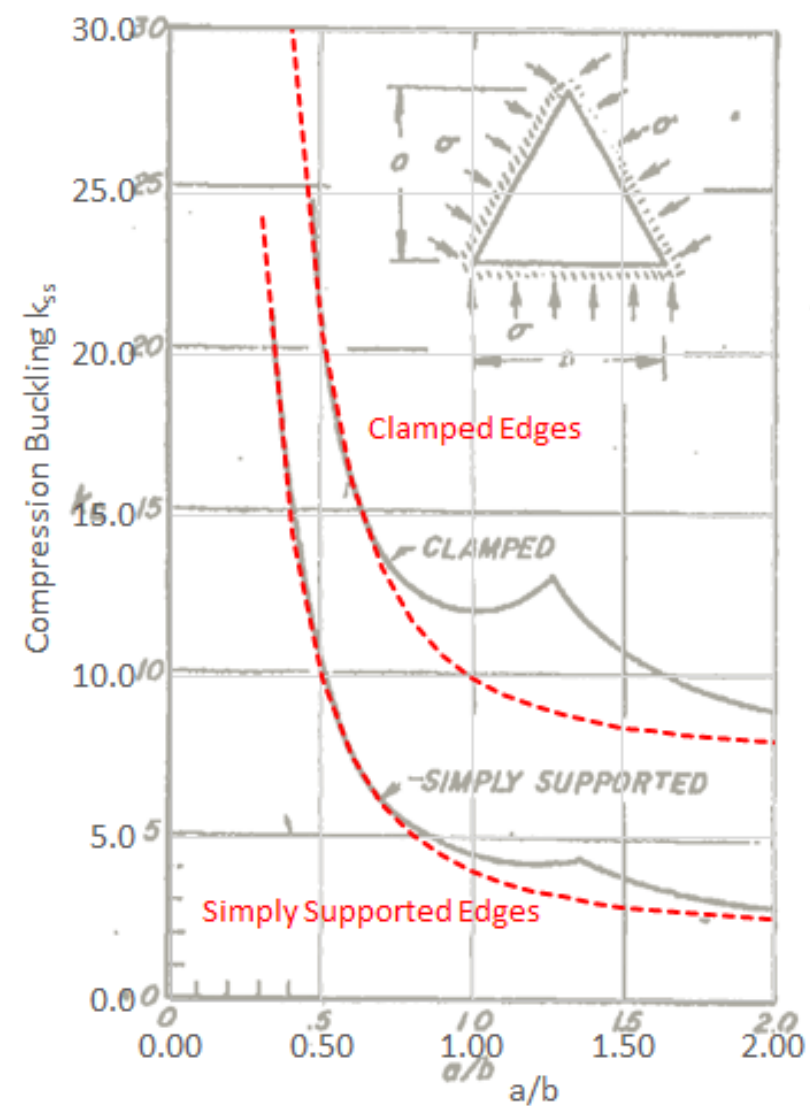


Figure 15.2.8-2: Compression Buckling Coefficient for Isosceles Triangular Panel in Compression – Approximate Curves

For the simply supported triangular panel the following expression can be used to calculate k:

$$k_{ss} = 2.0 + \frac{2.0}{(a/b)^2}$$

And for the clamped edge condition the following expression can be used:

$$k_{ff} = 7.5 + \frac{2.5}{(a/b)^{2.4}}$$

These approximations are available in this spreadsheet:



AA-SM-007-096 Mathematical Derivation of Triangular Plate Compression Buckling Coefficients

The values for k can be used in the classic buckling expression where b is the 'base' of the isosceles triangle:

$$F_{cr} = k \cdot \frac{\pi^2 \cdot E}{12 \cdot (1 - \nu_e^2)} \left(\frac{t}{b}\right)^2$$

There is no information available at this time on the plastic buckling of triangular panels in compression. It is advised to account for panel material plasticity, if F_{cr} exceeds F_{cy} then limit F_{cr} to F_{cy} . The buckling compression buckling analysis spreadsheet link is below:



AA-SM-007-052 Buckling of Flat Isotropic Plates - Compression Buckling of Triangular Panel

15.2.8.2. Shear Buckling of Triangular Panels

As before, this method is briefly covered in the excellent general reference (NACA-TN-3781, 1957):

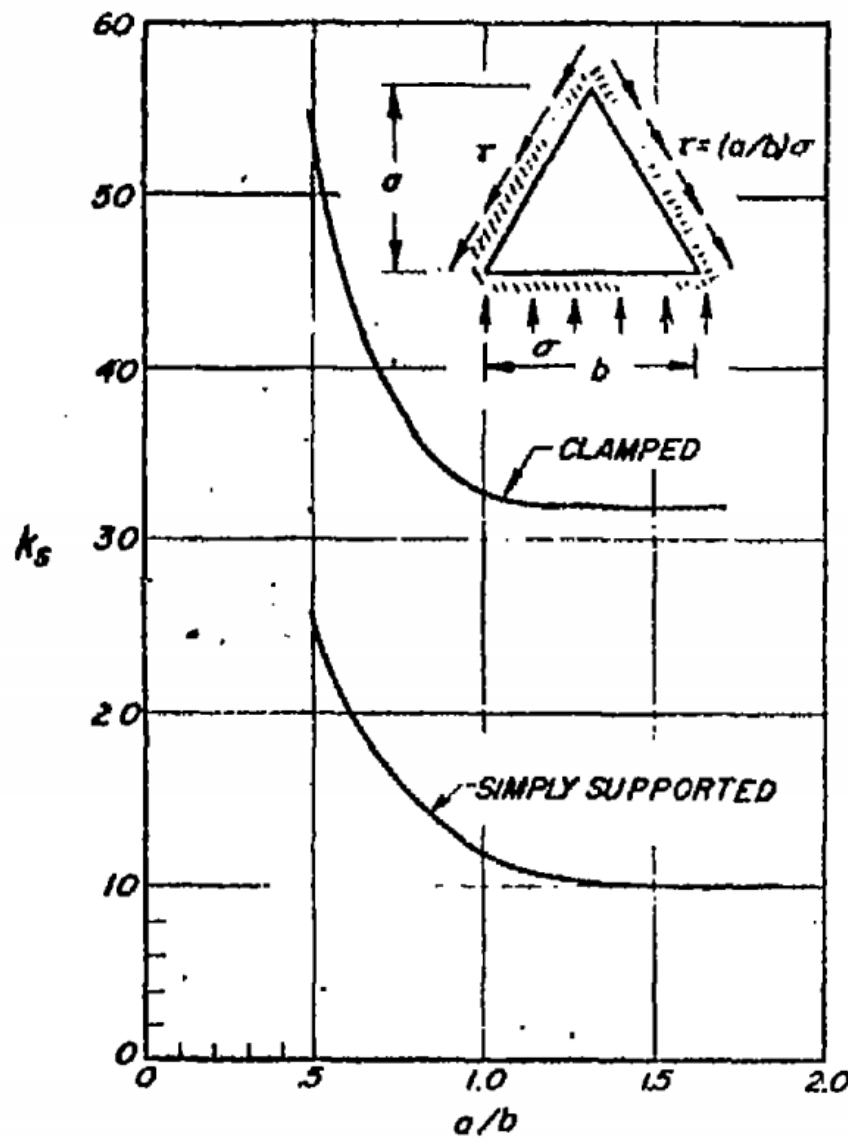


Figure 15.2.8-3: Shear Buckling Coefficient for Isosceles Triangular Panel in Compression. [\(NACA-TN-3781, 1957\)](#)

General curve fits have been done for the curves in Figure 15.2.8-3:

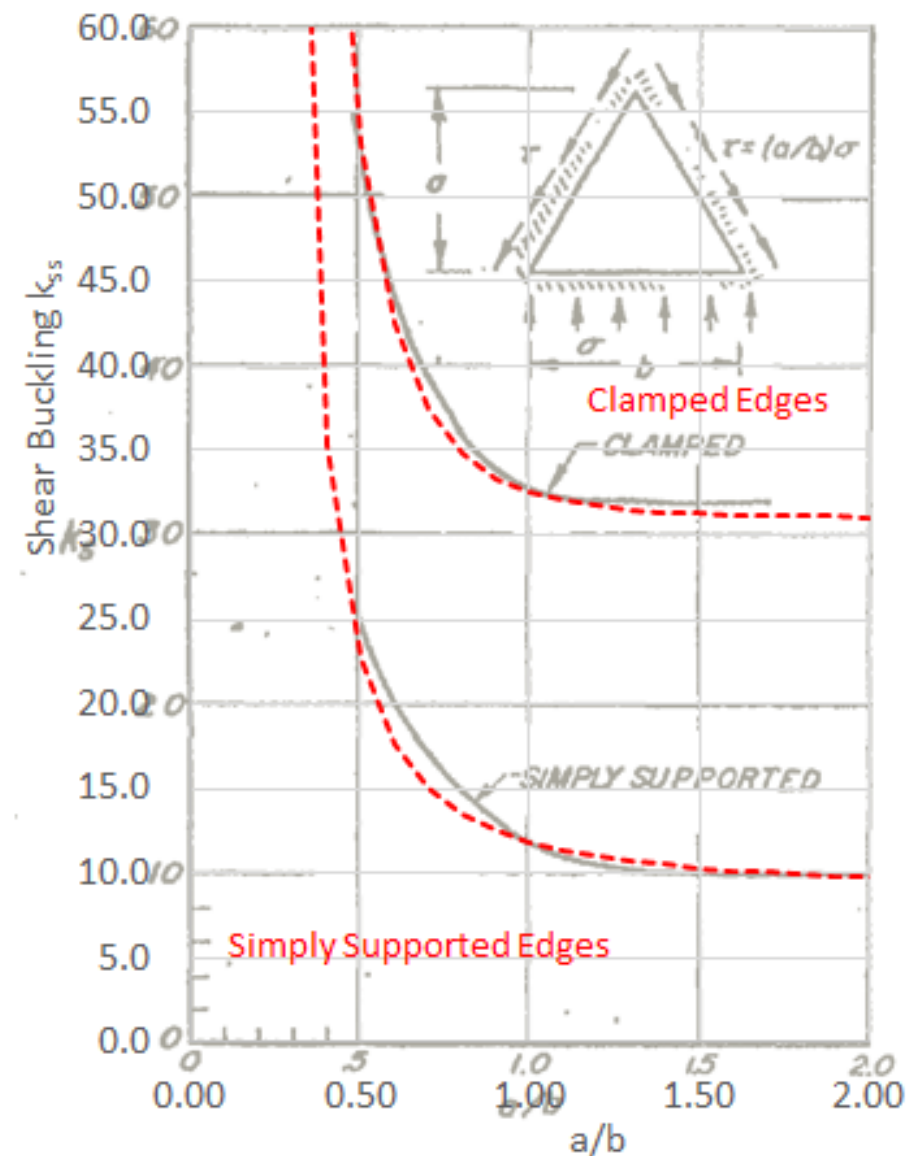


Figure 15.2.8-4: Shear Buckling Coefficient for Isosceles Triangular Panel in Compression – Approximate Curves.

For the simply supported triangular panel the following expression can be used to calculate k :

$$k_{ss} = 9.0 + \frac{2.0}{(a/b - 0.2)^{1.6}}$$

And for the clamped edge condition the following expression can be used:

$$k_{ff} = 31 + \frac{4.0}{(a/b - 0.21)^5}$$

These approximations are available in this spreadsheet:



AA-SM-007-095 Mathematical Derivation of Triangular Plate Shear Buckling Coefficients

The values for k can be used in the classic buckling expression where b is the 'base' of the isosceles triangle.

$$F_{cr} = k \cdot \frac{\pi^2 \cdot E}{12 \cdot (1 - \nu_e^2)} \left(\frac{t}{b} \right)^2$$

This method is available in a spreadsheet at the link below:



AA-SM-007-051 Buckling of Flat Isotropic Plates - Shear Buckling of Triangular Panel

15.2.9. Reduction Factors Due to Cladding

(NACA-TN-3781, 1957) is the best available reference (again) and gives a simple rational method for how to account for the presence of cladding.

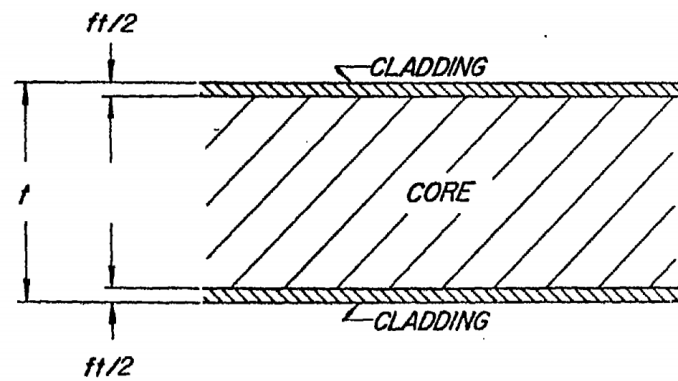


Figure 15.2.9-1: Cross Section of a Clad Plate (NACA-TN-3781, 1957)

The reducing in buckling due to the presence of cladding depends on two ratios:

$$\beta = \frac{\sigma_{cl}}{\sigma_{cr}}$$

Where:

σ_{cl} Yield stress of the cladding material, psi
 σ_{cr} Buckling stress of the panel, psi

And:

$$f = \frac{t_{cl}}{t_{pl}}$$

Where:

t_{cl} Total thickness of the cladding, in
 t_{pl} Total thickness of the clad plate, in

For different loading conditions and stress level the following terms apply.

Where:

σ_{pl} Yield stress of the clad plate material, psi

| Loading | $\sigma_{cl} < \sigma_{cr} < \sigma_{pl}$ | $\sigma_{cr} > \sigma_{pl}$ |
|------------------------------|---|-----------------------------|
| Short plate columns | $\frac{1 + (3\beta f / 4)}{1 + 3f}$ | $\frac{1}{1 + 3f}$ |
| Long plate columns | $\frac{1}{1 + 3f}$ | $\frac{1}{1 + 3f}$ |
| Compression and shear panels | $\frac{1 + 3\beta f}{1 + 3f}$ | $\frac{1}{1 + 3f}$ |

Figure 15.2.9-2: Reduction Factors Due to Cladding (NACA-TN-3781, 1957)

| Material designation | Cladding material | Total plate thickness, in. | Total cladding thickness, f, in. |
|----------------------|-------------------|----------------------------|----------------------------------|
| Alclad 2014 | 6053 | <0.040 ≥0.040 | 0.25 0.10 |
| Alclad 2024 | 1230 | <0.064 ≥0.064 | 0.10 0.05 |
| Alclad 7075 | 7072 | All thicknesses | 0.08 |

This label is incorrect, should read "Total Cladding Thickness, Fraction of Total Clad Plate Thickness"

Figure 15.2.9-3: Cladding of Thicknesses (NACA-TN-3781, 1957)

This method is available in this spreadsheet:



AA-SM-007-060 Buckling Reduction Factors due to Cladding

Note that in some circumstances, particularly for panels with low buckling allowables, a cladding reduction factor of greater than 1.00 can occur. In this circumstance a maximum value of 1.00 should be used.



15.2.10. Panel and Flange Buckling Summary

15.2.10.1. Rectangular Panel Buckling Coefficients

(NACA-TN-3781, 1957) gives the following summary for minimum buckling coefficient figures (infinitely long Panels):

| Loading | Edge support | Coefficient |
|-----------------|-----------------------------|-------------------------------------|
| Compression | SS on all edges | $k_c = 4.0$ NACA Rep. 733 |
| | C on all edges | $k_c = 6.98$ (ref. 29) |
| | SS on $y = 0, y = a, x = 0$ | |
| | F on $x = b$ | $k_c = 0.43$ NACA Rep. 734 (ref. 8) |
| | C on $y = 0, y = a, x = 0$ | |
| | F on $x = b$ | $k_c = 1.28$ |
| Shear | SS on all edges | $k_s = 5.35$ NACA TN 1222 (ref. 35) |
| | C on all edges | $k_s = 8.98$ NACA TN 1223 (ref. 43) |
| Bending | SS on all edges | $k_b = 23.9$ NACA TN 1323 (ref. 37) |
| | C on all edges | $k_b = 41.8$ |

Figure 15.2.10-1: Rectangular Panel and Flange Buckling Stress Coefficient Summary (NACA-TN-3781, 1957)

15.2.10.2. Rectangular Panel Plasticity Correction Factors

And the following summary for plasticity reduction factors:

$$\left[j = \frac{(E_s/E)(1 - v_e^2)}{(1 - v^2)} \right]$$

| Loading | Structure | η/j |
|-------------|---|--|
| Compression | Long flange, one unloaded edge simply supported | 1 |
| | Long flange, one unloaded edge clamped | $0.330 + 0.335 [1 + (3E_t/E_s)]^{1/2}$ |
| | Long plate, both unloaded edges simply supported | $0.500 + 0.250 [1 + (3E_t/E_s)]^{1/2}$ |
| | Long plate, both unloaded edges clamped | $0.352 + 0.324 [1 + (3E_t/E_s)]^{1/2}$ |
| | Short plate loaded as a column ($L/b \ll 1$) | $0.250 [1 + (3E_t/E_s)]$ |
| | Square plate loaded as a column ($L/b = 1$) | $0.114 + 0.886 (E_t/E_s)$ |
| | Long column ($L/b \gg 1$) | E_t/E_s |
| Shear | Rectangular plate, all edges elastically restrained | $0.83 + 0.17 (E_t/E_s)$ |

Figure 15.2.10-2: Rectangular Panel and Flange Buckling Plasticity Correction Factors (NACA-TN-3781, 1957)

15.2.10.3. Rectangular Panel Cladding Correction Factors

And the following summary for cladding reduction factors:

| Loading | $\sigma_{cl} < \sigma_{cr} < \sigma_{pl}$ | $\sigma_{cr} > \sigma_{pl}$ |
|------------------------------|---|-----------------------------|
| Short plate columns | $\frac{1 + (3\beta f/4)}{1 + 3f}$ | $\frac{1}{1 + 3f}$ |
| Long plate columns | $\frac{1}{1 + 3f}$ | $\frac{1}{1 + 3f}$ |
| Compression and shear panels | $\frac{1 + 3\beta f}{1 + 3f}$ | $\frac{1}{1 + 3f}$ |

Figure 15.2.10-3: Rectangular Panel and Flange Buckling Cladding Correction Factors (NACA-TN-3781, 1957)

| Material designation | Cladding material | Total plate thickness, in. | Total cladding thickness, f, in. |
|----------------------|-------------------|----------------------------|----------------------------------|
| Alclad 2014 | 6053 | <0.040 ≥.040 | 0.20 .10 |
| Alclad 2024 | 1230 | <0.064 ≥.064 | 0.10 .05 |
| Alclad 7075 | 7072 | All thicknesses | 0.08 |

Figure 15.2.10-4: Rectangular Panel and Flange Buckling Cladding Thicknesses (NACA-TN-3781, 1957)

15.2.10.4. Rectangular Panel Buckling Interactions

| Theory | Loading combination | Interaction equation | Figure |
|-----------|---|---|--------|
| Elastic | Biaxial compression | For plates that buckle in square waves, $R_x + R_y = 1$ | 28 |
| | Longitudinal compression and shear | For long plates, $R_c + R_s^2 = 1$ | 27 |
| | Longitudinal compression and bending | None | 28 |
| | Bending and shear | $R_b^2 + R_s^2 = 1$ | 27 |
| | Bending, shear, and transverse compression | None | 27 |
| | Longitudinal compression and bending and transverse compression | None | 28 |
| Inelastic | Longitudinal compression and shear | $R_c^2 + R_s^2 = 1$ | 29 |

Figure 15.2.10-5: Rectangular Panel and Flange Buckling Interactions
(NACA-TN-3781, 1957)

15.2.10.5. Triangular Panel buckling Coefficients

| Edge supports (a) | k_c | k_{s+} | k_{s-} |
|--|-------|----------|----------|
| All edges simply supported | 10.0 | 62.0 | 23.2 |
| Sides simply supported, hypotenuse clamped | 15.6 | 70.8 | 34.0 |
| Sides clamped, hypotenuse simply supported | 18.8 | 80.0 | 44.0 |

Figure 15.2.10-6: Rectangular Panel and Flange Buckling Interactions
(NACA-TN-3781, 1957)

15.2.11. Inter-Rivet Buckling

The common method for inter rivet buckling is based on Euler column behavior and does not include a correction for Poisson's ratio effect. There is a method defined in (NACA-TN-3785, 1957) that takes account of the Poisson's ratio effect and generates allowables about 10% greater than alternative methods.

The ruling equation is an adaptation of the classic plate buckling equation:

$$\sigma_i = \frac{e \cdot \pi^2 \cdot \eta \cdot \bar{\eta} \cdot E}{12 \cdot (1 - \nu^2)} \left(\frac{t_s}{p} \right)^2$$

Where:

- e End fixity coefficient
- η Plasticity reduction factor
- $\bar{\eta}$ Cladding reduction factor
- E Sheet material young's modulus, psi
- ν Sheet material Poisson's ratio
- t_s Sheet thickness, in
- p Fastener pitch, in

The value of the end fixity coefficient is given by the following table:

END-FIXITY COEFFICIENTS FOR INTERRIVET BUCKLING

| Fastener type | e | Reference |
|--------------------|-----|-----------|
| Flathead rivet | 4 | 8 |
| Spotwelds | 3.5 | 10 |
| Brazier-head rivet | 3 | 10 |
| Countersunk rivet | 1 | 11 |

Figure 15.2.11-1: Inter-Rivet Buckling Coefficients (NACA-TN-3785, 1957)

The plasticity correction factor can be assumed to be the same as it is for a panel in compression as defined in section 15.2.4.4.

The cladding reduction factor is defined in section 15.2.9.

A spreadsheet of this method, including plasticity reduction factors, is available here:

ABBOTT AEROSPACE SEZC LTD
SPREADSHEETS
ABBOTTAEROSPACE.COM
AA-SM-007-080 Inter-Rivet Buckling

ADVERT: TECHNICAL LIBRARY

TECHNICAL LIBRARY

SEE MORE

PUBLIC DOMAIN
TECHNICAL DATA



Analysis and Design of Composite and Metallic Flight Vehicle Structures



The only fully featured free structures engineering text book

Used by thousands of Engineers all over the world

 **ABBOTT
AEROSPACE**
SEZC LTD

15.3. Column Buckling

This section is in part based on the following references:

[\(NACA-TN-306, 1929\)](#), [\(NACA-TN-2163, 1950\)](#), [\(AFFDL-TR-69-42, 1986\)](#)

These analysis methods are applicable to isotropic materials. These methods can be adopted for composite laminate materials as long as the structures being analyzed are close to quasi-isotropic. Any application of analysis methodologies developed for isotropic materials applied to composite laminar structures must be confirmed by test as soon as is practical.

15.3.1. Euler Approach for Elastic Column Buckling

The simplest approach for column strength that is generally applicable to long, elastic columns with stable cross sections is the Euler method:

The Euler long strut formula:

$$\frac{P}{A} = \frac{\pi^2 \cdot E}{((L/\sqrt{C})/R)^2}$$

Where:

| | |
|----------|---|
| P | Load, lbs |
| A | Cross sectional area of strut, in ² |
| C | Fixity coefficient (See section 15.3.3) |
| E | Young's modulus of strut material, psi |
| L | Length of strut, in |
| R | Least radius of gyration of the strut cross section, in |

The term (L/R) is called the slenderness ratio, or S , and the effective slenderness ratio is the slenderness ratio modified by the fixity coefficient in the following way: $(L/\sqrt{C})/R$, this gives the basic term for the squared denominator of the Euler equation.

Plotting the Euler column allowable is for a given material stiffness over a range of effective slenderness ratio values gives the following result.

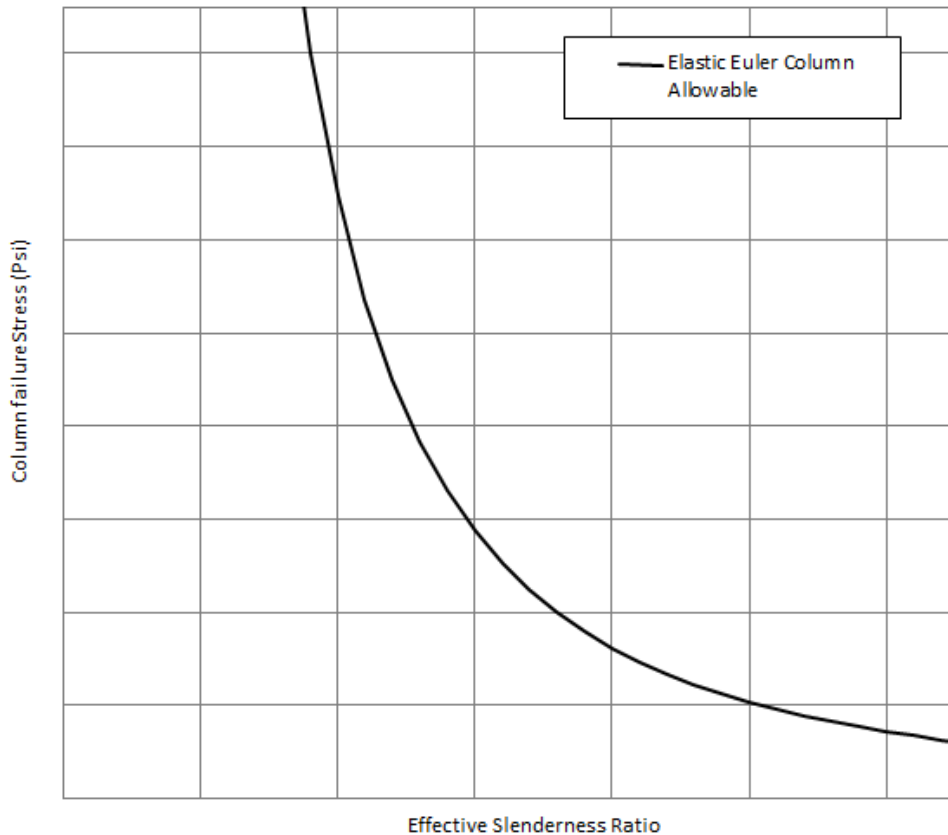
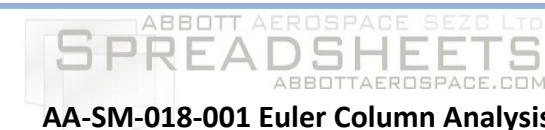


Figure 15.3.1-1: Euler Column Buckling Allowable Curve

Note that as the effective slenderness ratio reduces the strength of the column increases at an increasing rate. At low effective slenderness ratios the Euler approach gives unrealistic results as the allowable stress exceeds the elastic limit of the material.

The Euler allowable can also exceed the ultimate strength of the material. The spreadsheet method includes a 'cap' to the Euler allowable of F_{tu} , however in reality it is almost certain that the column will fail at some stress value below F_{tu} :



15.3.2. Johnson-Euler approach for Elastic-Plastic Column Behavior

The Johnson approach conservatively predicts column strength for short columns where inelastic behavior can have a significant effect on the column strength.

The Johnson short strut formula:

$$\frac{P}{A} = f_{cy} - \frac{f_{cy}^2}{4 \cdot \pi^2 \cdot E} \left(\frac{(L/\sqrt{C})}{R} \right)^2$$

Where:

| | |
|----------|---|
| P | Load, lbs |
| A | Cross sectional area of strut, in ² |
| C | Fixity coefficient (See section 15.3.3) |
| E | Young's modulus of strut material, psi |
| L | Length of strut, in |
| R | Least radius of gyration of the strut cross section, in |
| f_{cy} | Strut material compressive yield strength, psi |

Comparing the Johnson and the Euler column buckling curves for the same material gives the following result:

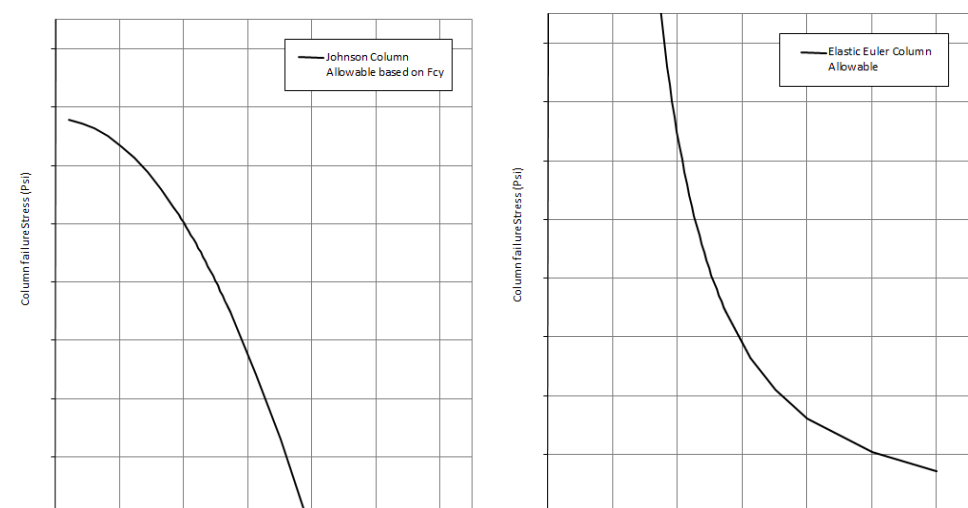


Figure 15.3.2-1: Johnson Column and Euler Column Buckling Allowable Curves

The Johnson and the Euler curves intersect at the L/R value of:

$$\frac{L}{R} = \sqrt{\frac{2 \cdot C \cdot \pi^2 \cdot E}{f_{cy}}}$$

The full material range column behavior can be approximated by taking the Johnson curve for effective slenderness ratios less than the intersection point and the Euler curve for effective slenderness ratios less than the intersection point. This produces a curve as follows:

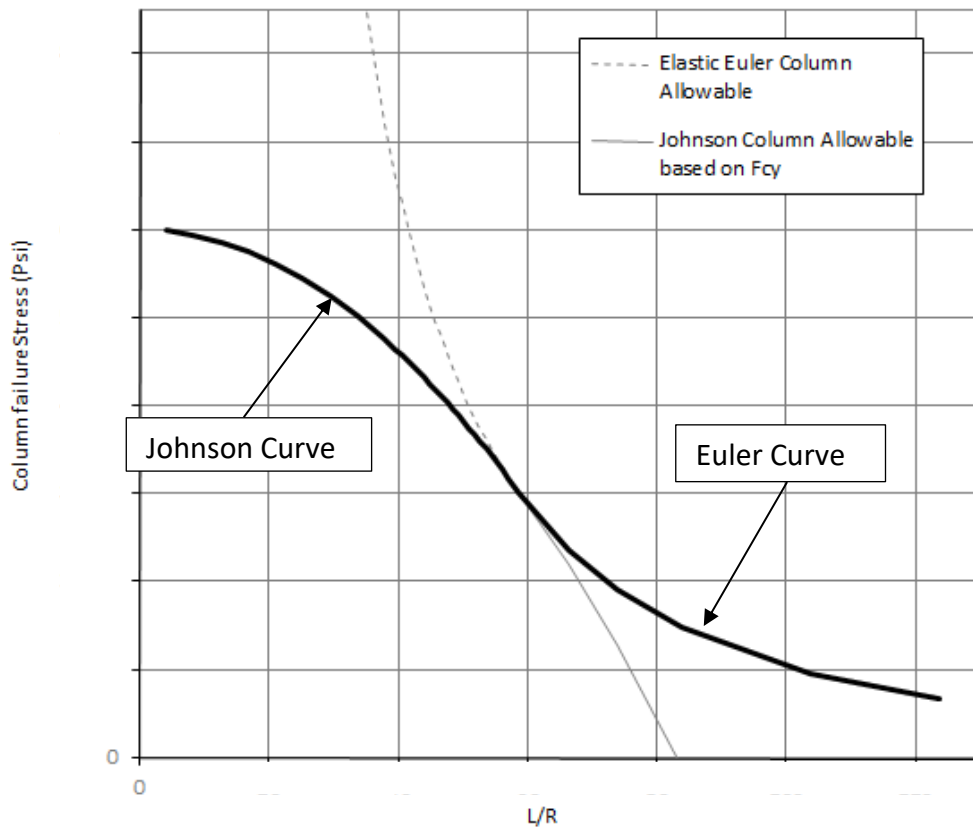


Figure 15.3.2-2: Johnson Column and Euler Column Buckling Allowable Curves Superimposed

For a relatively simple approach to column strength where full elasto-plastic material characteristics are not available it is recommended that the Johnson F_{cy} limit column strength is used for low slenderness ratios and the Euler column allowable is used for columns with high slenderness ratios. This approach is shown by the heavy line in Figure 15.3.2-2.

This method is defined in this spreadsheet:



15.3.3. Column Fixity Coefficient, C

| Type of Fixity | C | Type of Fixity | C |
|----------------|------|----------------|------|
| | .25 | | 2.05 |
| | 1.00 | | 4.00 |

Table 15.3.3-1: Column Fixity Coefficients [\(AFFDL-TR-69-42, 1986\)](#)

15.3.4. Tangent Modulus approach for Elastic-Plastic Column Behavior

If the slenderness ratio of a column is low enough that some its fibers are no longer in the elastic range at the time of failure the Euler formula no longer holds. In this instance the tangent modulus can be used in place of the Young's Modulus in the Euler equation:

$$\frac{P}{A} = \frac{\pi^2 \cdot E_T}{(C \cdot L/R)^2}$$

This produces results that are generally less conservative than the Johnson column allowable based on F_{cy} .

The effect of the tangent modulus on the buckling allowable can be derived analytically using the Ramberg-Osgood approximation for the plastic stress-strain curve.

In the authors experience, for typical isotropic structural materials, the effect of the shape factor rarely reduces the buckling allowable lower than that of the Johnson Buckling Curve:

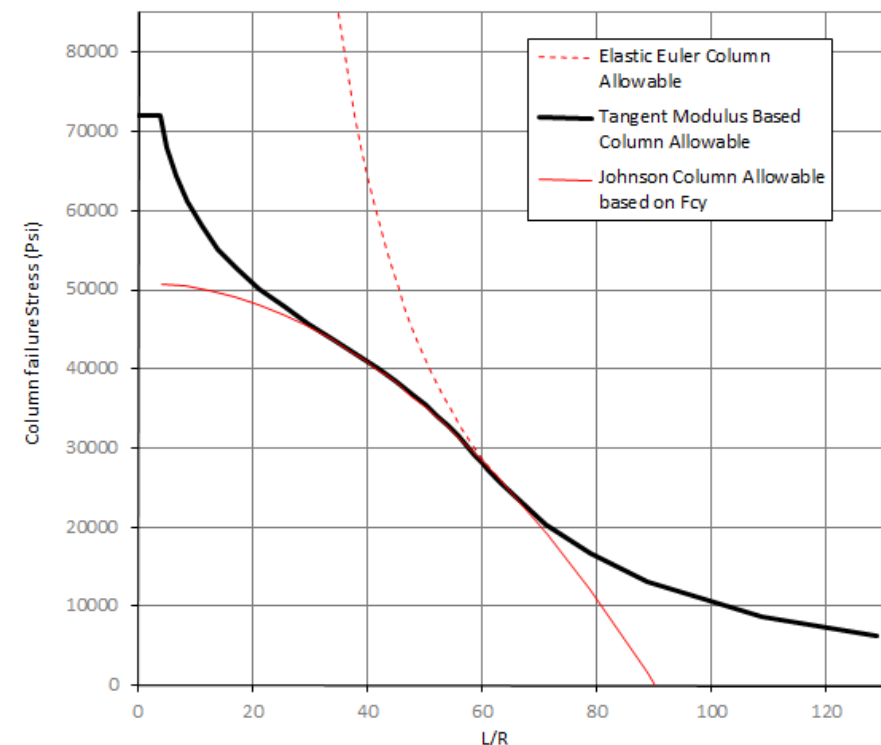


Figure 15.3.4-1: Tangent Modulus Column Buckling Curve for Sample Ductile Material n=10

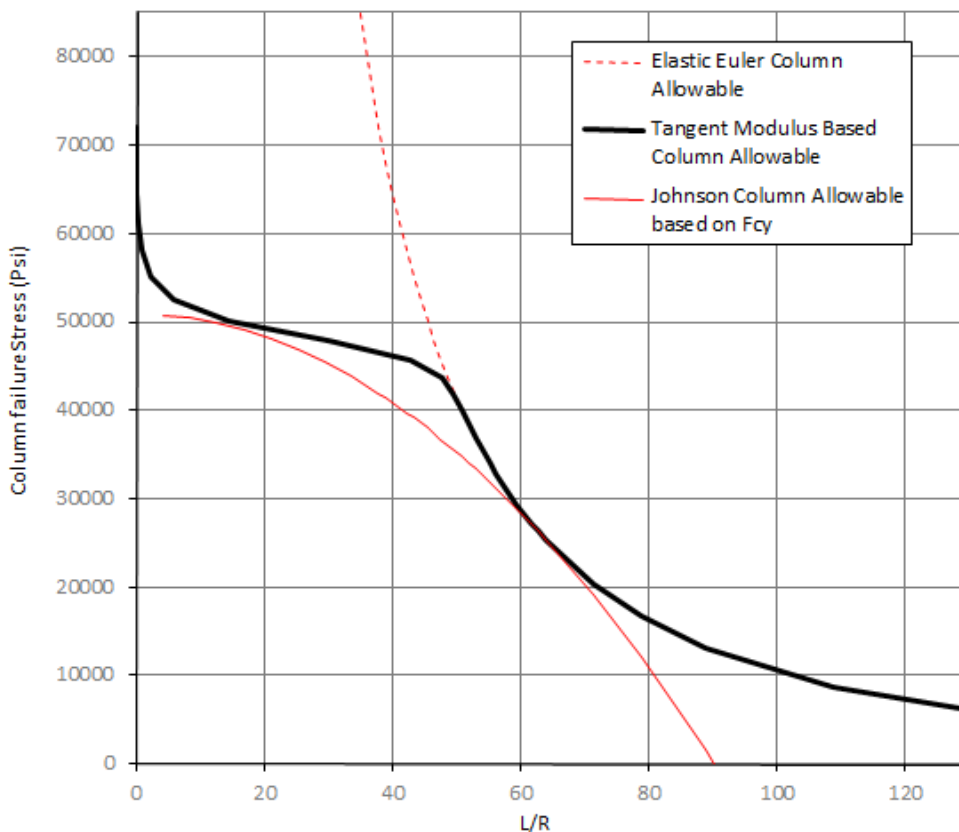


Figure 15.3.4-2: Tangent Modulus Column Buckling Curve for Sample Ductile Material n=40

The figures above show that for a sample. Typical ductile material the tangent modulus curve with shape factors between 10 and 40 lie between the Euler and the Johnson Buckling Curves and do not exhibit a lower value than the Johnson Curve.

This implies that for inelastic columns with stable cross sections the Johnson curve can be used as a conservative sizing allowable.

For materials with very low shape factors (less than 10) it is advisable to carry out a full tangent modulus analysis.

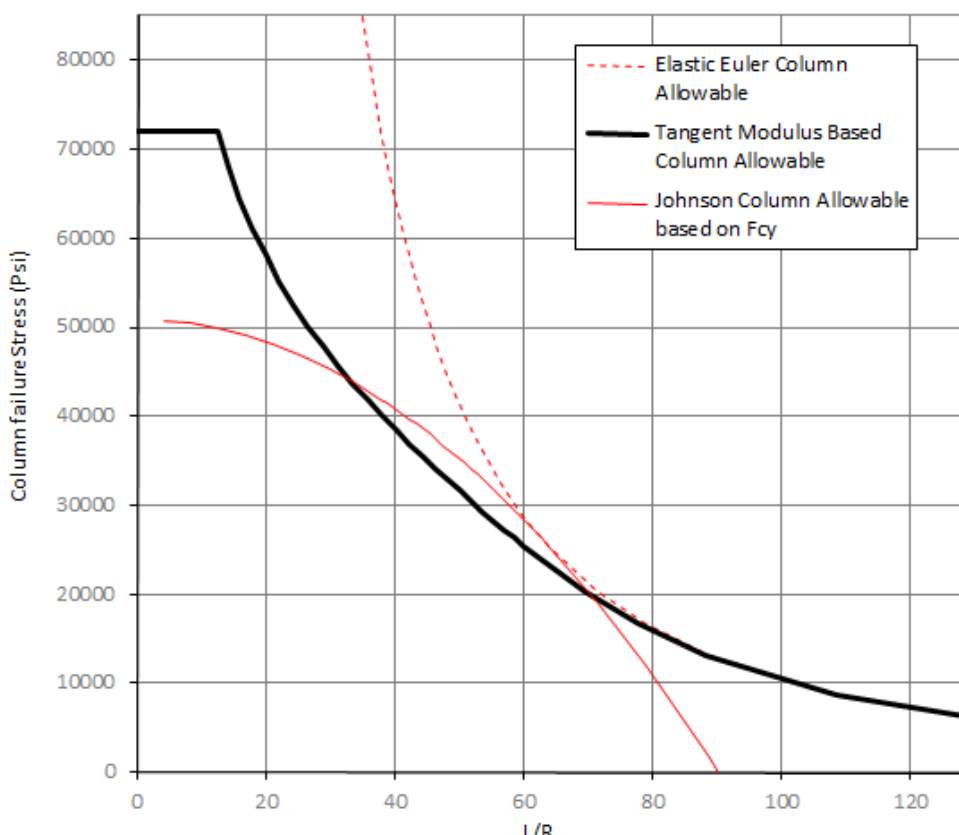


Figure 15.3.4-3: Tangent Modulus Column Buckling Curve for Sample Ductile Material n=5

Figure 15.3.4-3 shows that a ductile material with a shape factor of 5 exhibits column strength significantly lower over a significant slenderness ratio range than the Johnson Buckling Curve. This method is covered in the following spreadsheet:



15.3.5. Limits to Column Buckling Strength

There are limitations to the column strength of a compression member, these can include local buckling, crippling, a welded joint within the column or any other feature that reduces the failure load of the member. This limitation appears as a horizontal line on the column strength graph:

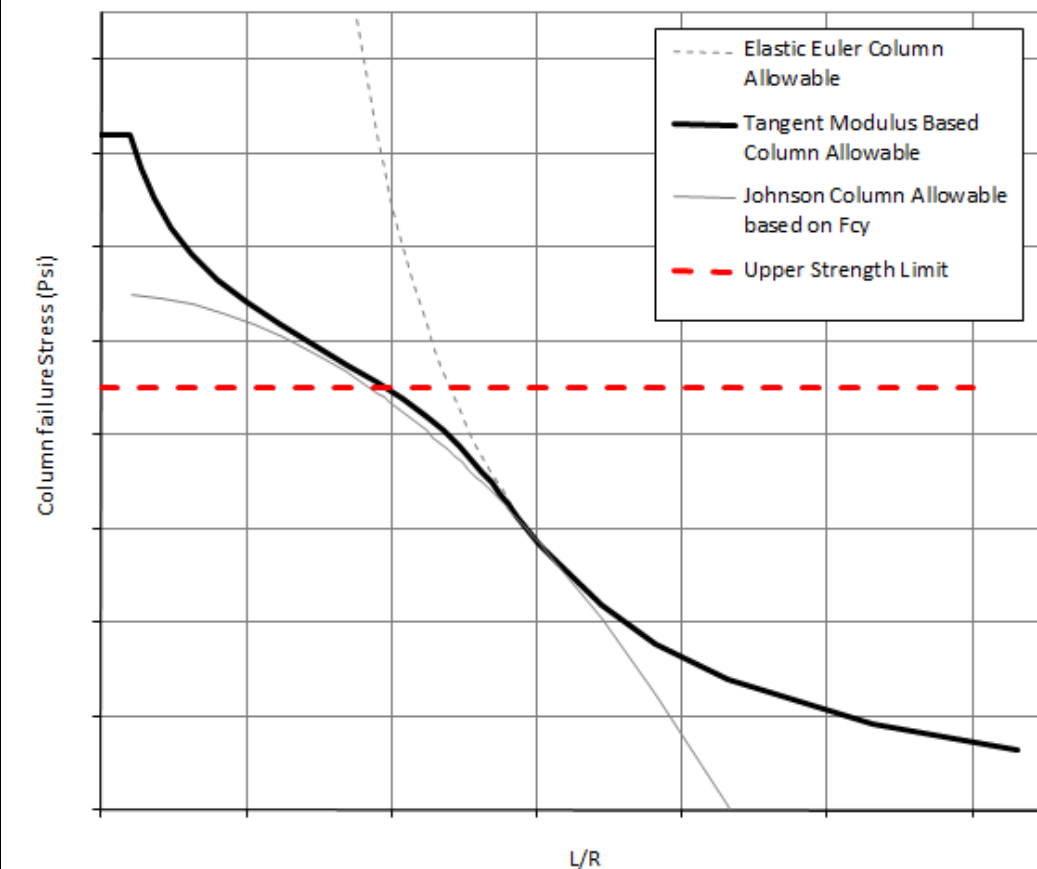
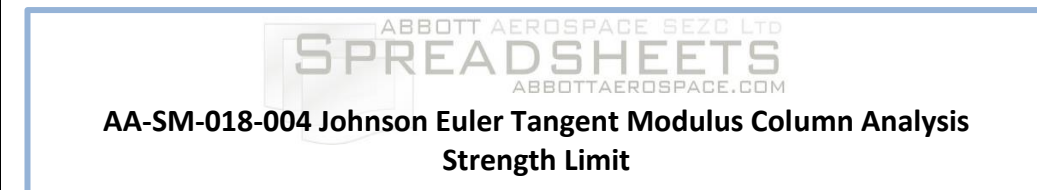


Figure 15.3.5-1: Tangent Modulus Column Buckling Curve for Sample Ductile Material Showing Upper Strength Limit

This method is covered in the following spreadsheet:



15.3.6. Beam Column Analysis

The method discussed in this section is defined in Chapter 2.3.1.7 of [\(AFFDL-TR-69-42, 1986\)](#). In this reference the situation is described as "Bending Failure of Eccentrically Loaded Long Columns".

The bending effect can be generated from an eccentricity of the applied load – i.e. the load is applied some distance off axis from the axis of the column:

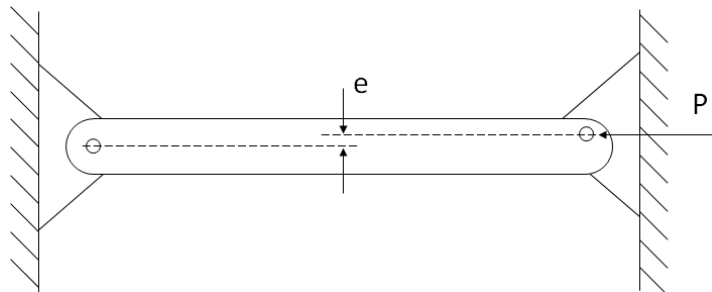


Figure 15.3.6-1: Beam Column with Moment created by Applied Load Eccentricity

Or the bending effect can be created by a deviation, or eccentricity, of the load path within the column member.

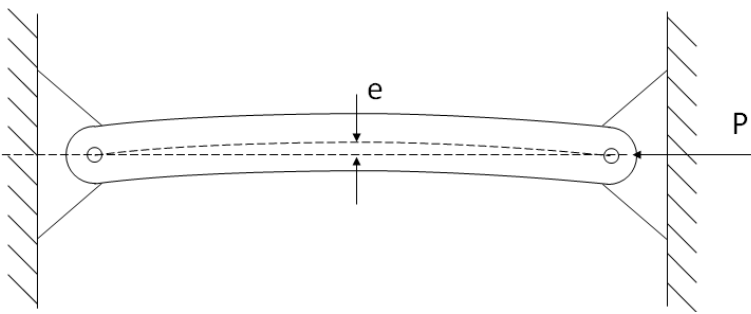


Figure 15.3.6-2: Beam Column with Moment Created by Column Member Geometry

In both cases the solution is the same.

In the case where an initial moment is applied combined with a compressive end load, the deflection caused by the bending moment can be calculated and the resulting deflection can be used as the initial eccentricity.

The solution to a beam column is achieved using the secant formula:

$$\frac{P}{A} = \frac{F}{1 + \frac{e \cdot c}{R^2} \cdot \sec \left[\frac{L'}{2 \cdot R} \cdot \sqrt{\frac{P}{A \cdot E}} \right]}$$

Where:

- P** Load, lb
- A** Cross sectional area of strut, in²
- c** Distance between the column neutral axis and the outer fiber of the concave side, in
- F** Strength of column without bending or eccentricity, psi
- e** eccentricity, in
- R** Least radius of gyration of the strut cross section, in
- L'** Effective length of the column = (L/\sqrt{C}) , Where 'C' (upper case) is the column fixity coefficient, in
- E** Column material young's modulus, psi

The solution to this equation is solved by either trial and error or iteratively for a value of P/A , which represents the reduced allowable for the beam-column, that satisfies the rearranged expression:

$$\frac{F}{1 + \frac{e \cdot c}{R^2} \cdot \sec \left[\frac{L'}{2 \cdot R} \cdot \sqrt{\frac{P}{A \cdot E}} \right]} - \frac{P}{A} = 0$$

Note that this methodology does not account for the increased propensity for local buckling failures due to the combination of compressive end load and bending effects.

All physical columns will have some accidental initial curvature due to imperfections. In these cases, an equivalent eccentricity may be used to approximate the effects of the imperfections. It is recommended that **L/400** is used as a conservative estimate for the equivalent eccentricity due to imperfections.

The spreadsheet for this method includes the tangent modulus column allowable combined with a beam column solution that is solved iteratively automatically.

ABBOTT AEROSPACE SEZC LTD
SPREADSHEETS
ABBOTTAEROSPACE.COM

AA-SM-018-005 Beam Column Analysis

ADVERT: ENGINEERING SERVICES

STRUCTURES DESIGN ENGINEERING SERVICES

[CONTACT US](#)



ABBOTT AEROSPACE
ABBOTTAEROSPACE.COM

15.4. Buckling – Specific Cases

15.4.1. Buckling of Thin Cylindrical Shells

Extract from: [\(NASA TM X-73306, 1975\)](#)

The application of theory to the design of actual cylindrical shells has been complicated by apparent discrepancies between theory and experiment.

For shells in which longitudinal compression of the cylinder wall predominates, the discrepancies can be quite large. For shells in which shear or circumferential compression predominates, the discrepancies are generally less severe but still large enough to require experimental programs to establish design data. The causes of such discrepancies are generally understood.

The primary source of error is the dependence of the buckling load of cylindrical shells on small deviations from the nominal circular cylindrical shape of the structure. Because the unloaded shape of a test specimen usually has not been stringently controlled, most test results for nominally identical specimens have larger scatter and fall below the theoretical values.

Another source of discrepancy is the dependence of buckling loads of cylindrical shells on edge values of longitudinal and circumferential displacements or forces. Also, because tangential edge conditions have not usually been precisely controlled in buckling tests, some of the scatter of test results can be attributed to this source. Current methods of establishing design data tend to treat both initial imperfections and edge conditions as random effects. Results from all available tests are considered together without regard to specimen construction or methods of testing and are analyzed to yield lower bound or statistical correction factors to be applied to simplified versions of the theoretical results. This technique has proved satisfactory to date for design purposes.

Within the limitations imposed by the state of the art, acceptable procedures for the estimation of critical loads on circular cylindrical shells are described in this section.

Analysis Terms:

| | |
|----------|--|
| r | Mean radius of the cylinder, in |
| t | Thickness of cylinder wall, in |
| L | Length of cylinder, in |
| E | Young's modulus of strut material, psi |
| ν | Sheet material Poisson's ratio |
| η | Plasticity reduction factor |
| γ | Correlation factor |
| ϕ | Correlation factor |

15.4.1.1. Buckling of Thin Simple Cylinders Under External Pressure

This section is taken from [\(AFFDL-TR-69-42, 1986\)](#) Section 8.3.1.3.1. This method is similar to that defined in [\(NASA TM X-73306, 1975\)](#) Section 3.1.1.5.

The formula for the critical stress in short cylinders ($L^2/r \cdot t < 100$) which buckle elastically under radial pressure is:

$$F_{cr} = \frac{k_y \cdot \pi^2 \cdot E}{12 \cdot (1 - \mu_e^2)} \cdot \left(\frac{t}{L}\right)^2$$

Where k_y is obtained from the figure below:

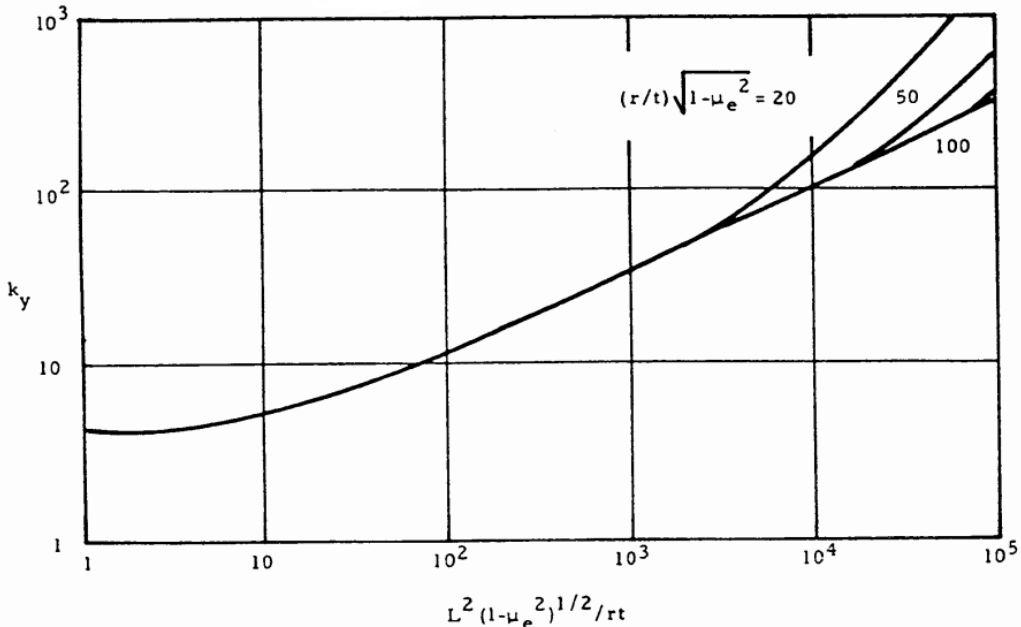


Figure 15.4.1-1: Coefficient for Buckling of Simply Supported Short Cylinders under Internal Pressure [\(AFFDL-TR-69-42, 1986\)](#)

The critical stress for long cylinders ($100 \cdot t/r < (L/r)^2 < 5 \cdot r/t$) under external radial pressure is:

$$F_{cr} = 0.93 \cdot E \cdot \left(\frac{t}{r}\right)^{3/2} \left(\frac{r}{L}\right)$$

For very long cylinders, ($(L/r)^2 > 5 \cdot r \cdot t$) the buckling stress is given by:

$$F_{cr} = \eta \cdot \frac{0.25 \cdot E}{(1 - \mu_e^2)} \cdot \left(\frac{t}{r}\right)^2$$

Where η is the plasticity reduction factor given in this case by:

$$\eta = \frac{E_s}{E} \cdot \frac{(1 - \mu_e^2)}{(1 - \mu^2)} \cdot \left(\frac{1}{4} + \frac{3}{4} \cdot \frac{E_t}{E_s}\right)$$

When the material remains in the elastic range the plasticity reduction factor = 1.0

The allowable stress can be converted to an allowable pressure load using the expression:

$$\text{Allowable Pressure} = \frac{F_{cr} \cdot t}{r}$$

This method is available in the linked spreadsheet below:

ABBOTT AEROSPACE SEZC LTD
SPREADSHEETS
ABBOTTAEROSPACE.COM

AA-SM-014-001 Buckling of Cylinder due to External Pressure



15.4.1.2. Buckling of Thin Simple Cylinders Under Axial Compression

This section is taken from [\(NASA TM X-73306, 1975\)](#) Section 3.1.1.1.

This method predicts local buckling of short cylinders, longer cylinders should be checked as a column per section 15.3.

The design allowable compression buckling stress for a circular cylinder subjected to axial compression is given by:

$$F_{cr} = \eta \cdot \frac{\gamma \cdot E}{\sqrt{3 \cdot (1 - \mu_e^2)}} \cdot \left(\frac{t}{r}\right)$$

The lower boundary of the experimental data for cylinders in axial compression is given by the following expression:

$$\gamma = 1.0 - 0.907 \cdot (1 - e^{-\phi})$$

Where:

$$\phi = \frac{1}{16} \cdot \sqrt{\frac{r}{t}} \quad \text{for } \frac{r}{t} < 1500$$

The relationship between γ and r/t is shown in the figure below:

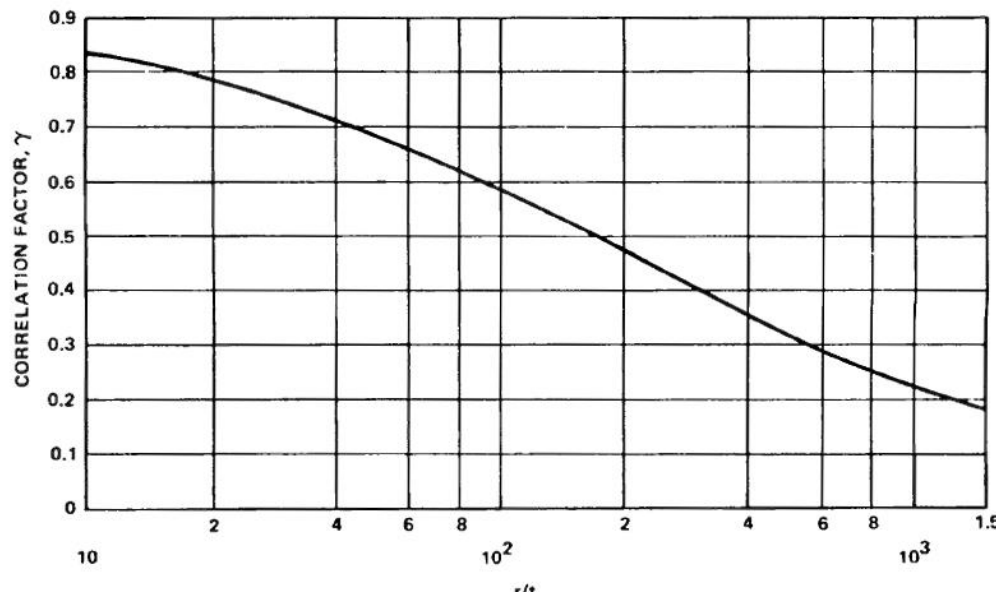


Figure 15.4.1-2: Coefficient for Buckling of Short Cylinders Axial Compression [\(NASA TM X-73306, 1975\)](#)

This method is available in the linked spreadsheet below:

ABBOTT AEROSPACE SEZC LTD
SPREADSHEETS
ABBOTTAEROSPACE.COM

AA-SM-014-002 Buckling of Cylinder due to Axial Compression

15.4.1.3. Buckling of Thin Simple Cylinders Under Axial Compression and Internal Pressure

This section is taken from [\(NASA TM X-73306, 1975\)](#) Section 3.1.1.2.

The modification to the buckling load is similar to the method in [\(NACA-Report-1027\)](#) which compares analytical predictions and experimental results.

Buckling and collapse coincide for internally pressurized circular cylinders in axial compression, just as in the case of the un pressurized cylinder. Pressurization increases the buckling load in the following ways:

1. The total compressive load must be greater than the tensile pressurization load $p \cdot \pi \cdot r^2$ before buckling can occur.
2. The destabilizing effect of initial imperfections is reduced.

The circumferential tensile stress induced by the pressurization inhibits the diamond buckling pattern, and, at sufficiently high pressurization the cylinder buckles in the classical axisymmetric mode at approximately the classical buckling stress.

It is recommended that the total load for buckling, unless substantiated by testing, be obtained by the addition of the pressurization load $p \cdot \pi \cdot r^2$, the buckling load for the unpressurized cylinder (Reference Section 15.4.1.2) and an increase in the buckling load caused by pressurization; that is:

$$P_{cr} = 2 \cdot \pi \cdot E \cdot t^2 \cdot \left(\frac{\gamma}{\sqrt{3 \cdot (1 - \mu_e^2)}} + \Delta\gamma \right) + p \cdot \pi \cdot r^2$$

Where $\Delta\gamma$ is obtained from figure below:

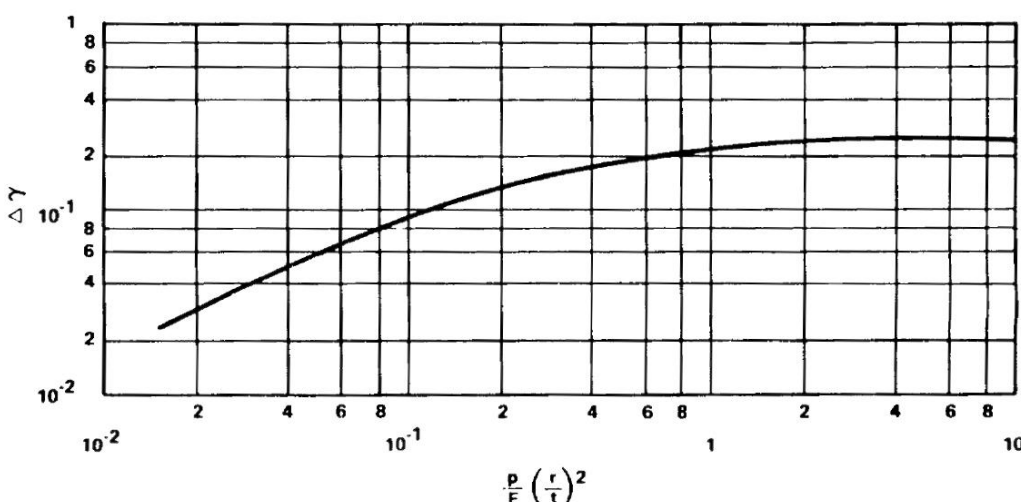


Figure 15.4.1-3: Coefficient for Buckling of Short Cylinders Axial Compression and Internal Pressure [\(NASA TM X-73306, 1975\)](#)

This method is available in the linked spreadsheet below:

ABBOTT AEROSPACE SEZC LTD
SPREADSHEETS
ABBOTTAEROSPACE.COM

AA-SM-014-003 Buckling of Cylinder due to Axial Compression and Internal Pressure

15.4.1.4. Buckling of Thin Simple Cylinders Under Bending

The design allowable bending buckling stress for a circular cylinder subjected to axial compression is given by:

$$F_{cr} = \eta \cdot \frac{\gamma \cdot E}{\sqrt{3 \cdot (1 - \mu_e^2)}} \cdot \left(\frac{t}{r}\right)$$

The procedure given for isotropic cylinders in axial compression may be used also to obtain the critical maximum stress for isotropic cylinders in bending, except that a correlation factor based on bending tests should be used. The correlation factor for the cylinder in bending is taken as:

$$\gamma = 1.0 - 0.731 \cdot (1 - e^{-\phi})$$

Where:

$$\phi = \frac{1}{16} \cdot \sqrt{\frac{r}{t}} \quad \text{for } \frac{r}{t} < 1500$$

The relationship between γ and r/t is shown in the figure below:

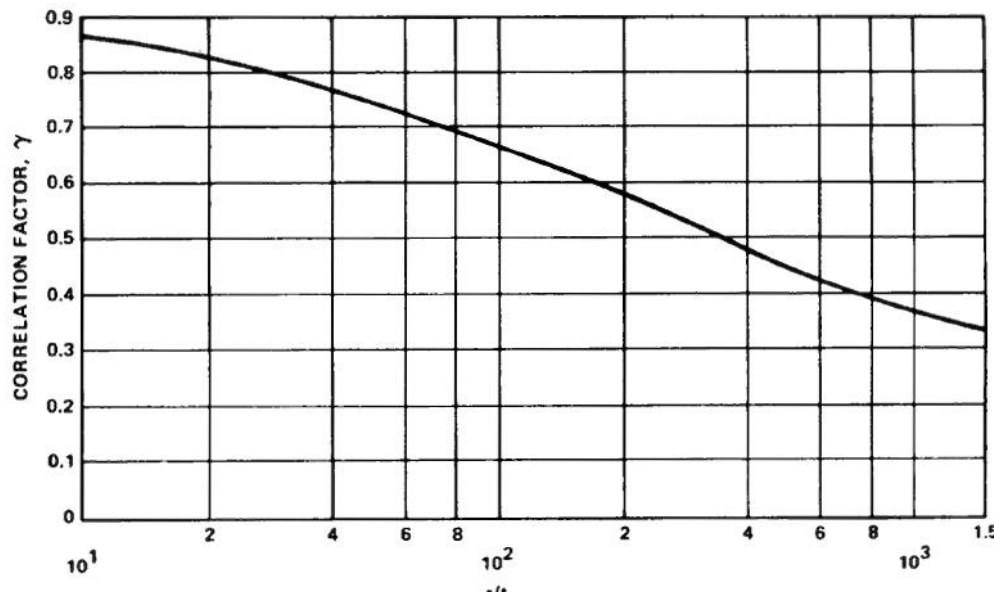


Figure 15.4.1-4: Coefficient for Buckling of Short Cylinders in Bending [\(NASA TM X-73306, 1975\)](#)

The Allowable Bending Moment can be calculated using the following expression:

$$M_{cr} = \pi \cdot r^2 \cdot F_{cr} \cdot t$$

This method is available in the linked spreadsheet below:

ABBOTT AEROSPACE SEZC LTD
SPREADSHEETS
ABBOTTAEROSPACE.COM

AA-SM-014-004 Buckling of Cylinder due to Bending

15.4.1.5. Buckling of Thin Simple Cylinders Under Bending and Internal Pressure

For thin-walled cylinders subjected to bending and internal pressure, it is recommended that the buckling moment be obtained by adding the moment-carrying capability of a pressurized membrane cylinder the buckling moment for the unpressurized cylinder:

$$M_{press} = \pi \cdot r \cdot E \cdot t^2 \cdot \left(\frac{\gamma}{\sqrt{3 \cdot (1 - \mu_e^2)}} + \Delta\gamma \right) + \frac{p \cdot \pi \cdot r^3}{2}$$

As with a cylinder in bending:

The correlation factor for the cylinder in bending is taken as:

$$\gamma = 1.0 - 0.731 \cdot (1 - e^{-\phi})$$

Where:

$$\phi = \frac{1}{16} \cdot \sqrt{\frac{r}{t}} \quad \text{for } \frac{r}{t} < 1500$$

Where $\Delta\gamma$ is obtained from figure 15.4.1.3.

This method is available in the linked spreadsheet below:

ABBOTT AEROSPACE SEZC LTD
SPREADSHEETS
ABBOTTAEROSPACE.COM

AA-SM-014-005 Buckling of Cylinder due to Bending and Internal Pressure

15.4.1.6. Buckling of Thin Simple Cylinders Under Shear or Torsion

This method is taken from [\(NACA-TN-1344, 1947\)](#).

The theoretical buckling coefficient for cylinders in torsion can be obtained from Figure 15.4.1-5. The straight-line portion of the curve is given by the equation:

$$k_{xy} = \frac{N_{xy} \cdot L^2}{\pi^2 \cdot D} = 0.85 \cdot (\gamma \cdot Z)^{3/4}$$

This rearranges to form the following expression:

$$N_{xy} = \frac{k_{xy} \cdot \pi^2 \cdot D}{L^2}$$

and

$$\tau_{xy} = \frac{k_{xy} \cdot \pi^2 \cdot D}{t \cdot L^2}$$

Where:

$$D = \frac{E \cdot t^3}{12 \cdot (1 - \mu^2)}$$

and:

$$Z = \frac{L^2}{r \cdot t} \cdot \sqrt{1 - \mu^2}$$

k_{xy} is the buckling coefficient. This can be estimated in the following way. For very short cylinders the shear stress buckling coefficient approached the value for a flat plate. **5.34** when the edges are simply supported and **8.98** when the edges are clamped.

For long cylinders the buckling coefficients can be approximated by the following expressions.

For simply supported edges:

$$k_{xy} = 0.85 \cdot Z^{3/4}$$

For clamped edges:

$$k_{xy} = 0.93 \cdot Z^{3/4}$$

The range of validity of these formulas is:

$$100 < Z < 10 \cdot \frac{r^2}{t^2}$$

For very high values of Z (< 20000) the value of k_{xy} increases slightly above the values predicted by the expressions above. This increase in k_{xy} is not characterized in this text, for more information see figure 1 of [\(NACA-TN-1344, 1947\)](#).

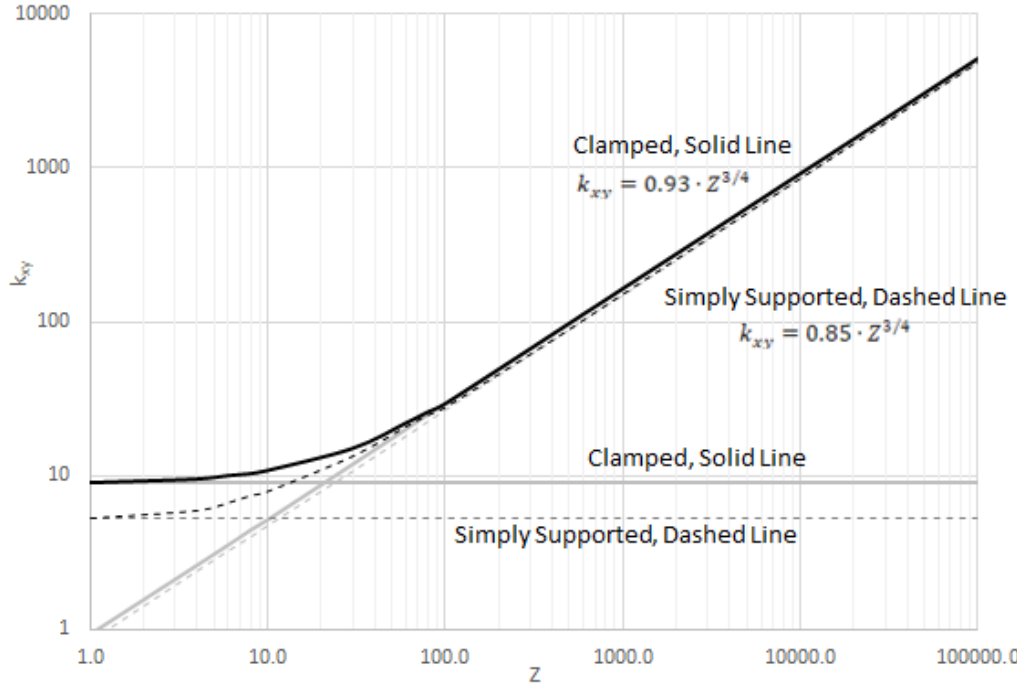


Figure 15.4.1-5: Coefficient for Buckling of Simply Supported Cylinders in Torsion [\(NACA-TN-1344, 1947\)](#)

ABBOTT AEROSPACE SEZC LTD
SPREADSHEETS
ABBOTTAEROSPACE.COM

AA-SM-014-006 Buckling of Cylinder due to Torsion

15.4.1.7. Combined Buckling of Thin Simple Cylinders

The interaction between load effects is calculated using combinations of reserve factors

Combined Compression and Bending: [\(NASA TM X-73306, 1975\)](#)

$$R_c + R_b = 1$$

Axial Compression and External Pressure: [\(NASA TM X-73306, 1975\)](#)

$$R_c + R_p = 1$$

Bending and Torsion: [\(NASA TM X-73306, 1975\)](#)

$$R_b + R_t^2 = 1$$

Axial Load and Torsion: [\(NACA-TN-1345, 1947\)](#)

For torsion/shear and compression

$$R_{xy}^2 + R_c = 1$$

Valid for simply supported and clamped edges in the range:

$$5 < Z < 7.7 \cdot \frac{r^2}{t^2}$$

For torsion/shear and tension

$$R_{xy} + 0.5R_t = 1$$

Valid for simply supported and clamped edges in the range:

$$30 < Z < 7.7 \cdot \frac{r^2}{t^2}$$

ABBOTT AEROSPACE SEZC LTD
SPREADSHEETS
ABBOTTAEROSPACE.COM

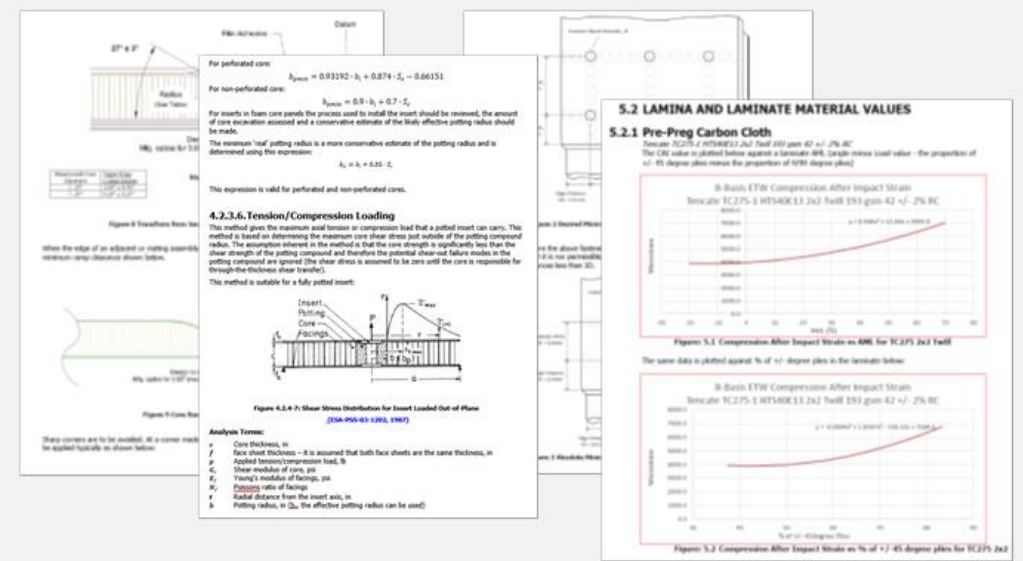
AA-SM-014-007 Combined Buckling of Cylinders

ADVERT: ENGINEERING SERVICES

ENGINEERING METHODS

CONTACT US

ENGINEERING
SERVICES



ABBOTT
AEROSPACE
SEZC LTD

15.5. Crippling

This method is taken from [\(AFFDL-TR-69-42, 1986\)](#) Section 2.3.2.4.

Crippling is a mode of failure that occurs due to compression effects. Typically, this is a check that is applied to thin walled columns where the local stability of the cross section may not allow the column to achieve its full column strength. The crippling strength of a cross section or feature can be used as a cut off on the column strength curve. See Figure 15.3.5-1.

Crippling strength checks are most commonly applied to angles or corner features.

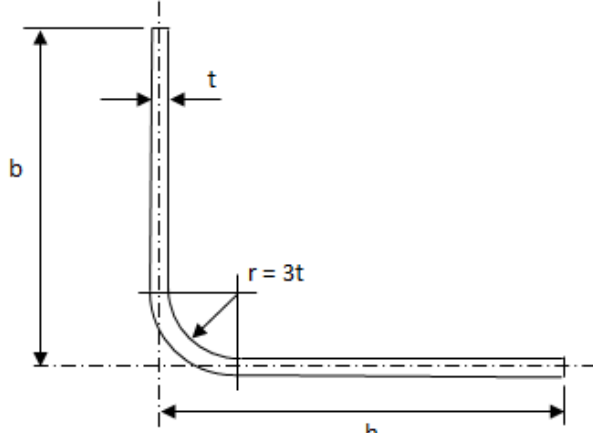


Figure 15.4.1-1: Angle Notation for Crippling Check

The basic crippling stress equation is:

$$\frac{F_{cc}}{\sqrt{F_{cy} \cdot E}} = \left[\frac{C_e}{\left(\frac{b'}{t}\right)^{0.75}} \right]$$

The Load at which the section above will cripple is given by the following expression:

$$P_{cc} = \left[C_e \cdot \frac{\sqrt{F_{cy} \cdot E}}{\left(\frac{b'}{t}\right)^{0.75}} \right] \cdot A$$

Where:

$b' = (h + b)/2$

t Angle thickness, in

b Minimum leg length, in

h Maximum leg length, in

F_{cy} Material compressive yield Strength, psi

E Material young's modulus, psi

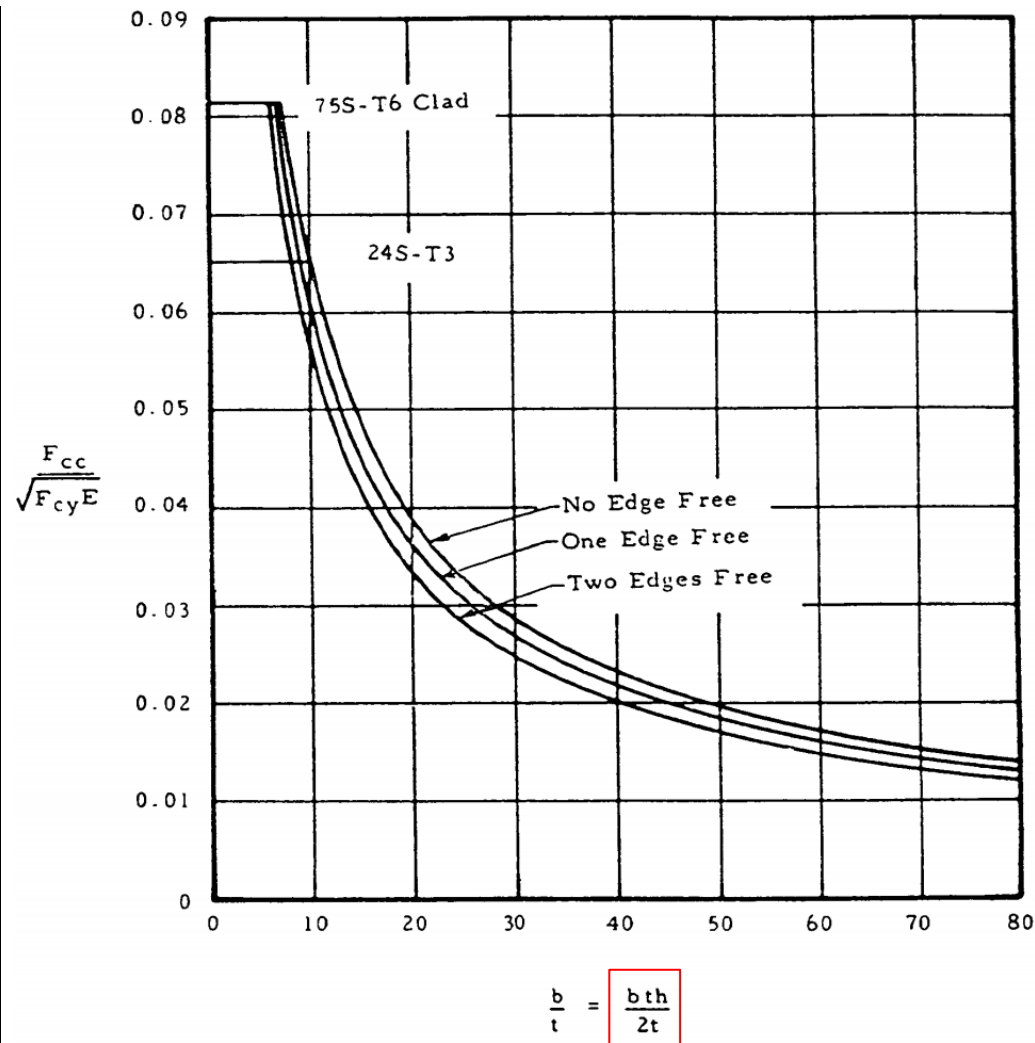
Cross Sectional Area – for the angle shown, $A = \left(\left(\frac{b'}{t}\right) - 0.214 \cdot \left(\frac{r}{t}\right) \right) \cdot 2 \cdot t^2$

$C_e = 0.316$ (two edges free)

$C_e = 0.342$ (one edge free)

$C_e = 0.366$ (no edge free)

These parameters can be used to construct the curves in the following figure:



This term includes an error from the original reference, this should read $(b+h)/2t$

Figure 15.4.1-2: Dimensionless Crippling Curves [\(AFFDL-TR-69-42, 1986\)](#)

The method is provided in the spreadsheet linked below:

ABBOTT AEROSPACE SEZC LTD
SPREADSHEETS
ABBOTTAEROSPACE.COM
AA-SM-012 Section Crippling - Needham Method

16. LOCAL STABILITY – COMPOSITE MATERIALS

16.1. Introduction

16.2. Buckling of Laminates

Once the basic integrity of the laminate to withstand the internal strains created by the external loads is established other forms of failure mode must be considered.

Panel buckling is a criterion that can be considered either as a critical failure mode or a change of state that allows residual strength beyond the onset of buckling.

A buckle forces a load redistribution and secondary in-plane and out-of-plane load effects. These secondary effects that occur at the time of buckling and the effect that they have on especially adhesively bonded structure can propagate wider structural failure.

For this reason, many composite aircraft projects consider local buckling to be an ultimate level failure and design for no buckling up to ultimate load.

To search the [Abbott Aerospace Technical Library](#) for 'Laminate Buckling' click on the link below:

ABBOTT AEROSPACE SEZC LTD
Library Subject Search: Laminate Buckling

16.2.1. Buckling of Un-Cored Laminates

The methods below are taken from [\(MIL-HDBK-17F Vol 3, 2002\)](#) Section 5.7 and [\(NASA-TN-D-7996, 1975\)](#). The following caveats apply to the applicability of this analysis method:

..... the closed form solutions of laminated orthotropic Panels are appropriate only when the lay-ups are **symmetrical and balanced**. Symmetrical implies identical corresponding plies about the Panel mid-surface. Balanced refers to having a minus _ ply for every plus _ ply on each side of the mid-surface. Symmetrical and balanced laminated Panels have B terms vanish and the D₁₆ and D₂₆ terms virtually vanish.....

Note that the buckling performance of a panel depends on the panel size, the rigidity of the panel edge constraints and the out-of-plane stiffness of the panel. The out-of-plane stiffness of the panel is expressed using the D matrix component of the laminate ABD matrix, see section 4.1.6.1 of this document for more information.

Note that these methods are not specifically limited to uncored laminates but the effect of the presence of core on the buckling solution can be significant depending on the characteristics of the core panel.

Classical Panel theory is based up on the Kirchhoff hypothesis: "Normals to the mid-plane of the un-deformed Panel remain straight and normal to the mid-plane during deformation". This assumption therefore ignores the transverse shear deformation. Consideration of the shear deformation results in added flexibility which becomes significant as the Panel thickness increases relative to the length and width. [\(AFWAL-TR-85-3069, 1985\)](#)

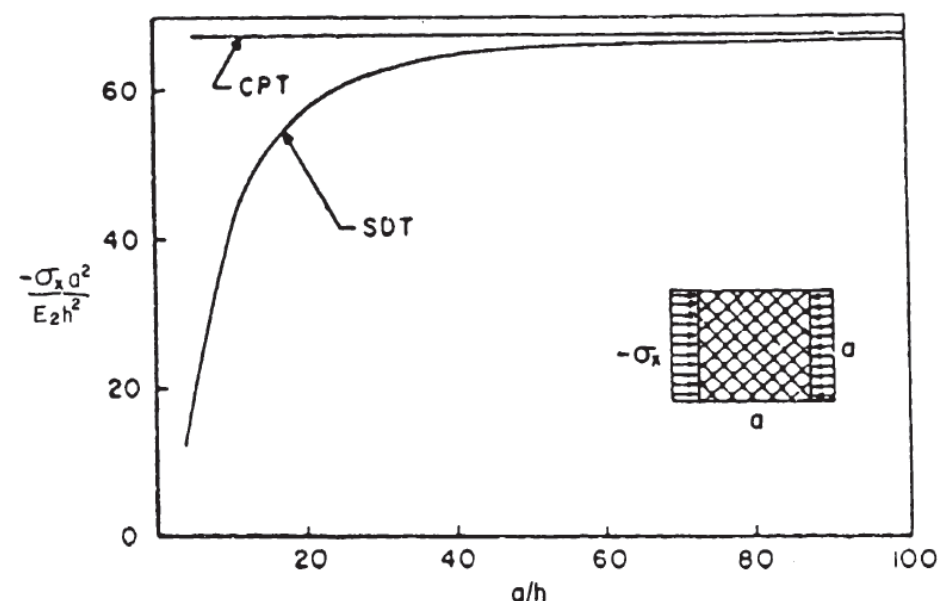


Figure 16.2.1-1: The effect of Panel size to Thickness Ratio (a/h) on the Transverse Shear Influence of the Uniaxial Compression Buckling Allowable [\(AFWAL-TR-85-3069, 1985\)](#)

However, there are buckling predictions specifically for cored laminate panels and these are examined in section 16.2.2 of this document.

It is recommended that the analyst uses multiple methods, if they are available, so the results can be compared and correlated. It is also useful when the opportunity comes to test structures that have been designed using these methods as the test results can be used to help select the 'best fit' analysis for future work.

Analysis Terms:

| | |
|---|--|
| <i>a</i> | Length, in |
| <i>b</i> | Width, in |
| <i>B_{ij}</i> | Stiffness coupling terms of laminated panel |
| <i>D_{ij}</i> | Flexural/twisting stiffness terms of laminated panel |
| <i>F_{x,cl}^{cr}</i> | Classical orthotropic longitudinal compressive buckling stress, psi |
| <i>F_{x,l}^{cr}</i> | Initial longitudinal compressive buckling stress from test, psi |
| <i>F_x^{cc}</i> | Longitudinal crippling stress from test, psi |
| <i>F_x^{cu}</i> | Longitudinal ultimate compressive stress of laminate, psi |
| <i>N_{x,cl}^{cr}, N_{y,cl}^{cr}</i> | Classical orthotropic longitudinal and transverse compressive uniform buckling load flows, respectively, lb/in |
| <i>N_{x,i}^{cr}</i> | Initial longitudinal uniform buckling load flow from test, lb/in |
| <i>N_{x,w}^{cr}</i> | Longitudinal compressive uniform buckling load flow based on anisotropic theory, including transverse shear effects, lb/in |
| <i>N_{x, N_y}</i> | Longitudinal and transverse applied uniform load flows, respectively, on a Panel, lb/in |
| <i>P_{x,i}^{cr}</i> | Total longitudinal initial buckling load from test, lb |
| <i>P_{x,i}^{cc}</i> | Total longitudinal crippling load from test, lb |
| <i>t</i> | Thickness, in |

Notes:

All of the following methods are for large aspect ratio panels. Note that for short aspect ratio panels these solutions will give conservative results.

These methods correlate well with test for b/t ratios greater than 35 – see figure on next page:

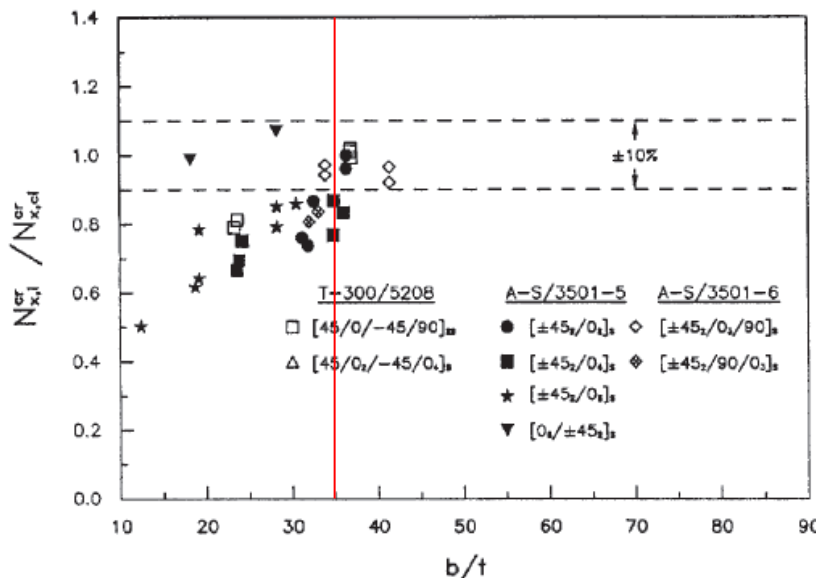


Figure 16.2.1-2: Predicted Classical Buckling Loads Compared to Experimental Data [\(MIL-HDBK-17F Vol 3, 2002\)](#)

For b/t ratios lower than 35, the $N_{x,I}^{cr} / N_{x,cl}^{cr}$ ratio shows that the following methods will be significantly optimistic.

For this method to be accurate for a laminate panel of 0.040in thickness the b dimension would have to be greater than $0.040 \times 35 = 1.4$ in.

This correlates to the difference in the predicted buckling performance between methods that account for transverse shear and those that do not, as shown in Figure 16.2.1-1. The inaccuracy in this methodology is strongly influenced by the out-of-plane shear effect.

16.2.1.1. Uniaxial Loading, Long Panel, All Sides Simply Supported

(Aspect ratio >4)

For long plates the loaded edges can also be clamped and the allowable buckling stress will not be affected.

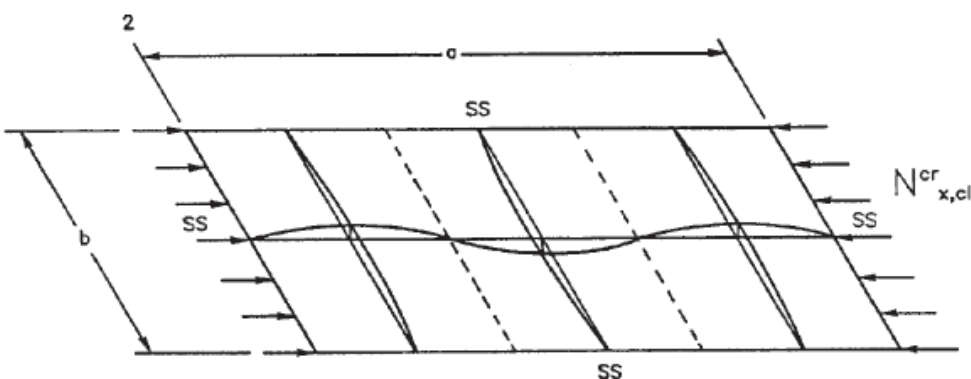


Figure 16.2.1-3: Uniaxial Loaded Panel, SS all sides, Compression Buckling [\(MIL-HDBK-17F Vol 3, 2002\)](#)

The end load flow (lb/in) for the point of initial buckling is given by the following expression:

$$N_{x,cl}^{cr} = \frac{2 \cdot \pi^2}{b^2} \cdot [(D_{11} \cdot D_{22})^{1/2} + D_{12} + 2 \cdot D_{66}]$$

This method is available in the following spreadsheet:

16.2.1.2. Effect of Central Circular Hole on Simply Supported Compression Buckling Allowable [\(NASA-TP-2528, 1986\)](#):

An approximate solution for the effect of a circular hole on the compression buckling performance of a square panel is given by the following method. This method is defined by the reduction in K, the compression buckling coefficient. The value of K for the panel without a hole can be generated from the calculated compression buckling allowable using the following expression:

$$K = \frac{N_x^{cr} \cdot W^2}{\pi^2 \cdot \sqrt{D_{11} \cdot D_{22}}}$$

Where W is the width of the loaded edge of the panel – 'b' in standard nomenclature.

The effect on the compression buckling allowable for a simply supported Panel is given by this figure:

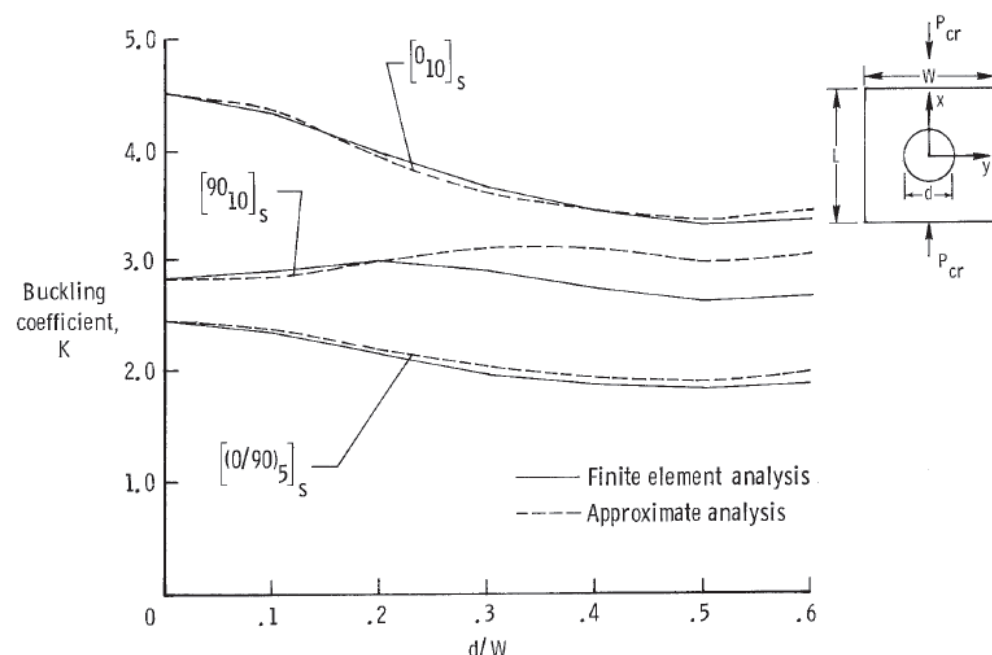


Figure 16.2.1-4: Effect of a Central Circular Hole on Axial Compression Buckling of a Simply Supported Orthotropic Panel [\(NASA-TP-2528, 1986\)](#)

The graph shows various results for different methods. The greatest overall reduction in K from all the curves will be used to generate a reduction factor that can be used to modify the K value or the compression buckling allowable directly.

This is expressed in the following figure:

(note that this reduction factor graph is in broad agreement with [\(AFWAL-TR-85-3069, 1985\)](#) Figure 7.2.

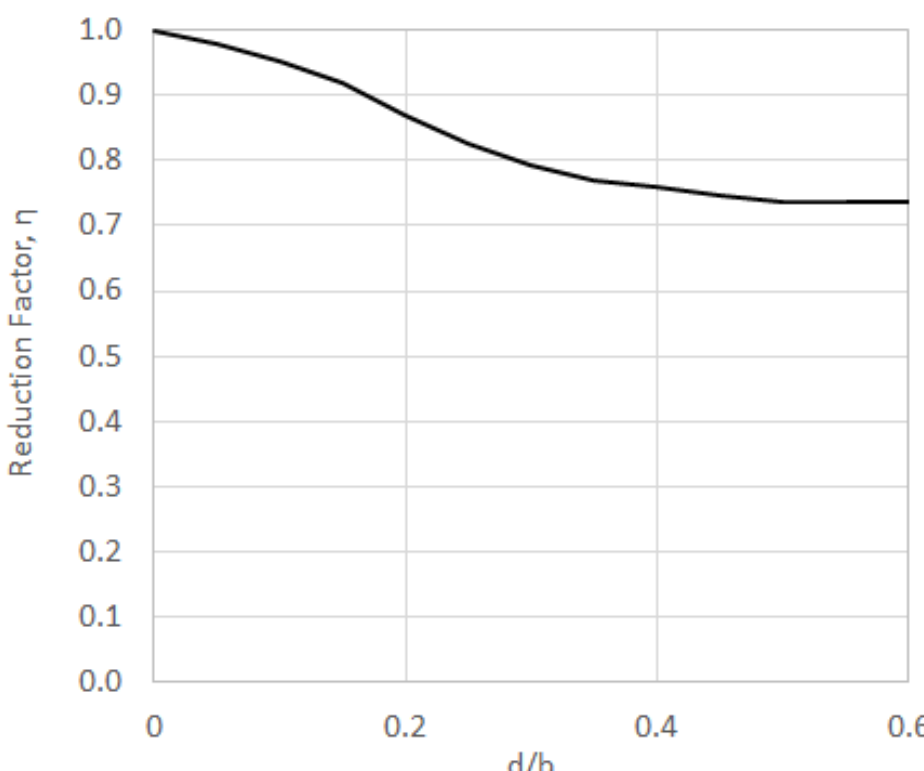


Figure 16.2.1-5: Effect of a Central Circular Hole on Axial Compression Buckling of a Simply Supported Orthotropic Panel

The end load flow for the point of initial buckling for a panel with a central circular hole becomes:

$$N_{x,cl}^{cr} = \eta \cdot \frac{2 \cdot \pi^2}{b^2} \cdot [(D_{11} \cdot D_{22})^{1/2} + D_{12} + 2 \cdot D_{66}]$$

This method is available in the following spreadsheet:

ABBOTT AEROSPACE SEZC LTD
SPREADSHEETS
ABBOTTAEROSPACE.COM

AA-SM-103-002-001 Composites - Buckling of Laminates - Uniaxial Long Plate SS with hole

16.2.1.3. Uniaxial Loading, long Panel, all sides Fixed

(Aspect ratio >4)

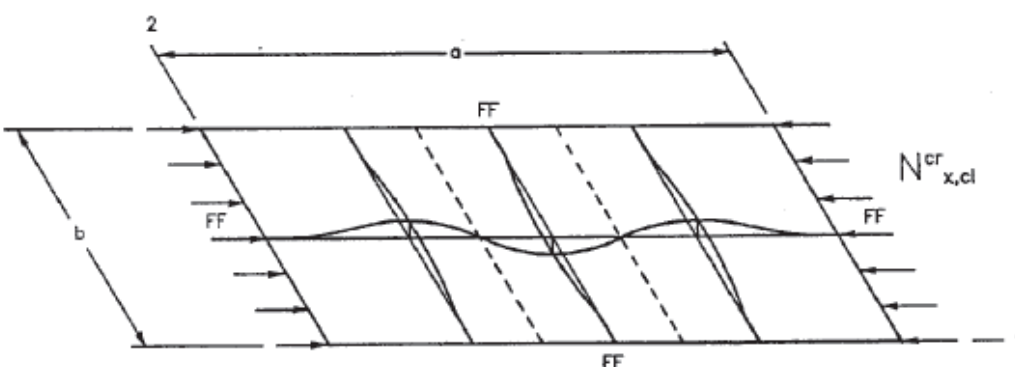


Figure 16.2.1-6: Uniaxial loaded Panel, SS all sides, Compression Buckling (MIL-HDBK-17F Vol 3, 2002)

The end load flow for the point of initial buckling is given by this expression:

$$N_{x,cl}^{cr} = \frac{\pi^2}{b^2} \cdot [4.6 \cdot (D_{11} \cdot D_{22})^{1/2} + 2.67 \cdot D_{12} + 5.33 \cdot D_{66}]$$

This method is available in the following spreadsheet:

ABBOTT AEROSPACE SEZC LTD
SPREADSHEETS
ABBOTTAEROSPACE.COM

AA-SM-103-002-002 Composites - Buckling of Laminates - Uniaxial Long Plate FF

16.2.1.4. Effect of Central Circular Hole on Fully Fixed Compression Buckling Allowable

An approximate solution for the effect of a circular hole on the compression buckling performance of a square panel with fully fixed edges is given by the following method:

The effect on the compression buckling allowable for a fully fixed Panel is given by this figure:

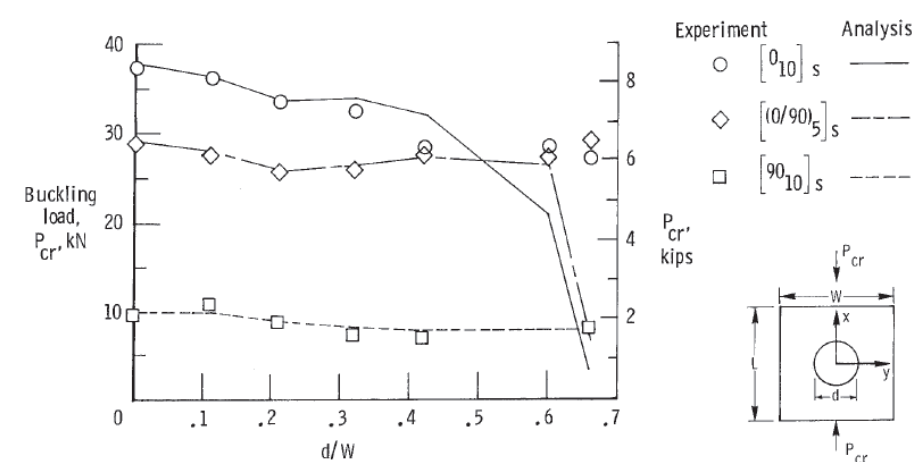


Figure 16.2.1-7: Effect of a Central Circular Hole on Axial Compression Buckling of Fully Fixed Orthotropic Panel (NASA-TP-2528, 1986)

The graph shows various results for different methods. It is recommended that the trace showing the greatest reduction is used. As there are a range of results comparing analysis and test methods, a conservative approximation over the critical data sets has been used with a cubic line of best fit:

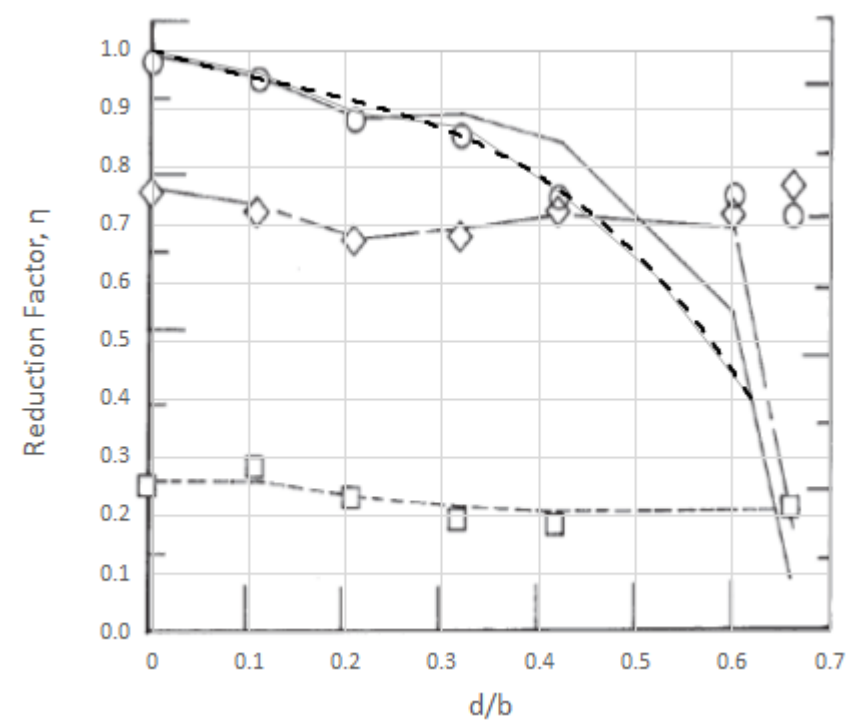


Figure 16.2.1-8: Effect of a Central Circular Hole on Axial Compression Buckling of a Fully Fixed Orthotropic Panel

The end load flow for the point of initial buckling for a panel with a central circular hole becomes:

$$N_{x,cl}^{cr} = \eta \cdot \frac{\pi^2}{b^2} \cdot [4.6 \cdot (D_{11}D_{22})^{1/2} + 2.67 \cdot D_{12} + 5.33 \cdot D_{66}]$$

This method is available in the following spreadsheet.



16.2.1.5. Uniaxial Loading, Long Panel, Three Sides Simply Supported and One Unloaded Edge Free

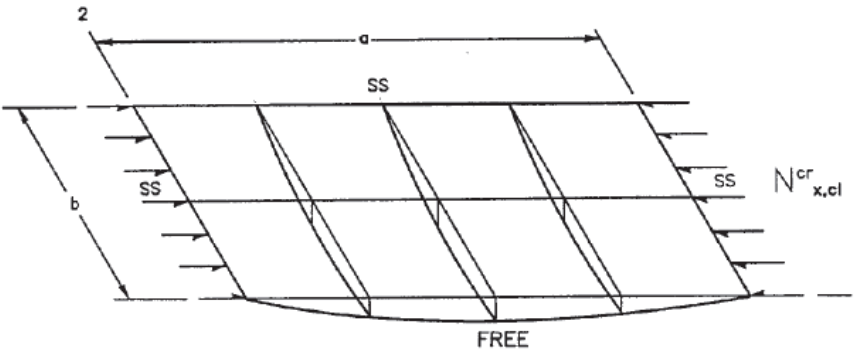


Figure 16.2.1-9: Uniaxial loaded Panel, SS three sides, Compression Buckling (MIL-HDBK-17F Vol 3, 2002)

The end load flow for the point of initial buckling:

$$N_{x,cl}^{cr} = \frac{12 \cdot D_{66}}{b^2} + \frac{\pi^2 \cdot D_{11}}{a^2}$$

This method is available in the following spreadsheet:



The following methods for shear buckling are more refined and give solutions for finite length panels covering a range of panel aspect ratios.

16.2.1.6. Shear Loading, Panel with all sides simply supported

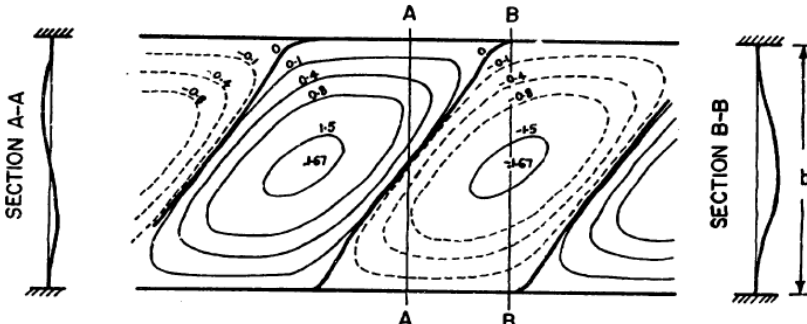


Figure 16.2.1-10: Shear Loaded Panel with Shear Buckle (AFWAL-TR-85-3069, 1985)

The shear buckling analysis method is taken from [\(NASA-TN-D-7996, 1975\)](#) which gives buckling solutions for shear and compression combinations. This paper gives the basic solution for shear buckling of a finite panel so we have used this as the best available reference. The general solution of the shear buckling equations can be expressed using the following parameter:

$$k_{ss} = \frac{b^2 \cdot N_x^{cr}}{\pi^2 \cdot \sqrt[4]{D_{11} \cdot D_{22}}^3}$$

The parameter k_s is a function of only two variables:

$$\Theta = \frac{\sqrt{D_{11} \cdot D_{22}}}{D_3}$$

Where: $D_3 = D_{12} + 2D_{66}$

And:

$$B = \frac{b}{a} \cdot \sqrt[4]{\frac{D_{11}}{D_{22}}}$$

To find the k_s for panel with simply supported edges see Figure 16.2.1-11:

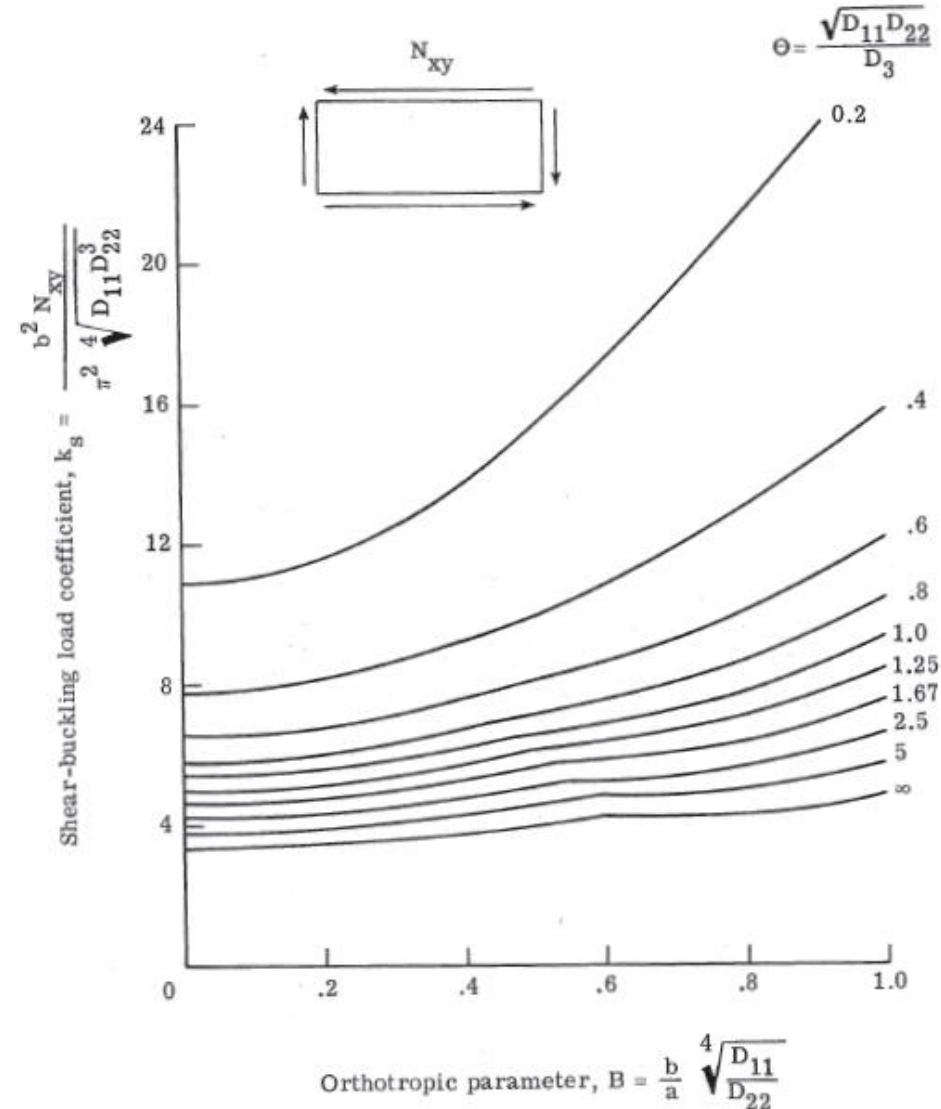


Figure 16.2.1-11: Graphical Solution for k_s – Shear Buckling of Simply Supported Panels [\(NASA-TN-D-7996, 1975\)](#)

Therefore:

$$N_{xy} = \frac{k_{ss} \cdot \pi^2 \cdot \sqrt[4]{(D_{11} \cdot D_{22})^3}}{b^2}$$

This method is available in the following spreadsheet:



To find the k_s for panel with fully fixed edges see Figure 16.2.1-12:

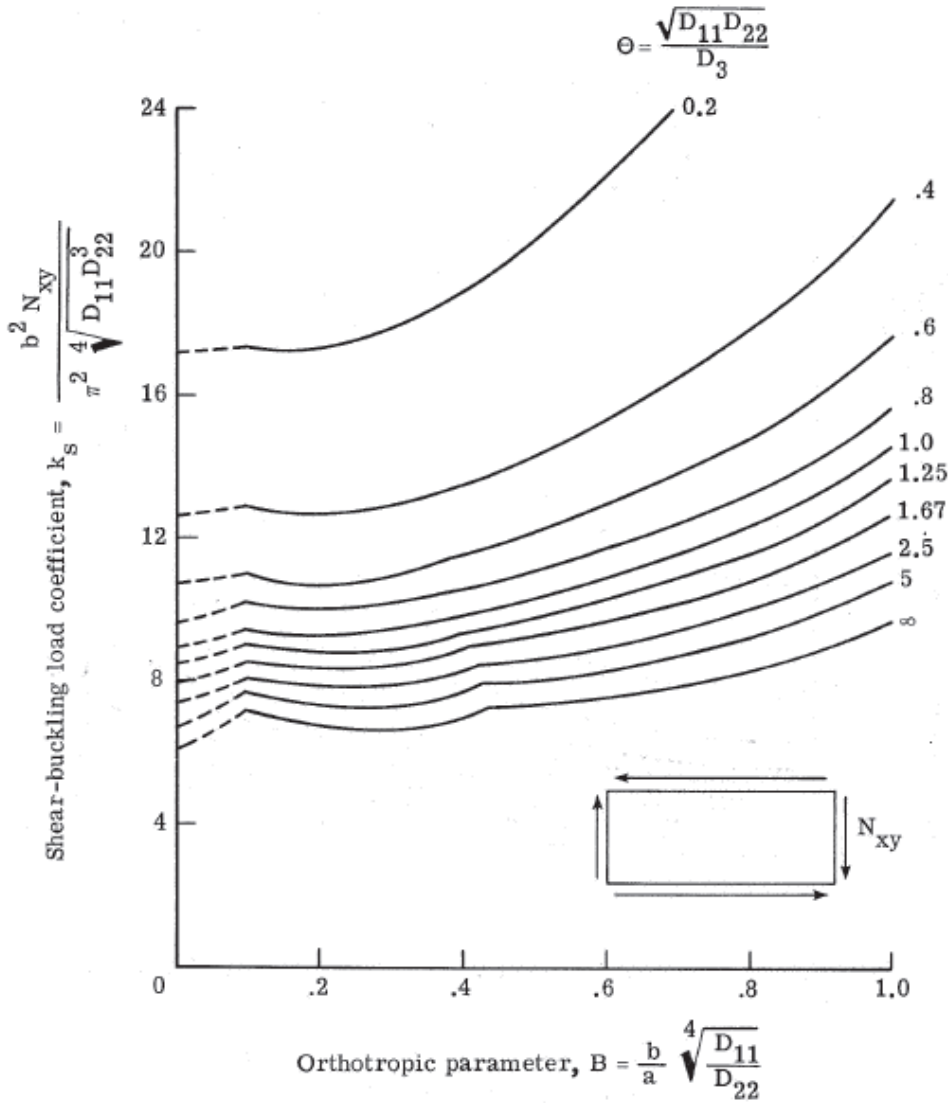


Figure 16.2.1-12: Graphical Solution for k_s – Shear Buckling of Fully Fixed Panels [\(NASA-TN-D-7996, 1975\)](#)

For a panel with edges fixed in rotation the spreadsheet method is available here:



Once K_s has been found graphically the equation for k_s can easily be rearranged to give the solution for N_{xy} :

$$N_{xy} = \frac{k_s \cdot \pi^2 \cdot \sqrt[4]{(D_{11} \cdot D_{22})^3}}{b^2}$$

Note that this equation is a similar form to the buckling equation for isotropic Panel buckling from [\(NACA-TN-3781, 1957\)](#), shown in its general form below:

$$\sigma_{cr} = \frac{k \cdot \pi^2 \cdot E}{12 \cdot (1 - \nu_e^2)} \cdot \left(\frac{t}{b}\right)^2$$

The equivalent terms that express the out-of-plane stiffness of the Panel are:

$$\sqrt[4]{(D_{11} \cdot D_{22})^3} \equiv \frac{E}{12 \cdot (1 - \nu_e^2)} \cdot \left(\frac{t}{b}\right)^2$$

$$\sqrt[4]{(D_{11} \cdot D_{22})^3} \equiv \frac{E \cdot t^2}{12 \cdot (1 - \nu_e^2)}$$

16.2.1.7. Interaction of Compression and Shear Buckling Effects

Ref. [\(NASA-TN-D-7996, 1975\)](#) shows comparison between a set of analyses and a linear/squared interaction. This demonstrates that using the mathematical approximation of the compression buckling reserve factor and the square of the shear buckling reserve factor is conservative.

This approach is confirmed in [\(NASA CR-2330, 1974\)](#).

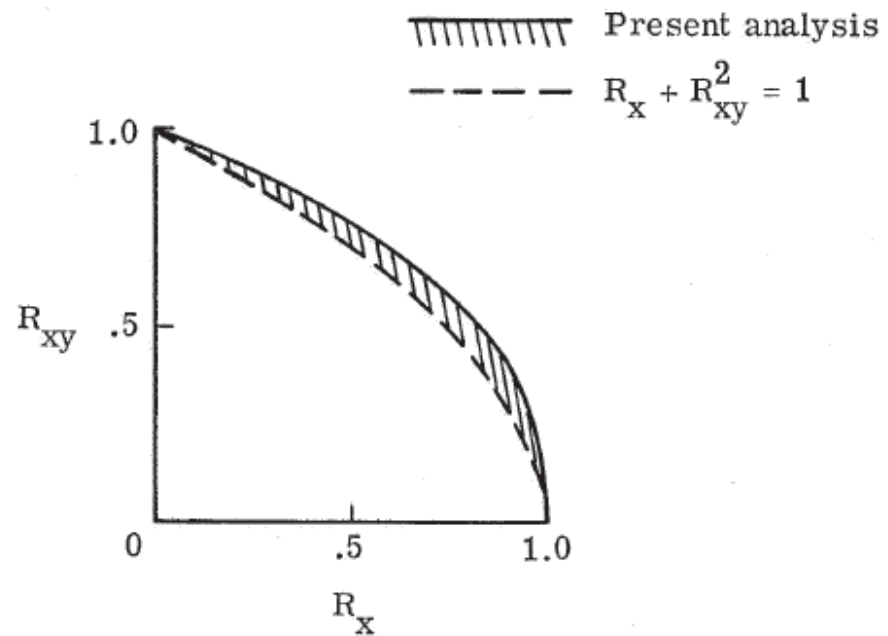


Figure 16.2.1-13: Graphical Comparison of Analysis vs Mathematical Solution for Compression and Shear Buckling Effects [\(NASA-TN-D-7996, 1975\)](#)

This interaction method is available as a spreadsheet solution here:



16.2.1.8. Note on Post-Buckling and Crippling

As noted at the start of this chapter it is common to keep composite structure non-buckling up to ultimate load. Post buckling effects will not be covered in this edition. Crippling is a post buckling failure mode thus it will not be covered.

It is recommended that all composite primary structure be kept non-buckling up to ultimate load.

16.2.2. Stability of Cored Laminates

16.2.2.1. Introduction

The fundamental purpose of cored laminate is to achieve a disproportionate increase in out-of-plane stiffness when compared to the weight increase. This particular increase in property makes cored panels more resistant to panel buckling effects.

Panel buckling is just one of a set of stability failure modes that cored laminates can experience. The critical failure mode depends on the type of core (honeycomb or foam), the thickness and material properties of the core, the material and thickness of the face sheets and the overall panel dimensions.

The failure modes that will be covered in this section are:

Global Mode: (Panel) Buckling



Figure 16.2.2-1: Sandwich Panel Buckling [\(NASA/CR-1999-208994, 1999\)](#)

Global Mode: Shear Crimping

Shear crimping appears to be a local mode of failure but is actually a form of general overall buckling in which the wavelength of the buckles is very small because of low core shear modulus. The crimping of the sandwich occurs suddenly and usually causes the core to fail in shear at the crimp. It may also cause shear failure in the bond between the facing and core.

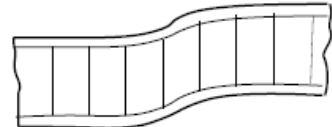


Figure 16.2.2-2: Sandwich Panel Shear Crimping [\(NASA/CR-1999-208994, 1999\)](#)

Crimping may also occur in cases where the overall buckle begins to appear and then the crimp occurs suddenly because of severe local shear stresses at the ends of the overall buckle. As soon as the crimp appears, the overall buckle may disappear. Therefore, although examination of the failed sandwich indicates crimping or shear instability, failure may have begun by overall buckling that finally caused crimping.

Local Mode: Facesheet Dimpling

If the core is of cellular (honeycomb) or corrugated material, it is possible for the facings to buckle or dimple into the spaces between core walls or corrugations as shown below:



Figure 16.2.2-3: Sandwich Panel Facesheet Dimpling [\(NASA/CR-1999-208994, 1999\)](#)

Dimpling may be severe enough so that the amplitude of the dimples may be large enough to cause the dimples to grow across the core cell walls and result in a wrinkling of the facings.

Local Mode: Facesheet Wrinkling

Wrinkling may occur if a sandwich facing subjected to edgewise compression buckles as a panel on an elastic foundation. The facing may buckle inward or outward, depending on the flatwise compressive strength of the core relative to the flatwise tensile strength of the bond between the facing and core. If the bond between facing and core is strong, facings can wrinkle and cause tension failure in the core. Thus, the wrinkling load depends upon the elasticity and strength of the foundation system; namely, the core and the bond between facing and core. Since the facing is never perfectly flat, the wrinkling load will also depend upon the initial eccentricity of the facing or original waviness.



Figure 16.2.2-4: Sandwich panel Facesheet Wrinkling [\(NASA/CR-1999-208994, 1999\)](#)

Other Local Failure modes:



Figure 16.2.2-5: Core Crushing [\(NASA CR-1457, 1969\)](#)

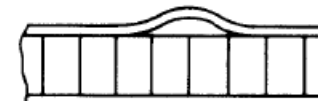


Figure 16.2.2-6: Tensile Rupture of Bond [\(NASA CR-1457, 1969\)](#)



Figure 16.2.2-7: Tensile Rupture of Core Proper [\(NASA CR-1457, 1969\)](#)

Note:

It is important to note that all of these failure modes can result in catastrophic global failure of the panel. A sandwich panel is dependent on the cohesion of the face sheets and the core and the local failure modes can initiate global failure modes. Because of the out-of-plane stiffness of the sandwich panel, the secondary loads generated by the buckling failure modes are often significant and catastrophic.

General Panel Nomenclature:

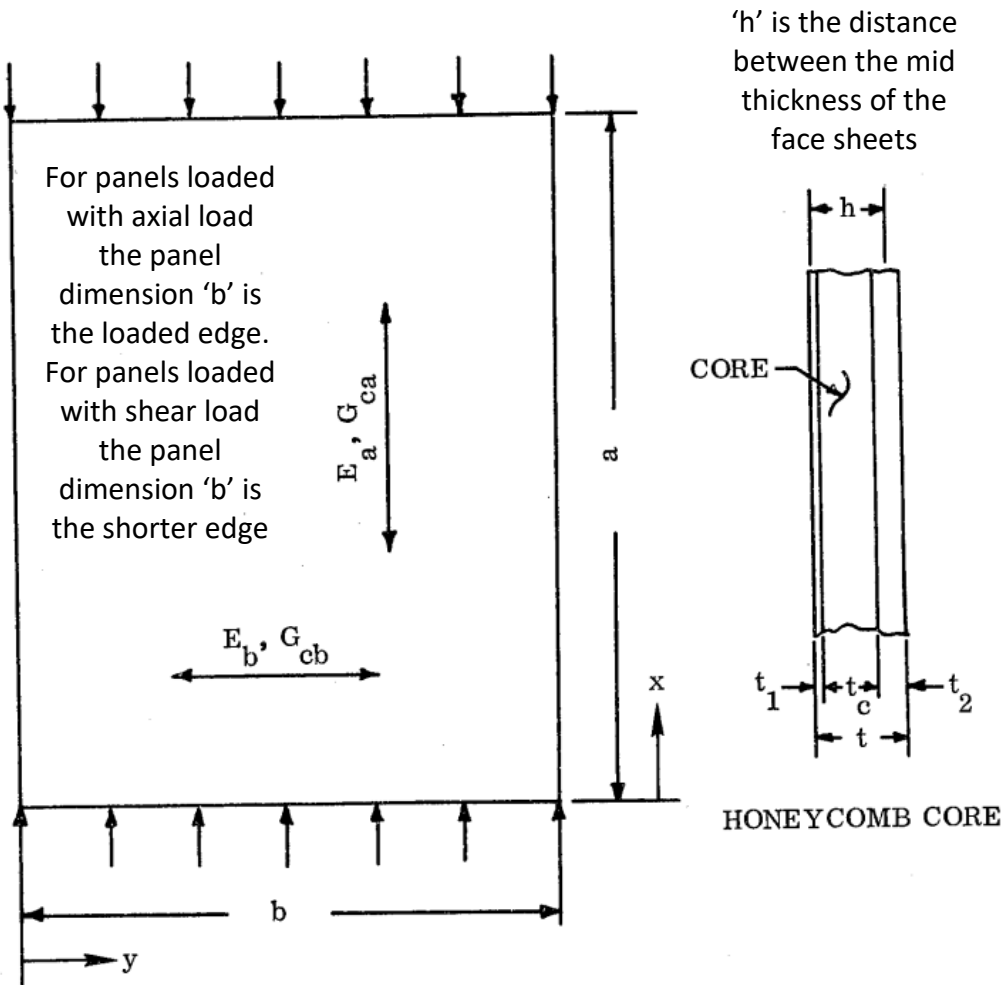


Figure 16.2.2-8: Sandwich Panel Nomenclature and Thickness Notation
(NASA CR-1457, 1969)

ADVERT: SOFTWARE

EXCEL ADD-IN: SOFTWARE TOOLS

[DOWNLOAD](#)

XL-VIKING

By Aerospace Stress Engineers for Aerospace Stress Engineers

Boost your Excel Performance

A silhouette of a fighter jet flying through clouds.

ABBOTT AEROSPACE SEZC LTD

16.2.2.2. Global Mode: Panel Buckling

The panel buckling methods are taken from [\(NASA CR-1457, 1969\)](#). This reference gives solutions for orthotropic and isotropic facings. Much of the work on buckling of sandwich panels, and the work on sandwich panels in general, originate in the US Forest Product Laboratory reports and their pioneering work done in the 1950s and 1960s. We have collected the relevant reports and host them on our website, they can be found [here](#).

16.2.2.3. Sandwich Panel Compression Buckling

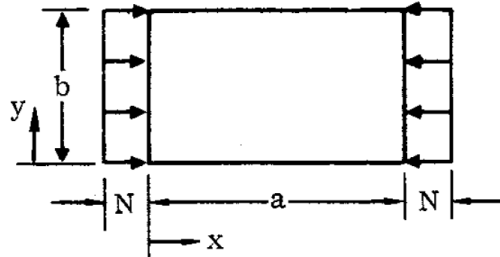


Figure 16.2.2-9: Shear Buckling Load Application and Nomenclature [\(NASA CR-1457, 1969\)](#)

The load per unit panel width at which buckling of a sandwich panel will occur is given by the theoretical formula:

$$N_{cr} = K \cdot \frac{\pi^2}{b^2} \cdot D$$

Where N_{cr} is the allowable load flow (lb/in).

The D_{11} term from the D matrix of the laminate can be used for 'D' in the expression above.

Solved for face sheet stresses:

$$F_{c1,2} = \pi^2 \cdot K \cdot \frac{E'_1 \cdot t_1 \cdot E'_2 \cdot t_2}{(E'_1 \cdot t_1 + E'_2 \cdot t_2)^2} \cdot \left(\frac{h}{b}\right)^2 \cdot \frac{E'_{1,2}}{\lambda}$$

For sandwich panels with equal face sheets:

$$F_{c1,2} = \frac{\pi^2 \cdot K}{4} \cdot \left(\frac{h}{b}\right)^2 \cdot \frac{E'_{1,2}}{\lambda}$$

Where:

- K buckling coefficient = $K_F + K_M$ (See section below)
- E' $(E'_a E'_b)^{0.5}$ = effective modulus of elasticity for orthotropic facings, psi
- $\lambda = (1 - \mu_a \mu_b)$
- μ_a, μ_b Poisson's ratio as measured parallel to the subscript direction
- $f_{1,2}$ subscripts denoting facings
- h, b Panel Dimensions, in - Figure 16.2.2-8

As noted above the buckling coefficient for the panel under this loading condition is given by the equation:

$$K = K_F + K_M$$

Where:

$$K_F = \frac{(E'_1 \cdot t_1^3 + E'_2 \cdot t_2^3)(E'_1 \cdot t_1 + E'_2 \cdot t_2)}{12 \cdot E'_1 \cdot t_1 \cdot (E'_2 \cdot t_2) \cdot h^2} \cdot K_{M0}$$

K_{M0} is given by the following figure:

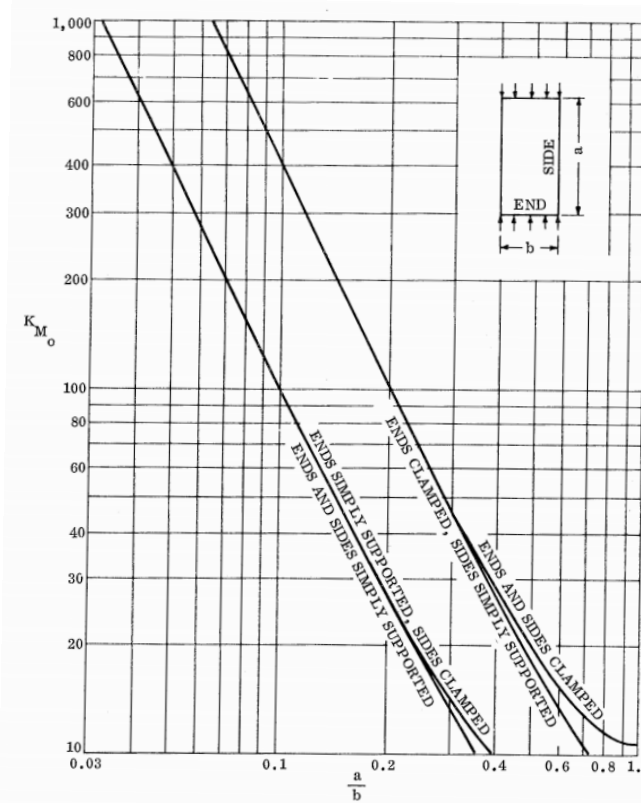


Figure 16.2.2-10: K_{M0} for Sandwich Panels with Isotropic Facings in Edgewise Compression [\(NASA CR-1457, 1969\)](#)

The values of K_F are generally small relative to K_M . As safe first approximation is to assume K_F is equal to zero unless the margin of safety is low.

For sizing it is safe to assume $K = K_M$.

$K_{M0} = K_M$ when $V = 0$, see definition of V below, and when $a/b > 1.0$ it can be assumed $K_F = 0$.

The value of K_M is related to the bending shear rigidity parameter V :

$$V = \frac{\pi^2 D}{b^2 U}$$

Where

U = Sandwich transverse shears stiffness, defined as:

$$U = \frac{h^2}{t_c} \cdot G_c \approx h \cdot G_c$$

V can also be defined in terms of the geometry and properties of the face sheets and core:

$$V = \frac{\pi^2 \cdot t_c \cdot E'_1 \cdot t_1 \cdot E'_2 \cdot t_2}{\lambda \cdot b^2 \cdot G_c \cdot (E'_1 \cdot t_1 + E'_2 \cdot t_2)}$$

Where:

$$\lambda = (1 - \mu_a \mu_b)$$

Having the necessary physical properties of the panel defined, the K value and the buckling allowable can be derived.

The basic cored panel physical properties can be calculated using this spreadsheet:

ABBOTT AEROSPACE SEZC LTD
SPREADSHEETS
ABBOTTAEROSPACE.COM

AA-SM-102-001 Composites - Cored Laminate Basic Stiffness Properties

Derivation of K_M for cored panels in compression

[\(FPL-070, 1964\)](#) gives a mathematical derivation of compression buckling coefficients for cored panels. The full derivation will not be given in this text but the math is implemented in the spreadsheet below. The curves for K_M have been developed using this reference and reference curves for isotropic core for $\alpha = 1.00$, $\beta = 1.00$ and $\gamma = 0.375$ are given in this spreadsheet:



The reference curves for cored panel compression buckling from [\(NASA CR-1457, 1969\)](#) are shown below. The general solution, mathematically derived per [\(FPL-070, 1964\)](#) for all panels is given in the following spreadsheet:

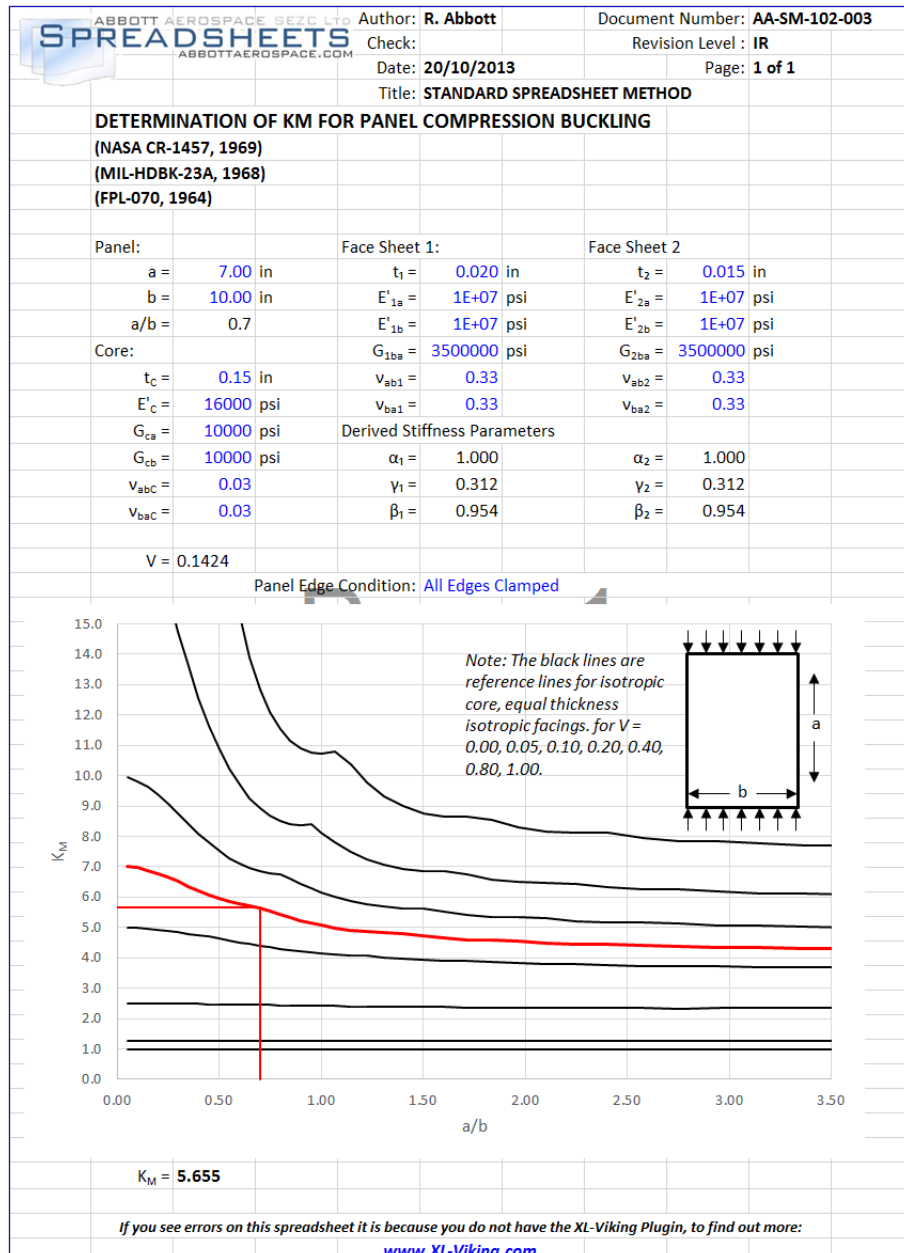
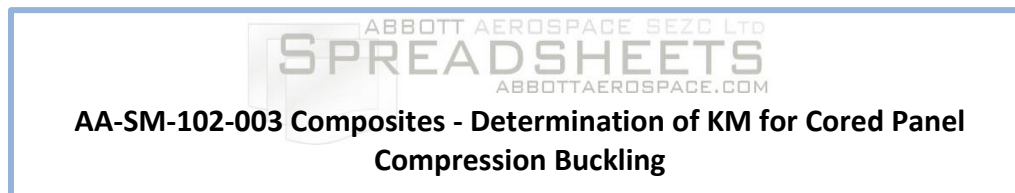


Figure 16.2.2-11: Spreadsheet for General Solution of K_M for Cored Panel Compression Buckling

The sandwich panel compression buckling coefficient figures are given below, it is recommended that the spreadsheet method is used to determine the compression buckling coefficient. The following figures should be used for comparison and checking.

In the following figures the term 'R' is used, this is the degree of core shear modulus orthotropicity (G_{ca}/G_{cb}).

16.2.2.4. Sandwich Panel Compression Buckling Coefficients for Panels with Isotropic Facings and Isotropic Core:

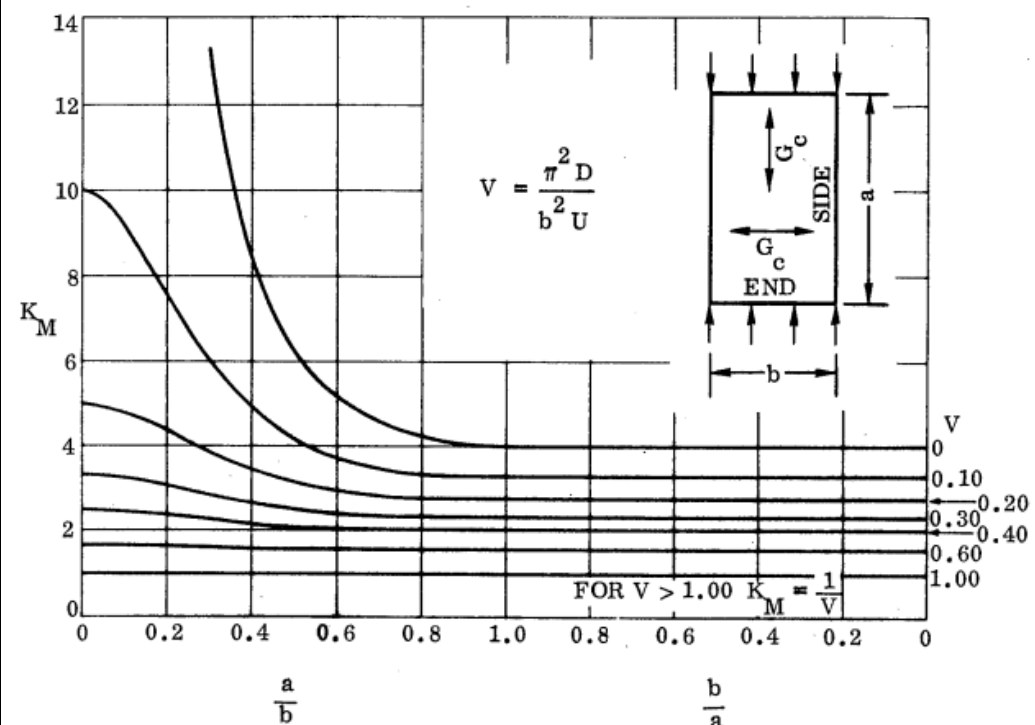


Figure 16.2.2-12: Sandwich Panel Compression Buckling, Isotropic Facings, Isotropic Core, All Sides Simply Supported [\(NASA CR-1457, 1969\)](#)

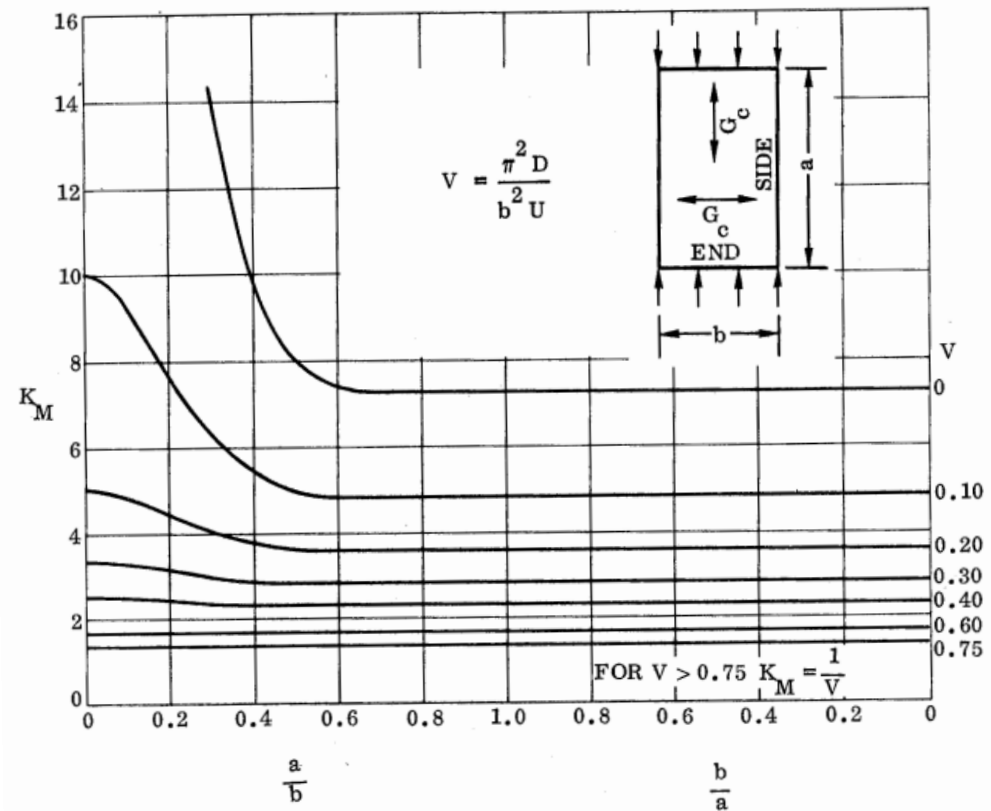
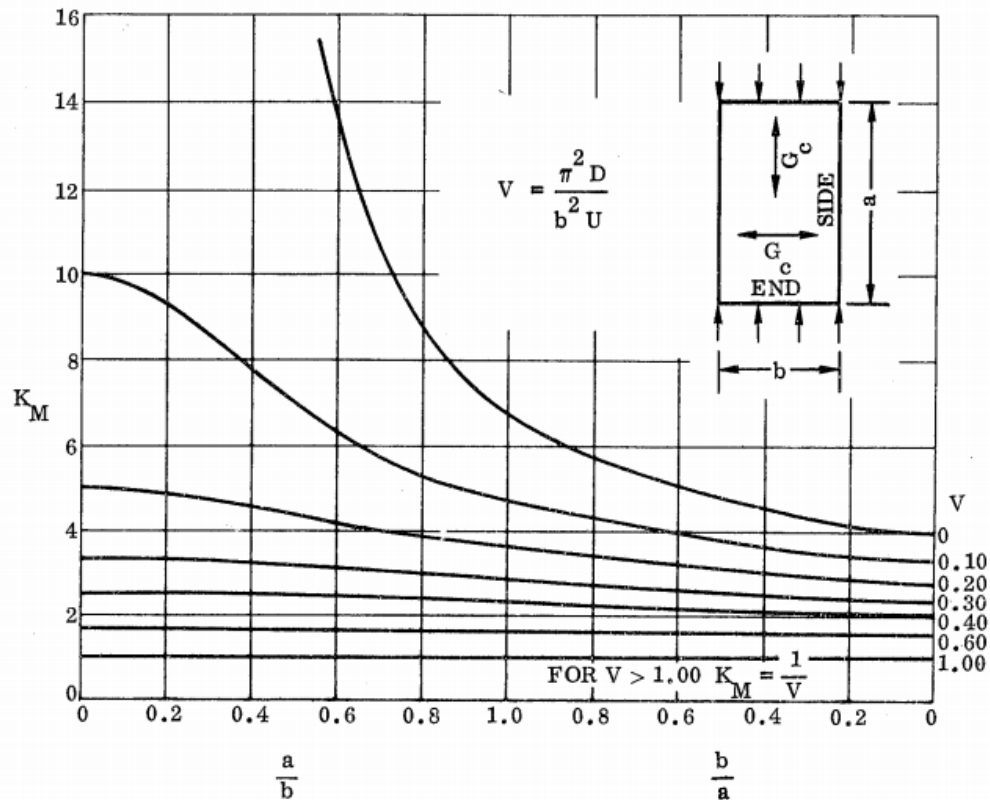
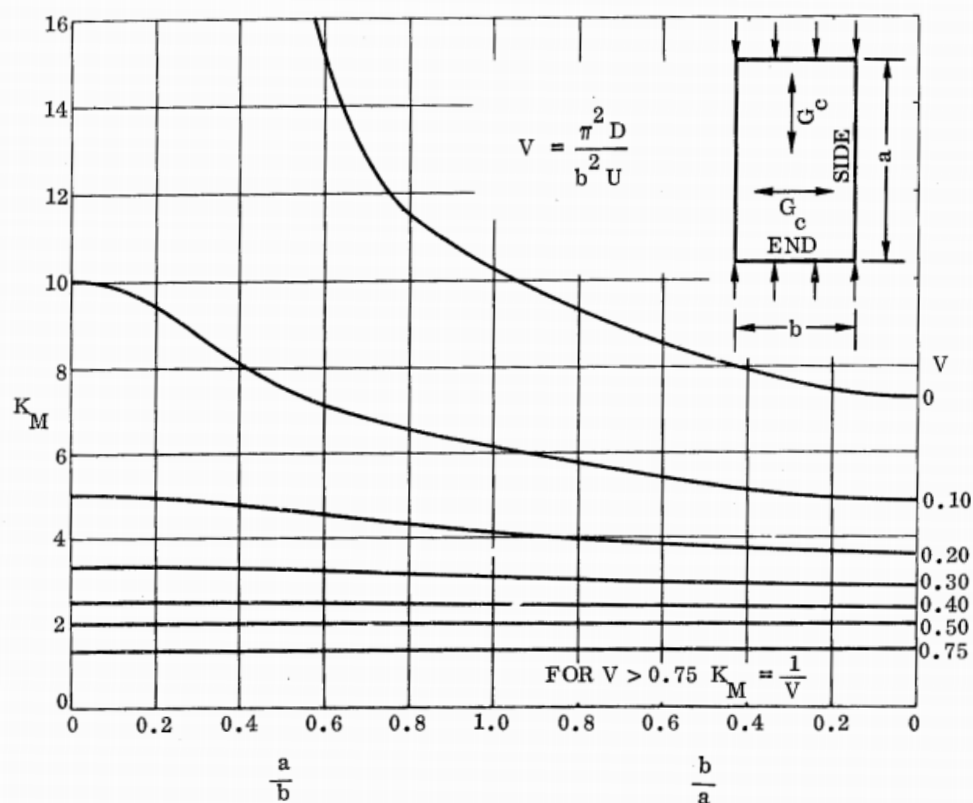


Figure 16.2.2-13: Sandwich Panel Compression Buckling, Isotropic Facings, Isotropic Core, Ends Simply Supported, Sides Clamped [\(NASA CR-1457, 1969\)](#)



**Figure 16.2.2-14: Sandwich Panel Compression Buckling, Isotropic Facings,
 Isotropic Core, Sides Simply Supported, Ends Clamped
 (NASA CR-1457, 1969)**



**Figure 16.2.2-15: Sandwich Panel Compression Buckling, Isotropic Facings,
 Isotropic Core, All Sides Clamped
 (NASA CR-1457, 1969)**

**16.2.2.5. Sandwich Panel Compression Buckling Coefficients
for Panels with Isotropic Facings and Orthotropic Core
(R=0.40):**

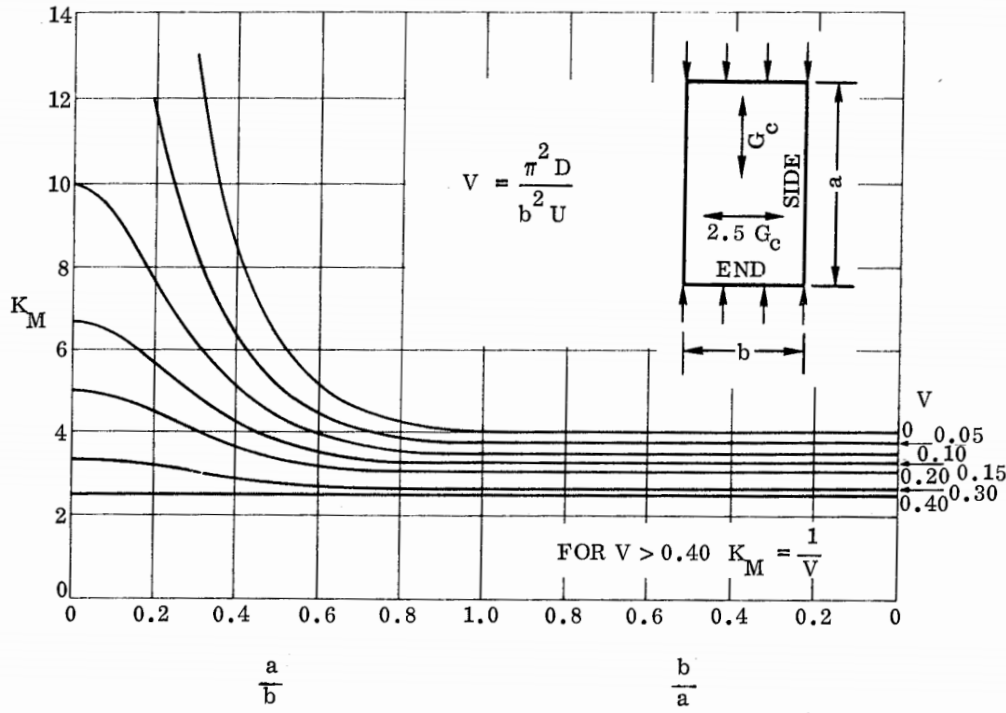


Figure 16.2.2-16: Sandwich Panel Compression Buckling, Isotropic Facings, Orthotropic Core (R=0.40), All Sides Simply Supported
(NASA CR-1457, 1969)

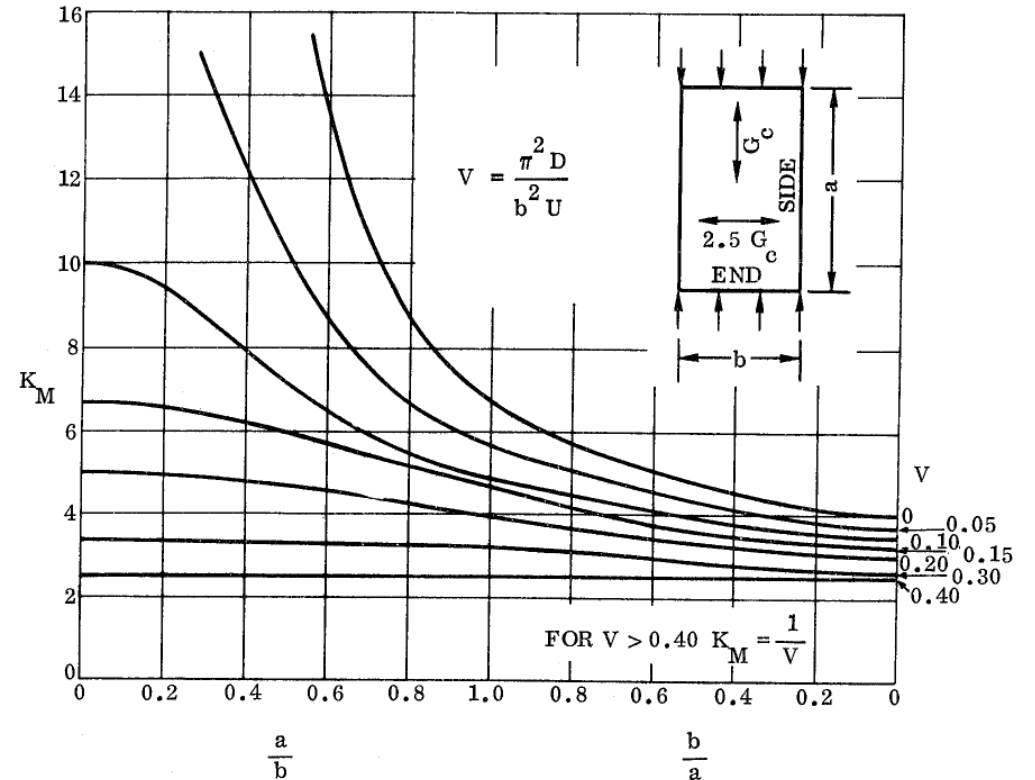


Figure 16.2.2-18: Sandwich Panel Compression Buckling, Isotropic Facings, Orthotropic Core (R=0.40), Sides Simply Supported, Ends Clamped
(NASA CR-1457, 1969)

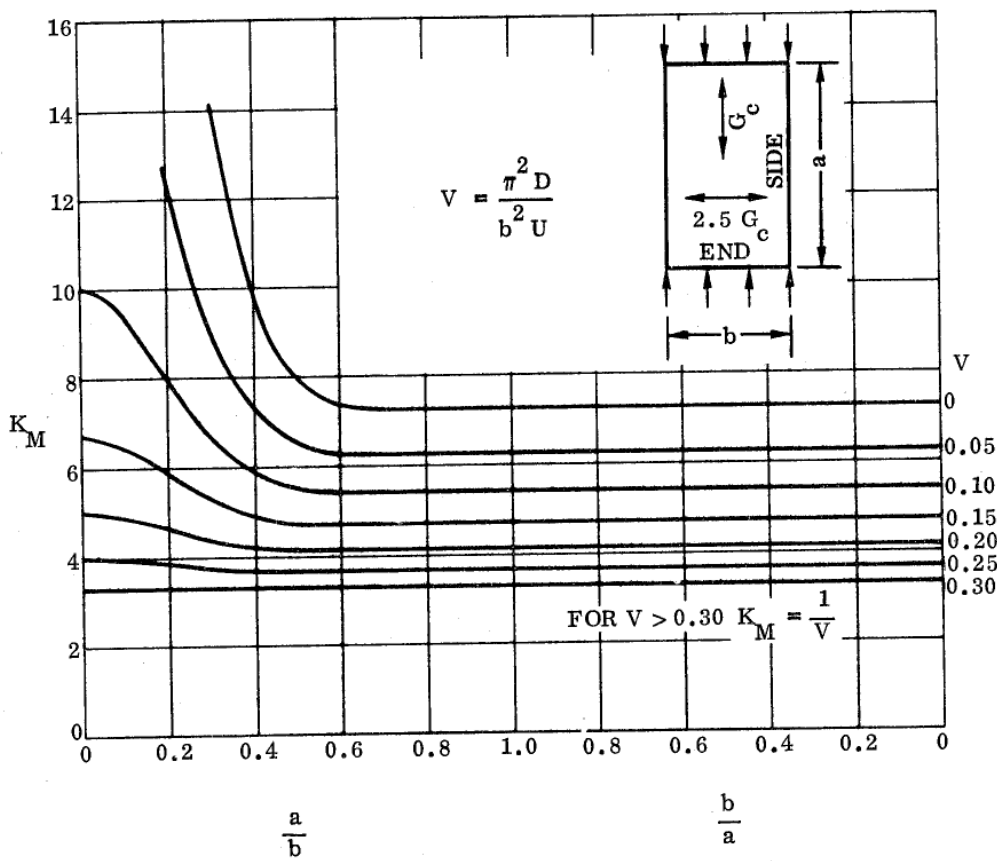


Figure 16.2.2-17: Sandwich Panel Compression Buckling, Isotropic Facings, Orthotropic Core (R=0.40), Ends Simply Supported, Sides Clamped
(NASA CR-1457, 1969)

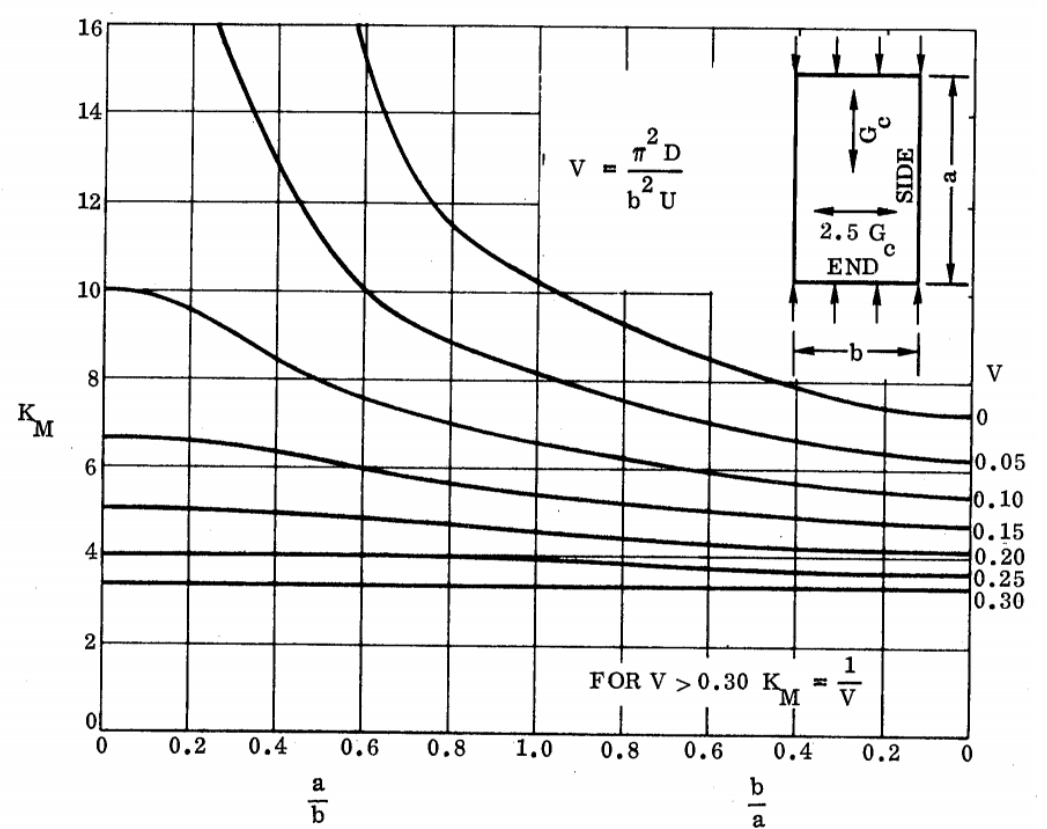


Figure 16.2.2-19: Sandwich Panel Compression Buckling, Isotropic Facings, Orthotropic Core (R=0.40), All Sides Clamped
(NASA CR-1457, 1969)

**16.2.2.6. Sandwich Panel Compression Buckling Coefficients
for Panels with Isotropic Facings and Orthotropic Core
(R=2.50):**

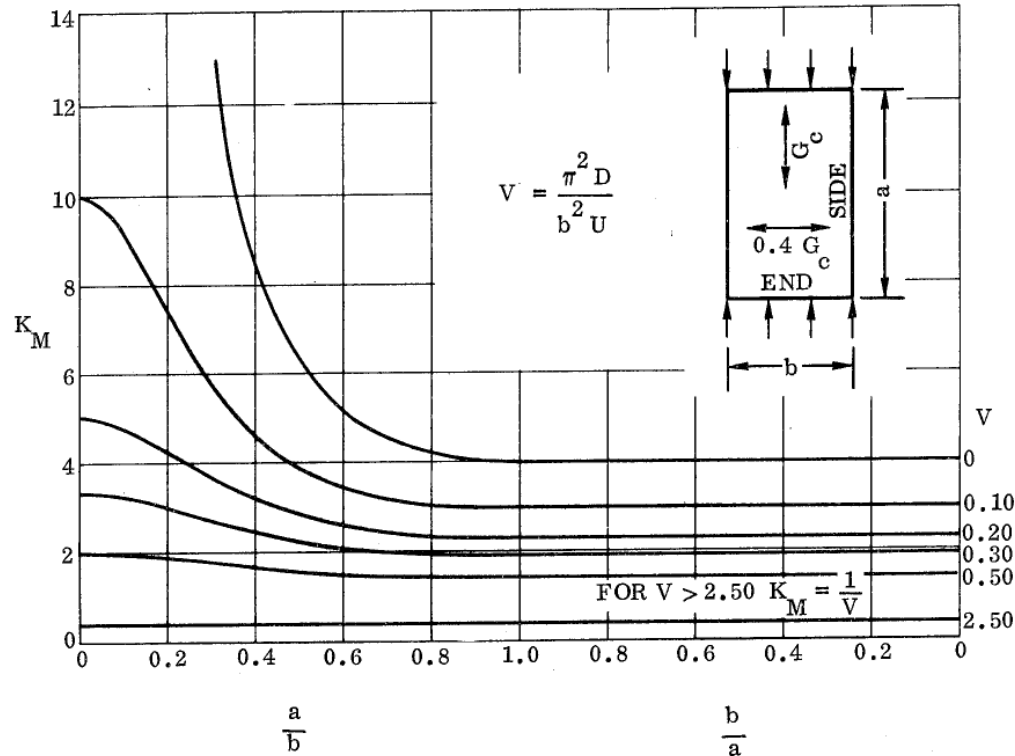


Figure 16.2.2-20: Sandwich Panel Compression Buckling, Isotropic Facings, Orthotropic Core (R=2.50), All Sides Simply Supported
(NASA CR-1457, 1969)

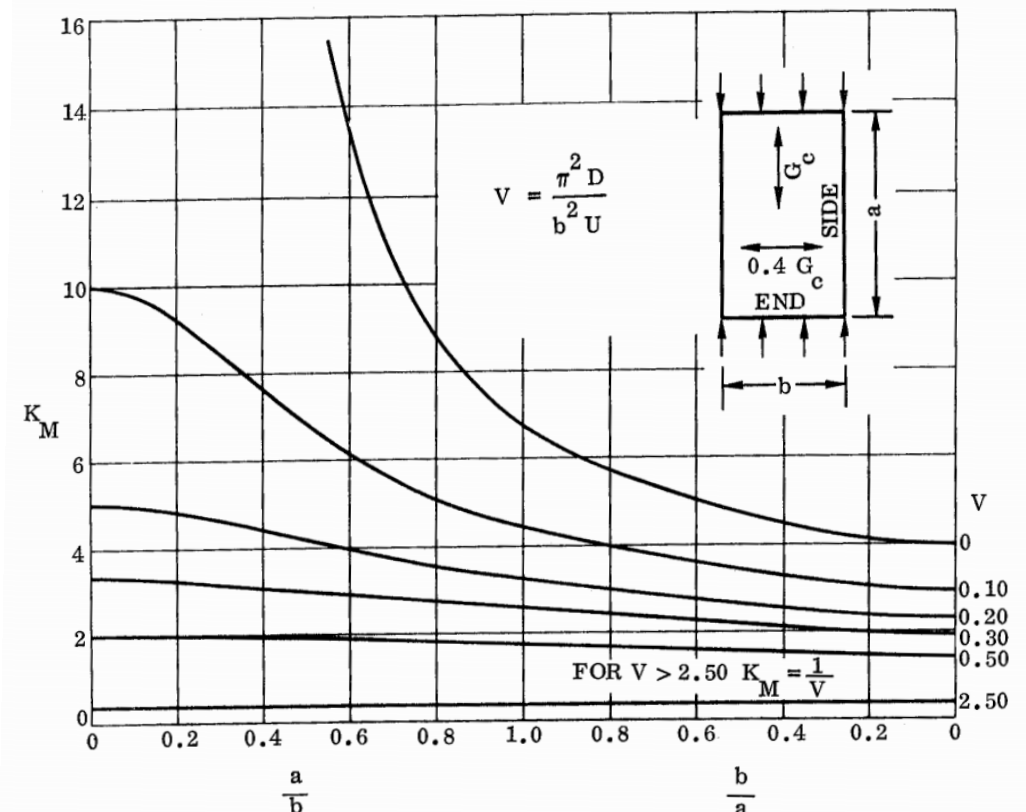


Figure 16.2.2-22: Sandwich Panel Compression Buckling, Isotropic Facings, Orthotropic Core (R=2.50), Sides Simply Supported, Ends Clamped
(NASA CR-1457, 1969)

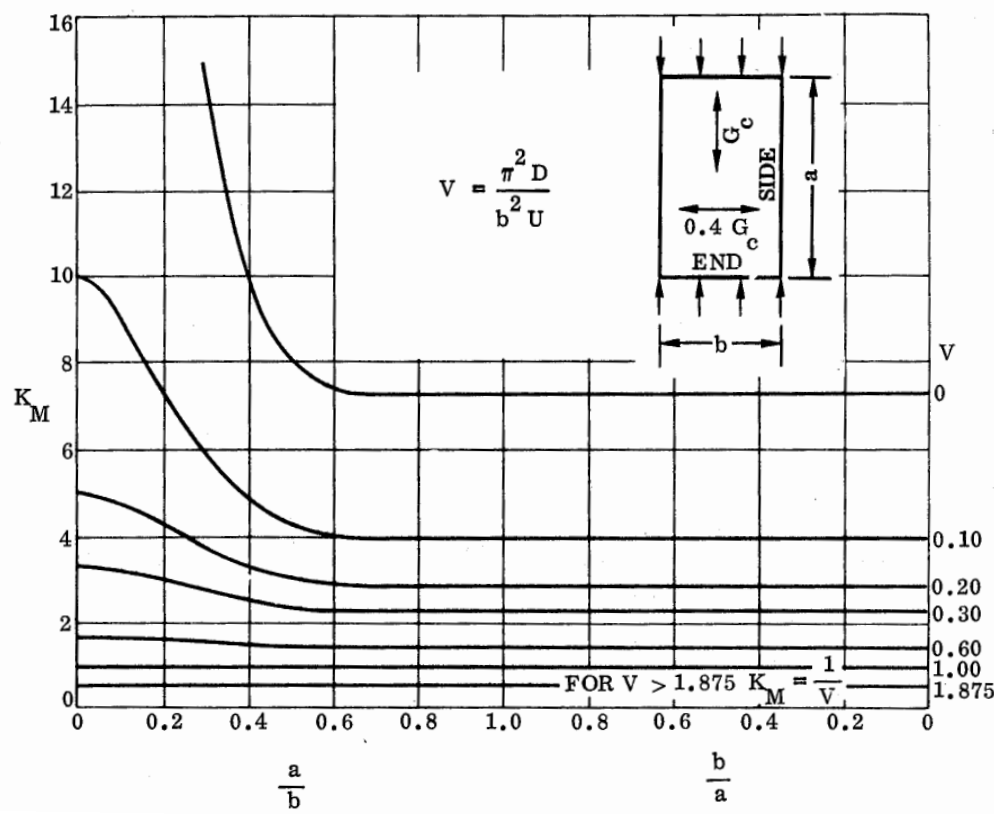


Figure 16.2.2-21: Sandwich Panel Compression Buckling, Isotropic Facings, Orthotropic Core (R=2.50), Ends Simply Supported, Sides Clamped
(NASA CR-1457, 1969)

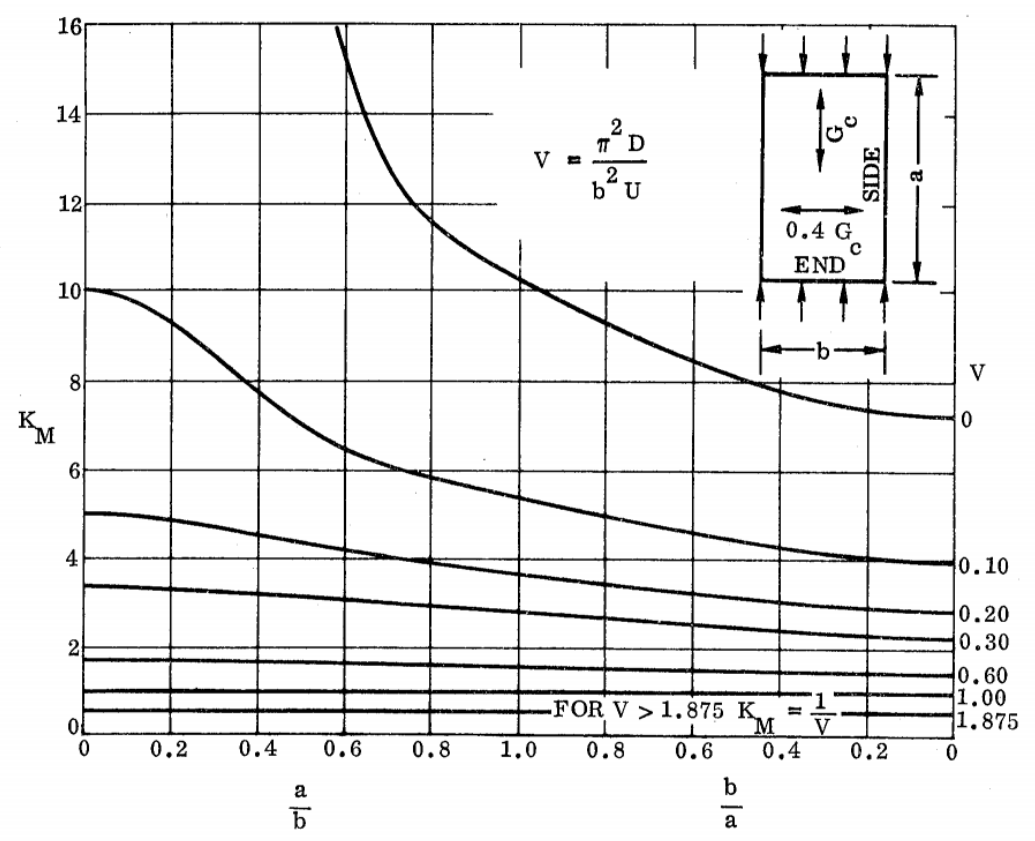


Figure 16.2.2-23: Sandwich Panel Compression Buckling, Isotropic Facings, Orthotropic Core (R=2.50), All Sides Clamped
(NASA CR-1457, 1969)

16.2.2.7. Sandwich Panel Shear Buckling

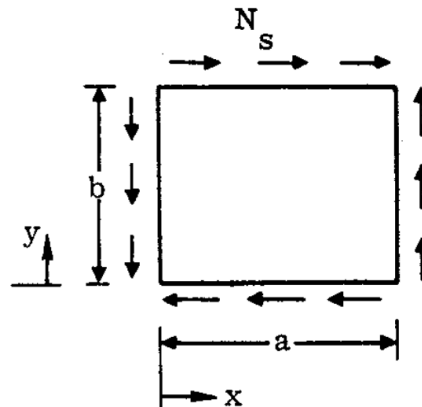


Figure 16.2.2-24: Shear Buckling Load Application and Nomenclature
(NASA CR-1457, 1969)

The base theory for the expression for buckling is the same as defined for the compression buckle in section 16.2.2.3.

The load per unit panel width at which shear buckling of a sandwich panel will occur is given by the theoretical formula:

$$N_{cr} = K_s \cdot \frac{\pi^2}{b^2} \cdot D$$

Where: N_{cr} is the allowable load flow (lb/in).

The D_{11} term from the D matrix of the laminate can be used.

Solved for face sheet stresses:

$$F_{c1,2} = \pi^2 \cdot K_s \cdot \frac{E'_1 \cdot t_1 \cdot E'_2 \cdot t_2}{(E'_1 \cdot t_1 + E'_2 \cdot t_2)^2} \cdot \left(\frac{h}{b}\right)^2 \cdot \frac{E'_f}{\lambda}$$

For isotropic face sheets this formula solved for the facing stress becomes:

Where:

- K** Buckling coefficient = $K_F + K_M$ (See section below)
- E'** $(E'_a E'_b)^{0.5}$ = effective modulus of elasticity for orthotropic facings, psi
- $\lambda = (1 - \mu_a \mu_b)$
- μ_a, μ_b Poisson's ratio as measured parallel to the subscript direction
- $f, 1, 2$ Subscripts denoting facings
- h** Figure 16.2.2-8
- b** Panel Minimum Dimension, in

As noted above the buckling coefficient for the panel under this loading condition is given by the equation:

$$K_s = K_F + K_M$$

Where:

$$K_F = \frac{(E'_1 \cdot t_1^3 + E'_2 \cdot t_2^3)(E'_1 \cdot t_1 + E'_2 \cdot t_2)}{12 \cdot E'_1 \cdot t_1 (E'_2 \cdot t_2) \cdot h^2} \cdot K_{M0}$$

And:

$K_{M0} = K_{FM}$ when $V = 0$ – This is the upper line from each of the curves.

As for compression buckling of cored panels, the values of K_F are generally small relative to K_M . As safe first approximation is to assume it is equal to zero unless the margin of safety is low.

For sizing it is safe to assume $K = K_M$, however for greater accuracy K_F can be calculated by taking the K_{M0} values from the curves on the following pages.

ADVERT: ENGINEERING SERVICES

STRUCTURES DESIGN

CONTACT US

ENGINEERING SERVICES

ABBOTT AEROSPACE SEZC LTD

16.2.2.8. Sandwich Panel Shear Buckling Coefficients for Panels with Isotropic Facings and Isotropic Core:

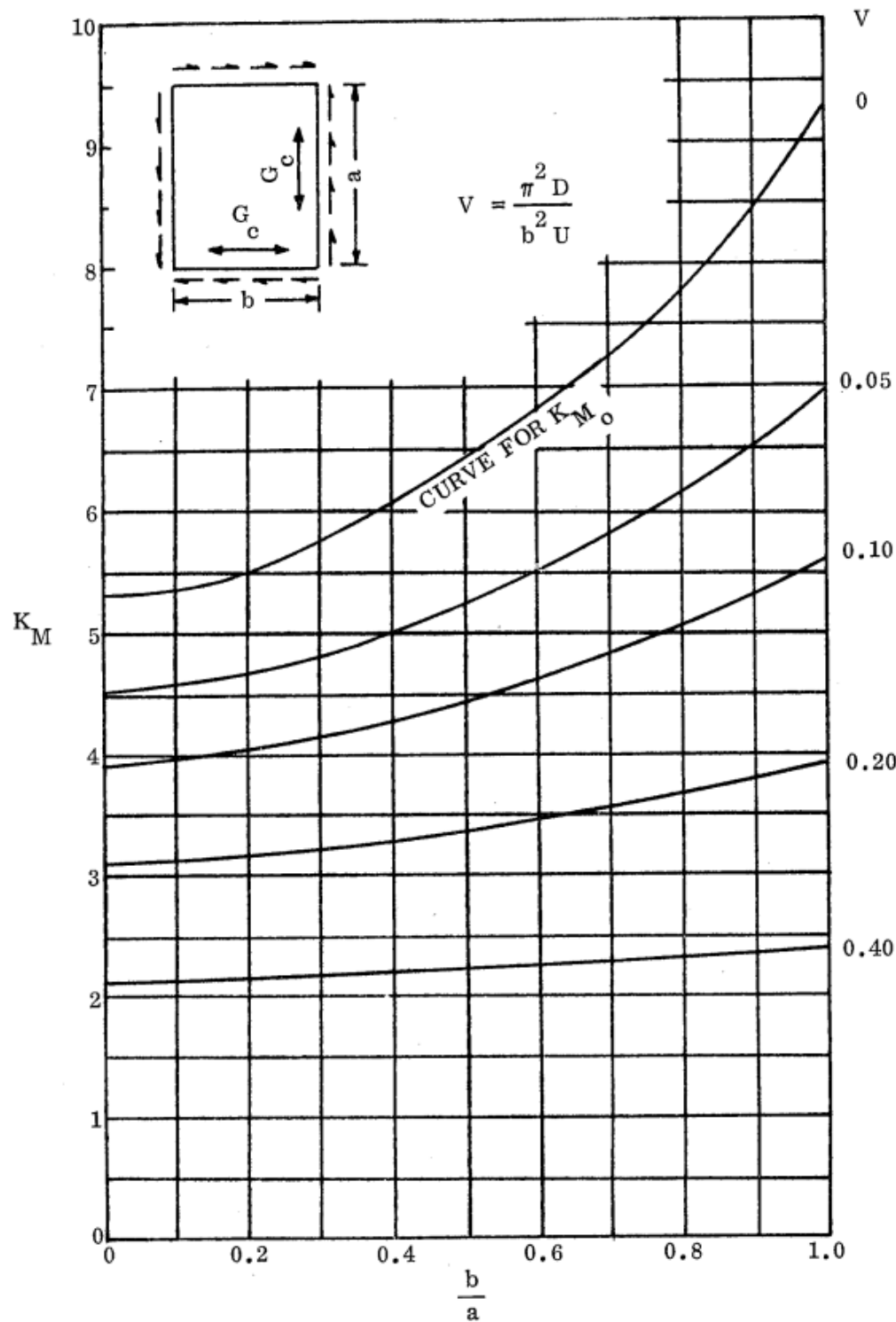


Figure 16.2.2-25: Sandwich Panel Shear Buckling, Isotropic Facings, Isotropic Core, All Sides Simply Supported [\(NASA CR-1457, 1969\)](#)

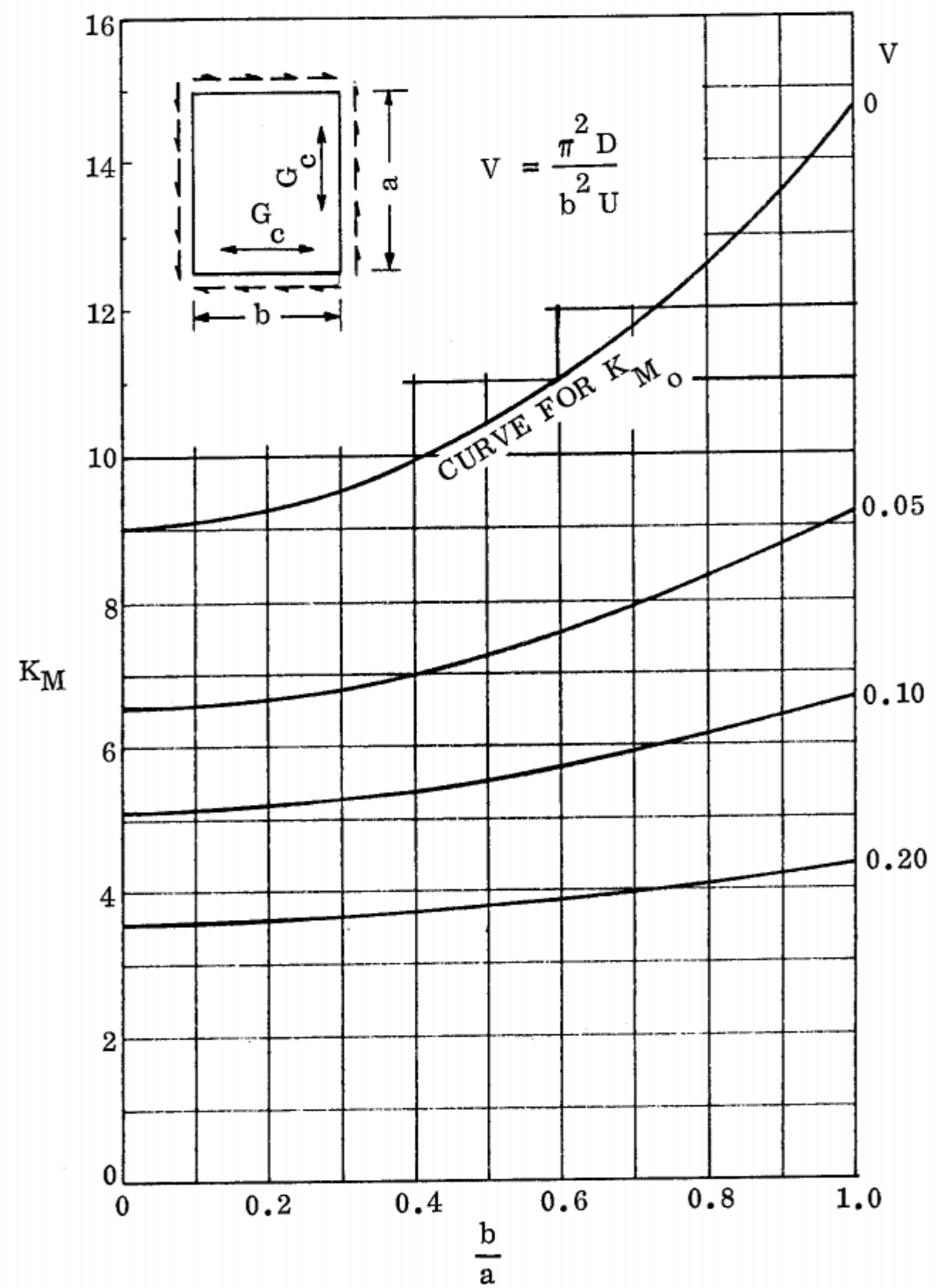


Figure 16.2.2-26: Sandwich Panel Shear Buckling, Isotropic Facings, Isotropic Core, All Sides Clamped [\(NASA CR-1457, 1969\)](#)

16.2.2.9. Sandwich Panel Shear Buckling Coefficients for Panels with Isotropic Facings and Orthotropic Core ($R=0.40$):

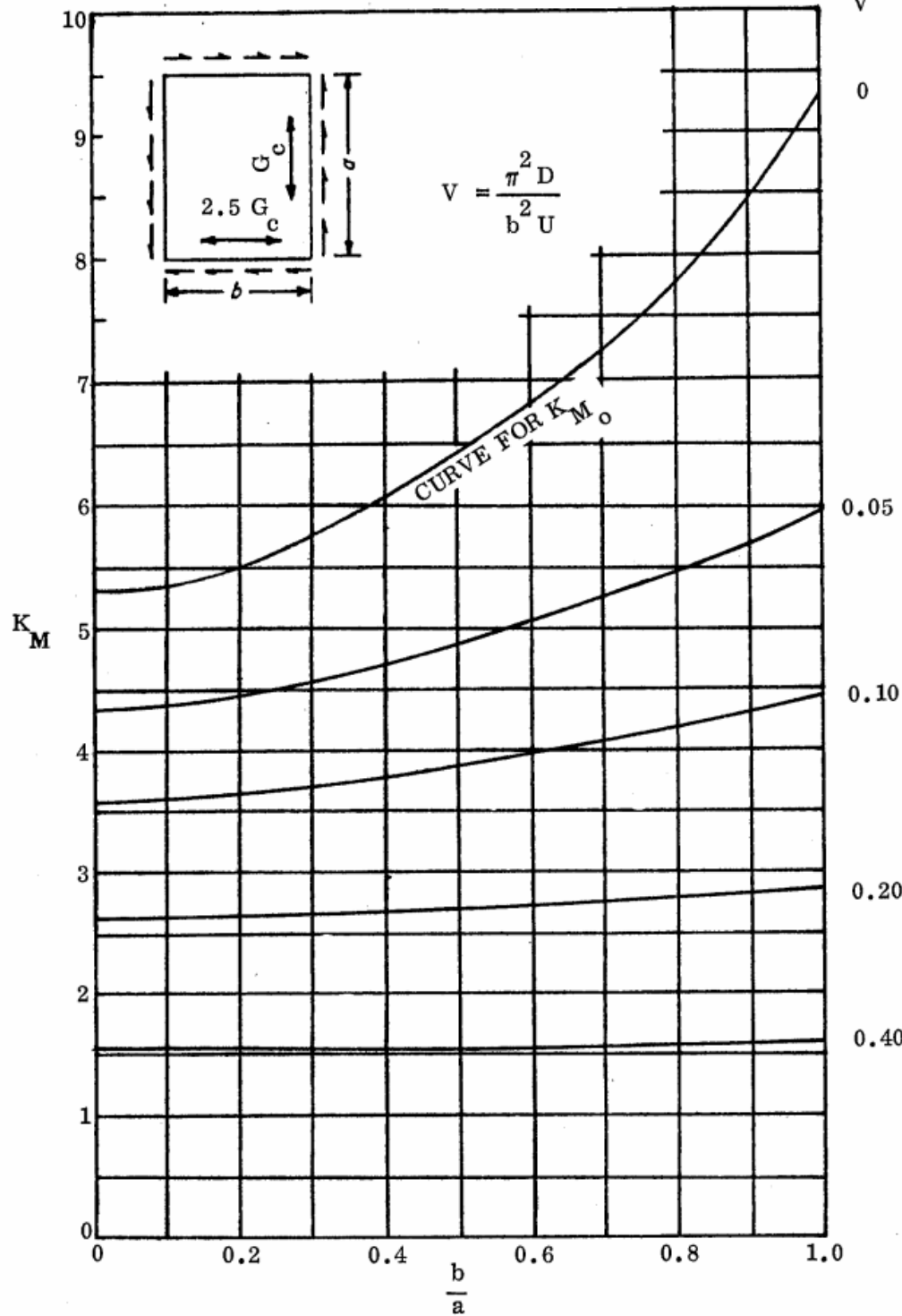


Figure 16.2.2-27: Sandwich Panel Shear Buckling, Isotropic Facings, Orthotropic Core ($R=0.40$), All Sides Simply Supported
(NASA CR-1457, 1969)

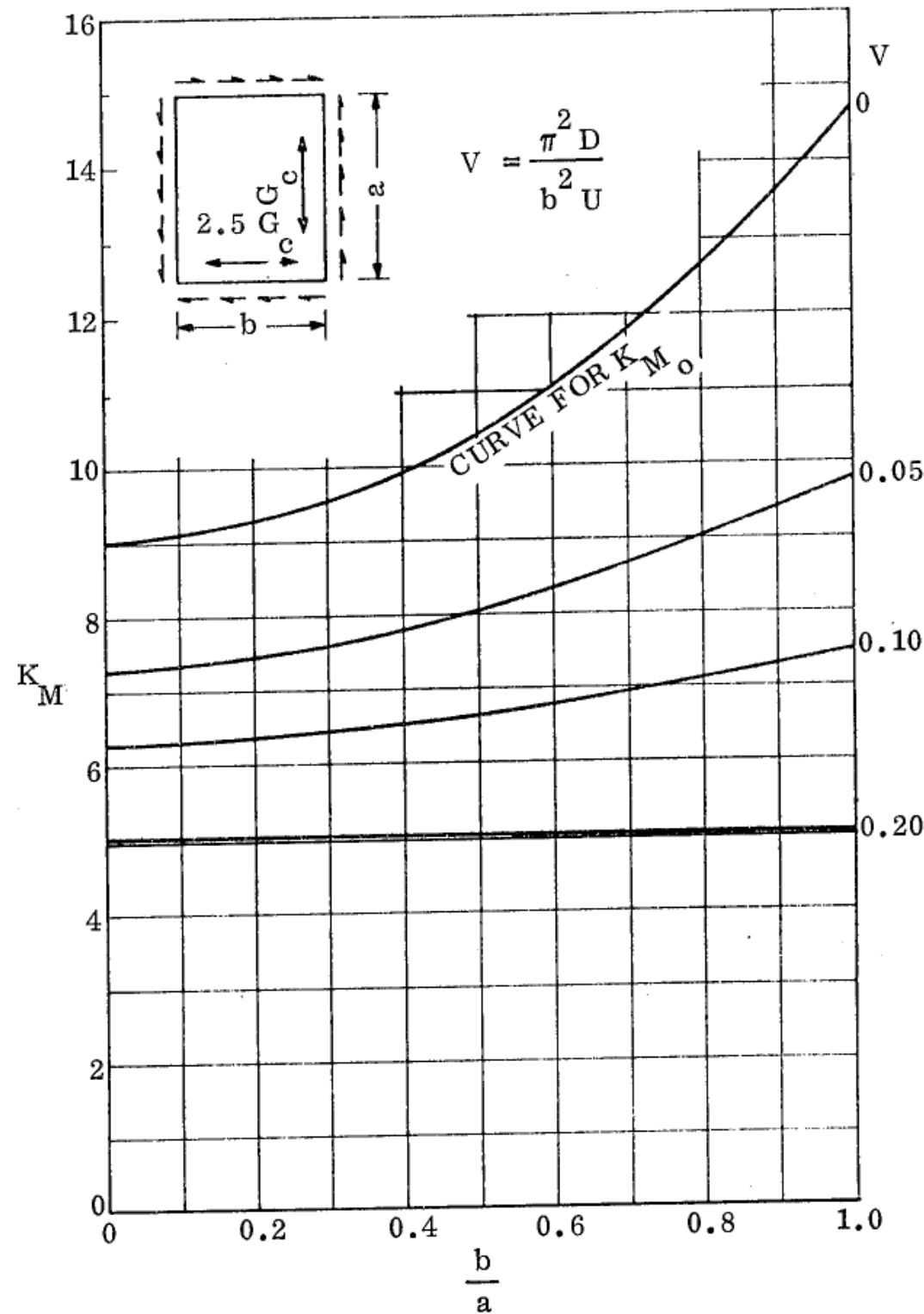


Figure 16.2.2-28: Sandwich Panel Shear Buckling, Isotropic Facings, Orthotropic Core ($R=0.40$), All Sides Clamped
(NASA CR-1457, 1969)

16.2.2.10. Sandwich Panel Shear Buckling Coefficients for Panels with Isotropic Facings and Orthotropic Core ($R=2.50$):

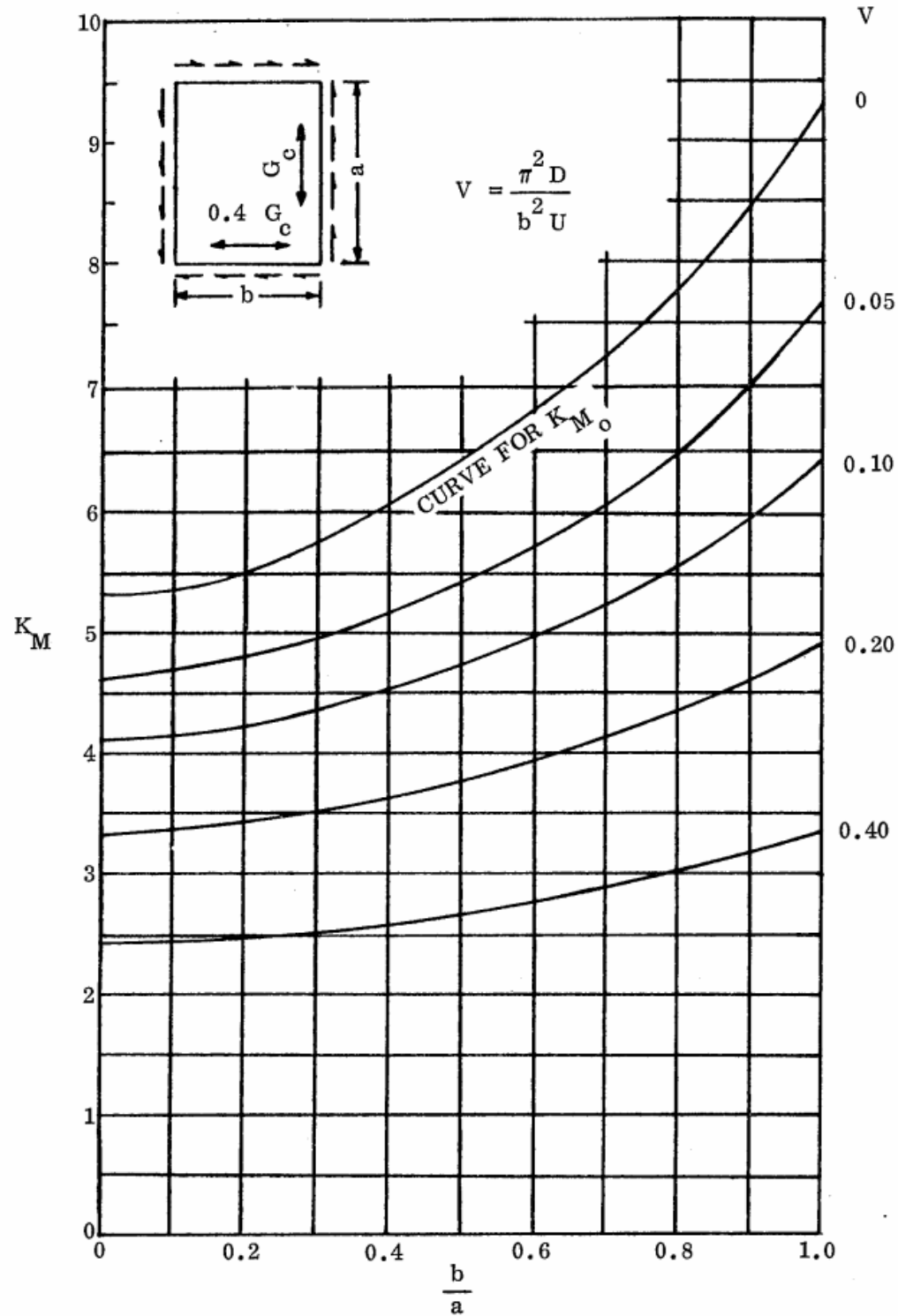


Figure 16.2.2-29: Sandwich Panel Shear Buckling, Isotropic Facings, Orthotropic Core ($R=2.50$), All Sides Simply Supported
(NASA CR-1457, 1969)

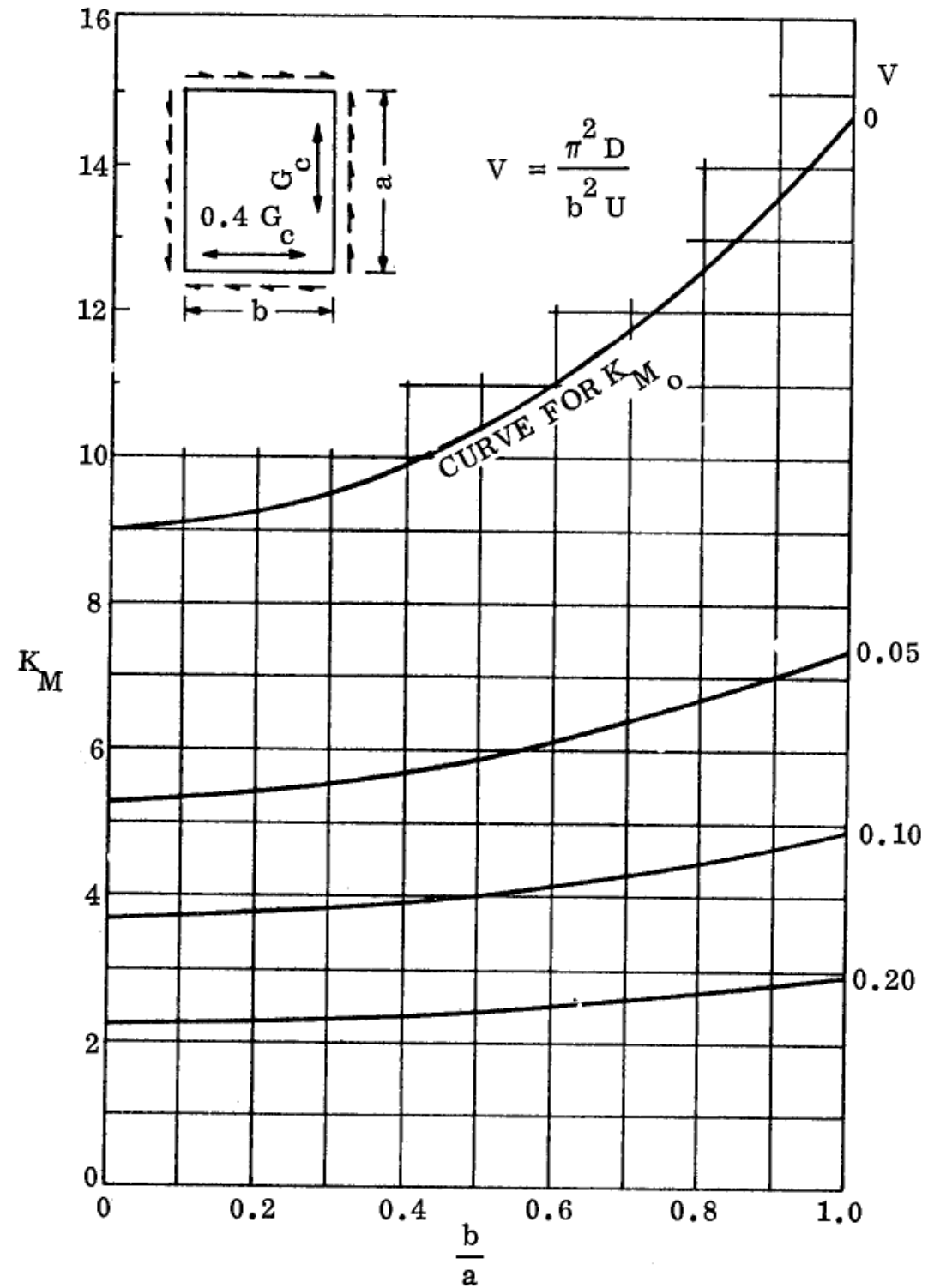


Figure 16.2.2-30: Sandwich Panel Shear Buckling, Isotropic Facings, Orthotropic Core ($R=2.50$), All Sides Clamped
(NASA CR-1457, 1969)

16.2.2.11. Sandwich Panel Bending Buckling

An in-plane bending load applied to a panel is generally less critical than the same panel in compression as the panel is stabilized by the half of the panel that is loaded in tension.

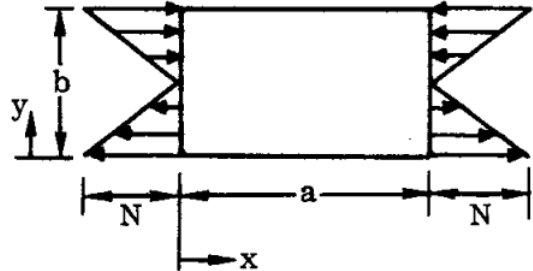


Figure 16.2.2-31: Bending Buckling Load Application and Nomenclature
 (NASA CR-1457, 1969)

The load per unit panel width at which bending buckling of a sandwich panel will occur is given by the theoretical formula:

$$N_{cr} = K_b \cdot \frac{\pi^2}{b^2} \cdot D$$

Where: N_{cr} is the allowable load flow (lb/in).

The D_{11} term from the D matrix of the laminate can be used.

Solved for face sheet stresses:

$$F_{c1,2} = \pi^2 \cdot K_b \cdot \frac{E'_1 \cdot t_1 \cdot E'_2 \cdot t_2}{(E'_1 \cdot t_1 + E'_2 \cdot t_2)^2} \cdot \left(\frac{h}{b}\right)^2 \cdot \frac{E'_f}{\lambda}$$

For isotropic face sheets this formula solved for the facing stress becomes:

Where:

- K** Buckling coefficient = $K_F + K_M$ (See section below)
- E'** $(E'_a E'_b)^{0.5}$ = effective modulus of elasticity for orthotropic facings, psi
- $\lambda = (1 - \mu_a \mu_b)$
- μ_a, μ_b Poisson's ratio as measured parallel to the subscript direction
- $f, 1, 2$ Subscripts denoting facings
- h** Figure 16.2.2-8
- b** Panel Minimum Dimension, in

As noted above the buckling coefficient for the panel under this loading condition is given by the equation:

$$K_b = K_F + K_M$$

Where:

$$K_F = \frac{(E'_1 \cdot t_1^3 + E'_2 \cdot t_2^3)(E'_1 \cdot t_1 + E'_2 \cdot t_2)}{12 \cdot E'_1 \cdot t_1 (E'_2 \cdot t_2) \cdot h^2} \cdot K_{M0}$$

And:

$K_{M0} = K_M$ when $V = 0$ – This is the upper line from each of the curves.

16.2.2.12. Sandwich Panel Shear Buckling Coefficients for Panels with Isotropic Facings:

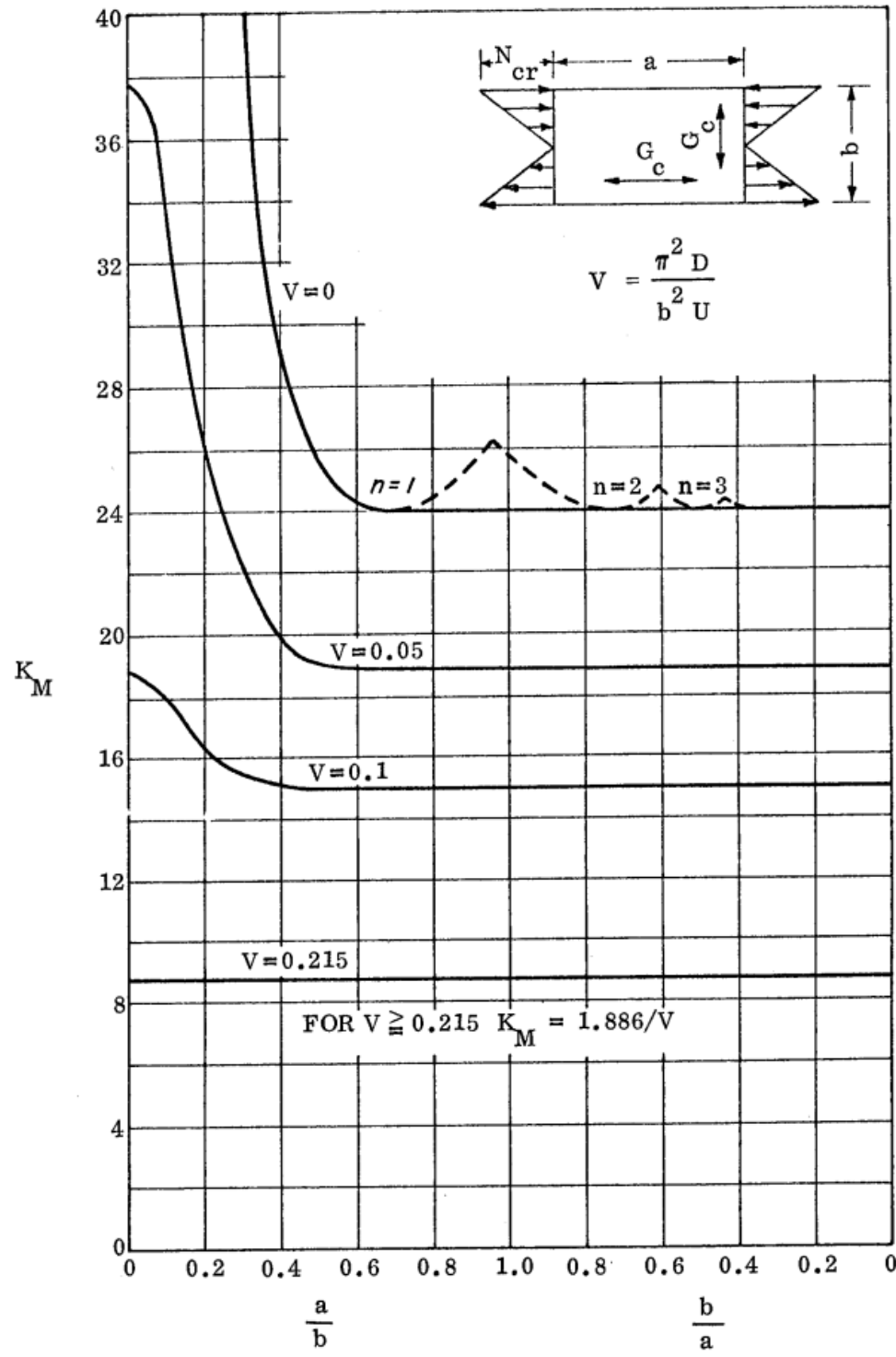


Figure 16.2.2-32: Sandwich Panel Bending Buckling, Isotropic Facings, Isotropic Core, All Sides Simply Supported [\(NASA CR-1457, 1969\)](#)

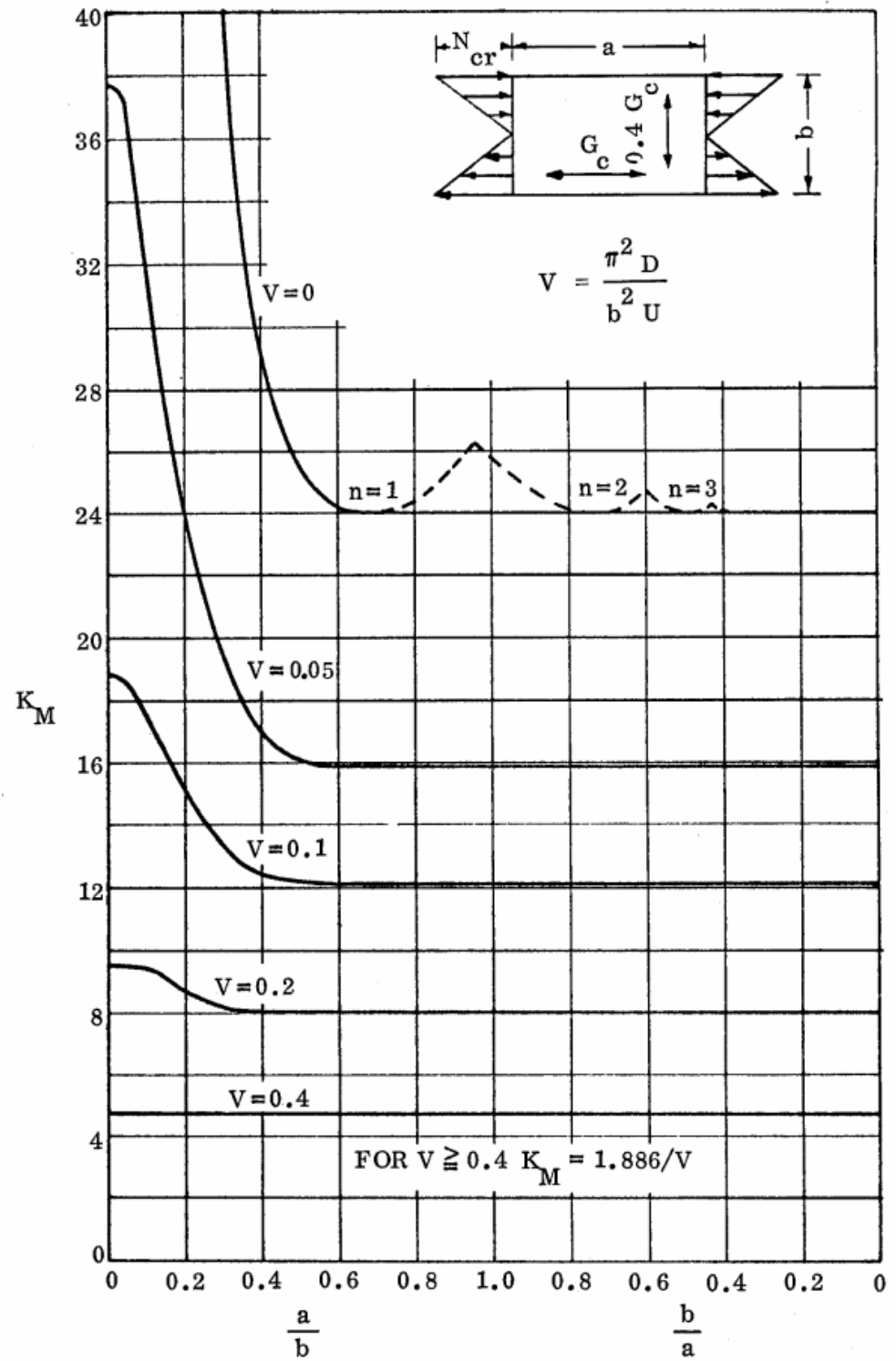


Figure 16.2.2-33: Sandwich Panel Bending Buckling, Isotropic Facings, Orthotropic Core ($R=0.40$), All Sides Simply Supported [\(NASA CR-1457, 1969\)](#)

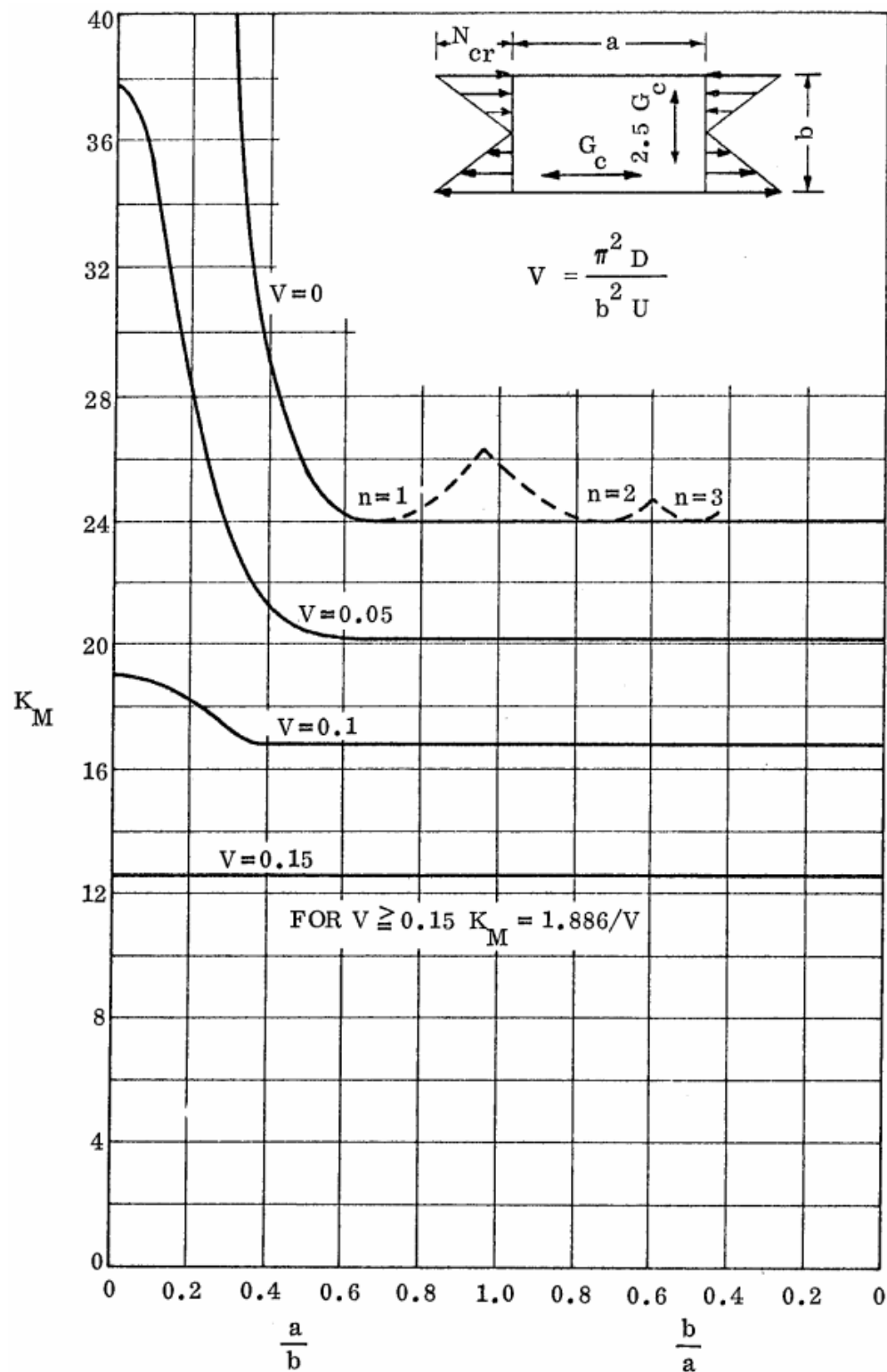


Figure 16.2.2-34: Sandwich Panel Bending Buckling, Isotropic Facings,
 Orthotropic Core ($R=2.50$), All Sides Simply Supported
 (NASA CR-1457, 1969)

16.2.2.13. Combined Loading Conditions for Sandwich Panels

The reference [\(NASA CR-1457, 1969\)](#) states that these interaction methods are for honeycomb cored panel. These methods can be assumed to apply for panels with isotropic cores.

Biaxial Compression:

$$R_{cx} + R_{cy} = 1$$

Where:

$R_{cx} = N/N_{cr}$ Compression reserve factor in the 'x' direction

$R_{cy} = N/N_{cr}$ Compression reserve factor in the 'y' direction

$$M.S = \frac{1}{R_{cx} + R_{cy}} - 1$$

This method is correct for square panels for which $V=0$, it is generally conservative for panels with larger aspect ratios and larger values of V (weaker core).

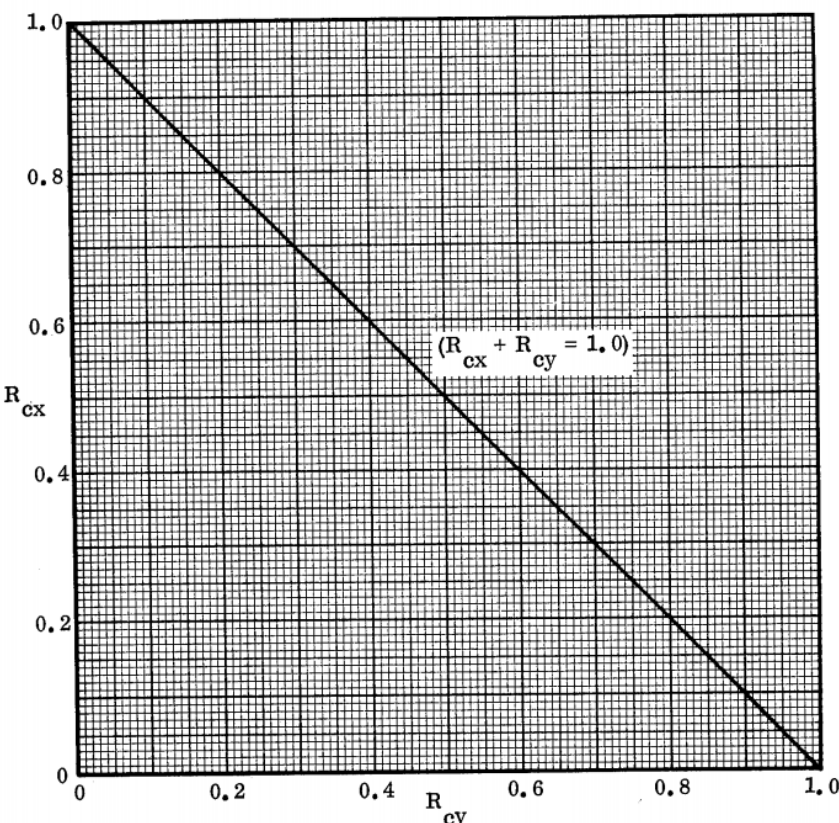


Figure 16.2.2-35: Interaction curve for Sandwich panel – Biaxial Compression
[\(NASA CR-1457, 1969\)](#)

Bending and Compression:

$$R_{cx} + (R_{Bx})^{3/2} = 1$$

Where:

$R_c = N/N_{cr}$ Compression Reserve Factor

$R_b = N/N_{cr}$ Bending Reserve Factor

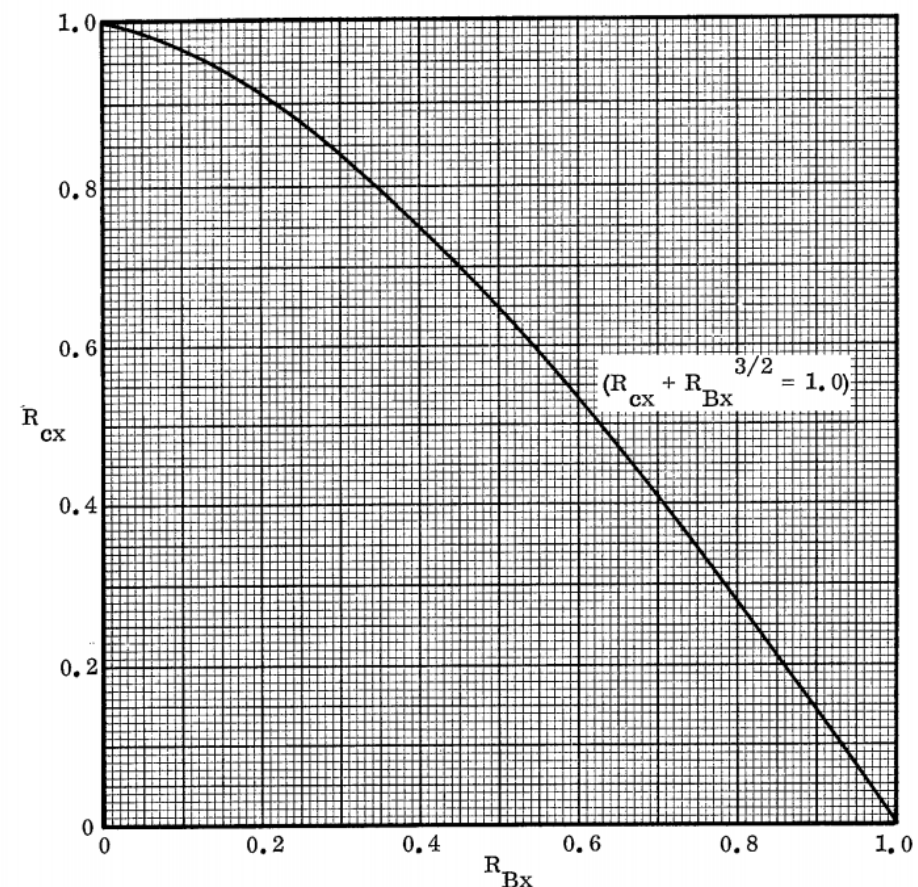


Figure 16.2.2-36: Interaction curve for Sandwich panel – Bending and Compression
[\(NASA CR-1457, 1969\)](#)

Compression and Shear:

$$R_c + (R_s)^2 = 1$$

Where:

$R_c = N/N_{cr}$ Compression Reserve Factor

$R_s = N/N_{cr}$ Shear Reserve Factor

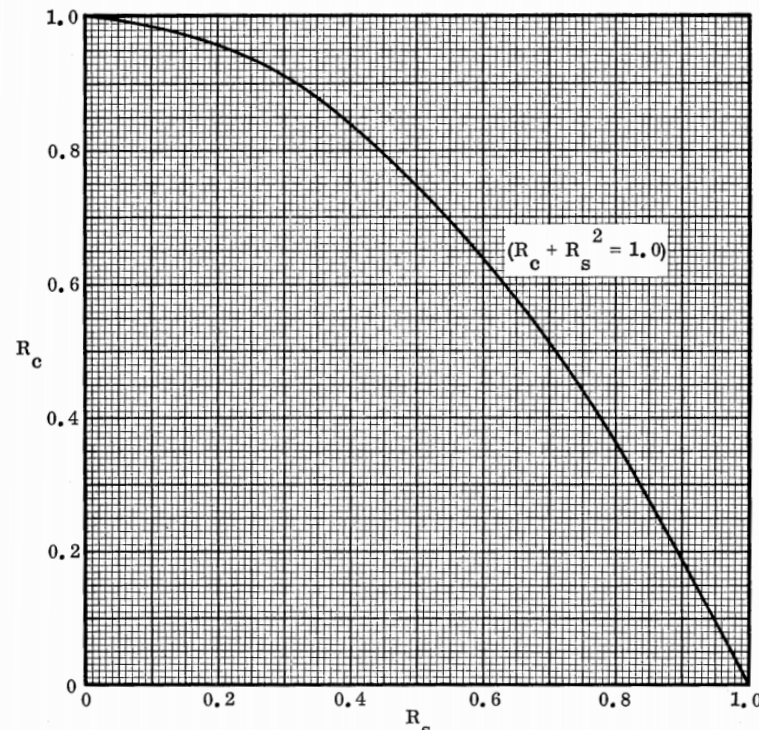


Figure 16.2.2-37: Interaction curve for Sandwich panel – Shear and Compression
[\(NASA CR-1457, 1969\)](#)

Bending and Shear:

$$(R_B)^2 + (R_S)^2 = 1$$

Where:

$R_B = N/N_{cr}$ Bending Reserve Factor

$R_S = N/N_{cr}$ Shear Reserve Factor

$$M.S = \frac{1}{\sqrt{(R_B)^2 + (R_S)^2}} - 1$$

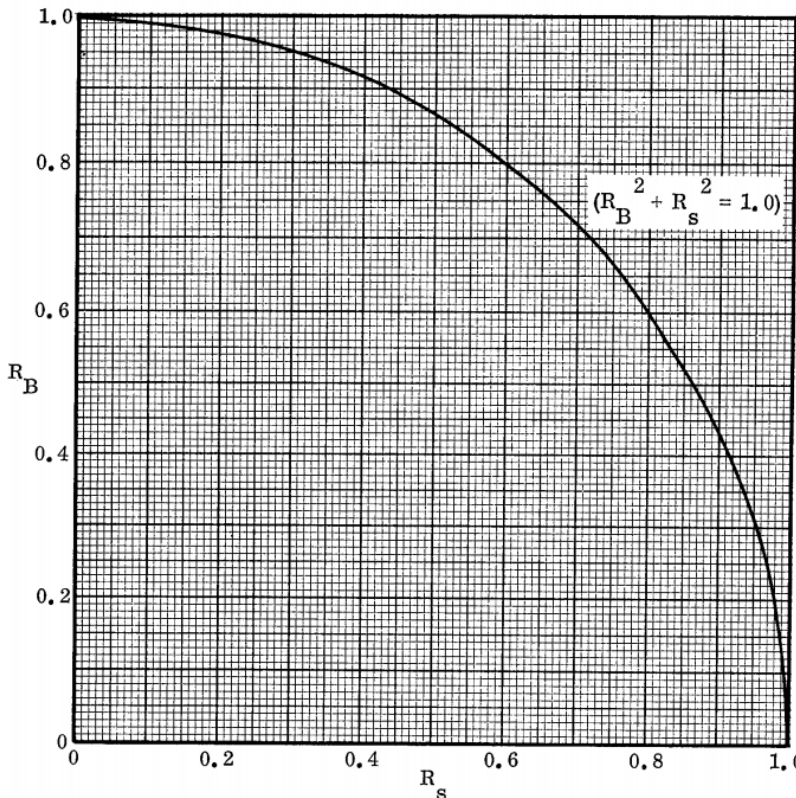


Figure 16.2.2-38: Interaction curve for Sandwich panel – Shear and Bending
(NASA CR-1457, 1969)

All of these interaction effects are available in the spreadsheet linked below:

ABBOTT AEROSPACE SEZC LTD
SPREADSHEETS
ABBOTTAEROSPACE.COM
AA-SM-102-081 Interaction of Cored Panel Buckling Effects

16.2.2.14. Global Mode: Shear Crimping

The shear crimping mode of failure can occur because of insufficient shear stiffness of the core.

For uniaxial compression acting co-planar with the facings:

$$\sigma_{cr} = \frac{h^2}{(t_1 + t_2)t_c} G_{ij}$$

Where G_{ij} is the core shear modulus of the plane perpendicular to the face sheets and parallel to the direction of loading.

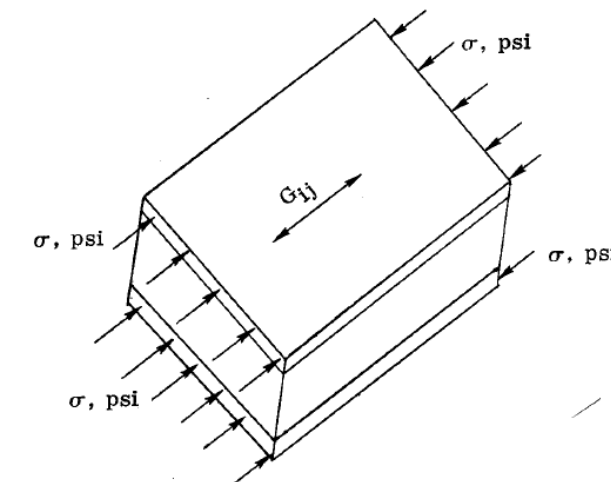


Figure 16.2.2-39: Shear Crimping Terminology for Uniaxial load
(NASA CR-1457, 1969)

For pure shear acting co-planar with the facings:

$$\tau_{cr} = \frac{h^2}{(t_1 + t_2)t_c} \sqrt{G_{xz}G_{yz}}$$

Where G_{xz} and G_{yz} are the core shear moduli of the plane perpendicular to the face sheets (z) and parallel to the direction of loading (x,y).

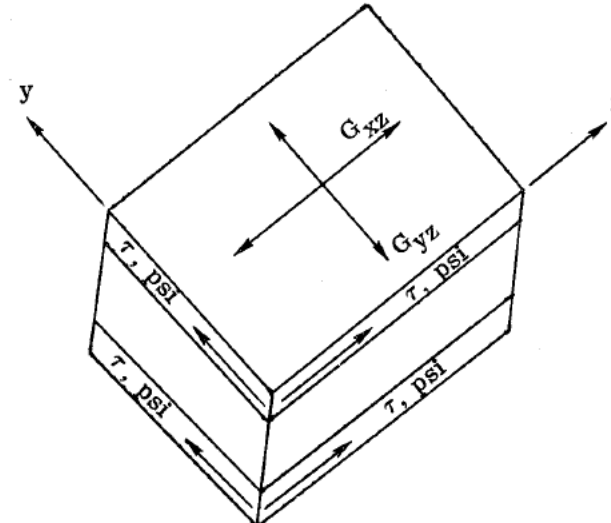


Figure 16.2.2-40: Shear Crimping Terminology for Shear load
(NASA CR-1457, 1969)

This method is available in the following spreadsheet:

ABBOTT AEROSPACE SEZC LTD
SPREADSHEETS
ABBOTTAEROSPACE.COM
AA-SM-102-010 Composites - Cored Panel Shear Crimping

16.2.2.15. Local Mode: Facesheet Dimpling (Intracellular Buckling)

From a practical viewpoint intracellular buckling can be regarded as flat Panel behavior. Even where curvature is present, as in the cases of cylinders and spheres, the honeycomb core size will usually be sufficiently small to justify such an assumption.

As noted from [\(NACA-TN-3781, 1957\)](#), the critical stress for flat Panels can be expressed in the form (note that this is for isotropic face sheets).

$$\sigma_{cr} = \frac{k \cdot \pi^2 \cdot \eta \cdot E_f}{12 \cdot (1 - \nu_e^2)} \cdot \left(\frac{t_f}{s}\right)^2$$

Where:

| | |
|---------------|--|
| σ_{cr} | Critical compressive stress, psi |
| k | Coefficient – depends on plate geometry, boundary conditions and loading |
| η | Plasticity reduction factor |
| E_f | Facing material young's modulus, psi |
| ν_e | Facing material elastic Poisson's ratio |
| t_f | Thickness of face sheets, in |
| s | Selected characteristic plate dimension, in |

For elastic cases and composite face sheets it can be assumed that $\eta = 1$.

[\(NASA CR-1457, 1969\)](#) recommends that a K value of 2.0 is used. However, it is noted that this value has been shown to be optimistic in some cases. A review of the experimental data shows that this may be particularly optimistic for honeycomb core. **It is therefore recommended that a K value of 1.5 is used.**

The dimension 's' is related to the cell size of the core. The recommended value of s is determined as follows:



Figure 16.2.2-41: Definition of Dimension 's' [\(NASA CR-1457, 1969\)](#)

The term for intracellular buckling therefore becomes:

$$\sigma_{cr} = 1.23 \cdot \frac{E_f}{(1 - \nu_e^2)} \cdot \left(\frac{t_f}{s}\right)^2$$

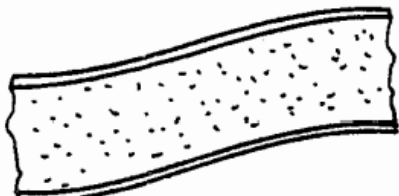
This method is available in the following spreadsheet:

ABBOTT AEROSPACE SEZC LTD
SPREADSHEETS
ABBOTTAEROSPACE.COM

AA-SM-102-011 Composites - Cored Panel Intracellular Buckling

16.2.2.16. Local Mode: Facesheet Wrinkling

Antisymmetric Wrinkling: Typical facesheet wrinkling failure mode in solid/foam cores [\(NASA CR-1457, 1969\)](#).



The stress in the face sheet at which face wrinkling will occur in sandwich constructions having solid or foam cores is given by:

$$\sigma_{wr} = Q \cdot \left[\frac{\eta \cdot E_f \cdot E_c \cdot G_c}{(1 - \nu_e^2)} \right]^{\frac{1}{3}}$$

[\(NASA CR-1457, 1969\)](#) gives guidance that in the absence of any other information the value of Q can be conservatively assumed to be 0.50. This is based on the results shown below.

For elastic cases it can be assumed that $\eta = 1$, in almost all cases for composite laminate face sheets they must remain elastic and therefore $\eta = 1$.

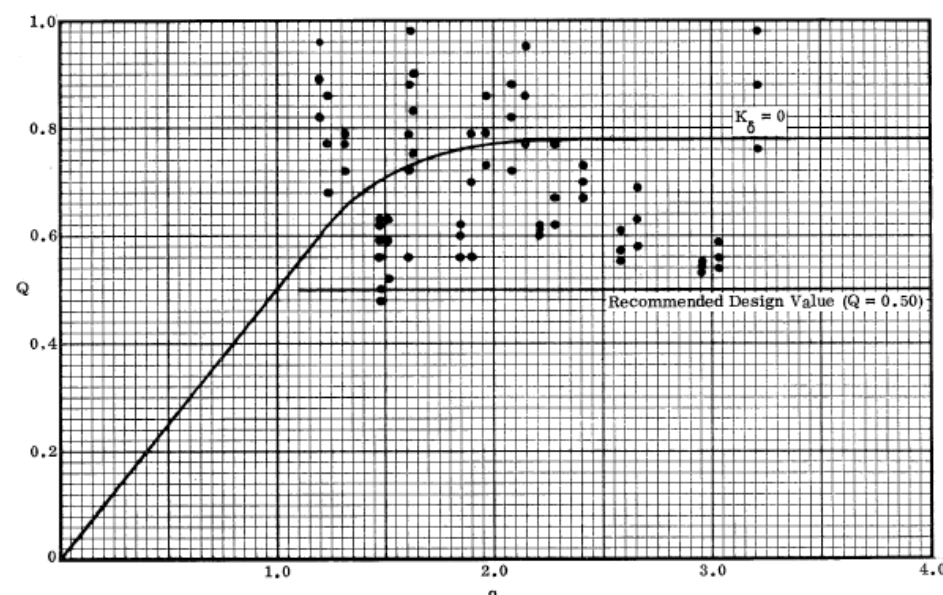


Figure 16.2.2-42: Survey of Analysis vs Test for Sandwich Panels having Solid or Foam Cores [\(NASA CR-1457, 1969\)](#)

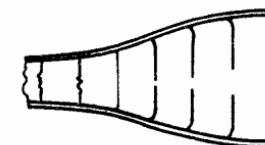
The precise value of Q can be calculated of the amplitude of the initial waviness in the facings is known. This is expanded on and explained in [\(NASA CR-1457, 1969\)](#).

It is recommended that unless the user has significant experience with this subject that a Q of 0.5 is used. Therefore, the expression becomes:

$$\sigma_{wr} = 0.5 \cdot \left[\frac{\eta \cdot E_f \cdot E_c \cdot G_c}{(1 - \nu_e^2)} \right]^{\frac{1}{3}}$$

For elastic cases and composite face sheets it can be assumed that $\eta = 1$. It is noted in the source material that this method is approximate and therefore should be used for initial sizing only.

Symmetric Wrinkling: Typical facesheet wrinkling failure mode *in honeycomb cores only* [\(NASA CR-1457, 1969\)](#).



For unknown initial waviness and for preliminary design use the following expression:

$$\sigma_{wr} = 0.33 \cdot \left[\frac{E_c \cdot t_f}{\eta \cdot E_f \cdot t_c} \right]^{\frac{1}{2}} \cdot (\eta \cdot E_f)$$

For elastic cases and composite face sheets it can be assumed that $\eta = 1$. It is noted in the source material that this method is approximate and conservative and therefore should be used for initial sizing only.

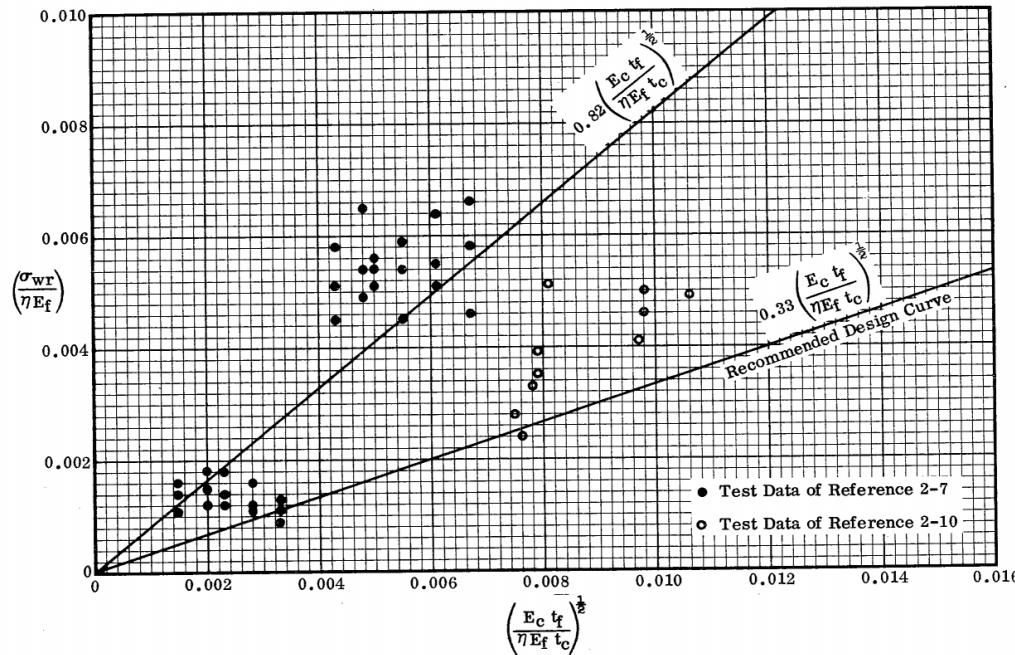
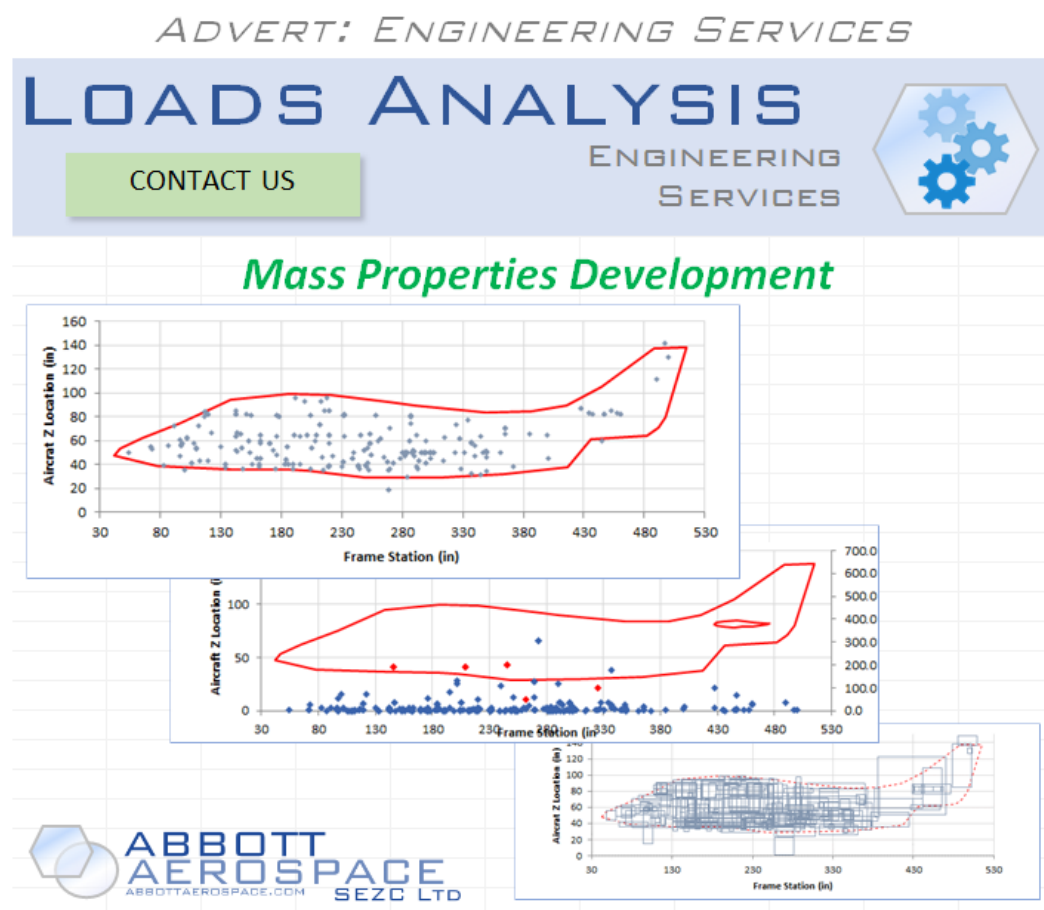


Figure 16.2.2-43: Comparison of Honeycomb Core Face Wrinkling test data with the Analytical Method (NASA CR-1457, 1969)

This method is available in the following spreadsheet:



17. RESERVED

17.1. Introduction

17.2. Reserved

17.3. Reserved

This section will be included in a later edition. This page is a placeholder only.

18. RESERVED

18.1. Introduction

18.2. Reserved

18.3. Reserved

This section will be included in a later edition. This page is a placeholder only.

19. FINITE ELEMENT MODELLING

19.1. Introduction

19.2. Reserved

19.3. Reserved

This section will be included in a later edition. This page is a placeholder only.

20. NOMENCLATURE

These are the common nomenclatures in use within this document and in general use in the industry. There are no rigid rules for the use of nomenclature, so a degree of caution must always be used to avoid misinterpretation and error.

| | |
|------------------------|--|
| <i>A</i> | Area of Cross Section, in ² , In-Plane Stiffness matrix for laminates |
| <i>a</i> | Subscript - Allowable |
| <i>B</i> | Slenderness Ratio, Coupling matrix for laminates |
| <i>b</i> | Width of Sections, Subscript - Bending |
| <i>br</i> | Subscript – Bearing |
| <i>C</i> | Circumference |
| <i>c</i> | Fixity Coefficient for columns, distance from neutral axis, Subscript - Compression |
| <i>cr</i> | Subscript - Critical |
| <i>D</i> | Diameter, Out-of-plane stiffness matrix for laminates |
| <i>d</i> | Depth or Height |
| <i>E</i> | Modulus of Elasticity |
| <i>e</i> | Elongation, percent, the minimum distance from a hole center to the edge of a sheet |
| <i>E'</i> | Effective Modulus of Elasticity |
| <i>E_c</i> | Compressive Modulus of Elasticity |
| <i>E_t</i> | Tangent Modulus of Elasticity |
| <i>E_s</i> | Secant Modulus of Elasticity |
| <i>F</i> | Allowable Stress |
| <i>f</i> | Calculated Stress |
| <i>F_b</i> | Allowable Bending Stress, Modulus of Rupture in Bending |
| <i>F_{bru}</i> | Allowable Ultimate Bearing Stress |
| <i>F_{bry}</i> | Allowable Yield Bearing Stress |
| <i>F_c</i> | Allowable Compression Stress |
| <i>F_{cc}</i> | Allowable Crushing or Crippling Stress |
| <i>F_{co}</i> | Allowable Column Stress |
| <i>F_{cu}</i> | Allowable Ultimate Compression Stress |
| <i>F_{cy}</i> | Allowable Yield Compression Stress |
| <i>F_{su}</i> | Allowable Ultimate Shear Stress |
| <i>F_{sy}</i> | Allowable Yield Shear Stress |
| <i>F_{scr}</i> | Allowable Shear Buckling Stress |
| <i>F_{ccr}</i> | Allowable Compression Buckling Stress |
| <i>F_{bcr}</i> | Allowable Bending Buckling Stress |
| <i>F_c</i> | Allowable Compression Stress |
| <i>F_{tu}</i> | Allowable Ultimate Tension Stress |
| <i>F_{ty}</i> | Allowable Yield Tension Stress |
| <i>G</i> | Modulus of Rigidity |
| <i>h</i> | Height or Depth |
| <i>I</i> | Moment of Inertia |
| <i>i</i> | Slope, due to Bending of a Beam |
| <i>J</i> | Torsion Constant |
| <i>K</i> | General Constant or Coefficient |
| <i>ksi</i> | 1000 pounds per square inch |
| <i>L</i> | Length (in), Longitudinal Grain Direction |
| <i>LT</i> | Longitudinal Transverse Grain Direction |

| | |
|----------------------|----------------------------------|
| <i>M</i> | Applied Bending Moment or Couple |
| <i>M_a</i> | Allowable Bending Moment |
| <i>P</i> | Applied Load, pounds |
| <i>P_a</i> | Allowable Load |
| <i>psi</i> | Pounds per Square Inch |
| <i>R</i> | Stress Ratio |
| <i>r</i> | Radius, Ratio |
| <i>S</i> | Shear Force |
| <i>s</i> | Subscript - Shear |
| <i>ST</i> | Short Transverse Grain Direction |
| <i>T</i> | Applied Torsion Moment |
| <i>T_a</i> | Allowable Torsion Moment |

21. NUMERICAL METHODS

21.1. Common Equations

21.1.1. Simple Unit Stresses

Tension

$$f_t = \frac{P}{A}$$

Compression

$$f_c = \frac{P}{A}$$

Bending

$$f_b = \frac{M \cdot y}{I} = \frac{M}{Z}$$

Average Direct Shear Stress

$$f_s = \frac{S}{A}$$

Longitudinal or Transverse Shear Stress

$$f_s = \frac{S \cdot Q}{I \cdot b}$$

Shear Stress in Round Tubes due to Torsion

$$f_s = \frac{T \cdot y}{I_p}$$

Shear Stress due to Torsion on thin Walled Structures of Closed Section. 'A' is the area enclosed by the median line of the section,

$$f_s = \frac{T}{2 \cdot A \cdot t}$$

Principal stresses

$$f_1 = \frac{f_x + f_y}{2} + \sqrt{\left(\frac{f_x - f_y}{2}\right)^2 + f_{xy}^2}$$

$$f_2 = \frac{f_x + f_y}{2} - \sqrt{\left(\frac{f_x - f_y}{2}\right)^2 + f_{xy}^2}$$

Max, Min Shear Stresses

$$f_{smax}, f_{smin} = \pm \sqrt{\left(\frac{f_x - f_y}{2}\right)^2 + f_{xy}^2}$$

Von Mises Stress

$$f_e = \sqrt{\frac{1}{2} \cdot [(f_1 - f_2)^2 + (f_2 - f_3)^2 + (f_3 - f_1)^2]}$$

21.1.1.1. Equations of Motion

Linear Motion

Where:

| | |
|-----|-----------------------|
| u | Initial Velocity |
| v | Final Velocity |
| s | Distance |
| a | Constant Acceleration |
| t | time |

$$v = u + a \cdot t$$

$$s = u \cdot t + \frac{1}{2} \cdot a \cdot t^2$$

$$s = \frac{1}{2} \cdot (u + v) \cdot t$$

$$v^2 = u^2 + 2 \cdot a \cdot s$$

Rotational Motion

Where:

| | |
|------------|-------------------------------|
| ω_0 | Initial Angular Velocity |
| ω | Final Angular Velocity |
| θ | Angular Displacement |
| α | Constant Angular Acceleration |
| t | time |

$$\omega = \omega_0 + \alpha \cdot t$$

$$\theta = \omega_0 \cdot t + \frac{1}{2} \cdot \alpha \cdot t^2$$

$$\theta = \frac{1}{2} \cdot (\omega_0 + \omega) \cdot t$$

$$\omega^2 = \omega_0^2 + 2 \cdot \alpha \cdot \theta$$

21.2. Unit Conversion

Reserved

21.3. Quadrilateral Analysis

Reserved

21.4. Intersection of Two Circles

Reserved

21.5. Intersection of a line and a Circle

Reserved

21.6. Curve Fits

Reserved

22. AIRCRAFT SPECIFIC DESIGN FEATURES AND DESIGN METHODS

22.1. Introduction

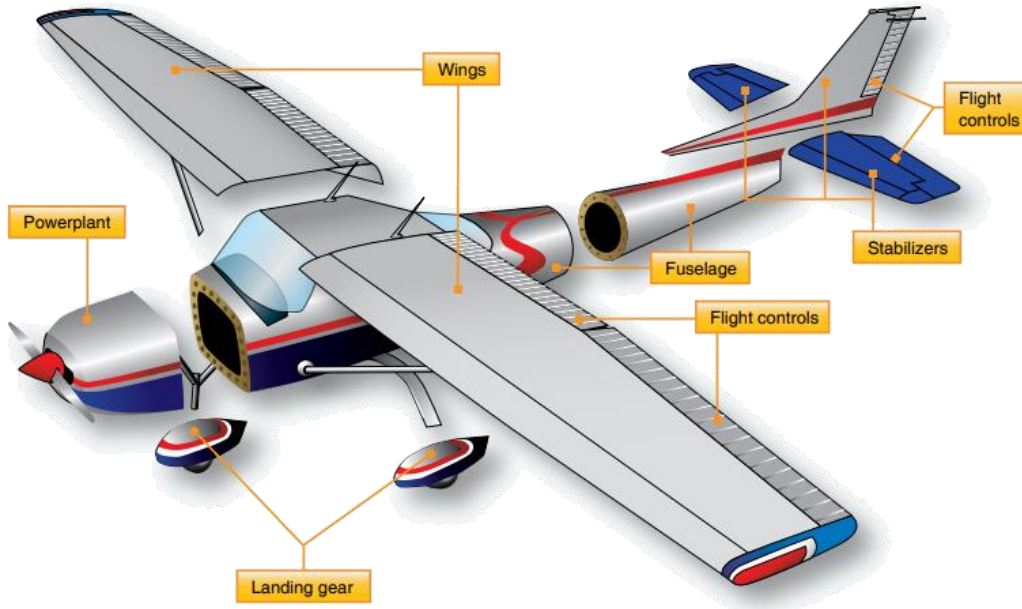


Figure 21.1.1-1: Principal Aircraft Structural Sub Assemblies [\(FAA-H-8083-31, 2012\)](#)

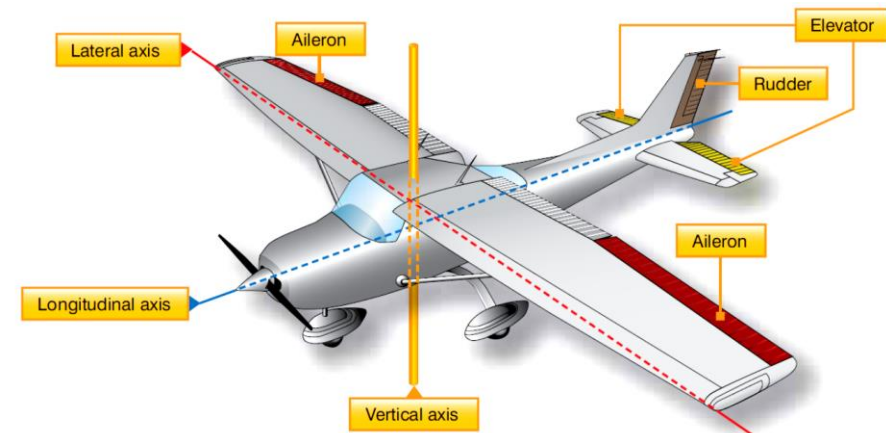


Figure 21.1.1-2: Definition of Aircraft Axis System [\(FAA-H-8083-31, 2012\)](#)

22.2. 06 Dimensions and Areas

Reserved

22.3. 07 Lifting and Shoring

Reserved

22.4. 08 Levelling and Weighing

Reserved

22.5. 09 Towing and Taxiing

Reserved

22.6. 25 Equipment and Furnishings (Interiors)

Reserved

22.7. 27 Flight Controls

The flight controls (ATA group 27) is concerned with the system between the pilot and the control surfaces. The control surfaces themselves fall under the ATA code section of the major sub assembly to which they attach.

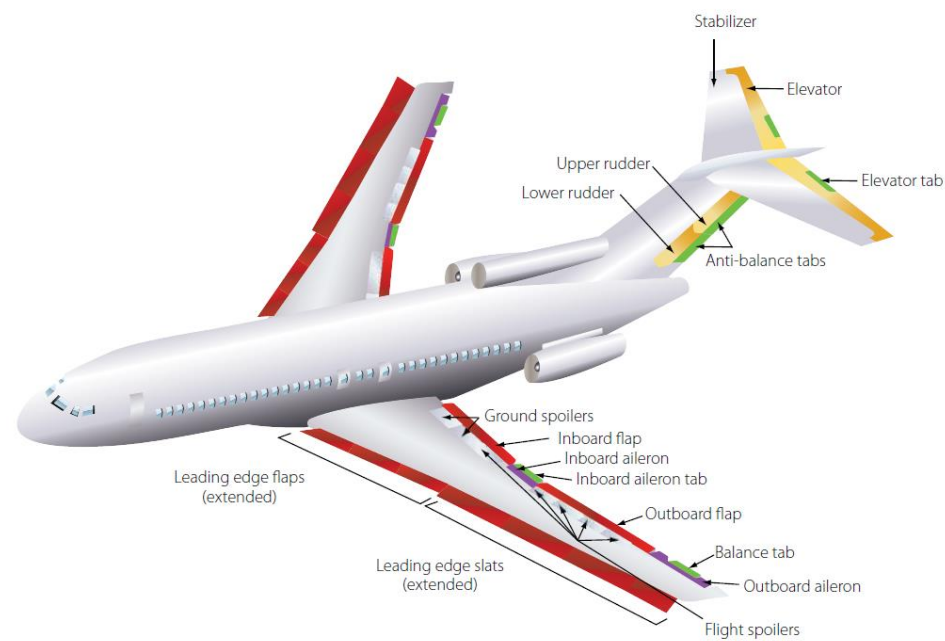


Figure 21.1.1-1: Identification of Flight Control Surfaces, Typical Transport Category Aircraft [\(FAA-H-8083-30, 2008\)](#)

22.8. 28 Fuel

Reserved

22.9. 29 Hydraulic Power

Reserved

22.10. 32 Landing Gear

Reserved

22.11. 52 Doors

Reserved

22.12. 53 Fuselage

The fuselage is the main structure or body of the fixed-wing aircraft. It provides space for cargo, controls, accessories, passengers, and other equipment. In single-engine aircraft, the fuselage houses the powerplant. In multiengine aircraft, the engines may be either in the fuselage, attached to the fuselage, or suspended from the wing structure. There are two general types of fuselage construction: truss and monocoque.

22.12.1. Truss Type

A truss is a rigid framework made up of members, such as beams, struts, and bars to resist deformation by applied loads. The truss-framed fuselage is generally covered with fabric or molded composite panels.

The truss-type fuselage frame is usually constructed of 4130 steel tubing welded together in such a manner that all members of the truss can carry both tension and compression loads, reference Figure 22.12.1-1. In some aircraft, principally the light, single engine models, truss fuselage frames may be constructed of aluminum alloy and may be riveted or bolted into one piece, with cross-bracing achieved by using solid rods or tubes.

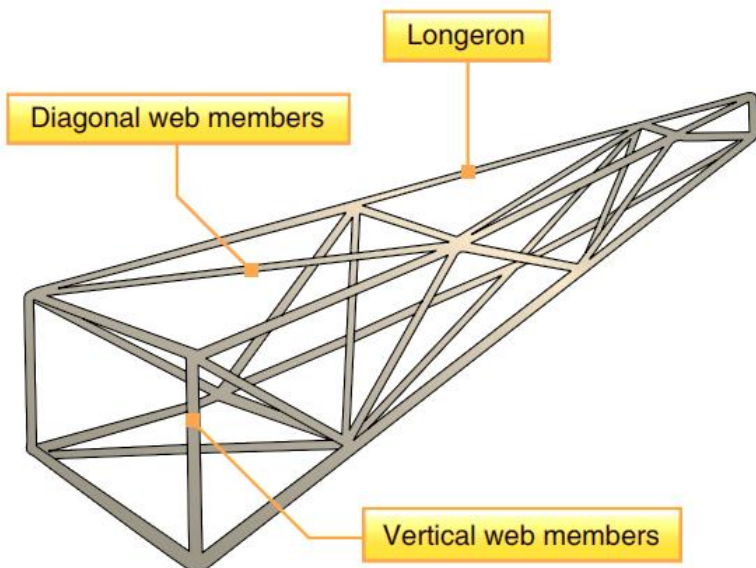


Figure 22.12.1-1: Truss Type Fuselage [\(FAA-H-8083-31, 2012\)](#)

22.12.2. Monocoque Type

The monocoque (single shell) fuselage relies largely on the strength of the skin or covering to carry the primary loads.

The design may be divided into two classes:

1. Monocoque
2. Semi monocoque

Different portions of the same fuselage may belong to either of the two classes, but most modern aircraft are of semi monocoque type construction.

22.12.2.1. True Monocoque Type

A true monocoque construction uses formers, frame assemblies, and bulkheads to give shape to the fuselage, reference Figure 22.12.2-1. The heaviest of these structural members are located at intervals to carry concentrated loads and at points where fittings are used to attach other units such as wings, powerplants, and stabilizers. Since no other bracing members are present, the skin must carry the primary stresses and keep the fuselage rigid. Thus, the biggest problem involved in monocoque construction is maintaining enough strength while keeping the weight within allowable limits.

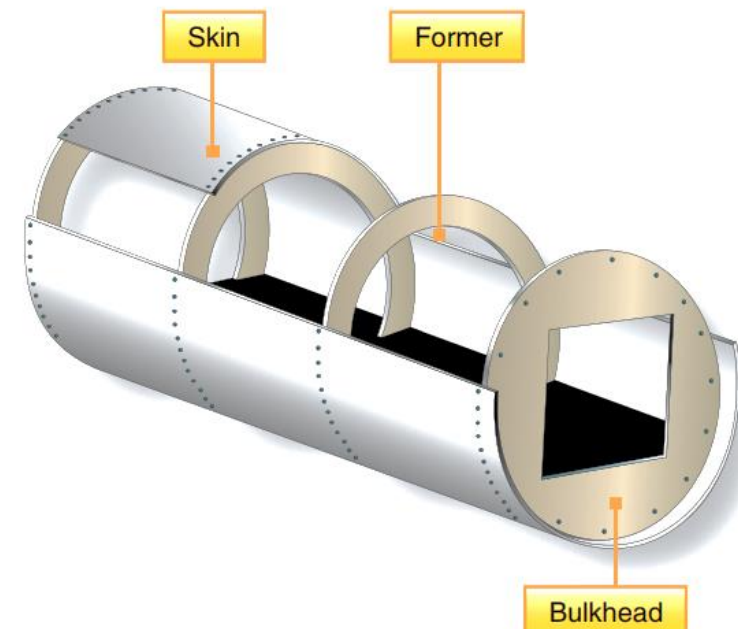


Figure 22.12.2-1: Monocoque Type Fuselage [\(FAA-H-8083-31, 2012\)](#)

22.12.2.2. Semi monocoque Type

To overcome the strength/weight problem of monocoque construction, a modification called semi monocoque construction was developed. It also consists of frame assemblies, bulkheads, and formers as used in the monocoque design but, additionally, the skin is reinforced by longitudinal members called longerons.

Longerons usually extend across several frame members and help the skin support primary bending loads. They are typically made of aluminum alloy either of a single piece or a built-up construction. Stringers are also used in the semi monocoque fuselage.

These longitudinal members are typically more numerous and lighter in weight than the longerons. They come in a variety of shapes and are usually made from single piece aluminum alloy extrusions or formed aluminum. Stringers have some rigidity but are chiefly used for giving shape and for attachment of the skin. Stringers, longerons and the skin resist fuselage bending.

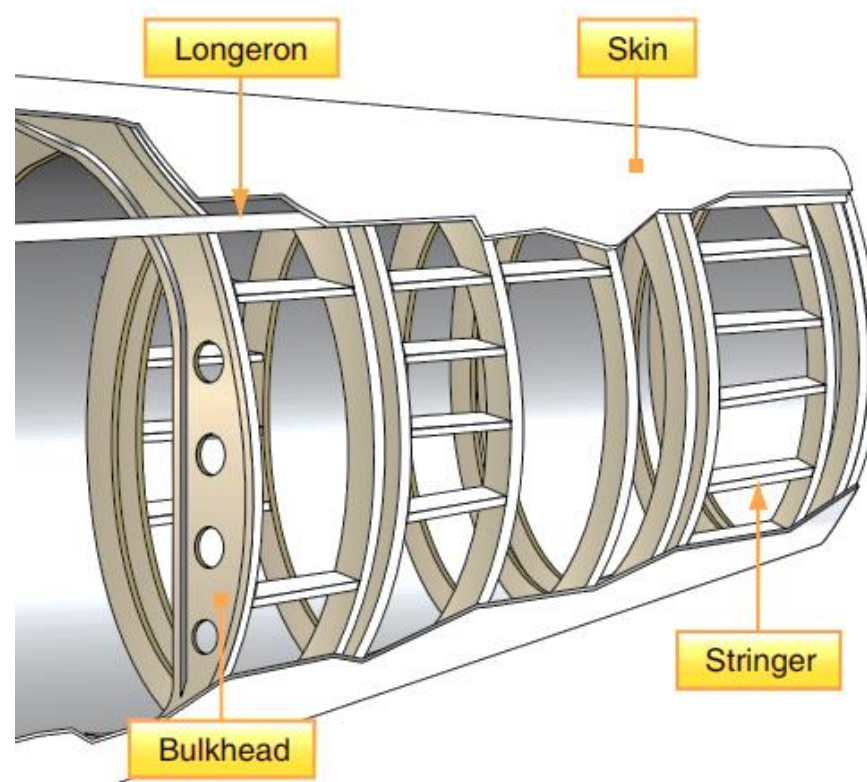


Figure 22.12.2-2: Semi-Monocoque Type Fuselage [\(FAA-H-8083-31, 2012\)](#)

Other bracing between the longerons and stringers can also be used. Often referred to as web members, these additional support pieces may be installed vertically or diagonally. It must be noted that manufacturers use different nomenclature to describe structural members. For example, there is often little difference between some rings, frames, and formers.

The semi monocoque fuselage is constructed primarily of alloys of aluminum and magnesium, although steel and titanium are sometimes found in areas of high temperatures. Individually, no one of the components is strong enough to carry the loads imposed during flight and landing. But, when combined, those components form a strong, rigid framework. This is accomplished with gussets, rivets, nuts and bolts, screws, and even friction stir welding. A gusset is a type of connection bracket that adds strength.

For semi monocoque structure made from aluminum the skin panels can be allowed to buckle above normal service loads. The longeron and stringers give adequate residual strength in the post buckled state. This design approach allows thin skin panels and generally produces the lightest weight structure.

Composite fuselage construction can be without any frames at all (relying on core to give the skin adequate stiffness), with frames or with frames, stringers and longerons, known as black metal as the design is very similar to semi-monocoque metal fuselage design but the carbon material gives it a black color. It is unusual to allow composite primary structure to buckle, therefore composite structure generally exhibits linear behavior up to ultimate load.

22.13. 54 Nacelles & Pylons

Nacelles (sometimes called “pods”) are streamlined enclosures used primarily to house the engine and its components. They usually present a round or elliptical profile to the wind thus reducing aerodynamic drag. On most single-engine aircraft, the engine and nacelle are at the forward end of the fuselage. On multiengine aircraft, engine nacelles are built into the wings or attached to the fuselage at the empennage (tail section).

Occasionally, an aircraft is designed with a nacelle in line with the fuselage aft of the passenger compartment. Regardless of its location, a nacelle contains the engine and accessories, engine mounts, structural members, a firewall, and skin and cowling on the exterior to fare the nacelle to the wind. Some aircraft have nacelles that are designed to house the landing gear when retracted.

Retracting the gear to reduce drag is standard procedure on high-performance/high-speed aircraft. The wheel well is the area where the landing gear is attached and stowed when retracted. Wheel wells can be in the wings and/or fuselage when not part of the nacelle. Figure 22.12.2-1 shows an engine nacelle incorporating the landing gear with the wheel well extending into the wing root.



Figure 22.12.2-1: An Engine Nacelle Firewall ([FAA-H-8083-31, 2012](#))

The framework of a nacelle usually consists of structural members like those of the fuselage. Lengthwise members, such as longerons and stringers, combine with horizontal/vertical members, such as rings, formers, and bulkheads, to give the nacelle its shape and structural integrity. A firewall is incorporated to isolate the engine compartment from the rest of the aircraft. This is usually a stainless steel or titanium bulkhead that contains a fire in the confines of the nacelle rather than letting it spread throughout the airframe. Figure 22.12.2-1.

Engine mounts are also found in the nacelle. These are the structural assemblies to which the engine is fastened. They are usually constructed from chrome/molybdenum 4130 or 4140 steel tubing in light aircraft and forged chrome/nickel/ molybdenum assemblies in larger aircraft, Figure 22.12.2-2.

The exterior of a nacelle is covered with a skin or fitted with a cowling which can be opened to access the engine and components inside. Both are usually made of sheet aluminum or magnesium alloy with stainless steel or titanium alloys being used in high-temperature areas, such as around the exhaust exit. Regardless of the material used, the skin is typically attached to the framework with rivets.

Cowling refers to the detachable panels covering those areas into which access must be gained regularly, such as the engine and its accessories. Cowl flaps are moveable parts of the nacelle cowling that open and close to regulate engine temperature.

Composite cowlings are also used, usually with a tumescent, heat sensitive internal coating that expands to create a temporary insulating layer in the event of an engine fire. The ‘scrubbing’ effect of the cooling air flow on the outside surface of the cowlings help maintain structural integrity in the event of an engine fire.

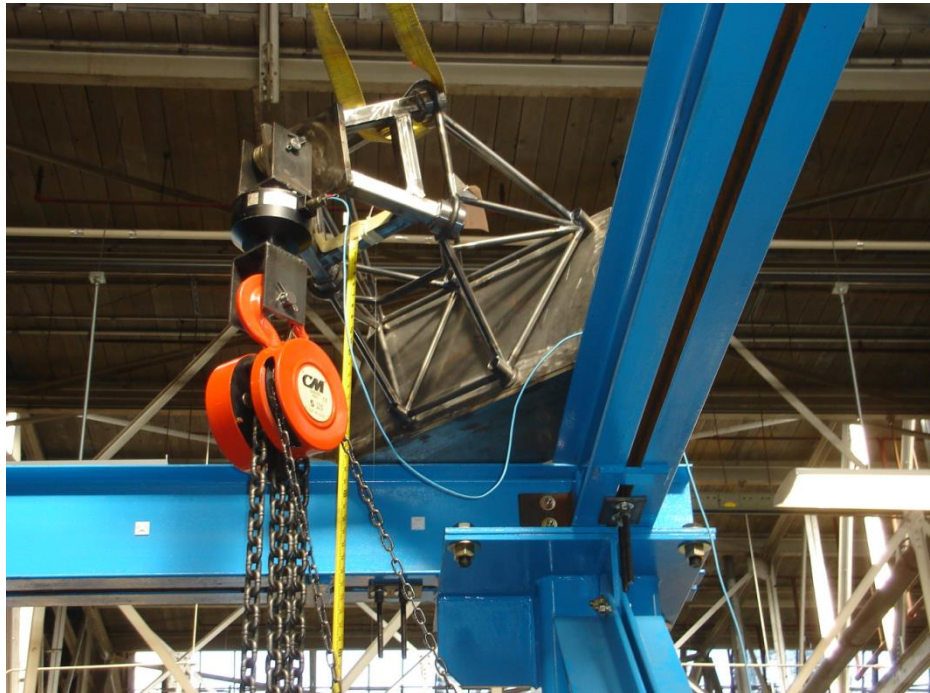


Figure 22.12.2-2: A 4130 Welded Steel Engine Mount for a Part 23 Aircraft Undergoing Certification Structural Testing (Author's Collection)

There are many engine cowl designs. Figure 22.12.2-3 shows an exploded view of the pieces of cowling for a horizontally opposed engine on a light aircraft.

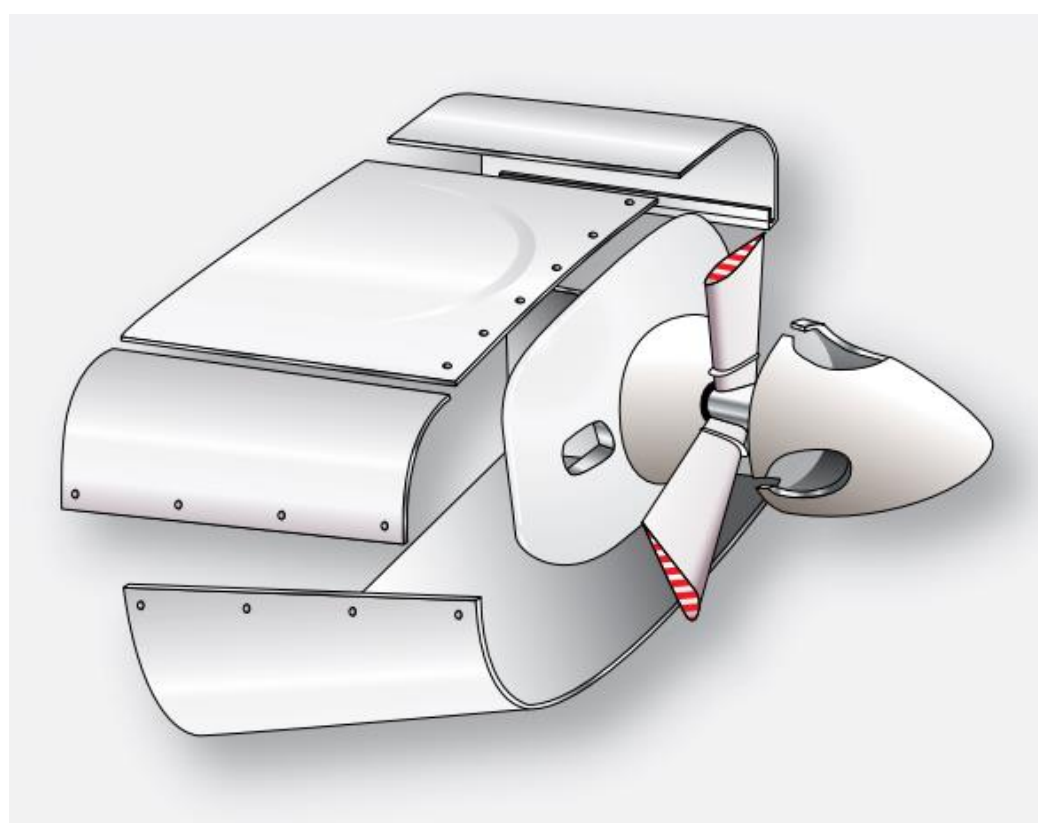


Figure 22.12.2-3: Typical Cowling for Horizontally Opposed Reciprocating Engine (FAA-H-8083-31, 2012)

The cowling is attached to the nacelle by means of screws and/or quick release fasteners. Some large reciprocating engines are enclosed by "orange peel" cowlings which provide excellent access to components inside the nacelle, Figure 22.12.2-4.

These cowl panels are attached to the forward firewall by mounts which also serve as hinges for opening the cowl. The lower cowl mounts are secured to the hinge brackets by quick release pins. The side and top panels are held open by rods and the lower panel is retained in the open position by a spring and a cable. All of the cowling panels are locked in the closed position by over center steel latches which are secured in the closed position by spring-loaded safety catches.

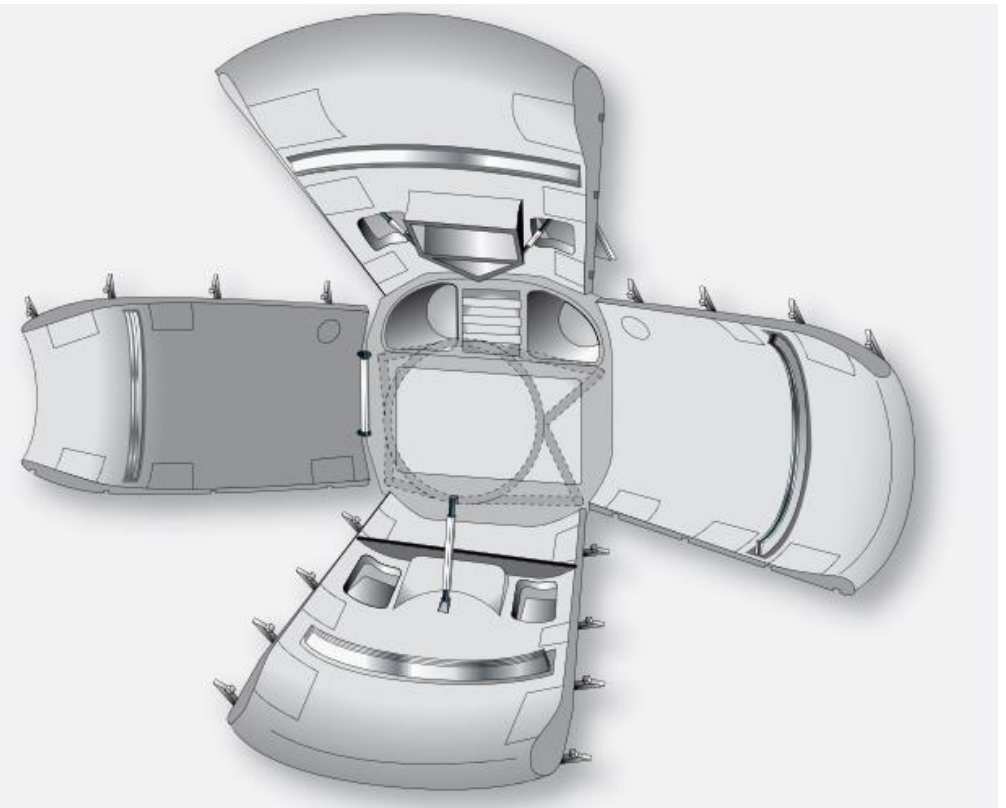


Figure 22.12.2-4: 'Orange Peel' Type Cowling for Large Radial Reciprocating Engine (FAA-H-8083-31, 2012)

An example of a turbojet engine nacelle can be seen in Figure 22.12.2-5. The cowling panels are a combination of fixed and easily removable panels which can be opened and closed during maintenance. A nose cowl is also a feature on a jet engine nacelle. It guides air into the engine.



Figure 22.12.2-5: Cowling on Transport Category Turbine Engine Nacelle (Courtesy Wikimedia Commons)

When the engine is buried inside the fuselage or tail of the aircraft the nose cowl or lip of the intake must be lengthened into a duct. In some cases the duct has to be split into a Y-Duct around the cabin area of the fuselage, Figure 22.12.2-6.



Figure 22.12.2-6 Air Intake Duct and Lip for Fuselage Internal Mounted Engine
(Author's Collection - Courtesy of [Stratos Aircraft](#))

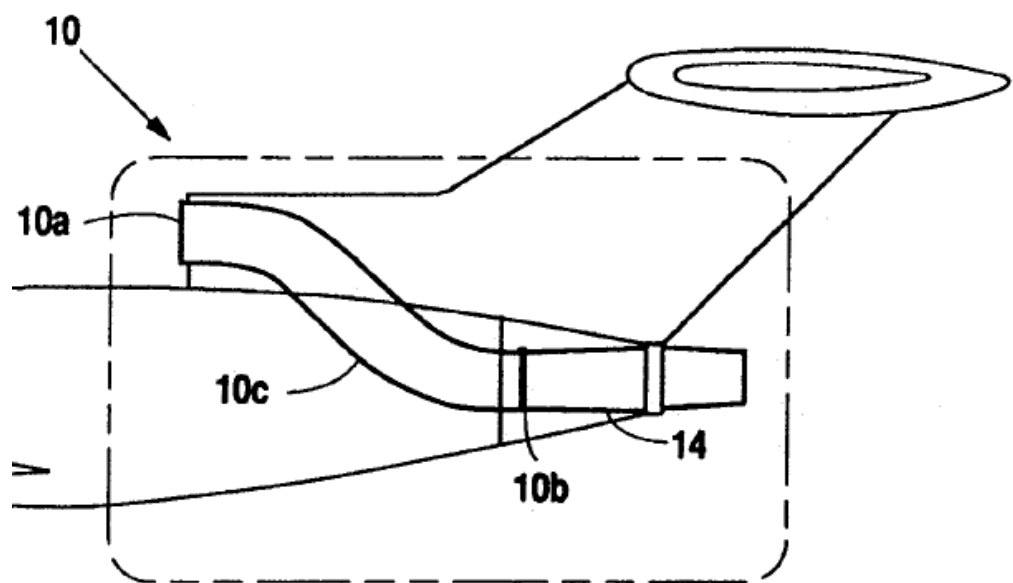


Figure 22.12.2-7 Air Intake Duct for Tail Mounted Engine (Dee Howard Company, Patent US5299760)

22.14. 55 Empennage/Stabilizers

The empennage of an aircraft is also known as the tail section. Most empennage designs consist of a tail cone, fixed aerodynamic surfaces or stabilizers, and movable aerodynamic surfaces.

The tail cone serves to close and streamline the aft end of most fuselages. The cone is made up of structural members like those of the fuselage; however, tail cones are usually of lighter construction since they transfer less load than the fuselage.

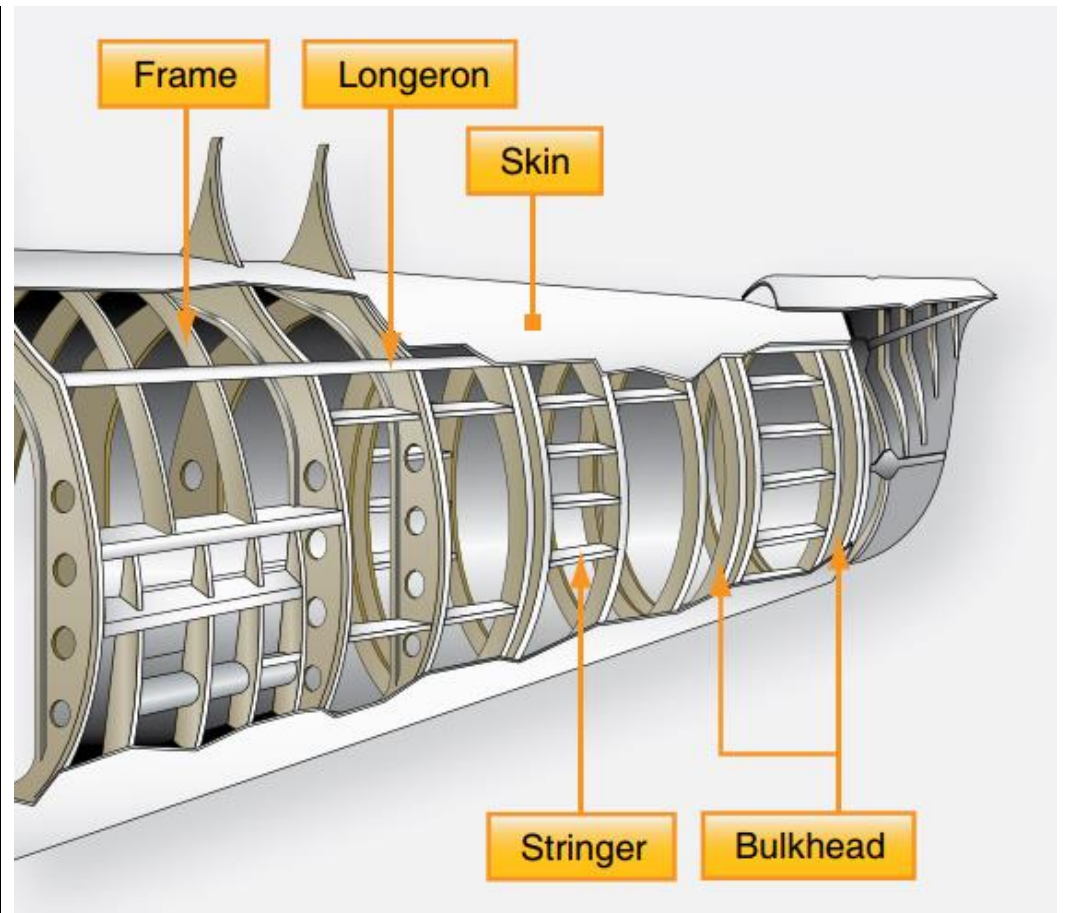


Figure 22.12.2-1 Typical Metal Tailcone Construction ([FAA-H-8083-31, 2012](#))

The other components of the typical empennage are of heavier construction than the tail cone. These members include fixed surfaces that help stabilize the aircraft and movable surfaces that help to direct an aircraft during flight. The fixed surfaces are the horizontal stabilizer and vertical stabilizer. The movable surfaces are usually a rudder located at the aft edge of the vertical stabilizer and an elevator located at the aft edge the horizontal stabilizer.

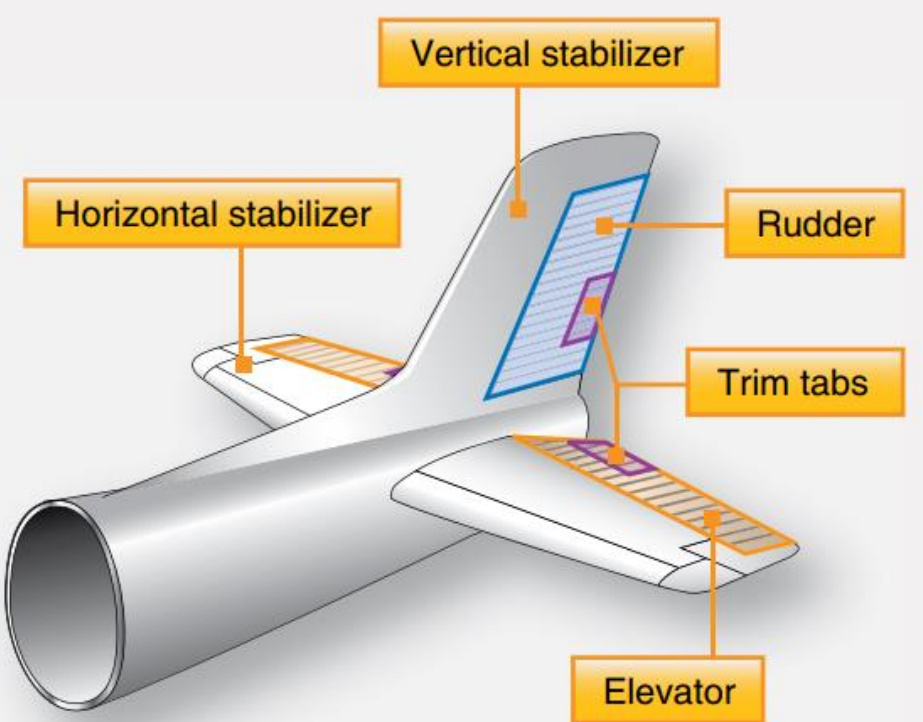


Figure 22.12.2-2: Components of a Typical Empennage ([FAA-H-8083-31, 2012](#))

The structure of the stabilizers is very similar to that which is used in wing construction. Figure 22.12.2-3 shows a typical vertical stabilizer. Notice the use of spars, ribs, stringers, and skin like those found in a wing. They perform the same functions shaping and supporting the stabilizer and transferring loads.

Bending, torsion, and shear created by air loads in flight pass from one structural member to another. A horizontal stabilizer is built the same way.

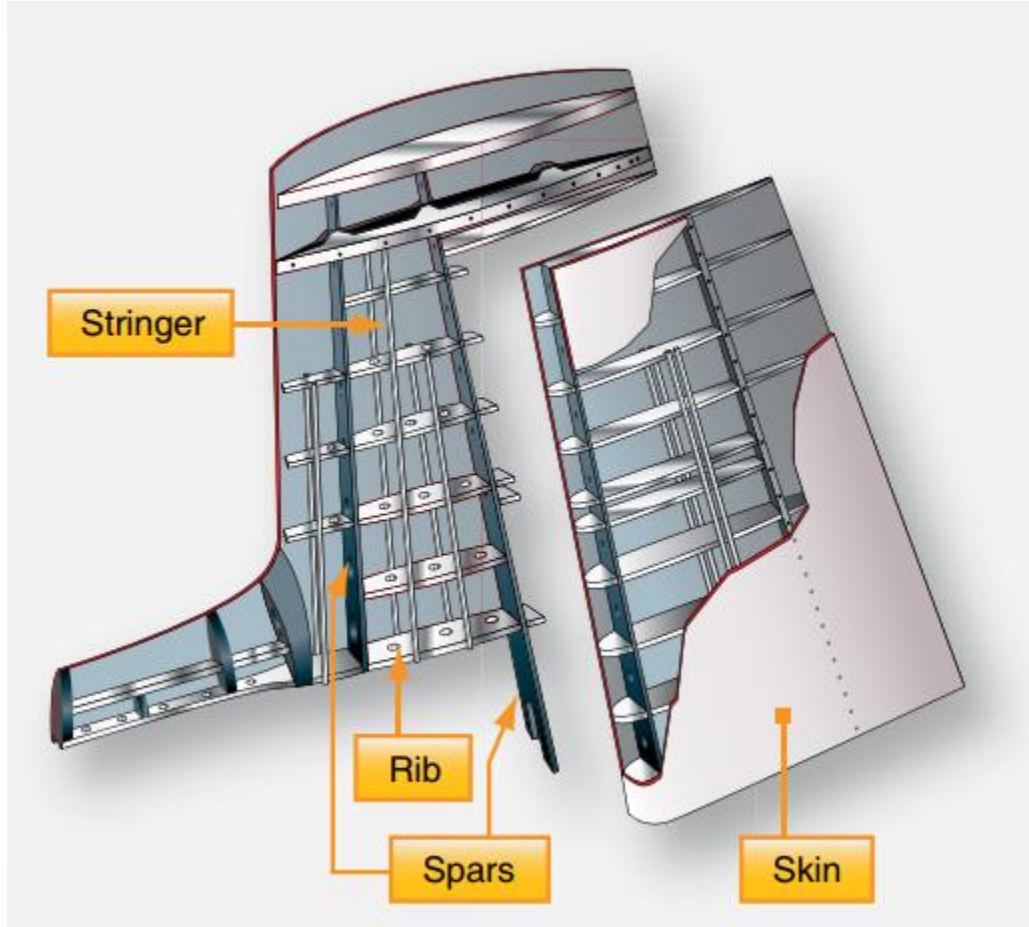


Figure 22.12.2-3: Vertical Stabilizer and Rudder Construction ([FAA-H-8083-31, 2012](#))

Where composite sub-assemblies with cored skin are used the structure becomes simpler with fewer parts required. The skin requires less intermediate support from ribs and there is a minimum of internal components required for structural integrity.



Figure 22.12.2-4: Internal Structure of a General Aviation wComposite Horizontal Stabilizer (Author's Collection - Courtesy of [Stratos Aircraft](#))

The rudder and elevator are flight control surfaces that are also part of the empennage.

22.14.1. Elevator

The elevator is the primary flight control surface that moves the aircraft around the horizontal or lateral axis. The elevator causes the nose of the aircraft to pitch up or down. The elevator is hinged to the trailing edge of the horizontal stabilizer and typically spans most or all of its width. It is controlled in the cockpit by pushing or pulling the control yoke or stick forward or aft.

Light aircraft use a system of control cables and pulleys or push pull tubes to transfer cockpit inputs to the movement of the elevator.

High performance and large aircraft typically employ more complex systems. Hydraulic power is commonly used to move the elevator on these aircraft. On aircraft equipped with fly-by-wire controls, a combination of electrical and hydraulic power is used.

22.14.2. Rudder

The rudder is the primary control surface that causes an aircraft to yaw or move about the vertical axis. Most aircraft have a single rudder hinged to the trailing edge of the vertical stabilizer. It is controlled by a pair of foot-operated rudder pedals in the cockpit. When the right pedal is pushed forward, it deflects the rudder to the right which moves the nose of the aircraft to the right. The left

pedal is rigged to simultaneously move aft. When the left pedal is pushed forward, the nose of the aircraft moves to the left.

As with the other primary flight controls, the transfer of the movement of the cockpit controls to the rudder varies with the complexity of the aircraft. Many aircraft incorporate the directional movement of the nose or tail wheel into the rudder control system for ground operation. This allows the operator to steer the aircraft with the rudder pedals during taxi when the airspeed is not high enough for the control surfaces to be effective. Some large aircraft have a split rudder arrangement. This is actually two rudders, one above the other. At low speeds, both rudders deflect in the same direction when the pedals are pushed. At higher speeds, one of the rudders becomes inoperative as the deflection of a single rudder is aerodynamically sufficient to maneuver the aircraft.

22.15. 56 Windows

Reserved

22.16. 57 Wings

22.16.1. General

Wings are airfoils that, when moved rapidly through the air, create lift. They are built in many shapes and sizes. Wing design can vary to provide certain desirable flight characteristics. Control at various operating speeds, the amount of lift generated, balance, and stability all change as the shape of the wing is altered. Both the leading edge and the trailing edge of the wing may be straight or curved, or one edge may be straight and the other curved.

One or both edges may be tapered so that the wing is narrower at the tip than at the root where it joins the fuselage. The wing tip may be square, rounded, or even pointed. Figure 22.16.1-1 shows several typical wing leading and trailing edge shapes.

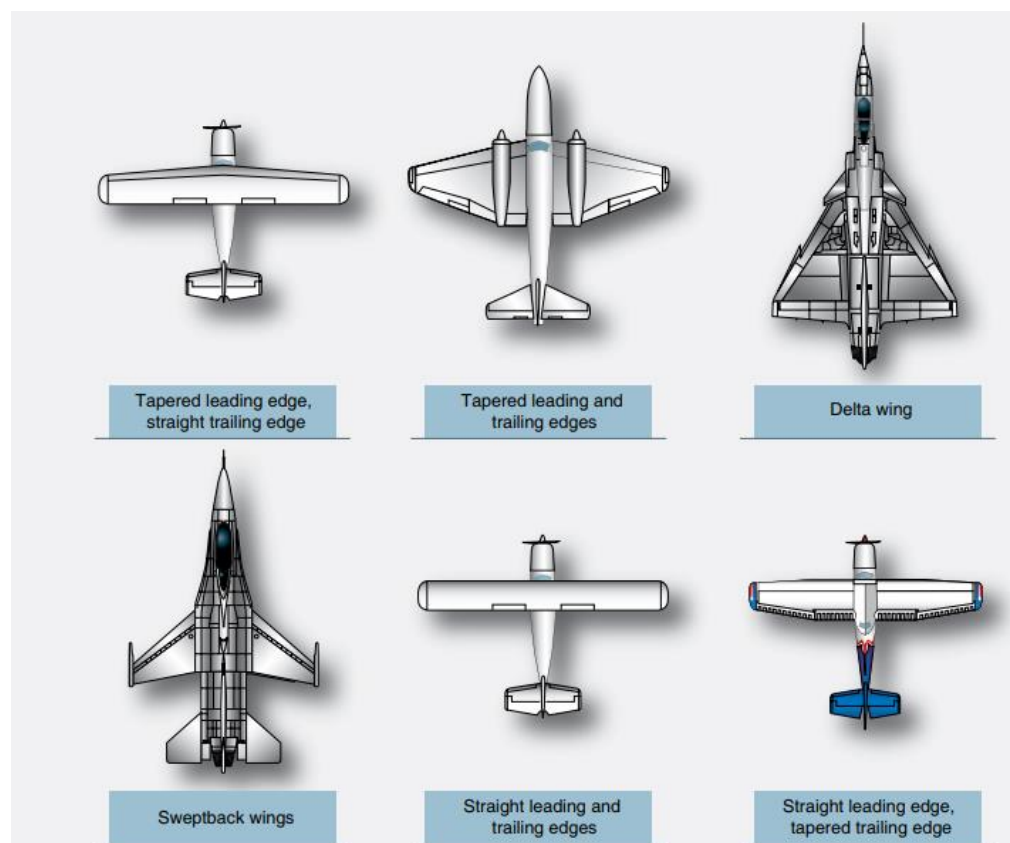


Figure 22.16.1-1: Various Wing Planform Shapes [\(FAA-H-8083-31, 2012\)](#)

The wings of an aircraft can be attached to the fuselage at the top, mid-fuselage, or at the bottom. They may extend perpendicular to the horizontal plain of the

fuselage or can angle up or down slightly. This angle is known as the wing dihedral. The dihedral angle affects the lateral stability of the aircraft. Figure 22.16.1-2 shows some common wing attach points and dihedral angle.

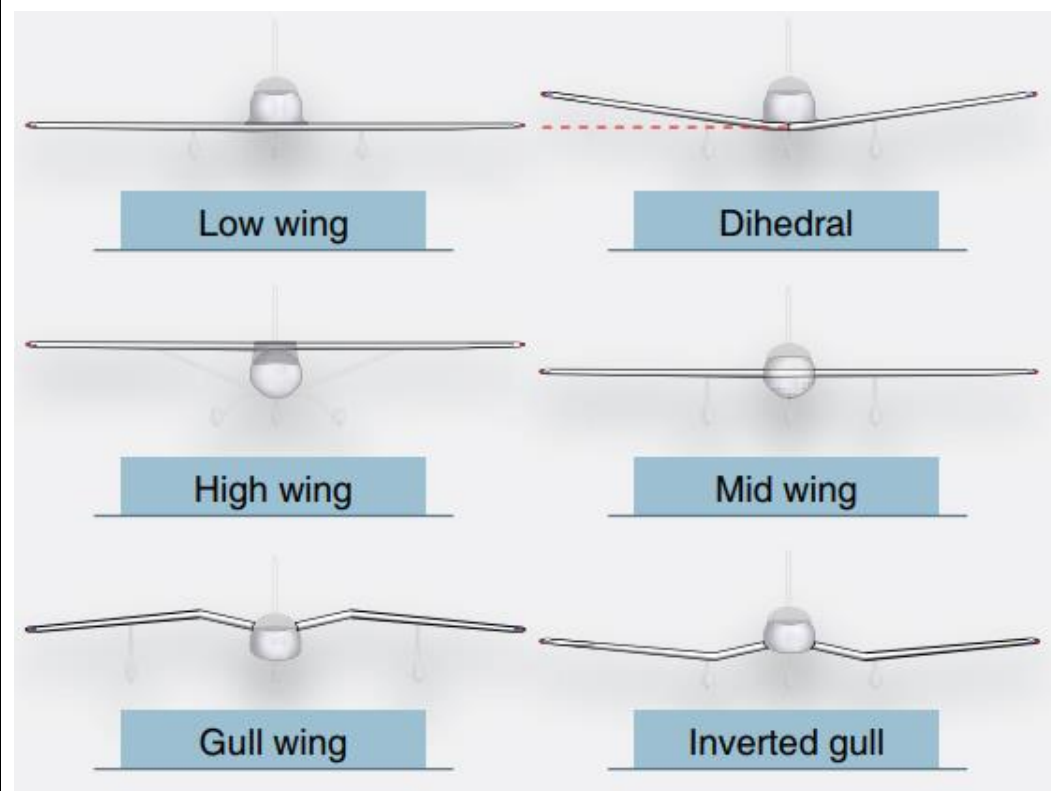


Figure 22.16.1-2: Wing Attach Points and Wing Angles [\(FAA-H-8083-31, 2012\)](#)

22.16.2. Main Wing Box

The wings of an aircraft are designed to lift it into the air and they carry the weight of the aircraft. The wing design for any given aircraft depends on a number of factors, such as size, weight, use of the aircraft, desired speed in flight and at landing, and desired rate of climb. The wings of aircraft are designated left and right, corresponding to the left and right sides of the operator when seated in the cockpit.

Often wings are of full cantilever design. This means they are built so that no external bracing is needed. They are supported internally by structural members (spars and ribs) assisted by the skin of the aircraft. Other aircraft wings use external struts or wires to assist in supporting the wing and carrying the aerodynamic and landing loads. Wing support cables and struts are generally made from steel. Many struts and their attach fittings have fairings to reduce drag. Short, nearly vertical supports called jury struts are found on struts that attach to the wings a great distance from the fuselage. This serves to subdue strut movement and oscillation caused by the air flowing around the strut in flight.

Figure 22.16.2-1 shows samples of wings using external bracing, also known as semi cantilever wings. Cantilever wings built with no external bracing are also shown.

Aluminum is the most common material from which to construct wings, but they can be wood covered with fabric, and occasionally magnesium alloys have been used.

Modern aircraft tend towards lighter and stronger materials throughout the airframe and in wing construction. Wings made entirely of carbon fiber or other composite materials exist, as well as wings made of a combination of materials for maximum strength to weight performance.

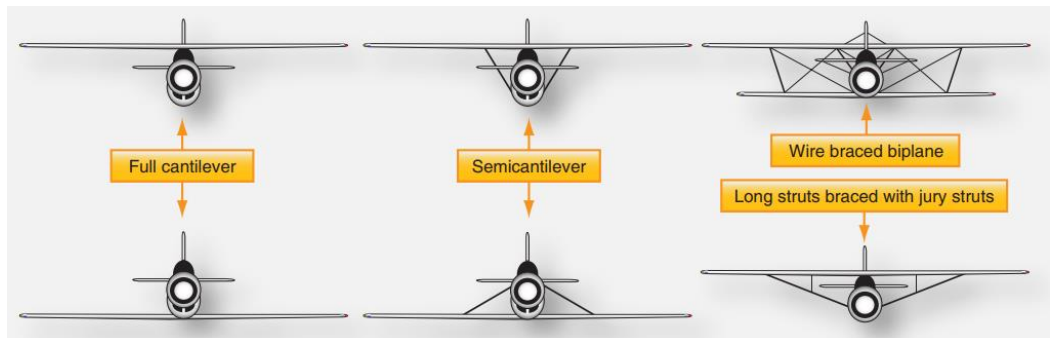


Figure 22.16.2-1: Different Methods of Wing Support [\(FAA-H-8083-31, 2012\)](#)

The internal structures of most wings are made up of spars and stringers running spanwise and ribs and formers or bulkheads running chordwise (leading edge to trailing edge). The spars are the principle structural members of a wing. They support all distributed loads, as well as concentrated weights such as the fuselage, landing gear, and engines.

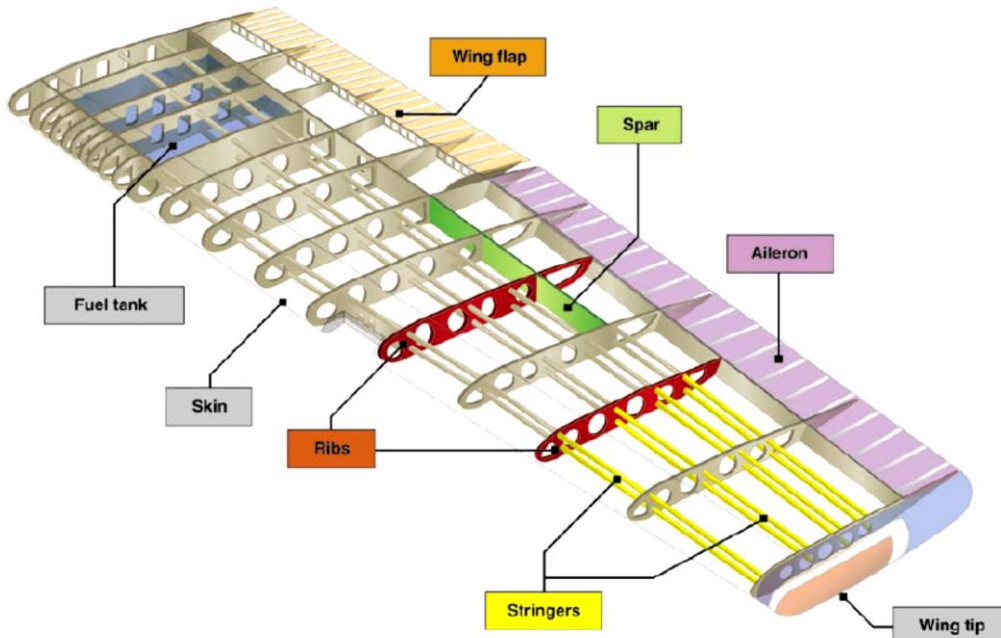


Figure 22.16.2-2: Various Wing Layout and Major Components [\(FAA-H-8083-25A, 2008\)](#)

The skin, which is attached to the wing structure, carries part of the loads imposed during flight. It also transfers loads to the wing ribs. The ribs, in turn, transfer the loads to the wing spars. Figure 22.16.2-4 In general, wing construction is based on one of three fundamental designs:

1. Mono-spar
2. Multi-spar
3. Box beam

Modification of these basic designs may be adopted by various manufacturers. The mono-spar wing incorporates only one main spanwise or longitudinal member in its construction.

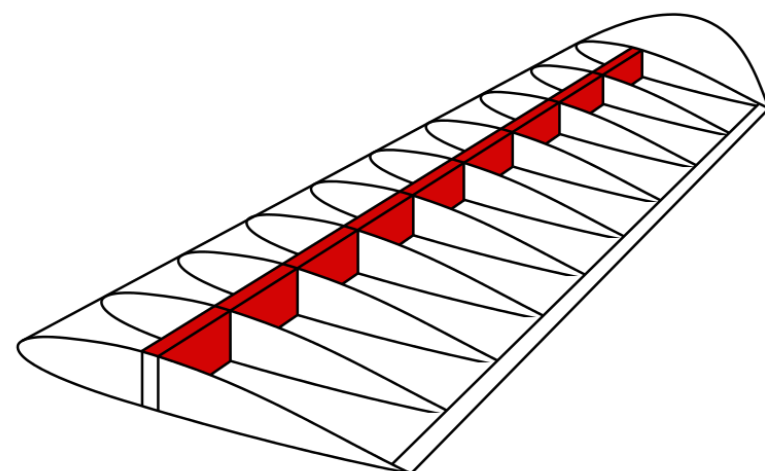


Figure 22.16.2-3: Single Spar or Mono-Spar Wing [\(By MLWatts \[CC0\], from Wikimedia Commons\)](#)

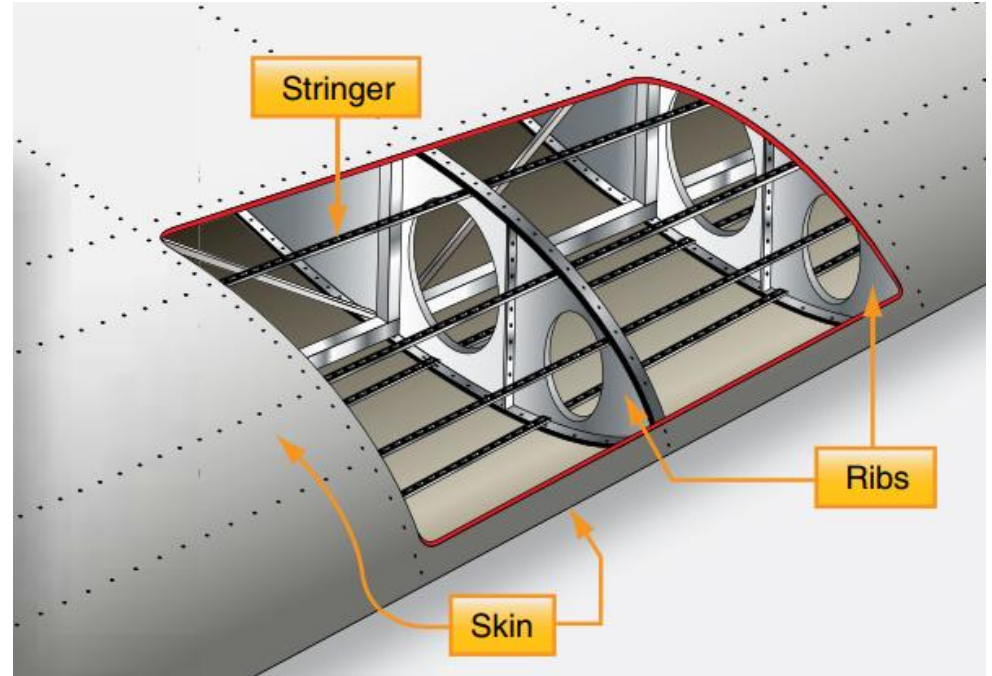
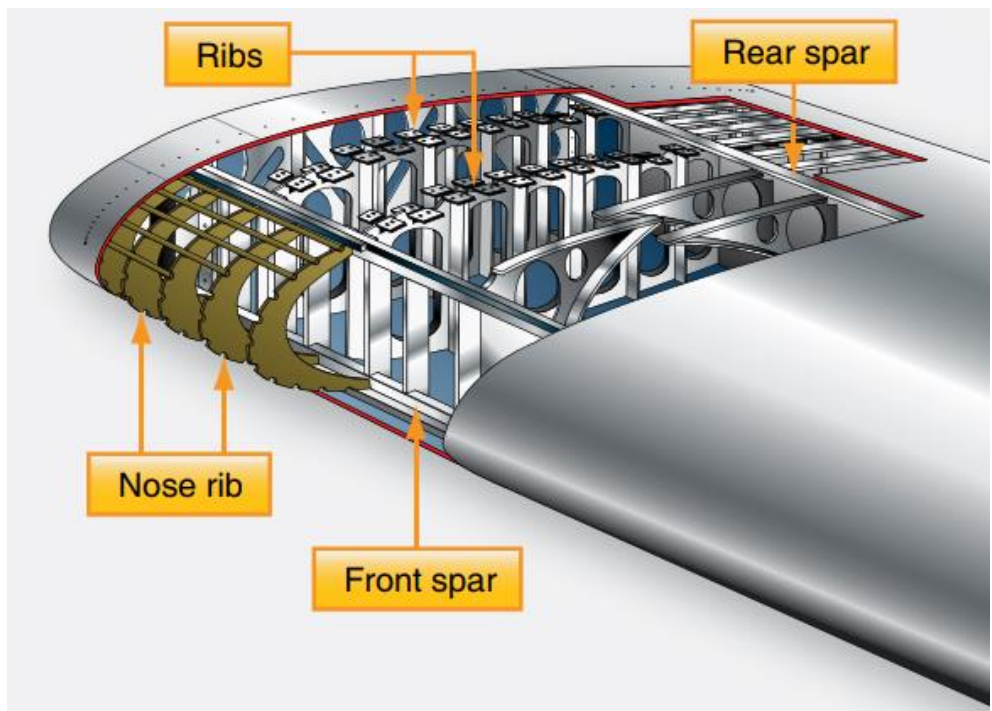


Figure 22.16.2-4: Wing Structure Nomenclature [\(FAA-H-8083-31, 2012\)](#)

Ribs or bulkheads supply the necessary contour or shape to the airfoil. Although the strict mono-spar wing is not common, this type of design modified by the addition of false spars or light shear webs along the trailing edge for support of control surfaces is sometimes used. The multi-spar wing incorporates more than one main longitudinal member in its construction. To give the wing contour, ribs or bulkheads are often included.

22.16.2.1. Wing Spars

Spars are the principal structural members of the wing. They correspond to the longerons of the fuselage. They run parallel to the lateral axis of the aircraft, from the fuselage toward the tip of the wing, and are usually attached to the fuselage by wing fittings, plain beams, or a truss. Spars may be made of metal, wood, or composite materials depending on the design criteria of a specific aircraft.

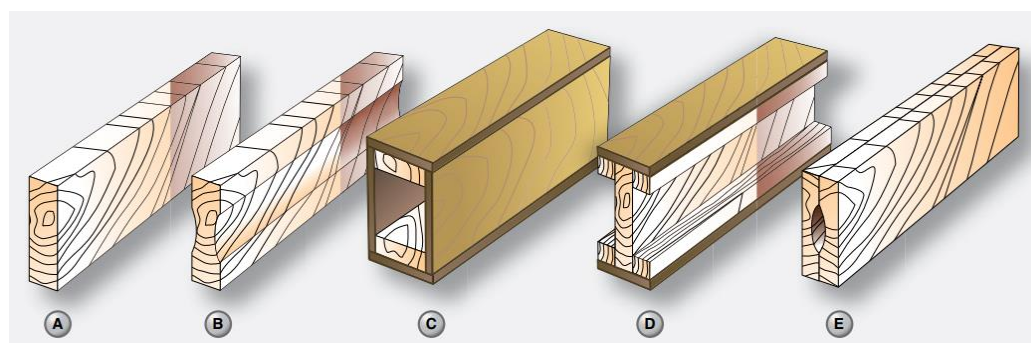


Figure 22.16.2-5: Typical Wooden Wing Spar Cross-Sections [\(FAA-H-8083-31, 2012\)](#)

Wooden spars are usually made from spruce. They can be generally classified into four different types by their cross-sectional configuration. As shown in Figure 22.16.2-5, they may be (A) solid, (B) box shaped, (C) partly hollow, or (D) in the form of an I-beam.

Lamination of solid wood spars is often used to increase strength. Laminated wood can also be found in box shaped spars. The spar in Figure 22.16.2-5 (E) has had material removed to reduce weight but retains the strength of a rectangular spar. As can be seen, most wing spars are basically rectangular with the long dimension of the cross-section oriented up and down in the wing.

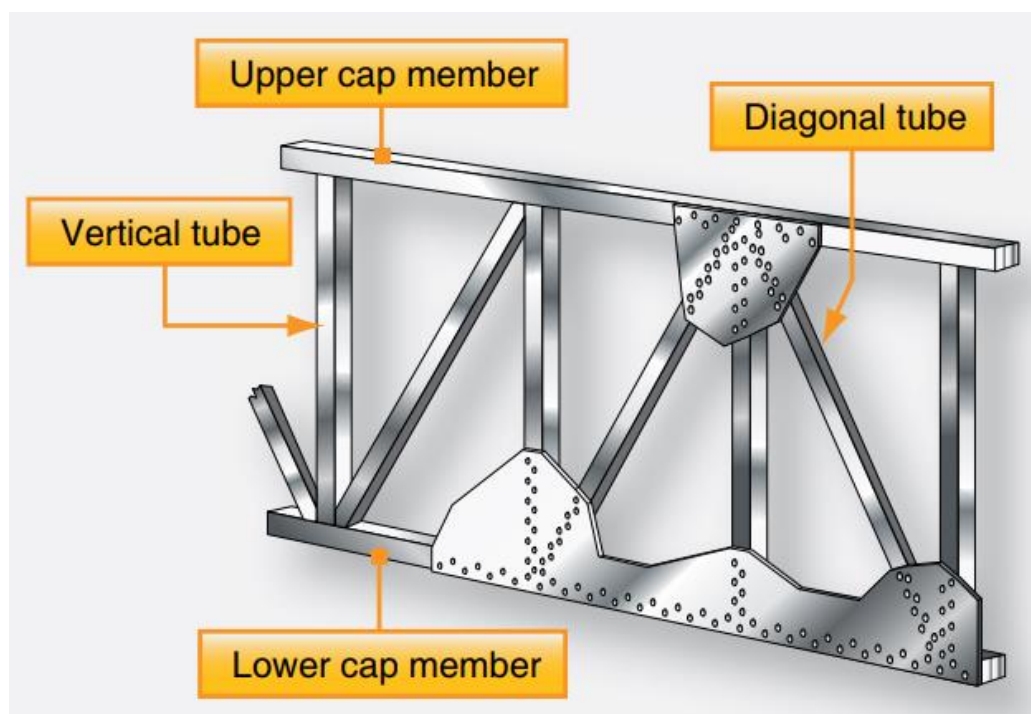


Figure 22.16.2-6: Truss Wing Spar [\(FAA-H-8083-31, 2012\)](#)

Currently, most manufactured aircraft have wing spars made of solid extruded aluminum or aluminum extrusions riveted together to form the spar.

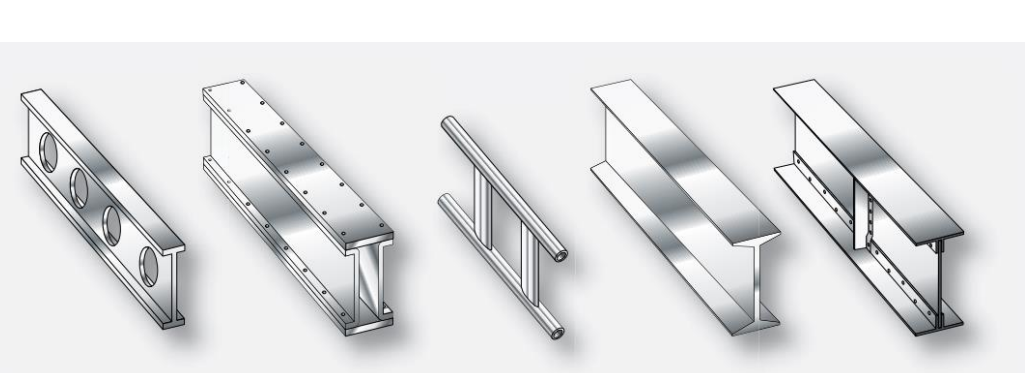


Figure 22.16.2-7: Examples of Metal Wing Spar Shapes [\(FAA-H-8083-31, 2012\)](#)

Figure 22.16.2-7 shows examples of metal wing spar cross-sections. In an I-beam spar, the top and bottom of the I-beam are called the caps and the vertical section is called the web. The entire spar can be extruded from one piece of metal but often it is built up from multiple extrusions or formed angles. The web forms the principal depth portion of the spar and the cap strips (extrusions, formed angles, or milled sections) are attached to it.

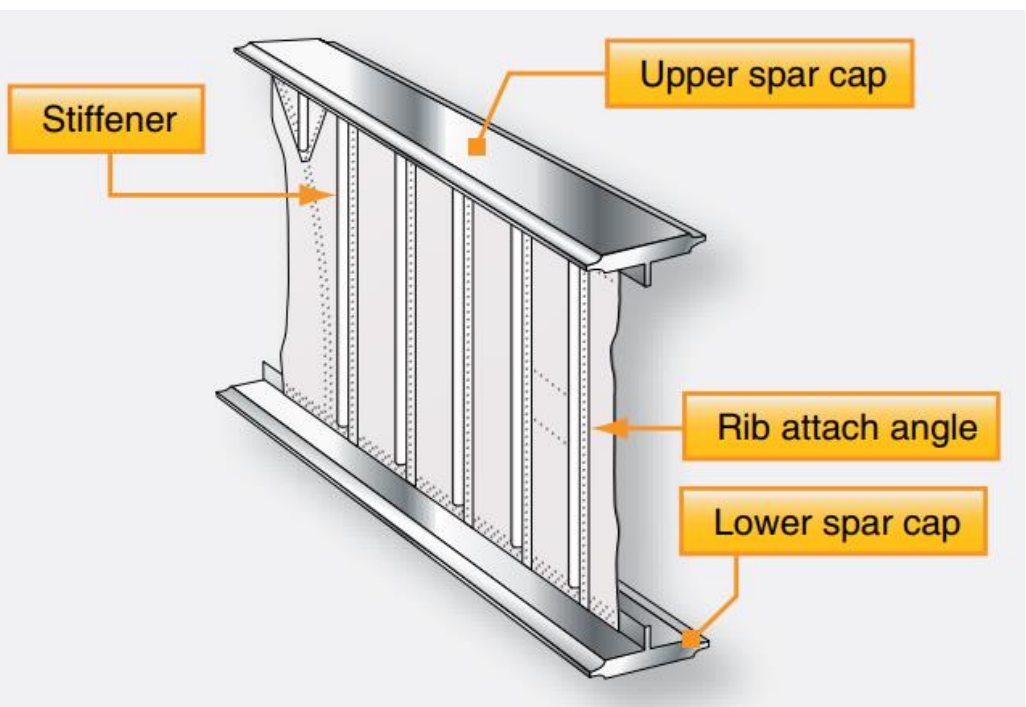


Figure 22.16.2-8: A Plate Web Wing Spar with Vertical Stiffeners [\(FAA-H-8083-31, 2012\)](#)

Together, these members carry the loads caused by wing bending, with the caps providing a foundation for attaching the skin. Although the spar shapes in Figure 22.16.2-7 are typical, actual wing spar configurations assume many forms. For example, the web of a spar may be a plate, or a truss as shown in Figure 22.16.2-6. It could be built up from lightweight materials with vertical stiffeners employed for strength. Figure 22.16.2-8.

It could also have no stiffeners but might contain flanged holes for reducing weight but maintaining stiffness. Some metal and composite wing spars retain the I-beam concept but use a sine wave web. Figure 22.16.2-10.

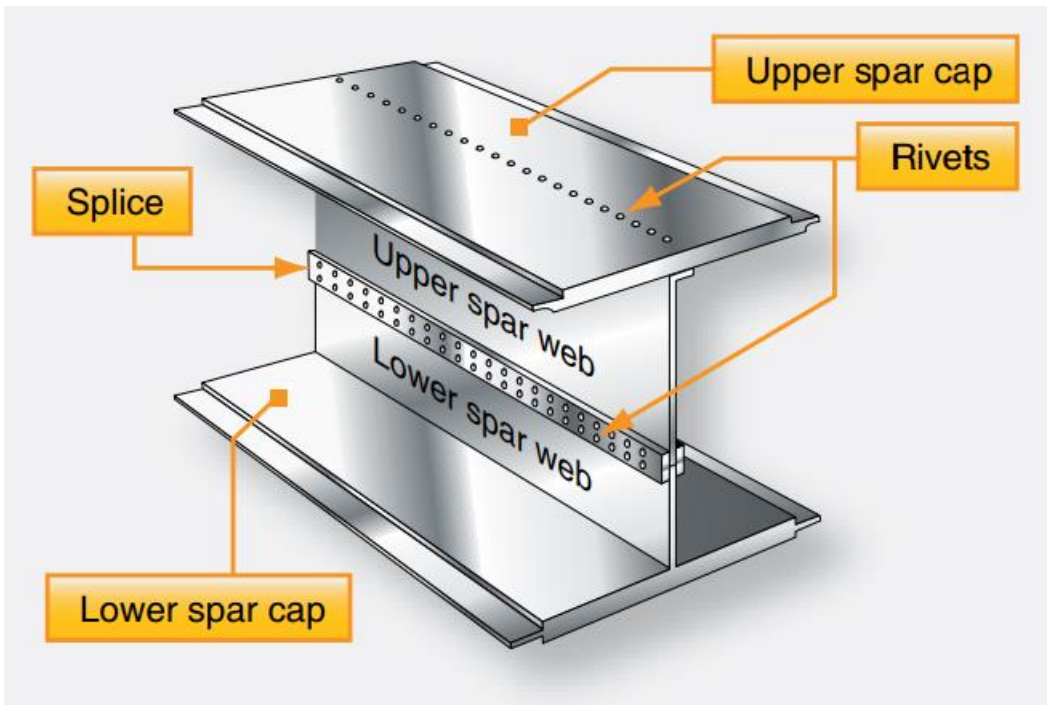


Figure 22.16.2-9: A Failsafe Spar with a Riveted Spar Web [\(FAA-H-8083-31, 2012\)](#)

Additionally, fail-safe spar web design exists. Fail-safe means that should one member of a complex structure fail, some other part of the structure assumes the load of the failed member and permits continued operation. A spar with failsafe construction is shown in Figure 22.16.2-9. This spar is made in two sections. The top section consists of a cap riveted to the upper web plate. The lower section is a single extrusion consisting of the lower cap and web plate.

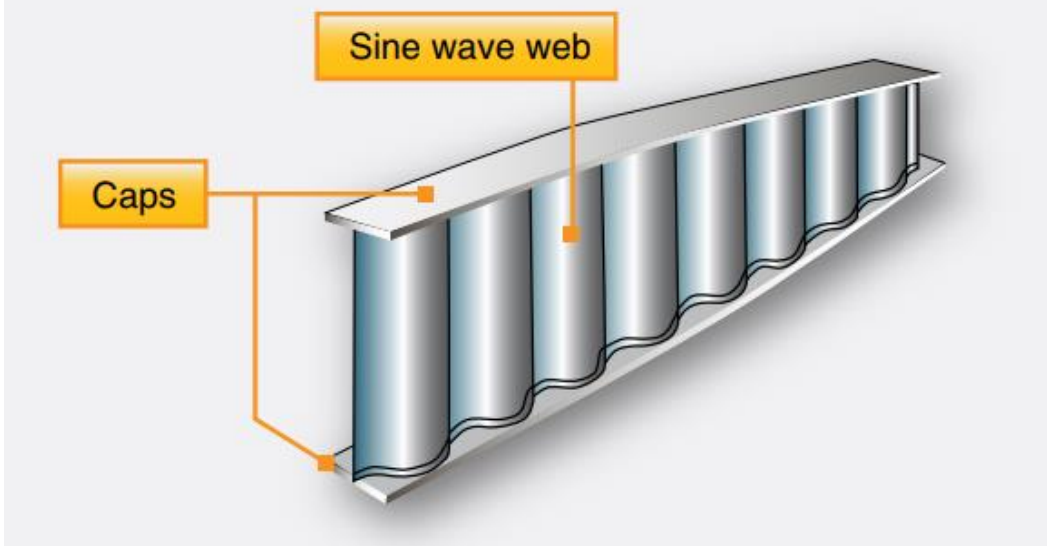


Figure 22.16.2-10: A Sine Wave Wing Spar [\(FAA-H-8083-31, 2012\)](#)

These two sections are spliced together to form the spar. If either section of this type of spar breaks, the other section can still carry the load. This is the fail-safe feature. Most wings have two spars. One spar is usually located near the front of the wing, and the other about two-thirds of the distance toward the wing's trailing edge. Regardless of type, the spar is the most important component of the wing. The spar carries the accumulated vertical load caused by the lift force on the wing. At the wing root this load can be very large. See Figure 22.16.2-11.

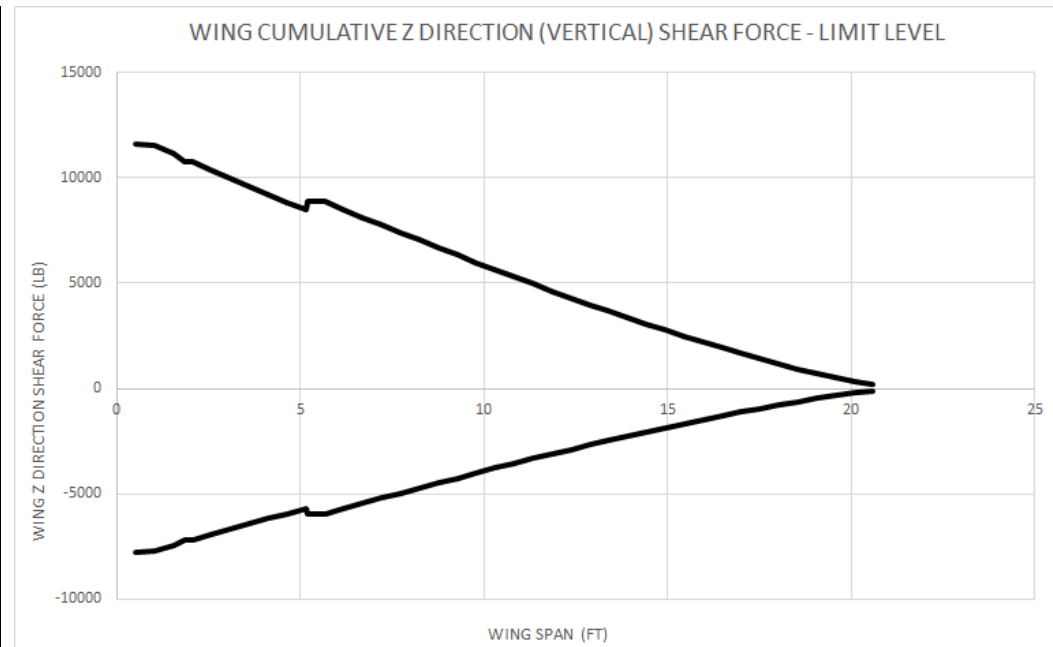


Figure 22.16.2-11: Wing Cumulative Vertical Shear Load Envelope for a Cantilevered Wing

Note that positive shear force indicates up-bending on the wing which results from a positive 'g' maneuver (pitching nose up) or positive gust event. Negative shear force indicates wing down-bending from a negative 'g' maneuver (pitching nose down) or negative gust event.

In general, is it idealized that the vertical load created by positive and negative lift on the wing is carried by the vertical web of the wing spar or spars.

The peak vertical shear force at the wing root is greatly reduced when using a strut to support the wing. See Figure 22.16.2-12.

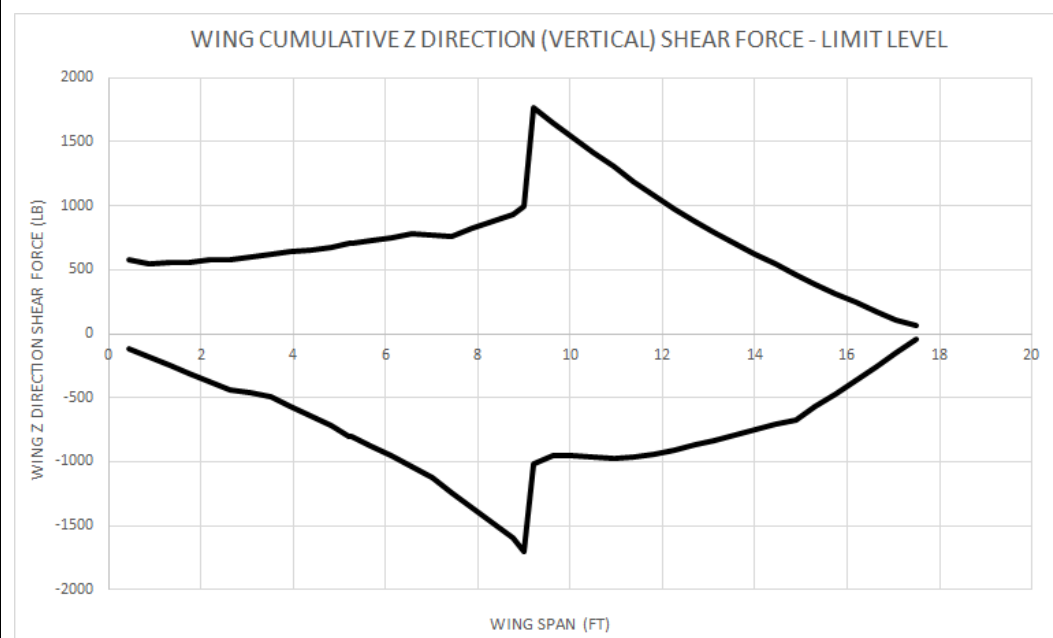


Figure 22.16.2-12: Wing Cumulative Vertical Shear Load Envelope for a Wing with Strut

Composite wing spars use high modulus carbon unidirectional fibers in the spar caps to carry the wing bending loads and to give maximum stiffness to the wing. The spar web is often biased towards +/- 45 degree woven composite carbon or glass to transfer the vertical shear loads.

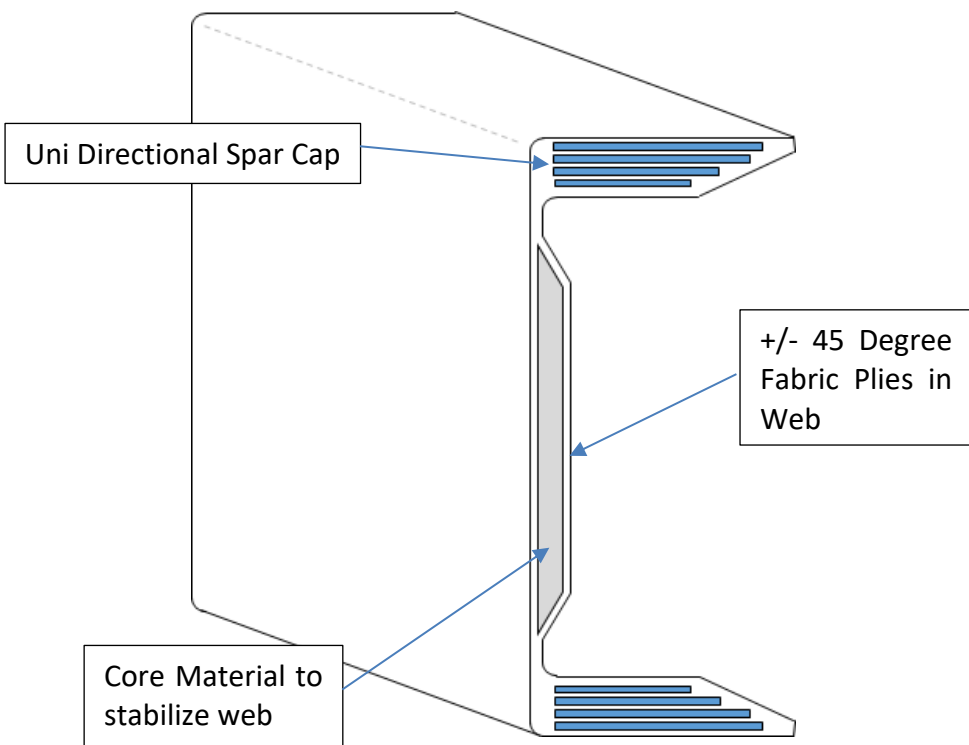


Figure 22.16.2-13: Typical Part 23 Composite Spar Configuration

The spar web can be stabilized for shear buckling with honeycomb or foam core, or with bonded or fastened stiffeners.

If the fuel is carried in the wing of the aircraft the same means of resisting buckling of the web help to add strength to resist the out of plane loads on the spar web caused by the hydrostatic pressure of the fuel.

22.16.2.2. Wing Ribs

Ribs are the structural crosspieces that combine with spars and stringers to make up the framework of the wing. They usually extend from the wing leading edge to the rear spar or to the trailing edge of the wing. The ribs give the wing its cambered shape and help to transmit the air load from the skin and stringers to the spars.

Wing ribs are also used to help resist the pressure loads cause by carrying fuel in the wing. They are also used to help stabilize the skin in shear and compression buckling. They are more effective in helping the skin resist shear buckling because the ribs are aligned perpendicular to the compression loads in the skin which act in the spanwise direction.

Similar ribs are also used in ailerons, elevators, rudders, and stabilizers.

Wing ribs are usually manufactured from wood, metal or composite. Aircraft with wood wing spars may have wood or metal ribs while most aircraft with metal spars have metal ribs. Wood ribs are usually manufactured from spruce. The three most common types of wooden ribs are the plywood web, the lightened plywood web, and the truss types.

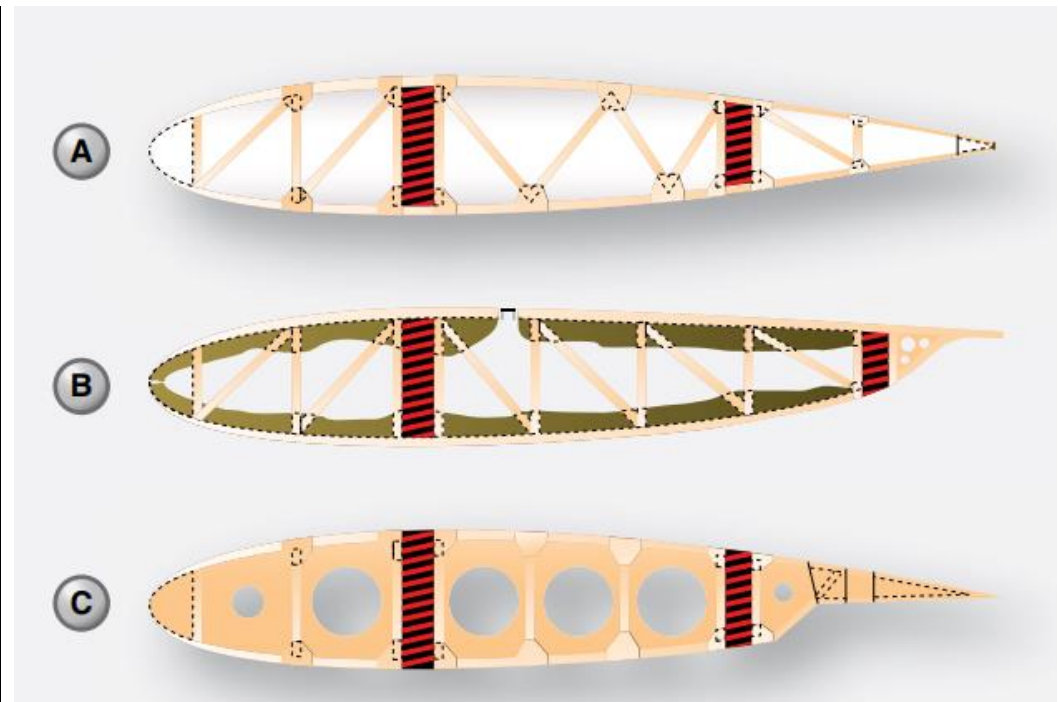


Figure 22.16.2-14: Examples of Wooden Wing Rib Design [\(FAA-H-8083-31, 2012\)](#)

Of these three, the truss type is the most efficient because it is strong and lightweight, but it is also the most complex to construct. Figure 22.16.2-14 shows wood truss web ribs and a lightened plywood web rib. Wood ribs have a rib cap or cap strip fastened around the entire perimeter of the rib. It is usually made of the same material as the rib itself. The rib cap stiffens and strengthens the rib and provides an attaching surface for the wing covering. In Figure 22.16.2-14 (A), the cross-section of a wing rib with a truss-type web is illustrated. The dark rectangular sections are the front and rear wing spars. Note that to reinforce the truss, gussets are used. In Figure 22.16.2-14 (B), a truss web rib is shown with a continuous gusset. It provides greater support throughout the entire rib with very little additional weight. A continuous gusset stiffens the cap strip in the plane of the rib. This aids in preventing buckling and helps to obtain better rib/skin joints where nail-gluing is used. Such a rib can resist the driving force of nails better than the other types.

Continuous gussets are also more easily handled than the many small separate gussets otherwise required. Figure 22.16.2-14 (C) shows a rib with a lightened plywood web. It also contains gussets to support the web/cap strip interface. The cap strip is usually laminated to the web, especially at the leading edge.

A wing rib may also be referred to as a plain rib or a main rib. Wing ribs with specialized locations or functions are given names that reflect their uniqueness. For example, ribs that are located entirely forward of the front spar that are used to shape and strengthen the wing leading edge are called nose ribs or false ribs. False ribs are ribs that do not span the entire wing chord, which is the distance from the leading edge to the trailing edge of the wing.

Wing butt ribs may be found at the inboard edge of the wing where the wing attaches to the fuselage. Depending on its location and method of attachment, a butt rib may also be called a bulkhead rib or a compression rib if it is designed to receive compression loads that tend to force the wing spars together. Since the ribs are laterally weak, they are strengthened in some wings by tapes that are woven above and below rib sections to prevent sidewise bending of the ribs. Drag and anti-drag wires may also be found in a wing. Figure 22.16.2-15, they are shown crisscrossed between the spars to form a truss to resist forces acting on the wing in the direction of the wing chord. These tension wires are also referred to as tie rods. The wire designed to resist the backward forces is called a drag wire; the anti-drag wire resists the forward forces in the chord direction. Figure 22.16.2-15 illustrates the structural components of a basic wood wing.

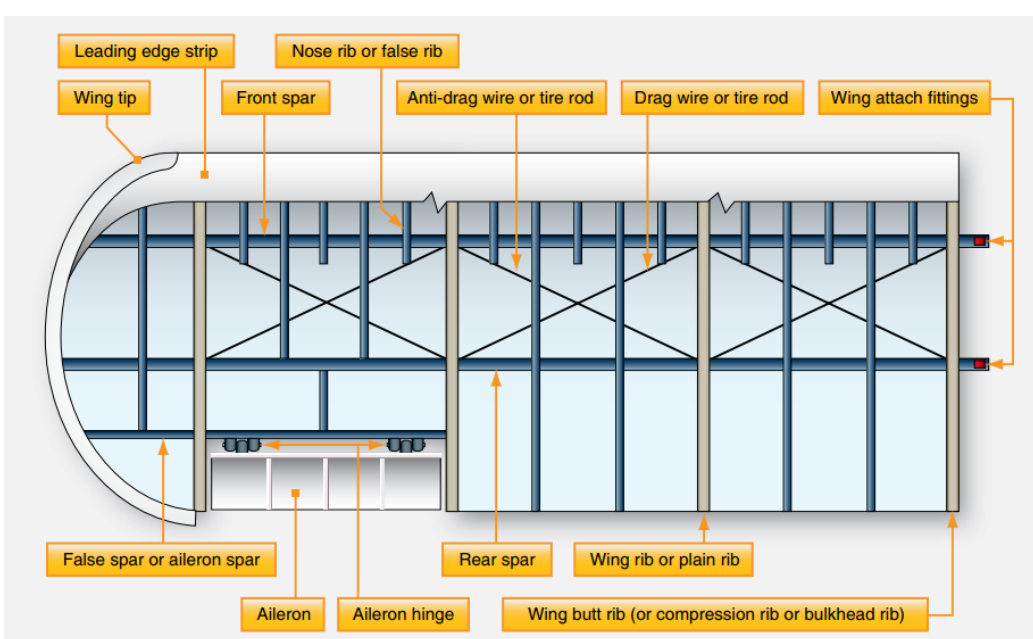


Figure 22.16.2-15: Basic Wood Wing Structure and Components [\(FAA-H-8083-31, 2012\)](#)

At the inboard end of the wing spars is some form of wing attach fitting as illustrated in Figure 22.16.2-15. These provide a strong and secure method for attaching the wing to the fuselage. The interface between the wing and fuselage is often covered with a fairing to achieve smooth airflow in this area.

22.16.2.3. Wing Skin

Often, the skin on a wing is designed to carry part of the flight and ground loads in combination with the spars and ribs. This is known as a stressed-skin design. The all-metal, full cantilever wing section illustrated in Figure 1-35 shows the structure of one such design. The lack of extra internal or external bracing requires that the skin share some of the load. Notice the skin is stiffened to aid with this function.

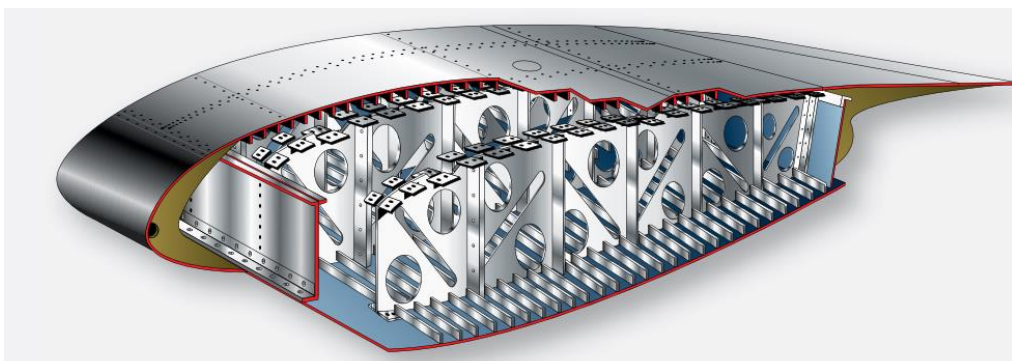


Figure 22.16.2-16: Metal Wing Design with Skin as Integral Load Carrying Member [\(FAA-H-8083-31, 2012\)](#)

Fuel is often carried inside the wings of a stressed-skin aircraft. The joints in the wing can be sealed with a special fuel resistant sealant enabling fuel to be stored directly inside the structure. This is known as wet wing design. Alternately, a fuel-carrying bladder or tank can be fitted inside a wing. Figure 1-36 shows a wing section with a box beam structural design such as one that might be found in a transport category aircraft. This structure increases strength while reducing weight. Proper sealing of the structure allows fuel to be stored in the box sections of the wing. The wing skin on an aircraft may be made from a wide variety of materials such as fabric, wood, or aluminum. But a single thin sheet of material

is not always employed. Chemically milled aluminum skin can provide skin of varied thicknesses.

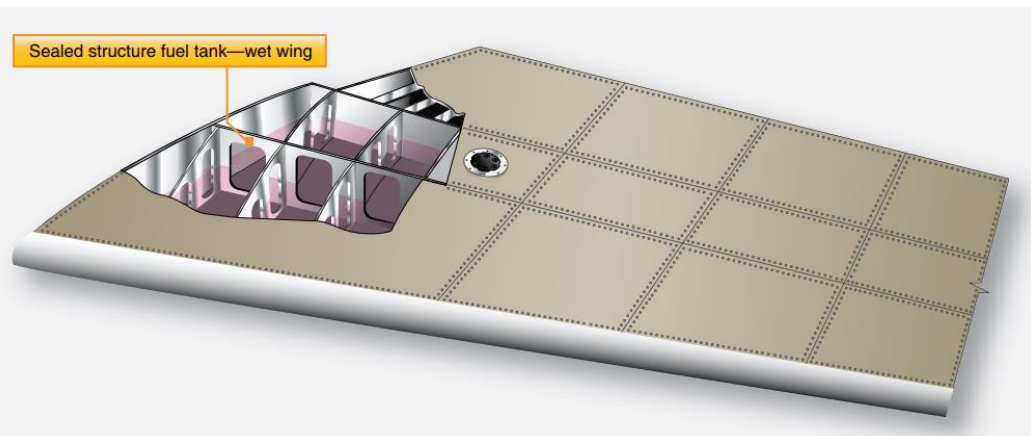


Figure 22.16.2-17: Fuel Region in Wing Structure [\(FAA-H-8083-31, 2012\)](#)

On aircraft with stressed-skin wing design, honeycomb structured wing panels are often used as skin. A honeycomb structure is built up from a core material resembling a bee hive's honeycomb which is laminated or sandwiched between thin outer skin sheets. Figure 1-37 illustrates honeycomb panes and their components. Panels formed like this are lightweight and very strong. They have a variety of uses on the aircraft, such as floor panels, bulkheads, and control surfaces, as well as wing skin panels. Figure 1-38 shows the locations of honeycomb construction wing panels on a jet transport aircraft.

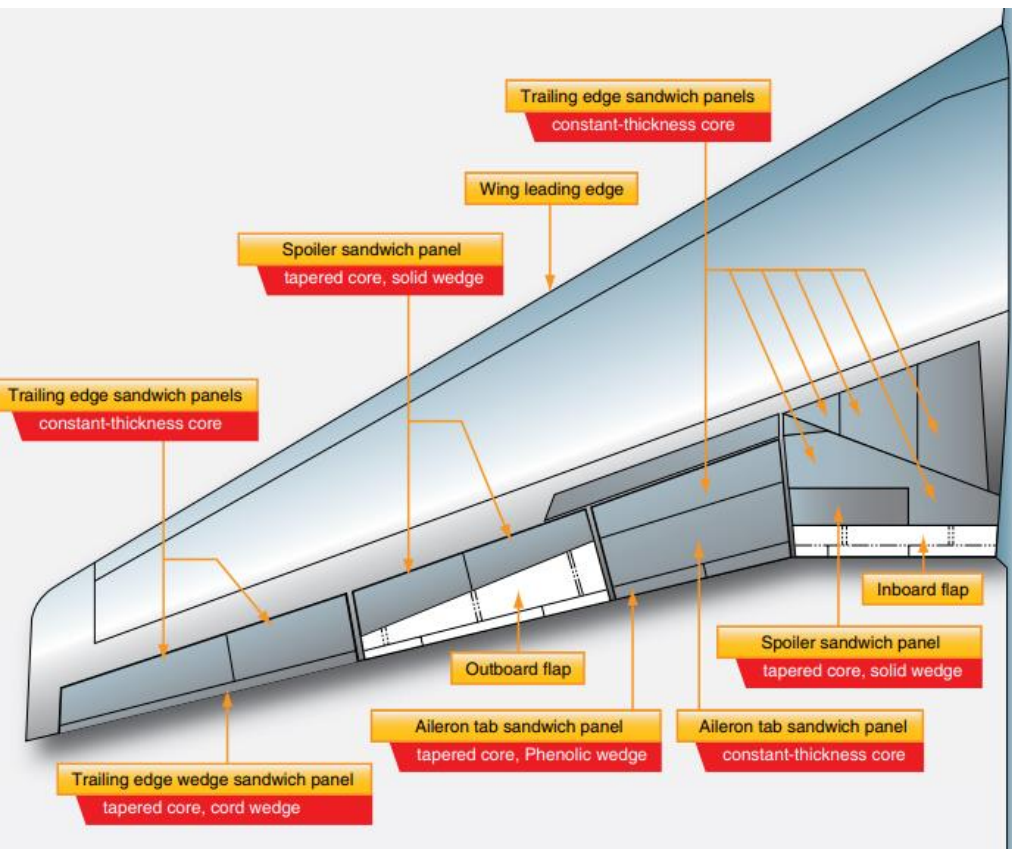


Figure 22.16.2-18: Honeycomb Structure on Transport Category Aircraft Wing [\(FAA-H-8083-31, 2012\)](#)

A honeycomb panel can be made from a wide variety of materials. Aluminum core honeycomb with an outer skin of aluminum is common. But honeycomb in which the core is an Arimid® fiber and the outer sheets are coated Phenolic® is common as well. In fact, a myriad of other material combinations such as those using fiberglass, plastic, Nomex®, Kevlar®, and carbon fiber all exist. Each honeycomb structure possesses unique characteristics depending upon the materials, dimensions, and manufacturing techniques employed. Figure 1-39 shows an entire wing leading edge formed from honeycomb structure.

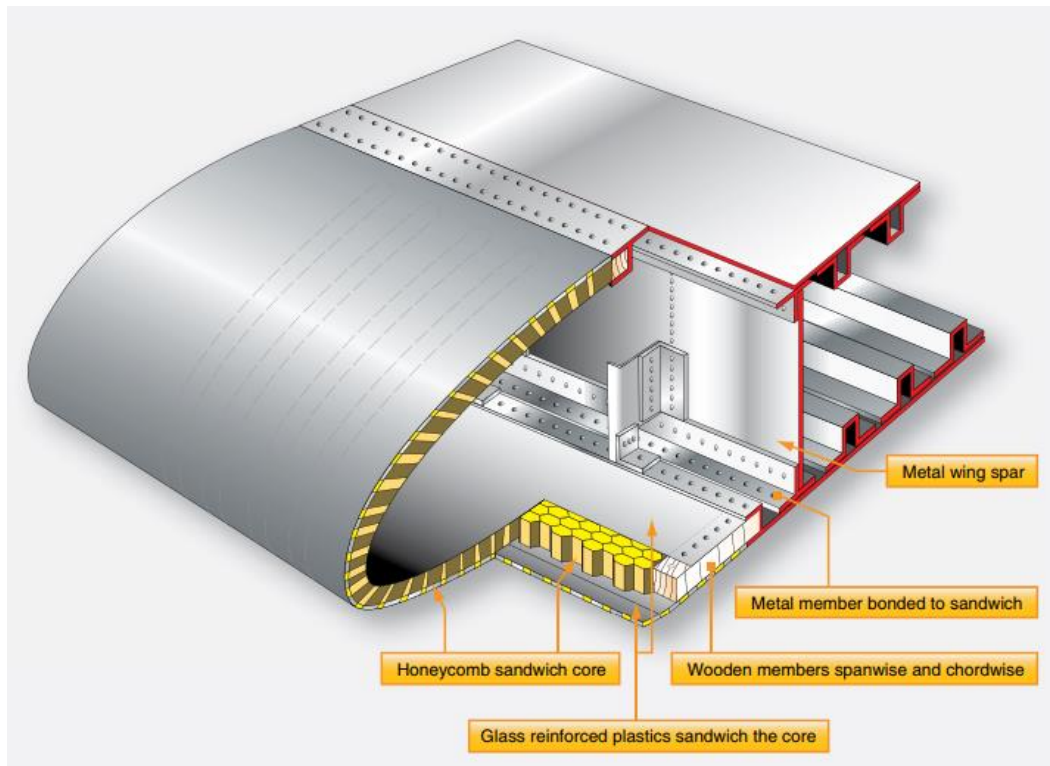


Figure 22.16.2-19: Honeycomb Leading Edge Structure on Metal Wing Box
(FAA-H-8083-31, 2012)

22.16.3. Wing Tip

The wing tip is often a removable unit, bolted to the outboard end of the wing panel. One reason for this is the vulnerability of the wing tips to damage, especially during ground handling and taxiing. Figure 1-34 shows a removable wing tip for a large aircraft wing. Others are different. The wing tip assembly is of aluminum alloy construction. The wing tip cap is secured to the tip with countersunk screws and is secured to the interspar structure at four points with $\frac{1}{4}$ -inch diameter bolts. To prevent ice from forming on the leading edge of the wings of large aircraft, hot air from an engine is often channeled through the leading edge from wing root to wing tip. A louver on the top surface of the wingtip allows this warm air to be exhausted overboard. Wing position lights are located at the center of the tip and are not directly visible from the cockpit. As an indication that the wing tip light is operating, some wing tips are equipped with a Lucite rod to transmit the light to the leading edge.

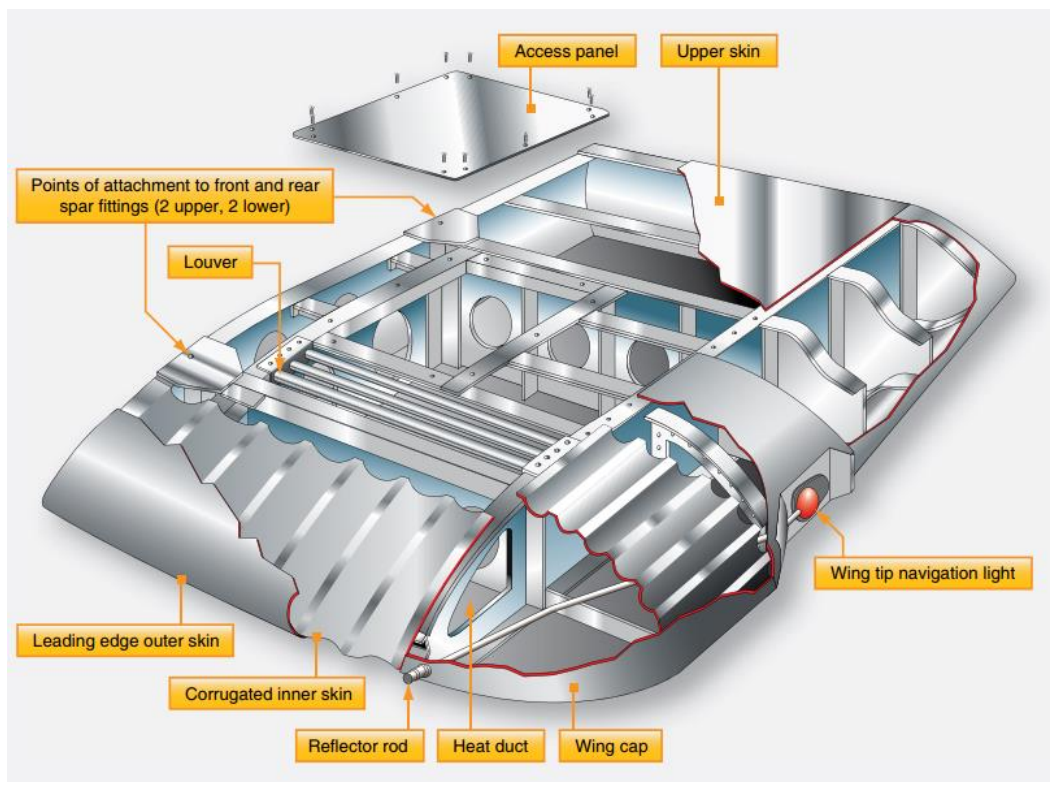


Figure 22.16.3-1: Removable Metal Wing Tip (FAA-H-8083-31, 2012)

22.16.3.1. Winglet

A winglet is an obvious vertical upturn of the wing's tip resembling a vertical stabilizer. It is an aerodynamic device designed to reduce the drag created by wing tip vortices in flight. Usually made from aluminum or composite materials, winglets can be designed to optimize performance at a desired speed.



Figure 22.16.3-2: B737-800 Winglet (Courtesy Wikimedia Commons, <https://commons.wikimedia.org/wiki/User:Dtom>)

There are several variations on the blended winglet that serve the same purpose for drag reduction.



Figure 22.16.3-3: Split "Scimitar" Winglets
(Courtesy Tony Higgett)

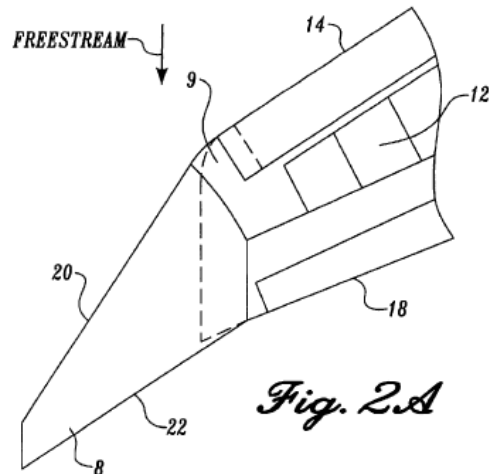


Fig. 2A

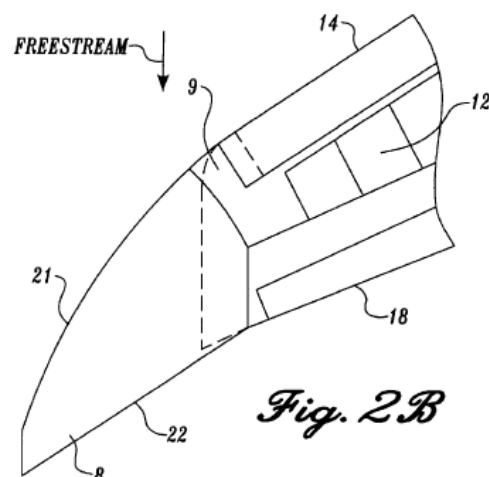


Fig. 2B

Figure 22.16.3-4: Blunt Leading Edge Raked Wingtips, The Boeing Company, Patent US9086502

22.16.4. Leading and Trailing Edge Devices

Flaps are found on most aircraft. They are usually inboard on the wings' trailing edges adjacent to the fuselage. The flaps are lowered to increase the camber of the wings and provide greater lift and control at slow speeds. They enable landing at slower speeds and shorten the amount of runway required for takeoff and landing. The amount that the flaps extend and the angle they form with the wing can be selected from the cockpit. Typically, flaps can extend up to 45–50°. Figure 22.16.4-1 shows various aircraft with flaps in the extended position.

Flaps are usually constructed of materials and with techniques used on the other airfoils and control surfaces of a particular aircraft. Aluminum skin and structure flaps are the norm on light aircraft. Heavy and high-performance aircraft flaps may also be aluminum, but the use of composite structures is also common. There are various kinds of flaps. Plain flaps form the trailing edge of the wing when the flap is in the retracted position. [Figure 1-63A] The airflow over the wing continues over the upper and lower surfaces of the flap, making the trailing edge of the flap essentially the trailing edge of the wing. The plain flap is hinged so that the trailing edge can be lowered. This increases wing camber and provides greater lift. A split flap is normally housed under the trailing edge of the wing. [Figure 1-63B] It is usually just a braced flat metal plate hinged at several places along its leading edge. The upper surface of the wing extends to the trailing edge of the flap. When deployed, the split flap trailing edge lowers away from the trailing edge of the wing. Airflow over the top of the wing remains the same. Airflow under the wing now follows the camber created by the lowered split flap, increasing lift.



Figure 22.16.4-1: Various Flaps on Different Aircraft (Courtesy Wikimedia Commons)

Fowler flaps not only lower the trailing edge of the wing when deployed but also slide aft, effectively increasing the area of the wing, reference Figure 22.16.4-2. This creates more lift via the increased surface area, as well as the wing camber. When stowed, the fowler flap typically retracts up under the wing trailing edge similar to a split flap. The sliding motion of a fowler flap can be accomplished with a worm drive and flap tracks. An enhanced version of the fowler flap is a set of flaps that contains more than one aerodynamic surface. Figure 22.16.4-3 shows a triple-slotted flap. In this configuration, the flap consists of a fore flap, a mid flap, and an aft flap. When deployed, each flap section slides aft on tracks as it lowers. The flap sections also separate leaving an open slot between the wing and the fore flap, as well as between each of the flap sections. Air from the underside of the wing flows through these slots. The result is that the laminar flow on the upper surfaces is enhanced. The greater camber and effective wing area increase overall lift.

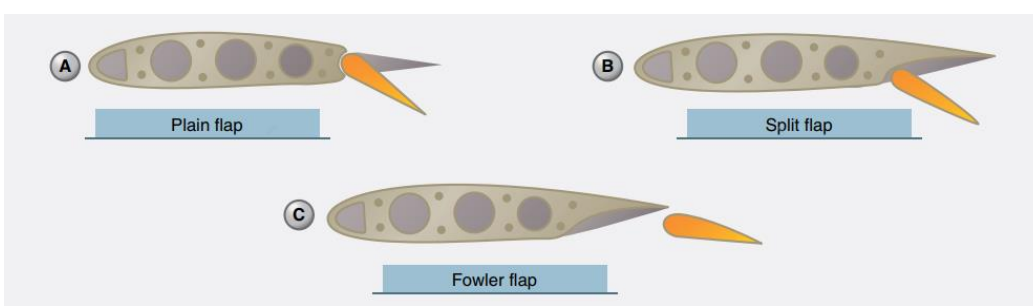


Figure 22.16.4-2: Different Types of Flap [\(FAA-H-8083-31, 2012\)](#)

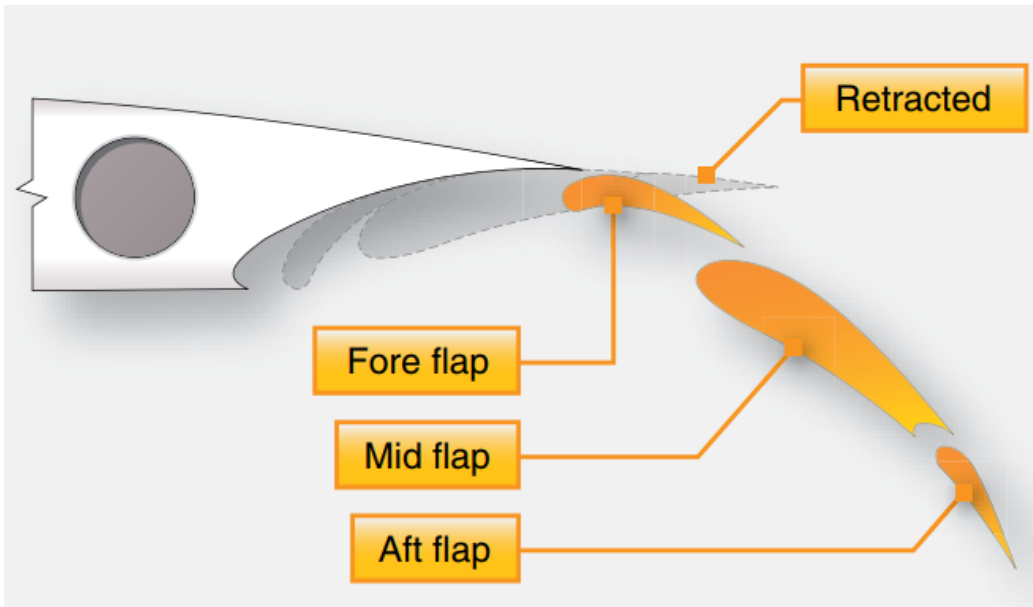


Figure 22.16.4-3: Triple Slotted Flap [\(FAA-H-8083-31, 2012\)](#)

The remainder of this section is taken directly from [\(NASA-CR-4746, 1996\)](#). This is an excellent reference written by Peter K. C. Rudolph. This reference contains more useful data than is shown here and the reader is strongly recommended to become familiar with the source material. The text in Italics is taken directly from the source without change.

22.16.4.1. Split Flap

The split flap was widely used in earlier days, especially on military airplanes. It is a good attitude and glideslope control device, but it does not produce much lift increase. However, as a speed brake it is better than a spoiler because it produces drag without losing lift. The split flap is not used on any modern airliner. It is used on low performance part 23 aircraft.

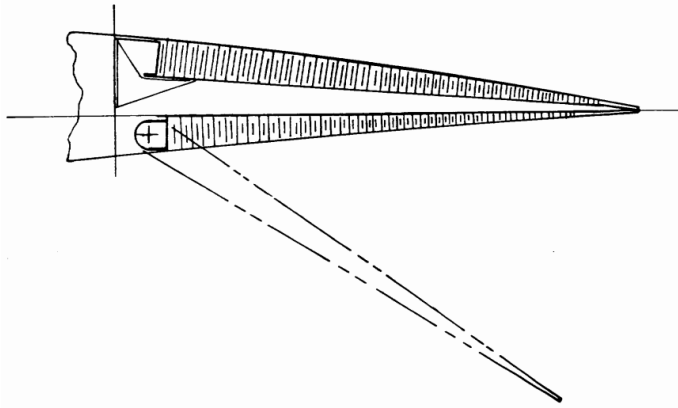


Figure 22.16.4-4: Split Flap [\(NASA-CR-4746, 1996\)](#)

22.16.4.2. Plain Flap

The plain flap has a panel with a rounded upper leading edge that deploys by downward rotation without opening a slot. The deployment angle is limited to about 20°; beyond that, the flow separates on the upper surface. Because this restriction limits its lift-producing capability, it is not used on any modern airliner. However, it has come in through the back door—any inboard or outboard aileron that is drooped at low speed (flaperon) is a plain flap.

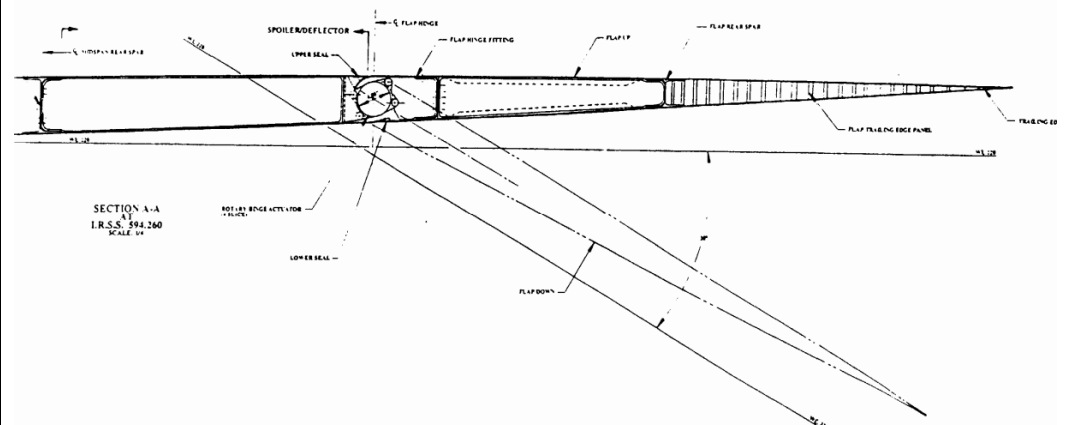


Figure 22.16.4-5: Plain Flap [\(NASA-CR-4746, 1996\)](#)

22.16.4.3. Simple Slotted Flap

The simple slotted flap has a flap panel with a fully developed aerodynamic leading edge. It is generally mounted on pivots a little below the lower wing surface and is deployed into a slotted down position of 30° to 35°. The simple slotted flap has very little flap overlap with the fixed trailing edge and hence develops only little Fowler motion, defined as aft travel of the flap that increases wing area.

Also, the flap motion does not move far enough away from the lower cove panel to develop a good entry into a slot. Therefore, it requires a rounded cavity on the lower surface, which is a solution suitable only for low-speed airplanes. For high-speed airplanes, the lower cove panel has to be rotated upward with a slave linkage, so the simple flap turns out to be not quite that simple. The simple slotted flap is not used on any modern airliner as a main flap concept, but the concept is used for flaperons.

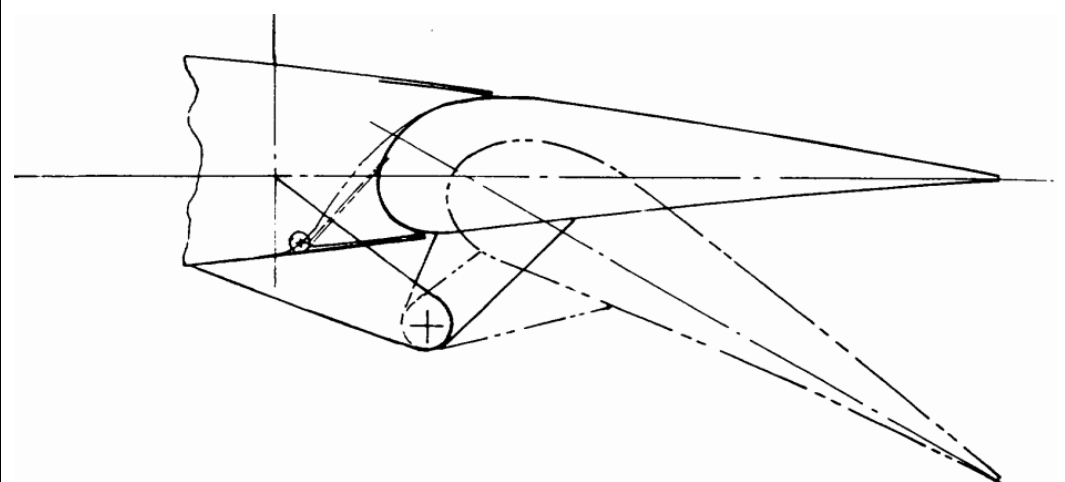


Figure 22.16.4-6: Simple Slotted Flap [\(NASA-CR-4746, 1996\)](#)

22.16.4.4. Single Slotted Fowler Flap

When stowed, Fowler flaps have significant overlap between flap and spoilers or the fixed upper cove panel. In the fully deployed position, this overlap is converted into Fowler motion by moving the flap aft, which effectively increases wing area. The single-slotted flap is the simplest of all Fowler flaps and therefore the most attractive one from a weight and cost point of view. With careful aerodynamic design, a single-slotted flap can be deflected to about 40°.

Single-slotted flaps were widely used in the early days of the jet age, then they were displaced by more sophisticated double- and triple-slotted flaps, and now they are making a comeback.

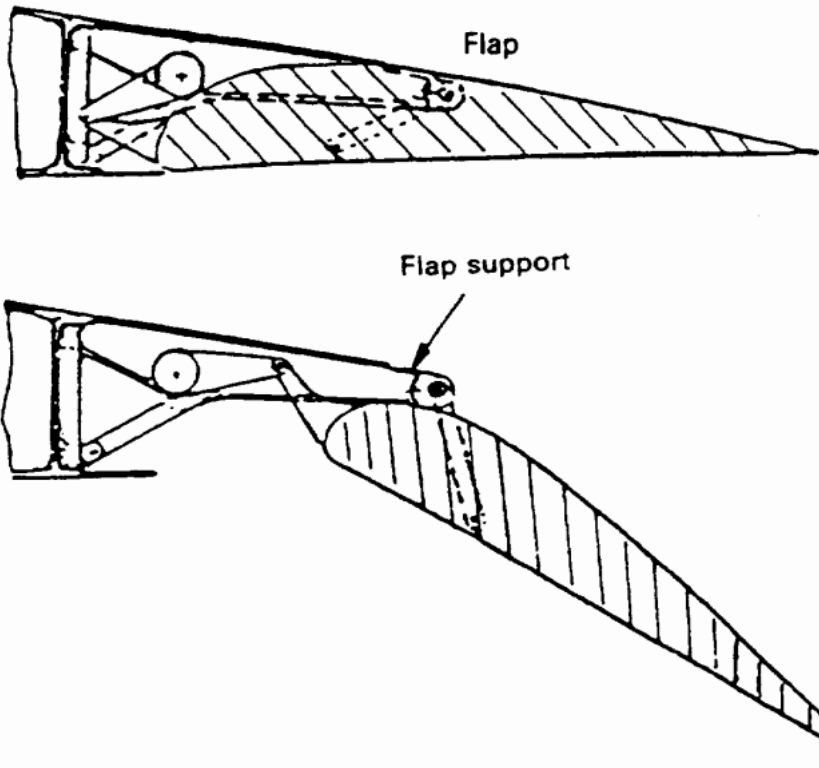


Figure 22.16.4-7: Boeing 747 SP - Single Slotted Fowler Flap [\(NASA-CR-4746, 1996\)](#)

22.16.4.5. Fixed Vane/Main Double Slotted Flap

The fixed vane/main flap has a vane rigidly attached to the main flap, which forms a fixed—geometry slot. When fully deployed, the flap is double-slotted and allows flap deflections of as much as 55°.

The vane in its stowed position is trapped between the spoiler above and a lower cove panel. Extracting the vane out of this slot imposes restrictions on the mechanism design. The fixed vane/main flap is only slightly heavier and costlier than the single-slotted flap, it produces a little more lift, and it helps adjust airplane attitude on landing approach.

For takeoff, it is generally desirable to have the vane sealed against the upper cove panel or spoilers because in this setup only the second slot is open and takeoff L/D is improved. However, with complex vane extraction from the cove and a second geometric constraint of providing a single-slotted takeoff position, very few mechanisms qualify for the fixed vane/main flap. Nonetheless, the fixed vane/main flap is used on many commercial airliners.

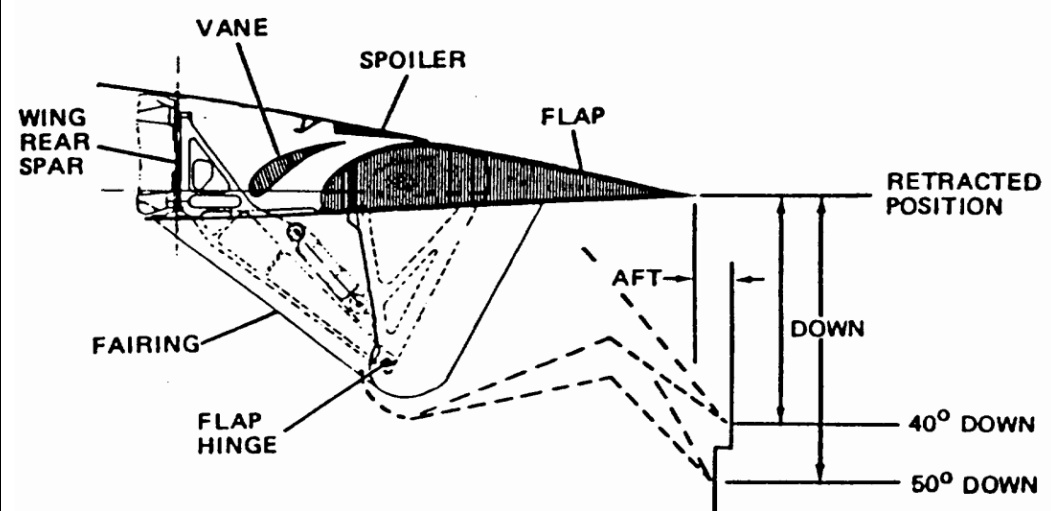


Figure 22.16.4-8 Douglas DC-9/MD-80 - Fixed Vane/Main Double Slotted Flap [\(NASA-CR-4746, 1996\)](#)

22.16.4.6. Articulating Vane/Main Double Slotted Flap

Making the vane retractable relative to the main flap creates a second overlap that can be used to increase both Fowler motion and the total developed wing chord relative to a fixed vane/main flap.

This step is accomplished with no change in the occupying space in the wing. However, the articulating vane/main flap adds quite a bit of complexity to the design.

Generally, vanes are not actively actuated but are spring-loaded into the deployed position and stowed by the stow stop and the actuating force of the main flap. The structural-vane-to-main—flap connections are generally either straight or circular arc tracks that penetrate the front spar of the main flap. If an active mechanism for moving the vane relative to the main flap is used, it is easier to provide a single-slotted takeoff position with the slot in front of the vane and the vane-to—main—flap slot closed.

However, this configuration reduces Fowler motion available for takeoff and increases complexity.

Both fixed and articulating vane/main flaps need “smart” mechanisms to take full advantage of their aerodynamic capabilities. The challenge is not only to extract the vane from the cove without slave linkages, but to keep the vane in contact with the upper-cove trailing edge (spoilers) during initial deployment for flap angles of 5° to 15° so that the flap stays single-slotted for typical takeoff settings for best takeoff L/D.

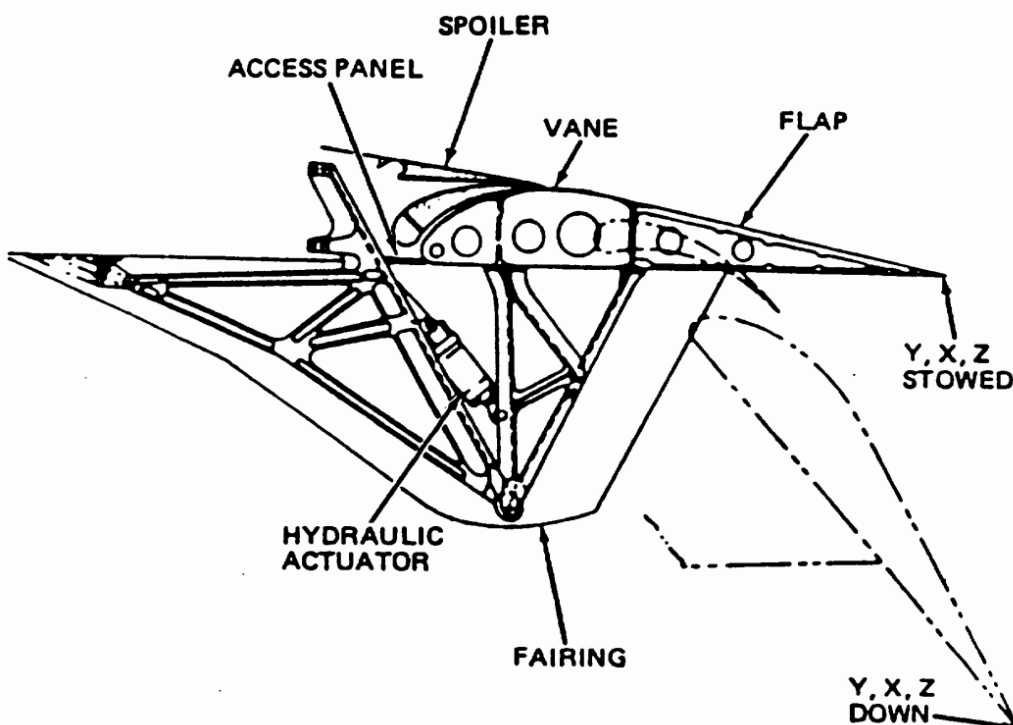


Figure 22.16.4-9 Douglas DC-10/MD-11 - Articulating Vane/Main Double Slotted Flap [\(NASA-CR-4746, 1996\)](#)

22.16.4.7. Main/Aft Double Slotted Flap

Main/aft double-slotted flap— The main/aft double-slotted flap is one step farther in complexity beyond the articulating vane/main flap. The forward or main flap is the larger element and the aft flap the smaller, and the main flap has its overlap with the wing cove while the aft flap overlaps with the aft end of the main flap. Typical flap deflection angles are 30° to 35° for the main flap and 28° to 30° for the aft flap, for a total deflection of 60° to 65°. A main/aft flap generally achieves more Fowler motion than an articulating vane/main flap with the same stowed chord length. Thus, it produces slightly more lift and helps adjust airplane landing attitude.

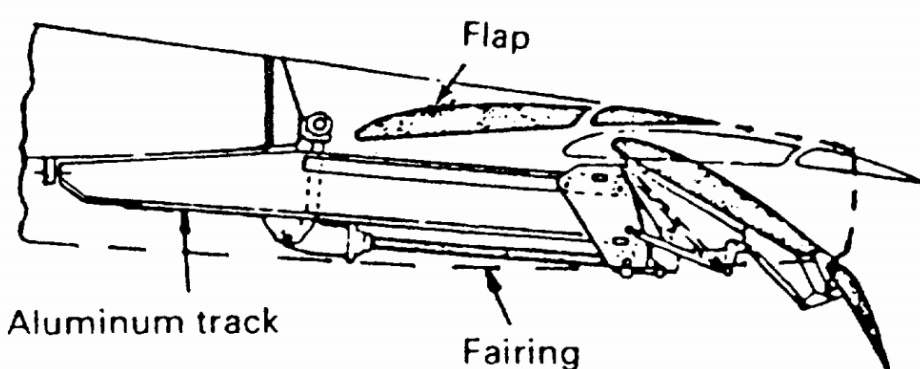


Figure 22.16.4-10 Airbus A300 Main/Aft Double Slotted Flap [\(NASA-CR-4746, 1996\)](#)

22.16.4.8. Triple Slotted Flap

A triple-slotted flap is like an articulating vane/main flap with an additional aft flap added to the main flap. Since it has three overlaps, it can provide very high Fowler motion, and the three slots allow deflections of the aft flap to as much as 80°.

Because all three of the flap elements have to be supported structurally and their motion somehow geared together, the triple-slotted flap is very complex and heavy. It produces higher sectional lift than the double-slotted flap, but edge

losses are very significant (one vortex per flap panel edge). The nose-down pitching moments are very high and need to be trimmed by a tail-down load, which further reduces its benefits. Three Boeing airplanes use triple-slotted flaps—the 727, 737, and 747.

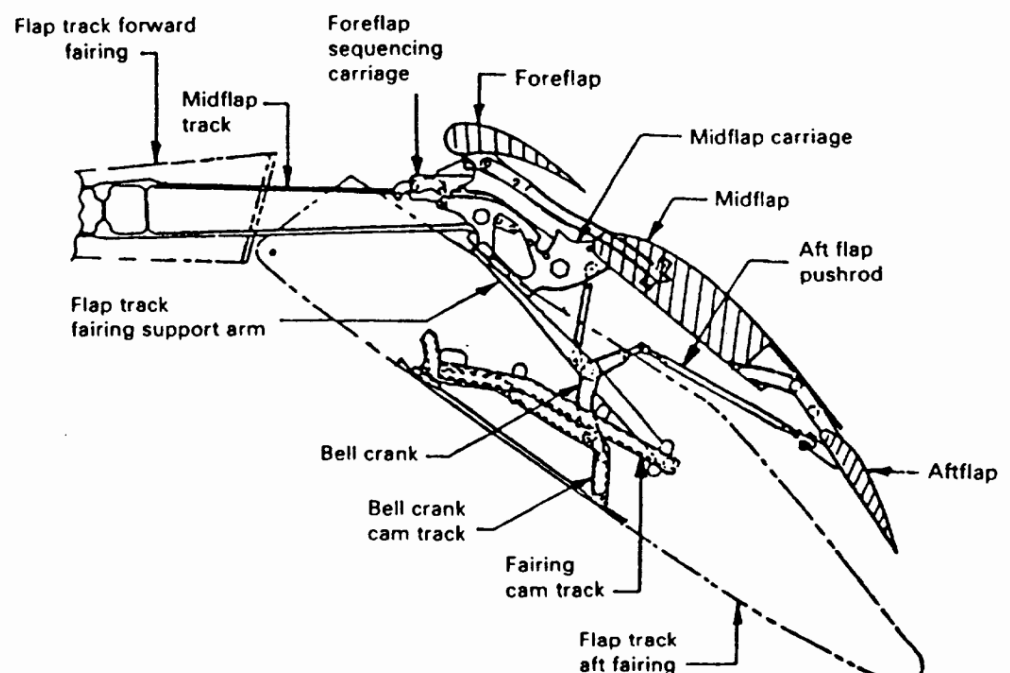


Figure 22.16.4-11 Boeing 737 - Triple Slotted Flap [\(NASA-CR-4746, 1996\)](#)

22.16.5. 5754 Leading Edge Devices

Leading edge devices can be split into the following types:

22.16.5.1. Hinged Leading Edge (Droop Nose)

Hinged leading edge (droop nose)— There is no known use of a hinged leading edge on a commercial subsonic airliner. Droop-nose leading edges have been used on some fighter airplanes.

The major drawback of the hinged leading edge is that the radius of curvature on the upper wing surface is too tight and causes flow separation. Flow separation is not a problem on a supersonic airplane, where a much higher leading-edge sweep angle triggers a stable vortex on the upper surface, which provides lift.

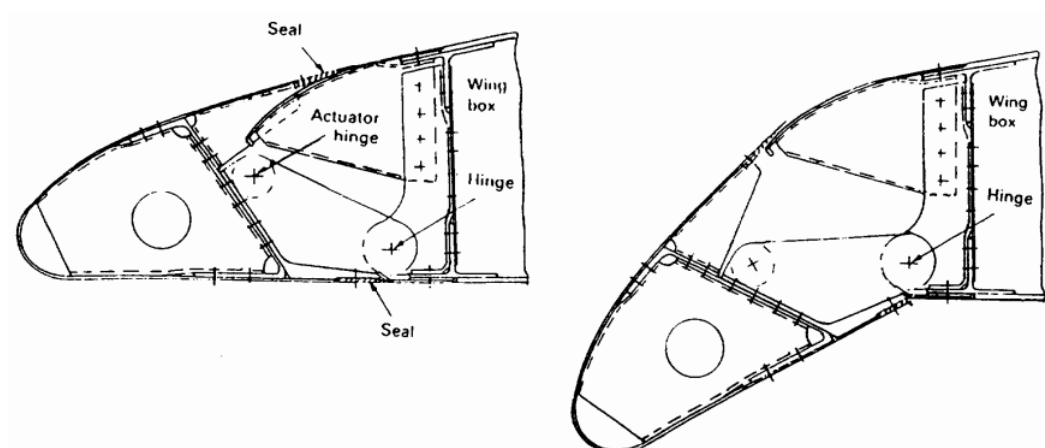


Figure 22.16.5-1: Hinged Leading Edge [\(NASA-CR-4746, 1996\)](#)

22.16.5.2. Variable Camber (VC) Leading Edge

A VC leading edge was successfully tested on NASA's Advanced Flight Technology Integration (AFT I) 111 experimental airplane. However, because low-speed, high-lift characteristics are not good, it is not in use on subsonic commercial airliners.

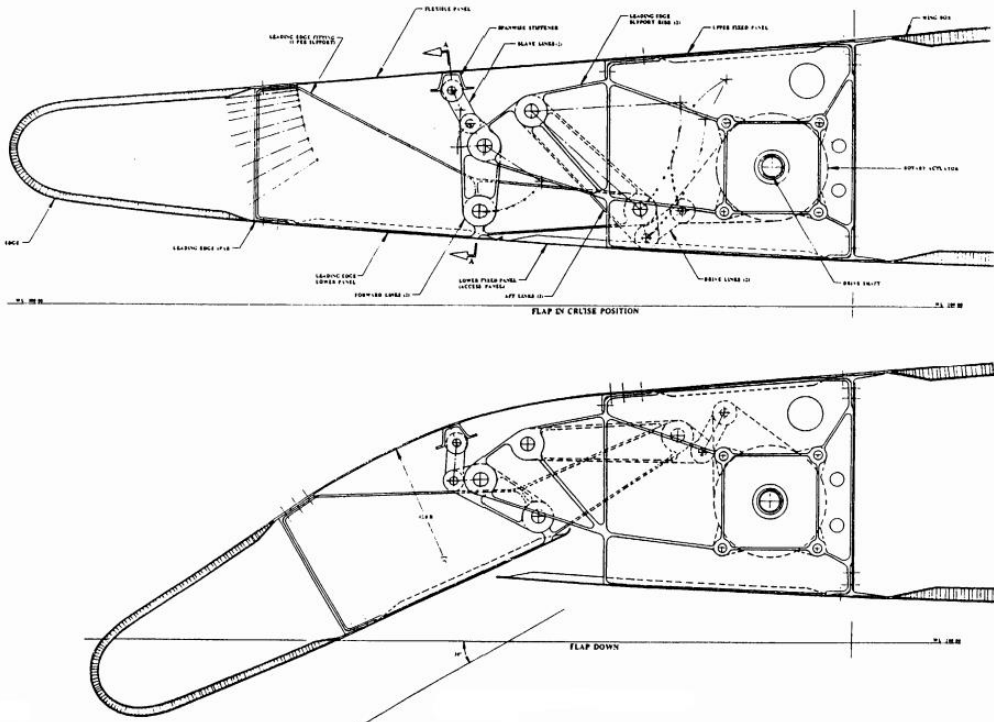


Figure 22.16.5-2: Variable Camber Leading Edge [\(NASA-CR-4746, 1996\)](#)

22.16.5.3. Fixed Slot

The fixed slot has been used successfully on short takeoff and landing (STOL) airplanes with slow cruise speeds. The drag penalty of fixed slots is unacceptable for a high-performance subsonic airliner.

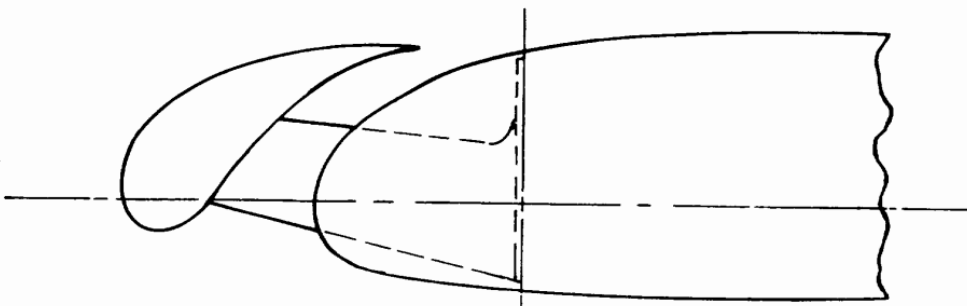


Figure 22.16.5-3: Fixed Slot [\(NASA-CR-4746, 1996\)](#)

22.16.5.4. Simple Krueger Flap

The simple Krueger flap consists of a panel on the lower side of the wing leading edge. A hinge on the forward end of the panel allows it to rotate first downward and then forward into a position where its forward edge seals against the lower surface of the fixed-wing leading edge. The panel is at an angle of 60° to 80° relative to a horizontal line. The simple Krueger flap is used on the inboard wing of the Boeing 707.

The Krueger flap is the simplest leading-edge device in use on high-performance airliners. Its high-lift performance is adequate for inboard wing sections, but its deficiency lies in its inability to accommodate varying angles of attack. During normal operation, there is generally a stagnation bubble on the upper aft portion of the Krueger panel.

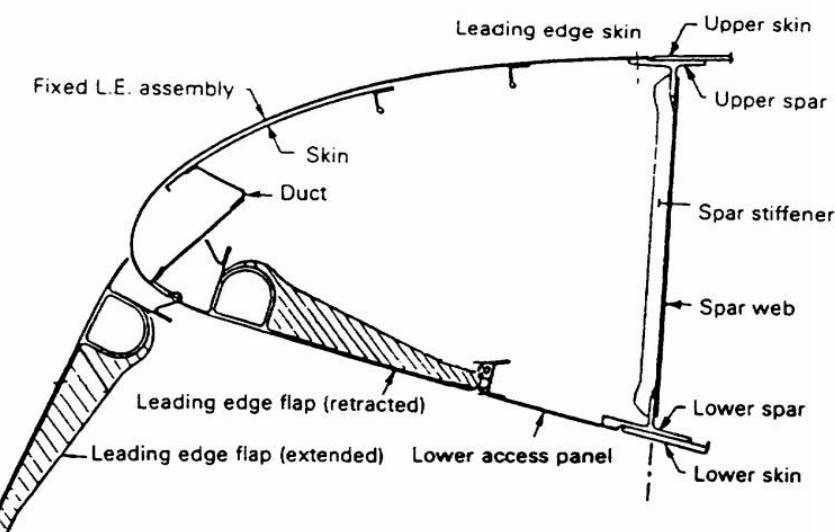


Figure 22.16.5-4: Simple Krueger Flap [\(NASA-CR-4746, 1996\)](#)

22.16.5.5. Folding, Bull-Nose (Rigid), Krueger Flap

The simple Krueger flap can be improved by adding a folding bull nose to it. Hinged to the aft end in the stowed position, the folding bull nose is a panel that runs the length of the main Krueger panel. It has a D-shaped cross section, and it is connected with a slave linkage that rotates to deploy the bull nose as the main Krueger panel deploys. Because of the rounded bull nose, the folding, bull-nose Krueger is more tolerant to changes in angle of attack. As a result, the flow on the upper surface of the Krueger is attached over a wider angle-of-attack range.

The folding, bull-nose Krueger has generally been used without a slot between the Krueger and a fixed-wing leading edge. The simple Krueger flap and the folding, bull-nose Krueger flap are generally used as two position devices with the deployed position biased toward an optimum landing configuration (CLmax). A third position that is more optimum for takeoff is possible, but it requires a more complex mechanism or fairing concept.

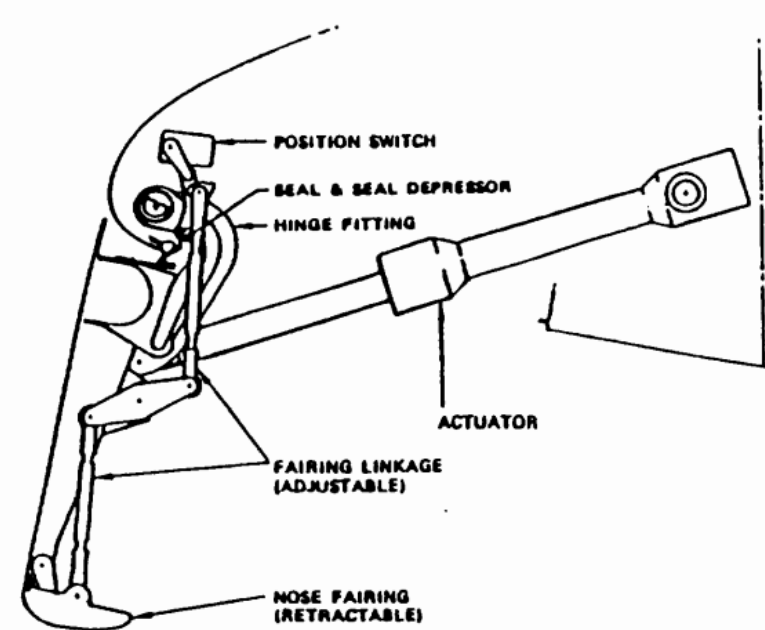


Figure 22.16.5-5: Boeing 727 - Folding, Bull-Nose (Rigid), Krueger Flap [\(NASA-CR-4746, 1996\)](#)

22.16.5.6. Variable Camber Krueger Flap

Figure 22.16.5-6 shows the VC Krueger flap, one attempt to improve the shape of the deployed Krueger flap.

The shapes of the simple Krueger flap and the main panel of the folding, bull-nose Krueger flap are dictated by the airfoil shape at the lower surface of the wing leading edge.

The VC Krueger changes the main Krueger panel from a rigid to a flexible panel, which improves the airfoil shape of the Krueger dramatically and also improves the aerodynamic performance of the Krueger.

This improvement, however, comes with a penalty. The linkage for the VC Krueger is a more complex 4-bar linkage, and the main Krueger panel has to be flexible in a line normal to the wing leading edge. This flexibility is accomplished with a fiberglass panel and only two stiffeners in the form of hat sections parallel to the leading edge.

As a result, the bending stiffness of this panel in the spanwise direction is limited. Whereas a rigid Krueger panel with two spanwise hinges can be designed for a span equivalent to the span of a slat (100 to 150 inches, depending on the size of the airplane), the practical span of a VC Krueger panel is limited to about half that. Therefore, about twice as many spanwise panels are needed for a VG Krueger as compared to a rigid Krueger or a slat, thus making the VC Krueger a complicated and expensive device. Rigging problems associated with the flexible panels are also present because the flexible panels tend to distort under high cruise air loads. A careful preloading of the flexible panels is required to avoid panel bulging with panel mismatch, which could cause cruise drag penalties.

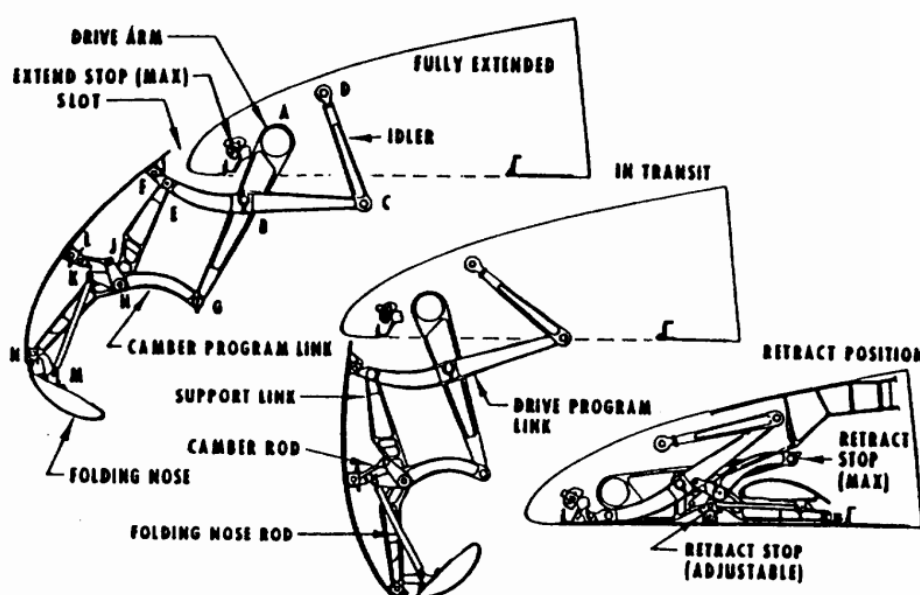


Figure 22.16.5-6: Boeing 747 - Variable Camber Krueger Flap [\(NASA-CR-4746, 1996\)](#)

So far, the VC Krueger flap has been exercised only as a two-position device with the deployed position biased toward an optimum landing configuration. Therefore, the takeoff lift/drag ratio (L/D) is not good. Attempts to make the VC Krueger a three-position device have not been successful.

22.16.5.7. Two Position Slat

The two-position slat has one stowed and one deployed position. The original two-position slat was the Handley Page slat, which was mounted on curved tracks, deployed with the help of aerodynamic forces, and stowed with the force of a preloaded spring. This design was also used on the F-84 fighter aircraft. No two-position slats are known to be in use on commercial airliners.

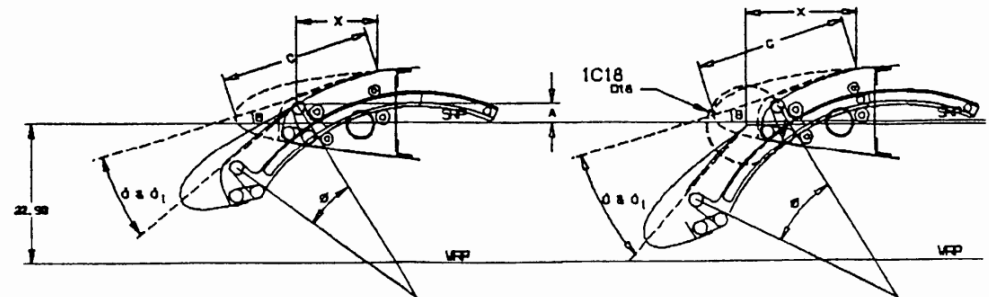


Figure 22.16.5-7: Boeing 777 - Two Position Slat [\(NASA-CR-4746, 1996\)](#)

22.16.6. Support and Actuation Concepts

The basic elements to guide and structurally support a moving element such as a flap or a slat panel are hinges, linkages, and tracks. Each panel is generally supported in two spanwise locations with two fixities in each location. Since a statically determinate system needs only three support points, the fourth support point is redundant and creates a potential for force fight. The best spanwise support location is generally at a point about 25 percent of the distance from the ends of a panel, but buried support systems sometimes require supports at the end of the panel. Also, the large spanwise dimension of an outboard flap panel and its limited thickness may require a third support location to avoid making two outboard flaps. The third support location has to be designed to avoid a force fight between flap and wing. Figure 22.16.6-1 shows a simple example of such an arrangement for the thin flap panel of a supersonic airplane. A panel with three hinges has two rigid hinges, with the third hinge on a swing link. As the wing box (the stronger and stiffer element) bends under a flight load, the three hinge points go out of alignment, and the swing link of the third hinge can rotate. This process still forces some bending into the flap panel, but the high-stress shear loads in the flap plane are avoided.

Actuation of high-lift devices can be done either individually for each support or panel, or it can be geared together with drive shafts powered by a centrally located power drive unit (PDU). For an individual drive, the hydraulic actuator is the most commonly used drive unit. If more than one actuator is used per panel, the panel has to become the synchronizing torque member in case of an actuator failure. This situation explains why multiple linear hydraulic actuators are found only on hinged panels or circular arc tracks where the panel can transmit torque. On flap mechanisms that provide good initial Fowler motion (translation), multiple linear actuators cannot be used because the panel translation cannot transmit torque.

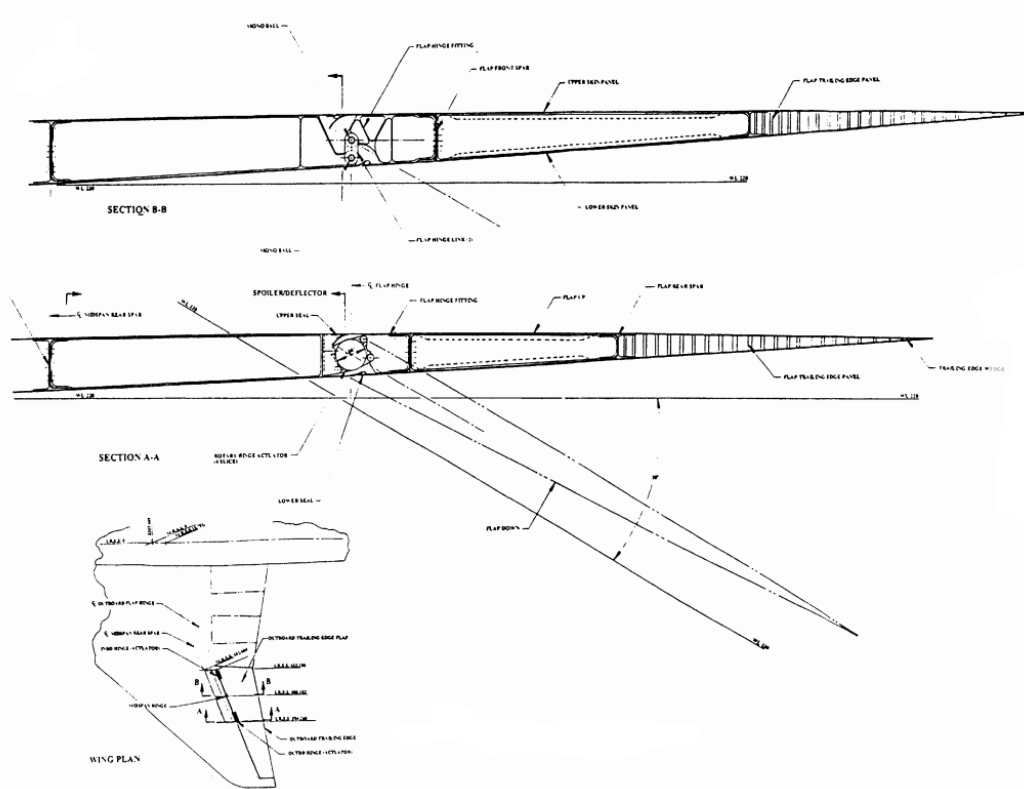


Figure 22.16.6-1: Flap with Three Hinge Points [\(NASA-CR-4746, 1996\)](#)

Centrally powered and synchronized actuation systems use screw jacks, rotary hinges, rotary actuators, or rack and pinion drives as actuators. This drive system has become the one most frequently used for trailing-edge and leading-edge flaps because it is the surest and safest way to synchronize flap deployment. Figure 22.16.6-2 shows the Boeing 737 trailing-edge-flap drive system.

A drive system of this nature has been used on the trailing-edge flaps of all Boeing airplanes since the 707 and on all Airbus airplanes. A similar drive system has been used for leading-edge actuation on all Boeing airplanes beginning with the 747 and on all Airbus airplanes. In addition to the synchronizing nature of the shafts, the high reduction ratios of the gearboxes make the system essentially self-locking. Shafting is generally designed to withstand jam failures. Therefore, additional brakes or no-backs and symmetry-sensing devices are redundant safety features. In other words, this actuation system is the safest one against asymmetric and passive failures. Dual motorson PDUs guarantee functional reliability on demand.

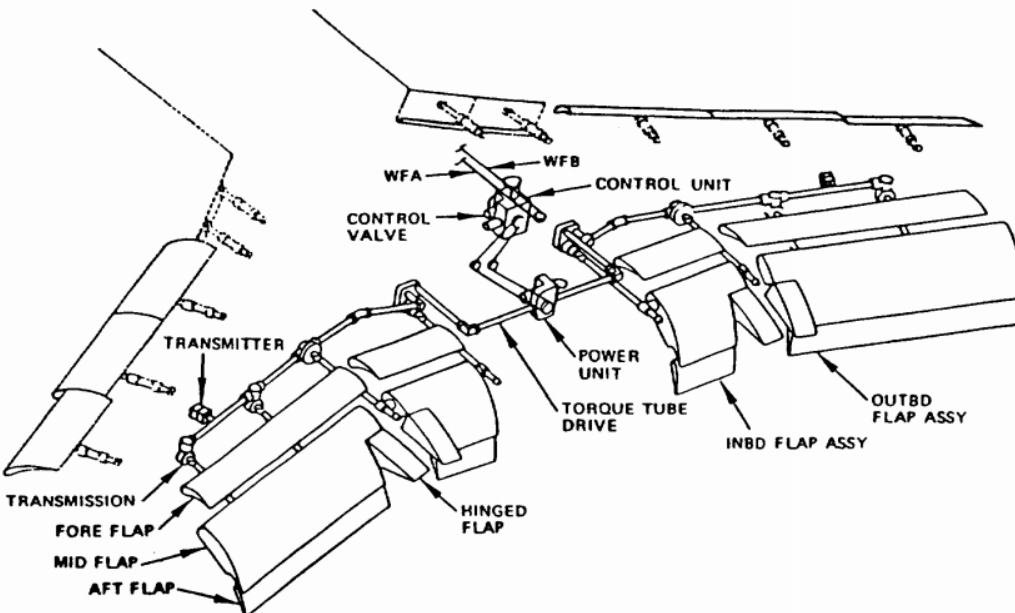


Figure 22.16.6-2: Boeing 737 – Trailing Edge Flap Drive System [\(NASA-CR-4746, 1996\)](#)

22.16.6.1. Trailing Edge Devices

Numerous support mechanisms are known for trailing-edge flaps, and new ones are being invented and reinvented all the time. Leaving out hinges and actuation systems for flaperons and simple flaps for supersonic airplanes, the emphasis here will be on conventional trailing-edge flap mechanisms.

Definition of Fowler Motion

Before describing trailing-edge flap mechanisms and their relative benefits, it is first appropriate to define one of the major goodness factors, namely Fowler motion. It is not clear how Mr. Fowler defined his motion. Most aerodynamicists today see the significant parameter to be the increase in developed wing chord, which means chord in space and not just the wing chord projected into the wing reference plane as shown in several publications. Using just projected chord change makes the Fowler motion of many flaps negative because the rotation shortens the projected flap chord. So, for this report, Fowler motion is defined as the incremental, developed chord measured in the wing chord plane for slats.

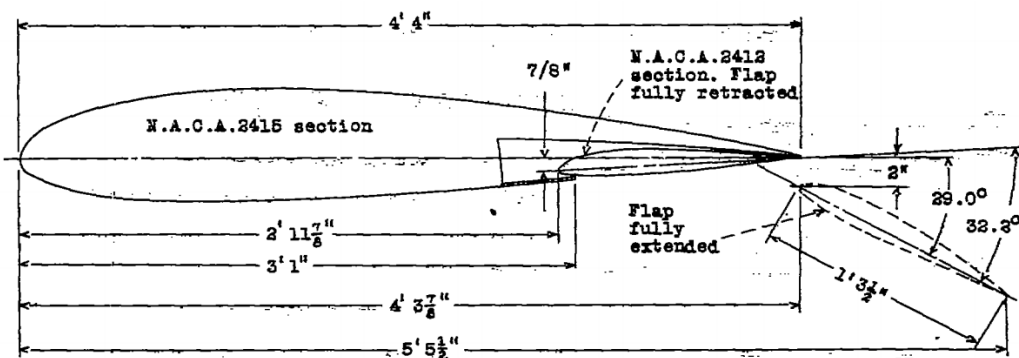


Figure 22.16.6-3: Section View of Fowler Flap Retracted and Extended [\(NACA-TN-578, 1936\)](#)

For trailing-edge flaps with multiple elements, Fowler motion is measured in linear increments in the chord plane of the respective upstream element, as shown in Figure 22.16.6-4. Measuring the Fowler motion in linear increments in chord planes is a practical approximation to the real chord extension as measured in a curve on the upper surface of the elements. The Fowler motion for landing, with the flaps in the fully deployed position, is independent of flap linkage, and therefore it is a function only of the flap overlap provided.

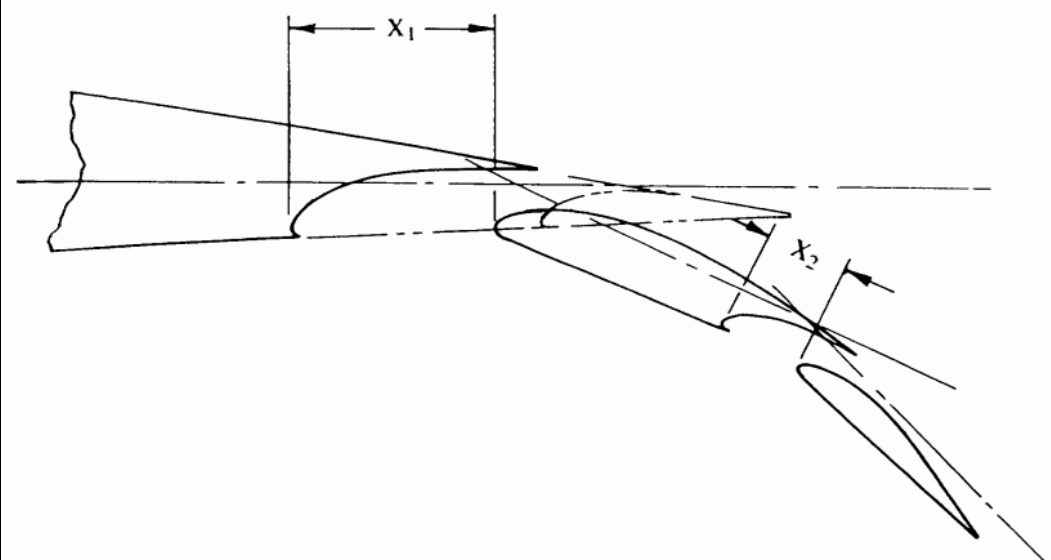


Figure 22.16.6-4: Definition of Trailing Edge flap Fowler Motion [\(NASA-CR-4746, 1996\)](#)

A "smart" flap mechanism provides most of the available Fowler motion in the initial flap deployment at low deflection angles. This area increase at low-flap-angle settings results in the best MD for takeoff.

Simple Hinge for Fowler Flap

Good performance for a hinged, overlapping flap requires a flap pivot far below the wing surface whether it is a single, vane/main, or main/aft double-slotted flap.

The words "simple pivot" used for this arrangement are not accurate; this concept requires a pivot far away from the wing box and requires a fairly deep, fixed hinge fitting. The flap hinge fitting is about the same size, and both fittings are encased in large, flat-sided fairings. (See Figure 22.16.4-9) The long and narrow hinge fittings cannot transmit the flap side loads, so another side-load reaction has to be provided, either in the form of A-frame-type links or a side-load track. The circular arc motion of a hinged flap develops Fowler motion proportional to the deployment angle. For low deployment angles required for high-gross-weight takeoff, the hinged flap develops little Fowler motion, and it is therefore not the best mechanism for this requirement. The simple hinge is an example of a "dumb" mechanism.

Yet another bad feature is associated with simple hinges. Hinged flaps are not easily adaptable to streamwise motion on swept, outboard wing trailing edges. The swept hinge axis of the simple hinge flap rotates the aft hinge fairing into a skewed angle inboard and out of the wake of the forward fixed fairing, which produces drag. Also, the inboard end of an outboard flap is not trimmed.

in a streamwise direction, so the skewed end rib is exposed to full ram pressure when the flap is deployed, producing still more drag (See Figure 22.16.6-5). This same characteristic makes sealing a swept, outboard flap against an unswept, inboard flap difficult.

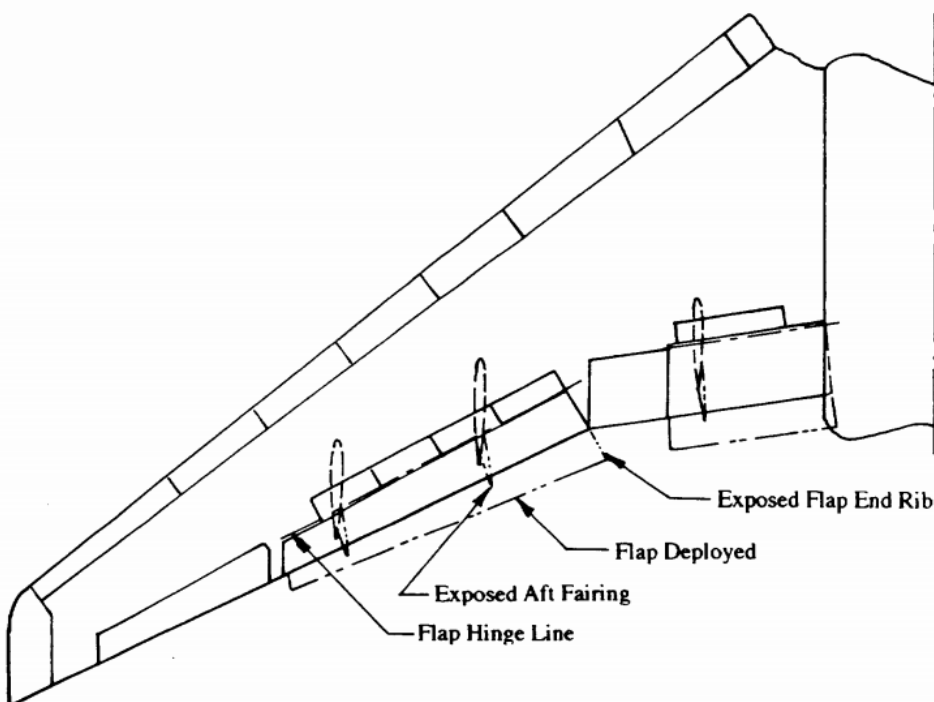
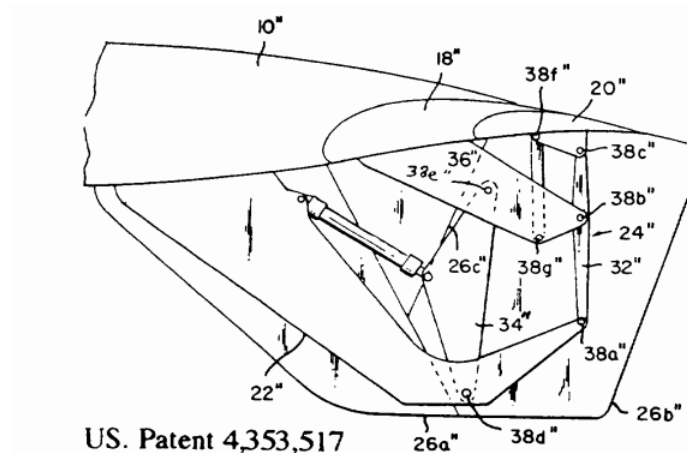


Figure 22.16.6-5: Deficiencies of a Simple Hinge [\(NASA-CR-4746, 1996\)](#)

Upright, Four Bar Linkage

The four-bar linkage with upright links reduces the fairing depth by 30 to 35 percent as compared to a simple hinge and improves the Fowler motion schedule. Figure 1.25 shows such a linkage exercised in three variations for a main/aft double-slotted flap. The results are somewhat better than those produced by a simple-hinge, double-slotted flap as used on the Boeing YC-14.



Common aft/aft link

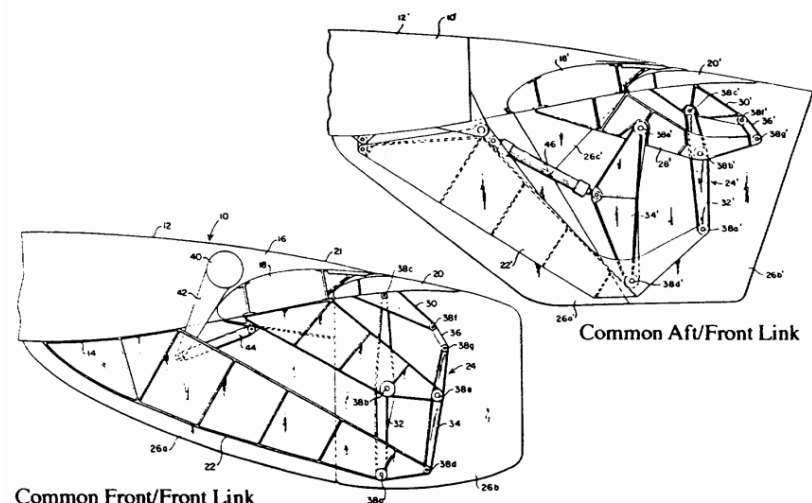


Figure 22.16.6-6: Variations of Upright, Four-Bar Linkages [\(NASA-CR-4746, 1996\)](#)

Upside-Down, Four-Bar Linkage

The upside-down, four-bar linkage has a much better potential for applications to trailing-edge flaps. The two links at any support location are hinged on a fixed structure at their upper end and to the flap or a flap carriage at their lower end. When used as an end support, the links can be buried completely inside an airfoil, with no need for flap support fairings.

This configuration, of course, means lower drag at both low and high speeds. For example, refer to the Boeing 747SP flap shown in Figure 22.16.4-7.

The upside-down linkage in its more compact form (shortest links) tends to drop the flap down and create some counterrotation during the initial part of deployment. It is therefore not advantageous for a vane/main flap that needs to extract the vane from the slot between the upper and lower cove unless the vane is made small and with little overlap, which is the case on the Douglas DC-8 (Figure 22.16.6-7). However, the DC-8 flap mechanism is not a plain four-bar linkage, but rather has the upper pivot of the aft link move aft in a short, straight track. This motion is slave-linked to the forward link. The upside-down, four-bar linkage is good for a single-slotted flap and for the main and aft flaps of a main/aft type double-slotted flap. McDonnell Douglas used this concept again on the YC-15 and the 017 for blown, double-slotted, main/aft-type flaps (Figure 22.16.6-8).

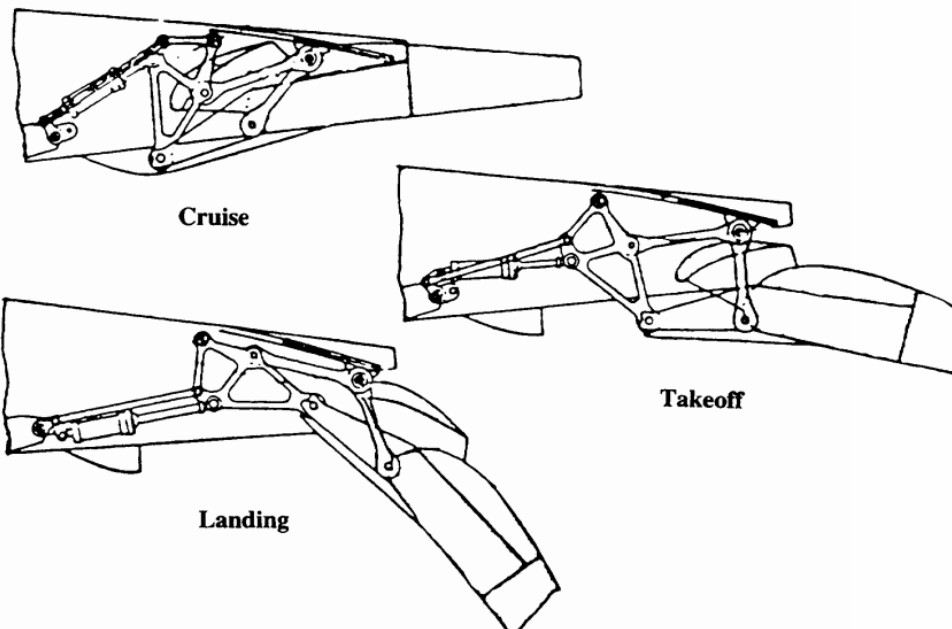


Figure 22.16.6-7: Douglas DC-8 Four Bar Trailing-Edge-Flap Linkage [\(NASA-CR-4746, 1996\)](#)

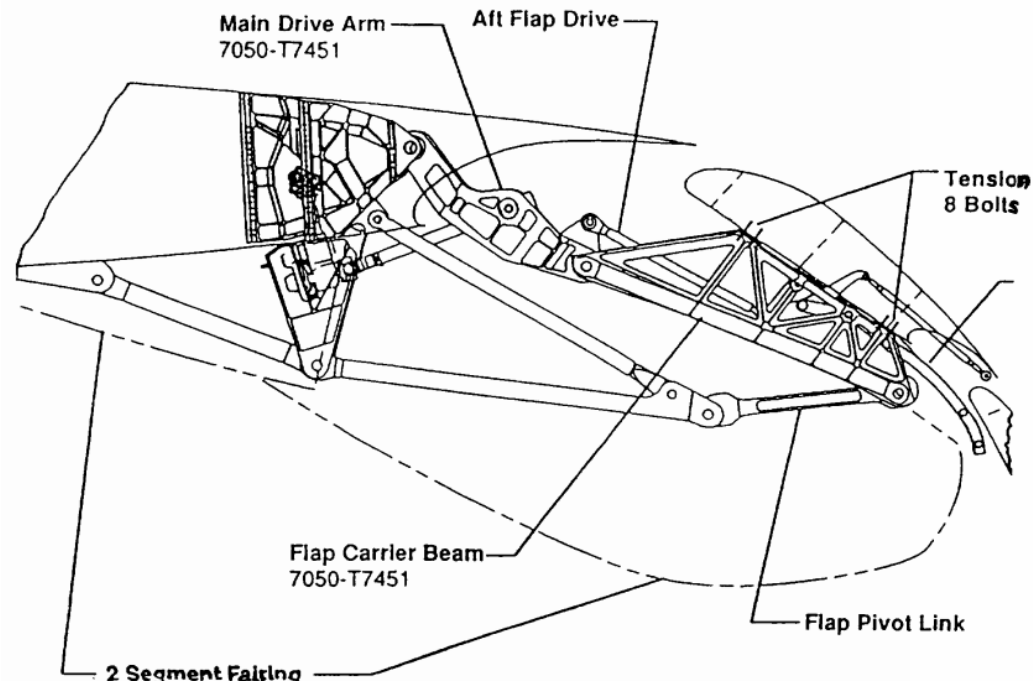


Figure 22.16.6-9: Boeing 777 Inboard Flap Mechanism [\(NASA-CR-4746, 1996\)](#)

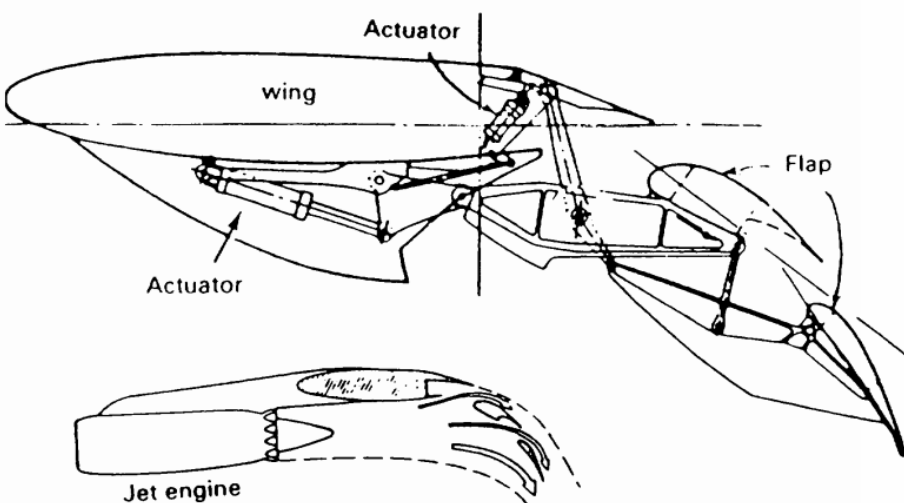


Figure 22.16.6-8: Douglas YC-15 Trailing Edge Flap [\(NASA-CR-4746, 1996\)](#)

The Fowler motion progression of the upside-down, four-bar linkage is quite good, achieving high Fowler motion at small flap deployment angles for good takeoff L/D. It is not clear who invented this linkage or used it first on a trailing-edge flap, but it has repeatedly been claimed as a novel linkage. The linkage can be adapted for streamwise conical motion, which is required to allow inboard and outboard flaps to seal against each other. Actuation power requirements can become quite high.

Upside-down/upright four-bar linkage

Of the two combinations possible within this concept, the arrangement with the upside-down link forward and the upright link aft seems to have the most promise. Whether this concept is better or worse than the pure upside-down linkage is not clear, but at first glance it looks about as good as the other concept. It can be easily adapted to conical, streamwise motion. The fairing size required to house the linkage is fairly deep, but short. Actuation power requirements are, as on the upside-down concept, fairly high. The upside-down/upright, four-bar linkage is used on the Boeing 777 inboard main flap and single-slotted outboard flap (Figure 22.16.6-9).

Complex four-bar linkages

Many recent attempts have been made to design more complex linkages for trailing-edge flaps. The design goal of most of these attempts has been to squeeze another percent or two of additional Fowler motion out of the concept for low-takeoff flap angles.

One of the more memorable attempts was called a “walking beam four-bar linkage,” where a beam located underneath the flap is moved aft with an upside-down linkage while the flap is moved aft and rotated with an upright, four-bar linkage that rides on the “walking beam.” The concept, of course, needs more slave links, and for fail-safe, every link is duplicated. The same linkage is then repeated for the aft flap with more slave links, and, as a result, the number of links and pivot points is about 20 per support location, which makes the concept very expensive to build and maintain. The major flaw of this kind of approach is that there are too many joints in series, which increases both the probability of failure and the chance that joint wear will result in a wiggly support.

One successful implementation of a complex linkage flap support, best described as a hinged-beam/upside-down/upright, four-bar linkage (Figure 22.16.6-10), is used on the Boeing 767 for the main flap panel of the inboard flap and the single-slotted outboard flap. The flap is mounted on an upside-down/upright, four-bar linkage with the forward, upside-down link hinged on a fixed structure and the upright, aft link hinged on the folding beam. The folding beam itself is hinged on a fitting on the lower surface of the wing box. As the four-bar linkage moves the flap aft and rotates it into the landing position, the hinged beam first moves down and then up.

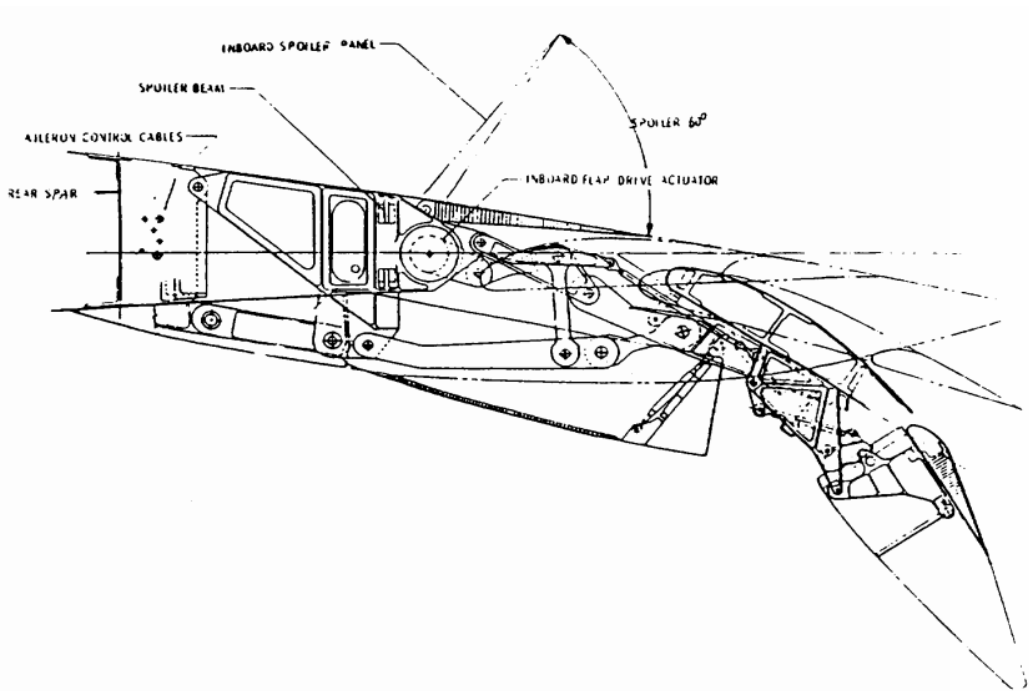


Figure 22.16.6-10: Boeing 767 Inboard Flap Mechanism [\(NASA-CR-4746, 1996\)](#)

This process negates some of the up-and-down motion of the aft link to avoid flap interference with the spoiler and to create proper flap gaps. The concept is ingenious because it creates a lot of Fowler motion at low flap angles. However, it has some of the flaws discussed earlier: The multiple links and joints in series require doubling of most links for fail-safe. This configuration adds to the complexity and cost of the design and makes it difficult, if not impossible, to accomplish streamwise deployment of the flaps. Therefore, the disadvantages of the simple hinge flap apply to the 767 linkage—a slanted end trim of the inboard end of the outboard flap that does not allow sealing with the inboard flap, and rotation of the slanted inboard-flap end rib and aft-flap fairing into the free stream. In addition, the duplicated linkage is wide and essentially normal to the rear spar. Hiding this normal linkage in a streamwise fairing makes for a wide fairing with a lot of slot blockage and reduced flap performance.

Hooked-track supports

Before discussing hooked-track supports, a discussion about the Boeing 707 circular—arc—flap support track is in order. This track is located forward of the flap inside the airfoil. It does not provide any fancy motion but deploys the flap from stowed to full extension. This mechanism is light and does not require any flap fairings. Details about this flap mechanism can be found in Chapter 2.

Hooked tracks used to deploy the main flaps of successive Boeing airplanes (727, 737, 747, and 757, Figure 22.16.6-11) have been quite successful. The forward end of this hooked track is essentially straight and slopes downward; therefore, initial flap motion is aft and slightly down. A good portion of Fowler motion can thus be obtained at low flap angles for takeoff. The aft end of the track is hooked down and accomplishes the major part of the flap rotation for the landing configuration. The hooked-track concept lends itself to conical streamwise flap deployment, which allows a sealed interface between a straight-motion, unswept, inboard flap and a conical-motion, swept, outboard flap.

The major drawback of the hooked-track concept is that the reaction to the flap air loads, which are generally aft of the carriage, results in a couple between the front and aft rollers of the roller carriage. For practical purposes, this couple is not very long, and the result is very high aft roller loads. Therefore, designing rollers and tracks for reasonable service life is not easy.

It is not clear who invented the hooked-track flap support. In addition to the use on four Boeing airplane models, it is used by British Aerospace on the BAe146 and RJ70/ 100/ 120 airplanes and by Airbus on the A310 airplanes.

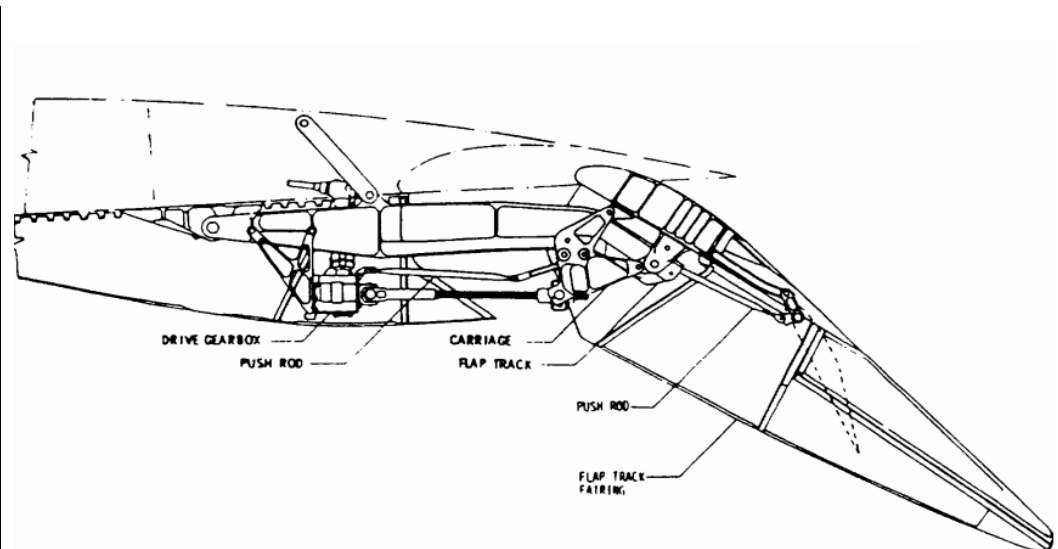


Figure 22.16.6-11: Boeing 757 Inboard Flap Mechanism [\(NASA-CR-4746, 1996\)](#)

Link/track mechanisms

Most of the linkage systems described in the previous paragraphs have the problem that one link wants to be quite long for ideal flap motion and does not fit into the minimum fairing envelope. It should be recognized that an infinitely long link can be simulated with a straight track. This thought process led to the evolution of several link/track mechanisms. For the link/track flap mechanism, the low overturning moment from the flap loads creates a couple between the roller carriage and the front link or aft link and drive rod. This setup reduces roller loads and provides good roller/track wear characteristics. The advantages of this arrangement were recognized at Boeing in the late 1970s, but it was not vigorously pursued. Airbus is using two of these concepts on the Airbus A320/321 and A330/340 airplanes.

Airbus A320 flaps use an upside-down, forward link in conjunction with a straight track on a fixed structure as aft support (Figure 22.16.6-12). The motion of this mechanism is very favorable for Fowler motion at lower takeoff flap angles and requires very low actuation power. In addition, the mechanism is adaptable to streamwise conical motion.

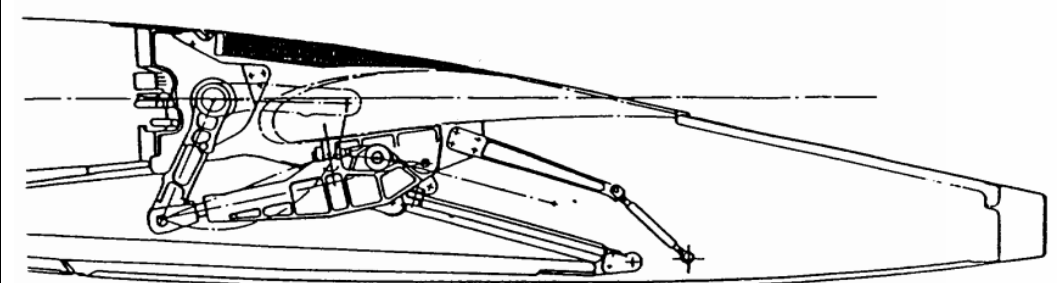


Figure 22.16.6-12: Airbus A320 Trailing-Edge Flap Mechanism [\(NASA-CR-4746, 1996\)](#)

The A330/340 flap mechanism uses similar elements, but in a different arrangement; it has a straight and sloped track on fixed structure as forward support and an upright link as aft support (Figure 22.16.6-13). Again, Fowler motion progression is very good, but no better than on the A320.

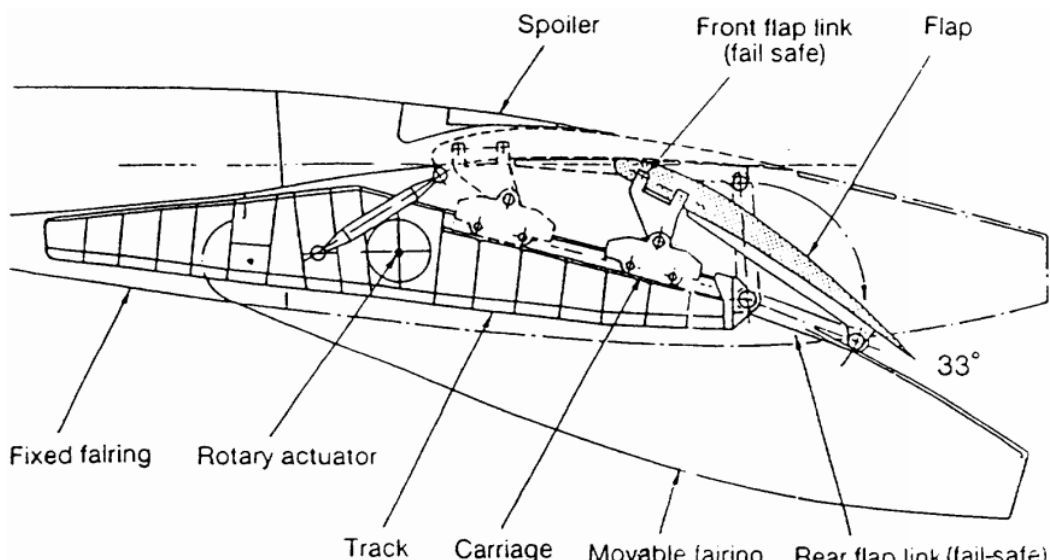


Figure 22.16.6-13: Airbus A330/340 Trailing-Edge Flap Mechanism [\(NASA-CR-4746, 1996\)](#)

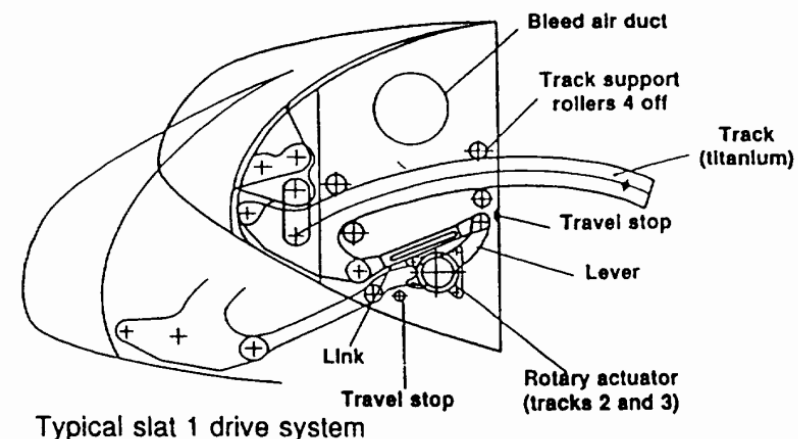


Figure 22.16.6-14: Airbus A340 Inboard Slat [\(NASA-CR-4746, 1996\)](#)

22.16.6.2. Leading Edge Devices

Slats

As mentioned earlier, most slats in service on commercial airliners are mounted on circular arc tracks with two tracks per slat panel. The tracks generally have an I-beam cross section. In the Boeing version, the rollers are engaged with the outside flanges of the I-beam, they are end-supported, and each roller reacts against either a down or an up load. Some Airbus airplanes use larger, cantilevered rollers that roll inside the flanges of the I-beam and react against both up and down loads. The air loads on a slat are essentially normal to the path of deployment by the circular arc tracks. Therefore, the magnitude of the actuation loads is low. Slats see air-load reversal at low angles of attack, generally on the ground.

Several different actuator arrangements for slat actuation are used on today's commercial airliners. The biggest number of in-service airliners, the Boeing 727 and 737 airplanes, use a single hydraulic actuator to deploy each slat. Today's design standards indicate that the single actuator is not sufficient, and two actuators are required to avoid racking of the slat panel in the tracks. However, practical experience indicates otherwise: none of the approximately 4500 Boeing 727 and 737 airplanes in service today have slat deployment problems. The slats have a programmed deployment/stow schedule that makes them deploy at different times, and symmetry is maintained with the help of electrical position signaling.

Other slat-actuation schemes use rotary actuators with drive links, as on the Boeing 767 and on the inboard slats of several other airplanes, including the Airbus A340. (Figure 22.16.6-14).

Screw jack drives are suitable as well to actuate slats; they are used on the Airbus A300 and A310 airplanes (Figure 22.16.6-15).

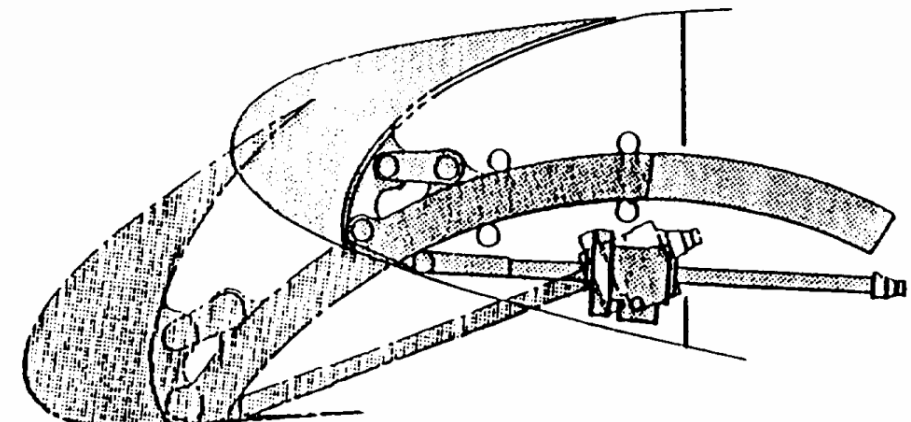


Figure 22.16.6-15: Airbus A300/310 Slat Actuation [\(NASA-CR-4746, 1996\)](#)

McDonnell Douglas and Fokker use cables to actuate slats. The slats have a conical motion, so travel at every track location is different. This configuration is accomplished using cables wrapped around drums with different diameters to achieve different lengths of travel. However, this system has many flaws: the difficulties of rigging the cables and maintaining preload in the system; the large number of pulleys; and a concern for safety since this drive system has no sure way to lock the slats in place in case of actuator failure. A Douglas DC-10/MD-II slat-actuation system is shown in Figure 22.16.6-16.

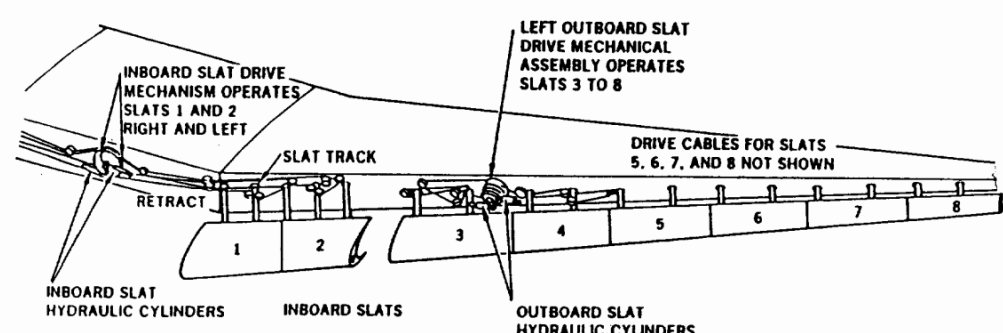


Figure 22.16.6-16: Douglas DC-10/MD-11 Slat Actuation System [\(NASA-CR-4746, 1996\)](#)

Lately, the rack and pinion drive (Figure 22.16.6-17) has become the most popular drive system for slats. First used on the Boeing 757 airplane, it has been copied by the Airbus A320/321, the A330/340, and the Boeing 777 airplanes. This drive uses a rotary hinge that has an outer rotating case and is configured as a spur gear to drive a rack. This rack is a structural part of the circular arc track, and

power comes from a centrally located PDU that also synchronizes the system between right- and left-hand sides of the airplane.

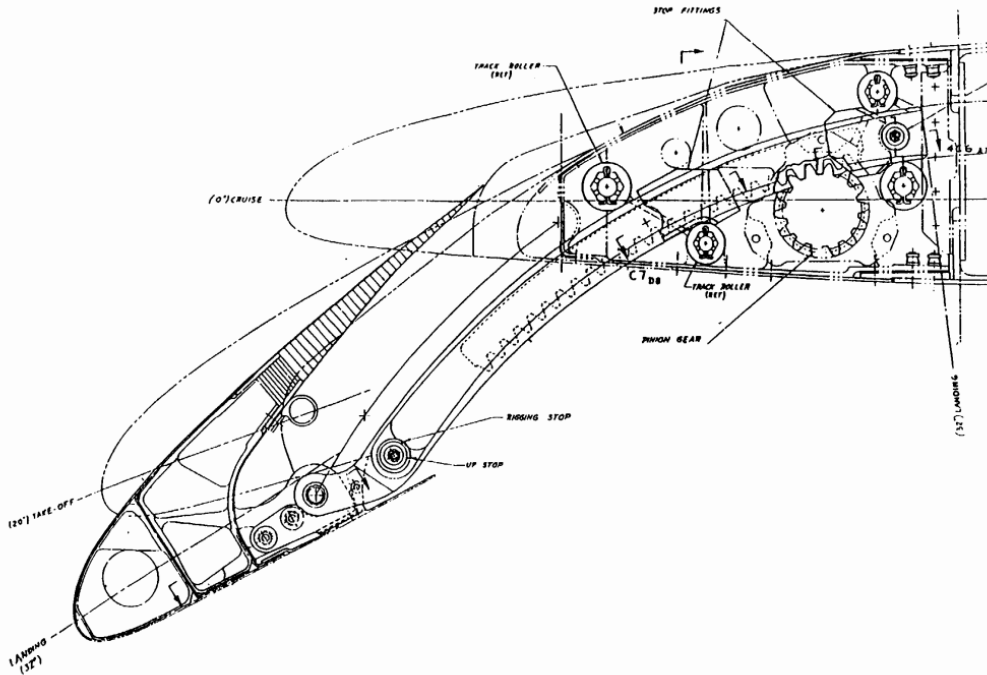


Figure 22.16.6-17: Boeing 757 Slat with Rack and Pinion Drive [\(NASA-CR-4746, 1996\)](#)

22.16.7. Ailerons & Elevons

Ailerons are the primary flight control surfaces that move the aircraft about the longitudinal axis. In other words, movement of the ailerons in flight causes the aircraft to roll. Ailerons are usually located on the outboard trailing edge of each of the wings. They are built into the wing and are calculated as part of the wing's surface area. Figure 1-53 shows aileron locations on various wing tip designs.

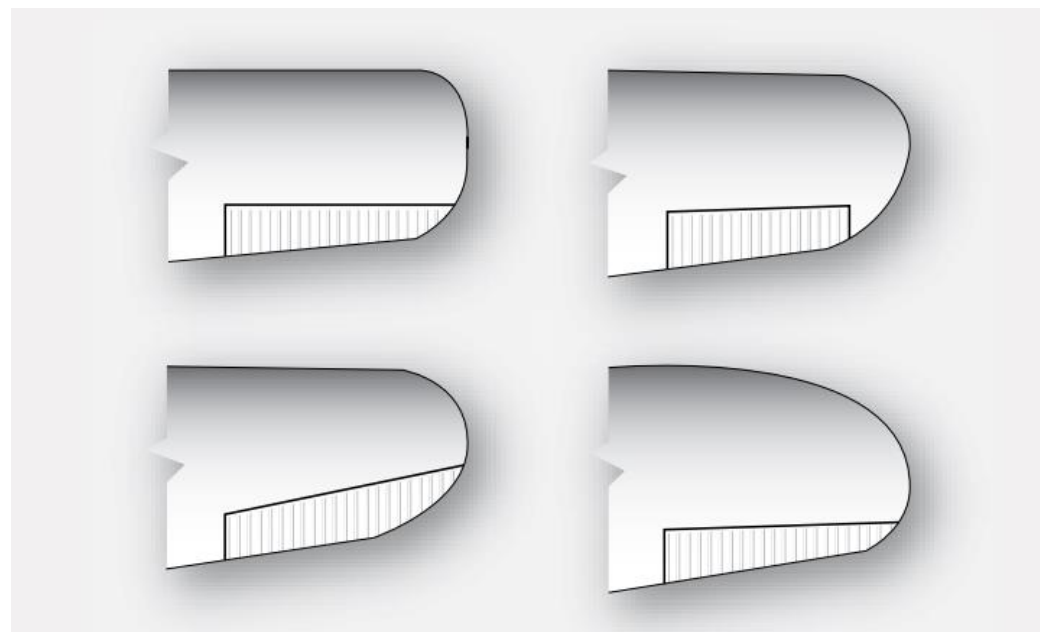


Figure 22.16.7-1: Different Aileron Layouts [\(FAA-H-8083-31, 2012\)](#)

Ailerons are controlled by a side-to-side motion of the control stick in the cockpit or a rotation of the control yoke. When the aileron on one wing deflects down, the aileron on the opposite wing deflects upward. This amplifies the movement of the aircraft around the longitudinal axis. On the wing on which the aileron trailing edge moves downward, camber is increased, and lift is increased. Conversely, on the other wing, the raised aileron decreases lift. [Figure 1-54] The result is a sensitive response to the control input to roll the aircraft.



Figure 22.16.7-2: Yoke and Relative Aileron Movements [\(FAA-H-8083-31, 2012\)](#)

The pilot's request for aileron movement and roll are transmitted from the cockpit to the actual control surface in a variety of ways depending on the aircraft. A system of control cables and pulleys, push-pull tubes, hydraulics, electric, or a combination of these can be employed.

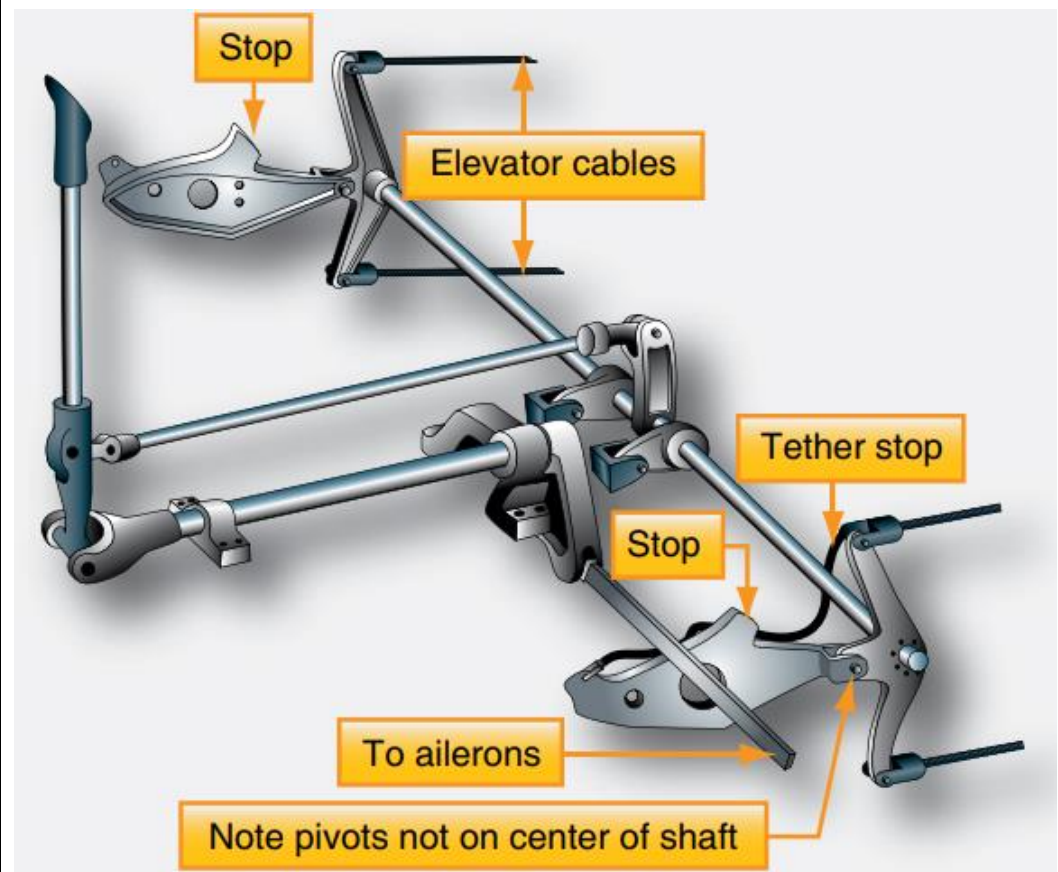


Figure 22.16.7-3: Typical Joystick Aircraft Control System [\(FAA-H-8083-31, 2012\)](#)

Simple, light aircraft usually do not have hydraulic or electric fly-by-wire aileron control. These are found on heavy and high-performance aircraft. Large aircraft and some high-performance aircraft may also have a second set of ailerons located inboard on the trailing edge of the wings. These are part of a complex system of primary and secondary control surfaces used to provide lateral control and stability in flight. At low speeds, the ailerons may be augmented using flaps and spoilers. At high speeds, only inboard aileron deflection is required to roll the

aircraft while the other control surfaces are locked out or remain stationary. Figure 1-56 illustrates the location of the typical flight control surfaces found on a transport category aircraft.

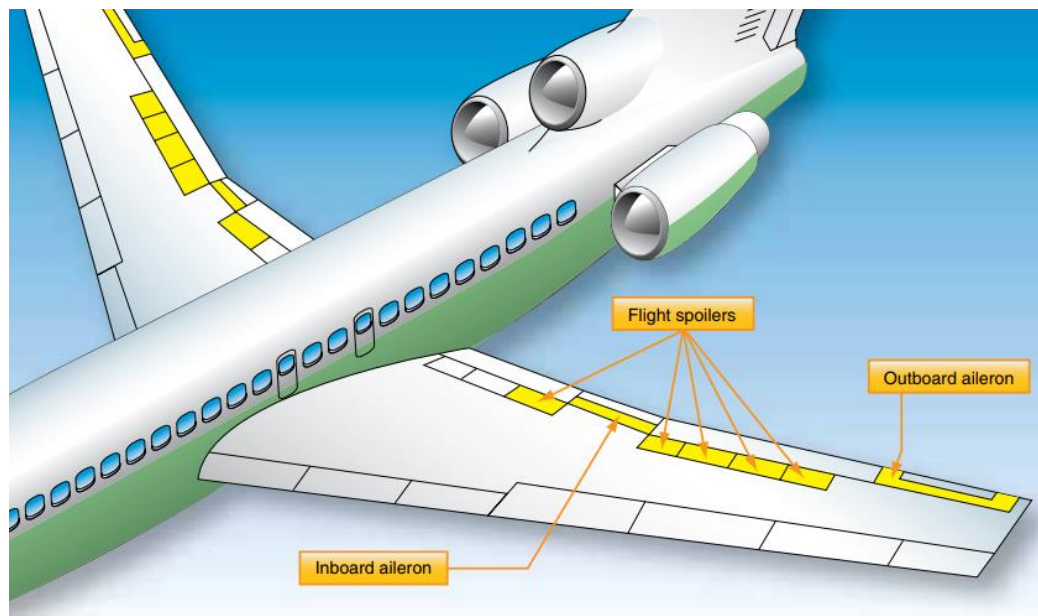


Figure 22.16.7-4: Typical Transport Category Aileron and Spoiler Layout [\(FAA-H-8083-31, 2012\)](#)

Figure 1-52 illustrates several aileron configurations with their hinge points well aft of the leading edge. This is a common design feature used to prevent flutter.

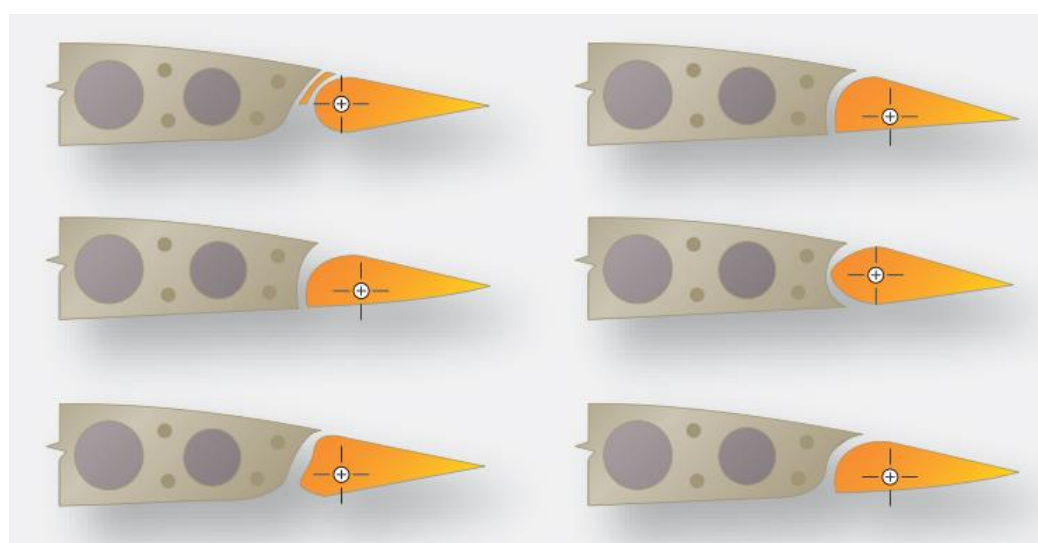


Figure 22.16.7-5: Different Aileron Hinge line Configurations [\(FAA-H-8083-31, 2012\)](#)

22.16.8. Spoilers

A spoiler is a device found on the upper surface of many heavy and high-performance aircraft. It is stowed flush to the wing's upper surface. When deployed, it raises up into the airstream and disrupts the laminar airflow of the wing, thus reducing lift.

Spoilers are made with similar construction materials and techniques as the other flight control surfaces on the aircraft. Often, they are honeycomb-core flat panels. At low speeds, spoilers are rigged to operate when the ailerons operate to assist with the lateral movement and stability of the aircraft. On the wing where the aileron is moved up, the spoilers also raise thus amplifying the reduction of lift on that wing. [Figure 1-68] On the wing with downward aileron deflection, the spoilers remain stowed. As the speed of the aircraft



Figure 22.16.8-1: Transport Category Aircraft Wing with Spoilers Deployed [\(FAA-H-8083-31, 2012\)](#)

22.16.9. Some Transport Wing Layouts

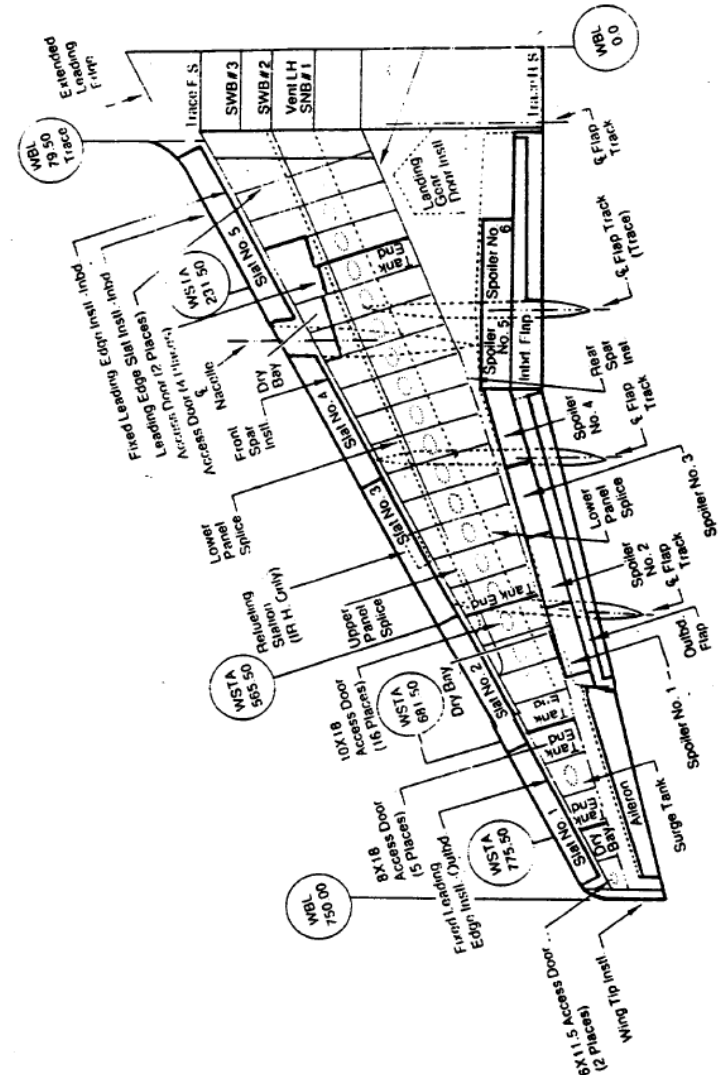


Figure 22.16.9-1: Boeing 757-200 Wing [\(NASA-CR-4746, 1996\)](#)

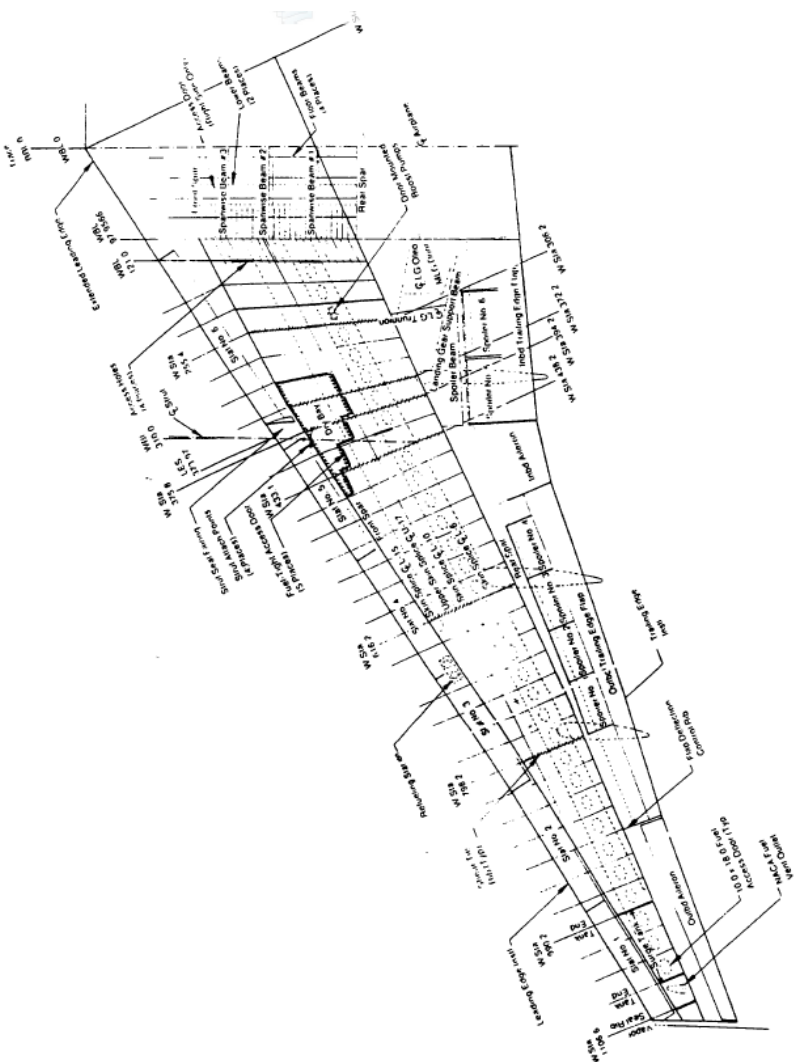


Figure 22.16.9-2: Boeing 767 Wing (NASA-CR-4746, 1996)

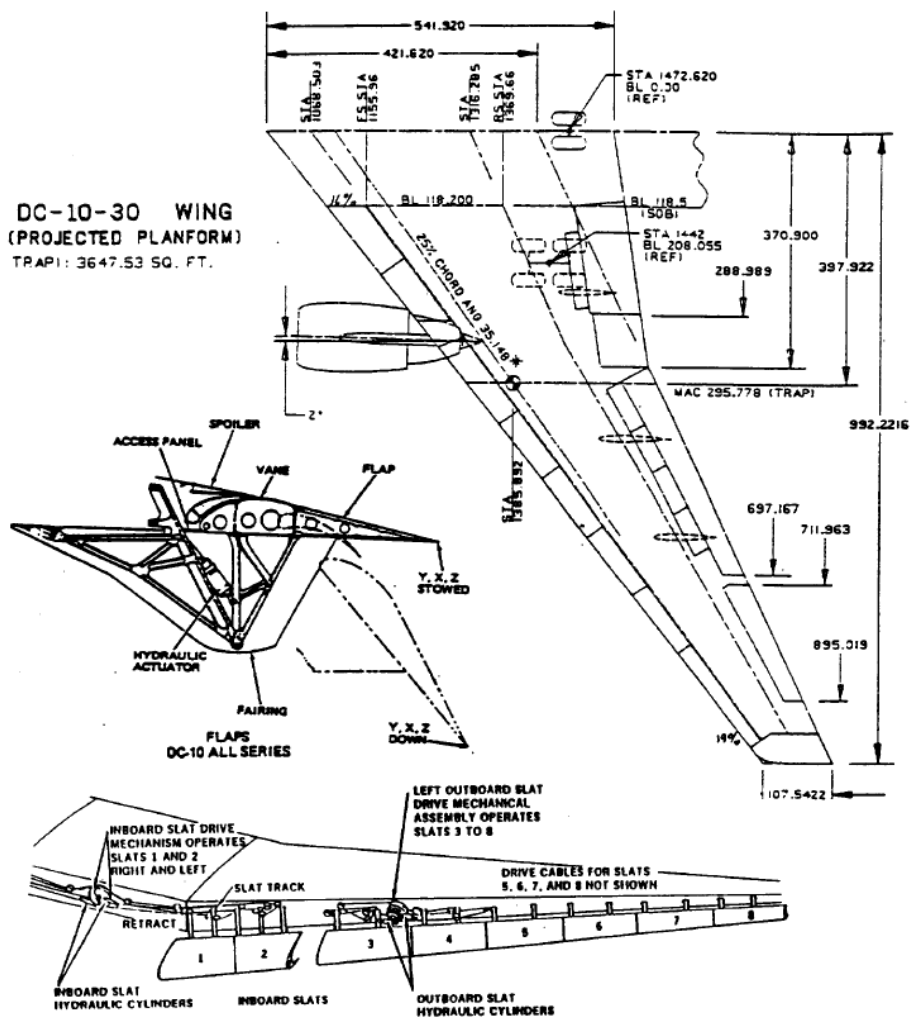


Figure 22.16.9-4: Douglas DC10 Wing [\(NASA-CR-4746, 1996\)](#)

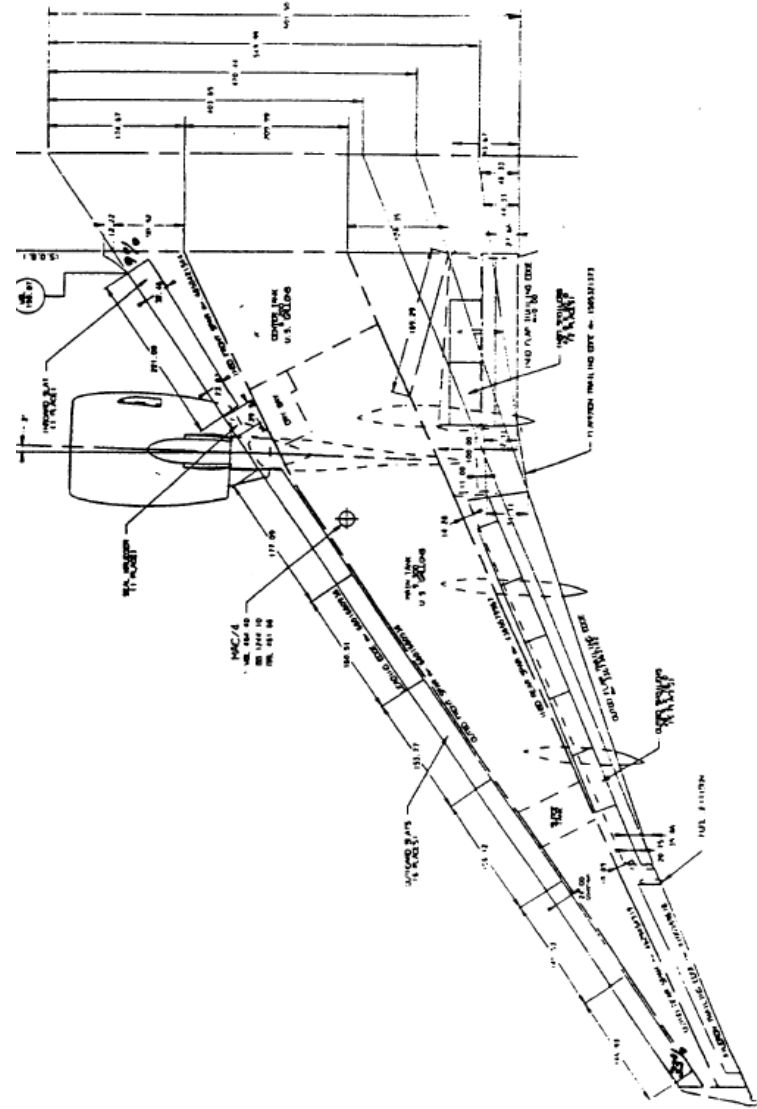


Figure 22.16.9-3: Boeing 777 Wing [\(NASA-CR-4746, 1996\)](#)

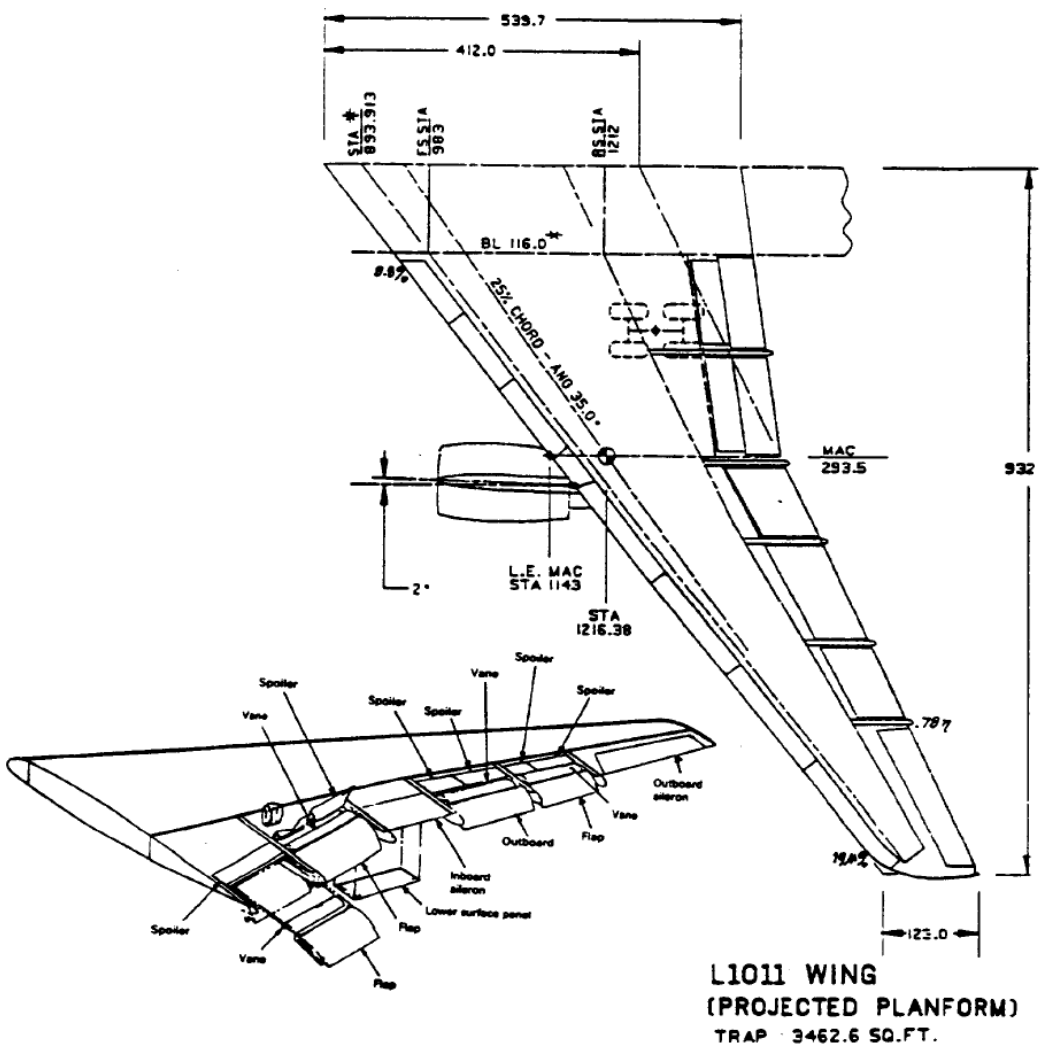


Figure 22.16.9-5: Lockheed L1101 Wing [\(NASA-CR-4746, 1996\)](#)

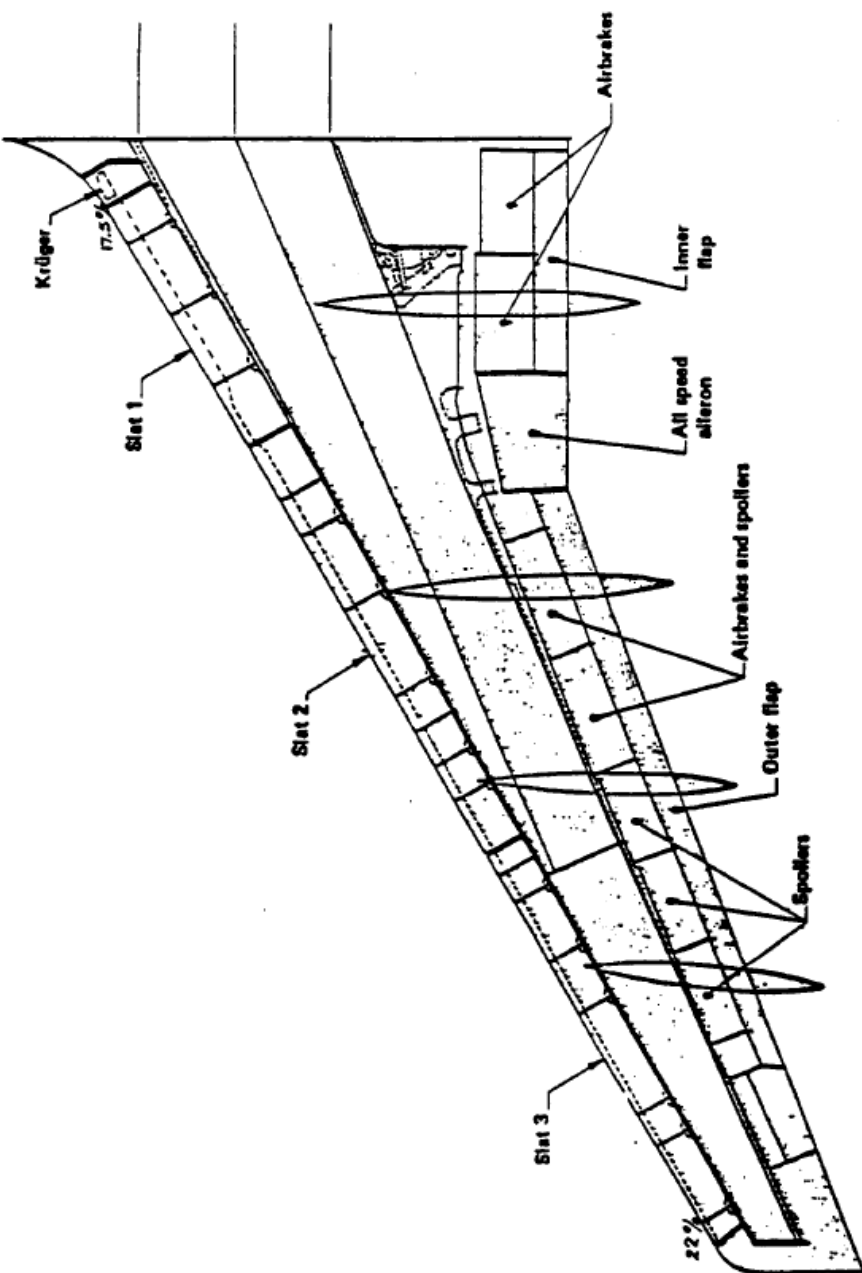


Figure 22.16.9-6: Airbus A310 Wing [\(NASA-CR-4746, 1996\)](#)

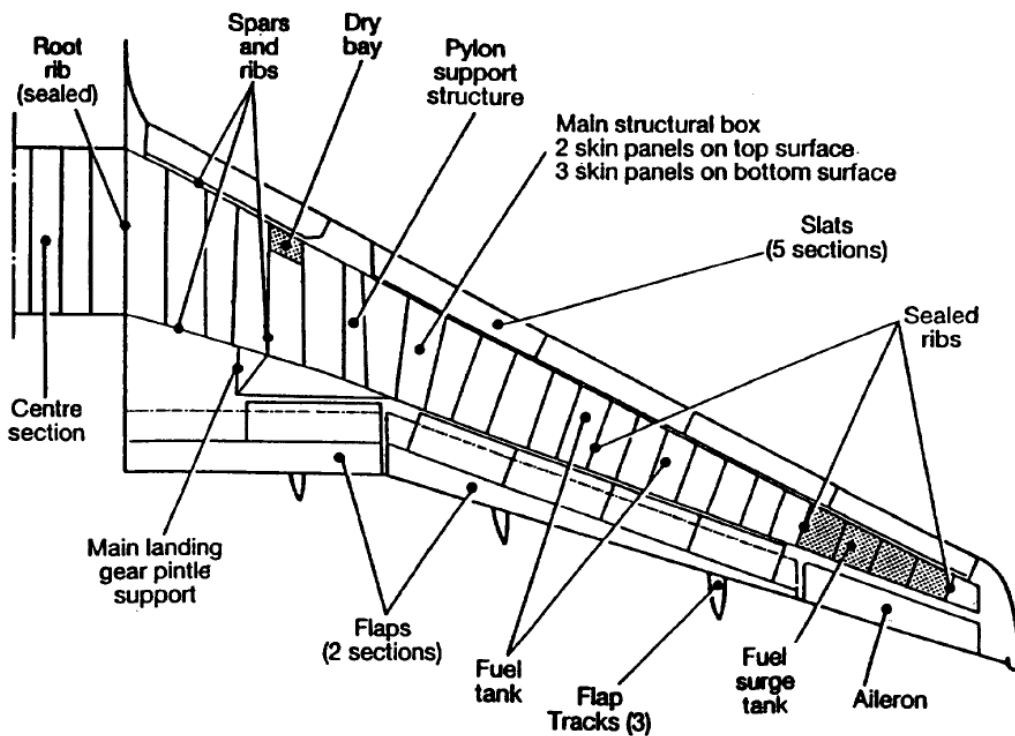


Figure 22.16.9-7: Airbus A320 Wing [\(NASA-CR-4746, 1996\)](#)

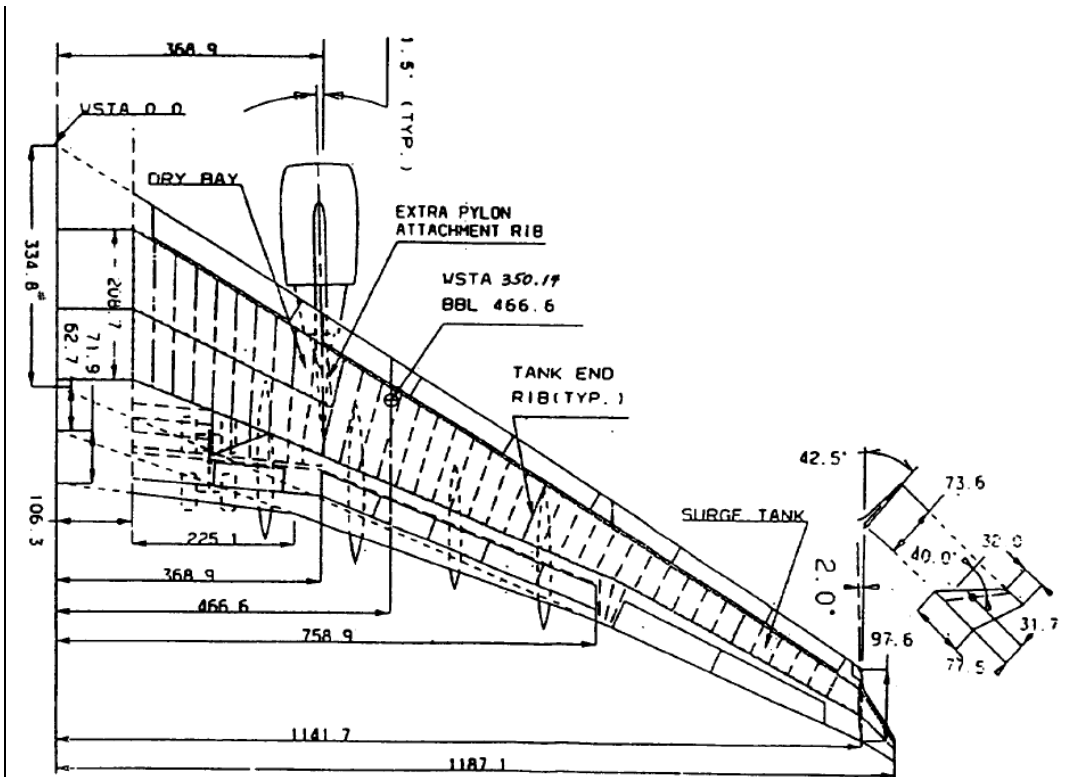


Figure 22.16.9-8: Airbus A330/340 Wing [\(NASA-CR-4746, 1996\)](#)

22.17. 71 Powerplant

Reserved

23. FIXED WING AIRCRAFT PERFORMANCE

23.1. Introduction

23.2. Reserved

23.3. Reserved

This section will be included in a later edition. This page is a placeholder only.

24. OTHER AIRCRAFT TYPES: DESIGN AND ANALYSIS

24.1. Introduction

24.2. Reserved

24.3. Reserved

This section will be included in a later edition. This page is a placeholder only.

25. CERTIFICATION

25.1. Introduction

25.2. Reserved

25.3. Reserved

This section will be included in a later edition. This page is a placeholder only.

26. MICROSOFT EXCEL AS A REPORT WRITING TOOL

26.1. Introduction



In writing this book I had to make what I consider to be a huge personal and professional concession. I had to use Microsoft Word. I started out writing this book in Excel but the problems with page formatting and section numbering and referencing issues were too great.

Word is great for writing resumes, letters and engineering textbooks. For engineering reports, it has several significant drawbacks. These problems include:

1. Word tries to do too much and can end up creating very large unstable files that get 'corrupted'. i.e. Word ends up doing something that even Word rejects and you end up losing data and time.
2. Word does not let you keep calculations 'live'. This results in time spent creating report updates for new loading, geometry or materials that take a significant amount of time as every numerical value must be updated manually.

We still use Word for writing reports when we have no choice. When a client has an internal reporting system that flows down to us and we must use Word, the whole team just has to knuckle down and live with the inefficiency and frustration.

To be fair, Microsoft Excel is a spreadsheet tool that was initially optimized for accounting. Excel has significant limitations:

1. Excel is not WYSIWYG and looks different at different screen magnifications and needs to be tailored for each different printer the report may be printed out on.
2. Excel has limitations on how subscript and superscript characters are processed (more on this later).
3. Excel is not a word processor or a graphics tool.

To use Microsoft Excel as an efficient technical reporting tool you must adopt a code of 'best practice'. Our 'best practice' is informed by our experience and the experience of other senior level technical people we have worked with.

Why not use Mathcad? Mathcad is a great tool, but it has several drawbacks:

1. It is expensive
2. It is not universally used

3. Mathcad is great at presenting math. My experience of work created and presented in Mathcad is that the user gets carried away with the beautiful mathematics and you end up with a report that consists of page after page of mystifying math with few diagrams and little commentary.

Having listed the main reasons why we do not use any other package and the negative points about Excel, let me list the positive aspects.

1. Excel is a universally used – almost everyone has an Excel license. Analysis files are easily shared and edited.
2. Excel is the most stable of the Microsoft Office suite of programs.
3. Excel is a *general* tool – it does many things moderately well.

Reports written in Word tend to have a lot of prose and not enough math. Report written in Mathcad tend to have a lot of math and not enough prose. Reports written in Excel tend to naturally strike a balance between prose and math because it is equally good (and bad) at both.

Excel can also be used as a database for FE output for storage and processing. We also use Excel to create input loads files for Finite Element models in the correct .bdf or .dat format. See section 26.2.6 for more information.

We also use Excel to create simple engineering drawings and for creating commercial logos and graphics for most of our company needs.

Excel mirrors good practical engineering traits:

Jack of all trades and master of none, But oft times better than a master of one.

Important Terms:

Workbook – a discrete Excel file, usually has .xlsx extension.

Worksheet – a sheet tab within a workbook, a workbook can contain hundreds of individual worksheets.

Cell – an individual referenceable item of data within a worksheet, cells are shown as a grid of rectangles on the worksheet..

Print Area – the area of the worksheet that is printed.

26.2. Excel as a Reporting Tool – The Basics

26.2.1. Choosing your Font

Font selection is important. It is important to select a font that looks clear on the screen and when printed out. It is preferable to select a font that is part of the windows native font package, so it need not be specially installed by everyone who wants to use your file. The font must be fully populated with the extended character set (more on this later). The font must have minimal scaling problems with Excel's display when you use different magnification levels.

We have settled on using Calibri and have been using it for the last 5 years and we are very happy with it. This document is written in Calibri and it is a clean, san-serif font that looks good in bold and italic.

We have developed a [custom font](#) that is part of the [XL-Viking package](#). This font is given away for free without having to make any purchase. We have populated this font with a set of superscript and subscript characters in the native font format that are not usually available.

It is important that attention is paid to the little things. Legibility, transferability and clarity are all key aspects of a technical report.

26.2.2. Page Break Preview and Print Area

Excel was created without consideration for authoring Letter or A4 page size reports in mind. Nevertheless, there are some useful tools built in that help you do this.

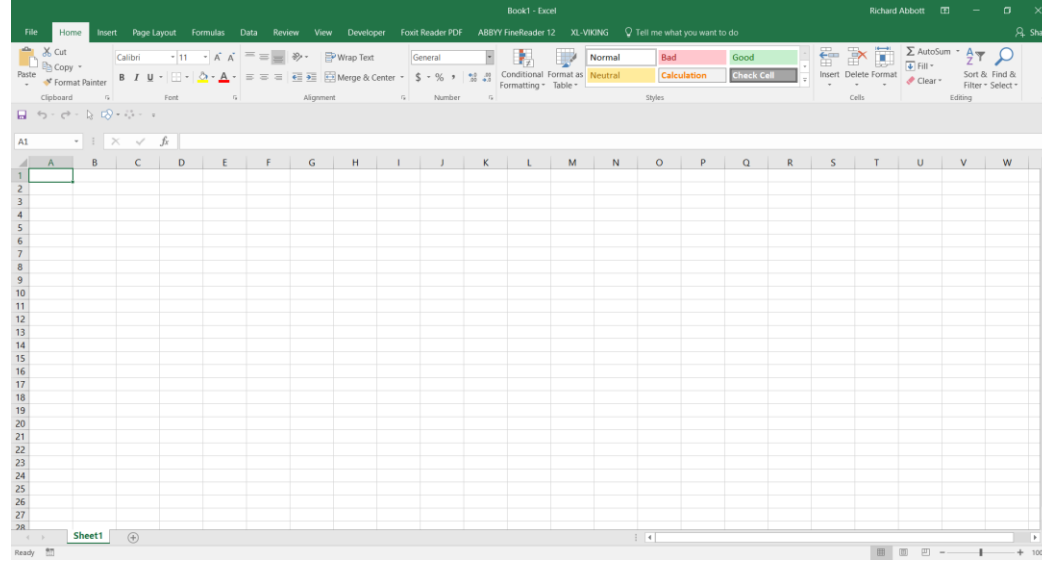


Figure 26.2.2-1: Excel When First Started

Figure 26.2.2-1 above is what you see when you start excel. In the lower RH corner there are 3 icons.

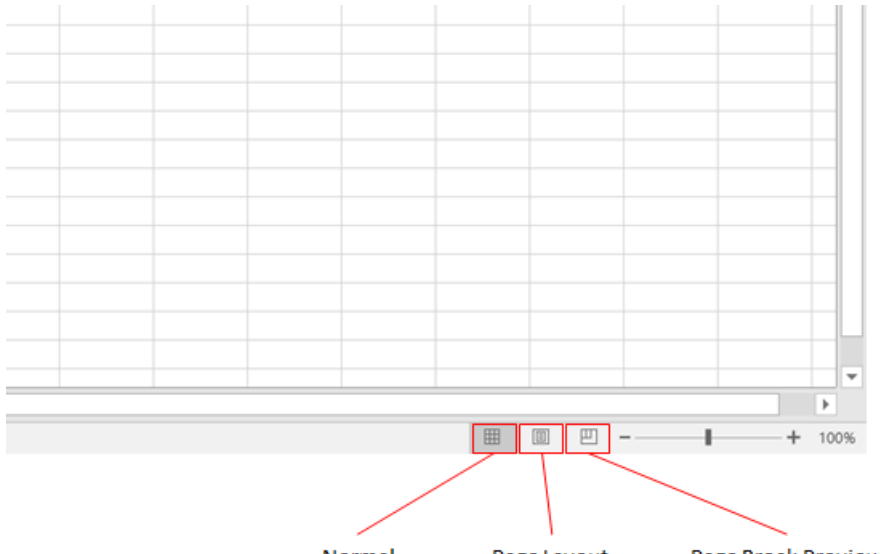


Figure 26.2.2-2: Page Layout Icons

For the report sheets (More on the use of sheets later) we only work in Page Break Preview.

If you click that icon your screen will change and will look like this:

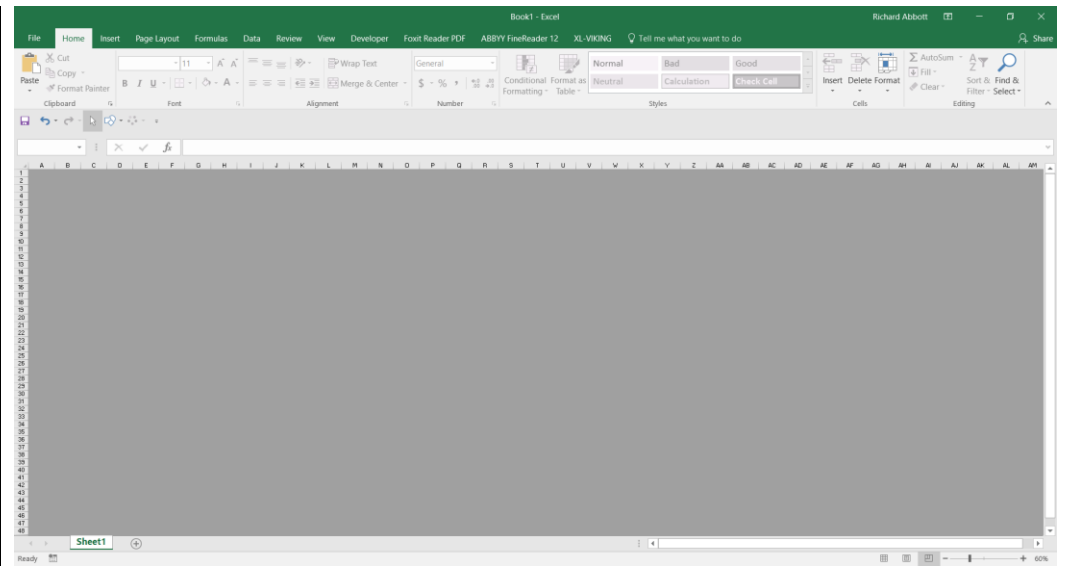


Figure 26.2.2-3: Excel Startup Page Break Preview

All the cells are ‘greyed-out’. This is because there is no defined *Print Area*. To define a *Print Area*, select a range of cells and go to the Page layout menu.

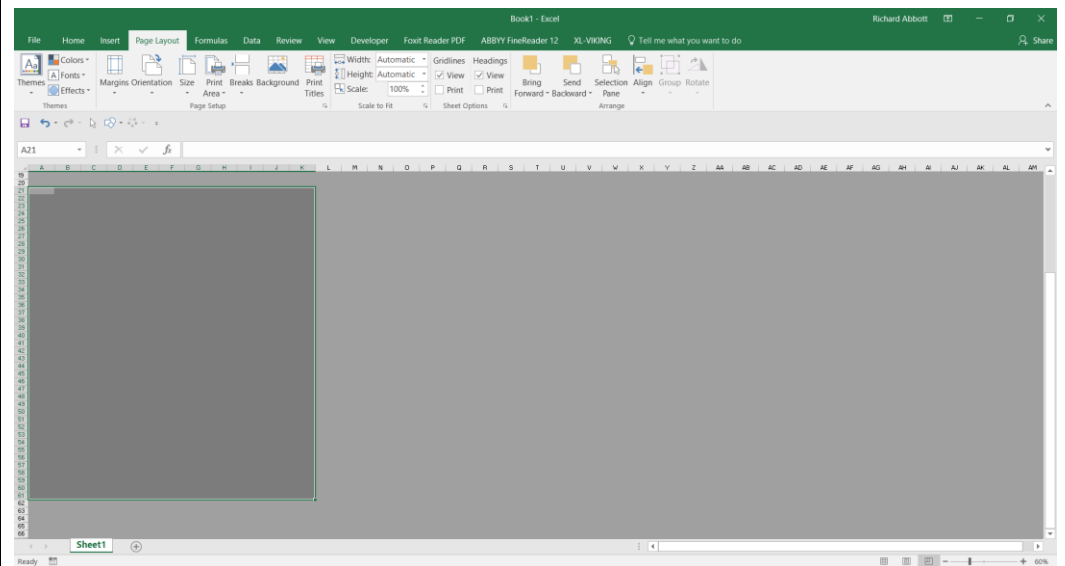


Figure 26.2.2-4: Selecting Cells to Define a Print Area

And click on the Print Area button:

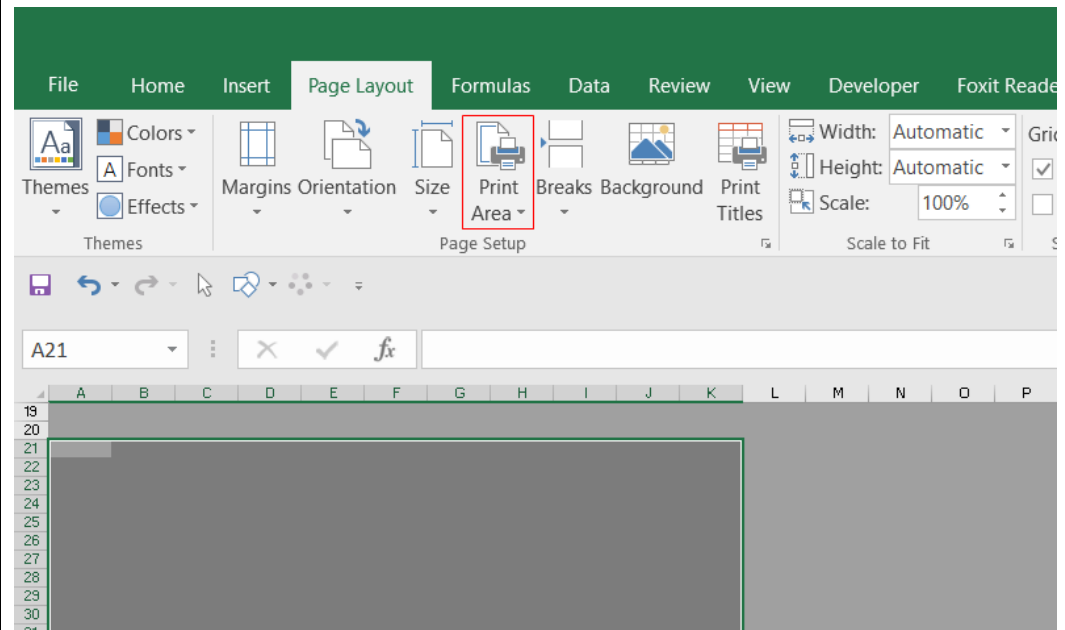


Figure 26.2.2-5: Print Area Button

And click ‘Set Print Area’. The screen will now look like this:

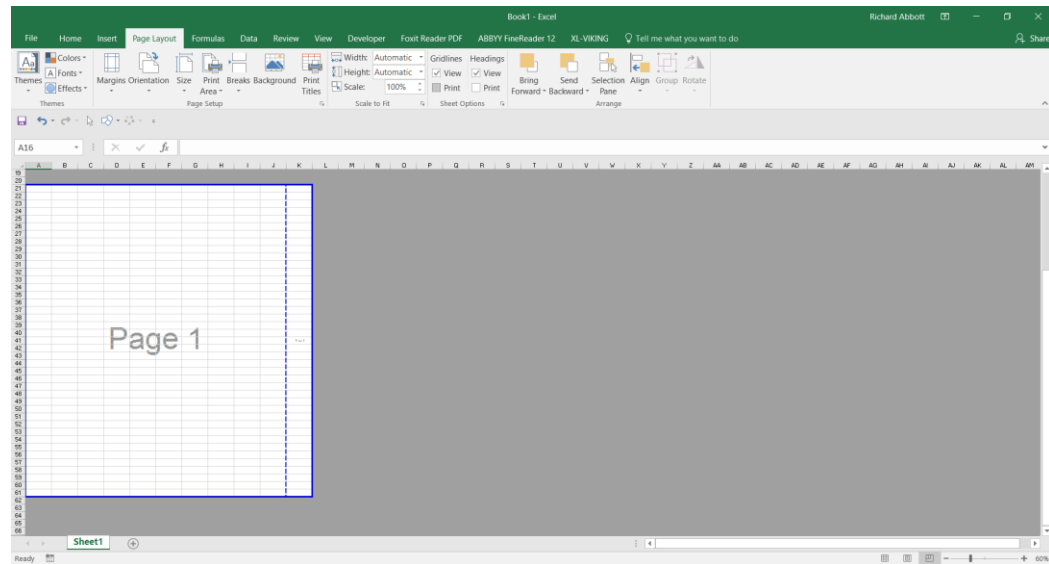


Figure 26.2.2-6: Print Area Defined

When Excel is used in this way only the area of the white cells is printed. The grey area is not printed. When the term ‘Printed’ is used it also applies to the creation of pdf files. When a pdf file is created, the pdf will only show the *Print Area* of the page.

This is very useful and allows you to display only the results of an analysis on the printed part of the report. We use this concept extensively in many of our [standard spreadsheets](#). The way you arrange and use your analysis within this framework is key and is covered in the next section.

26.2.3. Printing, Columns and Rules

Excel does not cope well with different printers and is bad at adapting page breaks and scaling from one printer to another. An important rule to adopt is to set up all your report spreadsheets printer to ‘Microsoft Print to PDF’. This is done in the file menu. Select print from the menu on the left hand side.

It is best to avoid printing your report directly from Excel to a printer. It is better to create a .pdf file and then print the .pdf file or the part of the file that you want.

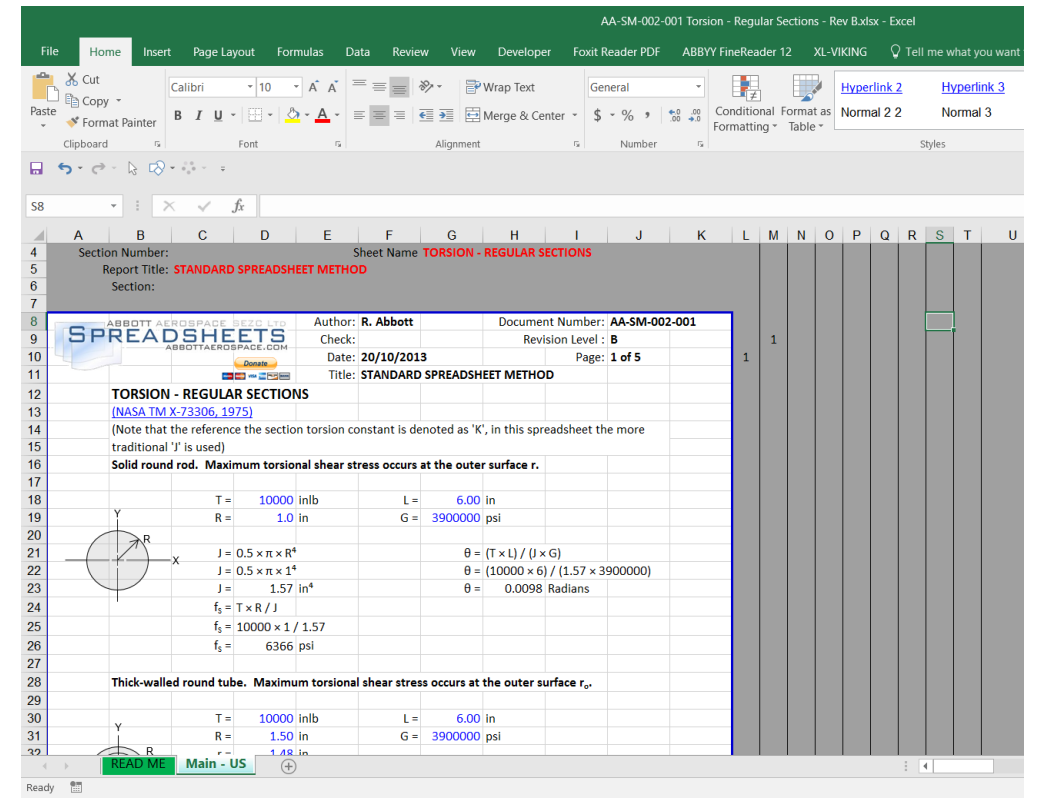


Figure 26.2.3-2: Abbott Aerospace Standard Column Sizing and Arrangement

Note that numeric values will not spread over to the neighboring cells like text does. A numeric value must fit all in a single cell. If a number is too large to fit in a single cell you can merge cells to display numbers with higher character counts.

In Figure 26.2.3-2 above you can see that to the right of the print area there are several columns that are narrower and marked with vertical border lines.

We use these columns to create figure and section numbering similar to Microsoft word.

We also reserve the first few rows of the sheet to contain sheet or document data. Note that both regions – the columns to the left of the page and the rows above the page – are not printed and are only visible to the analyst who is using the spreadsheet to create the report.

Other rules that we follow:

- Cell text color rule:** All cells that contain numerical input data for the analysis in the sheet have blue text. This way everyone who uses the spreadsheet knows which cells are ‘input’ values.
- Page Header Rule:** The top 4 or 5 rows of your page is the page header and contains the company information, report, subsection and page numbering information.
- Analysis off the page Rule:** The non-displayed analysis for each page is kept within the same rows as the page.
- Column widths Rule:** If you need a numerical value too large for your column width, merge cells across multiple columns.
- Do not use Visual Basic:** Visual basic is not recommended for use in report spreadsheets.
- Do not use Named Ranges:** Names ranges in excel can cause problems when copying sections between reports, duplicating sheets within a report and copying from standard methods into reports. We have ceased use of all named ranges. See later section for workarounds.
- Avoid Using the Solver:** Any process that must be triggered by the user that they cannot be intuitively aware of should be avoided. The Solver is the most common feature like this.

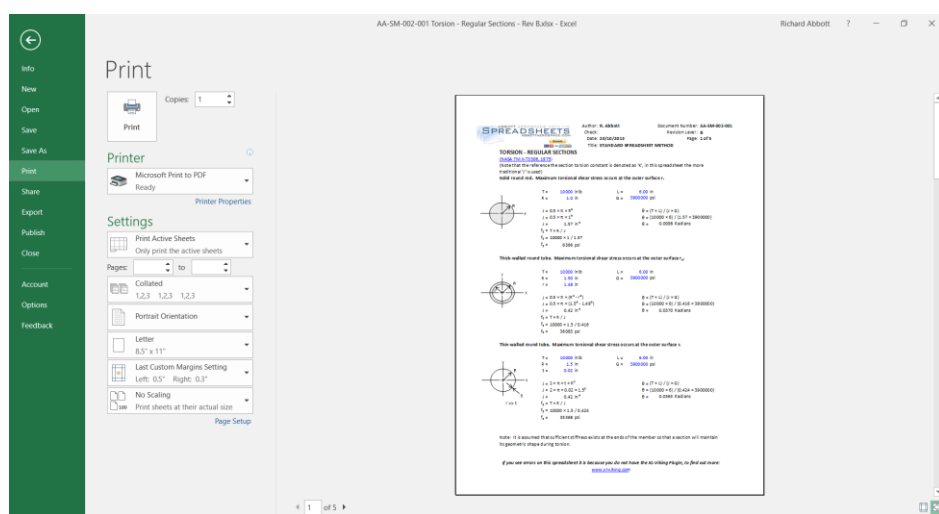


Figure 26.2.3-1: Changing your Printer to ‘Microsoft Print to PDF’

Column width should be set so when using the font and the size of font that works for your report you can display large numbers in individual cells.

The body text of our reports is 10 point Calibri and we base our page width on 11 columns. Each column is 81 pixels wide and an individual cell can display numbers up to 8 digits long.



26.2.3.1. Cell Text Color Rule and Managing Input Data

It is important that you track which cells have input data that is typed in. This is for two reasons.

1. In a large report, up to hundreds of pages long, it is easy to forget which cells contain raw data and which cells reference other cells. When it comes time to do changes or updates to the reports it is important to know which cells should be manually updated with the change in the analysis parameters.
2. When you pass the report on to your client or co-worker they should also know which cells have to be manually updated.

To get the most out of Excel as a report writing tool the author and the reader have to know what parts of the report are raw data and what parts are linked to the raw data.

For some reports, we will import finite element model output into one sheet, process it in another and write the report in a separate sheet. If the finite element model output data is kept in native format, updated runs of the finite element model can be written over the existing data and the report can update to the new input values automatically (with some judicious checking to ensure nothing went wrong along the way).

This kind of approach takes some forethought and careful setting up of how the imported finite element model output data is searched by the spreadsheet (using the INDEX and MATCH functions). When it is done properly it can save hours or days of time when inevitable loads or design updates occur.

We use blue text to denote inputs on the pages of the report section of the workbook.

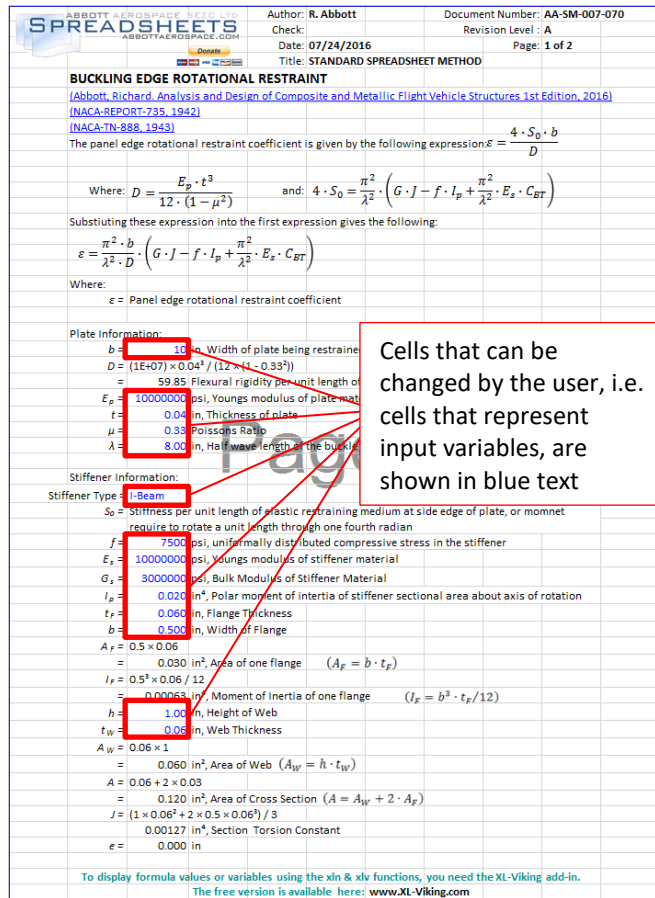


Figure 26.2.3-3: Example of Blue Input Cells for Analysis Spreadsheet

26.2.3.2. Page Header (and Footer) Rule

We use the first few rows at the top of each page to create the page header:

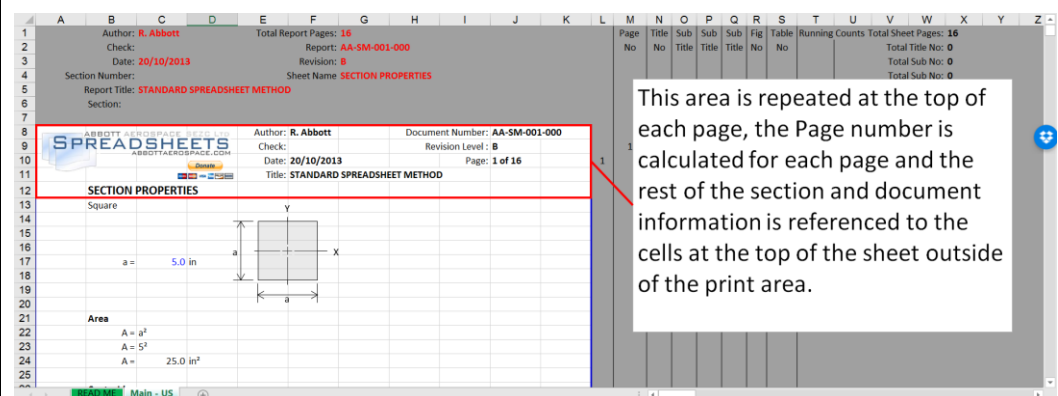


Figure 26.2.3-4: Page Header Definition

The page header can be formatted to suit any company report standard. Care must be taken to preserve this region of each page. It can easily be reconstituted by copying from an intact example, but it is good practice to consider this region of the page 'out of bounds'.

For our in-house templates we do not use a page footer. On the [standard analysis spreadsheets](#) on the [Abbott Aerospace website](#) we do have the footer advertisement for [XL-Viking](#), but this is an extra page element to manage so we avoid this where we can.

If you avoid the use of a footer on the worksheet then you can terminate pages early without having the footer change its position – a footer shown on the spreadsheet page will change position with the length of the page.

26.2.3.3. Analysis off the Page Rule

The art of creating a good report is to show only what you need to on the page of the report – and to show that information appropriately referenced and to the correct level of detail.

The area off to the right of the page is a region where you can place the workings of the analysis if it is not appropriate to show it on the page of the report. The area off to the right of the printed report page can be used as an area for rough calculations, to store a picture or scanned reference, or to place hyperlinks to online references. It can also be used to pass on notes to other people using the spreadsheet.

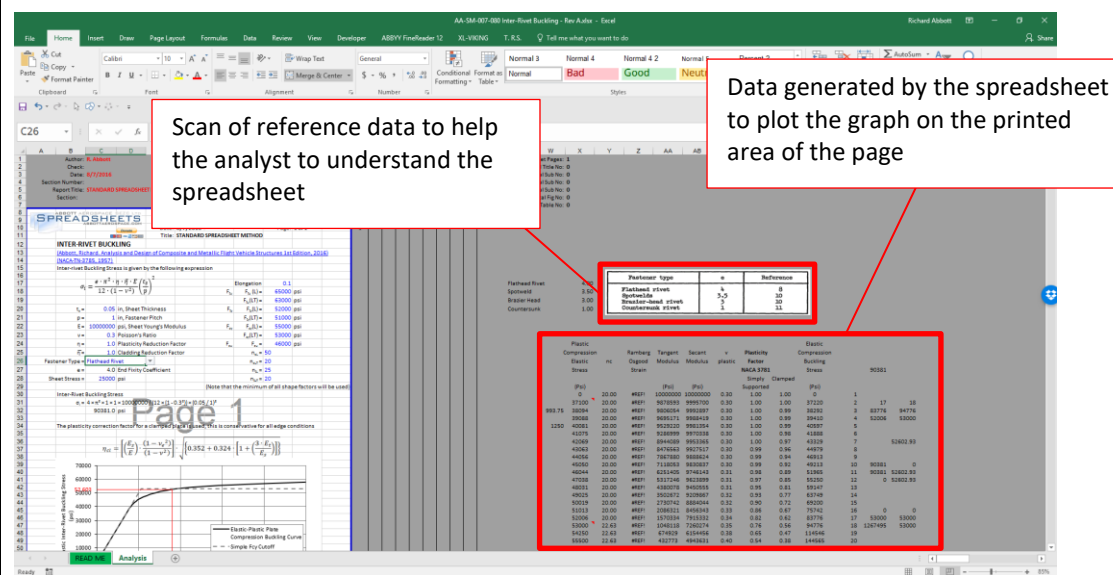


Figure 26.2.3-5: Analysis Sheet Example Showing Data off the Printed Area of the Page

However, the cardinal rule is to keep all of the off-page work in line with the analysis shown on the page. This makes it possible to copy a complete discrete analysis, all the working out and all of the references by copying complete rows to another place in the report, or into another report/excel workbook file.

26.2.3.4. Column Widths Rule

Once you set your column width and font size (see previous note) for general text you must keep all of your pages the same number of columns wide, keep all of your columns the same width and use the same font throughout.

This is essential to create trouble-free copying between worksheets or reports.

This approach also means that you will encounter the same problems associated with your choice of column width and will develop and use the same workarounds for the common problems you will encounter.

26.2.3.5. Do not use Visual Basic Rule

This is a difficult rule to follow and involves lateral thinking for complex analysis problems. Visual basic is a very powerful tool and can be used to add some very useful functionality. But, we have a rule – do not use visual basic.

This is a rule with a caveat – we do use it in a particular way that is very limited and discourages ‘everyday’ use of visual basic.

Let’s first cover why you would not use visual basic. We try to make everything we do transportable. i.e. you can copy a section out of one spreadsheet into any other spreadsheet and it will work without any further changes.

If your analysis method relies on visual basic that is attached to the workbook or worksheet when you copy a set of cells or rows out into another workbook the visual basic code is left behind. When this happens, the analysis will not work.

We have found that you can force native Excel functions, singly or in combination, to perform very complex and powerful analyses.

We do use visual basic in our project office in a very particular way. We will only use it in the form of user defined functions. When we develop a useful user defined function we add it to our in-house Excel add-in and make it available on all our machines. This makes it possible to share spreadsheets and standard methods within our office.

This approach works fine for sharing material and methods in house but makes it hard to share your spreadsheets with the rest of the world – unless you share your excel add-ins with the rest of the world.

To effectively share your work with the rest of the world it is best practice to avoid all use of visual basic.

You may note that our standard spreadsheets use a visual basic add-in to help display mathematics. We developed this add-in to create critical additional functionality that Excel does not have, and to keep functionality constant for all users.

26.2.3.6. Do not use Named Ranges Rule

We have stopped using named ranges. This functionality in excel allows you to give a single cell or a range of cells a name rather than a cell reference. The problem with using this is that if you copy from multiple excel workbooks to a single excel workbook several problems will occur.

- Common names can often be used across multiple excel sources. For example, ‘F’ for force. Excel will automatically rename these to avoid name duplicates in a single workbook.
- If you define a name and don’t use it, it still exists in excel and persists as you copy the source material to multiple new workbooks. We have found that over time a workbook that has been developed from multiple excel sources using names can accumulate hundreds of unused names and eventually this will reduce stability and encourage crashes to occur.

If you do use named ranges in your workbooks these is an excellent free excel add-in that improves Excel’s native name management. It is available from JKP Application Development Services and is free. You can download it here: <http://www.jkp-ads.com/officemarketplacenm-en.asp>

26.2.3.7. Avoid Using the Solver

The solver is a useful tool. However, every time the analysis input data is updated the solver had to be manually triggered. If the user does not know that the result of the analysis depends on the solver being used then the answer produced by the spreadsheet will be incorrect.

There are some work-arounds. Where an iterative solution is required this can be set up in a series of cells with a simple check for convergence built in.

Our [Beam-Column Analysis spreadsheet](#) uses a simple iteration solver to solve the expression for the modification to the column allowable for eccentricity.

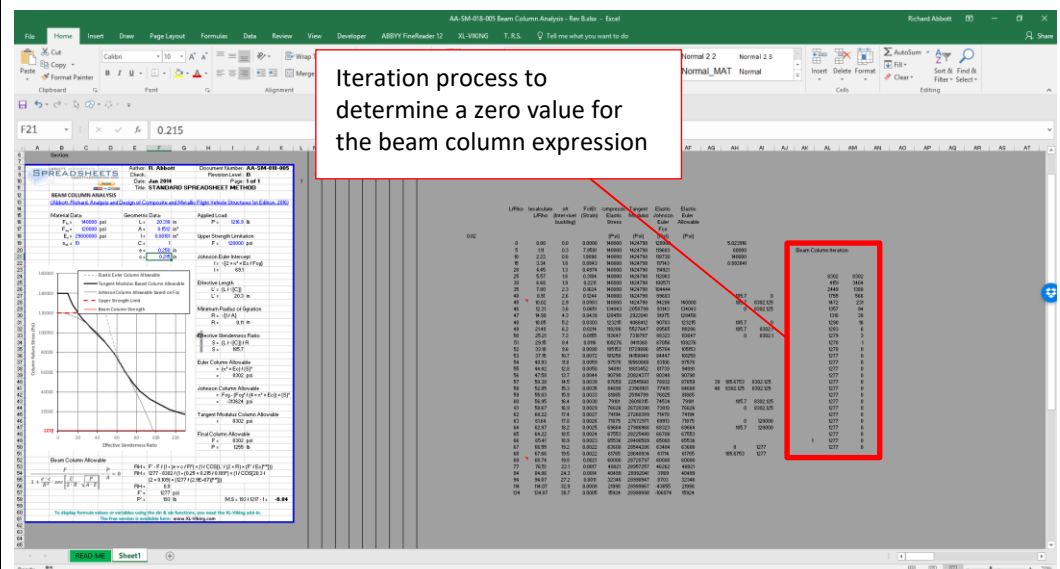


Figure 26.2.3-6: Example of Work-around for Solver Alternative

We have stopped using the solver (or the goal seek) and we have found an alternative and functioning solution every time where we would have used the solver.

26.2.4. Advanced Excel Methods

Reserved

26.2.5. XL-Viking

Reserved

26.2.6. Creating NASTRAN Input Files Using Microsoft Excel

This is one of my favorite and unexpected ways to integrate Excel with other analysis tools.

We typically use this method to process loads data from our loads analysis spreadsheets. But once the Bulk Data File format is known, any part of a finite element model can be created in excel, exported as a text file and imported into any NASTRAN pre-processor.

We use Excel to perform the loads analysis and generate the loads data at discrete points along the aircraft loads reference axes. We use excel again to generate aircraft loads envelopes and identify the critical loads cases. For most part 23 programs this is a set of 50-60 critical cases taken from an overall load set of 600-700 cases.

We use excel to generate the .bdf format file to be read into our NASTRAN pre-processor defined at the reference node locations.

The correct format can be created using the & operator. For example, this excel expression:

```
='NODE NUMBERS'!B3&","&'NODE NUMBERS'!C3&","&'NODE
NUMBERS'!D3&","&'NODE NUMBERS'!G3&","&'NODE
NUMBERS'!H3&","&ROUND('NODE NUMBERS'!M3,3)&","&ROUND('NODE
NUMBERS'!N3,3)&","&ROUND('NODE NUMBERS'!O3,3)
```

Becomes the following

```
FORCE,1,531037,0,1.,0,0,0,0
```

NASTRAN Force cards can be created in the correct format. Any applied loads can be done like this. With planning of the individual load application node numbers in the finite element model entire input decks can be created:

| A | B | C | D | E | F | G | H | I | J | K | L | M | N | O |
|----|---|---|---|---|---|---|---|---|---|---|---|---|---|---|
| 1 | S Femap with NX Nastran Load Set 1 : HT13+GVCMDWAL-20000, VERTICAL STABILIZER | | | | | | | | | | | | | |
| 2 | 33,3) | | | | | | | | | | | | | |
| 3 | FORCE,1,531038,0,1.,4.798,0.502,-21.652 | | | | | | | | | | | | | |
| 4 | FORCE,1,531039,0,1.,4.882,0.504,5.669 | | | | | | | | | | | | | |
| 5 | FORCE,1,531040,0,1.,4.96,0.506,5.718 | | | | | | | | | | | | | |
| 6 | FORCE,1,531041,0,1.,5.033,0.508,5.763 | | | | | | | | | | | | | |
| 7 | FORCE,1,531042,0,1.,5.102,0.509,5.803 | | | | | | | | | | | | | |
| 8 | FORCE,1,553201,0,1.,5.165,0.51,5.838 | | | | | | | | | | | | | |
| 9 | FORCE,1,553202,0,1.,5.223,0.511,5.869 | | | | | | | | | | | | | |
| 10 | FORCE,1,553203,0,1.,5.275,0.511,5.895 | | | | | | | | | | | | | |
| 11 | FORCE,1,553204,0,1.,5.323,0.511,5.917 | | | | | | | | | | | | | |
| 12 | FORCE,1,553205,0,1.,5.365,0.511,5.934 | | | | | | | | | | | | | |
| 13 | FORCE,1,553206,0,1.,5.403,0.511,5.947 | | | | | | | | | | | | | |
| 14 | FORCE,1,553207,0,1.,0,0,5.955 | | | | | | | | | | | | | |
| 15 | FORCE,1,553208,0,1.,5.435,0.51,5.958 | | | | | | | | | | | | | |
| 16 | FORCE,1,553209,0,1.,5.462,0.508,5.957 | | | | | | | | | | | | | |
| 17 | FORCE,1,553210,0,1.,5.484,0.507,5.951 | | | | | | | | | | | | | |
| 18 | FORCE,1,553211,0,1.,5.501,0.505,5.941 | | | | | | | | | | | | | |
| 19 | FORCE,1,553212,0,1.,5.512,0.503,5.926 | | | | | | | | | | | | | |
| 20 | FORCE,1,553213,0,1.,5.519,0.5,5.907 | | | | | | | | | | | | | |
| 21 | FORCE,1,553214,0,1.,5.52,0.497,5.883 | | | | | | | | | | | | | |
| 22 | FORCE,1,553215,0,1.,5.516,0.494,5.854 | | | | | | | | | | | | | |
| 23 | FORCE,1,553216,0,1.,5.502,0.49,5.821 | | | | | | | | | | | | | |

Figure 26.2.6-1: BDF Format Cell Entry in Excel

The input deck should be created so it looks exactly as the .bdf file should look on the screen.

The input deck should exist in a worksheet tab of its own and that worksheet should include no other data.

This individual worksheet can be saved as a text format file. However, first you should save the whole workbook as a spreadsheet.

Once the workbook has been saved, with the worksheet with the bdf input deck selected, you should select “Save As” and then choose “Text (MS-DOS)”.

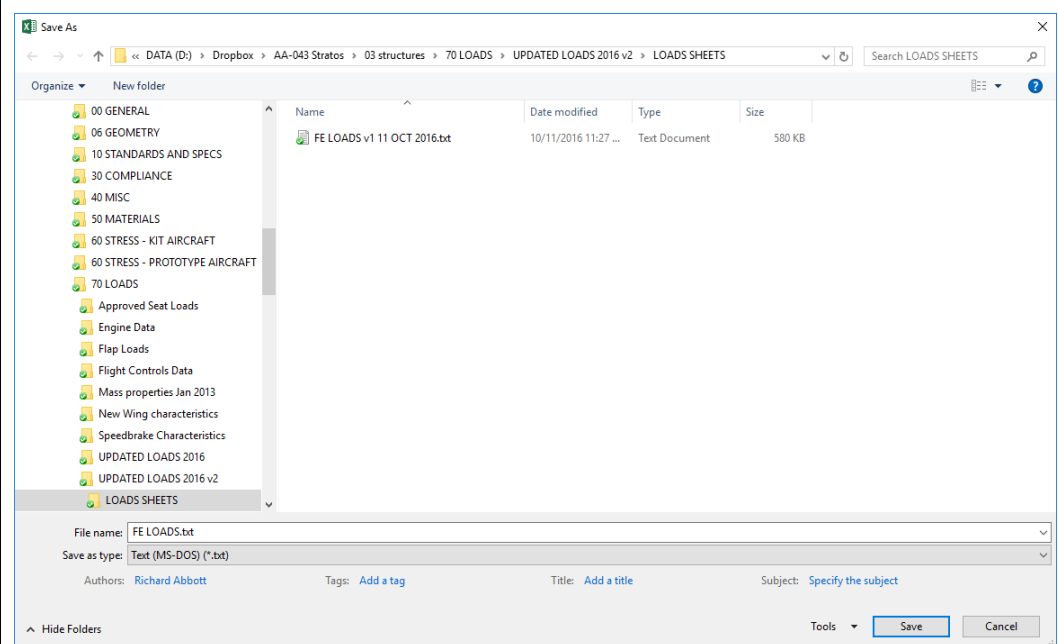


Figure 26.2.6-2: Save as Text File

Choose a file name and save slick save.

The following Dialog box will appear:

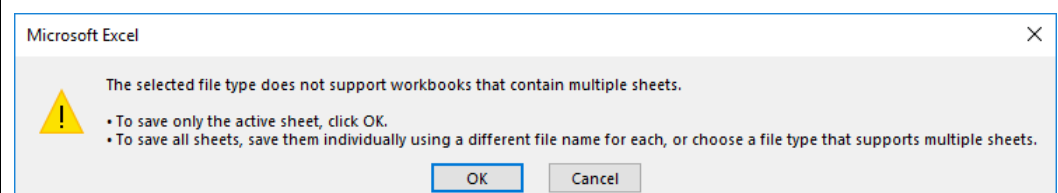


Figure 26.2.6-3: First Dialog Box

Click “OK”, then this Dialog box will appear:

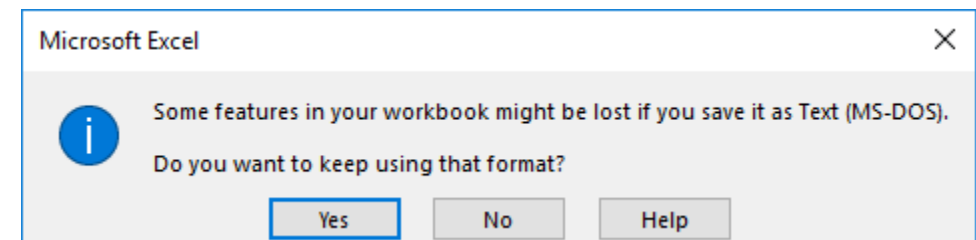


Figure 26.2.6-4: Second Dialog Box

Click “Yes”.

When you open up the text file that has been created it will look something like this:

```
FE LOADS.txt - Notepad
File Edit Format View Help
$ Femap with NX Nastran Load Set 1 : HT13+GVCMTWAL-20000, VERTICAL STABILIZER
"FORCE,1,531037,0,1.,0,0,0"
"FORCE,1,531038,0,1.,4.798,0.502,-21.652"
"FORCE,1,531039,0,1.,4.882,0.504,5.669"
"FORCE,1,531040,0,1.,4.96,0.506,5.718"
"FORCE,1,531041,0,1.,5.033,0.508,5.763"
"FORCE,1,531042,0,1.,5.102,0.509,5.803"
"FORCE,1,553201,0,1.,5.165,0.51,5.838"
"FORCE,1,553202,0,1.,5.223,0.511,5.869"
"FORCE,1,553203,0,1.,5.275,0.511,5.895"
"FORCE,1,553204,0,1.,5.323,0.511,5.917"
"FORCE,1,553205,0,1.,5.365,0.511,5.934"
"FORCE,1,553206,0,1.,5.403,0.511,5.947"
"FORCE,1,553207,0,1.,0,0,5.955"
"FORCE,1,553208,0,1.,5.435,0.51,5.958"
"FORCE,1,553209,0,1.,5.462,0.508,5.957"
"FORCE,1,553210,0,1.,5.484,0.507,5.951"
"FORCE,1,553211,0,1.,5.501,0.505,5.941"
"FORCE,1,553212,0,1.,5.512,0.503,5.926"
"FORCE,1,553213,0,1.,5.519,0.5,5.907"
"FORCE,1,553214,0,1.,5.52,0.497,5.883"
"FORCE,1,553215,0,1.,5.516,0.494,5.854"
"FORCE,1,553216,0,1.,5.508,0.49,5.821"
"FORCE,1,553217,0,1.,5.494,0.486,5.783"
"FORCE,1,553218,0,1.,5.474,0.482,5.74"
"FORCE,1,553219,0,1.,5.45,0.477,5.693"
"FORCE,1,553220,0,1.,5.421,0.473,5.642"
"FORCE,1,553221,0,1.,5.386,0.467,5.586"
"FORCE,1,553222,0,1.,5.346,0.462,5.525"
"FORCE,1,553223,0,1.,5.301,0.456,5.459"
"FORCE,1,553224,0,1.,5.251,0.45,5.39"
"FORCE,1,553225,0,1.,5.196,0.443,5.315"
```

Figure 26.2.6-5: Raw Text File Output from Excel

Note that each individual line of text is surrounded by quotation marks. These can be removed from the entire file by the 'find and replace' operation in Notepad, the Windows default text editor:

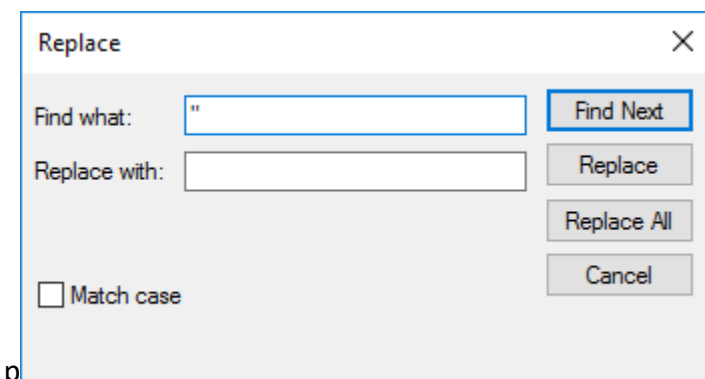


Figure 26.2.6-6: Replace Dialog Box in Notepad

When this operation is complete the file will have the correct syntax:

```
FE LOADS.txt - Notepad
File Edit Format View Help
$ Femap with NX Nastran Load Set 1 : HT13+GVCMTWAL-20000, VERTICAL STABILIZER
FORCE,1,531037,0,1.,0,0,0
FORCE,1,531038,0,1.,4.798,0.502,-21.652
FORCE,1,531039,0,1.,4.882,0.504,5.669
FORCE,1,531040,0,1.,4.96,0.506,5.718
FORCE,1,531041,0,1.,5.033,0.508,5.763
FORCE,1,531042,0,1.,5.102,0.509,5.803
FORCE,1,553201,0,1.,5.165,0.51,5.838
FORCE,1,553202,0,1.,5.223,0.511,5.869
FORCE,1,553203,0,1.,5.275,0.511,5.895
FORCE,1,553204,0,1.,5.323,0.511,5.917
FORCE,1,553205,0,1.,5.365,0.511,5.934
FORCE,1,553206,0,1.,5.403,0.511,5.947
FORCE,1,553207,0,1.,0,0,5.955
FORCE,1,553208,0,1.,5.435,0.51,5.958
FORCE,1,553209,0,1.,5.462,0.508,5.957
FORCE,1,553210,0,1.,5.484,0.507,5.951
FORCE,1,553211,0,1.,5.501,0.505,5.941
FORCE,1,553212,0,1.,5.512,0.503,5.926
FORCE,1,553213,0,1.,5.519,0.5,5.907
FORCE,1,553214,0,1.,5.52,0.497,5.883
FORCE,1,553215,0,1.,5.516,0.494,5.854
FORCE,1,553216,0,1.,5.508,0.49,5.821
FORCE,1,553217,0,1.,5.494,0.486,5.783
FORCE,1,553218,0,1.,5.474,0.482,5.74
FORCE,1,553219,0,1.,5.45,0.477,5.693
FORCE,1,553220,0,1.,5.421,0.473,5.642
FORCE,1,553221,0,1.,5.386,0.467,5.586
FORCE,1,553222,0,1.,5.346,0.462,5.525
FORCE,1,553223,0,1.,5.301,0.456,5.459
FORCE,1,553224,0,1.,5.251,0.45,5.39
FORCE,1,553225,0,1.,5.196,0.443,5.315
```

Figure 26.2.6-7: Excel Created BDF File – Correct Syntax

The text file can be saved and the file extension can be changed to .dat or .bdf to aid importing into a NASTRAN preprocessor.

This example is limited to generating load input decks but any type of FE model data can be created in the same way.

The advertisement features sections on Acrylic Material Properties, Variation of Strength Modulus with Temperature, and Pre-Preg Carbon Cloth (F4279-COTM) Lay-up reliability for Bulk Insulation. It includes graphs showing strength and modulus vs temperature, and tables for triangular load calculations.

ABBOTT AEROSPACE
ABBOTTAEROSPACE.COM SEZC LTD

27. COMMON AIRCRAFT HARDWARE

27.1. Rivets

| Rivet Number | Description |
|-----------------|---|
| AN427 | Rivet, 100° csk. Head steel, monel, copper |
| AN430 | Rivet, round head al. Alloy |
| AN441 | Rivet, tinner's Head, steel, ss, monel |
| AN456 | Rivet, brazier head, aluminum alloy |
| AN123151-123750 | Rivet, universal head & 100° steel, Inconel |
| NAS 1200 | Rivet, solid, 100° flush shear head |
| NAS 1241 | Rivet, solid, 100° flush head |
| NAS 1242 | Rivet, solid universal head |
| NAS 1398 | Rivet, blind, protruding head, locked spindle |
| NAS 1399 | Rivet, blind, 100° csk. Head, locked spindle |

| Rivet Number | Description |
|------------------|--|
| NAS 1738-1739 | Rivet, blind, protruding & flush hd., mech. locked spindle, bulbed |
| NAS1806-1816 | Rivet, hi-shear, flathead., ti. alloy |
| NAS1906-1916 | Rivet, hi-shear, 100° hd., ti. alloy |
| AN124951-125550 | Rivet, solid universal head & 100° csk. head, cres. steel, inconel |
| AN125551-1255700 | Rivet, solid universal head, steel |
| AN426 MS20426 | Rivet, solid, csk. 100° head al. alloy |
| AN470 MS20470 | Rivet, solid, universal head, al. & al. alloy |
| MS9319 | Rivet, solid univ. head, AMS 7233 |
| MS9403 | Rivet, solid, universal head, AMS 5737 |
| MS16535 | Rivet, tubular, oval head |

| Rivet Number | Description |
|---------------|--|
| MS16536 | Rivet, tubular, 100° flat csk. head |
| MS20426 | Rivet, solid, csk., 100° al. alloy |
| MS20427 | Rivet, solid, csk., 100° flush hd., AMS 7233 |
| MS20470 | Rivet, solid, universal head, al. alloy |
| MS20600 | Rivet, blind, pull stem, protruding head |
| MS20601 | Rivet, blind, pull stem, 100°, flush head |
| MS20602-20603 | Rivet, blind, explosive |
| MS20604-20605 | Rivet, blind nonstructural univ. and 100° flush head |
| MS20613-20615 | Rivet, solid, monel, universal hd., steel, ss, brass, copper |
| NAS452-453 | Rivnut, 100° csk. head & flathead |
| NAS454-455 | Rivet blind, al. alloy |

| Rivet Number | Description |
|--------------|---|
| NAS508 | Rivet, universal head, monel |
| NAS1054 | Rivet, hi-shear, protruding head |
| NAS1055 | Rivet, hi-shear, 100° flush head |
| NAS1097 | Rivet, solid, 100° flush shear head, al. Alloy |
| NAS1198 | Rivet, solid, universal head |
| NAS1199 | Rivet, solid, 100° flush head |

27.2. Screws

| Screw MS, AN, or NAS Number | Description |
|--------------------------------|--|
| AN255 | Screw, external relieved body |
| AN500 & 501 | Screw, machine fillister head |
| AN502 & 503 | Screw, machine, fill. Head, drilled, coarse & fine |
| AN504 | Screw, tapping, thread cutting rnd. Head, mach. Thread |

| Screw MS, AN, or NAS Number | Description |
|-----------------------------|--|
| AN505 | Screw, machine, flathead, 82° coarse thread |
| AN506 | Screw, tapping, type F, coarse & fine |
| AN507 | Screw, machine, flathead, 100° |
| AN508 | Screw, machine, round head |
| AN509 | Screw machine, 100° structural |
| AN510 | Screw, machine, flathead, 82° fine thread |
| AN515 & AN520 | Screw, machine, round head |
| AN525 | Screw, washer head |
| AN526 | Screw, machine buttonhead |
| AN530 | Screw-tapping, thread cutting, rnd. hd. |
| AN531 | Screw, tapping, thread forming or cutting, 82° flathead. |

| Screw MS, AN, or NAS Number | Description |
|-----------------------------|---|
| AN535 | Drive screw, round head |
| AN545 | Screw, wood, round head |
| AN550 | Screw, wood, flathead, 82° |
| AN565 | Setscrew, hex. & fluted socket |
| AN115401-115600 | Screws, flat fill. head, steel, .190-.375 |
| AN115601-115800 | Drilled shank Screw flat fill. head, steel, .190-.375 |
| AN115801-116150 | Screw, flat fill. head, steel, .190-.375 |
| AN116901-117080 | Screw, oval fill. head, steel |
| MS9016 | Bushing Screw, plain |
| MS9017 | Bushing Screw, slotted |
| MS9122-9123 | Screw, machine slotted hex. hd. |

| Screw MS, AN, or NAS Number | Description |
|--------------------------------|--|
| MS9177-9178 | Screw, dbl. hex. head, cres. |
| MS9183-9186 | Screw, machine, steel, drilled 12 pt. hd., cad. plate |
| MS9187-9188 | Screw, drilled dbl. hex. head, cres. |
| MS9189-9192 | Screw, machine, steel, 12 pt. hd., black oxide |
| MS9206-9214 | Screw, dbl. hex. ext. washer head, diffused nickel cad. plate |
| MS9215-9223 | Screw, dbl. hex. ext. washer head, diffused nickel cad. plate, drilled |
| MS9281-9291 | Screw, machine, hex. hd., AMS 6322 black oxide |
| MS9292-9302 | Screw, machine, hex. hd., AMS 6322 blk. oxide, drilled |
| MS9316-9317 | Screw, machine, steel slotted hex. head |
| MS9438-9439 | Screw, mach. steel AMS 6304 diffused nickel cad. hex. hd., one hole |
| MS9631-9639 | Screw, mach., hex. hd. one hole, full shank, titanium AMS 4967 |

| Screw MS, AN, or NAS Number | Description |
|--------------------------------|---|
| MS16198 | Screw, wood, slotted RH austenitic corr. res. steel |
| MS16199 | Screw, wood, slot flat-head, copper silicone |
| MS16995 | Screw, cap, socket head hex., corr. resisting steel UNC-3A |
| MS16996 | Screw, cap, socket head, hex., corr. resisting steel UNF-3A |
| MS16997 | Screw, cap, socket head, hex., alloy steel cad. UNC-3A |
| MS16998 | Screw, cap, socket head, hex., alloy steel, cad. UNF-3A |
| MS18063-18068 | Setscrew, self-locking, cup, flat, cone pts., steel & stainless |
| MS18211 | Screw, machine, flat-head, plastic, nylon |
| MS18212 | Screw, machine, pan-head, plastic, nylon |
| MS21090 | Screw, self-lock, pan-head, cross recessed |
| MS21207 | Screw, tapping, 100° clk. flathead., steel, cres. steel |

| Screw MS, AN, or NAS Number | Description |
|-----------------------------|--|
| MS21262 | Screw, self-lock, int. wrenching |
| MS21277-21285 | Screw, machine, double hex., ext. washer head |
| MS21286-21294 | Screw, machine, double hex., ext. washer head |
| MS21295 | Screw, self-lock, int. wrenching |
| MS21318 | Screw, drive, round head, Type U |
| MS21342 | Setscrew, fluted socket, cup and flat point |
| MS24615-24618 | Screw, tapping, phillips recessed, pan & 82° flathead Type A |
| MS24619-24622 | Screw, tapping, phillips recessed, pan & 82° flathead Type B |
| MS24623-24626 | Screw, tapping, cross recessed pan & 82° flathead, Type BF or BT |
| MS24627-24630 | Screw, tapping, thread cutting cross recessed pan & 82° flathead, Type F |
| MS24667 & 24671 | Screw, cap socket hd., flat, csk. |

| Screw MS, AN, or NAS Number | Description |
|-----------------------------|---|
| MS24673-24678 | Screw, cap socket hd., flat, drilled |
| MS24693 | Screw, machine, flat csk. head, 100° cross recess |
| MS24694 | Screw, machine, csk. flathead., 100° cross recess, structural |
| MS27039 | Screw, machine, panhead, structural, cross recessed |
| MS35190-35203 | Screw, machine 82° flathead., cross recessed, steel, brass, alum. |
| MS35206-35219 | Screw, machine, panhead, cross recessed, steel, brass, alum. |
| MS35223-35234 | Screw, machine, panhead, slotted, SS steel, steel |
| MS35239-35243 | Screw, machine, flathead., slotted, steel |
| MS35265-35278 | Screw, machine, drilled fillister head, slotted, SS steel, brass, alum. |
| MS35492-35493 | Screw, wood, flathead, cross recessed |
| MS35494-35495 | Screw. wood, flat & round hd., slotted |

| Screw MS, AN, or NAS Number | Description |
|-----------------------------|--|
| MS35914 | Insert, screw, thread, self-tapping |
| MS51017-51047 | Setscrew, hex. socket SS & steel half dog, cone, flat, cup pt. |
| MS51861 | Screw, tapping, type AB, panhead, cross recessed |
| MS51862 | Screw, tapping, type AB, flathead., cross recessed |
| MS51957-51958 | Screw, machine, panhead, cross recessed |
| MS51959-51960 | Screw, machine, flat-head, cross recessed |
| MS51963-51966 | Setscrew, hex. socket, cup & flat point |
| MS51973-51974 | Setscrew, hex. socket, cone point |
| MS51975 | Screw, shoulder, socket head |
| MS51976-51977 | Setscrew, hex. socket, half dog point |
| MS51981-51982 | Setscrew, hex. socket, oval point |

| Screw MS, AN, or NAS Number | Description |
|-----------------------------|---|
| NAS220-237 | Screw, brazier hd. philips recessed |
| NAS384-385 | Screw, oval head, philips recessed 100°, 82°, steel |
| NAS387-388 | Screw, machine, oval hd., 100°, 82°, steel |
| NAS514 | Screw, machine, 100° flathead., fully threaded, al. steel |
| NAS517 | Screw, 100° flathead, close tol. 160,000 psi |
| NAS548 | Screw, 100° flathead, type B tapping |
| NAS560 | Screw, machine, 100° structural, hi-temp |
| NAS600-606 | Screw, machine, aircraft, panhead phillips recessed, full thr., steel |
| NAS608-609 | Screw, hex. socket cap, plain & self-locking, drilled head |
| NAS623 | Screw, panhead. thr. short, 160,000 psi |
| NAS720 | Screw, panhead, assembled |

| Screw MS, AN, or NAS Number | Description |
|--------------------------------|---|
| NAS1081 | Setscrew, hex. socket, self-locking |
| NAS1096 | Screw, hex. head, recess, full thr. |
| NAS1100 | Screw, machine, panhead, full thread, torq.-set |
| NAS1101 | Screw, machine, flat fill hd. full thread |
| NAS1102 | Screw, machine, 100° flathead. full thr. torq.-set |
| NAS1121-1128 | Screw, machine, flat fill hd., short thread, torq.-set |
| NAS1131-1138 | Screw, machine, pan hd., short thread, torq.-set |
| NAS1141-1148 | Screw, machine, panhead. modified, short thread torq.-set |
| NAS1151-1158 | Screw, machine, 100° flathead., sort thread, torq.-set |
| NAS1161-1168 | Screw, machine, 100° flathead., shear, torq.-set |
| NAS1171-1178 | Screw, panhead., shear, self-lock., torq.-set |

| Screw MS, AN, or NAS Number | Description |
|--------------------------------|--|
| NAS1181-1188 | Screw, flat fill hd., self-locking, torq.-set |
| NAS1189 | Screw, flat 100° hd., full thread, self-locking |
| NAS1190 | Screw, panhead., self-locking, full thread |
| NAS1191 | Screw, flat fill. hd., full thread, self-locking |
| NAS1216 | Screw, panhead hi-torque, full thread |
| NAS1217 | Screw, panhead, hi-torque, short thread |
| NAS1218 | Screw, panhead, hi-torque, short thread |
| NAS1219 | Screw, 100° csk. hd., hi-torque, full thread |
| NAS1220 | Screw, 100° csk. hd., hi-torque, short thread |
| NAS1221 | Screw, 100° clk. hd., hi-torque, long thread |
| NAS1298 | Screw, shoulder, brazier head |

| Screw MS, AN, or NAS Number | Description |
|--------------------------------|---|
| NAS1299 | Screw, shoulder, 100° flathead |
| NAS1300 | Thumbscrew, drilled/undrilled |
| NAS1301 | Screw, panhead, as- sembled washers phil- lips recess |
| NAS1351-1352 | Socket Capscrew, hex. head, drilled/undrilled |
| NAS1393 | Screw, 82° flathead, torq-set |
| NAS1402-1406 | Screw, panhead, phil- lips recess |
| NAS1579 | Screw, panhead., full thread, 1200° F |
| NAS1603-1610 | Screw, flush head, .0312 O.S. |
| NAS1620-1628 | Screw, machine, 100° flat short thread, torq-set |
| NAS1630-1634 | Screw, machine, panhead., short thread, torq.-set |
| NAS1635 | Screw, panhead cross recessed, full thread |

| Screw MS, AN, or NAS Number | Description |
|--------------------------------|---|
| NAS5000-5006 | Screw, panhead, tri-wing recess, short thr., alloy stl. |
| NAS5100-5106 | Screw, panhead, tri-wing recess, short thr., cres. |
| NAS5200-5206 | Screw, panhead, tri-wing recess, short thr., cres. |
| NAS5300-5306 | Screw, fillister head, tri-wing recess, full thr., alloy stl. |
| NAS5400-5406 | Screw, fillister hd., tri-wing recess, full thr., cres. |
| NAS5500-5506 | Screw, fillister hd., tri- wing recess, full thr., titanium |
| NAS5600-5606 | Screw, 100° head, tri-wing recess, full thr., alloy stl. |
| NAS5700-5706 | Screw, 100° head, tri-wing recess, full thr., cres. |
| NAS5800-5806 | Screw, 100° head, tri-wing recess, full thr., titanium |
| NAS5900-5903 | Screw, hex. Head, tri-wing recess, full thr., alloy stl. |
| NAS6000-6003 | Screw, hex. Head, tri-wing recess, full thr., cres. |

| Screw MS, AN, or NAS Number | Description |
|-----------------------------|---|
| NAS6100-6103 | Screw, hex head, tri-wing recess, full thr., titanium |
| NAS6500-6506 | Screw, 100° oval hd., tri-wing recess, full thr., cres. |
| NAS6900-6904 | Screw, panhead, tri-wing recess, full thr., cres. |

27.3. Bolts

| Bolt Number | Description |
|-------------|--------------------------------|
| AN3-20 | Bolt, machine |
| AN21-36 | Bolt, clevis |
| AN42-49 | Bolt, eye |
| AN73-81 | Bolt, machine, drilled |
| AN173-186 | Bolt, aircraft Close tolerance |
| AN774 | Bolt, flared tube |
| AN775 | Bolt, universal fitting |

| Bolt Number | Description |
|-----------------|---|
| AN148551-149350 | Bolt, socket head, 6-hole drilled, .190-.625 |
| AN101001-101900 | Bolt, hex, steel, head |
| AN101901-102800 | Bolt, hex., drilled shank, steel |
| AN102801-103700 | Bolt. Drilled hex. Head, (one hole), steel |
| AN103701-104600 | Bolt, drilled hex. Head, steel, (six holes) |
| AN104601-105500 | Bolt, hex. Head, corrosion-resistant steel |
| AN105501-106400 | Bolt, hex. Head, drilled shank, corrosion-resistant steel |
| AN106401-107300 | Bolt, hex., drilled head, (one holes), corrosion-resistant steel |
| AN107301-108200 | Bolt, hex., drilled head, (six holes), corrosion-resistant steel |
| MS9033-9039 | Bolt, machine 12pt. Head, 130,000 psi min. T.S. |
| MS9060-9066 | Bolt, machine 12pt. Double hex. 130,000 psi min. T.S. ext. washer head, drilled |

| Bolt Number | Description |
|-------------|--|
| MS9088-9094 | Bolt, machine, steel, drilled 12 pt. head |
| MS9110-9113 | Bolt, machine, double hex., ext. washer head, close tolerance |
| MS9146-9152 | Bolt, steel, 12 pt. hd. black oxide 125,000 psi min. T.S. |
| MS9157-9163 | Bolt, steel, 12pt. hd. black oxide 125,000 psi min. T.S. |
| MS9169-9175 | Bolt, steel, 12 pt. drilled hd., black oxide 125,000 psi min. T.S. |
| MS9224 | Bolt, 12 pt. head, heat resistant |
| MS9397-9402 | Bolt, tee head, AMS 6322, chamfered cad. pl. |
| MS9432-9437 | Bolt, tee head AMS 5735 chamfered |
| MS9440-9448 | Bolt, mach. steel. AMS 6304 diffused nickel cad. hex. hd., 3 holes |
| MS9449-9459 | Bolt, mach. steel, AMS 6304 diffused nickel cad., hex. head |
| MS9487-9497 | Bolt, mach. hex. hd. full shank, AMS 5731 |

| Bolt Number | Description |
|-------------|---|
| MS9498-9508 | Bolt, mach. hex. hd., 1 hole, full shank |
| MS9516-9526 | Bolt, mach., steel AMS 6322 cad. 1 hole hex. hd. |
| MS9527-9537 | Bolt, mach., steel AMS 6322 cad. 1 hole hex. hd. |
| MS9554-9562 | Bolt, mach., dbl. hex. ext. wash. hd., PD shank, AMS 5731 |
| MS9563-9571 | Bolt, mach., dbl. hex. ext. wash. hd. drilled, AMS 5731 |
| MS9572-9580 | Bolt, mach., dbl. hex. ext. wash. hd., drilled, PD shank AMS 5731 silver plated |
| MS9583-9591 | Bolt, mach., hex. hd. 6 holes full shank, AMS 5731 |
| MS9622-9630 | Bolt, mach., hex. hd. 1 hole, PD shank, titanium AMS 4967 |
| MS9641-9648 | Bolt, mach., hex. hd., 1 hole, full shank titanium AMS 4967 |
| MS9649-9652 | Bolt, mach., hex. hd. full shank, titanium AMS 4967 |
| MS9676-9679 | Bolt, mach., dbl. hex. ext. wash. hd., cup washer locked, cres. AMS 5731 |

| Bolt Number | Description |
|-------------|---|
| MS9680-9683 | Bolt, mach., dbl. hex. ext. wash. hd., cup washer locked, steel AMS 6322 cad. |
| MS9685-9693 | Bolt, mach., hex. hd. 1 hole, PD shank, steel AMS 6304 diffused nickel cad. |
| MS9694-9702 | Bolt mach. dbl. hex. ext. wash. hd. AMS 5708 |
| MS9703-9711 | Bolt, mach., dbl. hex. ext. wash. hd., drilled, AMS 5708 |
| MS9712-9720 | Bolt, mach. dbl. hex. ext. wash. hd. drilled, AMS 5708 silver plate |
| MS9730-9738 | Bolt, mach., dbl. hex. ext. wash. hd. PD shank, cres. AMS 5643 |
| MS9739-9747 | Bolt, mach. dbl. hex. ext. wash. hd. drilled, PD shank, cres. AMS 5643 |
| MS9748-9756 | Bolt, mach. dbl. hex. ext. wash. hd. PD shank, titanium AMS 4967 |
| MS9757-9765 | Bolt, mach., dbl. hex. ext. wash. hd., PD shank, drilled, titanium AMS 4967 |
| MS9781-9791 | Bolt, hex. hd., mach. full shank, AMS 5643 |
| MS9792-9802 | Bolt, mach., hex. hd. 1 hole, full shank, AMS 5643 |

| Bolt Number | Description |
|---------------|---|
| MS9803-9813 | Bolt, mach., hex. Hd. 1 hole, full shank, AMS 5643 |
| MS9814-9824 | Bolt, mach., hex. Hd. 1 hole, PD shank, AMS 5643 |
| MS9883-9891 | Bolt, mach., dbl. Hex. Ext. wash. Hd., AMS 5616 |
| MS9892-9900 | Bolt mach., dbl. Hex. Ext. wash. Hd., AMS 5616 drilled |
| MS9912-9920 | Bolt, mach., dbl. Hex. Ext. wash. Hd., PD shank, steel AMS 6322 cad. |
| MS9921-9929 | Bolt, mach., dbl. Hex. Ext. wash hd. PD shank, steel AMS 6322 cad. Drilled |
| MS9930-9938 | Bolt, mach., dbl. Hex. Ext. wash. Hd., full shank, steel AMS 6322 cad. |
| MS9939-9946 | Bolt, mach., dbl. Hex. Ext. wash. Hd., drilled, full shank, steel AMS 6322 cad. |
| MS20004-20024 | Bolt, int. wrench, 160 KSI |
| MS20033-20046 | Bolt, machine, hex. Head, 1200 °F |
| MS20073-20074 | Bolt, machine, aircraft, drilled hd., fine & coarse thr. |

| Bolt Number | Description |
|---------------|---|
| MS21091-21093 | Bolt, self-lock., 100° flush head, cross recessed |
| MS21094-21095 | Bolt, self-lock., hex. head |
| MS21096-21097 | Bolt, self-lock., pan-head, crass recessed |
| MS21098-21099 | Bolt, self-lock., 12 pt. ext. wrenching |
| MS21250 | Bolt, 12 pt., ext. wrenching |
| NAS144-158 | Bolt, internal wrenching, steel, 1/4-28 thru 1-1/8-12 |
| NAS333-340 | Bolt, 100°, close tolerance, hi-strength |
| NAS428 | Bolt, adjusting, crowned hex. hd. |
| NAS464 | Bolt, shear, close tolerance |
| NAS501 | Bolt, hex. head, drilled & undrilled |
| NAS551 | Bolt, universal fitting |

| Bolt Number | Description |
|--------------|--|
| NAS563-572 | Bolt, full thread, fully identified head |
| NAS583-590 | Bolt, 100° head, hi-torque, close tol. 160,000 psi |
| NAS624-644 | Bolt, twelve point external wrench, 180000 psi |
| NAS653-658 | Bolt, hex. head, close tolerance, ti. alloy |
| NAS663-668 | Bolt, full thread, fully identified head |
| NAS673-678 | Bolt, hex. head, close tolerance, ti. alloy |
| NAS1003-1020 | Bolt, machine, hex. head |
| NAS1053 | Eye Bolt Assembly, Shoulder nut |
| NAS1083 | Bolt, 100° flathead, titanium alloy |
| NAS1103-1120 | Bolt, machine, hex. head |
| NAS1202-1210 | Bolt, 100° phil. recessed, close tolerance, 16,000 psi |

| Bolt Number | Description |
|--------------|--|
| NAS1223-1235 | Bolt, self-locking, hex. head 250 °F |
| NAS1236 | Bolt, universal, Tube-end, flareless |
| NAS1243-1250 | Bolt, 100° head, hi-torq. 1600 psi |
| NAS1253-1260 | Bolt, 100° head, flush hd., .0312 O.S. hi-torque |
| NAS1261-1270 | Bolt, hex. head, short thread |
| NAS1271-1280 | Bolt, 12 point hd., external wrenching |
| NAS1297 | Bolt, shoulder, hex. head |
| NAS1303-1320 | Bolt, hex. head, close tolerance, 160,000 psi |
| NAS1414-1422 | Lock bolt, shear 100° head, all. steel |
| NAS1424-1432 | Lock bolt, shear protruding head, steel |
| NAS1503-1510 | Bolt, 100° flush head, hi-torq. |

| Bolt Number | Description |
|--------------|---|
| NAS1516-1522 | Lock Bolt, 100° head, pull type, al. Alloy |
| NAS1578 | Bolt, shear panhead, 1200 °F |
| NAS1580 | Bolt, tension, flush hd., 1200 °F |
| NAS1581 | Bolt, shear reduced 100 °F flush head, 1200 °F |
| NAS1586 | Bolt-tension, 1200 °F, 12 point, external wrenching |
| NAS1588 | Bolt, tension, flush hd., 1200 °F |
| NAS1703-1710 | Bolt, 100° head, .0156 O.S. shank, |
| NAS2005-2012 | Bolt lock, protruding head, ti. Alloy |
| NAS2105-2112 | Bolt, lock, 100° head, ti. Alloy |
| NAS2206-2210 | Bolt, lock, stump type, protruding head, ti. Alloy |
| NAS2306-2310 | Bolt, lock, stump type, 100° head, ti. Alloy |

| Bolt Number | Description |
|--------------|---|
| NAS2406-2412 | Bolt, lock, shear protruding head, ti. alloy |
| NAS2506-2512 | Bolt, lock, 100°head, ti. alloy |
| NAS2606-2612 | Bolt, lock, shear protruding head, ti. alloy |
| NAS2706-2712 | Bolt, lock, shear 100° head, ti. alloy |
| NAS2803-2810 | Bolt, lock, 100° hd., torq-set 180,000 psi |
| NAS2903-2920 | Bolt, hex. head, .0156 O.S. shank, 160,000 psi |
| NAS3003-3020 | Bolt, hex. head, .0312 O.S. shank, 160,000 psi |
| NAS3103-3110 | Bolt, U type |
| NAS3203-3210 | Bolt, hook |
| NAS3303-3305 | Bolt, U strap type |
| NAS4104-4116 | Bolt, 100° head, tri-wing recess, long thr., alloy stl. |

| Bolt Number | Description |
|--------------|---|
| NAS4204-4216 | Bolt, 100°head, tri-wing recess, long thr., cres. |
| NAS4304-4316 | Bolt, 100° head, tri-wing recess, long thr., titanium |
| NAS4400-4416 | Bolt, 100° head, tri-wing recess, short thr., alloy stl. |
| NAS4500-4516 | Bolt, 100° head, tri-wing recess, short thr., cres. |
| NAS4600-4616 | Bolt, 100° head, tri-wing recess, short thr., titanium |
| NAS4703-4716 | Bolt, 100° reduced, tri-wing recess, short thr., alloy stl. |
| NAS4803-4816 | Bolt, 100° reduced, tri-wing recess, short thr., cres. |
| NAS4903-4916 | Bolt, 100° reduced, tri-wing recess, short thr., titanium |
| NAS6203-6220 | Bolt, hex. head, short thread, alloy steel |
| NAS6303-6320 | Bolt, hex. head, short thread, cres. |
| NAS6403-6420 | Bolt, hex. head, short thread, titanium |

| Bolt Number | Description |
|--------------|--|
| NAS6604-6620 | Bolt, hex head, long thread, alloy steel |
| NAS6704-6720 | Bolt, hex. head, long thread, cres. |

27.4. Nuts

| Nut Part Number | Description |
|-----------------|--------------------------------------|
| AN256 | Nut, self-lock right angle plate |
| AN310 | Nuts, castellated |
| AN315 | Nut, plain |
| AN316 | Nut, check |
| AN320 | Nut, castle shear |
| AN335 | Nut, plain, hex, nonstructural |
| AN340 | Nut, plain, hex., n-s, course thread |
| AN341 | Nut, plain, hex. |

| Nut Part Number | Description |
|-----------------|---|
| AN345 | Nut, plain, hex., n-s, fine thread |
| AN350 | Nut, plain, wing |
| AN355 | Nut, engine, slotted |
| AN356 | Nut, stamped |
| AN360 | Nut, plain, engine |
| AN361 | Self-locking nut plate, countersunk 100°, 550 °F. |
| AN362 | Nut, plate, self-locking, noncounters., 550°F. |
| AN363 | Nut, self-locking, 550 °F. |
| AN364 | Nut, self-locking, thin, 250 °F. |
| AN365 | Nut, self-locking 250°F. |
| AN366 | Nut, plate, noncounters., 250°F. |

| Nut Part Number | Description |
|-----------------|--|
| AN373 | Countersunk nut, plate 100°, 250°F. |
| AN805 | Nut, union |
| AN817 | Nut, coupling |
| AN818 | Nut, coupling |
| AN924 | Nut, flared tube |
| AN3054 | Nut, coupling, elec. conduit |
| AN3066 | Nut, plain, hex. conduit coupling |
| AN6289 | Nut, flared tube universal fitting |
| AN121501-121550 | Nut, plain or cres. steel |
| AN121551-121600 | Nut, castel., hex. |
| MS9099-9100 | Nut, hex., boss connection, aluminum & cres. |

| Nut Part Number | Description |
|-----------------|--|
| MS9197-9199 | Nut, tube coupling |
| MS9200-9201 | Nut, plain, hex., boss connection |
| MS9356-9357 | Nut, plain hex., A-286 |
| MS9358-9359 | Nut, castellated hex., A-286 |
| MS9360 | Nut, plain hex. Drilled, A-286 |
| MS9361-9362 | Nut, plain hex. Check, A-286 |
| MS9363-9364 | Nut, slotted hex. Shear hd., A-286 |
| MS9553 | Nut, hex. Boss connection, cres. |
| MS9766-9767 | Nut, dbl. Hex. Cup washer locked, AMS 5737 cres. And AMS 6322 cad. |
| MS9881 | Nut, plain, hex. AMS 6322, cad. Plate |
| MS9882 | Nut, plain, hex., drilled, AMS 6322, cad. Plate |

| Nut Part Number | Description |
|-----------------|--|
| MS9951 | Nut, spanner, end slots, cup washer locked, AMS 6322 |
| MS16203 | Nut, plain, hex. Nonmagnetic |
| MS17825-17826 | Nut, self-locking, castle, hex. Regular and thin |
| MS17828 | Nut, self-locking, nylon insert, 250°, regular ht., monel |
| MS17829-17830 | Nut, self-locking, nylon insert, 250°, regular ht., cres. Steel, steel |
| MS19067-19068 | Nut, plain, round, retaining |
| MS20341 | Nut, electrical, plain, hex. |
| MS20364 | Nut, self-locking, 250 °F, thin |
| MS20365 | Nut, self-locking, 250° F, regular |
| MS20501 | Nut, plate, self-locking, two lug |
| MS21025 | Nut, castellated bearing, retaining |

| Nut Part Number | Description |
|-----------------|---|
| MS21047-21048 | Nut, self-locking, plate, two lug, low ht. |
| MS21049-21050 | Nut, self-locking, plate, two lug, 100° csk., low ht. |
| MS21051-21052 | Nut, self-locking, plate, one lug, low ht. |
| MS21053-21054 | Nut, self-locking, plate, one lug, 100° csk. |
| MS21055-21056 | Nut, self-locking, plate, corner, low ht. |
| MS21057-21058 | Nut, self-locking, plate, corner, 100° csk. |
| MS21059-21060 | Nut, self-locking, plate, two lug, floating, low ht. |
| MS21061-21062 | Nut, self-locking, plate, floating low ht., one lug |
| MS21069-21070 | Nut, self-locking, plate, two lug, low ht., reduced rivet spacing |
| MS21071-21072 | Nut, self-locking, plate, one lug, low ht., reduced rivet spacing |
| MS21073-21074 | Nut, self-locking, plate, corner, reduced rivet spacing |

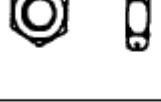
| Nut Part Number | Description |
|-----------------|---|
| MS21078 | Nut, self-locking, plate, two lug, nylon insert |
| MS21080 | Nut, self-locking, plate, one lug, nylon insert |
| MS21081 | Nut, self-locking, plate, corner, nylon insert |
| MS21083 | Nut, self-locking, hex., nylon insert |
| MS21340 | Nut, plain, hex., electrical, thin, wire holes |
| MS21917 | Nut, sleeve coupling, flareless |
| MS21921 | Nut, sleeve coupling, flareless |
| MS24679-24680 | Nut, plain cap, low & high crown |
| MS25082 | Nut, plain, thin, hex., electrical |
| MS27040 | Nut, plain square |
| MS27128 | Nut, plain, welding |

| Nut Part Number | Description |
|-----------------|---|
| MS27130-27131 | Nut, blind, rivet, flathead., open and closed end |
| MS27151 | Nut, stamped |
| MS27955 | Nut, spanner, plain, round |
| MS35425-35426 | Nut, wing, plain & drilled |
| MS35649-35650 | Nut, plain hex. |
| MS35690-35691 | Nut, plain hex. |
| MS35692 | Nut, slotted hex. |
| MS51967-51972 | Nut, plain, hex. |
| MS90415 | Nut, self-locking, 12 point captive washer |
| MS172236-172270 | Nut, spanner, bearing, retaining |
| MS172321-172370 | Nut, spanner |

| Nut Part Number | Description |
|---|--------------------------------------|
| NAS395-396 | Nut, U type |
|  | |
| NAS443 | Nut, self-locking, int. wrenching |
|  | |
| NAS444-445 | Nut, double lug, anchor type, offset |
|  | |
| NAS446 | Nut, flat type |
|  | |
| NAS447-448 | Nut, plate, self-locking |
|  | |
| NAS449 | Nut, anchor type |
|  | |
| NAS450 | Nut, plate, self-locking |
|  | |
| NAS463 | Shim, plain anchor nut |
|  | |
| NAS487 | Nut, instrument mount |
|  | |
| NAS500 | Shim, anchor nut, csk. |
|  | |
| NAS509 | Nut, drilled |
|  | |

| Nut Part Number | Description |
|---|--|
| NAS577-578 | Nut, self-locking floating barrel retainer |
|  | |
| NAS671 | Nut, plain hex., small pattern |
|  | |
| NAS680-681 | Nut, plate, self-locking, two lug |
|  | |
| NAS682-683 | Nut, plate, self-locking, one lug |
|  | |
| NAS684-685 | Nut, plate, corner, self-locking |
|  | |
| NAS686 | Nut, plate, self-locking, two lug, floating |
|  | |
| NAS687 | Nut, plate, self-locking, one lug |
|  | |
| NAS688-695 | Nut Assembly, self-locking, gang channel |
|  | |
| NAS696 | Nut, plate self-locking, one lug, miniature |
|  | |
| NAS697 | Nut, plate, self-locking, two lug, miniature |
|  | |
| NAS698 | Nut, plate, corner, self-locking, miniature |
|  | |

| Nut Part Number | Description |
|---|--|
| NAS1021-1022 | Self-locking Nut, hex., regular and low ht. |
|  | |
| NAS1023-1024 | Nut, plate, self-locking, two lug |
|  | |
| NAS1025-1026 | Nut, plate, self-locking, one lug |
|  | |
| NAS1027-1028 | Nut, plate, corner, self-locking |
|  | |
| NAS1029-1030 | Nut, plate, self-locking, one lug, two lug |
|  | |
| NAS1031 | Nut, plate, self-locking, two lug, floating |
|  | |
| NAS1032 | Nut, plate, self-locking, one lug, floating |
|  | |
| NAS1033 | Nut, plate, right angle, floating, self-locking |
|  | |
| NAS1034-1041 | Nut Assembly, self-locking, gang channel |
|  | |
| NAS1067 | Nut, plate, self-locking, one lug, miniature |
|  | |
| NAS1068 | Nut, plate, floating, self-locking, two lug, miniature |
|  | |

| Nut Part Number | Description |
|---|--|
| NAS1098 | Nut, tube fitting |
|  | |
| NAS1287-1288 | Nut, hexagonal, self-locking, nut and washer shear pin |
|  | |
| NAS1291 | Nut, hexagonal, self-locking, low height |
|  | |
| NAS1329 | Nut, blind rivet, flathead, internal thread |
|  | |
| NAS1330 | Nut, blind rivet, csk. Head, internal thread |
|  | |
| NAS1408-1409 | Nut, hexagonal, self-locking, regular height, coarse and fine thr. |
|  | |
| NAS1410 | Nut, tube fitting |
|  | |
| NAS1423 | Nut, plain, thin hex., drilled jamnut |
|  | |
| NAS1473 | Nut, plate, self-locking, two lug, cap floating |
|  | |
| NAS1474 | Nut, plate, self-locking, two lug, cap floating, reduced rivet spacing |
|  | |
| NAS1512-1513 | Nut, plate, self-locking gang channel |
|  | |

| Nut Part Number | Description |
|-----------------|---|
| NAS8679 | Nut, self-locking, low height 550 °F, 800 °F |

27.5. Washers

| Washer Number | Description |
|-----------------|---|
| AN935 | Washer, lock, spring |
| AN936 | Washer, tooth lock |
| AN950 and 955 | Washer, ball socket, ball seat |
| AN960 | Washer, flat |
| AN961 | Washer, flat electrical (Brass, silver or tin-plated) |
| AN970 | Washer, flat, wood |
| AN975 | Washer, flat |
| AN8013 | Washer, insulator |
| AN122576-122600 | Washer, plain steel |

| Washer Number | Description |
|---------------|---|
| MS9081 | Washer, key dbl. Bearing retaining |
| MS9274 | Washer, key, dbl. Bearing ret. Cres. |
| MS9276 | Washer, key, cres. AMS 5510 180° locking |
| MS9320-9321 | Washer, flat AMS 6350 and 5510 |
| MS9482 | Washer, flat, steel AMS 6437 or AMS 6485 diffused nickel cad. Csk |
| MS9549 | Washer, flat, AMS 5510 |
| MS9581 | Washer, key, cres. AMS 5510 90° locking |
| MS9582 | Washer, key, cres. AMS 5510 270° locking |
| MS9684 | Washer, cup, lock cres. AMS 5510 |
| MS9768 | Washer, flat, cres. AMS 5525 and AMS 5737 csk. |
| MS9880 | Washer, cup, lock cres. AMS 5510 |

| Washer Number | Description |
|---------------|--|
| MS9952 | Washer, cup, lock, spanner nut, cres. AMS 5646 |
| MS15795 | Washer, flat, metal |
| MS17811 | Washer, thrust, steel |
| MS19069-19070 | Washer, key, retaining |
| MS20002 | Washer, plain, csk., hi-strength |
| MS21258 | Washer, key, retaining, steel |
| MS25081 | Washer, key |
| MS27051 | Washer, slotted |
| MS27111 | Washer, finishing, countersunk |
| MS27129 | Washer, finishing, csk., 80°, 82° |
| MS27183 | Washer, flat, round |

| Washer Number | Description |
|-----------------|--|
| MS28777 | Washer, hydraulic, packing backup |
| MS35333-35334 | Washer, lock, flat internal tooth, light and heavy |
| MS35335-35336 | Washer, lock, flat and csk., external tooth |
| MS35337-35340 | Washer, lock, med., light, heavy |
| MS35790 | Washer, lock, 100° csk., ext. tooth |
| MS122026-122075 | Washer, lock spring |
| MS172201-172235 | Washer, key, single bearing, retaining |
| MS172271-172320 | Washer, key, single |
| NAS70 | Washer, plain |
| NAS143 | Washer, csk. and plain |
| NAS390-391 | Washer, finishing |

| Washer Number | Description |
|---------------|---|
| NAS460 | Washer, tab type |
| NAS513 | Washer, rod end locking, steel |
| NAS549 | Washer, flat, resin fiber |
| NAS620 | Washer, flat, reduced O.D. |
| NAS1061 | Washer, hi-temp, lock, spring |
| NAS1099 | Washer, bevel 9 1/2° |
| NAS1169 | Washer, dimpled 100° |
| NAS1197 | Washer, flat, 5052 aluminum |
| NAS1252 | Washer, flat |
| NAS1401 | Washer, radius, al. Alloy, steel, cres. Steel |
| NAS1515 | Washer, plastic and rubber |

| Washer Number | Description |
|---------------|-----------------------------------|
| NAS1587 | Washer, 1200 °F, plain and csk. |
| NAS1598 | Washer, sealing |
| NAS1636 | Washer, key dual tab |
| NAS1640 | Washer, lock, spring, nonmagnetic |

27.6. Pins

| Pin Number | Description |
|-------------|--------------------|
| AN253 | Pin, hinge |
| AN380 & 381 | Pin, cotter |
| AN385 | Pin, plain taper |
| AN386 | Threaded taper pin |
| AN392-406 | Pin, flathead |
| AN415 | Pin, lock |

| Pin Number | Description |
|-----------------|--|
| AN416 | Pin, retaining safety |
| AN122676-122775 | Pin, dowel steel |
| AN121601-121925 | Pin, flathead clevis .125 -.500 drilled shank |
| AN150201-150400 | Pin, lock, steel, brass |
| MS9047 | Pin, spring, steel, phosphated finish |
| MS9048 | Pin, spring, steel, cadmium plate |
| MS9105 | Pin, lock |
| MS9164 | Pin, straight, steel, headless, oversize |
| MS9245 | Pin, cotter, cres. AMS 7211 |
| MS9389 | Pin, straight, headless, lock, AMS 5735 |
| MS9390 | Pin, straight, headless, cres. AMS 5735, dowel std. & O.S. |

| Pin Number | Description |
|---------------|---|
| MS9462-9468 | Pin, straight hd. AMS 5735 |
| MS9486 | Pin, straight, headless, lock, AMS 5132 |
| MS9842-9848 | Pin, straight, headed, AMS 5616 |
| MS16555 | Pin, straight, headless .0002 over nominal size |
| MS16556 | Pin, straight, headless .001 over nominal size |
| MS16562 | Pin, spring, tubular, slotted |
| MS17984-17990 | Pin, quick release, positive lock |
| MS20253 | Pin, hinge |
| MS20392 | Pin, straight, headed, drilled |
| MS24665 | Pin, cotter |
| MS35671-35679 | Pin, grooved, headless, tapered groove |

| Pin Number | Description |
|-----------------|--|
| MS35810 | Pin, clevis, headed |
| MS39086 | Pin, spring, tubular coiled |
| MS51923 | Pin, spring, tubular coiled |
| MS51987 | Pin, tubular coiled |
| MS171401-171900 | Pin, spring, SS, steel |
| NAS427 | Pin, pulley guard, steel, al. Alloy |
| NAS561 | Pin, spring slotted and coiled, heavy duty |
| NAS574 | Pin, rear mounting |
| NAS607 | Pin, headless, dowel, steel |
| NAS1292-1296 | Pin, shear thread 100° flush head |
| NAS1322 | Pin, shear thread, protruding head |

| Pin Number | Description |
|--------------|---|
| NAS1332-1346 | Pin, quick release |
| NAS1353-1366 | Pin, quick release, positive locking, double acting |
| NAS1407 | Pin, spring, coiled |
| NAS1436-1442 | Pin, swage lock, 100° shear head, pull type, steel |
| NAS1446-1452 | Pin, swage lock, protruding head, pull type, steel |
| NAS1456-1462 | Pin, swage lock, 100° head, pull type, steel |
| NAS1465-1472 | Pin, swage lock, protruding head, pull type, steel |
| NAS1475-1482 | Pin, swage lock, 100° head, pull type, steel |
| NAS1486-1492 | Pin, swage lock, 100° head, stump type, steel |
| NAS1496-1502 | Pin, swage lock, protruding head, stump type, steel |
| NAS1525-1532 | Pin, swage lock, protruding head, al. alloy |

| Pin Number | Description |
|--------------|---|
| NAS1535-1542 | Pin, swage lock, 100° hd., tension, pull type, alum. |
| NAS1546-1552 | Pin, swage lock, 100° hd., tension, stump type, alum. |
| NAS1583 | Pin, 100° csk. hd., hi-shear rivet, 1200 °F |
| NAS1584 | Pin, flathead, hi-shear rivet, 1200 °F |

ABBOTT AEROSPACE SEZC LTD

We provide clean sheet engineering definition to detail design and analysis of composite and metallic structures.



STRATOS
AIRCRAFT

Our expertise includes compliance planning, structures, mechanical systems, landing gear and loads engineering.



We advise Innovation based startups on financial and risk management strategy

Contact us to find out how we can reduce risk, maximize your potential and help your project take flight.



CONTACT US